Mechanistic Investigation into the Pd-Catalysed C–H Bond Functionalisation of Fluoroarenes: Reaction Kinetics and Intermediate Characterisation

George Makoto Henry Platt

Doctor of Philosophy

University of York

Chemistry

September 2016

Abstract

This thesis reports on the results from mechanistic experiments performed on the Pd-catalysed direct arylation of iodoarenes with fluoroarenes. The C–H bond activation step of the reaction had originally been reported to undergo ambiphilic metal-ligand activation (AMLA) transition state (TS) based on DFT calculations. The proposed mechanism highlighted the potential of utilising combination of weak interactions to access typically inert C–H bonds. The key developments and the mechanistic studies of relevance in the field are initially highlighted for reactions supporting AMLA pathway (Chapter 1).

As a study of non-kinetic nature, the effects of reaction conditions on the product yields were investigated to understand the role played by the different reaction components (Chapter 2). The scope of the model reaction was studied for a series of polyfluoroarenes. The synthesis and characterisation of hypothesised catalytic intermediates were also reported.

Kinetic observations were made monitoring the reaction progress by *in situ* FT-IR spectroscopy (Chapter 3). The catalysis followed zeroth-order kinetics in ArI, first-order kinetics in C_6F_5H and between half- and first-order kinetics in the Pd catalyst. The reaction mechanism was complicated by a second competing reaction pathway independent of the C_6F_5H concentration. Experimental evidence confirmed the rate-limiting step of the main reaction pathway was the C–H bond cleavage of the fluoroarene by σ-aryl Pd species, via highly ordered TS with slight negative charge build up. The kinetic parameters of the reaction were determined from temperature dependence of the reaction rate. Evidence-driven optimisation of the catalytic cycle was also attempted using alternative catalyst systems.

The key catalytic intermediates were characterised by *in situ* NMR spectroscopy and *ex situ* MS analysis (Chapter 4). Dinuclear $[Pd(Ar)(\mu\text{-}OAc)(PPh_3)]_2$ was identified as the major intermediate of the reaction with trace quantities of mononuclear $Pd(Ar)(OAc)(PPh_3)_n$ (n = 1 or 2) also formed. These Pd species were successfully reacted with C_6F_5H in stoichiometric reaction and reported as competent catalysts. Rate acceleration was observed for reaction conditions with the $Pd(Ar)(OAc)(PPh_3)_n$ (n = 1 or 2) as the major intermediates.

A mechanism consistent with the experimental evidence was proposed for the two reaction pathways (Chapter 5). The main catalytic cycle reacted via AMLA(6)-TS with active on-cycle mononuclear Pd species in equilibrium with off-cycle reservoir of stable dinuclear Pd species. Although the exact identities of the second competing reaction pathways remain uncertain, possible mechanistic scenarios were suggested.

List of Contents

List of Tables

List of Figures

List of Schemes

Acknowledgements

I would like to thank my two amazing supervisors Professor Robin Perutz and Professor Ian Fairlamb for their support over the years. Their knowledge and experience were essential to the project. I also appreciate their patience and consideration, allowing me to take the project down the path of my interest. Of the many valuable lessons learned, Robin has taught me that research is incremental and Ian has taught me to always be enquiring. Furthermore, I am now a firm believer in the potential of catalytic nanoparticles. After 4 years, I could not have asked for better supervisors.

During my time at York I was blessed with the good fortune of meeting and working alongside incredible people. There are too many people to name individually here, but a number of friends played a crucial role in helping me continue pushing forwards with the research: Barbara Procacci (one reliable constant in the lab), Dan Smith (DaS), Sarah Pike (biscuit club), Jessica Milani (The Killers), Tom Ronson (-−–), Martin Voelkel (Discovery), Josh Bray (*in situ* FT-IR buddy), Alan Reay (Captain America to my Iron Man), Lyndsay Ledingham (GBBO), Kate Appleby (bestie), Ben Aucott (Geoffrey Boycott lover), Mary Kagoro (Mrs Reflux), and Lars Anders Hammarbäck (Madden and Sunday Night Football with Ali G's). I appreciate all the work done by the past group members, for building up the knowledge within the group and creating the friendly work environment. The openness of the chemistry department also allowed me to become friends with people outside of the inorganic group. Thank you to the distinguished members of the Lunch Soc: Mary Wheldon, Sarah Chambers, Aimee Clarke, Matt Lloyd, Ryan Gorman and Thomas Sanderson. Additionally, the technical support provided at York and the people in charge were fantastic: Naser Jasim (dry solvents and jokes), Charlotte Elkington (*in situ* FT-IR spectroscopy), Pedro Aguiar (HR-MAS NMR spectroscopy, but more importantly being a good friend. Go Pack Go!), Heather Fish (NMR spectroscopy) and Karl Heaton (MS).

The most influential person throughout my years of academic study has been Dr Maisha Jabeen. She has taught me the joy of working hard and inspires me every day to achieve the best I can. I am excited for where the future will take us, but for now, thank you for everything you have done for me.

Finally, I would like to thank Ian Platt, Sachiko Platt, Emma Platt, Anne Platt, George Platt (grandfather), Noriko Takahashi, Shigeko Takahashi and Sabro Takahashi for all the moral and financial support over the years. Thank you Emma for looking out for me. Thank you mum for all the work you do for the family. Thank you dad for always encouraging me to learn, and spending hours teaching me English, this thesis is dedicated to you.

Author’s Declaration

I declare that this thesis is a presentation of original work and I am the sole author, except where referenced or clearly indicated in the body of the text. The content has not previously been presented for an award at this, or any other, University. The work was carried out at the University of York between October 2012 and September 2016.

Chapter 1: Introduction

1.1 Benefits of Fluorine Substitution in the Aromatic System

The effect of a fluorine substituent in a molecule has been exploited in the agrochemical[1, 2], materials[3], and pharmaceutical[4, 5] industries, with 5–15% of all drug molecules produced globally in the last 50 years containing fluorine atoms (**Figure 1**). One of the earliest examples of a fluorinated-drug molecule is 5-fluoro-uracil (trademark name Efudex^{TM}), reported by Heidelberger and co-workers in 1957 for its anti-tumour properties not observed in 5-bromo-uracil.[6] Furthermore, the NMR active spin-½ ^{19}F-nucleus possesses an optimal gyromagnetic ratio for NMR spectroscopic analysis with 100% naturally occurring abundance. This provides a convenient method for isotopically labelling drug molecules.[7] The lack of any fluorinated biological compound or water signal simplifies analysis using ^{19}F NMR spectroscopy.[8]

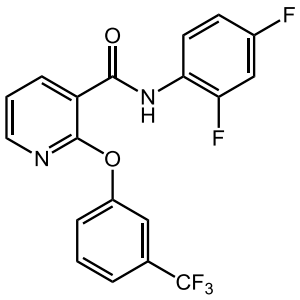

1

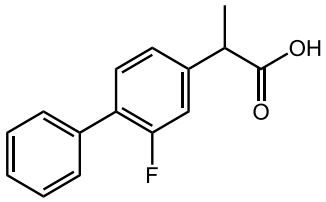

2

Figure 1. Examples of commercially available fluorine-containing compounds. Phytoene desaturase (PDS)-inhibiting herbicide **1** (Diflufenican, Bayer Cropscience Ltd)[9] and non-steroidal anti-inflammatory drug **2** (Ansaid, Pfizer Inc.).[10]

The incorporation of a fluorine atom into a molecule can have profound effect on its properties, summarised as the fluorine-substitution effect.[11, 12] The fluorine atom has been assigned the highest electronegativity of all the atoms with a value of 4.0 on the Pauling scale. As a consequence, changes in the electronic property of neighbouring carbons, the molecule's dipole moment, and the pKa are commonly observed. For example, a substitution of fluorine near a basic group such as amine allows for controlled reduction in basicity which improves metabolic stability and bioavailability of the whole molecule.[13] The electron deficiency caused by the σ-inductive effect of fluorine generally decreases overall polarizability of a molecule, resulting in improved solubility in fat and cell membrane penetration. Furthermore, the dipole of a C–F bond often enhances the binding selectivity and affinity to receptors and enzymes via favourable multipolar interactions.[14]

Contrary to some reports, a recent study by Mueller and co-workers suggests that C–F bonds are poor H-bond acceptors.[15] However, in fluorobenzene the hydrogen atoms in the *ortho*-positions are positively polarized, resulting in stronger C–H --- X (with X = O, N) and C–H --- π-interaction compared with non-fluorinated benzene.[16, 17]

Substitution of a fluorine atom for a hydrogen atom is a common bioisosteric replacement.[18] Although the Van der Waals radius of a fluorine atom (1.47 Å) is larger than a hydrogen atom (1.20 Å) and closer to a hydroxyl oxygen atom (1.52 Å), studies have shown fluorine to cause minimum conformational distortion when substituted for a hydrogen atom.[19-21] The introduction of C–F bond provides thermal and oxidative stability. It is one of the strongest carbon single bonds known (*e.g.* C–F bond dissociation energy for $X–C_6H_5$ = 525.5 ± 8.4 kJ mol^{-1}) compared with a C–H bond (*e.g.* C–H bond dissociation energy for $X–C_6H_5$ = 472 ± 2.2 kJ mol^{-1}).[22, 23] However, in the past, the fluorine-induced stability has caused sodium fluoroacetate, a metabolic poison used as pesticide, to accumulate as environmental pollution.[24, 25]

1.2 Preparation of Fluorinated Organic Molecules

Fluorinated-organic molecules are extremely rare in natural biological systems due to the low concentration of fluoride ions compared with chloride ions found in nature.[26-28] For this reason, organofluorine compounds are almost exclusively prepared synthetically.[29, 30] One method of preparation is by using an electrophilic or nucleophilic fluorine source.[31] A variety of relatively mild fluorinating reagents such as 1-chloromethyl-4-fluoro-1,4-diazoniabicyclo[2,2,2]octane bis(tetrafluoroborate) (Selectfluor®), bis(2-methoxyethyl)-aminosulfur trifluoride (Deoxo-Fluor®), anhydrous tetramethylammonium fluoride[32, 33] and 1,3-bis(2,6-diisopropylphenyl)-2,2-difluoro-2,3-dihydro-1*H*-imidazole (PhenoFluor™)[34, 35] have been utilised to avoid the use of highly hazardous F_2 and HF. However, the Balz-Schiemann reaction with arenediazonium salts remain the only practical method for fluoroarene preparation without the use of costly and toxic metals (*e.g.* Tl[9], Pb[10]) or reagents (*e.g.* diaryliodonium salt) in stoichiometric quantities.[36, 37] On the other hand, the metal-catalysed preparation of fluoroarenes requires milder reaction conditions and provides good functional group compatibility without undesired oxidation.[38-40] However, the thermal decomposition of metal-aryl-fluoride complexes can be complicated by dimerisation and kinetically-favoured P–F bond-forming reactions.[37] Buchwald and co-workers used [Pd^{II}(Ph)(F)(^{t}BuBrettPhos)] to successfully fluorinate limited examples of arenes, by creating a unique steric environment at the Pd^{II} metal centre.[41, 42] More recently, Ichiishi and co-workers have reported the transition metal-catalysed preparation of fluoroarenes using KF as the fluorinating reagent.[43-45] The application of late-stage

fluorination[46] for a rapid synthesis of aromatic ^{18}F-labeled probe molecules for ^{18}F positron emission tomography (PET) was reported by Lee and co-workers.[47]

Alternatively, readily fluorinated small molecules may be combined together using standard synthetic methods. These methods provide good control, despite being limited by the range of small molecules available. Perhaps one of the greatest achievements in the field of transition metal-catalysed synthetic chemistry has been the development of carbon-carbon bond-forming reactions. These transformations involve highly controlled bond formation between two carbon atoms and allow the construction of a complex molecular skeleton. An example such transformations are the Mizoroki-Heck reactions[48-50] where organohalides are reacted with terminal alkenes in the presence of a base. Some of the most general and widely applied methods for C–C bond formation are the cross-coupling reactions. Cross-coupling reactions commonly require an organohalide or a pseudohalide, and an organometallic transmetallating reagent as a counterpart. Many named coupling-reactions exist today classified by the transmetallating reagent used (**Scheme 1**).[51] These include, but are not limited to, Kumada-Corriu (Grignard reagents and organolithiums),[52-56] Sonogashira (terminal alkynes),[57-59] Negishi (organozincs),[60-62] Stille (organostannanes),[63-65] Suzuki-Miyaura (organoboronic acids),[66-69] and Hiyama (organosilanes).[70-72] Modifications and improvements to the reactions have been made with improved product yields and substrate scope. Of the many transition metals used in C–C bond forming reactions, Pd has been one of the most applied and studied metals to date, often with the advantage of good air and moisture tolerance.

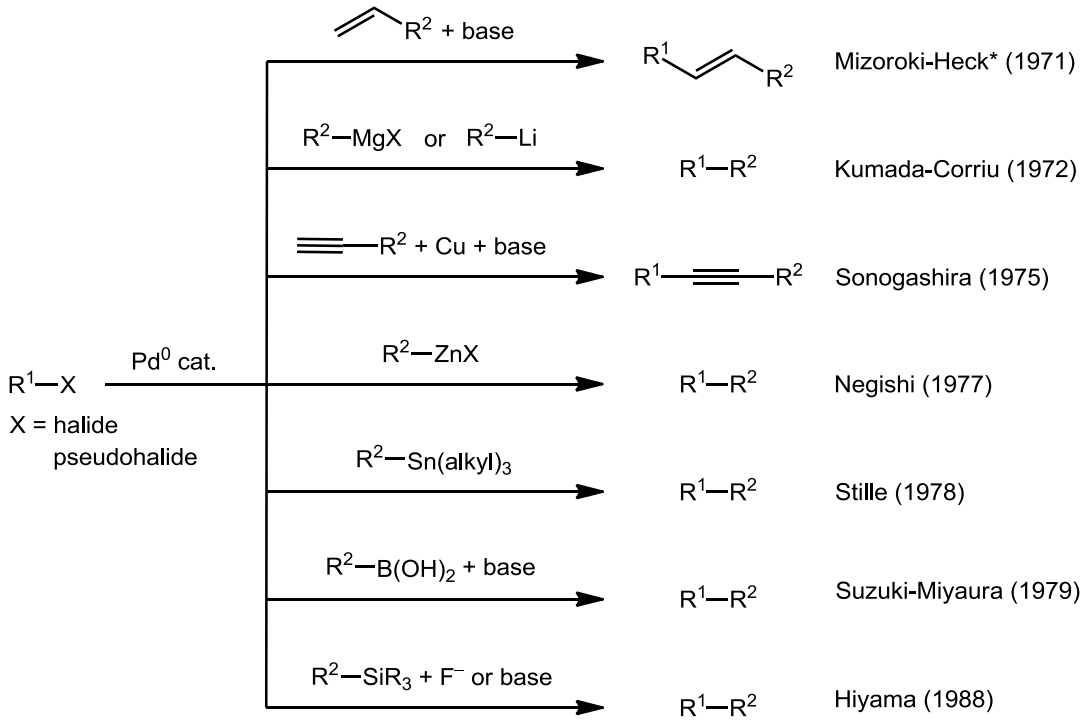

Scheme 1. Simplified examples of the original named Pd-catalysed C–C bond forming cross-coupling reactions and the year of publication (* not formally a cross-coupling reaction).

Pd-catalysed coupling reactions have been applied extensively in the preparation of industrially significant molecules on kilogram scales.[73] The synthesis of clinical candidates for the inhibition of stress-activated kinase p38α **3** (**Scheme 2**)[74] and the treatment of peripheral artery disease (PAD) **5** (**Scheme 3**)[75] were achieved by Suzuki-Miyaura and Mizoroki-Heck reactions respectively. Both examples demonstrate the high efficiency and the general applicability of the methodology for the preparation of fluorine-containing molecules. The importance of the field was acknowledged in 2010 through the award of the Nobel Prize in Chemistry to Heck, Suzuki and Negishi.[76]

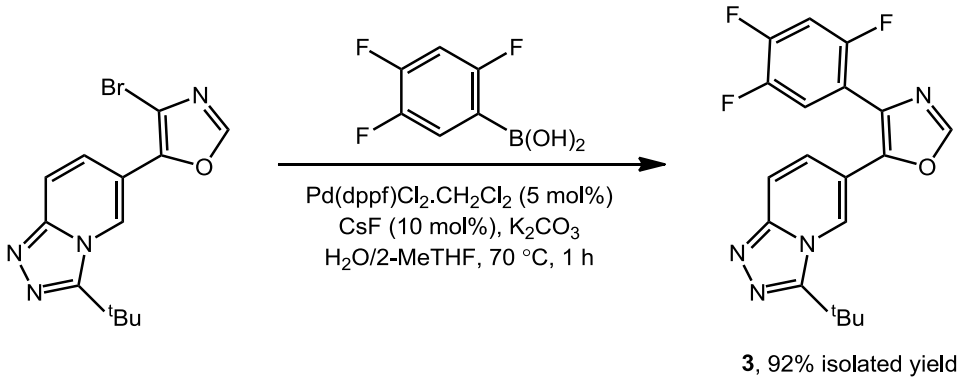

Scheme 2. Suzuki-Miyaura cross-coupling applied to the final step in the scalable synthesis of kinase inhibitor **3** reported by Pfizer Global R&D (Li and co.).[74]

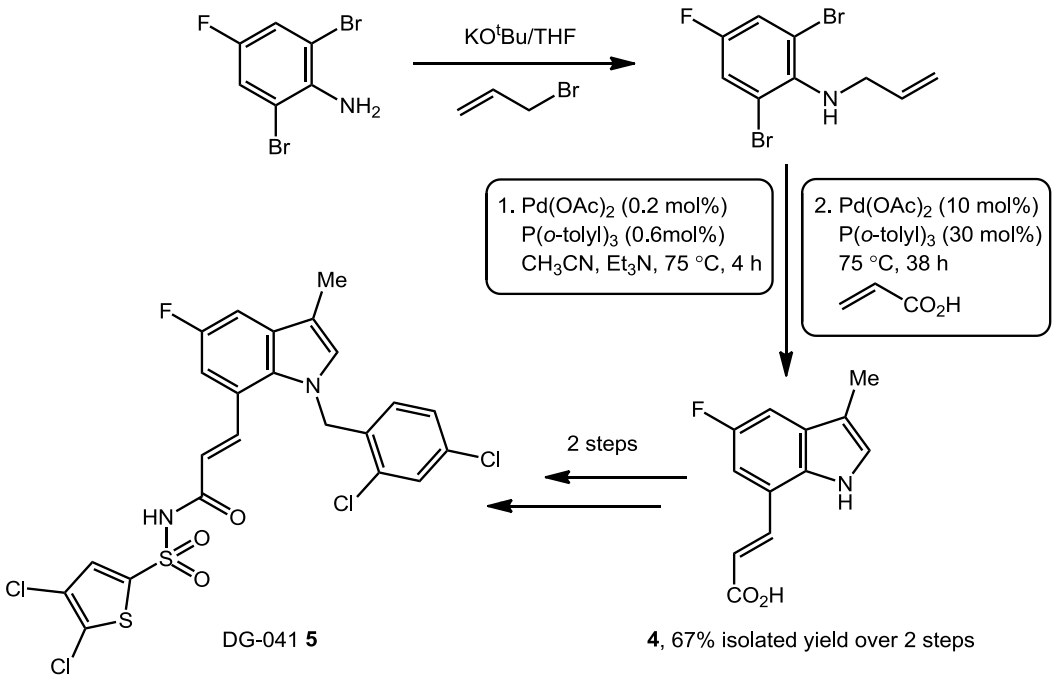

Scheme 3. One-pot synthesis of prostaglandin E2 receptor 3 (EP3) receptor antagonist DG-041 **5** utilising sequential Mizoroki-Heck reaction (highlighted in the boxes) for the synthesis of intermediate **4** (Zegar and co.).[75]

Functionalisation of pentafluorobenzene has been reported in the literature for the nucleophilic substitution reaction of the corresponding Grignard or alkyllithium reagents[77] and dimethyl zinc mediated allylic polyfluoroarylation reaction.[78] However, cross-coupling reaction of pentafluorobenzene is typically achieved by using pentafluorobenzyl halide[79-81], due to the low reactivity of electron-deficient polyfluorinated transmetallating reagents[82, 83] and the competitive hydrodeboration reaction.[84] Alternatively, C–F bond activation of polyfluoroarenes has been utilised as a method of accessing fluorinated molecules.[85-89] Braun and co-workers reported a Ni-catalysed chemo- and regio-selective functionalisation of 2,3,5,6-tetrafluoropyridine **6a** and pentafluoropyridine **6b** for accessing the 2-vinyl derivatives **7a** and **7b** (**Scheme 4**).[90]

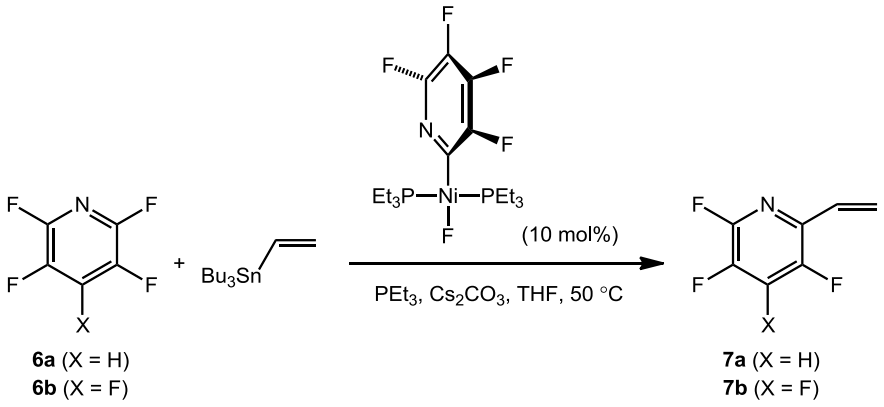

Scheme 4. Ni-catalysed Stille cross-coupling reaction via C–F bond activation (Braun and co.).[90]

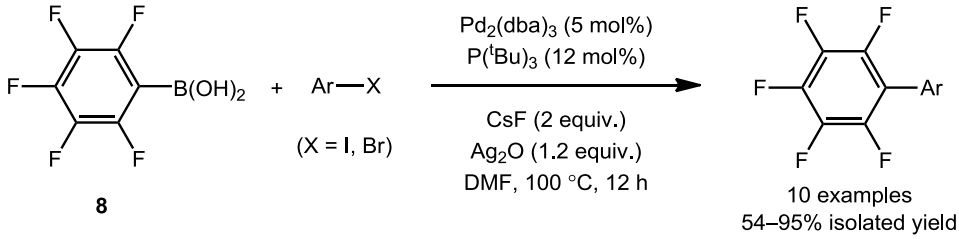

Scheme 5. Suzuki-Miyaura cross-coupling reaction of pentafluorophenylboronic acid **8** with aryl halide (Korenaga and co.).[91]

An example of Pd-catalysed Suzuki-Miyaura cross-coupling reaction of pentafluoro-phenylboronic acid **8** was reported by Korenaga and co-workers (**Scheme 5**).[91] The Ag_2O additive is a known promoter for Suzuki-Miyaura cross-coupling.[92, 93] Silver(I) is proposed to adsorb the reaction intermediates and enhance the electrophilicity of the Pd, allowing for the aryl transfer from weakly nucleophilic transmetallating reagents.[94] Frohn and co-workers have also reported the synthesis of polyfluorinated biaryls using $K[C_6F_5BF_3]$[95-97] and $Li[C_6F_5B(OMe)_3]$[98] as reagents which are more stable in basic condition compared with boronic acids. Alternatively, a synthesised pre-catalyst **9** was used by Kinzel and co-workers for the coupling reaction of polyfluoroboronic acids (**Scheme 6**).[99]

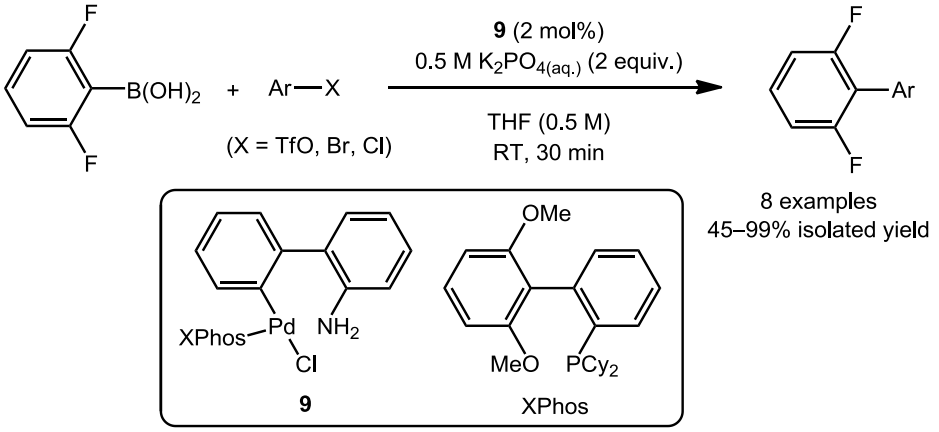

Scheme 6. Suzuki-Miyaura cross-coupling using synthesised pre-catalyst **9** (Kinzel and co.).[99]

1.3 Mechanism of Pd-Catalysed C–C Bond Formation Reactions

The mechanism for the Pd-catalysed C–C bond cross-coupling reactions depends on the variables of specific reaction condition.[100] However, the generally accepted homogeneous catalytic cycle (first model proposed by Stille[64]) begins with the oxidative addition of organohalide R-X (X = halide or pseudohalide) to the Pd^0 metal centre (**Scheme 7**). The resulting Pd^{II} species react with the different transmetallating reagents [M]-R^2 to form *trans*-biaryl Pd species which undergoes isomerisation to give *cis*-biaryl Pd complex. Reductive elimination of the biaryl product regenerates Pd^0 complex to complete the

catalytic cycle. It is important to note that nanoparticulate metals can often play significant roles in catalytic reactions proposed as homogeneous catalysis.[101, 102]

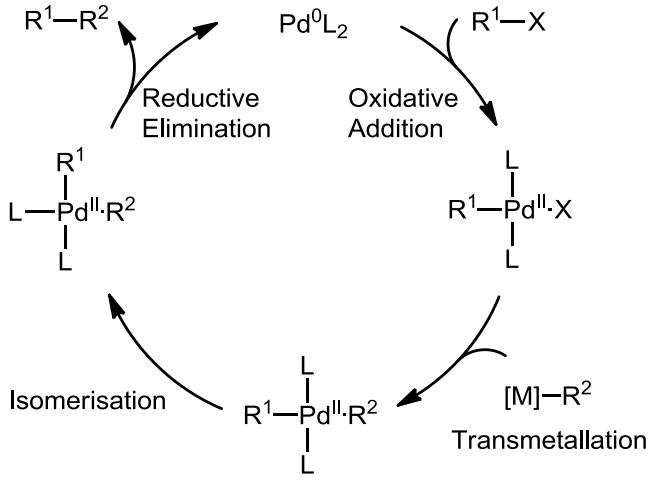

Scheme 7. General mechanism of the Pd^0/Pd^{II}-catalysed C–C bond-forming cross-coupling reactions.

The major differences between the cross-coupling reactions are the organometallic nucleophiles involved (*i.e.* hard or soft). Many mechanistic studies have been published with focus on identifying the intermediates and the transition states (TS) involved in the catalytic cycle, important factors to consider for evidence-driven reaction optimisation. The transmetallation step of Stille coupling reaction is one such example. In the original publication, an electrophilic cleavage of the Sn–C bond (*i.e.* S_E2) with "open" TS **10**[64] was proposed. However, a competing mechanism involving "closed" TS **11**[103, 104] was later suggested with the reaction pathway depending on the X ligand and the polarity of the solvents (**Scheme 8**). Experimental evidence indicated that the "open" TS **10** was favoured in coordinating solvents with X ligands incapable of acting as a bridging group (*e.g.* TfO, L) and the "closed" TS **11** was favoured in non-coordinating solvents with X ligands capable of acting as a bridging group (*e.g.* Cl, Br, I).[105-107] The two transition states **10** and **11** affect the stereochemistry of the reaction products, therefore, the understanding of the mechanism allows the reaction condition to be tailored for the preparation of a desired target molecule.

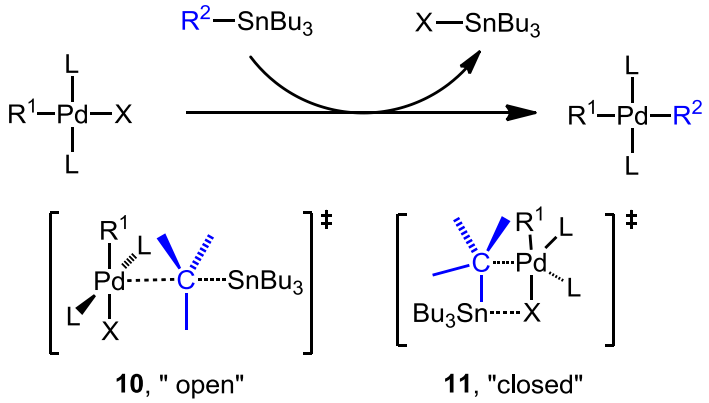

Scheme 8. Proposed "open" **10** and "closed" **11** transition states for Stille cross-coupling reactions.

The critical role of base additive in the Suzuki-Miyaura cross-coupling was studied by Amatore and co-workers.[108] The base was initially considered to be involved in the formation of aryl hydroxyborates $R^2B(OH)_2(OR)^-$ and $Pd^{II}R^1L_2$-OR (R = H, Me etc.) species as the reactive intermediates of the catalytic cycle. However, it was demonstrated by kinetic studies and stoichiometry reactions, that OH^- was required for the formation of the active complex *trans*-$[Pd(R^1)(OH)(L)_2]$ **12**, but also inhibited the reaction by forming poorly reactive anionic $R^2B(OH)_3^-$ **13** (**Scheme 9**). This was highlighted by the bell-shaped dependence of the reaction rate on the OH^- concentration. For reaction optimisation, it was then necessary to determine the concentration of the base additive required for generating maximum concentration of the active P^{II}-OH **12** and minimum concentration of $R^2B(OH)_3^-$ **13**.

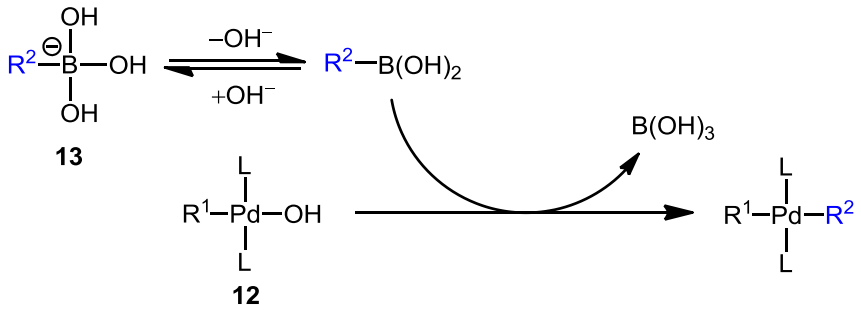

Scheme 9. Transmetallation step involved in the Suzuki-Miyaura cross-coupling reactions.

Unlike the cross-coupling reactions, Mizoroki-Heck reactions do not proceed through a transmetallation step. Instead, the key step for the reaction is the stereoselective *syn*-insertion of alkene into the Pd–C bond, followed by the β-hydride elimination (**Scheme 10**).[109] The reaction was proposed as proceeding through two pathways starting with the dissociation of either anionic (X) or neutral (L) ligands.[110] The difference in the electrophilicity of the resulting intermediates is one of the factors affecting the regioselectivity of the product formed.

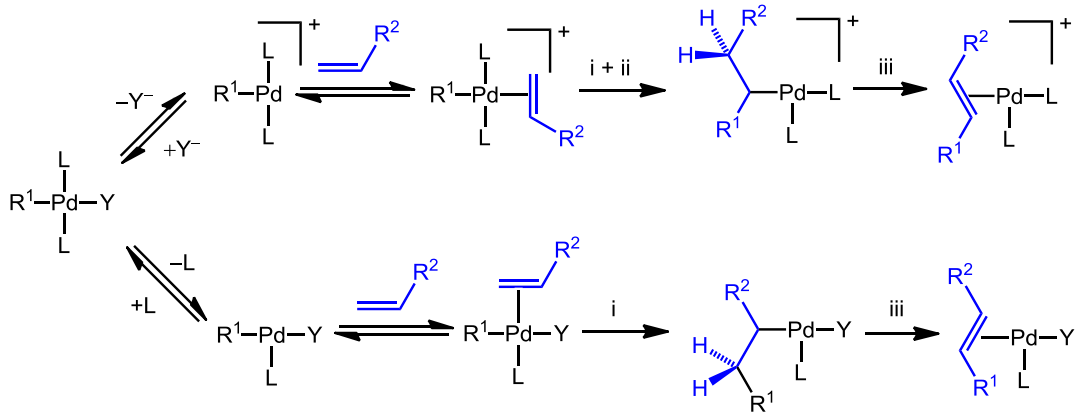

Scheme 10. Alkene insertion **(i)**, isomerisation **(ii)**, and β-hydride elimination **(iii)** steps in the Mizoroki-Heck reaction.

1.4 Pd-Mediated C–H Bond Functionalisation Reaction

Metal-mediated direct C–H bond functionalisation reactions have been studied extensively in the past decade as cost-effective, eco-friendly and sustainable alternatives to conventional cross-coupling reactions, with better atom economy and less metal waste.[111] Synthetic methodologies such as oxidative direct arylation, direct arylation and dehydrogenative arylation all involve the activation of C–H bonds to a varying degree with the latter making the preparation of the organometallic reagent redundant (**Scheme 11**). The strategies are most commonly applied to aryl-aryl bond formation as it avoids the pre-functionalisation of aromatics with electropositive heteroatoms.[112, 113]

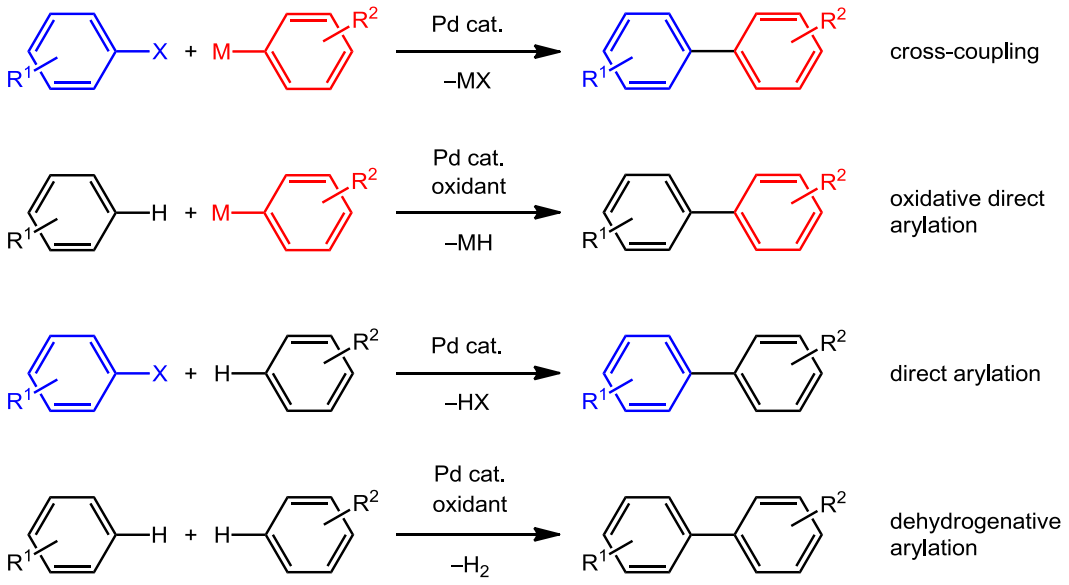

Scheme 11. Pd-catalysed methodologies for the synthesis of biaryls.

Although dehydrogenative arylation is considered the most atom-efficient C–C bond forming reaction, controlling the regioselectivity of two substrates with diverse C–H bond groups in an intermolecular reaction is a major problem.[114] In this regard, direct arylation methodology provides a better control by using readily available aryl halides or pseudohalides.[115] Over the last decade, a wide range of aromatic hydrocarbons have been shown to undergo C–H bond functionalisation reactions in the presence of carboxylates.[116] The strategy has been successfully applied to the functionalisation of electron-rich (*e.g.* indole)[117, 118], neutral (*e.g.* benzene)[119], and poor (*e.g.* pyridine *N*-oxide)[120] aromatic systems. The direct arylation of a fluoroarene is an example with significant industrial interest for the potential in accessing fluorinated compounds without pre-synthesised organometallic species.[121] The technique provides an additional tool for synthetic chemists to incorporate the fluorine atom into the target structure via intra- and inter-molecular reactions. The original work by Lafrance and co-workers reported on the synthetic methodology and the mechanism of the reaction based on density functional theory (DFT) calculations.[122] Direct arylation of aryl halides **15** with polyfluorobenzenes **14** was catalysed by combination of $Pd(OAc)_2$ and the HBF_4 salt of di(*tert*-butyl)methylphosphine, in the presence of K_2CO_3 (**Scheme 12**). The polyfluorinated biaryl products **16** were mostly isolated in good to excellent yields. The reaction has since been reported for Au[123], Ru[124] and Cu[125] catalysts, and for modified reaction conditions[126, 127], and utilised to access complex molecular structures.[128]

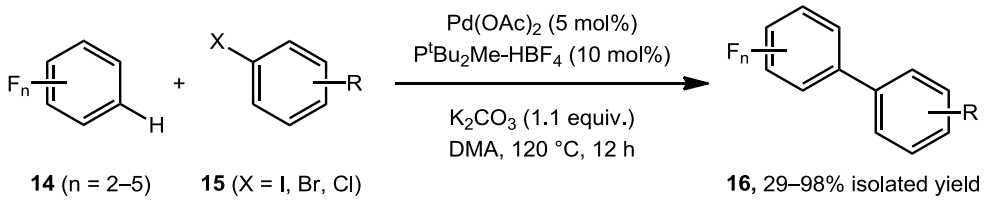

Scheme 12. Direct arylation of aryl halide **15** with polyfluoroarene **14** (Lafrance and co.).[122]

There are many examples of transition metal-catalysed intra- and inter-molecular C–H bond activation reactions reported to date with extensive mechanistic and kinetic investigation.[129] A range of different reaction pathways have been proposed from Heck-type[130-133], oxidative additions, σ-bond metathesis to electrophilic aromatic substitution (S_EAr)[117, 118, 134], with the S_EAr mechanism commonly reported for the direct arylation of electron-rich arenes such as benzoxazole and indolizine.[135] More recently, a mechanism involving ambiphilic metal-ligand activation (AMLA) between an aryl-Pd κ^1-carboxylate intermediate and an aromatic reactant has been proposed.[136, 137] The AMLA(6)-TS is characterised by the simultaneous coordination of hydrogen atom of the aromatic substrate to the intramolecular carboxylate and the stabilisation of the carbanion by the metal

(**Figure 2** a). The numbers in the bracket specifying the number of atoms involved in the cyclic TS. The earliest examples of AMLA(6) transition states were observed in stoichiometric reactions of mercuration[138, 139] and cyclopalladation[140-142] (**Figure 2** b and **Figure 2** c). The mechanism of AMLA(6) highlights the potential of enhancing the reactivity of typically inert bond by combination of multiple weak interactions working in synergy.[137] As suggested by the name of the TS, the activation process of the C–H bond involves both the metal and the ligand. The H-bonding interaction between the C–H bond and the acetate increases the electron density on the C–H bond. The resulting enhancement in the agnostic interaction polarises the C–H bond and increases the acidity of the proton, making it easier to cleave. A variety of terms such as "internal electrophilic substitution" (IES)[143, 144] and "concerted metalation deprotonation" (CMD)[137, 145, 146] have been coined to describe the mechanism involving range of ligands and other transition metals (*e.g.* Ru and Ir).

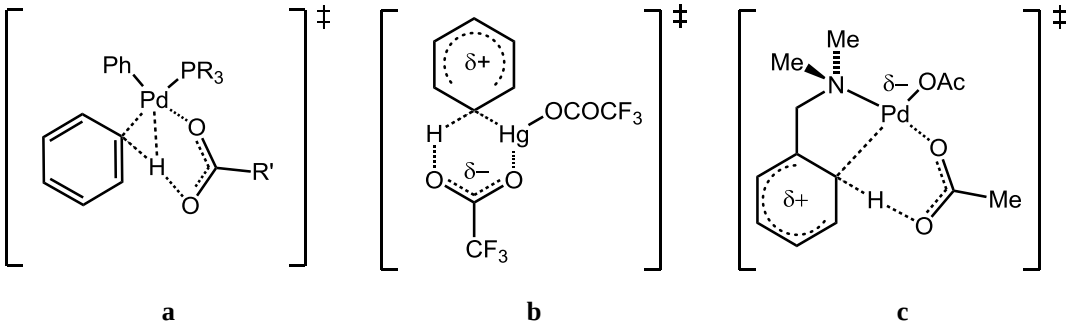

a **b** **c**

Figure 2. Ambiphilic metal-ligand activation (AMLA) transition states for **(a)** direct arylation reaction, **(b)** mercuration reaction, **(c)** cyclopalladation reaction.[116]

The mechanism for the direct arylation of polyfluoroarenes was proposed by Lafrance and co-workers (**Scheme 13**).[122] The catalytic cycle is similar to the cross-coupling reaction, starting with the oxidative addition of aryl halide to Pd^0 species. Following the ligand exchange of the halide with the carbonate anion, the resulting κ^2-CO_3 complex was hypothesised to react with polyfluoroarenes via AMLA(6)-TS to form the bisaryl-Pd complex. Similar to the Mizoroki-Heck reaction, the oxidation state of the Pd^{II} remains unchanged upon the addition of the second substrate.[147] The reductive elimination of the product biaryl completed the catalytic cycle with the regeneration of the Pd^0 species.

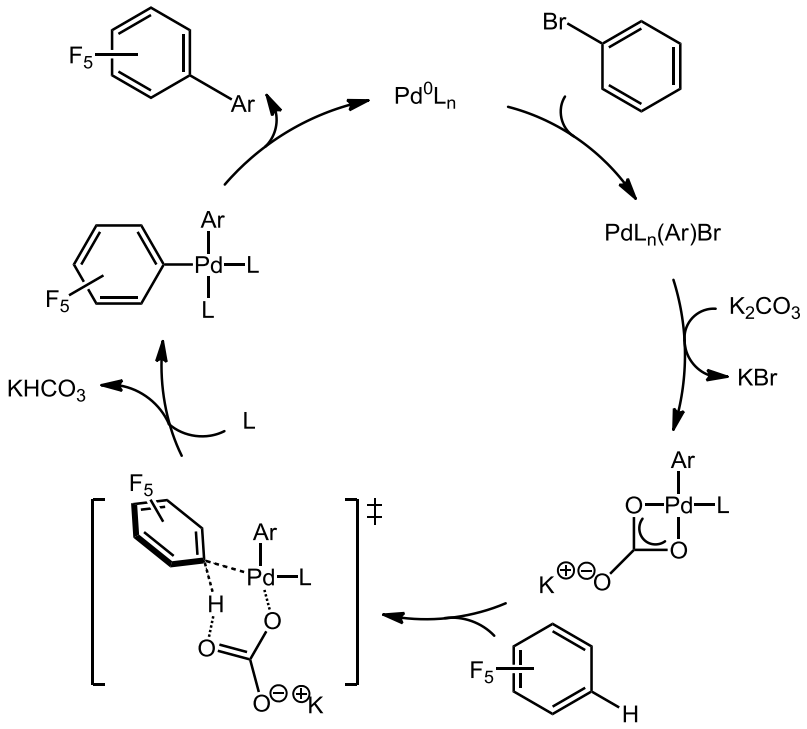

Scheme 13. Proposed catalytic cycle for the direct arylation of aryl halide with polyfluorobenzene (Lafrance and co.).[122]

The challenge of intermolecular direct C–H bond functionalisation reaction, just like any C–H bond functionalisation, is to control the regioselectivity of the C–H bond cleaved in the process. One of the most common methods to overcome this obstacle is by using substrates with metal-coordinating functional groups that can act as a directing group (DG) (**Figure 3**).[115, 148-150]

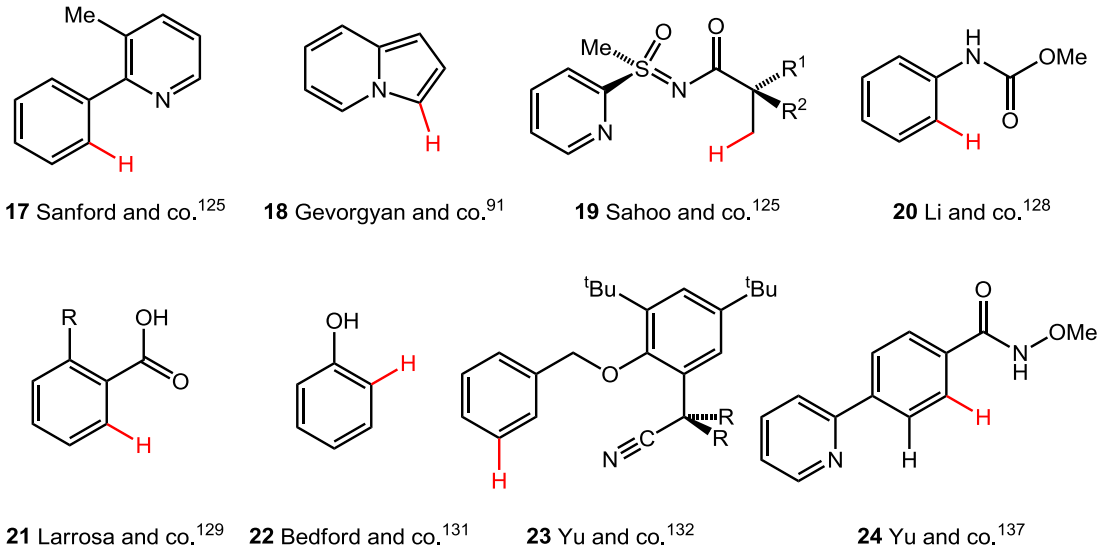

Figure 3. Examples of substrates reported in Pd-catlaysed, regioselective, DG assisted direct C–H bond functionalisation. The functionalised C–H bonds are highlighted in red.

The formation of cyclopalladated intermediate by the Lewis basic DG (*e.g.* nitrogen, sulfur, phosphorus and oxygen) facilitates an intramolecular C–H bond cleavage of substrates such as 2-phenylpyridine **17**[151] and indolizine **18**, often *ortho* to the DG.[117] Reactions taking advantage of removable DG have also been reported. An example of this strategy was highlighted by Sahoo and co-workers using *S*-methyl-*S*-2-pyridyl-sulfoximine (MPyS) **19** as an easily removable and reusable DG.[152, 153] Simpler structural motifs such as aniline carbamate **20**[154], and carboxylic acids **21** have also been utilised as removable DG post functionalisation.[155] While the removal of aniline carbamate from compound **20** results in 1° amine, the protodecarboxylation of compound **21** provides a method to functionalise in the *meta*-position to the R-group. Luo and co-workers also demonstrated a one-pot *meta*-selective direct arylation of phenol **22** by performing carboxylation of the substrate under high pressure of carbon dioxide (**Scheme 14**).[156] The reaction of phenol **22** under normal reaction conditions results in *ortho*-functionalisation as reported by Bedford and co-workers.[157]

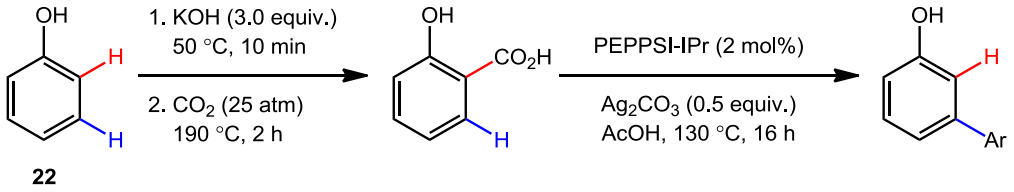

Scheme 14. One-pot *meta*-selective direct arylation of phenol **22** utilising CO_2 as transient DG (Luo and co.).[156]

Another strategy employed in the DG driven C–H bond functionalisation is to use a molecular structure designed to provide a versatile template for the desired transformation.[158] The *meta*-arylation of toluene derivatives **23**, aniline, phenol and heterocycles were achieved by Yu and co-workers using nitrile-based DG.[159-162] The same group have also demonstrated the functionalisation of C–H bond in the *ortho*-position to the *N*-methoxy amide (CONHOMe) **24** was favoured over the C–H bond in the *ortho*–position to the pyridine.[163] The use of *N*-methoxy amide **24** overcame the structural limitation of having multiple coordinating functional groups in the substrate and provided a synthetic route to functionalise medicinally important heterocyclic substrates.

The success of DG assisted C–H bond functionalisation reactions has vastly expanded the application of direct arylation methodology. Despite the advantages of controlling the regioselectivity of the transformation, the functional group coordinating to the catalyst can often result in catalyst poisoning. Additionally, it is desirable to have regioselective reactions without the directing groups.[164] Polyfluoroarenes are one of the few known group

of substrates to undergo regioselective functionalisations driven by the electronic and steric properties of the arenes.

The substituent effects on intramolecular C–H bond cyclisation were studied by Garcia-Cuadrado and co-workers comparing the regioselectivity in a molecule **25** capable of coupling to fluorinated and non-fluorinated arenes (**Scheme 15** a).[165] Experimental and computational DFT calculations suggested the fluorine atom was able to act as a directing-group with 14:1 regioselectivity favouring the *ortho*-position to the fluorine. Similar results were obtained for the intermolecular reactions, notably the coupling of 1,3-difluorobenzene **26** and 4-bromotoluene **27** which affords C2 substituted biaryl **28** in 85% yield (**Scheme 15** b).[122] Competition experiments confirmed that the C–H bond between two *ortho*-fluorines to be more reactive than the C–H bond adjacent to one *ortho*-fluorine. Dehydrogenative cross-coupling of polyfluorobenzenes were reported by Li and co-workers, utilising the *ortho*-fluorine induced regioselectivity to form the desired products **30** from fluoroarene **26** and benzene **29** (**Scheme 15** c).[166, 167]

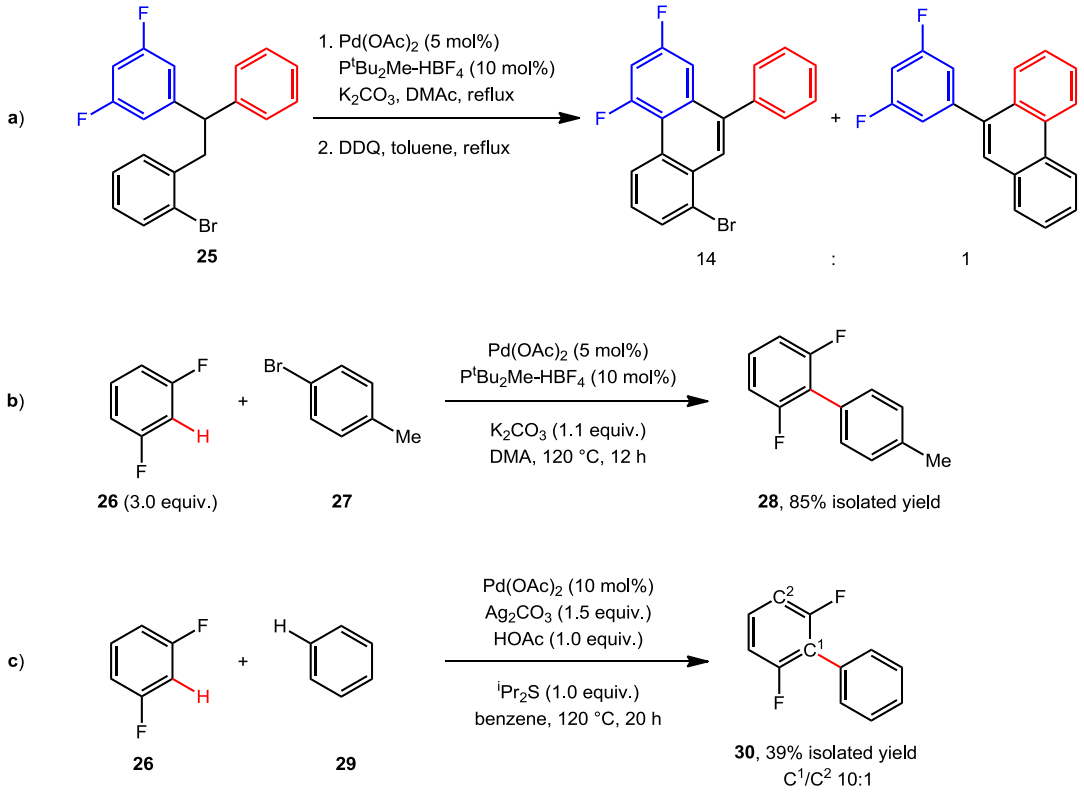

Scheme 15. **(a)** Pd-catalysed intramolecular direct arylation of fluorine substituted bromobenzyldiarylmethanes **25** (Echavarran and co.).[165] **(b)** Pd-catalysed direct arylation reaction of 1,3-difluorobenzene **26** with 4-bromotoluene **27** to form the 2,6-difluoro-4′-(methyl)biphenyl **28** (Lafrance and co.).[122] **(c)** Pd-catalysed dehydrogenative cross-coupling of 1,3-difluorobenzene **26** with benzene **29** to regioselectively form the 2,6-(difluoro)biphenyl **30** (Li and co.).[166]

The fluorine-induced regioselectivity is commonly referred to as the *ortho*-fluorine effect. The best explanation for the origin of this effect has been illustrated by the correlation between the calculated energy barrier for AMLA(6)-TS and relative dissociation energies of the Pd–C bond formed (**Figure 4** a).[168] The substrates were successfully classified into three groups based on the number of fluorine atoms in the *ortho*–position to the activated C–H bond. An attempt has been made by Gorelsky and co-workers to link the regioselectivity to the pKa and thus the C–H bond dissociation energies of the Ar^F–H bond.[169] However, the reagent classification by this method failed to clearly distinguish between the three classes of fluoroarenes (**Figure 4** b), and incorrectly predicted the regioselectivity of pyridine and 3-methylindolizine C–H bond functionalisation. Therefore, the acidity is unlikely to be a decisive factor for substrate reactivity, but rather a general trend that is observed.

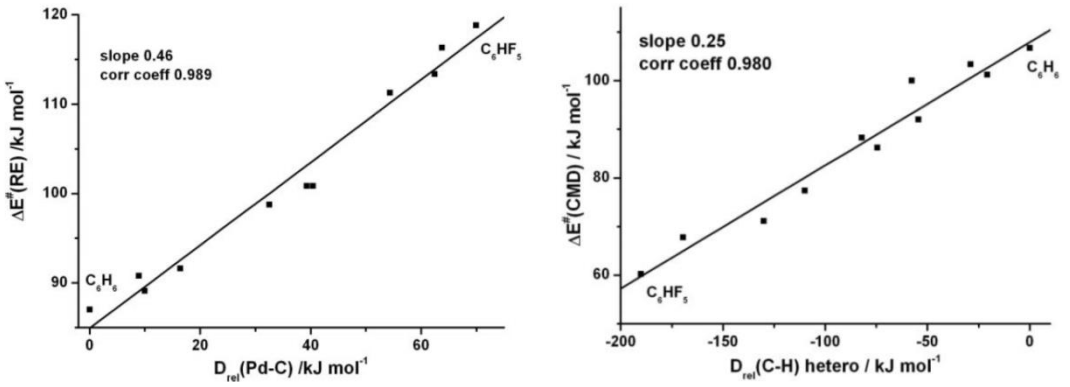

a **b**

Figure 4. Correlation between calculated energy barriers and **(a)** dissociation energies of Pd–C bond, **(b)** the relative C–H bond dissociation energies of the Ar^F–H bond.[168] (Reprinted with permission from J. Guihaumé, E. Clot, O. Eisenstein and R.N. Perutz, *Dalton Trans*., 2010, **39**, 10510–10519. Copyright 2016 Royal Society of Chemistry.).

1.5 Mechanistic Studies on the AMLA Pathway

The properties of metal complexes able to activate C–H bond and their modes of action are of great interest in understanding how to react conventionally inert bonds. Pioneering work on acetate-ligand-assisted C–H bond activation at Pd metal was reported by Ryabov and co-workers.[141] The formation of cyclopalladated acetato-bridged dinuclear species **32** was observed in a mixture of trinuclear $Pd_3(OAc)_6$ and substituted *N*,*N*-dimethylbenzenes **31** (**Scheme 16**). The *ortho*-selective C–H bond activation was directed by the amine coordination and driven by the proximity effects. The *ortho*-palladation involving C–H bond cleavage was identified as the rate-limiting (RL) step from the primary kinetic isotope effect (KIE) of $k_H/k_D = 2.2 \pm 0.2$. A highly ordered TS was proposed based on the large negative activation entropy (*ca.* –250 J K^{-1} mol^{-1}) of the reaction. The slope of the

Hammett plot obtained by varying the R^1 and R^2 substituents on compound **31** was $\rho = -1.6$, indicating positive charge build-up during the TS. Based on this experimental evidence, TS **33** involving inner-sphere C–H bond cleaveage of metal arenium by the acetate was proposed. However, DFT calculations on the possible reaction pathways performed by Davies and co-workers indicated the reaction involved TS **34** with agostic C–H bond interaction[170] instead of the originally proposed Wheland intermediate **33**.[142] The activation energy for the reaction with AMLA(6)-TS was calculated as 54 kJ mol^{-1}, close to the experimentally determined activation enthalpy of 46 kJ mol^{-1}. For some examples of cyclometalation reactions, the initial step of κ^2-κ^1 displacement of the acetate was shown to be the RL-step instead of the C–H bond activation step.[136]

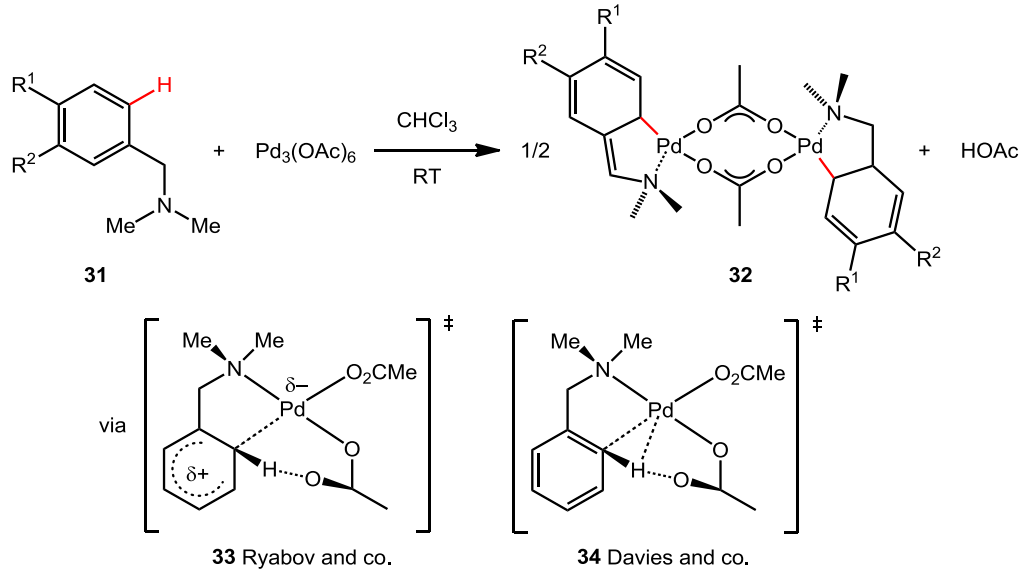

Scheme 16. Cyclopalladation of substituted *N*,*N*-dimethylbenzenes **31**, and the proposed transition states **33** (Ryabov and co.)[141] and **34** (Davies and co.).[170]

In addition to the development of Pd-mediated stoichiometric C–H bond activation reactions, Ru-mediated reactions have been studied extensively. Detailed experimental and computational mechanistic studies on the cyclometalation reaction of complex **35** for the synthesis of ruthenium metathesis catalysts **36** were reported by Cannon and co-workers (**Figure 5**).[171] The reaction was first-order in ruthenium dicarboxylate species generated *in situ* with increased rate for carboxylates (O_2CR) with more electron donating R-groups. A primary KIE of $k_H/k_D = 8.1 \pm 1.7$ was also reported. The kinetic observations made on the intramolecular methylene C(sp^3)–H bond activation were consistent with AMLA(6) pathway involving inner-sphere carboxylates.

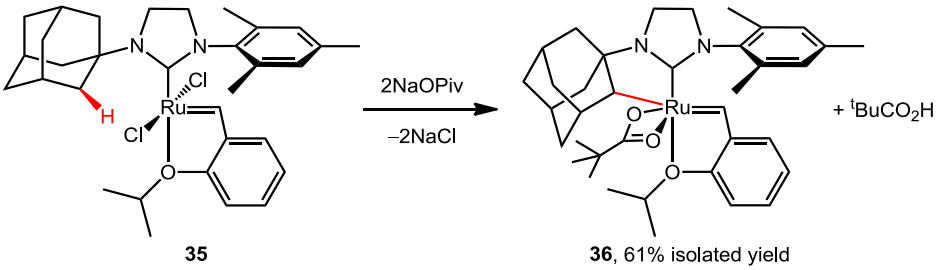

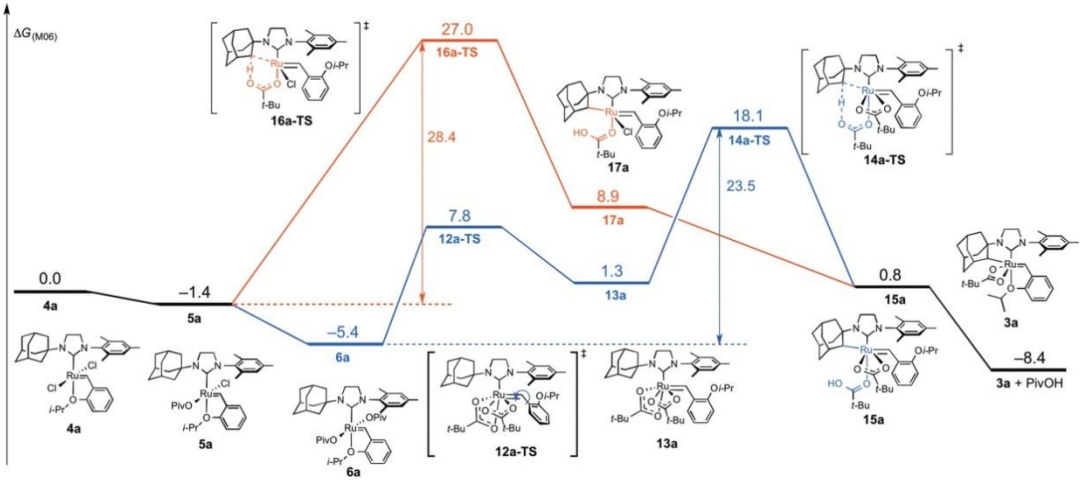

Figure 5. The structures and the free energies of potential intermediates involved in the cyclometalation of Ru-alkylidene complex **35** via AMLA(6) pathway. The energies are in kcal mol^{-1} at 25 °C.[171] (Reprinted with permission from J.S. Cannon, L. Zou, P. Liu, Y. Lan, D.J. O'Leary, K.N. Houk and R.H. Grubbs, *J. Am. Chem. Soc.*, 2014, **136**, 6733–6743. Copyright 2016 American Chemical Society.).

An increasing number of catalytic reactions involving different substrate and conditions have been proposed to take place via the AMLA(6) pathway based on DFT calculations.[145] However, detailed experimental mechanistic studies of direct arylation are still limited, with the Pd-catalysed reaction of pyridine *N*-oxide **37** and arylbromide **38** being one of them (**Scheme 17**).[172] Studies by ^{1}H NMR spectroscopy showed first-order kinetics in pyridine *N*-oxide **37** and half-order kinetics in Pd(P^{t}Bu$_3$)$_2$ catalyst concentration, suggesting an off-cycle equilibrium of mononuclear and dinuclear Pd species.[172] The Arrhenius and the Hammett plots were also reported with the E_a = 77 kJ mol^{-1} and ρ = +1.53 for 4-substituted pyridine *N*-oxides.

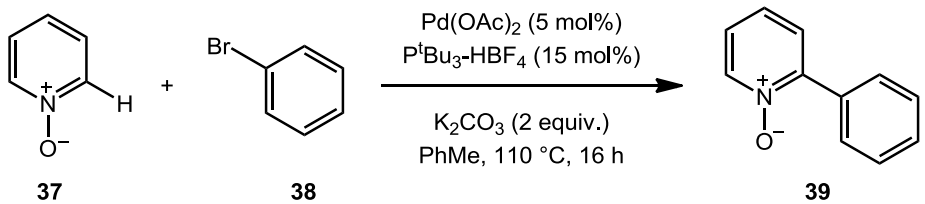

Scheme 17. Direct arylation of bromobenzene **38** with pyridine *N*-oxide **37** (Sun and co.).[172]

A half-order dependence in dinuclear Pd complex [Pd(μ-OAc)(^{t}Bu$_2$PCMe$_2$CH$_2$)]$_2$ **40** was later confirmed for the same reaction by Tan and co-workers.[173] This complex was thought to be in equilibrium with the cyclometalated-κ^2-acetato-Pd^{II} monomer **41**. Contrary to the earlier report by Sun and co-workers[172], the mechanism was suggested to involve two merging catalytic cycles (A and B) with two separate Pd centres (**Scheme 18**). The cycle A involved the oxidative addition of the arylbromide **38** to Pd^0 complex. The C–H bond activation of pyridine *N*-oxide **37** was facilitated by the mononuclear complex **41** in equilibrium with the dinuclear species **40** in cycle B. The transmetallation of the aryl group from the complex **42** of cycle B to the oxidative addition product **43** in cycle A results in the biaryl complex Pd(Ar)(2-pyridyloxide)(P^{t}Bu$_3$) **44** which forms the product **39** by reductive elimination. Further evidence for the coorperative mechanism was provided by Duric and co-workers.[174] Since the reaction rate was unaffected by the nature of the aryl halide and Pd–Ar complex, it was concluded that the Pd–Ar complex is not involved in the RL-step of the direct arylation reaction.

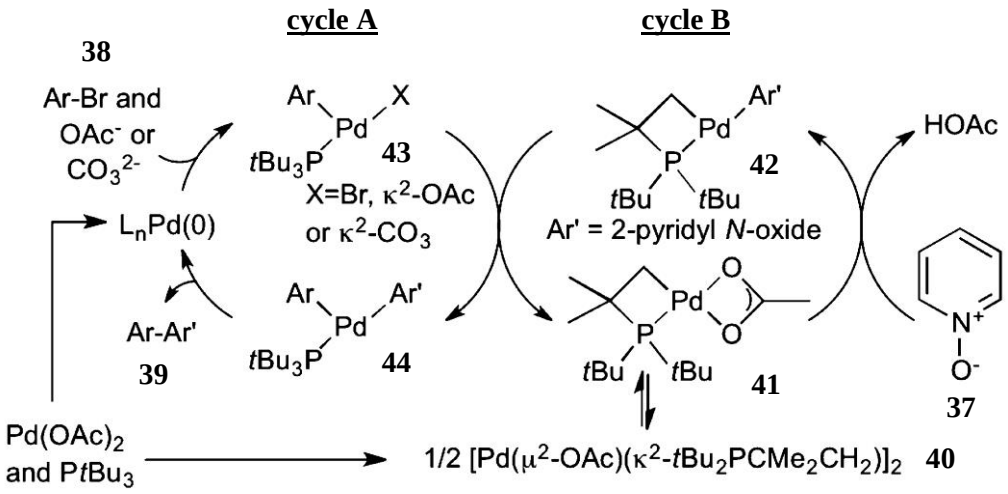

Scheme 18. Cooperative catalytic cycles involving Pd species, proposed as the mechanism for the reaction shown in **Scheme 17**.[173] (Adapted with permission from Y. Tan, F. Barrios-Landeros and J.F. Hartwig, *J. Am. Chem. Soc.*, 2012, **134**, 3683–3686. Copyright 2016 American Chemical Society.)

In another study by Wakioka and co-workers, dinuclear [Pd(Ar)(μ-OAc)(PPh$_3$)]$_2$ (Ar = Ph, 2-MeC$_6$H$_4$, 2,6-Me$_2$C$_6$H$_3$) **45** complex was successfully reacted with 3-methylthiophene **46** in 43% NMR yield (**Scheme 19**).[175] Following reductive elimination of the biaryl product **47**, formation of Pd precipitate, AcOH and PPh$_3$ were observed in the absence of any added base. The build-up of PPh$_3$ in the reaction mixture was rationalised to result in the formation of catalytically inactive Pd(Ar)(κ^1-OAc)(PPh$_3$)$_2$ **48** as a by-product which was formed in 47% NMR yield. Based on the proposed AMLA(6) pathway, a delayed formation of the Pd by-product **48** was expected. However, a kinetic study to clarify on this

hypothesis was not reported. The RL-step of the reaction was identified as the reductive elimination step based on lack of notable KIE.

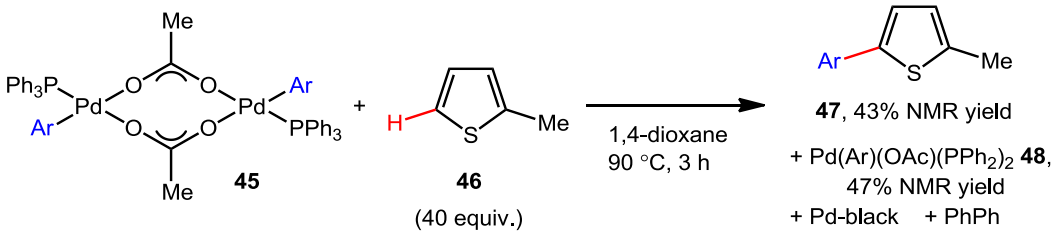

Scheme 19. Stoichiometric reaction of dinuclear complex **45** (Ar = Ph, 2-MeC_6H_4, 2,6-$Me_2C_6H_3$) with 2-methylthiophene **46**. The product yields based on NMR integration (Wakioka and co.).[175]

Wakioka and co-workers also reported the isolation of a stable monomeric Pd complex with *N*-bound benzothiazole **50** from a mixture of [Pd(2,6-$Me_2C_6H_3$)(μ-OAc)(PPh_3)]$_2$ **45** and benzothiazole **49** (**Figure 6**).[176] Further heating at 65 °C achieved 50% NMR yield to the C2-arylated benzothiazole product. The primary KIE of k_H/k_D = 3.3–5.5 and DFT calculations supported RL-step involving AMLA(6)-TS with complex **50** as the intermediate following C–H bond activation. Furthermore, the key catalytic intermediate of the reaction, a monomeric Pd complex Pd(Ar)(κ^2-OAc)(PPh_3) **51**, was shown to exist in equilibrium with the dinuclear complex **45** in solution (**Scheme 20**).

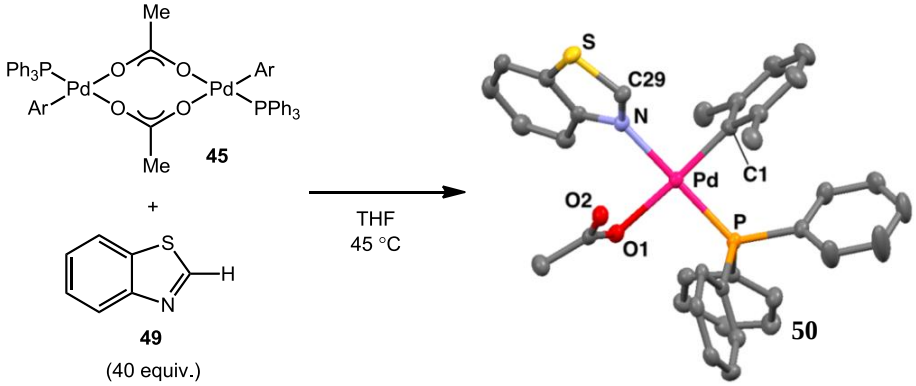

Figure 6. X-ray crystal structure of [Pd(Ar)(*N*-BT)(κ^1-OAc)(PPh_3)] **50** (BT = benzothiazole), a monomeric Pd complex with *N*-coordinated benzothiazole **49** with 50% probability ellipsoids.[176] (Adapted with permission from M. Wakioka, Y. Nakamura, Y. Hihara, F. Ozawa and S. Sakaki, *Organometallics*, 2013, **32**, 4423–4430. Copyright 2014 American Chemical Society.)

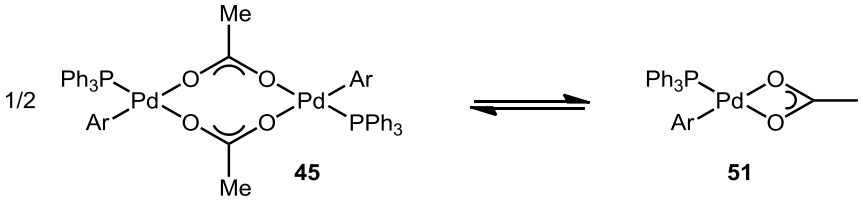

Scheme 20. Equilibrium between dinuclear [Pd(Ar)(μ-OAc)(PPh_3)]$_2$ (Ar = Ph, 2-MeC_6H_4, 2,6-$Me_2C_6H_3$) **45** and mononuclear Pd(Ar)(κ^2-OAc)(PPh_3) **51** in solution.

The kinetic investigation of Ru^{II} facilitated C–H bond activation of 2-phenylpyridine was reported by Ferrer Flegeau and co-workers.[177] Three key observations were made regarding the role of the acetate anion in the reaction. Firstly, irreversible C–H bond cleavage was observed with no deuterium incorporation into the substrate in the presence of deuteron AcOH. Secondly, the reaction was accelerated by increased concentration of carboxylic acid, suggesting the involvement of non-coordinating acetate in the RL-step of the mechanism. Thirdly, an acetate-coordinated Ru complex [Ru-C_6H_4-Py(OAc)(*p*-cymene)] **A** was observed during the reaction prior to the solvent coordinated complex [Ru-C_6H_4-Py(S)(*p*-cymene)] $\mathbf{B}^+$. Based on these observations, an autocatalytic mechanism involving irreversible C–H bond cleavage by intermolecular carboxylate was proposed (**Scheme 21**). In contrast, the equivalent Pd-catalysed reaction was not accelerated by the addition of AcOH and concluded to react via intramolecular process [*i.e.* AMLA(6)].[178]

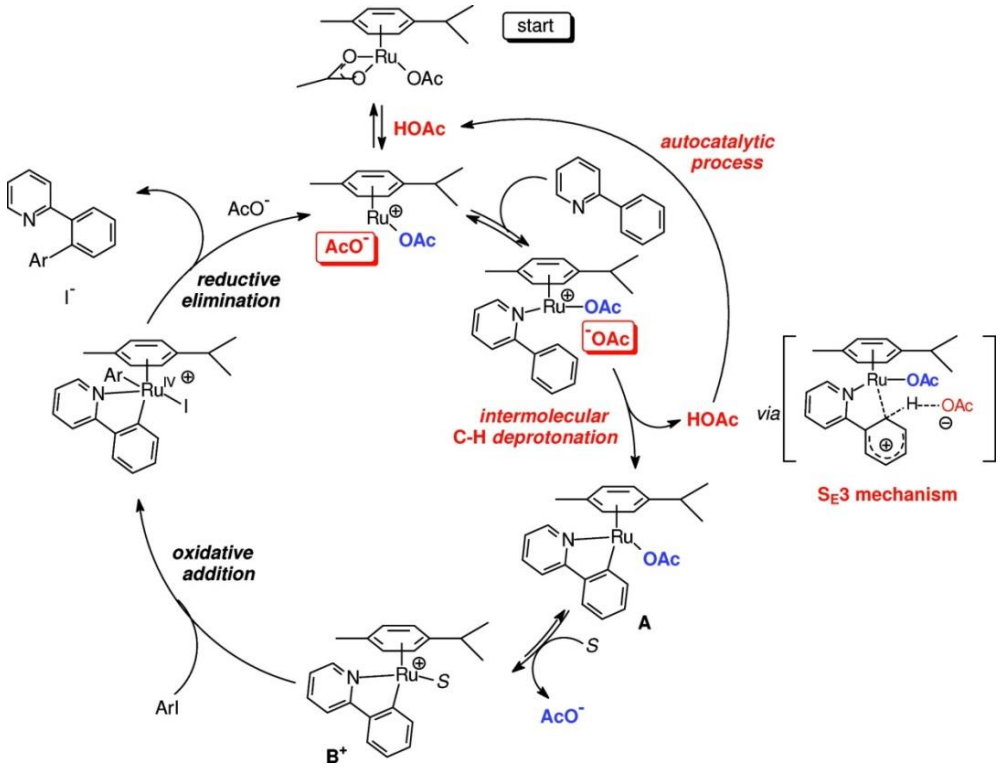

Scheme 21. Catalytic cycle for the Ru-catalysed direct arylation of phenyl pyridine.[177] (Reprinted with permission from E.F. Flegeau, C. Bruneau, P.H. Dixneuf and A. Jutand, *J. Am. Chem. Soc*., 2011, **133**, 10161–10170. Copyright 2016 American Chemical Society.)

The regioselective direct arylation reaction of iodoarene **53** with activated monofluoroarene **52** (by non-covalent π-complexation with $Cr(CO)_3$) was reported by Ricci and co-workers (**Scheme 22**).[179] The reaction conditions suffer from poor atom economy. However, the approach provides a strategy for enhancing the reactivity of arenes previously inert towards direct C–H bond activation reactions. The product **54** was further functionalised at the C–F bond by nucleophilic aromatic substitution reactions. Additionally, the reaction conditions

were successfully applied to the direct arylation of unsubstituted benzene to form the product in 42% yield.

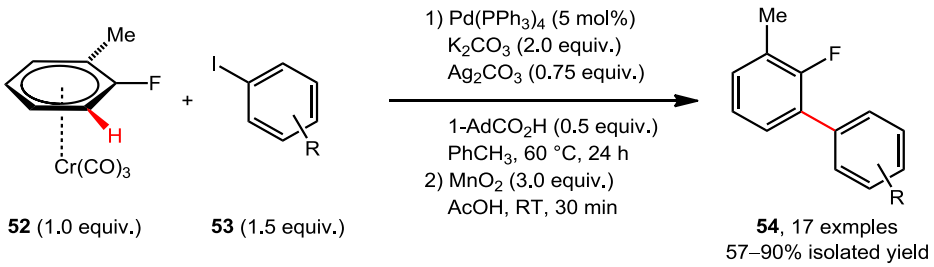

Scheme 22. Pd-catalysed direct arylation of iodoarene **53** with fluoroarene-$Cr(CO)_3$ complex **52** to form biaryl product **54** (Ricci and co.).[179]

The mechanistic investigation of the reaction revealed zeroth-order kinetics in the iodoarene **53** and Pd, with positive order dependence in the fluoroarene **52**, Ag, and PPh_3. The C–H bond cleavage was identified as the RL-step of the reaction based on the primary KIE (*ca.* 2.3) observed. Since the $AgAdCO_2(PPh_3)$ generated *in situ* was capable of reacting with the C–H bond of the substrate **52**, a cooperative heterobimetallic catalytic cycles involving Ag and Pd species was proposed (**Scheme 23**).[180] In a similar study, Lotz and co-workers demonstrated AgC_6F_5, formed from the reaction of AgOPiv and pentafluorobenzene via AMLA(6)-TS, as a transmetallating reagent in a Pd-catalysed reaction.[181] It is important to note these studies were specifically concerned with $AdCO_2^-$ and $PivO^-$ as the inner-sphere base involved in the C–H bond activation.

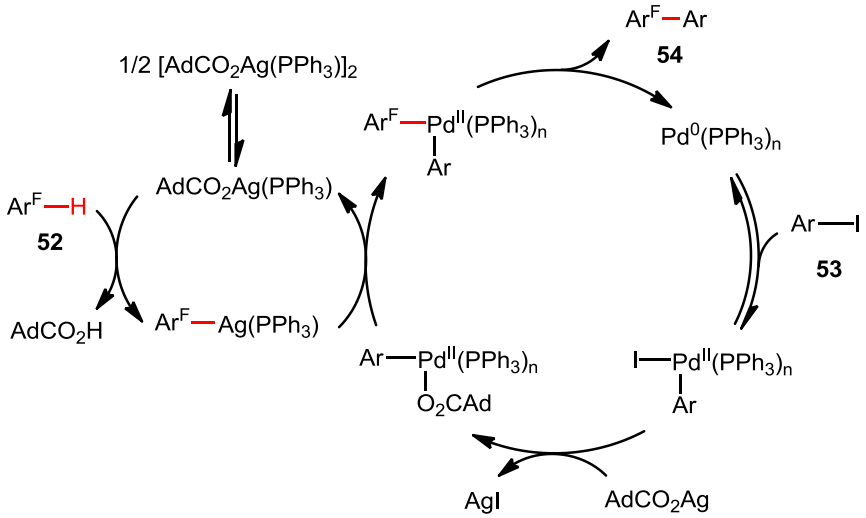

Scheme 23. Cooperative heterometallic catalytic cycles involving Ag and Pd species proposed as the mechanism for the reaction shown in **Scheme 22** (Whitaker and co.).[180] (Adapted with permission from D. Whitaker, J. Burés and I. Larrosa, *J. Am. Chem. Soc.*, 2016, 138, 8384–8387. Copyright 2016 American Chemical Society.)

The improved understanding of AMLA(6)-TS has inspired some creative modifications to the direct C–H bond functionalisation reaction. One such example is the catalytic direct borylation of heteroarenes (*i.e.* furans, pyrroles and electron-rich thiophenes) under metal-free conditions reported by Légaré and co-workers.[182] The mononuclear form of the frustrated Lewis pair **55** was designed to mimic the AMLA(6)-TS of metal-catalysed reactions (**Scheme 24**). The RL-step of the reaction was the C–H bond activation step of the heteroarenes and the resulting intermediate was proposed to react with pinacolborane (HBpin) via σ-bond metathesis. The reaction provides a method for synthesising products without using precious metals and free of toxic trace metal impurities.

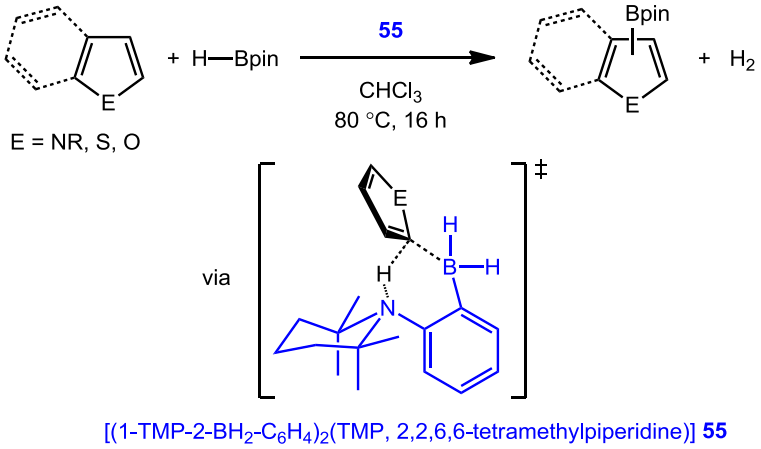

[(1-TMP-2-BH_2-C_6H_4)$_2$(TMP, 2,2,6,6-tetramethylpiperidine)] **55**

Scheme 24. AMLA(6)-TS inspired metal-free catalytic direct borylation reaction catalysed by molecule **55** (Légaré and co.).[182]

1.6 Project Aims and Objectives

The aim of the project was to propose a reaction mechanism for the Pd-catalysed direct arylation of fluoroarenes based on rigorous mechanistic experiments. The focus was placed on the C–H bond activation step of the catalytic cycle, which provided access to the unique reactivity. In order to achieve this goal, the experiments were designed with following objectives:

I. The limitations and factors affecting the reaction efficiency were highlighted with main focus on the pre-catalyst and the additives used (Chapter 2).

II. Suitable experimental methods for monitoring the reaction progress by *in situ* FT-IR spectroscopic analysis were developed and mechanistic information was elucidated from the kinetic measurements (*e.g.* substrate and catalyst order dependence, KIE, temperature dependence etc.) (Chapter 3).

III. The key catalytic reaction intermediates were identified using combination of *in situ* and *ex situ* analytical techniques and the reactivity of these species were tested in stoichiometric and catalytic reactions (Chapter 4).

IV. A mechanistic scenario for the catalytic cycle consistent with the experimental observations was proposed (Chapter 5).

Chapter 2: Scope of Fluoroarene Direct Arylation and the Synthesis of Pd Complexes

2.1 Selecting the Standard Model Reaction Condition

There are two main parameters used in organometallic chemistry to describe the efficiency and the robustness of catalysis.[183] The first, quantified as the turn-over-frequency (TOF), is the number of catalytic cycle completed per unit time. The second, described as the turn-over-number (TON), is the maximum number of moles of the target product formed per mole of the catalyst until decay of activity. While TOF is related to the reaction rate, TON determines the reaction yield and dictates the minimum catalyst loading necessary to achieve quantitative conversion of the starting material to the desired product under specific reaction conditions. Periodical monitoring of reactions allows for either of these parameters to be determined. However, performing kinetic investigations on every reaction condition is a highly inefficient approach in mechanistic study. Therefore, the effect of reaction condition on the yield of the product formation after constant heating time was studied, while acknowledging the possibility of slow, but high yielding reaction conditions being ignored.

The direct arylation of 4-iodotoluene **57** with pentafluorobenzene **56** was selected as the model reaction system (**Scheme 25**).[126] Unless otherwise stated, the reaction was based on 0.9 mmol scale of 4-iodotoluene **57** with 1.5 equivalents of pentafluorobenzene **56**, 5 mol% of $Pd(OAc)_2$, 10 mol% of PPh_3 and 0.75 equivalents of Ag_2CO_3 in 2.5 cm^3 degassed DMF. The solvent was selected on the merit of high product yield and overlap-free IR spectrum suitable for monitoring the reaction progress (see Chapter 3.2.1). Control experiments confirmed $Pd(OAc)_2$, PPh_3 and Ag_2CO_3 to be essential parts of the catalysis.

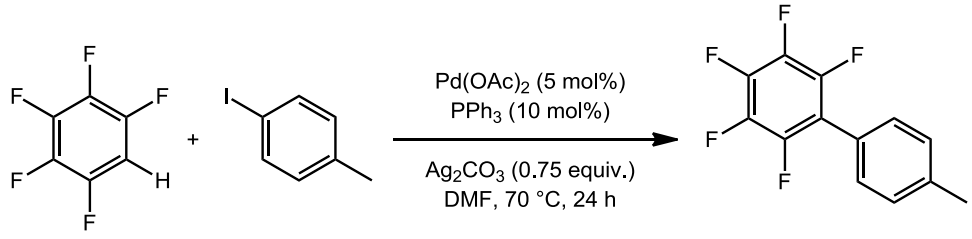

56 (1.5 equiv.) **57** **58**, quant. (84%)

Scheme 25. Direct arylation of 4-iodotoluene **57** with pentafluorobenzene **56**. Quantitative conversion of substrate **57** was observed and the product **58** was isolated in 84% yield.

The methyl group of reagent **57** provided a suitable ^1H NMR handle outside the aromatic region of the spectrum. An aliquot of the reaction mixture was collected after 24 hours of heating, and diluted in chloroform-d. Conversion of 4-iodotoluene **57** was determined from

integration of methyl ^{1}H signals of the starting material **57** and the product **58** at δ 2.31 and 2.44 respectively. The yield of the isolated product was determined after purification by flash column chromatography on silica gel using petroleum-ether 40–60 °C as the eluent. Under the model reaction conditions, 2,3,4,5,6-pentafluoro-4′-(methyl)biphenyl **58** was isolated in 84% yield with quantitative conversion of 4-iodotoluene **57**. Although the same reaction with 4-bromotoluene **27** resulted in 49% conversion of 4-bromotoluene **27** and 35% yield of the isolated product **58**, the reaction of 4-chlorotoluene only resulted in a trace quantity of product **58** observed by ^{1}H NMR spectroscopic analysis.

The homocoupling side-product **59** was formed in trace quantity for reactions with over 10 mol% of catalyst loading or without Ag. The methyl protons of this biaryl **59** was observed at δ 2.40 and did not interfere with the other methyl ^{1}H signals of interest. The synthesis of compound **59** under conditions similar to the model reaction was reported in the literature using Cs_2CO_3 and benzoin additives (**Scheme 26**).[184] The reaction gave the isolated product **59** in 96% yield with full conversion of the starting material **57**. The reaction was also successful using Ag_2CO_3 instead of Cs_2CO_3, but the starting material **57** conversion dropped to 75%, as determined by ^{1}H NMR spectroscopic analysis.

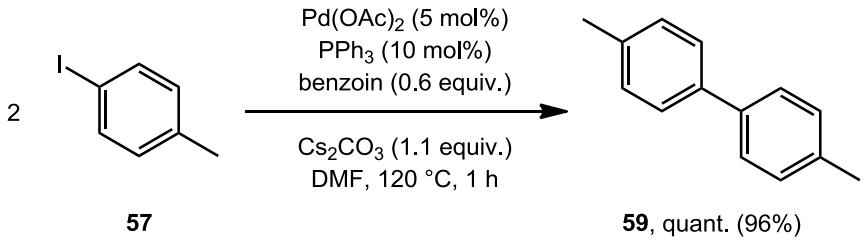

Scheme 26. Synthesis of 4,4′-(dimethyl)biphenyl **59** by a homocoupling reaction.[184]

2.2 Effect of Pre-Catalyst on the Yield of the Product 58

The effect of catalyst loading on the conversion of 4-iodotoluene **57** and the yield of the isolated product **58** was studied (**Table 1**). Quantitative conversion of starting material **57** was achieved at 3.4 mol% catalyst loading (Entry 5). At the lower loading, the yield did not improve with prolonged heating (*i.e.* 72 hours), which suggested a deactivation pathway for the catalyst – most likely by nanoparticle formation and precipitation (Entry 2). The conversion and the yield of the reaction followed a bell-curve trend, reaching a maximum of 84% around 5 mol% $Pd(OAc)_2$ (Entry 6) and dropping to 7% for 1 equivalents of $Pd(OAc)_2$ (Entry 9). The average TON of the catalyst determined from the reaction achieving partial conversion of reagent **57** was 105. For the reaction of 4-bromotoluene **27**, the use of 20 mol% Pd loading improved the isolated yield from 35% to 47%.

Table 1. Conversions of 4-iodotoluene **57** and yield of the isolated product **58** obtained for reaction shown in **Scheme 25** using different $Pd(OAc)_2$ pre-catalyst loading.

Entry	$Pd(OAc)_2$ / mol%	PPh_3 / mol%	%Conversion [a] (%Yield [b])
1	0.25	0.5	27 (23)
2	0.5	1.0	59 (52) / 52 (50) [c]
3	1.0	2.0	88 (70)
4	2.0	4.0	83 (70)
5	3.4	6.7	quant. (82)
6	5.0	10	quant. (84) / (35) [d]
7	11	22	90 (71)
8	20	40	69 (52) / (47) [d]
9	1 equiv.	2 equiv.	23 (7)

[a] Determined from integration of methyl ^{1}H NMR peaks of the reagent **57**, product **58** and side-products. [b] After purification by flash chromatography. [c] Heated for 72 h. [d] Reaction for 4-bromotoluene **27**.

The low conversion and the yield of product **58** were not accounted for by the homocoupling side-product **59**. Alternative side-reactions involving substrate **57** were considered. Comparing the methyl region of the ^{1}H NMR spectra (*i.e.* δ 2.60–2.00), additional signals were observed for reactions using higher catalyst loading (**Figure 7**). For reactions with 0.25 mol% and 5 mol% $Pd(OAc)_2$ catalyst loadings, only the product **58** and the starting material **57** peaks were observed at δ 2.43 and 2.30 respectively. At increased catalyst loading of 20 mol% $Pd(OAc)_2$ and 40 mol% PPh_3, an additional peaks were observed at δ 2.18. Although this peak (*i.e.* 24%) remained unassigned, integration with the product **58** peak (*i.e.* 52 %) seemed to make up for the number of missing protons. Interestingly, the peak at δ 2.18 was not observed under any of the other reaction conditions. Further methyl peaks of significance were observed at δ 2.54, 2.42, 2.39 (side-product **59**), 2.38, and 2.08 for the reaction with 1 equivalents of $Pd(OAc)_2$ and 2 equivalents of PPh_3. The signal at δ 2.54 was assigned to the methyl protons of triphenyl(4-tolyl)phosphonium iodide **60**. Formation of this side-product was expected as a consequence of reversible aryl-aryl exchange of Pd^{II}–Ar with PPh_3.[185] The side-product at δ 2.08 was hypothesised as a 4-tolyl-group containing Ag phosphine complex.

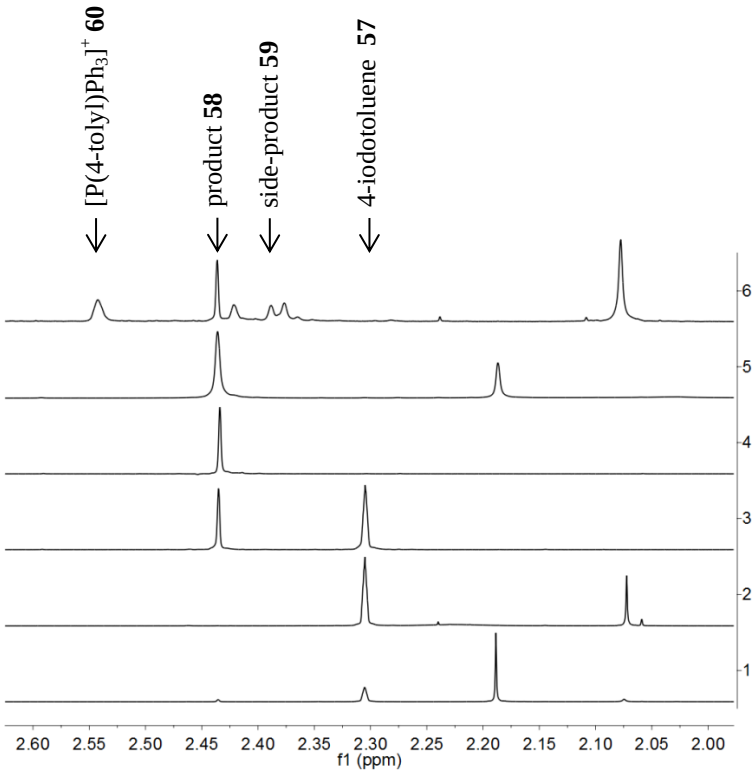

Figure 7. Stacked ^{1}H NMR of the crude reaction mixture diluted in chloroform-d. **(1)** 20 mol% $Pd(OAc)_2$ + 0 mol% PPh_3, **(2)** 0 mol% $Pd(OAc)_2$ + 40 mol% PPh_3, **(3)** 0.25 mol% $Pd(OAc)_2$ + 0.5 mol% PPh_3 **(4)** 5 mol% $Pd(OAc)_2$ + 10 mol% PPh_3, **(5)** 20 mol% $Pd(OAc)_2$ + 40 mol% PPh_3 and **(6)** 1 equiv. $Pd(OAc)_2$ + 2 equiv. PPh_3.

During the initial study, changes in the colour of the reaction mixture were observed. Starting from opaque yellow, the colour darkened over time to khaki, and after 24 hours of heating, the reaction mixture had become a yellow solution with a black precipitate (**Figure 8**). The black precipitate was only observed when the reaction was complete and hypothesised to be Pd aggregate, commonly referred to as Pd black. The shade of the mixture after reaction completion was darker for those reactions with higher catalyst loading.

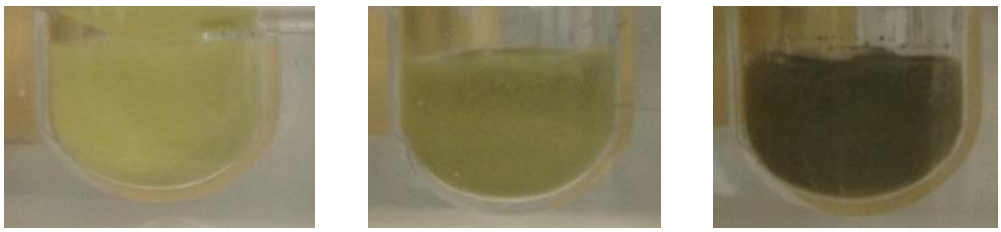

5 min 60 min 320 min

Figure 8. Progressive change in the colour of reaction mixture heated at 70 °C.

The use of preformed Pd nanoparticles (Pd-NPs) as an alternative to $Pd(OAc)_2$ pre-catalyst was examined in order to establish the type of catalyst (homogeneous and/or heterogeneous) involved in the reaction (**Table 2**). Direct arylation reaction of

polyfluorobenzene catalysed by heterogeneous Pd nanocrystals stabilised by curcurbit[6]uril, have been reported by Cao and co-workers.[127] The catalytic activities of Pd-NPs supported on polyvinylpyrrolidone (PVP) of different polymer weights and particle sizes were tested. The mass quantity of the catalyst added to the reaction mixture was changed to maintain the mol quantity of the Pd at 5 mol%. The reaction at 70 °C required PPh_3 and the yields were lower compared to using $Pd(OAc)_2$ pre-catalyst (*i.e.* 84%) (Entries 1–6). Reactions are often described as homogeneous or heterogeneous catalysis based on the pre-catalyst used.[101] However, this ignores the possibilities of pre-catalyst undergoing *in situ* transformation. For example, heterogeneous Pd on charcoal has been shown to generate catalytically-active homogeneous species in the presence of phophines.[186] Improved yields were obtained at elevated temperature of 100 °C, even without PPh_3 (Entries 7 and 8). The frequency of Pd leaching is expected to increase with elevated temperature.[187-189] A similar yield was obtained when 5 mol% $Pd(OAc)_2$ was reacted under ligand-free condition at 100 °C (Entry 9). Although the exact nature of the catalyst involved is difficult to confirm as completely homogeneous or heterogeneous, the product **58** formation was favoured under reaction conditions commonly associated with homogeneous catalysis. This was further demonstrated by the significantly different kinetic profile observed for the reactions catalysed with Pd-NPs stabilised by DMF solvation when compared to the standard reaction condition using $Pd(OAc)_2$ (see Chapter 3).

Table 2. Yields of isolated product **58** formed for the reaction shown in **Scheme 25** using Pd-NPs on PVP support as the pre-catalyst.

Entry	Condition			%Yield [a]
	Catalyst	Ligand	T / °C	
1	2wt% Pd-NPs on 29K-PVP	-	70	Trace
2	8wt% Pd-NPs on 29K-PVP	-	70	Trace
3	2wt% Pd-NPs on 10K-PVP	PPh_3	70	55
4	2wt% Pd-NPs on 29K-PVP	PPh_3	70	67
5	8wt% Pd-NPs on 29K-PVP	PPh_3	70	59
6	2wt% Pd-NPs on 55K-PVP	PPh_3	70	48
7	8wt% Pd-NPs on 29K-PVP	-	100	21
8	2wt% Pd-NPs on 55K-PVP	-	100	10
9	5 mol% $Pd(OAc)_2$	-	100	25

[a] Yield of the isolated product **58** after purification by flash chromatography.

In literature, Pd-catalysed C–H bond functionalisation reactions often start with $Pd(OAc)_2$ pre-catalyst in the presence of a base additive, commonly metal carbonates.[116] Under such conditions, the identity of the base directly involved in the C–H bond cleavage is unclear

between the two carboxylates in the reaction mixture (*i.e.* acetate anion from the pre-catalyst and the carbonate anion from the base). Studies have suggested the acetate anion to be the primary base that is regenerated from the AcOH by-product by the carbonate anion acting as a 'proton-shuttle'.[119] Computational calculations on the direct arylation of pyridine *N*-oxide **37** have also shown marginal 3.3 kJ mol^{-1} higher energy for AMLA(6)-TS involving deprotonation by inner-sphere carbonate anion at Pd compared to the acetate anion.[172]

The role of the acetate ligands on the pre-catalyst $Pd(OAc)_2$ was studied by comparing the product **58** yields for reactions using $Pd(PPh_3)_4$, $Pd(PPh_3)_2Cl_2$ and $PdCl_2$ pre-catalysts (**Table 3**). Results comparable with $Pd(OAc)_2$ were obtained for reactions catalysed by $Pd(PPh_3)_4$ (Entry 2) and $Pd(PPh_3)_2Cl_2$ (Entry 3). The $Pd(PPh_3)_4$ pre-catalyst in the presence of AcO^- is known to exist primarily as $[Pd(OAc)(PPh_3)_3]^-$ with traces of reactive $[Pd(OAc)(PPh_3)_2]^-$ in solution.[190] Oxidative addition of ArI results in a mixture of $Pd(Ar)(\kappa^1\text{-}OAc)(PPh_3)_2$ and $Pd(Ar)(I)(PPh_3)_2$ in equilibrium with $[Pd(Ar)(PPh_3)_2]^+$.[191] The same transformation may take place for CO_3^{-2} with the formation of $[Pd(Ar)(\kappa^1\text{-}CO_3)(PPh_3)_2]^-$ complex. If an identical catalytic cycle is assumed for all the pre-catalysts, these results highlight the carbonate anion as a competent base for C–H bond activation of pentafluorobenzene **56** via AMLA(6) pathway. It was interesting that reactions using 5 mol% $PdCl_2$ pre-catalyst with 10 mol% PPh_3 (Entry 4) and 5 mol% $Pd(PPh_3)_2Cl_2$ pre-catalyst without added PPh_3 (Entry 5) resulted in similar partial substrate **57** conversions. It is proposed that the presence of 4 equivalents of PPh_3 per Pd-atom was required for the complete activation of these pre-catalysts. In the absence of PPh_3, the reaction starting with $Pd(OAc)_2$ pre-catalyst worked with very poor yield (Entry 6). The ligand PPh_3 is understood to play a role in the activation of Pd^{II} to Pd^0 and the stabilisation of the oxidative addition complex by σ-electron donation.[192] It must be noted that the exact identity of the active catalyst depends on the pre-catalyst used, and the reaction mechanism can differ between them.[100]

Without added base, no product **58** was observed for either 1.5 mol% $Pd(OAc)_2$ or $PdCl_2$ (Entries 7 and 8). However, the product **58** was isolated in 14% yield in the absence of Ag_2CO_3 using 20 mol% $Pd(OAc)_2$ (Entry 9). In contrast, no product **58** was formed at 20 mol% $PdCl_2$ (Entry 10) or $Pd(PPh_3)_4$ (Entry 11). These observations suggested the acetate ligands of $Pd(OAc)_2$ was also capable of acting as an inner-sphere base for AMLA(6) pathway.

Table 3. Conversions of 4-iodotoluene **57** and the yields of the isolated product **58** obtained for reaction shown in **Scheme 25** under conditions designed to highlight the role of carboxylate anions.

Entry	Variable [a]	%Conversion [b] (%Yield [c])
1	5 mol% $Pd(OAc)_2$	quant. (84)
2	5 mol% $Pd(PPh_3)_4$	quant. (85)
3	5 mol% $Pd(PPh_3)_2Cl_2$	quant. (87)
4	5 mol% $PdCl_2$	72 (61)
5	5 mol% $Pd(PPh_3)_2Cl_2$, no PPh_3	60 (57)
6	20 mol% $Pd(OAc)_2$, no PPh_3	(5) / 0 [d]
7	1.5 mol% $Pd(OAc)_2$, no Ag_2CO_3	0
8	1.5 mol% $PdCl_2$, no Ag_2CO_3	0
9	20 mol% $Pd(OAc)_2$, no Ag_2CO_3	(14) / (7) [d]
10	20 mol% $PdCl_2$, no Ag_2CO_3	0
11	20 mol% $Pd(PPh_3)_4$, no Ag_2CO_3	0

[a] 0.75 equiv. Ag_2CO_3 present unless stated otherwise. [b] Determined from integration of methyl ^1H NMR peaks of the reagent **57** and the product **58**. [c] After purification by flash chromatography. [d] Reaction for 4-bromotoluene **27**.

2.3 Effect of Base Additive on the Yield of the Product 58

Of the metal carboxylates tested, Ag_2CO_3 resulted in the highest conversion of substrate **57** and the yield of the isolated product **58** (**Table 4**, Entry 1). The Lewis acid characteristic of Ag^I cation is known to strongly interact with halides to form insoluble Ag salts and provide the driving force for chemical transformations.[193] In the catalytic cycle, the Ag^I was hypothesised to act as a halide scavenger for the ArI oxidative addition intermediates.[191, 194] The high yield achieved for Ag_2CO_3 over K_2CO_3 and Cs_2CO_3 suggested the possibility of organosilver species involved in the mechanism. However, for the reaction of 4-bromotoluene **27**, K_2CO_3 and Cs_2CO_3 were better additives than Ag_2CO_3 (Entries 1–3).

The TON of the reactions depended on the amount of carbonate added. Increasing the quantity of Ag_2CO_3 resulted in increased product **58** formation, with quantitative conversion achieved between 0.25–0.75 equivalents of Ag_2CO_3 (**Table 4**, Entries 4 and 5). It was noticed that the yields generally were twice the equivalents of Ag_2CO_3 added (*i.e.* quantitative conversion expected at 0.5 equivalents of Ag_2CO_3). This was most likely because 1 equivalents of Ag^I was required to abstract the iodide for catalyst turnover and 0.5 equivalents of the dibasic carbonate anion (CO_3^{-2}) was required to scavenge 1 equivalents of proton generated from the reaction. Changing the base to AgOAc resulted in lower yields (Entry 6), and the presence of equivalent Ag^I atoms (*i.e.* 1.5 equivalents of AgOAc) did not improve the outcome in DMF or DMAc (Entries 7 and 8). A similar result

was obtained for the reaction using $Pd(PPh_3)_4$ pre-catalyst (Entry 9). Similar to 4-iodotoluene **57**, the reaction of 4-bromotoluene **27** with KOAc additive (Entry 10) resulted in a lower yield compared to K_2CO_3 additive (Entry 2). However, unlike 4-iodotoluene **57**, $Pd(PPh_3)_4$ was not a suitable pre-catalyst for 4-bromotoluene (Entries 11 and 12).

Table 4. Conversions of 4-iodotoluene **57** and the yields of the isolated product **58** obtained for the reaction shown in **Scheme 25** using different metal carboxylates.

Entry	Variable	%Conversion [a] (%Yield [b])
1	Ag_2CO_3	quant. (84) / 49 (35) [c]
2	K_2CO_3	40 (26) / 92 (68) [c]
3	Cs_2CO_3	70 (31) / 91 (73) [c]
4	0.25 equiv. Ag_2CO_3	56 (45)
5	1.5 equiv. Ag_2CO_3	quant. (82)
6	0.75 equiv. AgOAc	35 (25)
7	1.5 equiv. AgOAc	31 (23)
8	1.5 equiv. AgOAc in degassed DMAc	33 (25)
9	1.5 equiv. AgOAc, $Pd(PPh_3)_4$	38 (24)
10	1.5 equiv. KOAc	47 (37) [c]
11	1.5 equiv. KOAc, $Pd(PPh_3)_4$	2 (1) [c]
12	K_2CO_3, $Pd(PPh_3)_4$	5 (1) [c]

[a] Determined from integration of methyl ^{1}H NMR peaks of the reagent **57** and the product **58**. [b] After purification by flash chromatography. [c] Reaction for 4-bromotoluene **27**.

Testing the reactivity of other Ag additives, 0.75 equivalents of Ag_2O was shown to give the desired product **58** in high yield (**Table 5**, Entries 1 and 2). A similar result was obtained when using 5 mol% $Pd(PPh_3)_4$ instead of $Pd(OAc)_2$ (Entry 3). These reactions were not Ag catalysed as reagent **57** was fully recovered in the absence of Pd (Entry 4).

Table 5. Conversions of 4-iodotoluene **57** and the yields of the isolated product **58** obtained for the reaction shown in **Scheme 25** using different Ag additives.

Entry	Variable	%Conversion [a] (%Yield [b])
1	0.75 equiv. $AgNO_3$	1 (1)
2	0.75 equiv. Ag_2O	quant. (72)
3	0.75 equiv. Ag_2O, 5 mol% $Pd(PPh_3)_4$, no PPh_3	(75)
4	0.75 equiv. Ag_2O without Pd	0
5	0.75 equiv. Ag_2O, bottle DMF, no PPh_3	0
6	0.75 equiv. Ag_2O, 5 mol% $Pd(PPh_3)_4$, in NMP	(81)
7	0.75 equiv. Ag_2O in bottle DMF	88 (72)

[a] Determined from integration of methyl ^{1}H NMR peaks of the reagent **57** and the product **58**. [b] After purification by flash chromatography.

The reaction mechanism involving Ag_2O as the additive and $Pd(PPh_3)_4$ as the pre-catalyst did not fit the model represented by the carboxylate anion directly involved in the C–H bond cleavage. Fang and co-workers had reported a direct arylation of potassium 4-tolyltrifluoroborate **61** with pentafluorobenzene **56** to yield the product **58** in 83% isolation under similar reaction condition (**Scheme 27**).[195] The model reaction catalysed by 5 mol% $Pd(PPh_3)_4$ with 0.75 equivalents of Ag_2O in NMP was also high yielding (Entry 6).

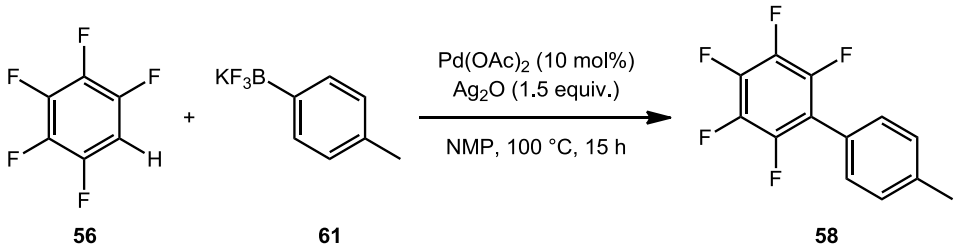

56 **61** **58**

Scheme 27. Pd-catalysed direct arylation reaction of potassium 4-tolyltrifluoroborate **61** with pentafluorobenzene **56** in the presence of Ag_2O additive (Fang and co.).[195]

The proposed mechanism for this reaction involves $Pd^{II}(OAc)_2$-catalysed intramolecular acetate-mediated AMLA(6)-TS, with Ag^{I}-oxidising Pd^{0} formed after reductive elimination of the product **58**. However, this failed to account for the high yield obtained for the reaction in the absence of carboxylate (Entry 3) and the lack of reaction in the absence of PPh_3 which is not required for Pd^{II}-catalysed reaction (Entry 5).

A possible catalytically-active Pd complex is proposed: a water-activated $Pd(Ar)(OH)(PR_3)_2$ complex. Takemoto and co-workers reported a room-temperature activation of a CF_3–H bond by [Pd(Ph)(OH)(dppp)].[196] The formation of AgOH from the reaction of Ag_2O and H_2O is a well-documented equilibrium.[197] The degassed DMF used in the reaction contained 110 ppm water by mass (established by coulometer), which equated to 6 mM in the reaction mixture. This was a significant quantity considering the 18 mM Pd used in the reaction to catalytically arylate 360 mM 4-iodotoluene **57** with pentafluorobenzene **56** (1.5 equiv., 540 mM). Using reagent-grade DMF with 1400 ppm water by mass (*i.e.* 73 mM) also resulted in good yield of product **58** (**Table 7**, Entry 9).

The effect of using non-Ag containing base was studied as a more environmentally friendly and cost effective alternative (**Table 6**). Arroniz and co-workers reported the use of $[Me_4N]OAc$ as an excellent substitute for AgOAc in the direct arylation reactions of iodoarenes with sp^2 and sp^3 C–H bonds.[198] This organic salt was effective for replacing Ag_2CO_3 in the model system, achieving quantitative conversion of the starting material **57** (Entry 1). On the other hand, using tetramethylammonium salts with bromide (Entry 2) and

chloride (Entry 3) counter-ions resulted in no reaction. The catalysis was less effective with [$^{n}Bu_4N$]OAc than [Me_4N]OAc, achieving partial conversion of the reagent **57** (Entries 4–6).

Table 6. Conversions of 4-iodotoluene **57** and the yields of the isolated product **58** obtained for the reaction shown in **Scheme 25** using different amine base additives.

Entry	Variable	%Conversion [a] (%Yield [b])
1	1.5 equiv. [Me_4N]OAc	quant. (82)
2	1.5 equiv. [Me_4N]Br	0
3	1.5 equiv.[Me_4N]Cl	0
4	0.75 equiv. [$^{n}Bu_4N$]OAc	(26)
5	1.5 equiv. [$^{n}Bu_4N$]OAc	48 (21)
6	5 equiv. [$^{n}Bu_4N$]OAc	(2)

[a] Determined from integration of methyl ^{1}H NMR peaks of the reagent **57** and the product **58**. [b] After purification by flash chromatography.

2.4 Effect of the Solvent on the Yield of the Product 58

The transition metal-catalysed direct reaction of a C–H bond is an improvement on the atom efficiency from cross-coupling reaction. Many advances have been made in increasing the substrate scope and achieving the desired transformation under milder reaction conditions. This includes an effort to move away from the commonly employed high boiling point, polar, aprotic solvents such as *N*,*N*-dimethylformamide (DMF), *N*-methylpyrrolidin-2-one (NMP) and *N*,*N*-dimethylacetamide (DMAc) that are considered to be hazardous.[199] These solvents are understood to allow the inorganic salt to dissolve as well as play a role in the catalytic cycle via coordination. Unfortunately, DMF is reported to be a highly toxic solvent that can be easily absorbed through the skin with association to liver damage and cancer.[200] Environmental concerns over disposal method and potential NO_X formation also make replacement with low risk and environmentally benign solvent inevitable.[111]

Alternative solvents utilised in the literature for C–H bond functionalisation reactions include dialkyl carbonates, PEG and water.[201] Rene and co-workers have reported excellent yields obtained for direct arylation of polyfluorobenzene under similar condition to the model reaction in biphasic solvent-system of EtOAc and H_2O at room temperature.[202] Furthermore, the model reaction was originally reported as a transformation in water.[126] For these reasons, alternative solvents for the reaction were considered together with possible effect of non-inert atmosphere and using bottle solvents (**Table 7**).

The polar aprotic solvents such as DMAc (Entry 1) and NMP (Entry 2) resulted in comparable yield to DMF as expected. Other solvents commonly used in direct arylation reaction, such as toluene (Entry 3) and 1,4-dioxane (Entry 4), were less effective. Use of ethylene carbonate (Entry 5) and propylene carbonate (Entry 6) afforded the product **58** in reasonable yields. Propylene carbonate was also an effective solvent for the reaction starting with $Pd(PPh_3)_4$ pre-catalyst (Entry 7). Therefore, the low-cost and biodegradable cyclic carbonates[203] were shown to be suitable replacements for DMF in the model reaction.

Although many Pd-catalysed reactions are reported under inert atmosphere, it is often an unnecessary precaution. The yield of the model reaction was not affected by the presence of air (Entry 8) or water (Entry 9). These results, however, do not suggest that the reactions follow the same rates. Study of the $Pd(OAc)_2$-catalysed Suzuki-Miyaura cross-coupling reaction by Adrio and co-workers demonstrated a kinetic profile in which a higher starting material conversion was achieved in the presence of O_2, but with a slower reaction rate.[204] The effect of air and water on the rate of the reaction was reported in Chapter 3.

Table 7. Effect of solvent and air on the conversions of 4-iodotoluene **57** and the yields of the isolated product **58** obtained for the reaction shown in **Scheme 25**.

Entry	Variable	%Conversion [a] (%Yield [b])
1	DMAc	quant. (79)
2	NMP	(67)
3	toluene	0
4	1,4-dioxane	28 (15)
5	ethylene carbonate	(50)
6	propylene carbonate	87 (51)
7	5 mol% $Pd(PPh_3)_4$ in propylene carbonate	79 (40)
8	prepared under air	quant. (78)
9	bottle DMF	quant. (82)

[a] Determined from integration of methyl ^{1}H NMR peaks of the reagent **57** and the product **58**. [b] After purification by flash chromatography.

2.5 Substrate Scope of the Model Reaction Condition

The original work by Chen and co-workers on the model system focused on the reaction optimisation and the substrate scope.[126] Good to high yields (*i.e.* 40–96%) were reported for a variety of pentafluorophenyl-aryls formed from the corresponding iodoarenes. Both electron-donating (*i.e.* OMe and Me) and electron-withdrawing (*i.e.* Ph, Br, F, and NO_2) substituents in the *para*-position of iodobenzene were tolerated. Furthermore, the reaction was successful for direct arylation of 5-iodo-1,3-benzodioxole, ethyl 3-iodobenzoate, and 3-iodothiophene.

With the results already reported in mind, the iodoarene suitable for the model reaction in DMF was studied (**Table 8**). Good yields (*i.e.* 68–84%) were obtained for the products formed from iodobenzene **64** and *para*-substituted-iodobenezes with electron withdrawing substituents (*i.e.* F **65**, CF_3 **66** and NO_2 **67**). However, biaryl **58** was the only successful product formed for iodobenzene with electron-donating *para*-substituent (products **62** and **63** were not formed). This was possibly due to catalyst inhibition by coordination of the 1° amine and the hydroxyl groups. Attempted synthesis of products formed from pentalfuoro-iodobenzene **68** and 2-iodotoluene **69** were unsuccessful possibly due to the steric bulk in the *ortho*-position. Further experimental evidences are necessary to validate these hypotheses. The comparison of the reaction kinetics for the different *para*-substituted iodobenzenes was discussed in Chapter 3.

Table 8. Yields of the isolated product **58**, **62–69** for the direct arylation of iodoarenes with pentafluorobenzene **56**.

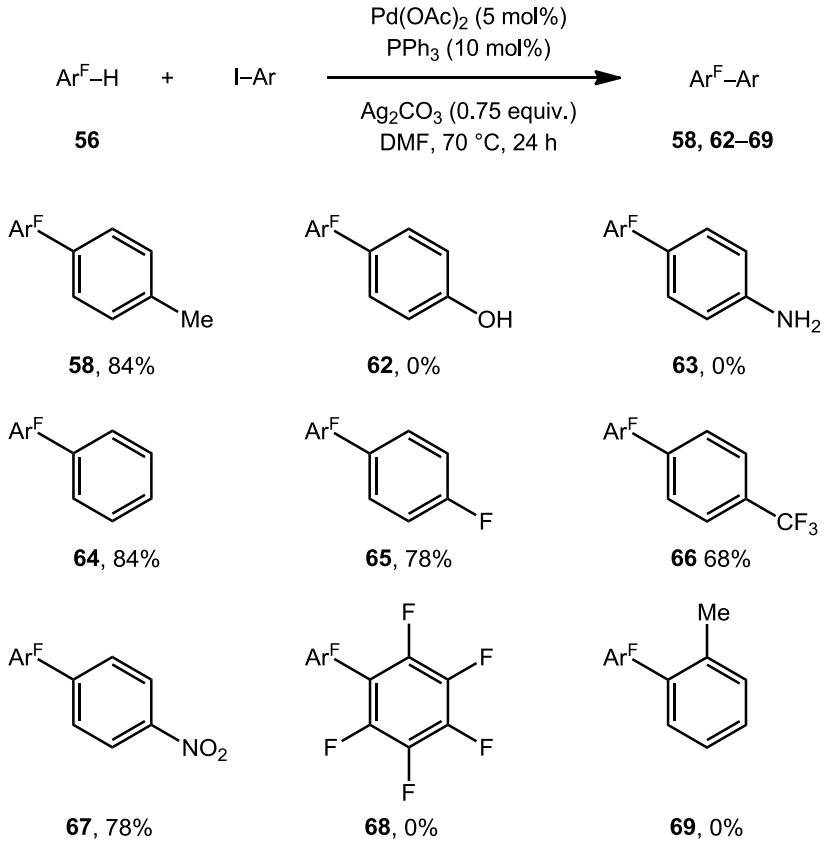

The reactivity of different polyfluoroarenes was also reported by Chen and co-workers.[126] Good yields (*i.e.* 36–86%) were achieved for range of tri- and tetra-fluorobenzenes. The reaction of 2,3,5,6-tetrafluoropyridine and 1-substituted-2,3,5,6-tetrafluorobenzenes with electron-donating (*i.e.* Me) and electron-withdrawing (*i.e.* Br, CF_3 and CN) substituents resulted in identical yields within experimental error. This observation suggested the reaction yield was unaffected by a change in the C1-position of 1-substituted-2,3,5,6-

tetrafluorobenzene. The only difluorobenzene reported in the work was 2,4-difluoro-1-nitrobenzene which achieved 78% product isolation in DMF. For substrates with low reactivity in water, improved yields were achieved in DMF.

A variety of polyfluorinated arenes were tested in the direct arylation of 4-iodotoluene **57** in DMF (**Table 9**). The results confirmed the observations reported by Chen and co-workers.[126] The tri- and tetra-fluorobenzenes successfully formed the mono-, di- and tri-substituted products **70** and **71** respectively), with partial conversion of 4-iodotoluene **57**. No product was formed for the reaction of difluorobenzenes (**72** and **28**), monofluorobenzene **73**, trifluorotoluene **74**, or benzene **75**. Quantitative conversion of 4-iodotoluene **57** was achieved for the 1-substituted-2,3,5,6-tetrafluorobenzenes to form products **76–80** in high yields. These substrates were used to characterise the electronic effect of the fluoroarenes on the reaction rate in Chapter 3.

Table 9. Conversions of 4-iodotoluene **57** and the yields of the isolated products **28**, **70–80** (in parentheses) for the direct arylation with fluoroarenes.

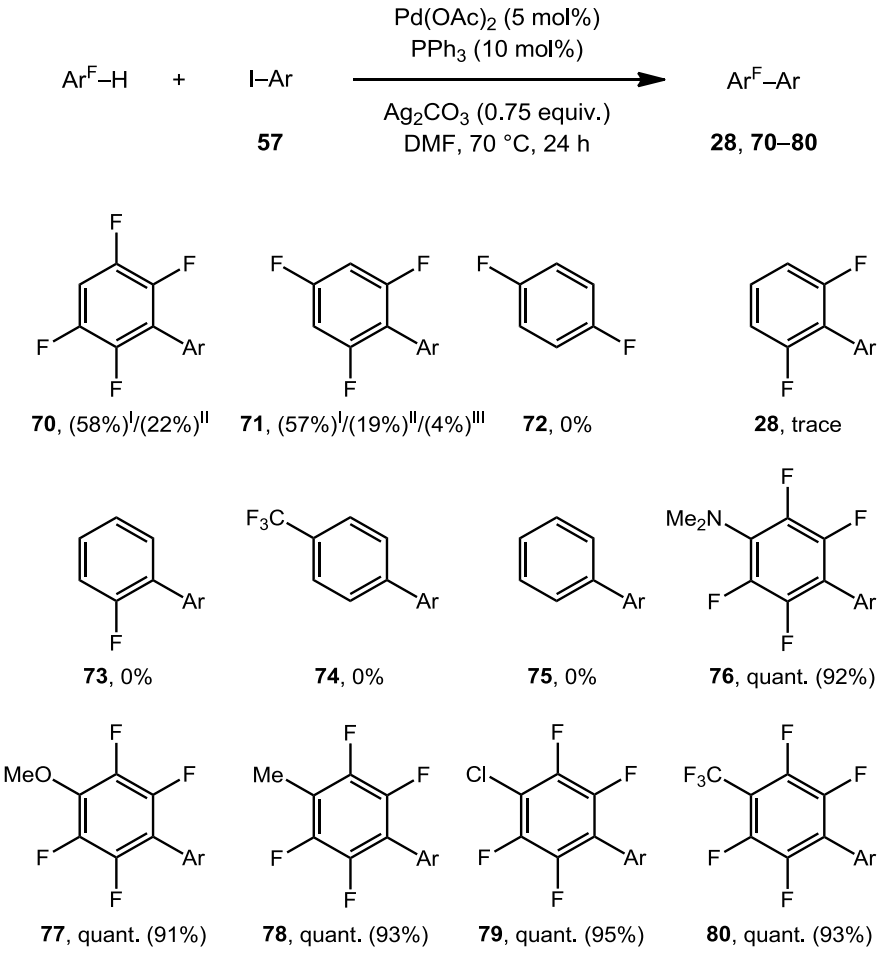

[I] Monosubstituted. [II] Disubstituted. [III] Trisubstituted.

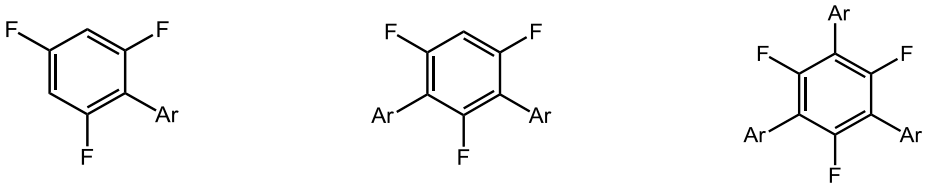

I **II** **III**

An attempt was made to improve on the limited substrate scope of the reaction. The reaction temperature was increased to 75 °C, with large excess of fluoroarenes **26** and increased amount of PPh_3 (15 mol%) (**Scheme 28**). Under these modified reaction conditions 1,3-difluorobenzene **26** was successfully functionalised regiospecifically at the C2-position *ortho* to the two fluorine atoms to form the product **28** in 68% isolated yield. The reactivity of other fluoroarene (*i.e.* 1,2-difluorobenzene, 1,4-difluorobenzene and fluorobenzene) under the modified reaction conditions was also tested, but these reactions only resulted in trace quantities of the respective biaryl products. The result was in agreement with the higher reactivity of the C–H bond between two fluorine atoms over single fluorine atom.

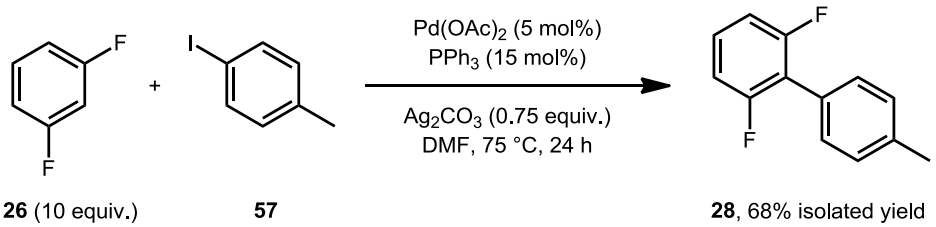

Scheme 28. Direct arylation reaction of 4-iodotoluene **57** with 1,3-difluorobenzene **26**.

2.6 Synthesis of Potential Catalytic Pd Intermediates

The identities of the catalytic intermediates are often unravelled by the kinetics of the stoichiometric reactions of isolated intermediate species.[205] A range of mononuclear and dinuclear Pd-containing complexes were hypothesised as potential on-cycle and off-cycle intermediates of the catalytic cycle. Literature procedures were followed for the synthesis of these complexes. The structures and the purity were determined based on characterisation data from ^{1}H NMR, ^{31}P NMR, FT-IR spectroscopy and MS.

Firstly, the oxidative addition products of Pd into iodobenzene **81** and 4-iodotoluene **57** were prepared by stirring a mixture of $Pd_2dba_3.CHCl_3$, PPh_3 and ArI in DCM at ambient temperature (**Scheme 29**).[206] The phenyl and the 4-tolyl analogues of the product with the general formula $Pd(Ar)(I)(PPh_3)_2$ (Ar = Ph **82a** and 4-tolyl **82b**) were isolated in 49% and 80% yields respectively. The ^{1}H and ^{31}P NMR spectra of the products were in agreement with the published data. The species **82a** and **82b** were detected by ESI(+)-MS as the

molecular ion $[M-I]^+$ at m/z 707.13 and 721.14 respectively with characteristic isotopic pattern of mononuclear Pd species.

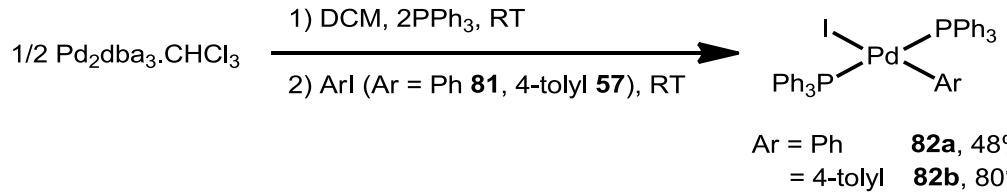

Scheme 29. Synthesis and isolated yields of $Pd(Ar)(I)(PPh_3)_2$ (Ar = Ph **82a** and 4-tolyl **82b**) from $Pd_2dba_3.CHCl_3$ and ArI (Ar = Ph **81** and 4-tolyl **57**).

In catalysis, dinuclear transition metal complexes are often considered to act as a stable reservoir for the active mononuclear catalyst complex.[207, 208] However, mechanisms involving on-cycle dinuclear complexes as the active catalytic species have been proposed in the literature. For example, Harakat and co-workers reported a dinuclear chloride bridged Pd complex as the active catalyst for the Wacker oxidation of alkenes based on an ESI-MS study.[209] This was further supported by the reaction kinetics between first and second-order in the Pd pre-catalyst as determined by GC based kinetic study. Widenhoefer and co-workers have also proposed a halide bridged dinuclear Pd species as the on-cycle species in the Buchwald-Hartwig amination based on study of stoichiometric reactions.[210]

Computational DMF calculations on the structure of AMLA(6)-TS often suggest involvement of carboxylate-coordinated Pd species, such as $Pd(Ar)(\kappa^2\text{-}OAc)(PPh_3)$ **51**. The stoichiometric C–H bond functionalisation of 2-methylthiophene **46** with acetate-bridged dinuclear $[Pd(Ar)(\mu\text{-}OAc)(PPh_3)]_2$ **45** was reported by Wakioka and co-workers.[175] The mononuclear acetate ligated Pd complex **51** was proposed as the active species in equilibrium with the stable dinuclear Pd species **45**.

In-order to synthesise the dinuclear complex **45**, the hydroxo-analogue $[Pd(Ar)(\mu\text{-}OH)(PPh_3)]_2$ **83** was prepared as the precursor.[211] A biphasic reaction mixture of $Pd(PPh_3)_2Cl_2$ and ArI (Ar = Ph **81** and 4-tolyl **57**) in aqueous KOH and benzene were heated to reflux under continuous flow of nitrogen for 3 h (**Scheme 30**). The phenyl analogue **83a** was isolated in 81% yield as air and moisture-stable white solid. However, the reaction of 4-tolyl resulted in a mixture of inseparable Pd-complexes with trace quantity of product $[Pd(4\text{-tolyl})(\mu\text{-}OH)(PPh_3)]_2$ **83b** observed by NMR spectroscopic analysis.

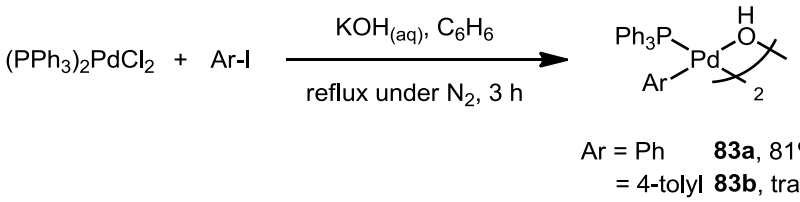

Scheme 30. Synthesis and isolated yields of dinuclear [Pd(Ar)(μ-OH)(PPh_3)]$_2$ (Ar = Ph **83a** and 4-tolyly **83b**).

An alternative synthetic route reported by Grushin and co-workers was followed for the preparation of the desired dinuclear complex **83b**.[211] A degassed suspension of complex [Pd(Ph)(μ-OH)(PPh_3)]$_2$ **83a** and 4-iodotoluene **57** in benzene was stirred under an atmosphere of CO (**Scheme 31**). The resulting red solution was degassed by three-cycles of freeze-pump-thaw and stirred under atmosphere of argon following the addition of 4-iodotoluene **57** and aqueous KOH solution for 27 hours. Purification of the product **83b** from excess 4-iodotoluene **57** was best achieved by recrystallization from chloroform and pentane to give isolated product **83b** in 50% yield. The mechanism of this reaction is thought to involve the *in situ* generation of highly active '$Pd^0(PPh_3)$' complex capable of oxidative addition.[211] The analysis of the product **83b** by LIFDI-MS confirmed the successful formation of the complex [Pd(4-tolyl)(μ-OH)(PPh_3)]$_2$ **83b** (m/z 954.14). However, the observation of PPh_3(4-tolyl)$^+$ **60** (m/z 352.88) highlighted the potential aryl exchange reaction between Pd–Ar and P–Ph. This would result in the formation of inseparable dinuclear Pd–Ar **83b** and Pd–Ph **83a** mixture. Unfortunately, the overall yield of the isolated complex [Pd(4-tolyl)(μ-OH)(PPh_3)]$_2$ **83b** was unfavourable for performing further study on the reactivity. Therefore, the synthetic effort was focused on phenyl containing Pd species.

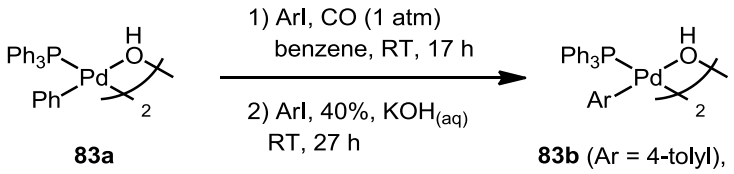

Scheme 31. Synthesis and isolated yield of of dinuclear [Pd(4-tolyl)(μ-OH)(PPh_3)]$_2$ **83b** under atmosphere of CO.

The structure of the dinuclear complex **83a** was confirmed by characteristic spectroscopic data. The OH-groups bridging the two Pd metal centres absorb at 3610 cm^{-1} in the IR spectrum and appear in the negative ppm region of the ^{1}H NMR spectrum. The *trans*- and *cis*-isomers were obtained in 3:1 ratio as also confirmed by both ^{1}H and ^{31}P NMR spectroscopic analysis (**Figure 9**). In solution the complexes did not isomerise, but gradually decomposed. These dinuclear structure of [Pd(Ph)(μ-OH)(PPh_3)]$_2$ **83a** was

confirmed by the LIFDI-MS with peak at m/z 926.09 showing characteristic isotopic pattern of dinuclear Pd complex. Additional peaks were observed for Pd(Ph)(PPh_3) (m/z 444.81), PPh_4^+ (m/z 338.93), and PPh_3 (m/z 261.84).

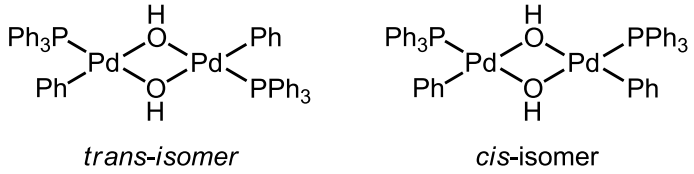

Figure 9. *Trans*- and *cis*-isomers of [Pd(Ph)(μ-OH)(PPh_3)]$_2$ **83a** obtained in 3:1 ratio.

The acetato-bridged dinuclear [Pd(Ph)(μ-OAc)(PPh_3)]$_2$ **84** species was successfully synthesised and isolated in 76% yield following the addition of excess AcOH to a suspension of [Pd(Ph)(μ-OH)(PPh_3)]$_2$ **83a** in benzene (**Scheme 32**). [212] The methyl group of the acetato-bridge was observed at δ 1.59 by ^{1}H NMR spectroscopic analysis, and the strong IR absorption of the carbonyl group was observed between 1577–1415 cm^{-1}. Analysis of the compound **84** by LIFDI-MS confirmed the dinuclear structure with isotopic pattern of dinuclear Pd species observed at m/z 1010.12. Additional peaks for Pd(Ph)(κ^1-OAc)(PPh_3)–Pd(PPh_3) (m/z 873.91), Pd(Ph)(OAc)(PPh_3) (m/z 503.93), and PPh_4^+ (m/z 338.98) were also detected. However, analysis by ^{31}P NMR spectroscopy confirmed the presence of single phosphine species at δ 29.9 in benzene-d_6 solution.

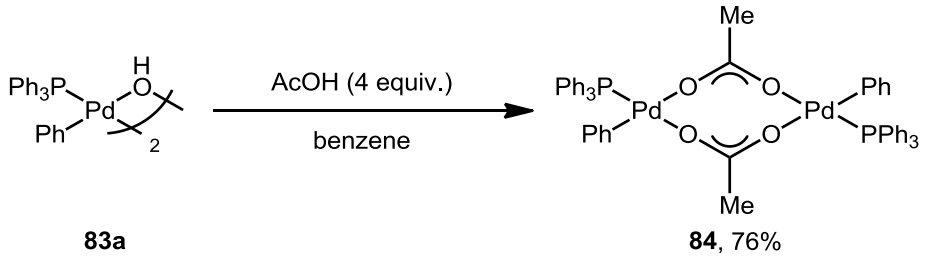

Scheme 32. Synthesis and isolated yield of dinuclear [Pd(Ph)(μ-OAc)(PPh_3)]$_2$ **84**.

The mononuclear Pd(Ph)(κ^1-OAc)(PPh_3)$_2$ **85** species was synthesised by addition of excess PPh_3 to a suspension of dinuclear [Pd(Ph)(μ-OAc)(PPh_3)]$_2$ **84** species in benzene (**Scheme 33**).[212] Addition of ice cold hexane to the resulting colourless solution resulted in isolation of the product **85** as a crystalline white solid in 81% yield. The ^{1}H NMR signals of the acetate methyl group was observed at δ 0.86 and a single ^{31}P NMR signal was detected at δ 20.6. The analysis of the product by LIFDI-MS revealed the presence of mononuclear species Pd(Ph)(OAc)(PPh_3)$_2$ (m/z 766.12), Pd(Ph)(OAc)(PPh_3) (m/z 503.90) and Pd(PPh_3)$_3$ (m/z 892.27), as well as PPh_3 (m/z 261.82) and PPh_4^+ (m/z 338.89).

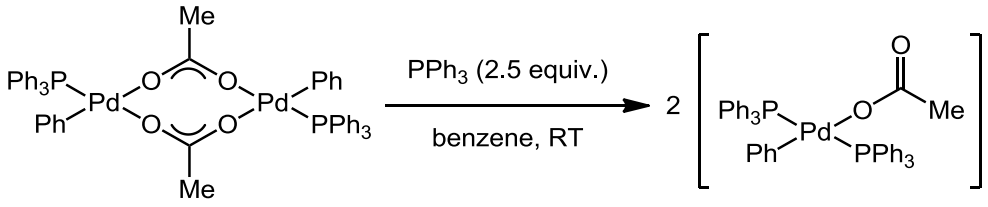

84 **85**, 81%

Scheme 33. Synthesis and isolated yield of mononuclear Pd(Ph)(κ^1-OAc)(PPh_3)$_2$ **85**.

The iodide-bridged dinuclear Pd complex [Pd(Ph)(μ-I)(PPh_3)]$_2$ **86** was prepared in 79% yield from complex **83a** in the presence of excess sodium iodide in DCM solution (**Scheme 34**).[211] The ^{1}H and ^{31}P NMR spectroscopic analysis of the complex **86** in CD_2Cl_2 matched the characterisation data reported by Grushin and co-workers.[211] A broad signal observed at δ 27.4 by ^{31}P NMR spectroscopic analysis was resolved into two singlets at δ 28.3 and δ 27.6 with integration of 1:2 upon decreasing the temperature to −20 °C. The signal averaging observed by ^{31}P NMR spectroscopic analysis suggests the dinuclear complex **86** underwent rapid *cis-trans* isomerisation in solution. This observation was consistent with rapid dissociation of dinuclear [Pd(Ph)(μ-I)($AsPh_3$)]$_2$ complex into the mononuclear species in DMF reported by Amatore and co-workers during the mechanistic study on the reaction of Pd(Ph)(I)($AsPh_3$)$_2$ with vinyl stannane.[207] Iodo-bridged dinuclear Pd species have also been reported as effective pre-catalysts in cross-coupling reactions.[213]

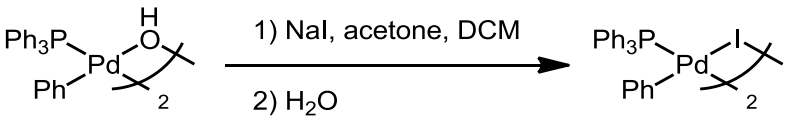

83a **86**, 79%

Scheme 34. Synthesis and isolated yield of dinuclear [Pd(Ph)(μ-I)(PPh_3)]$_2$ **86**.

The synthesised mononuclear and dinuclear Pd species were stored at −20 °C in the glovebox under an atmosphere of argon. The reactivity under stoichiometric reaction condition and suitability as the catalysts are reported and discussed for the phenyl containing Pd complexes (**82a**, **83b**, **84**, **85** and **86**) in Chapter 4.

2.7 Conclusions

The direct arylation reaction of 4-iodotoluene **57** with pentafluorobenzene **56** was selected as the benchmark model reaction for the mechanistic work. The yield of the product **58** formed under various reaction conditions revealed that the reported conditions were already optimised for the system at 5 mol% $Pd(OAc)_2$ catalyst loading. Homocoupling side-product **59** was formed in trace quantity under reaction conditions using over 10 mol% catalyst loading, or in the absence of Ag. However, this side-reaction was negligible under the

majority of the reaction conditions tested. Observations were made regarding different pre-catalysts, additives, solvents, and starting materials in order to understand the reaction condition necessary for effective C–H bond functionalisation.

The suitability of Pd-NPs catalysed direct arylation reaction with pentafluorobenzene **56** was demonstrated. A range of PVP stabilised Pd-NPs with different polymer sizes and particle sizes were tested. The catalyst required PPh_3 at 70 °C which was the highest temperature applied during the kinetic experiments. However, at elevated temperature of 100 °C the Pd-NPs were capable of forming the biaryl product **58** under ligand-free conditions. A similar result was obtained using $Pd(OAc)_2$ without PPh_3 at 100 °C. The product **58** formation was concluded to favour reaction conditions commonly associated with homogeneous catalysis.

The reaction was successfully catalysed by pre-catalysts other than $Pd(OAc)_2$. Quantitative conversion of substrate **57** was achieved for reactions using $Pd(PPh_3)_4$ and $Pd(PPh_3)_2Cl_2$ pre-catalysts. Results indicated 4 equivalents of PPh_3 per Pd-atom were required for the complete activation of these pre-catalysts. Furthermore, experimental evidence suggested both carboxylate anions present in the reaction mixture (*i.e.* acetate and carbonate anions) were capable of being directly involved in the AMLA(6) pathway. Of the metal carbonates tested, the highest yield was achieved using Ag_2CO_3 for the reaction of 4-iodotoluene **57** whereas K_2CO_3 or Cs_2CO_3 were better suited for 4-bromotoluene **27**. The conversion of the substrate **57** depended on the quantity of the Ag_2CO_3 added, highlighting the significant role played by the additive. Ag_2O and tetramethylammonium acetate were also shown to be comparably effective additives.

Alternative solvents for the model reaction were considered in order to reduce the health risk and environmental impact of using DMF. Polar solvents were required for successful product **58** formation and the yield was unaffected by the presence of air or water. Ethylene carbonate and propylene carbonate, both biodegradable cyclic carbonates, were reported to be effective solvents with the product **58** isolated in 50% and 51% yields respectively.

The substrate scope for the model reaction conditions was investigated. For the iodoarenes, the direct arylation of *para*-substituted-iodobenzenes with pentafluorobenzene **56** successfully formed the desired product for R = Me **58**, H **64**, F **65**, CF_3 **66** and NO_2 **67**. No product formation was observed for R = OH **62** and NH_2 **63**. For the fluoroarenes, the quantitative conversion of 4-iodotoluene **57** was achieved for reaction with 1-substituted-2,3,5,6-tetrafluorobenzenes (R = NMe_2 **76**, OMe **77**, Me **78**, Cl **79**, and CF_3 **80**). The reaction of 4-iodotoluene **57** with tetra- and tri-fluorobenzenes (**70** and **71** respectively)

successfully formed the mono-, di- and tri-substituted products. No product was formed for di- and mono-fluorobenzenes under the model reaction conditions. However, stereospecific direct arylation of the 1,3-difluorobenzene **26** in the C2 position was achieved to give 2,6-difluoro-4′-(methyl)biphenyl **28** in 68% isolated yield under modified reaction conditions with excess reagent **26** and 15 mol% PPh_3 at 75 °C.

Potential phenyl-containing catalytic Pd intermediates of the reaction were synthesised in good yields following literature procedures. The mononuclear Pd species (*i.e.* Pd(Ar)(I)$(PPh_3)_2$ **82a/82b** and Pd(Ph)(κ^1-OAc)$(PPh_3)_2$ **85**) and the dinuclear Pd species (*i.e.* [Pd(Ph)(μ-OH)(PPh_3)]$_2$ **83a/83b**, [Pd(Ph)(μ-OAc)(PPh_3)]$_2$ **84** and [Pd(Ph)(μ-I)(PPh_3)]$_2$ **86**) were characterised by ^{1}H NMR, ^{31}P NMR, FT-IR spectroscopy and MS. The reactivity of these Pd complexes under stoichiometric reaction conditions and their capability to act as the catalyst were reported and discussed in Chapter 4. The studies on the isolated 4-tolyl-containing Pd species were abandoned due to poor overall yield of the reactions and the presence of inseparable impurities.

Chapter 3: Kinetic Observations

3.1 Reaction Mechanism Studied by in situ FT-IR Spectroscopy

Infrared absorption spectroscopy is a powerful technique for studying heterogeneous catalysis.[214] In the past, *in situ* FT-IR spectroscopy has been applied extensively to studying surface chemistry of heterogeneous catalysis such as water-gas-shift reactions and methane, acetone, CO oxidations.[215, 216] The ability to obtain quantitative and qualitative information in real-time makes *in situ* FT-IR spectroscopy a powerful technique for process development and process control in industry. Analysis of homogeneous catalysis has also been reported, but often focused on monitoring reaction progress, compound decomposition and intermediate identification.

This approach was highlighted by the mechanistic study by He and co-workers on the copper-catalysed arylation of iodoarene **87** with β-diketone **88** (**Scheme 35**).[217] The sequential stoichiometric reaction of β-diketone **88**, K_3PO_4 and CuI in DMSO was monitored by the *in situ* FT-IR spectroscopy (**Figure 10**). Gradual formation of K(acac) was observed in a solution of K_3PO_4 and β-diketone **88**. Upon addition of CuI, instantaneous loss of K(acac) and formation of an unidentified peak was observed. This unknown species, which was shown to convert into $Cu^{II}(acac)_2$, was proposed to be the active catalyst $[Cu^{I}(acac)_2]^-$ based on additional experimental study and computational calculations based on DFT methodology.

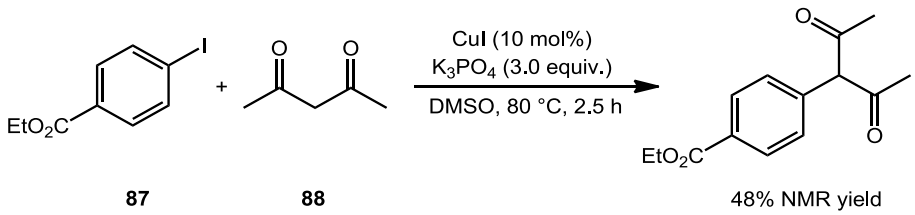

Scheme 35. Cu-catalysed C–C bond coupling reaction of iodoarene **87** with β-diketone **88** (He and co.).[217]

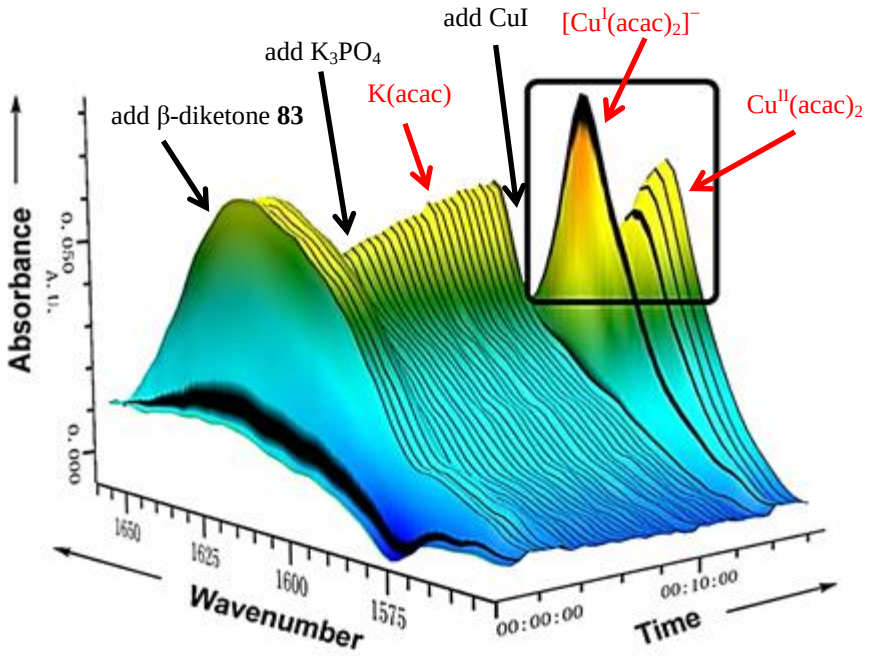

Figure 10. Three-dimensional FT-IR spectrum of the reaction shown in **Scheme 35**, with the moments of reagent addition in black and assignment of intermediate peaks in red.[217] (Adapted with permission from C. He, G.H. Zhang, J. Ke, H. Zhang, J.T. Miller, A.J. Kropf, A.W. Lei, *J. Am. Chem. Soc.* 2013, **135**, 488–493. Copyright 2014 American Chemical Society).

In 2012, Sheikh and co-workers reported enantioenriched synthesis of general 2-substituted-2-phenylpyrrolidines **89** and piperidines **90** with quaternary stereocentres (**Scheme 36**).[218] The lithiation step was directed by the C=O bond of the Boc ($CO_2{}^tBu$) protecting-group, and the free rotation of *N*-Boc bond was required for high yield of lithiation. Furthermore, for high stereoselectivity, the lithiated intermediates had to be configurationally stable. The reaction condition was optimised from the observations made monitoring the transformation by *in situ* FT-IR spectroscopy.

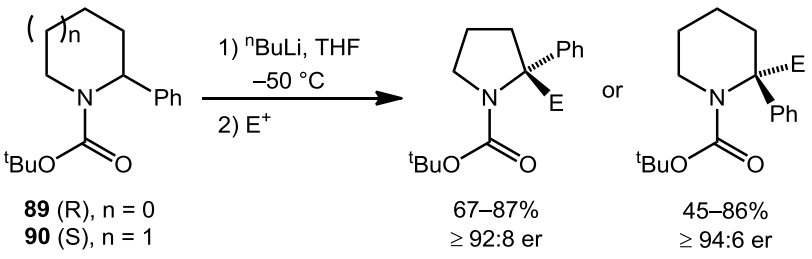

Scheme 36. Optimised reaction condition for the general synthesis of 2-substituted-2-phenylpyrrolidines **89** and piperidines **90** (Sheikh and co.).[218]

Detailed kinetic study of reaction between acid chloride **91** and imine **92** to form β-lactams **93** and **94** was reported by Lynch and co-workers (**Scheme 37**).[219] *In situ* FT-IR spectroscopy at low temperature (*i.e.* −22 °C) was used to follow the IR bands of the acid

chloride **91** (1800 cm^{-1}) and the β-lactams **93** and **94** (1750 cm^{-1}). The reaction was first-order in the concentrations of acid chloride **91** and *N*,*N*-diisopropylethylamine (DIEA). The reaction rate was found to be independent of the imine **92** concentration. The kinetic analysis showed that the reaction proceeded via ketene intermediate formed from the reaction of acid chloride **91** with DIEA.

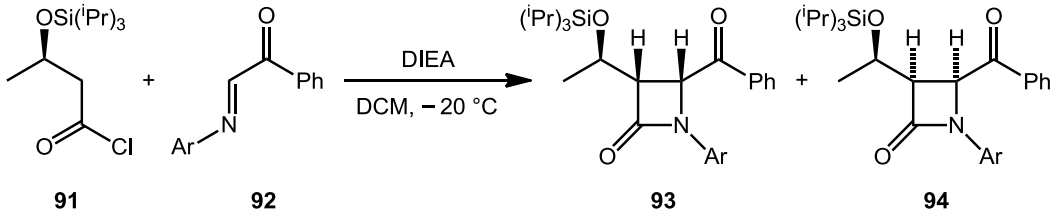

Scheme 37. Synthesis of β-lactams **93** and **94** from acid chloride **91** and imine **92** (Lynch and co.).[219]

Use of *in situ* FT-IR system for determination of a kinetic model of acid-catalysed hydrolysis of sucrose to fructose and glucose was reported by Pintar and co-workers (**Scheme 38**).[220] The effects of initial sucrose concentration, hydrogen ion concentration, and reaction temperature on the reaction rates were studied. The reaction was first-order with respect to the concentration of the sucrose, and first-order in the concentration of the hydrogen chloride in the presence of excess water. The second-order rate constant (k) was calculated as 1.22×10^{-2} mol^{-1} min^{-1} at 25 °C and the E_a was 95.0 kJ mol^{-1}. This study established that *in situ* FT-IR was capable of obtaining high quality kinetic data of reactions in solution.

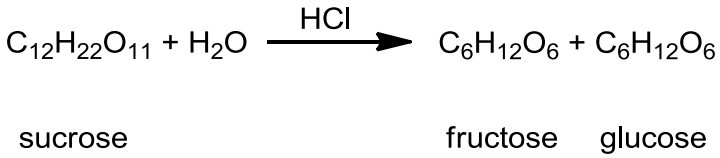

Scheme 38. Acid-catalysed hydrolysis of sucrose to fructose and glucose (Pintar and co.).[220]

Blackmond and co-workers have utilised *in situ* FT-IR spectroscopy as a powerful technique in the development of reaction progress kinetics analysis (RPKA).[221]

3.2 Kinetic Study using in situ FT-IR Spectroscopic Analysis

3.2.1 Experimental Set-Up

The IR activity of the reaction species in DMF was analysed to determine the suitability of the spectroscopic technique for studying kinetics of the model reaction system (**Scheme 39**). Strong IR absorptions around 1500 cm^{-1} (*i.e.* pentafluorobenzene **56** at 1533 cm^{-1} and 1513 cm^{-1}, 4-iodotoluene **57** at 1485 cm^{-1}, and product **58** at 1528 cm^{-1}, 1511 cm^{-1} and 1495 cm^{-1}) were unsuitable due to reagent and solvent peak overlap. However, distinctive absorption bands were identified for compounds **56**, **57** and **58** at 944–957 cm^{-1}, 1009 cm^{-1} and 989 cm^{-1} respectively (**Figure 11**). These bands lie within the 1020–900 cm^{-1} region of DMF where the solvent does not absorb the IR radiation. Of the polar solvents tested, DMF was the only example with flat absorbance in this region of interest (*ca.* 900–1050 cm^{-1}).

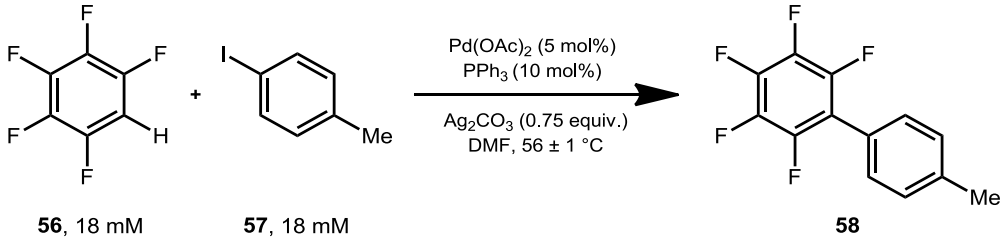

Scheme 39. Direct arylation reaction condition selected for study by the *in situ* FT-IR spectroscopy.

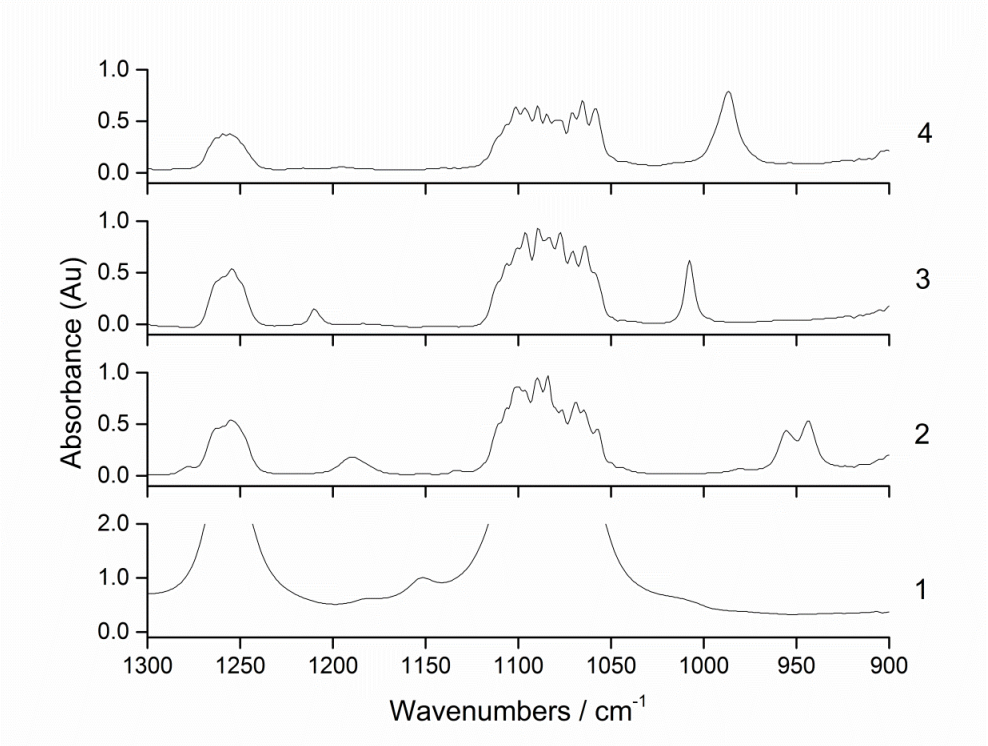

Figure 11. Overlaid FT-IR spectra of **(1)** DMF, and DMF solutions of **(2)** pentafluorobenzene **56**, **(3)** 4-iodotoluene **57** and **(4)** the product **58** in the solution cell.

The band assignment for pentafluorobenzene **56** with C_{2v} symmetry has been made by Steele and co-workers with the frequency at 957 cm^{-1} given as class b_2 fundamental based on type-A contours with P- and R-bands with medium strength Q-band in between.[222, 223] Garrigoulagrange and co-workers studied the vibrational frequencies of various *para*-disubstituted benzenes including 4-iodotoluene **57** which has C_{2v} symmetry. In this work, the band observed at 1009 cm^{-1} was assigned as class a_1 fundamental.[224, 225] The IR spectrum of the product **58** with C_{2V} symmetry had not been reported in the literature.

The *in situ* FT-IR spectroscopic measurements were recorded by the ReactIR™ equipped with a silicon ATR sensor at a resolution of 4 cm^{-1} with 167 scans per minute (**Figure 12**). The greatest advantages of *in situ* FT-IR spectroscopy using ATR probe is the convenience of monitoring the reaction progress. Since the probe is only required to be submerged below the solvent surface, the technique allows reaction mixtures with insoluble solids to be studied while being stirred. The IR absorptions of substrates (*i.e.* **56** and **57**) and the product **58** were unaffected by being in the reaction mixture (*i.e.* 944–957 cm^{-1}, 1009 cm^{-1} and 989 cm^{-1} respectively). Since FT-IR spectroscopy is an integral measurement, the IR absorptions were used to calculate the substrate conversions (*i.e.* $1-(A/A_0)$) and the concentrations during the reaction. The reaction was initiated by the addition of pentafluorobenzene **56** to a mixture of 4-iodotoluene **57**, $Pd(OAc)_2$, PPh_3 and Ag_2CO_3 under continuous flow of nitrogen. The reaction temperature was monitored using an electronic thermometer with a K-type thermocouple submerged in the reaction mixture. The data were analysed by subtracting the spectrum of degassed DMF at the relevant reaction temperatures, and using two baseline-offset points at *ca.* 1015 cm^{-1} and 915 cm^{-1}. The experimental results were treated as *in situ* rather than *in operando* as IR bands of the catalytic species were not observed.[226, 227]

Figure 12. Experimental set-up for following the kinetics of the reaction shown in **Scheme 39** using the ReactIR™, an *in situ* FT-IR instrument.

3.2.2 Initial Kinetic Measurements and Observations

The reaction profile generated by following the changes in IR absorptions at 1009 cm^{-1}, 989 cm^{-1} and 957 cm^{-1} showed rapid consumption of starting materials (*i.e.* **56** and **57**) and the formation of product **58** (**Scheme 13** and **Figure 14**). Instantaneous formation of product **58** was observed without any detectable induction period. This does not eliminate the possibility of an induction period for catalyst activation outside of the spectroscopic time-frame. However, it was not a problem for analysing the reaction rate, as the main interest lies in the steady-state characteristics of the catalysis. No intermediate species were detected on the time scale of the method. The reaction achieved quantitative conversion of 4-iodotoluene **57** (pentafluorobenzene **56** was in slight excess), with overall first-order kinetics with $k_{obs} = (7.14 \pm 0.03) \times 10^{-5}\ s^{-1}$ at 56 ± 1 °C (Eq. 1).

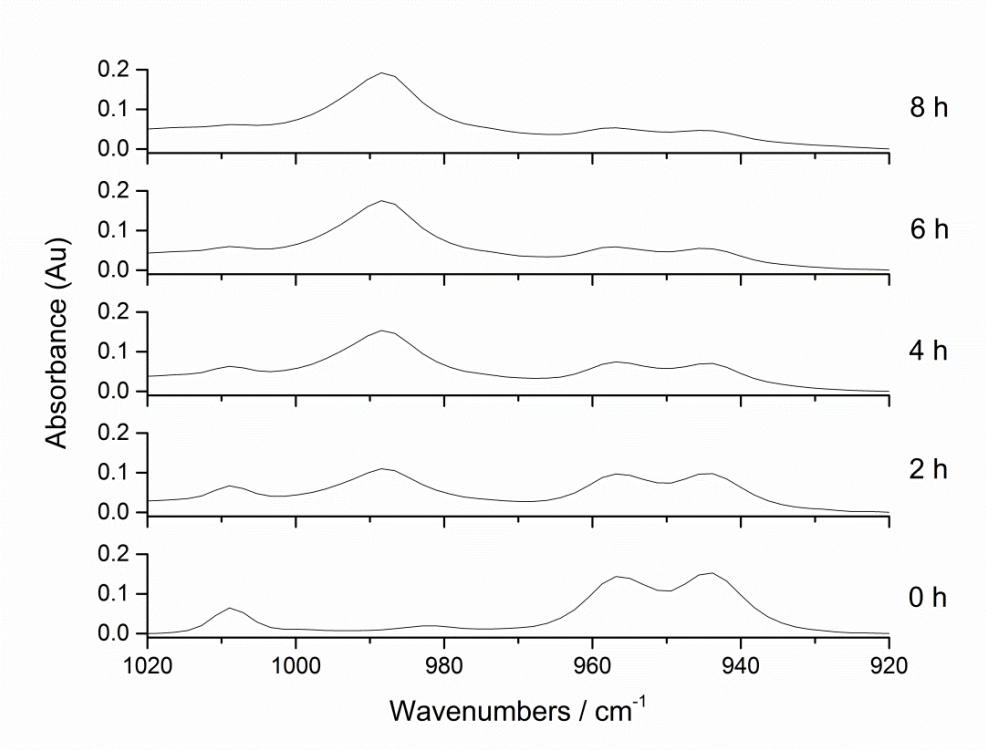

Figure 13. Stacked FT-IR spectra of the reaction mixture shown in **Scheme 39** between 0–8 h reaction time generated by *in situ* FT-IR spectroscopic analysis. Absorbance observed for 4-iodotoluene **57** (1009 cm^{-1}), the biaryl product **58** (989 cm^{-1}) and pentafluorobenzene **56** (957 cm^{-1} and 944 cm^{-1}).

$$rate = \frac{-d[ArI\ \mathbf{57}]}{dt} = \frac{-d[C_6F_5H\ \mathbf{56}]}{dt} = \frac{+d[P\ \mathbf{58}]}{dt} = \frac{1}{t} ln\left(\frac{[ArI\ \mathbf{57}]_0}{[ArI\ \mathbf{57}]_t}\right) \qquad (1)$$

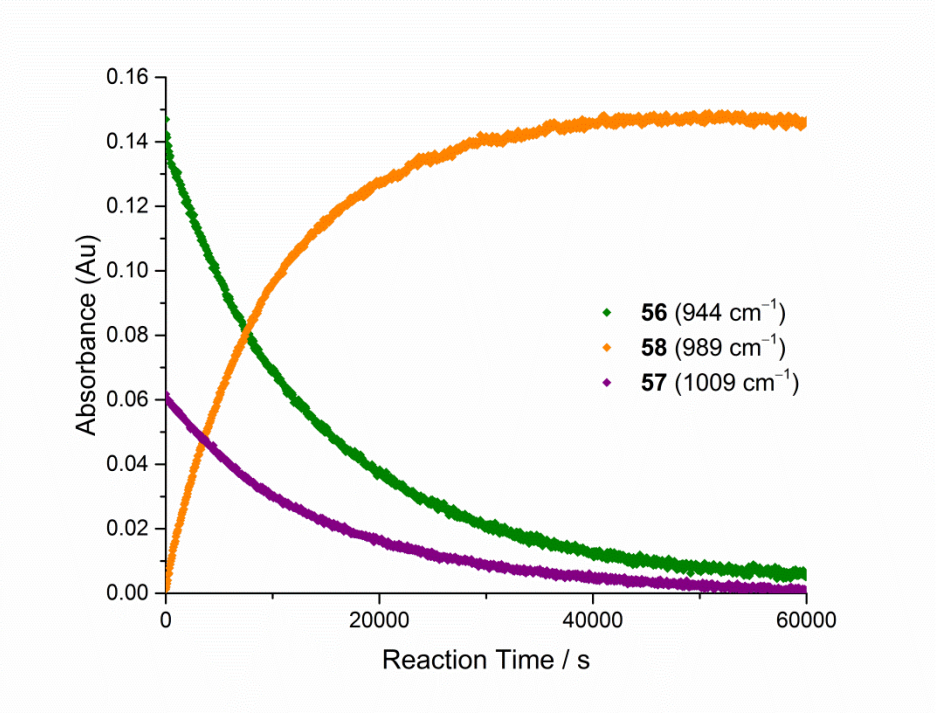

Figure 14. Changes in the IR absorbance observed during the reaction shown in **Scheme 39**.

The direct arylation reaction of 0.18 M C_6F_5H **56** with 0.018 M 4-iodotoluene **57** was monitored simultaneously by *in-situ* FT-IR spectroscopic analysis and *ex situ* NMR spectroscopic analysis. The percentage conversion of 4-iodotoluene **57** to the product **58** during the reaction was determined from integrating the methyl peaks observed by ^1H NMR spectroscopic analysis of reaction mixture aliquots sampled at regular interval. The side-products were not observed under the reaction conditions employed for the kinetic investigation. The kinetic profiles observed by the two techniques (*i.e.* FT-IR and NMR) were in very good agreement confirming the *in situ* FT-IR spectroscopic analysis to be a viable and convenient method for studying the kinetics of the reaction (**Figure 15**). Furthermore, the concentrations of the starting material **57** and the product **58** during the reaction can be calculated successfully by correlating the change in the corresponding IR absorbance to the %conversion determined by ^1H NMR spectroscopic analysis. However, the main disadvantage of the technique was the inability to detect short-lived intermediates or species in low concentration.

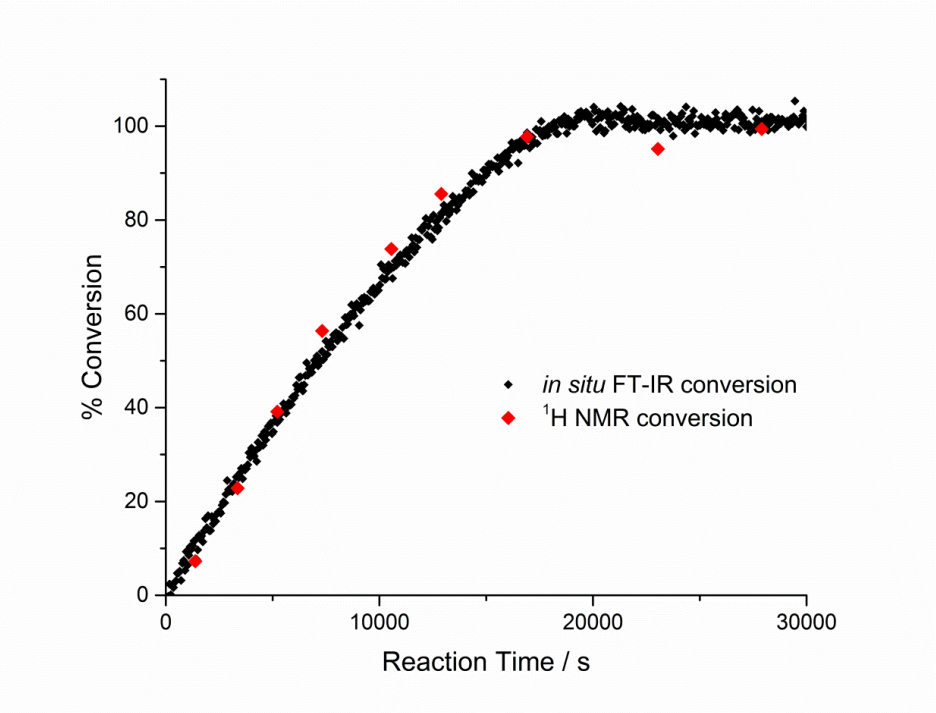

Figure 15. Progress of the reaction shown in **Scheme 39** with 10-fold excess of substrate **56** (*i.e.* 0.18 M) generated by **(Black)** *in situ* FT-IR spectroscopy and **(Red)** conversion determined by NMR spectroscopic analysis of sampled reaction mixture aliquots.

Alternative methods of initiating the reaction were tested in order to establish the best approach for detailed kinetic study. An attempt was made to start the reaction by the addition of $Pd(OAc)_2$ solution in DMF to a heated mixture of starting materials **56** and **57**, PPh_3 and Ag_2CO_3 in DMF (**Figure 16**). However, no reaction was observed between the addition of $Pd(OAc)_2$ and one hour of heating at 56 ± 1 °C. Interestingly, the reaction failed to start upon the addition of further 10 mol% of solid PPh_3. The reaction was finally initiated by the simultaneous addition of solid $Pd(OAc)_2$ (5 mol%) and PPh_3 (10 mol%). This result suggests the decomposition of $Pd(OAc)_2$ and PPh_3 in the absence of the counterpart.

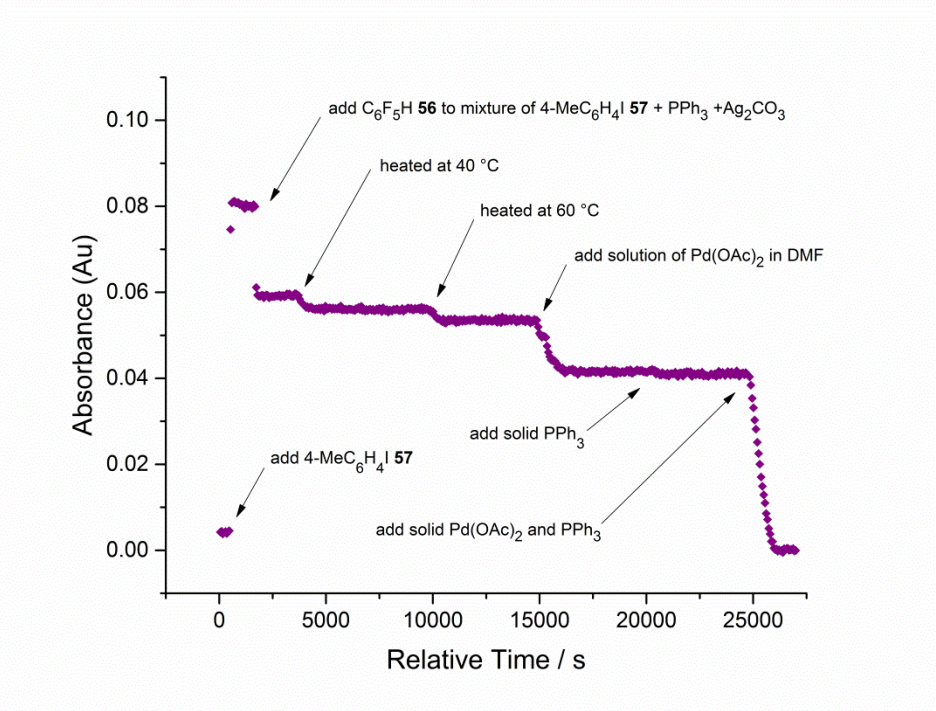

Figure 16. Changes in the IR absorbance of 4-iodotoluene **57** at 1009 cm^{-1} during the attempted initiation of reaction shown in **Scheme 39** by the addition of $Pd(OAc)_2$ solution in DMF.

The reaction initiated by the addition of 4-iodotoluene **57** showed trace quantity of product **58** formation, but did not match the rate observed when initiated by pentafluorobenzene **56**. Furthermore, the experiment suffered baseline shifting, most likely due to formation of Pd black. The complex formed between $Pd(OAc)_2$ and PPh_3 was potentially unstable in the absence of 4-iodotoluene **57**.

The reaction was successfully initiated by the addition of pre-mixed solution of $Pd(OAc)_2$ and PPh_3 in DMF. The k_{obs} = (4.56 ± 0.08) × 10^{-4} s^{-1} determined from the experiment was in agreement with what was obtained previously for the reaction initiated by the additon of pentafluorobenzene **56**, k_{obs} = (4.39 ± 0.14) × 10^{-4} s^{-1}. Furthermore, identical k_{obs} was obtained for reaction where DMF solution of the substrates (*i.e.* **56** and **57**) was transferred into the reaction vessel with the solid reagents (*i.e.* $Pd(OAc)_2$, PPh_3 and Ag_2CO_3). Under this preparation method (see Chapter 6.2 General Procedures), an induction period was observed (*ca.* 4 min) after the reaction was at 56 ± 1 °C. It was therefore concluded that the reaction can be initiated either by the (1) addition of pentafluorobenzene **56** to a mixture of 4-iodotoluene **57**, $Pd(OAc)_2$, PPh_3 and Ag_2CO_3 in DMF or (2) by the addition of pre-mixed solution of $Pd(OAc)_2$ and PPh_3 in DMF or (3) mixing all the reagents together, to provide identical kinetic results. The consistent kinetic results highlighted the excellent reproducibility of the experimental data obtained by the estabilished *in situ* FT-IR spectroscopic analysis methodologies.

Observations were made on the changes in the appearance of the $Pd(OAc)_2$ and PPh_3 catalyst mixture in DMF prior to addition (**Figure 17**). The sequence of colour changes observed suggests the *in situ* formation of Pd^0 from the reduction of Pd^{II} by PPh_3. The Pd^0PPh_3 most likely formed in the red solution is oxidised upon exposure to air (**Figure 18**). However, this complex was expected to form a stable oxidative addition complex $Pd^{II}(Ar)(I)(PPh_3)$ in the presence of 4-iodotoluene **57**.

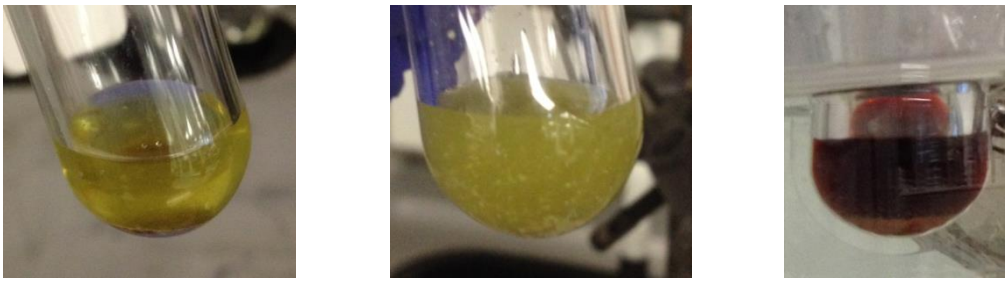

Stirred 1 min **Stirred 3 min** **Heated 10 min**

Figure 17. Changes in the colour observed for the solution of $Pd(OAc)_2$ and PPh_3 in DMF.

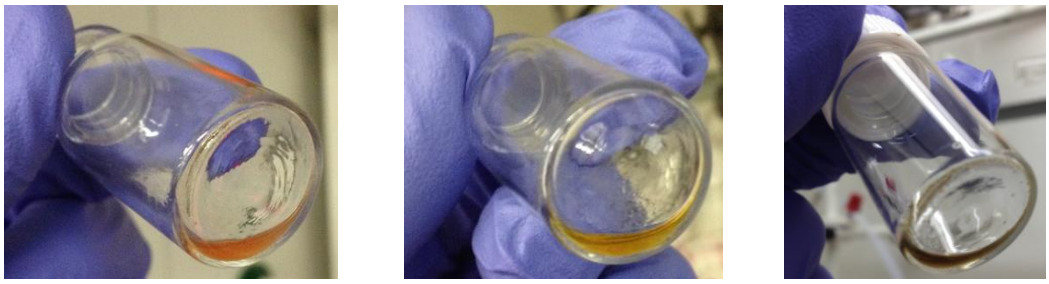

0 min - red **20 min - yellow** **1 day - black**

Figure 18. Changes in the colour of solution seen in **Figure 17** after exposure to air.

The effects of water and air on the reaction kinetics were considered. The reaction in the presence of 50-fold excess H_2O (k_{obs} = (8.83 ± 0.16) × 10^{-7} mol dm^{-3} s^{-1}) was at half the rate compared with the reaction without added H_2O (k_{obs} = (1.68 ± 0.02) × 10^{-6} mol dm^{-3} s^{-1}). Comparing the k_{obs} for a reaction under continuous flow of nitrogen and a reaction open to air, it was revealed that the kinetics were unaffected by the reaction atmosphere. In order to maintain consistency of data, all of the kinetic experiments were performed in commercially purchased dried DMF, degassed and stored over 3Å molecular sieves, under continuous flow of nitrogen.

3.3 Modern Kinetic Analysis: Reaction Progress Kinetic Analysis and Variable Time Normalisation Analysis

3.3.1 General Consideration and Kinetic Data

Initial kinetic investigations were made following instructions provided by Blackmond for carrying out reaction progress kinetic analysis (RPKA)[205, 222] and Burés for performing variable time normalisation analysis (VTNA).[228, 229] These methodologies have been successfully applied for kinetic analysis of organic reactions and transition metal-catalysed transformations in recent years.[230-236] The technique utilises all the data obtained from continuous reaction monitoring techniques and provide kinetic evidence based on visual graphical overlaps, with fewer experiments than classical kinetic analysis. Since RPKA and VTNA do not require the pseudo-nth-order conditions, they provide kinetic data under synthetically realistic reaction conditions. The information obtained from these methods were later compared and combined with the results from classical kinetic analysis approaches (see Chapter 3.4). The reaction with 93 mM [ArI **57**] and 140 mM [C_6F_5H **56**] (*i.e.* excess of 47 mM) catalysed by 4.6 mM $[Pd]_{TOT}$ at 56 ± 1 °C was selected as the standard conditions for both analyses (**Table 10**, Entry 1).

Table 10. Reaction conditions selected for performing the RPKA and the VTNA.

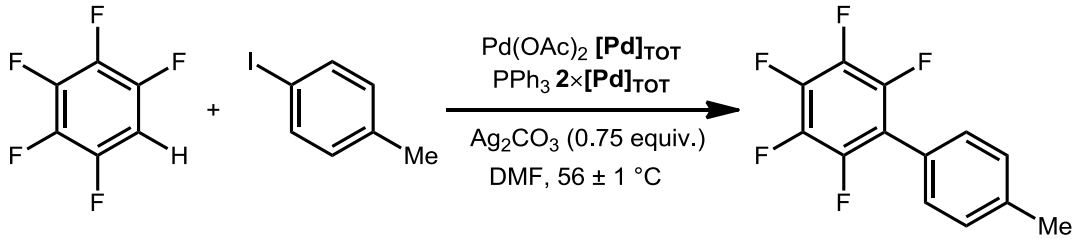

[C_6F_5H 56] **[ArI 57]** **[P 58]**

Entry	Condition	Concentration / mM				
		[ArI 57]	**[C_6F_5H 56]**	**$[Pd]_{TOT}$**	**[P 58]**	**[xs]** [a]
1	Standard	93	140	4.6	0	47
2	Different [xs]	93	93	4.7	0	0
3	Different [xs]	93	280	4.7	0	187
4	Different [xs]′	280	93	4.7	0	187 [b]
5	Different $[Pd]_{TOT}$	93	140	9.2	0	47
6	Same [xs]	47	93	4.6	0	46
7	Same [xs] + [P **58**]	47	93	4.6	47	46

[a] [xs] = [C_6F_5H **56**] − [ArI **57**]. [b] [xs]′ = [ArI **57**] − [C_6F_5H **56**].

3.3.2 Reaction Progress Kinetic Analysis

Unlike the classic method of kinetic investigation, RPKA can provide kinetic information on reactions with two changing substrate concentrations. This is achieved by utilising a parameter called the "excess" concentration and analysing plots of reaction rate against substrate concentration by "graphical rate equations". The experiments were designed with different amounts of ["excess"] or [xs] defined as the difference in the concentrations of the two substrates. The standard reaction (**Table 10**, Entry 1) was repeated with two different amounts of [xs] pentafluorobenzene **56** (Entries 2 and 3) and the same amount of [xs], starting with 47 mM [ArI **57**] and 93 mM [C_6F_5H **56**] (Entry 6). The reaction achieved faster completion under higher concentration of C_6F_5H **56** (**Figure 19**). However, no rate enhancement was observed with 187 mM excess concentration of 4-iodotoluene **57** (Entry 4). Therefore the reaction rate was dependent on the concentration of pentafluorobenzene **56**, but not the 4-iodotoluene **57**.

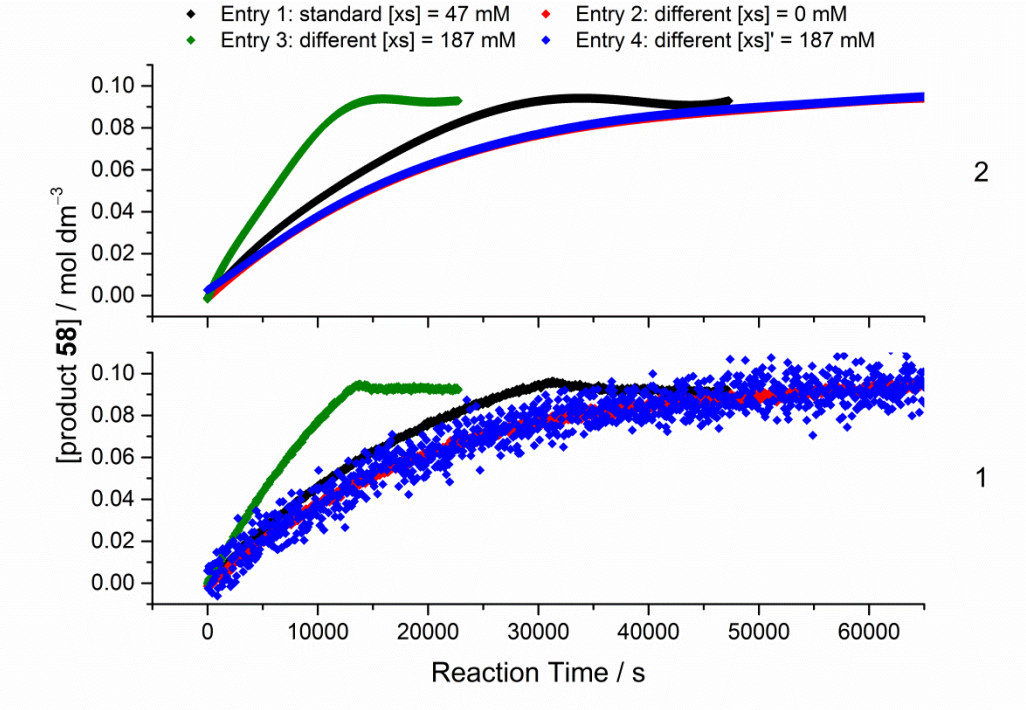

Figure 19. Kinetic profiles of the product **58** formation for the reaction shown in **Table 10** with different values of excess (where [xs] = [C_6F_5H **56**] − [ArI **57**] and [xs]′ = [ArI **57**] − [C_6F_5H **56**]). **(1)** Experimental data and **(2)** arbitrary polynomials fitted to the experimental data.

The concentrations versus time data collected by the *in situ* FT-IR spectrometer at 56 ± 1 °C were fitted to an arbitrary polynomial function (**Figure 19**). The reaction rates at each experimental data point were derived by the differential method of kinetic data analysis (*i.e.* differentiating the polynomial equations fitted to the experimental data). The calculated rates were significantly affected by the closeness of the fit. In order to improve the accuracy

of the rate profiles, the cells in the Excel spread sheets were referenced into the calculations to incorporate all decimal places. Additionally, suitable degrees of polynomial (up to n = 16th) were applied, based on trial and error. Therefore, it is acknowledge that the error introduced from the aforementioned mathematical transformations may be significant.

The calculated reaction rates were plotted against the concentration of the 4-iodotoluene **57** over the course of the reaction to give the simplest form of the graphical rate equation (**Figure 20**). The reaction progress is shown from right to left in graphical rate equations. The kinetic data between 20–80% product **58** formation were analysed for the steady-state catalytic cycle. In addition to visualising the increase in reaction rate with increased pentafluorobenzene **56** concentration, this plot provided a relationship between change in rate and the change in [ArI **57**]. Firstly, the rates of the reactions under different excess [C_6F_5H **56**] values decreased linearly with similar gradients, m (**Table 11**). Secondly, a sharp drop in the rates was observed towards the end of the reactions when [xs] ≠ 0 mM. This was highlighted by the significant nonzero y-intercepts, c, present for the lines-of-best-fit of these reactions. The graph also demonstrated that the reaction was dependent on the substrate **56** concentration in some way, as a reaction with zeroth-order in the two substrates would result in overlapping horizontal lines.

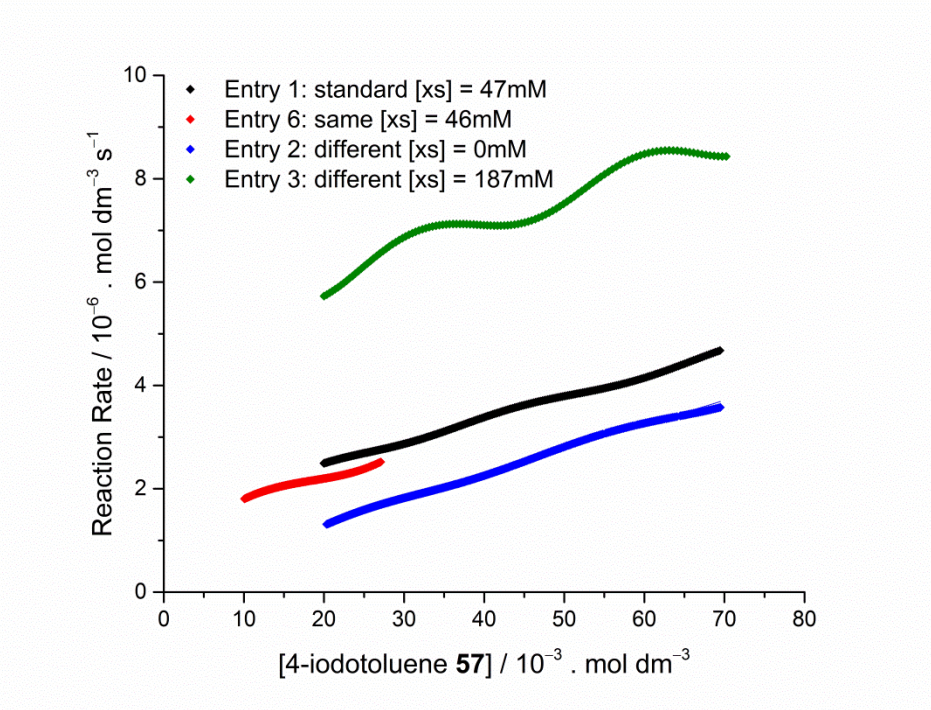

Figure 20. Graphical rate equations of selected reactions shown in **Table 10** with the rate plotted against [4-iodotoluene **57**] for 20–80% reaction completion. The reaction rates from the standard [xs] experiment was compared to the results from same [xs] and different [xs] experiments (where [xs] = [C_6F_5H **56**] − [ArI **57**]).

Table 11.Values of the lines-of-best-fit for the graphical rate equations plotted in **Figure 20**.

Entry	[xs] [a] / mM	m / 10^{-5} . dm^3 mol^{-1} s^{-1}	c / 10^{-6} . s^{-1}	m•[xs] [a] / s^{-1}
1	47	4.31 ± 0.02	1.62 ± 0.01	2.03×10^{-6}
2	47	3.55 ± 0.04	1.50 ± 0.01	1.67×10^{-6}
3	0.14	4.75 ± 0.01	0.389 ± 0.006	6.84×10^{-9}
4	187	5.40 ± 0.13	4.99 ± 0.06	1.01×10^{-5}

[a] [xs] = [C_6F_5H **56**] − [ArI **57**]

The observations made by RPKA discussed above, are characteristics of reaction with first-order kinetics in [C_6F_5H **56**] and zeroth-order kinetics in [ArI **57**] (Eq. 2). Assuming constant [xs] during the reaction and substrate consumption consistent with the reaction stoichiometry, the concentration of [C_6F_5H **56**] at any point in the reaction is the sum of the [ArI **57**] and the [xs] (Eq. 3). Therefore, the plot of rate versus [ArI **57**] was linear with the slope of k and the y-intercept of k[xs] (Eq. 4).

$$rate = k[C_6F_5H\ \mathbf{56}] \tag{2}$$

$$[C_6F_5H\ \mathbf{56}] = [ArI\ \mathbf{57}] + [xs] \tag{3}$$

$$rate = k[ArI\ \mathbf{57}] + k[xs] \tag{4}$$

The order in the substrates can be determined by utilising normalised rates, derived from normalisation of Eq. 2 by a substrate concentration (Eq. 5 and 6). One of the advantages of the RPKA is the visual determination of kinetic information based on graphical overlay and the plot shape. Overlapping of curves of the graphical rate equations normalised by the pentafluorobenzene **56** concentration suggests stable catalyst concentrations with first-order kinetics in C_6F_5H **56** concentration (**Figure 21**). Furthermore, the horizontal shapes indicate that the reaction is independent of changes in the 4-iodotoluene **57** concentration. These observations were consistent with the result obtained from the graphical rate equations normalised by the 4-iodotoluene **57** concentration (**Figure 22**).

$$pentafluorobenzene\ \mathbf{56}\ normalised\ rate = \frac{rate}{[C_6F_5H\ \mathbf{56}]} = k \tag{5}$$

$$4-iodotoluene\ \mathbf{57}\ normalised\ rate = \frac{rate}{[ArI\ \mathbf{57}]} = \frac{k[C_6F_5H\ \mathbf{56}]}{[ArI\ \mathbf{57}]} \tag{6}$$

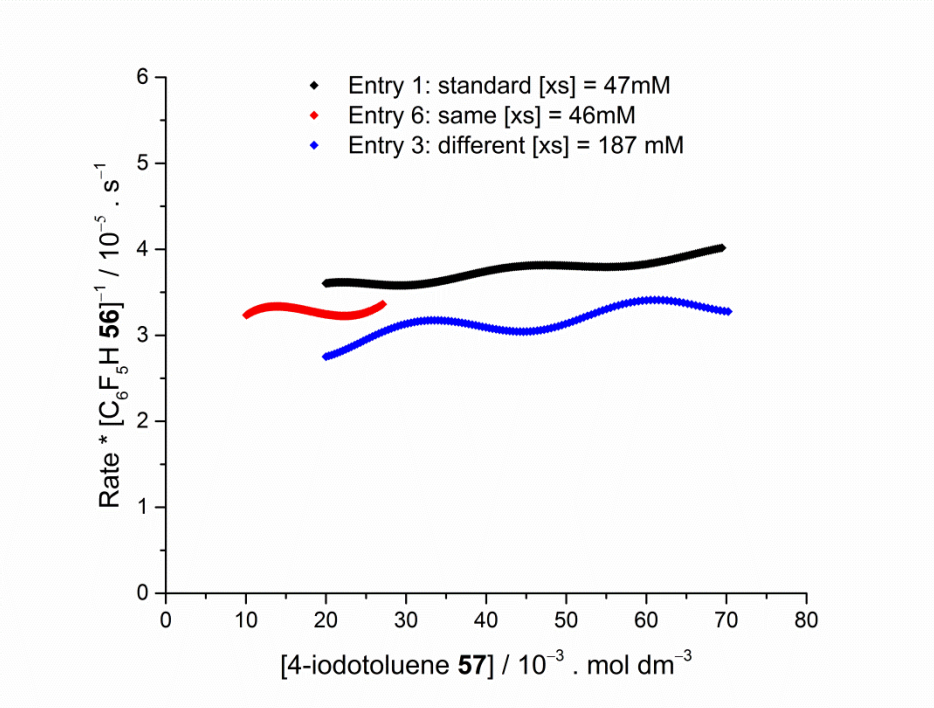

Figure 21. Graphical rate equation (Eq. 5) of selected reactions shown in **Table 10** normalised to substrate **56** concentration**.** The reaction rates from the standard [xs] experiment was compared to the results from same [xs] and different [xs] experiments (where [xs] = [C_6F_5H **56**] − [ArI **57**]).

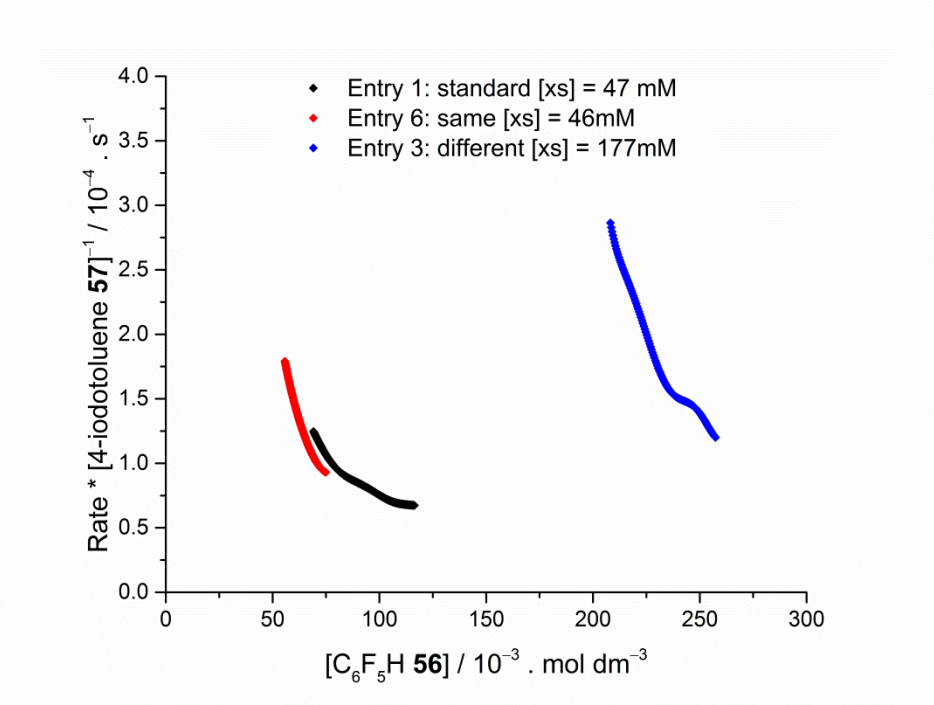

Figure 22. Graphical rate equation (Eq. 6) of selected reactions shown in **Table 10** normalised to substrate **57** concentration. The reaction rates from the standard [xs] experiment was compared to the results from same [xs] and different [xs] experiments (where [xs] = [C_6F_5H **56**] − [ArI **57**]).

The reaction at standard condition was repeated with increased catalyst loading at 9.2 mM (**Table 10**, Entries 5). Graphical rate equations can be used to determine the order with respect to the catalyst by plotting the turn-over-frequencies (TOF) against the concentrations of 4-iodotoluene **57**. The best overlap was achieved for the plot of rate divided by catalyst concentration raised to the power of a half (**Figure 23**). This is characteristics of half-order kinetics in the catalyst concentration where an on-cycle mononuclear species are in equilibrium with off-cycle dinuclear species.[205, 237-241]

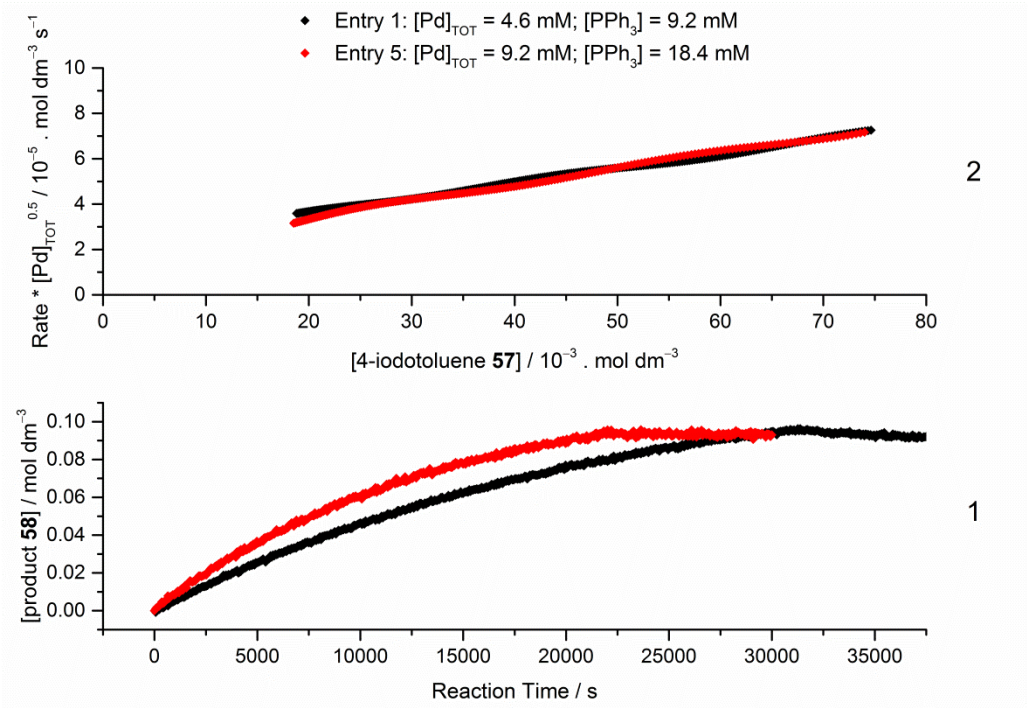

Figure 23. **(1)** Experimental data showing the kinetic profiles of the product **58** formation for the reaction shown in **Table 10** with different catalyst loadings **(2)** Graphical rate equations plotting the TOF of half-order catalyst against [ArI **57**]. Other variables in the reaction were kept consistent with [ArI **57**] = 93 mM, [C_6F_5H **56**] = 140 mM and [xs] = 47 mM (where [xs] = [C_6F_5H **56**] − [ArI **57**]).

3.3.3 Variable Time Normalisation Analysis

A more suitable method for analysing the conversion reaction profiles obtained by *in situ* FT-IR spectroscopy is the variable time normalisation analysis (VTNA). The kinetic data was treated by the normalised time scale method, where the time axis was replaced with the multiple of the reaction time and the initial concentration of the reaction component of interest raised to the n^{th}-power. This allowed the kinetic contribution of the respective reaction components to be removed from the kinetic profiles. The overlapping kinetic profiles were achieved for first-order kinetics in pentafluorobenzene **56** (**Figure 24**), zeroth-order kinetics in 4-iodotoluene **57** (**Figure 25**) and 0.5-order kinetics in the Pd catalyst (**Figure 26**).

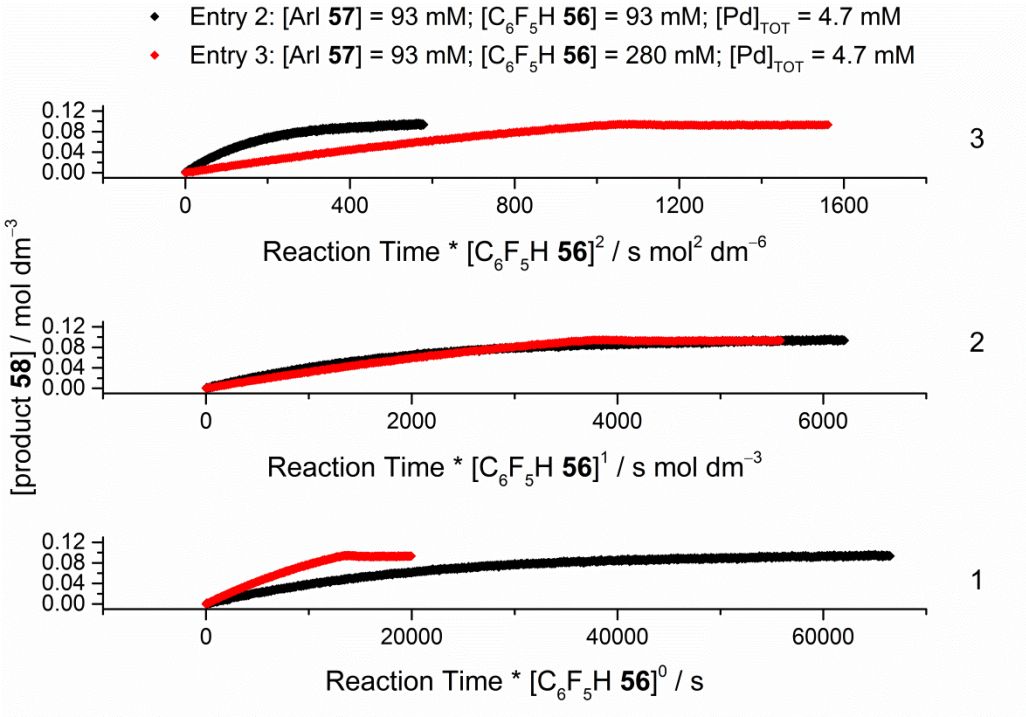

Figure 24. Kinetic profiles of the product **58** formation for the reaction shown in **Table 10**, normalised to the concentration of pentafluorobenzene **56** for **(1)** zeroth-order, **(2)** first-order, and **(3)** second-order kinetics.

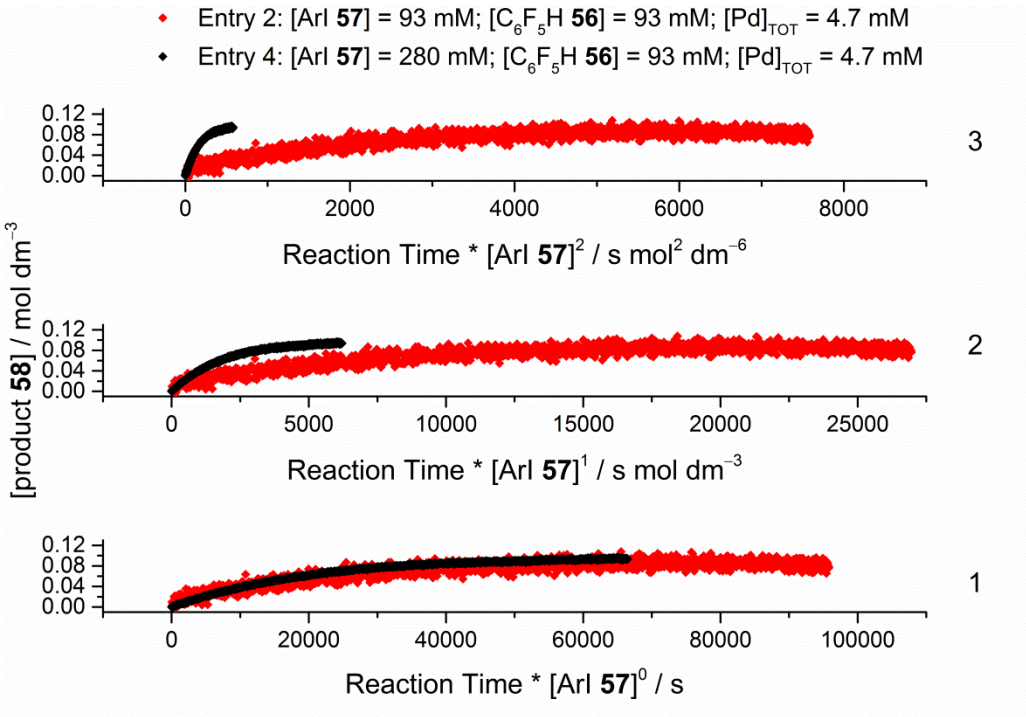

Figure 25. Kinetic profiles of the product **58** formation for the reaction shown in **Table 10**, normalised to the concentration of 4-iodotoluene **57** for **(1)** zeroth-order, **(2)** first-order, and **(3)** second-order kinetics.

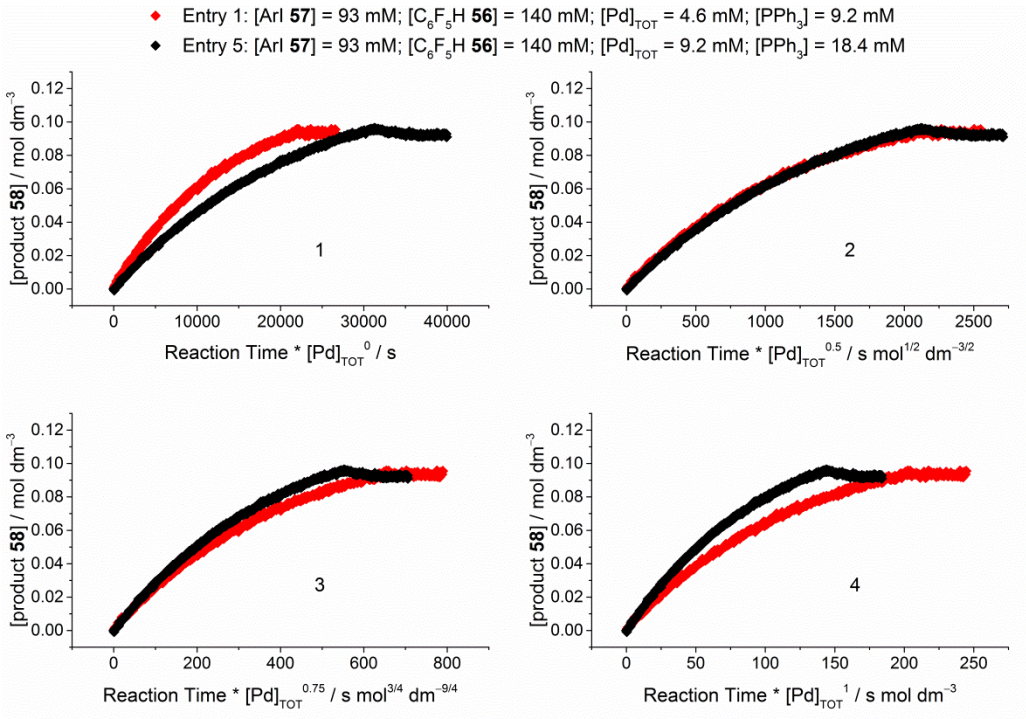

Figure 26. Kinetic profiles of the product **58** formation for the reaction shown in **Table 10**, normalised to the concentration of the catalyst for **(1)** zeroth-order, **(2)** 0.5-order, **(3)** 0.75-order, and **(4)** first-order kinetics.

3.3.4 Catalyst Robustness

The results obtained from three "same [xs]" experiments (**Table 10**, entries 1, 6 and 7) were studied to understand the robustness of the catalyst. Firstly, the standard condition reaction with initial concentrations of 93 mM [ArI **57**] and 140 mM [C_6F_5H **56**] were compared to a reaction with initial concentrations of 47 mM [ArI **57**] and 93 mM [C_6F_5H **56**] (**Figure 27**). The start of the latter reaction replicated the reaction condition of the former at 50% completion. The differences between the two reactions were the number of turn-overs made by the catalyst and the concentration of the product **58** in the reaction mixture. A change in the kinetic profile would suggest loss of catalytic activity or inhibition by the product **58** formed from 50% conversion of the starting material **57**. In order to differentiate between these two possibilities, "the same [xs]" experiment was also repeated with 47 mM [product **58**] added at the start of the reaction. The overlapping kinetic profiles of the product **58** formation from the three experiments suggested that neither catalyst deactivation nor product inhibition was taking place under the reaction condition of interest. Furthermore, kinetic data obtained with 2 equivalents of product **58** added to the reaction mixture confirmed the rate to be independent of product concentration and not auto-catalytic.

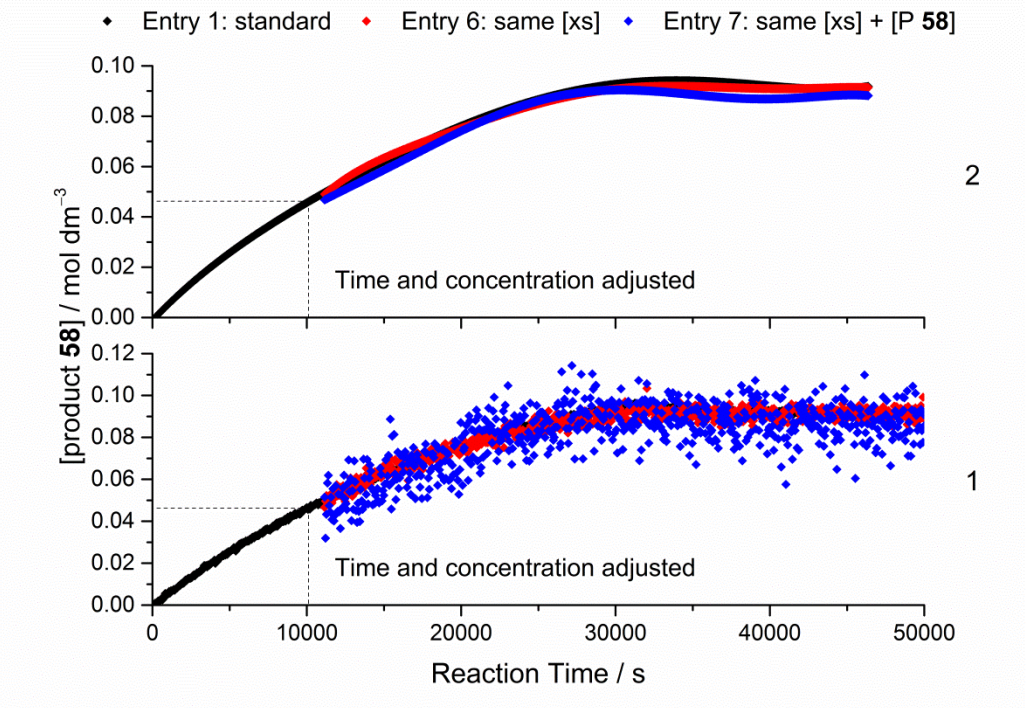

Figure 27. Time and concentration adjusted kinetic profile of the product **58** formation of the reaction shown in **Table 10**. **(1)** Experimental data and **(2)** arbitary polynomials fitted to the experimental data. **(Black)** [ArI **57**] = 93 mM; [C_6F_5H **56**] = 140 mM; $[Pd]_{TOT}$ = 4.6 mM; [xs] = 47 mM. **(Red)** [ArI **57**] = 47 mM; [C_6F_5H **56**] = 93 mM; $[Pd]_{TOT}$ = 4.6 mM; [xs] = 46 mM. **(Blue)** [ArI **57**] = 47 mM; [C_6F_5H **56**] = 93 mM; $[Pd]_{TOT}$ = 4.6 mM; [P **58**] = 47 mM; [xs] = 46 mM (where [xs] = [C_6F_5H **56**] − [ArI **57**]).

3.3.5 Overall Rate Law Based on Modern Kinetic Analysis

The kinetic results from RPKA and VTNA suggested the rate law of the reaction to be first-order in pentafluorobenzene **56**, zeroth-order 4-iodotoluene **57** and half-order in Pd catalyst concentrations. Based on these results, the proposed catalytic cycle was simplified to represent a mechanism involving transformation of two-substrates catalysed by Pd species generated from an off-cycle dinuclear complex (**Scheme 40**). The oxidative addition of aryl iodide and the subsequent iodide abstraction was assumed to be very fast and essentially irreversible with intermediate complex Pd1 fully saturated. The acetate ligand isomerisation of Pd1 to create a vacant site for pentafluorobenzene **56** coordination was assumed to be kinetically negligible.[231] Furthermore, any loss and gain of PPh_3 ligand was omitted. The kinetic data provide no information on the structure of the Pd species (*i.e.* cat, Pd1, Pd2 and D).

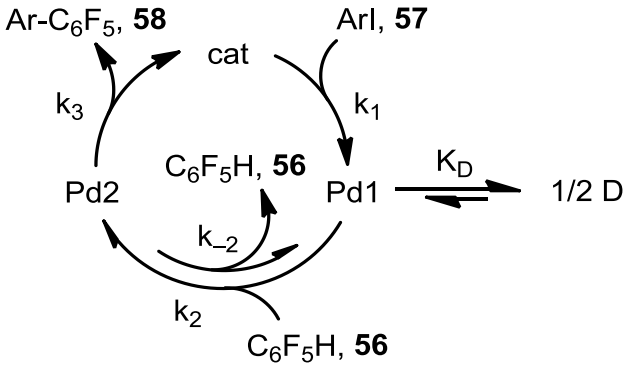

Scheme 40. Simplified mechanism for the model direct arylation shown in **Table 10** (ArI **57** + C_6F_5H **56** –> Ar-C_6F_5 **58**).

The overall rate law for the catalytic cycle shown above (**Scheme 40**) was derived by applying steady-state approximation to the elementary steps (Eq. 7 and 8) and applying quasi-equilibrium assumption between on/off-cycle species (Eq. 9). The total concentration of Pd intermediates involved in the reaction was assumed equal to the total concentration of the Pd pre-catalyst, $[Pd]_{TOT}$ (Eq. 10).

$$\frac{+d[cat]}{dt} = k_3[Pd2] - k_1[ArI\ \mathbf{57}][cat] \approx 0 \tag{7}$$

$$\frac{+d[Pd2]}{dt} = k_2[C_6F_5H\ \mathbf{56}][Pd1] - (k_3 + k_{-2})[Pd2] \approx 0 \tag{8}$$

$$K_D = \frac{[D]}{[Pd1]^2} \tag{9}$$

$$[Pd]_{TOT} = [cat] + [Pd1] + [Pd2] + 2[D] \tag{10}$$

$$\frac{+d[P\ \mathbf{58}]}{dt} = k_3[Pd2] \tag{11}$$

$$rate = \frac{+d[P\ \mathbf{58}]}{dt} = \frac{2k_3[Pd]_{TOT}}{b + \sqrt{b^2 + 4a[Pd]_{TOT}}} \tag{12}$$

$$a = 2K_D\left(\frac{k_3 + k_{-2}}{k_2[C_6F_5H\ \mathbf{56}]}\right)^2$$

$$b = \frac{k_2k_3[C_6F_5H\ \mathbf{56}] + k_1(k_3\ +\ k_{-2})[ArI\ \mathbf{57}] + k_1k_2[ArI\ \mathbf{57}][C_6F_5H\ \mathbf{56}]}{k_1k_2[ArI\ \mathbf{57}][C_6F_5H\ \mathbf{56}]}$$

An identical model catalytic cycle was reported by Rosner and co-workers for the Mizoroki-Heck reaction of aryl halide **95** and olefin **96** with off-cycle dinuclear Pd species (**Scheme 41**).[239] The order in the catalyst was shown to depend on the concentration of the Pd (**Figure 28**), rate constants, equilibrium constant for the on/off-cycle Pd species and substrate **96** concentration.[228]

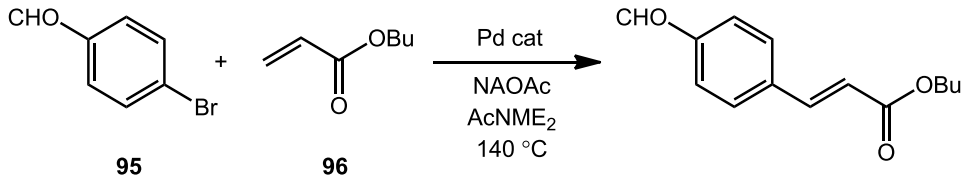

Scheme 41. Mizoroki-Heck reaction of 4-bromobenzaldehyde **95** with butyl acrylate **96** catalysed by palladacycle (Rosner and co.).[239]

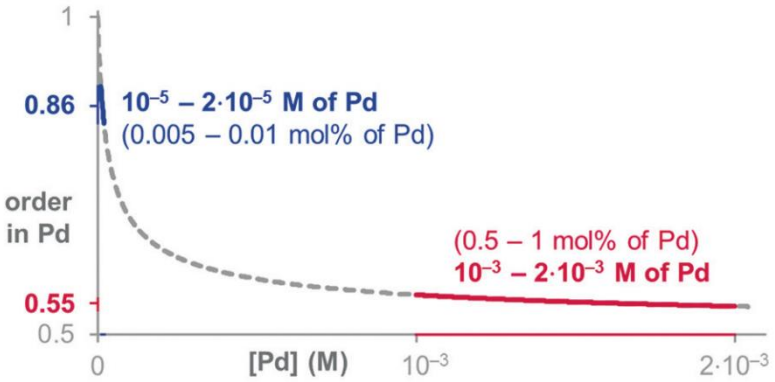

Figure 28. Effect of Pd concentration on the reaction order in Pd (Reprinted with permission from J. Burés, *Angew. Chem.-Int. Ed.*, 2016, **55**, 2028–2031. Copyright 2016 John Wiley and Sons).

When dinuclear complex D is the dominant Pd species in the reaction (*i.e.* term a in Eq. 12 is dominant), the overall rate equation simplifies to give exactly half-order kinetics in the catalyst concentration with kinetically negligible contribution from the oxidative addition step (Eq. 13).[237] The overall one-and-a-half order rate law was consistent with results from RPKA and VTNA. The rate constants and the equilibrium constant were all included in the rate constant of the overall reaction (k_r).

$$v(t) = \frac{+d[P\ \mathbf{58}]}{dt} = k_r[C_6F_5H\ \mathbf{56}][Pd]_{TOT}{}^{1/2} \quad (13)$$

$$k_r = \frac{k_2 k_3}{(k_{-2} + k_3)\sqrt{2K_D}} \quad (14)$$

$$when\ k_3 > k_{-2} \quad (15)$$

$$k_r = \frac{k_2}{\sqrt{2K_D}} \quad (16)$$

The rates of catalytic iodoarene cross-coupling reactions are often limited by the slow transmetallation step.[242] Similarly, the RL-step of the Pd-catalysed direct arylation of iodoarene with fluoroarene was hypothesised to be the AMLA(6) step, not the ligand exchange or the reductive elimination step. The rate constant of the overall reaction simplifies further under these conditions (Eq. 16). This equation was applied as the trial rate law in analysing the model reaction system.

3.4 Classical Kinetic Analysis

3.4.1 Isolation Method and Initial Rate

The order with respect to the substrates and the catalyst was successfully determined by the modern kinetic analysis of the experimental data (see Chapter 3.3). However, further kinetic study was required for the values of the rate constants to be calculated. Of the different strategies for studying chemical kinetics, the classic kinetic approach of isolation method was employed to simplify the determination of the empirical rate law of the model reaction system.[243] In this method, the order of each reactant is obtained under conditions where the concentration of all but the reactant of interest, is constant or nearly constant. The concentration factors assumed to be constant during the experiment can be included in the observed rate constant (k_{obs}) to simplify the rate equation. This forces the rate law to take n^{th}-order form, known as pseudo-n^{th}-order rate law where the term-n corresponds to the order dependence on the isolated substrate with changing concentration during the reaction.[243] The concentration of the Pd catalyst was assumed to stay constant without deactivation. Furthermore, the concentration of Ag_2CO_3 was assumed to be quasi-constant and low throughout the reaction due to poor solubility in DMF.

One of the disadvantages of the isolation method is the distorted concentration conditions that are applied in the experiments. For example, a reaction with 10-fold excess of pentafluorobenzene **56** (*e.g.* 0.93 M) involves 1.0 cm^3 of the reagent **56** under the conditions studied by the modern kinetic analysis. Even at this lowest excess concentration of pentafluorobenzene **56** required for generating a pseudo-n^{th}-order kinetics, the reaction medium was a v/v 9:1 mixture of DMF and pentafluorobenzene **56**. This is not truly representative of the reaction under normal conditions and the effects of non-ideality are high with the potential of affecting the reaction kinetics. In order to minimise the effect of excess substrate on the reaction composition, the concentration of the reaction was diluted from the RPKA and VTNA experiments to make the concentration of limiting reagent 18 mM which still presented acceptable signal-to-noise ratio (**Scheme 42**).

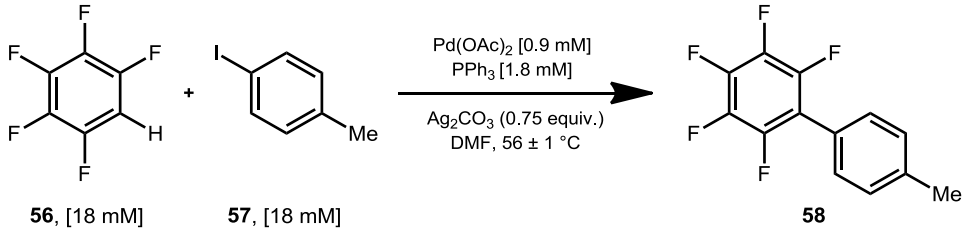

Scheme 42. The standard reaction conditions set for kinetic study by isolation method.

The kinetic data were collected from t = 0 s to reaction completion as change in concentration of reactants (*i.e.* **56** and **57**) and the product **58** as a function of time. The temperatures of the reactions were maintained at 56 ± 1 °C unless otherwise stated. The rates of the reactions were derived following the integration method of kinetic data analysis. The Excel Solver was used to determine the best integrated form of the rate law for fitting the experimental data and thus the order of the reaction, based on the lowest coefficients of determination (R^2).[244-246] The observed rate constants (k_{obs}) were calculated from the initial rate measurements, based on the line-of-best-fit between t = 300 s to half of the final %conversion achieved for the reaction conditions. The product **58** concentration was calculated by correlating the change in the IR absorbance at 989 cm^{-1} with the %conversion determined by ^1H NMR spectroscopic analysis. The standard error of the gradient and the y-intercept of the lines-of-best-fits were deduced using Excel linear least-squares curve fitting (LINEST) function.

Each of the reactants **56** and **57** were isolated in turn by adding 10-fold or more counterparts in excess. With reagent **57** added in 10-fold excess, the absorbance, and therefore [4-iodotoluene **57**], was nearly constant during the reaction (**Figure 29**). The change in the concentration of pentafluorobenzene **56** determined from the depletion of IR absorption at 957 cm^{-1} revealed the exponential decay of the reagent over time. This is

characteristic of pseudo-first-order rate law following the rate equation $-d[C_6F_5H$ **56**$]/dt = k_{obs}[C_6F_5H$ **56**$]$. The pseudo-first-order rate constant determined from the plot of the integrated rate law (Eq. 18, see Appendix 1 for full derivation) was $k_{obs} = (5.93 \pm 0.02) \times 10^{-5}$ s^{-1} (**Figure 30**). The apparent first-order dependence in $[C_6F_5H$ **56**$]$ was consistent with the result from the modern kinetic analysis. The half-life ($t_{1/2}$) of the reaction was 1.16 $\times 10^4$ s and the overall rate constant was $k_r = 5.85 \times 10^{-4}$ $dm^{3/2}$ $mol^{-1/2}$ s^{-1} (with $[Pd]_{TOT} =$ 10.27 mM).

$$\frac{-d[C_6F_5H\ \mathbf{56}]}{dt} = k_{obs}[C_6F_5H\ \mathbf{56}] \tag{17}$$

$$ln[C_6F_5H\ \mathbf{56}]_t = -k_{obs}t + ln[C_6F_5H\ \mathbf{56}]_0 \tag{18}$$

$$k_{obs} = k_r[Pd]_{TOT}{}^{1/2} \tag{19}$$

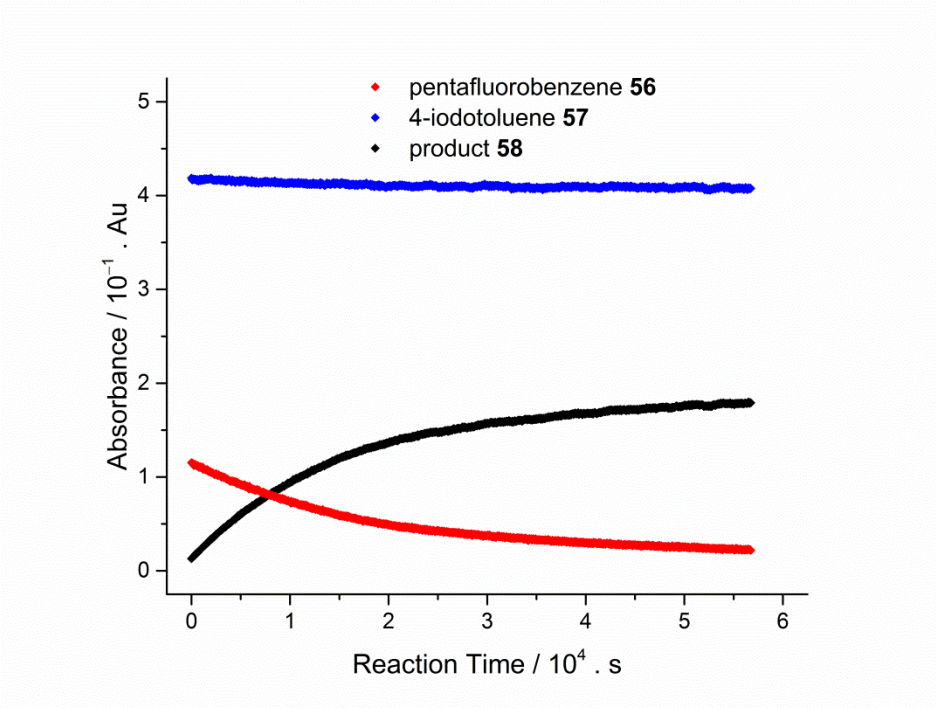

Figure 29. Isolation method of kinetic analysis with 10-fold excess of reagent **57**.

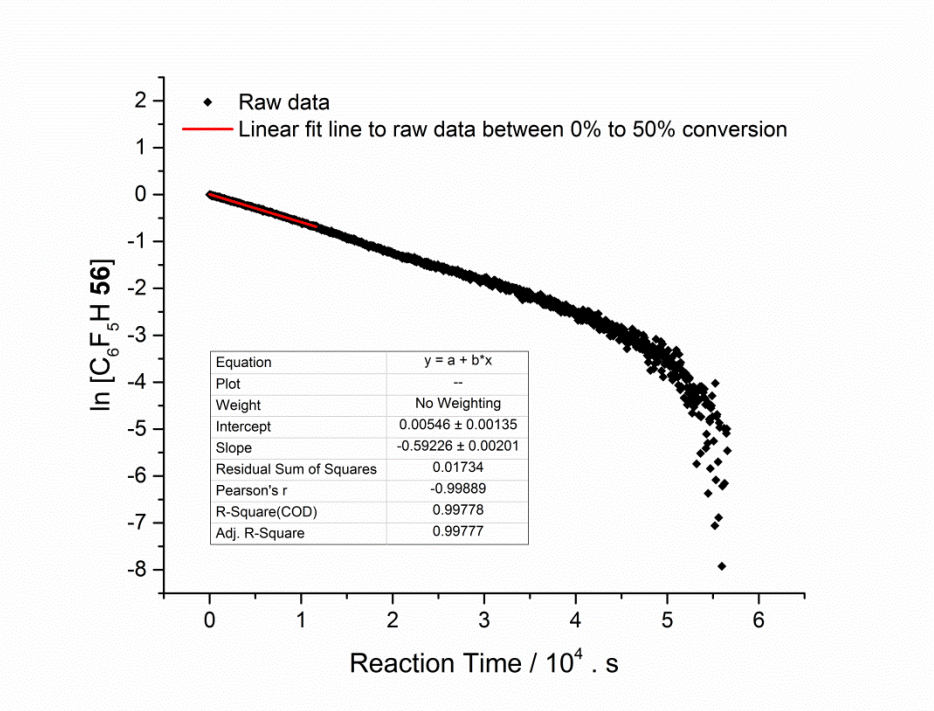

Figure 30. Absorbance decay of pentafluorobenzene **56** under pseudo-first-order conditions.

With reagent **56** added in 10-fold excess, the absorbance, and therefore [C_6F_5H **56**], was nearly constant during the reaction (**Figure 31**). Linear decay in the concentration of 4-iodotoluene **57** was observed based on the IR absorption at 1009 cm^{-1} following the rate law $-d$[ArI **57**]/dt = k_{obs}. The pseudo-zeroth-order rate constant calculated from the plot of the integrated rate law (Eq. 21) was k_{obs} = (5.78 ± 0.07) × 10^{-5} mol dm^{-3} s^{-1} (**Figure 32**). The observed zero-order dependence in [4-iodotoluene **57**] was in agreement with the result from the modern kinetic analysis. The overall rate constant k_r = 2.68 × 10^{-4} $mol^{1/2}$ $dm^{-3/2}$ s^{-1} (with $[C_6F_5H\ \mathbf{56}]_{ave}$ = 2.07 M and $[Pd]_{TOT}$ = 10.27 mM) was lower than k_r calculated from experiment where the concentration of pentafluorobenzene **56** was isolated.

$$\frac{-d[ArI\ \mathbf{57}]}{dt} = k_{obs} \tag{20}$$

$$[ArI\ \mathbf{57}] = -k_{obs}t + [ArI\ \mathbf{57}]_0 \tag{21}$$

$$k_{obs} = k_r[C_6F_5H\ \mathbf{56}]_{ave}[Pd]_{TOT}{}^{1/2} \tag{22}$$

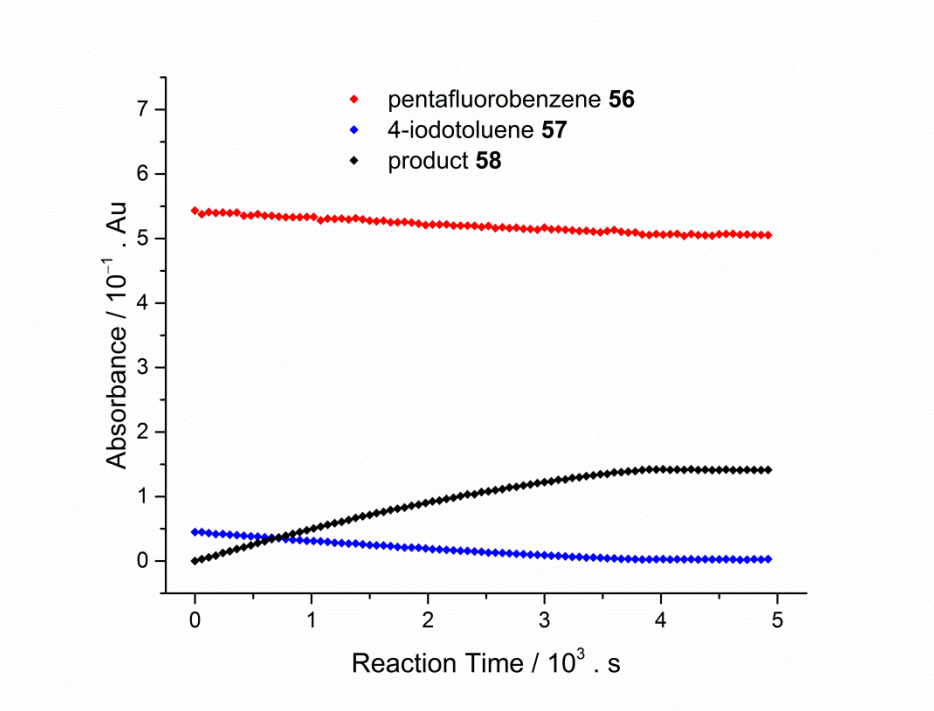

Figure 31. Isolation method of kinetic analysis with 10-fold excess of reagent **56**.

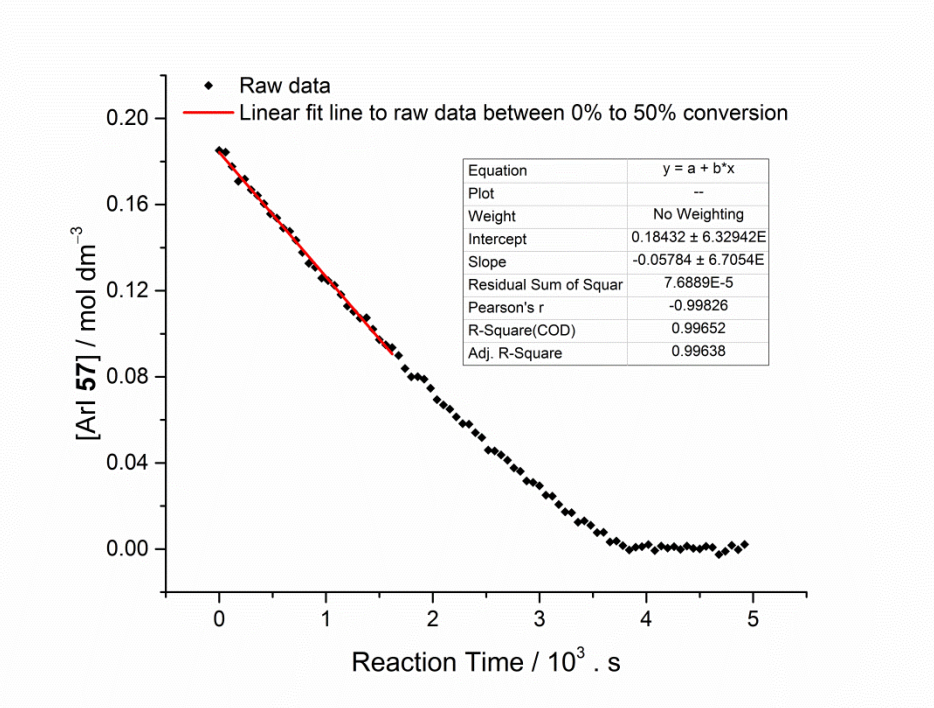

Figure 32. Absorbance decay of 4-iodotoluene **57** under pseudo-zeroth-order conditions.

Despite the different reaction conditions, the rate constant calculated from isolation methods were expected to be identical, assuming an accurate trial rate law. However, significant differences were observed in the overall rate constants, k_r, determined from isolated [C_6F_5H **56**] (5.85×10^{-4} mol$^{1/2}$ dm$^{-3/2}$ s^{-1}) and isolated [4-iodotoluene **57**] (2.68×10^{-4} mol$^{1/2}$ dm$^{-3/2}$ s^{-1}). Rosner and co-workers demonstrated that the half-order in Pd

catalyst depended on the total concentration of the catalyst, the ratios of the catalytic intermediates, and the equivalents of the substrates.[239] The kinetics shifted towards first-order in the catalyst at lower $[Pd]_{TOT}$ because a higher percentage of the total Pd atom is in the active on-cycle mononuclear form. Deviation from half-order kinetics in the total Pd concentration was also observed when Pd2 was the dominant catalytic intermediate instead of Pd1 (**Scheme 40**). Additionally, the half-order kinetics in the catalyst changed at higher excess of butyl acrylate **96** (**Scheme 41**). Therefore, the order with catalyst was expected to differ under different synthetic conditions. It is likely that the artificially large concentration of pentafluorobenzene **56** (*i.e.* 10-fold excess) affected the order dependence on the Pd catalyst by increasing the magnitude of deviation from half-order kinetics in $[Pd]_{TOT}$. For example, the rate constant k_r calculated for reaction with 0.65-order kinetics in Pd concentration would be 5.27×10^{-4} $dm^{3/2}$ $mol^{-1/2}$ s^{-1}. Therefore, the study of the concentration dependence of the Pd catalyst and pentafluorobenzene **56** under the isolation method may vary from results obtained by the modern kinetics analysis.

3.4.2 Reaction Rate Dependence on the Concentration of Pd

The rate dependence in $[Pd]_{TOT}$ at 56 ± 1 °C was measured between 0.19 mM to 14.8 mM catalyst concentration under pseudo-zeroth-order reaction condition with 10-fold excess of pentafluorobenzene **56** (*i.e.* 0.18 M) to 4-iodotoluene **57** (*i.e.* 18 mM) (**Table 12**). The $Pd(OAc)_2/PPh_3$ ratio was maintained at 1:2 for each kinetic measurements.

Table 12. The k_{obs} obtained at varying total concentration of the Pd catalyst for the direct arylation reaction of 4-iodotoluene **57** at 56 ± 1 °C, as shown in **Scheme 42** (with $[C_6F_5H$ **56]** = 180 mM).

Entry	mol% Equiv.	$[Pd]_{TOT}$ / 10^{-3} . mol dm^{-3}	k_{obs} / 10^{-6} . mol dm^{-3} s^{-1}
1	1.0	0.19	0.352 ± 0.003
2	2.5	0.46	0.790 ± 0.006
3	5.0	0.92	1.69 ± 0.02
4	10	1.86	1.84 ± 0.04
5	20	3.70	3.61 ± 0.13
6	40	7.43	5.73 ± 0.23
7	80	14.8	11.4 ± 0.1

The order with respect to the Pd concentration was determined from the double-logarithmic plot of log k_{obs} against log $[Pd]_{TOT}$ (**Figure 33**). This was based on the mathematical determination of the order with respect to the reaction components involved in the trial rate law (Eq. 23). The concentration of Pd atom was used as the Pd catalyst concentration as the

trinuclear $Pd_3(OAc)_6$ pre-catalyst is understood to dissociate readily to the mononuclear form in DMF.[204, 247] The reaction kinetics was (0.75 ± 0.04)-order in $[Pd]_{TOT}$ under the reaction condition studied. The deviation from half-order kinetics in $[Pd]_{TOT}$ caused by the 10-fold excess concentration of pentafluorobenzene **56** ($[C_6F_5H$ **56**$]_{ave}$ = 0.18 M) was expected to be constant. However, the effect of changing Pd concentration on the catalyst order could not be determined.

$$k_{obs} = k_r[C_6F_5H\ \mathbf{56}]_{ave}{}^{a}[Pd]_{TOT}{}^{b} \tag{23}$$

$$log(k_{obs}) = log(k_r[C_6F_5H\ \mathbf{56}]_{ave}{}^{a}[Pd]_{TOT}{}^{b})$$

$$log(k_{obs}) = log(k_r) + a \cdot log[C_6F_5H\ \mathbf{56}]_{ave} + b \cdot log[Pd]_{TOT}$$

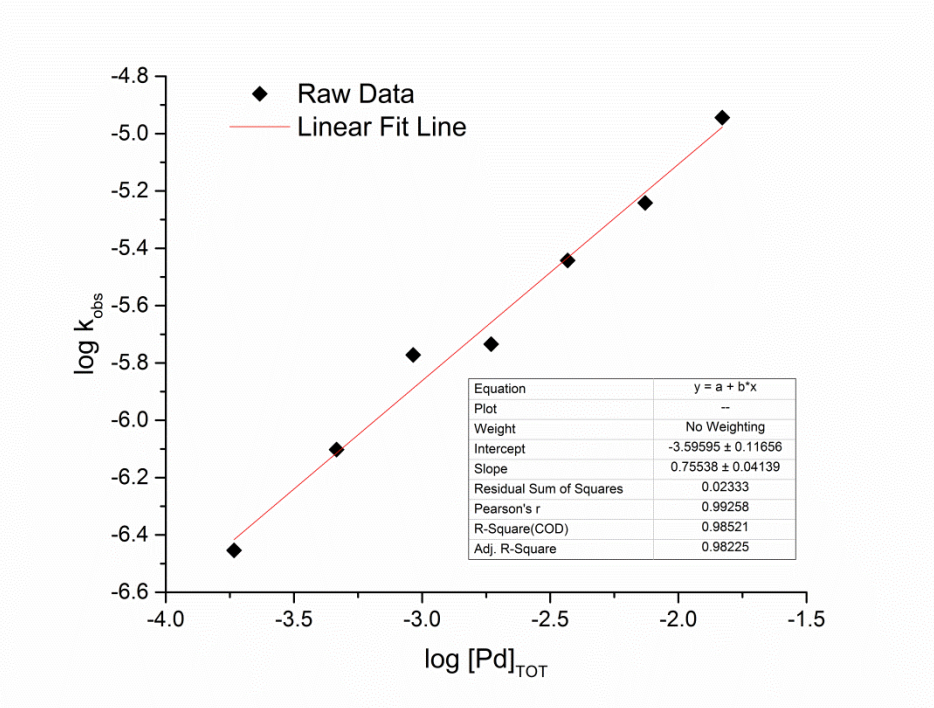

Figure 33. Plot of log k_{obs} against log $[Pd]_{TOT}$ to determine the order in Pd for the direct arylation reaction of 4-iodotoluene **57** at 56 ± 1 °C, as shown in **Scheme 42**. Graph constructed using data from **Table 12**.

The k_{obs} dependence on the $[Pd]_{TOT}$ were analysed graphically by plotting k_{obs} against 0.75-order in $[Pd]_{TOT}$ to determine the rate constant k (**Figure 34**). A positive linear dependence with slope of (2.61 ± 0.13) × 10^{-4} $mol^{1/4}$ $dm^{-3/4}$ s^{-1} was obtained. Attempt at calculating the rate constants were unsuccessful due to uncertainty in the rate equation under 0.75-order kinetics in the catalyst concentration.

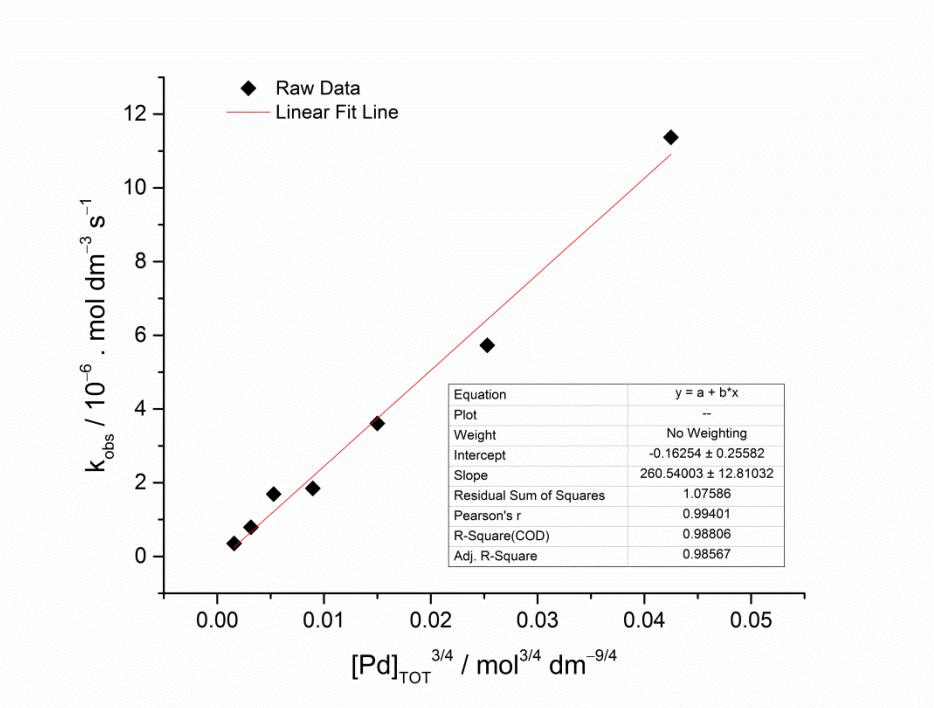

Figure 34. Plot of k_{obs} against $[Pd]_{TOT}^{3/4}$ between 0.19 mM and 14.8 mM for the direct arylation reaction of 4-iodotoluene **57** at 56 ± 1 °C, as shown in **Scheme 42**. Graph constructed using data from **Table 12**.

One of the parameters commonly used to describe the efficiency of catalysis is the TOF. Here the TOF was calculated as the number of substrate molecule reacted per Pd atom (*i.e.* active site) in unit time, assuming homogeneous catalysis.[183, 248] The TOF values at 50% reaction completion were determined for reactions with different concentrations of Pd pre-catalyst at 56 ± 1 °C (**Figure 35**). An increase in TOF was observed at low Pd concentration. For homogeneous catalysis, higher TOF achieved at lower catalyst concentration is characteristics of off-cycle high order Pd species being the catalyst resting state or the TOF-determining-intermediate (TDI).[239, 249, 250] This is rationalised as there being higher percentage of total Pd atoms in the catalytically active on-cycle mononuclear form at lower $[Pd]_{TOT}$. Similar trends have been observed for reactions associated with catalysis involving nano-particles.[251-253]

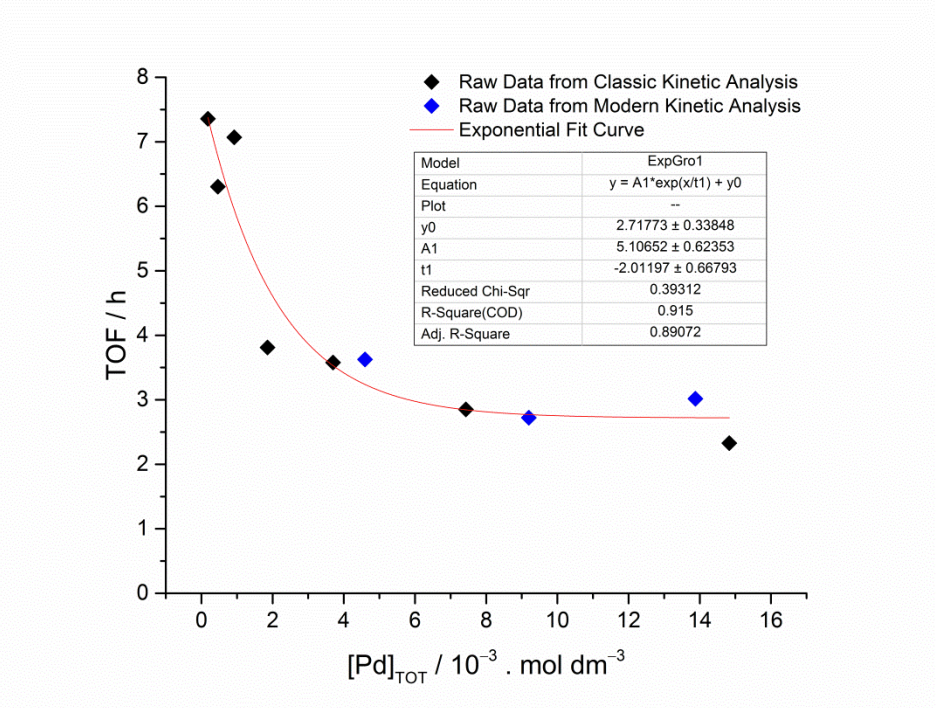

Figure 35. The dependence of TOF, determined at 50% reaction completion, on the concentration of Pd catalyst in the direct arylation reaction of 4-iodotoluene **57** with pentafluorobenzene **56** at 56 ± 1 °C, as shown in **Table 10** and **Scheme 42** (with [C_6F_5H **56]** = 180 mM).

3.4.3 Reaction Rate Dependence on the Concentration of Pentafluorobenzene 56

The pseudo-zeroth-order rate constant of the reaction at concentrations of [C_6F_5H **56**]$_{ave}$ between 0.18 M and 0.92 M at 56 ± 1 °C were measured (**Table 13**). The initial concentrations of 4-iodotoluene **57** and the pre-catalyst were maintained at 18 mM and 0.92 mM respectively. The mean concentrations of the excess pentafluorobenzene **56**, [C_6F_5H **56**]$_{ave}$, during the reaction were calculated for each reaction conditions. At 50-fold excess concentration of pentafluorobenzene **56**, the reaction mixture consists of 1.0 cm^3 reagent **56** and 8.7 cm^3 DMF. The effect of change in the solvent composition at high pentafluorobenzene **56** concentration and the degree of deviation from half-order kinetics in the Pd remained unknown.

Table 13. The k_{obs} obtained at varying concentration of pentafluorobenzene **56** for the direct arylation reaction of 4-iodotoluene **57** at 56 ± 1 °C, as shown in **Scheme 42**.

Entry	Equivalents	$[C_6F_5H$ **56**$]_{ave}$ / mol dm^{-3}	k_{obs} / 10^{-6} . mol dm^{-3} s^{-1}
1	10	0.18	1.68 ± 0.02
2	20	0.36	2.06 ± 0.03
3	30	0.55	2.56 ± 0.04
4	40	0.73	3.19 ± 0.06
5	50	0.92	4.04 ± 0.07

The results were further analysed graphically by plotting k_{obs} against $[C_6F_5H$ **56**$]_{ave}$ (**Figure 36**). The reaction rate showed a linear dependence on the concentration of pentafluorobenzene **56**. However, the nonzero y-intercept suggested the observed rate constants consisted of multiple rate constants which were pentafluorobenzene **56** concentration dependent (slope) and independent (y-intercept).

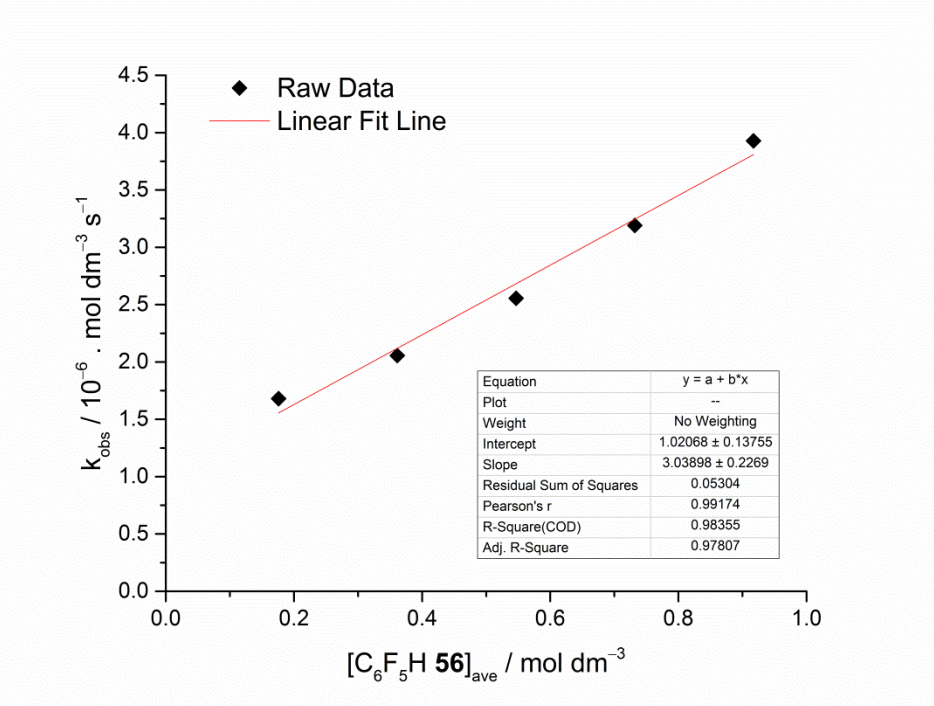

Figure 36. Plot of k_{obs} against $[C_6F_5H$ **56**$]_{ave}$ between 0.18 M and 0.92 M for the direct arylation of 4-iodotoluene **57** at 56 ± 1 °C, as shown in **Scheme 42**. Graph constructed using data from **Table 13**.

The values of rate constants under pseudo-zeroth-order kinetics were calculated from the graph of k_{obs} against $[C_6F_5H$ **56**$]_{ave}$ based on the Eq. 25. Division of the gradient and the y-

intercept by $[Pd]_{TOT}^{1/2}$ gave $k_2(2K_D)^{-1/2} = (9.99 \pm 0.75) \times 10^{-5}$ $dm^{3/2}$ $mol^{-1/2}$ s^{-1} (Eq. 26) and $k' = (3.36 \pm 0.45) \times 10^{-5}$ $mol^{1/2}$ $dm^{-3/2}$ s^{-1} (Eq. 27) respectively.

$$rate = k_{obs} \tag{24}$$

$$k_{obs} = \frac{k_2}{\sqrt{2K_D}}[Pd]_{TOT}{}^{1/2}[C_6F_5H\ \mathbf{56}]_{ave} + k'[Pd]_{TOT}{}^{1/2} \tag{25}$$

$$\frac{k_2}{\sqrt{2K_D}} = \frac{(3.04 \pm 0.23) \times 10^{-6}\ s^{-1}}{[Pd]_{TOT}{}^{1/2}} = (9.99 \pm 0.75) \times 10^{-5}\ dm^{3/2}\ mol^{-1/2}\ s^{-1} \tag{26}$$

$$k' = \frac{(1.02 \pm 0.14) \times 10^{-6}\ mol\ dm^{-3}\ s^{-1}}{[Pd]_{TOT}{}^{1/2}} = (3.36 \pm 0.45) \times 10^{-5}\ mol^{1/2}\ dm^{-3/2}\ s^{-1} \tag{27}$$

The calculation of the rate constants based on the kinetic data obtained by the isolation method was complicated by the uncertainties in the reaction order in $[Pd]_{TOT}$. Therefore, the values of $k_2(2K_D)^{-1/2}$ and k' were calculated for 0.5–1.0 order kinetics in Pd (**Table 14**). The exact value of the rate constant for the C–H bond activation step k_2 could not be determined as the value of the equilibrium constant K_D was unknown. However, the values of $k_2(2K_D)^{-1/2}$ was *ca.* 3 times larger than k'. Changes in the reaction order with increased Pd and pentafluorobenzene **56** concentrations were unknown and may account for the discrepancies observed between the modern kinetic analysis and the classic kinetic analysis.

Table 14. The values of $k_2(2K_D)^{-1/2}$ and k' calculated for different order dependence in the Pd concentration.

Entry	n^{th}-Order in $[Pd]_{TOT}$	$k_2(2K_D)^{-1/2}$ / 10^{-4} . dm^{3n} mol^{-n} s^{-1}	$k' \cdot 10^{-4}$
1	0.5	0.999 ± 0.075	0.336 ± 0..45 $mol^{1/2}$ $dm^{-3/2}$ s^{-1}
2	0.75	5.73 ± 0.43	1.92 ± 0.26 $mol^{1/4}$ $dm^{-3/4}$ s^{-1}
3	1	32.8 ± 2.5	11.1 ± 1.5 dm^3 mol^{-1} s^{-1}

3.4.4 Kinetic Study on the Direct Arylation Reaction of Iodobenzene 81 with Pentafluorobenzene 56

The syntheses of possible Pd intermediates with 4-tolyl substituents were attempted following a literature procedure (see Chapter 2.6).[211] However, the preparation of the complexes in quantity and purity required for kinetic study were unsuccessful. Therefore, the phenyl analogues of the Pd species were synthesised. The change in the substrate from 4-iodotoluene **57** to iodobenzene **81** was not expected to affect the mechanism of the catalysis. Furthermore, similar reaction kinetics were expected unless the oxidative addition becomes the RL-step of the catalytic cycle.

In order to confirm the consistency in the reaction mechanism between the two substrates (*i.e.* **57** and **58**), the kinetic experiments were repeated for the direct arylation reaction of iodobenzene **81** with pentafluorobenzene **56** (**Scheme 43**). The concentrations of the limiting reagent **81** of the reactions was increased to 55 mM (from 18 mM used for the 4-iodotoluene **57** study) to accommodate for the lower peak intensities observed for iodobenzene **81** (at 1016 cm^{-1}) and the biaryl product **64** (at 989 cm^{-1}).

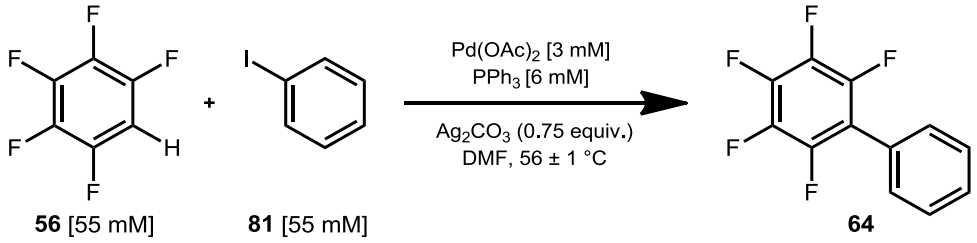

Scheme 43. Direct arylation of iodobenzene **81** with pentafluorobenzene **56**.

The stoichiometric reaction of iodobenzene **81** with pentafluorobenzene **56** followed first-order kinetics at 56 ± 1 °C. In the presence of 10-fold excess of pentafluorobenzene **56** (*i.e.* 0.55 M), the reaction followed a pseudo-zeroth-order kinetics. These observations were consistent with the kinetic results for the reaction of 4-iodotoluene **57** where the reaction followed first-order kinetics in pentafluorobenzene **56** concentration and zeroth-order kinetics in iodobenzene **57** concentration. The pseudo-zeroth-order rate constants at 56 ± 1 °C were measured for the concentrations of Pd between 2.8 mM and 16.7 mM in the presence of 0.55 M pentafluorobenzene **56** (**Table 15**). The reaction kinetics was half-order in the concentration of Pd, consistent with the non-integer order in catalyst observed for 4-iodotoluene **57** (**Figure 37**).

Table 15. The k_{obs} obtained at varying total concentration of the Pd catalyst for the direct arylation reaction of iodobenzene **81** with pentafluorobenzene **56** at 56 ± 1 °C, as shown in **Scheme 43**.

Entry	mol% Equiv.	$[Pd]_{TOT}$ / 10^{-3} . mol dm^{-3}	k_{obs} / 10^{-5} . mol dm^{-3} s^{-1}
1	5	2.79	0.999 ± 0.011
2	10	5.51	1.61 ± 0.01
3	20	11.0	2.18 ± 0.03
4	30	16.7	2.41 ± 0.04

Reaction orders in $[Pd]_{TOT}$ were different between the reaction of 4-iodotoluene **57** [(0.75 ± 0.04)-order)] and iodobenzene **81** [(0.48 ± 0.12)-order)] under kinetic conditions required for the isolation method. Despite the difference in the magnitude of deviation from first-order behaviour, the non-integer order dependence on the $[Pd]_{TOT}$ was consistent with off-cycle equilibrium in the reaction mechanism.

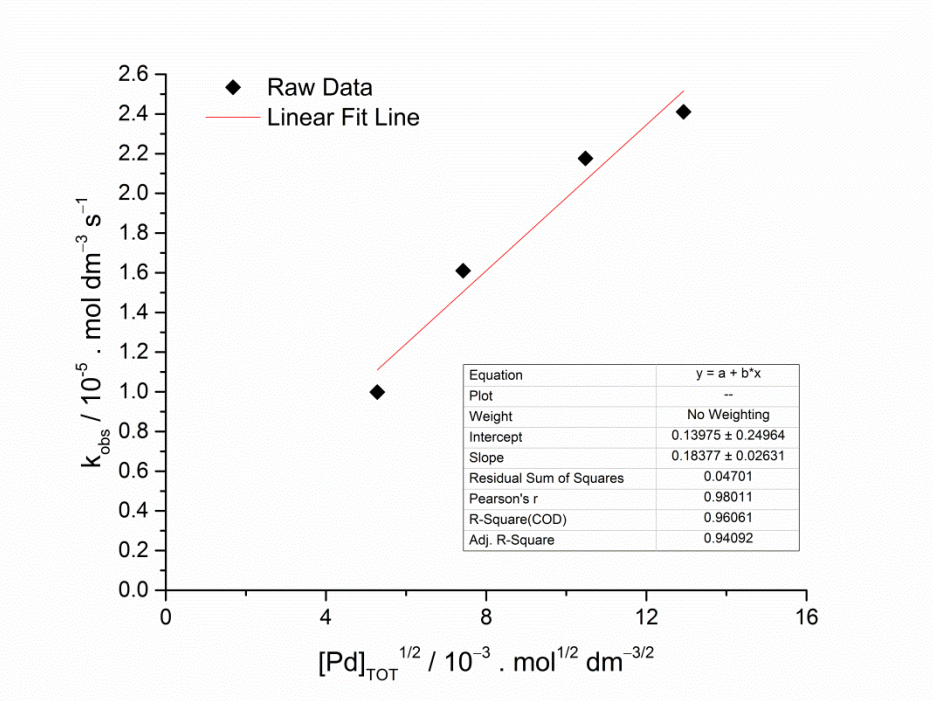

Figure 37. Plot of k_{obs} against $[Pd]_{TOT}^{1/2}$ between 2.8 mM and 16.7 mM for the direct arylation reaction of iodobenzene **81** at 56 ± 1°C, as shown in **Scheme 43**. Graph constructed using data from **Table 15**.

The observed rate constants at concentrations of pentafluorobenzene **56** between 0.53 M and 2.19 M were also determined for the reaction at 56 ± 1 °C with 2.8 mM catalyst (**Table 16**). The reaction rate was positively dependent on the concentration of pentafluorobenzene **56** (**Figure 38**). Similar to the 4-iodotoluene **57** experiments, a significant nonzero y-

intercept was observed signifying the reaction rate consisted of multiple rate constants which were pentafluorobenzene **56** concentration dependent (slope) and independent (y-intercept).

Table 16. The k_{obs} obtained at varying concentration of pentafluorobenzene **56** for the direct arylation reaction of iodobenzene **81** at 56 ± 1 °C, as shown in **Scheme 43**.

Entry	Equivalents	$[C_6F_5H\ 56]_{ave}$ / mol dm^{-3}	k_{obs} / 10^{-5} . mol dm^{-3} s^{-1}
1	10	0.53	0.999 ± 0.011
2	20	1.08	1.24 ± 0.02
3	30	1.63	1.57 ± 0.02
4	40	2.19	2.07 ± 0.05

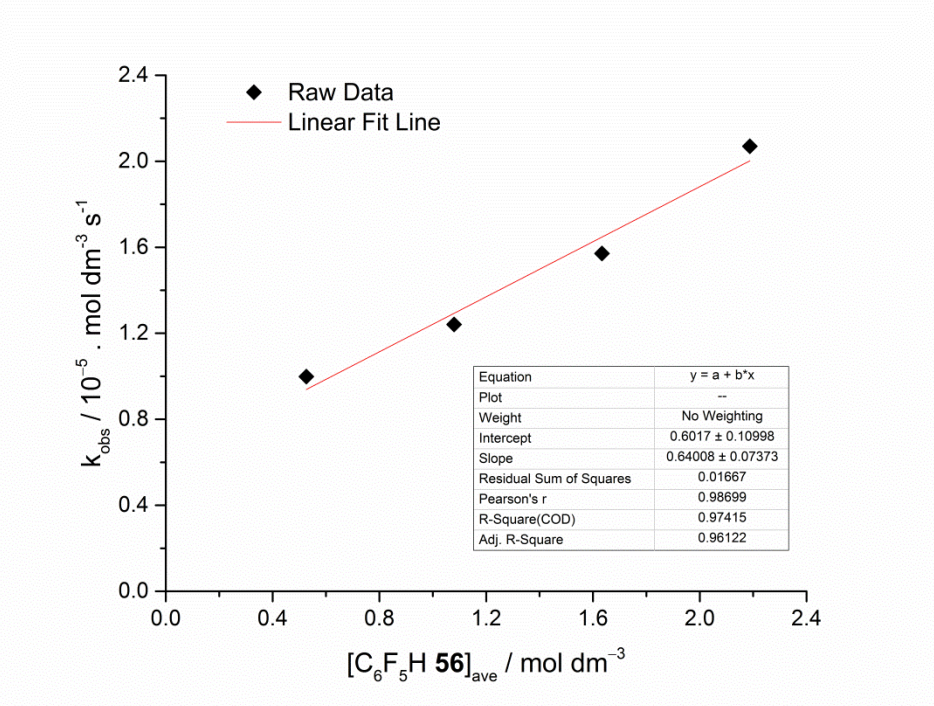

Figure 38. Plot of k_{obs} against $[C_6F_5H\ \mathbf{56}]_{ave}$ between 0.18 M and 1.19 M for the direct arylation reaction of iodobenzene **81** at 56 ± 1°C, as shown in **Scheme 43**. Graph constructed using data from **Table 16**.

The rate constants $k_2(2K_D)^{-1/2}$ and k′ were calculated for the direct arylation of iodobenzene **81** based on the Eq. 25. For half-order kinetics in Pd, the values of $k_2(2K_D)^{-1/2}$ and k′ were (1.21 ± 0.14) × 10^{-4} $dm^{3/2}$ $mol^{-1/2}$ s^{-1} and (1.14 ± 0.21) × 10^{-4} $mol^{1/2}$ $dm^{-3/2}$ s^{-1} respectively. Since the order dependence on Pd catalyst was unspecified under the isolation method, the values of $k_2(2K_D)^{-1/2}$ and k′ were calculated for 0.5–1.0 order kinetics in Pd (**Table 17**). The ratio of $k_2(2K_D)^{-1/2}$ and k′ was calculated as *ca.* 1.

Table 17. The values of $k_2(2K_D)^{-1/2}$ and k′ calculated for different orders in the Pd concentration.

Entry	n^{th}-Order in $[Pd]_{TOT}$	$k_2(2K_D)^{-1/2}$ / 10^{-4} . dm^{3n} mol^{-n} s^{-1}	k′ / 10^{-4}
1	0.5	1.21 ± 0.14	1.14 ± 0.21 $mol^{1/2}$ $dm^{-3/2}$ s^{-1}
2	0.75	5.29 ± 0.61	4.98 ± 0.92 $mol^{1/4}$ $dm^{-3/4}$ s^{-1}
3	1	23.1 ± 2.7	21.7 ± 4.0 dm^3 mol^{-1} s^{-1}

The values of $k_2(2K_D)^{-1/2}$ and k′ were compared between the reactions of iodobenzene **81** and 4-iodotoluene **57**. Differences were observed in the ratio of the rate constants ($k_2(2K_D)^{-1/2}$/k′) which were 3:1 for 4-iodotoluene **57** and 1:1 for iodobenzene **81**. Therefore the k′ in the rate was more significant for iodobenzene **81**. Despite the disparity highlighted above, the reaction mechanism between 4-iodotoluene **57** and iodobenzene **81** were shown to be consistent. Therefore the results obtained from studying the reactivity of potential catalytic intermediates with phenyl-substituents can be extended to the reaction of 4-iodotoleuene **57**.

3.4.5 Effect of PPh_3 Quantity on the Reaction Rate

For any chemical transformation, it is favourable to have milder reaction conditions with minimum additives. The development of ligand-free aryl-aryl coupling reactions has been successful in this regard.[48, 49] However, there are many examples in the literature where multiple additives are required for the best outcome but with great uncertainty regarding their role. This situation also applies to the model direct arylation reaction starting with $Pd(OAc)_2$ pre-catalyst, with the ligand and a base additive being essential components for the reaction.

The use of $Pd(OAc)_2$ and $nPPh_3$ ($n \geq 2$) mixture in catalytic C–C bond formation reaction is well documented, especially for the Mizoroki-Heck reaction.[254-256] The reaction between $Pd(OAc)_2$ and PPh_3 in DMF was studied by Amatore and co-workers.[257] The initial formation of $Pd(OAc)_2(PPh_3)_2$ was followed by intramolecular reduction to $[Pd^0(OAc)(PPh_3)]^-$ complex. A dinuclear and mononuclear species were formed depending on the equivalents of PPh_3 (**Scheme 44**). The formation of mononuclear species from dinuclear species was also highlighted by the synthesis of $Pd(Ph)(\kappa^1\text{-}OAc)(PPh_3)_2$ **85** complex from $[Pd(Pd)(\mu\text{-}OAc)(PPh_3)]_2$ **84** in the presence of excess PPh_3.[212] Therefore, increased equivalents of ligand are expected to accelerate the rate of reactions involving off-cycle multinuclear species by increasing the concentration of on-cycle mononuclear

species. This is unlike catalytic cycles without multinuclear species, where addition of excess ligand results in reaction inhibition.

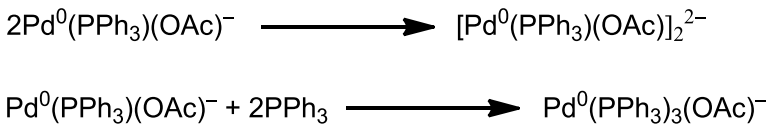

Scheme 44. Formation of $[Pd^0(OAc)(PPh_3)]_2^{2-}$ and $[Pd^0(OAc)(PPh_3)_3]^-$ from $[Pd^0(OAc)(PPh_3)]^-$.[60]

The *in-situ* FT-IR spectroscopic analysis was used to study the effect of changing the ligand-to-Pd ratio on the pseudo-zeroth-order rate constants (**Table 18**). The concentration of Pd catalyst was maintained at 0.93 mM. Quantitative conversion of 4-iodotoluene **57** was achieved in every reaction, except for 5 mol% PPh_3 which terminated at 76% conversion (Entry 1). Increased formation of triphenyl(4-tolyl)phosphonium iodide side-product **60** was not observed by ^1H or ^{31}P NMR spectroscopic analysis.

Table 18. The k_{obs} obtained for the direct arylation reaction of 4-iodotoluene **57** with pentafluorobenzene **56** at varying ratio of Pd-ligand at 56 ± 1 °C.

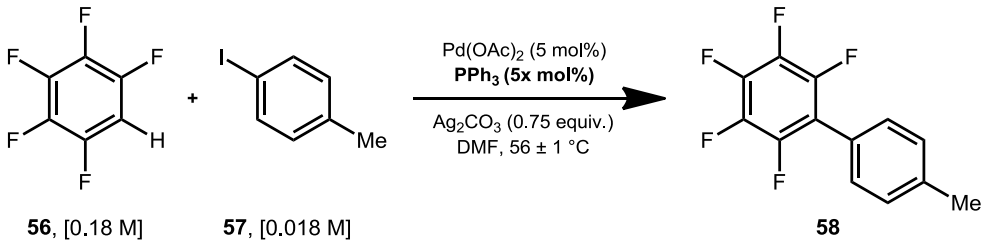

56, [0.18 M] **57**, [0.018 M] **58**

Entry	PPh_3 quantity / mol%	$[PPh_3]$ / $[Pd(OAc)_2]$ [a]	k_{obs} / 10^{-6} . mol dm^{-3}
1	5	1.01	0.604 ± 0.007
2	10	2.00	1.68 ± 0.02
3	15	3.04	2.78 ± 0.03
4	20	4.00	3.73 ± 0.08
5	25	5.01	2.72 ± 0.05
6	30	6.12	2.67 ± 0.04
7	40	8.03	2.71 ± 0.06

[a] $[Pd(OAc)_2]$ = 0.93 mM

Significant rate enhancement was observed up to 20 mol% of PPh_3 (*i.e.* 4:1 ratio of $PPh_3/Pd(OAc)_2$) (**Figure 39**). The rate decreased slightly and reached a plateau at 25 mol% PPh_3 (*i.e.* 5:1 ratio of $PPh_3/Pd(OAc)_2$) with average $k_{obs} = (2.70 \pm 0.05) \times 10^{-6}$ mol dm^{-3} s^{-1}. Further inhibition was not observed at higher phosphine concentration. It was realised that the standard model condition using 10 mol% PPh_3 was not optimised in terms of the reaction rate.

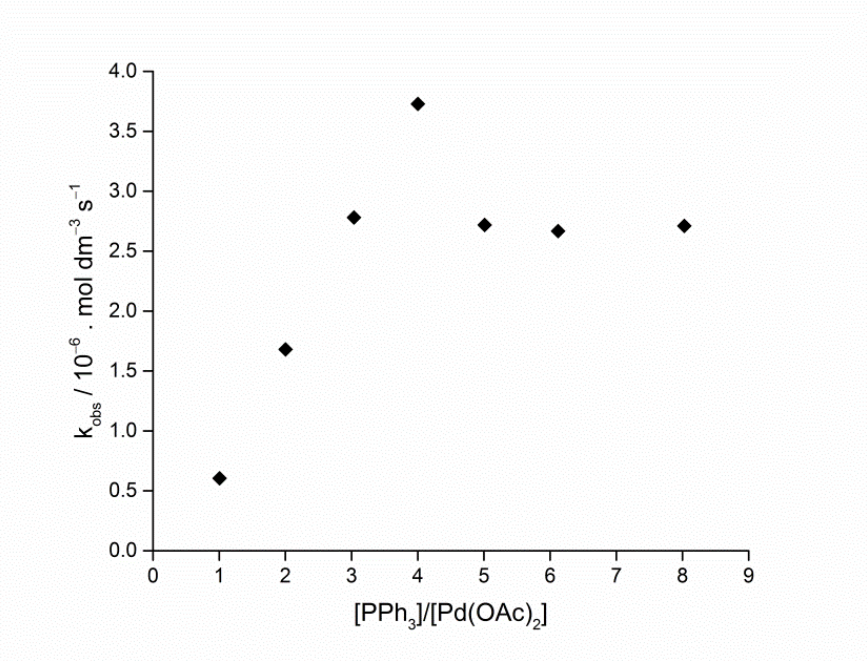

Figure 39. Plot of k_{obs} against [PPh_3]/[$Pd(OAc)_2$] ratio for the reaction shown in **Table 18** at 56 ± 1 °C.

One possible explanation involves the reaction between Ag_2CO_3 and PPh_3, and a potential role of Ag^I salts in C–H bond activation of polyfluoroarenes. A colourless solution of $AgBF_4$ and PPh_3 (2 equivalents) in DMF was prepared in an NMR tube equipped with a Young's tap. The mixture was left overnight at ambient temperature. Two peaks were observed by ^{31}P NMR spectroscopic analysis at δ 25.6 ($O=PPh_3$) and at δ 10.7 (Ag-phosphine complex). The full conversion of PPh_3 (expected at δ –0.54) explained the lack of reaction when $Pd(OAc)_2$ was added to a pre-stirred mixture of pentafluorobenzene **56**, 4-iodotoluene **57**, Ag_2CO_3 and PPh_3 in DMF (**Figure 16**). The chemical shift was similar to complexes reported in the literature such as $Ag(PPh_3)ClO_4$ (δ 11.0 in chloroform-d), $Ag(PPh_3)NO_3$ (δ 8.0 in chloroform-d) and $[Ag(PPh_3)_4]BF_4$ (δ 7.5 in methylene chloride-d_2).[258] Analysis of the reaction mixture by ESI-MS in the positive mode showed $Ag(PPh_3)_3^+$ (*m/z* 895.18) as the major product and $Ag(PPh_3)_2^+$ (*m/z* 631.08) as the minor product. The adduct of $Ag(PPh_3)^+$ and DMF was also observed as a minor product (*m/z* 444.05).

The rate acceleration observed with increased concentration of PPh_3 may result from the formation of the activated Ag polyfluoroarene species (*e.g.* $Ag(PPh_3)_n$-C_6F_5). Two independent studies led by Whitaker[180] and Lotz[181] have demonstrated Ag-carboxylates (*i.e.* Ag-CO_2Ad and Ag-OPiv) as a capable C–H bond activation reagent for electron deficient arenes such as pentafluorobenzene **56** in toluene, THF and dioxane. The resulting Ag-C_6F_5 species has a ^{19}F NMR signal at δ −105 in THF. This complex was then successfully reacted with $Pd(OAc)_2$(dtbpy) to yield a mixture of $Pd(C_6F_5)$(OR)(dtbpy) (R = Ac or Piv)

and $Pd(C_6F_5)_2$(dtbpy). The reaction rate increased with the concentration of PPh_3, explained as the formation of soluble $Ag(PPh_3)$-CO_2Ad species. Differences are expected between the carbonate anion CO_3^{2-} and the bulky carboxylates employed. This was highlighted by the reaction condition requiring both Ag_2CO_3 and 1-$AdCO_2H$. If Ag-C_6F_5 was generated in the model reaction condition, transmetallation with Pd-arene species could provide a faster alternative RL-step to the product **58**. However, no evidence for the presence of $Ag(PPh_3)_n$-C_6F_5 species were observed in any of the experimental data. It was noted that mechanisms of C–H bond activation involving heterodimetalic Pd-Ag species have also been proposed based on computational calculations using DFT methodologies.[160, 259]

3.4.6 Effect of Ag_2CO_3 Quantity on the Reaction Rate

Under the model reaction condition, the Ag_2CO_3 additive was considered to have two roles in the catalytic cycle; the Ag^I as an iodide scavenger and the carbonate anion as the base involved in the C–H bond cleavage together with the acetate anion. The effect of Ag_2CO_3 quantity on the reaction rate was investigated (**Table 19**). Since the concentration of Ag_2CO_3 in the reaction mixture was unknown, this was represented as the number of equivalents of Ag_2CO_3 added relative to 4-iodotoluene **57**. Quantitative conversion of 4-iodotoluene **57** was achieved for reactions with 0.49 or greater equivalents of Ag_2CO_3 (Entries 3–6).

Table 19. k_{obs} obtained for the direct arylation reaction of 4-iodotoluene **57** with pentafluorobenzene **56** at varying equivalents of Ag_2CO_3 (x = 0.1 to 2.25 equivalents) added relative to substrate **57** at 56 ± 1 °C.

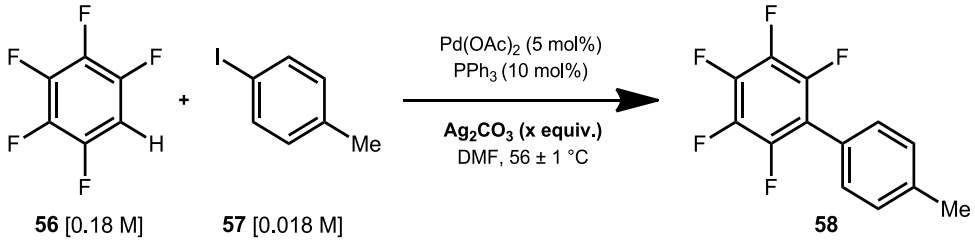

56 [0.18 M] **57** [0.018 M] **58**

Entry	Equivalents relative to 4-iodotoluene 57	%Conversion	k_{obs} / 10^{-6} . mol dm^{-3} s^{-1}
1	0.10	9	0.42 ± 0.04
2	0.24	39	0.79 ± 0.02
3	0.49	quant.	1.35 ± 0.01
4	0.74	quant.	1.68 ± 0.02
5	1.47	quant.	1.65 ± 0.02
6	2.24	quant.	1.71 ± 0.01

Increases in the reaction rates were observed up to 0.75 equivalents of Ag_2CO_3, after which the observed rate reached a plateau (**Figure 40**). The average value of k_{obs} at the plateau was $k_{obs} = (1.68 \pm 0.02) \times 10^{-6}$ mol dm^{-3} s^{-1}. The sudden independence of the rate on the quantity of Ag_2CO_3 suggests that the effect of the additive saturates at *ca.* 0.75 equivalents in DMF at 56 ± 1 °C. This was unexpected as all the experiments followed pseudo-zeroth-order kinetics.

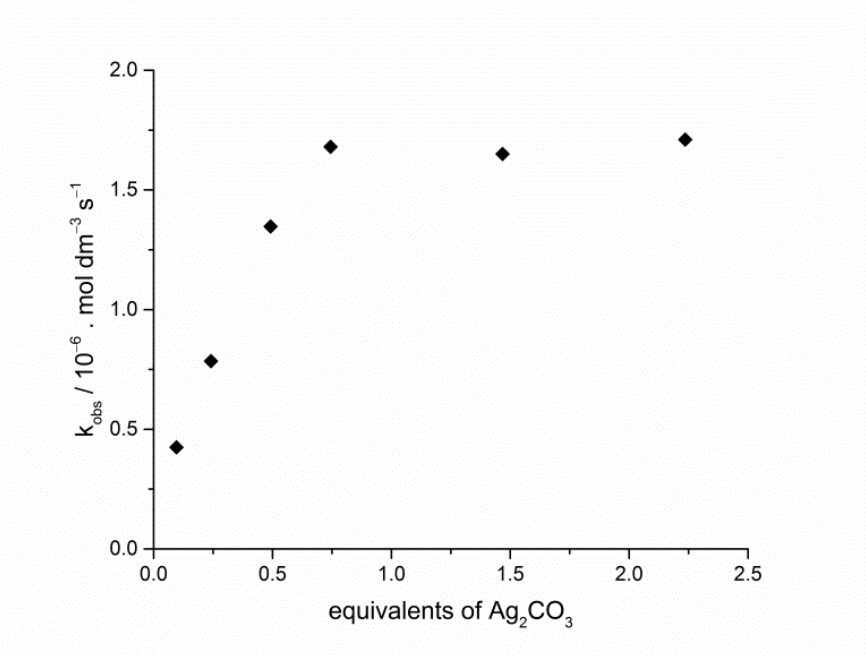

Figure 40. Plot of k_{obs} against equivalents of Ag_2CO_3 added relative to 4-iodotoluene **57** for the reaction shown in **Table 19** at 56 ± 1 °C.

The solubility of Ag_2CO_3 in DMF at 56 ± 1 °C remains unknown. However, some idea was obtained by looking at the solubility of different Ag and potassium salts in water and DMF calculated from published values of solubility products (K_{sp}) (**Table 20**).[260, 261] The maximum concentration of Ag_2CO_3 assuming complete dissolution under the standard reaction condition would be 1.38×10^{-2} M (1.34×10^{-4} mol in 9.7 cm^3). The solubility of the salts compared was generally lower in DMF compared with H_2O with the exception of AgI. Therefore assuming a quasi-constant concentration of Ag_2CO_3 in DMF during the reaction is reasonable.[134] However, the actual solubility of the Ag_2CO_3 will be higher at the reaction temperature and may be even greater in the presence of phosphine with the formation of Ag phosphine complex.

Table 20. Solubility limit of selected Ag and potassium salts in H_2O and DMF at 25 °C.

Salt	Solubility [a] / mol dm^{-3}	
	H_2O	**DMF**
silver carbonate (Ag_2CO_3)	1.28×10^{-4}	N/A
silver acetate (AgOAc)	6.31×10^{-2}	7.94×10^{-6}
silver chloride (AgCl)	1.26×10^{-5}	5.62×10^{-8}
silver bromide (AgBr)	7.08×10^{-7}	3.16×10^{-8}
silver iodide (AgI)	1.00×10^{-8}	1.26×10^{-8}
potassium carbonate (K_2CO_3)	8.11	N/A
potassium chloride (KCl)	0.36	1.99×10^{-3}
potassium bromide (KBr)	4.49	0.063
potassium iodide (KI)	7.68	1.78

[a] Calculated from published K_{sp} values.

3.5 Kinetic Isotope Effect of the Functionalised C–H Bond

Isotopic labelling is a powerful experimental technique where a naturally abundant isotope in the reaction mixture is substituted by an alternative isotope. Some of the common isotopes used include ^{2}H, ^{13}C and ^{17}O. There are two major ways in which an isotopic label can provide useful insight into the reaction mechanism. Firstly, by selecting a spectroscopically active isotope it is possible to tag the atom and follow the structural transformation taking place during the reaction. This may be achieved by *in situ* observation of the intermediates or by characterisation of the products. Secondly, isotopic labelling can be used to aid in the identification of the RL-step. The effect of isotope substitution, at or near the reaction site, on the reaction rate is called the kinetic isotope effect (KIE).[262] The KIE is calculated by the ratio of the rate constants for the reaction with naturally abundant isotope (*e.g.* k_H) over the reaction with the altered isotope (*e.g.* k_D) (Eq. 28). Different conclusions regarding the RL-step can be made based on the magnitude of the calculated KIE.

$$KIE = \frac{k_{light}}{k_{heavy}} \tag{28}$$

Where k_{light} = rate constant for reaction with naturally abundant isotope, *e.g.* ^{1}H

k_{heavy} = rate constant for reaction with altered isotope, *e.g.* D or ^{2}H

Since every C–H bond activation and functionalisation reactions involve the breaking of a C–H bond, the detrermination of KIE is an essential part of a mechanistic study. In reactions proposed to undergo AMLA(6)-TS, the C–H bond cleavage is often the RL-step characterised by a primary KIE. However, no KIE was observed for the direct arylation reaction of 2-methylthiophene **46** as the reductive elimination of the product **47** was the RL-step.[176] In the case of the direct arylation reaction of pentafluorobenzene **56**, the independence of the reaction rate on the concentration of 4-iodotoluene **57** suggests the resting state of the catalyst exists after the oxidative addition step. Based on the proposed catalytic cycle, this is either the ligand exchange, AMLA(6), or the reductive elimination steps. Determination of the KIE would allow the RL-step to be identified.

Lafrance and co-workers have reported the KIE of a direct arylation reaction of 4-bromotoluene **27** with fluoroarene based on a competition experiment involving 1.1 equivalents each of 1-ethoxy-2,3,5,6-tetrafluorobenzene **97** and 1-methoxy-2,3,5,6-tetrafluoro-4-deuterobenzene **98** (**Scheme 45**).[122] It is noted that the 1.1 equivalents of the two substrates is not enough to accurately determine the KIE. Furthermore, the KIE determined from a competition experiment does not conclusively mean the C–H bond cleavage is in the RL-step.[263]

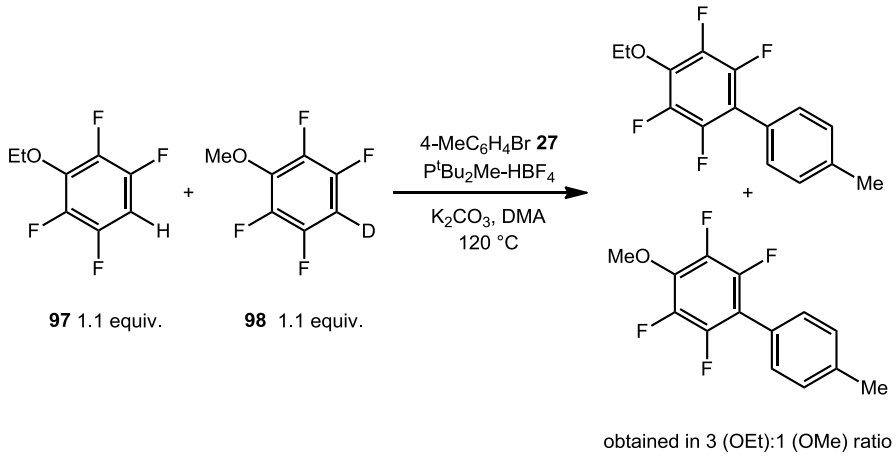

Scheme 45. KIE of the direct arylation reaction of 4-bromotoluene **27** with fluoroarenes determined by intermolecular competition of reagents **97** and **98** (Lafrance and co.).[122]

The KIE analysis of the functionalised C–H bond of the selected reaction system required the synthesis of pentafluorodeuterobenzene (C_6F_5D) **100**. The compound **100** was prepared by decomposition of pentafluoromagnesiumbromide (C_6F_5MgBr) **99** generated *in situ* with D_2O (**Scheme 46**).[264] The purity of the product **100** was confirmed by ^1H, ^2H and ^{19}F NMR spectroscopic analysis.

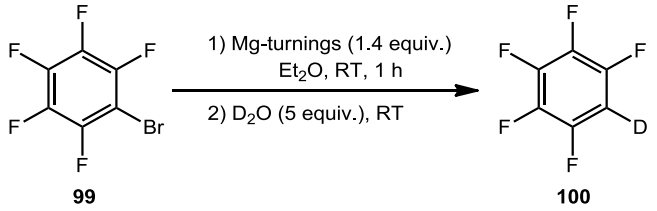

Scheme 46. Synthesis of deuteropentafluorobenzene **100**.

The reactions under pseudo-zeroth-order kinetics with 10-fold excess (*i.e.* 0.18 M) of deuteropentafluorobenzene (C_6F_5D) **100** at 56 ± 1 °C was monitored by *in situ* FT-IR spectroscopy (**Scheme 47**). The IR spectrum of C_6F_5D **100** was significantly different from that of C_6F_5H **56**. The characteristic 4-iodotoluene **57** peak at 1009 cm^{-1} previously observed overlapped with the band of C_6F_5D **100** at 1007 cm^{-1}. However, it was possible to follow the reaction progress by observing the peak of the product **58** at 989 cm^{-1}. The k_{obs} of separate reactions of C_6F_5H **56** ($k_{obs(H)}$) and C_6F_5D **100** ($k_{obs(D)}$) were obtained from the gradient (+*d*[P **58**]/*d*t) between steady-state of the catalytic cycle (*i.e.* 20–80% formation of the product **58**) (**Figure 41**). The KIE calculated from the ratio of $k_{obs(H)}$ to $k_{obs(D)}$ was 4.36 ± 0.06 at 56 ± 1 °C, making this a primary KIE with the cleavage of the C–H bond conclusively involved in the RL-step of the reaction.[263]

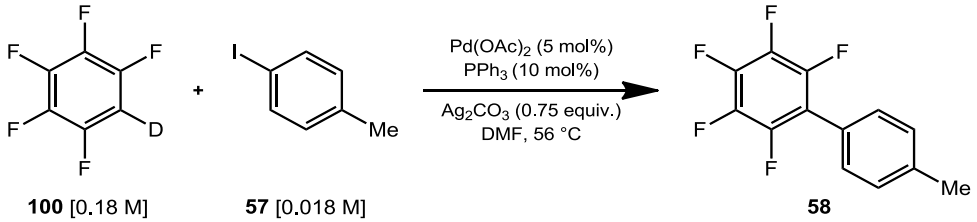

Scheme 47. Direct arylation reaction of 4-iodotoluene **57** with pentafluorodeuterobenzene **100**.

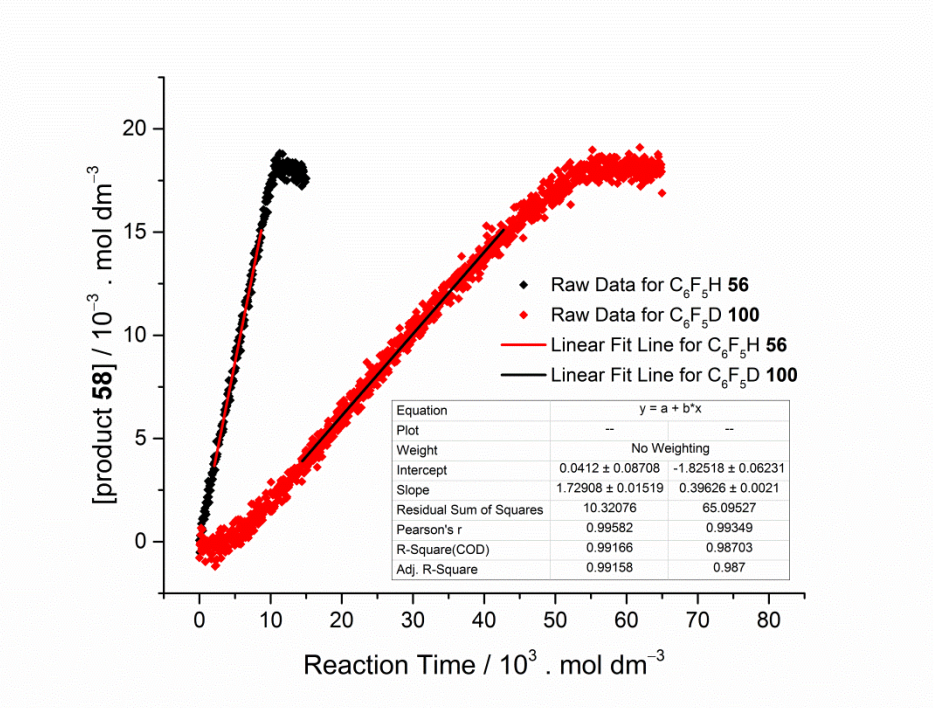

Figure 41. Change in the concentration of product **58** over time for the reaction of 4-iodotoluene **57** with 10-fold excess of **(Black)** C_6F_5H **56** and **(Red)** C_6F_5D **100**.

Change in the KIE was observed at different temperatures and different concentrations of the fluoroarene substrates (*i.e.* **56** and **100**) (**Table 21**). These are known variables for KIE measurements included in the Standards for the Reporting of Enzymological Data (STRENDA) guideline.[265, 266] Comparing the KIE at 40 ± 1 °C and 56 ± 1 °C, the values decreased with increased temperature for the reactions at the same concentrations of polyfluorobenzenes **56** and **100**. Based on the partition-function formulation of transition-state theory, KIE is expected to dependent on the temperature (Eq. 29).[267, 268] The inverse relationship between the temperature and the KIE was also reported by Cannon and co-workers for the C–H bond activation at Ru^{II} benzylidene complex.[171] The increase in the KIE at lower temperature excluded significant proton tunnelling involvement in the C–H bond cleavage of the selected model reaction system. Proton tunnelling is a quantum mechanical process of proton penetration through the activation energy barrier with little dependence on the temperature.[269, 270] Temperature dependent tunnelling has been observed in enzymatic hydride transfer where the process is affected by protein dynamics.[271-273] However, the observed KIE values of 2–5 were too low to be considered a tunnelling process which often results in KIE above 50.

$$KIE = \frac{k_H}{k_D} = \frac{\kappa_H}{\kappa_D} \frac{Q^{\ddagger}{}_H}{Q_H} \frac{Q_D}{Q^{\ddagger}{}_D} e^{-\Delta ZPE/RT} \quad (29)$$

Where κ = transmission coefficient (assumed to be 1), $Q^{\ddagger}$ = partition function for the TS, Q = partition coefficient for the reagents, ZPE = zero-point energy, R = ideal gas constant, T = absolute temperature.

Table 21. The KIE for the direct arylation reaction shown in **Scheme 47** determined by comparing the k_{obs} for the reaction of pentafluorobenzene **56** and deuteropentafluorobenzene **100** at different reaction temperatures and different polyfluorobenzene concentrations [Ar^F].

Entry	T / °C	$[Ar^F]_{ave}$ / mol dm^{-3}	Isotope	k_{obs} / 10^{-7} . mol dm^{-3} s^{-1}	KIE [a] ($k_{obs(H)}/k_{obs(D)}$)
1	40 ± 1	0.18	H	4.19 ± 0.02	5.47 ± 0.05
2			D	0.765 ± 0.002	
3		0.73	H	9.50 ± 0.12	2.97 ± 0.05
4			D	3.20 ± 0.02	
5	56 ± 1	0.18	H	17.3 ± 0.2	4.36 ± 0.06
6			D	3.96 ± 0.02	
7		0.73	H	29.4 ± 0.3	2.30 ± 0.04
8			D	12.8 ± 0.1	

[a] k_{obs} obtained under pseudo-zeroth-order rate law with [ArI **57**] = 18 mM.

An inverse relationship was also observed between the KIE and the concentration of polyfluorobenzenes (*i.e.* **56** and **100**). The substrate concentration dependence on KIE was a result of the rate law of the reaction having a rate constant k′ independent of the concentration of polyfluorobenzenes (*i.e.* **56** and **100**) (Eq. 32). Interesting observation was made from the preliminary analysis of the k_{obs} against [C_6F_5D **100**]. Based on the 4 data points available, it appears as though the reaction pathway dependent on the concentration of the deuteropentafluorobenzene **100** is more dominant compared with the competing pathway independent of the concentration of the deuteropentafluorobenzene **100**. Further experiments are required to confirm this finding (see Chapter 5.2). However, as a result the magnitude of the rate constant contribution to the overall KIE was affected by the concentration of polyfluorobenzenes (*i.e.* **56** and **100**).

$$k_{obs(H)} = [Pd]_{TOT}{}^{1/2}(k_{1(H)} + k_{2(H)}[C_6F_5H\ \mathbf{56}]) \quad (30)$$

$$k_{obs(D)} = [Pd]_{TOT}{}^{1/2}(k_{1(D)} + k_{2(D)}[C_6F_5D\ \mathbf{100}]) \quad (31)$$

$$KIE = \frac{k_{obs(H)}}{k_{obs(D)}} = \frac{[Pd]_{TOT}{}^{1/2}(k_{1(H)} + k_{2(H)}[C_6F_5H\ \mathbf{56}])}{[Pd]_{TOT}{}^{1/2}(k_{1(D)} + k_{2(D)}[C_6F_5D\ \mathbf{100}])} \quad (32)$$

The magnitude of KIE has been used to describe the degree of C–H bond cleavage or the symmetry of the activated complex.[274] The treatment of KIE based on k_H/k_D is known to be a simplification which only takes the changes in the zero-point energies (ZPE) between C–H/D bond stretching frequencies into account.[275] However, many interpretations of the KIE have been published, including the characterisation of the TS geometry by Kwart and co-workers based on TDKIE (temperature dependent KIE).[276, 277] This treatment of KIE compares the Arrhenius parameters between the protio- and deutero-substrates to determine the symmetry of the TS. The observation of a concerted TS by studying TDKIE would provide a strong evidence for AMLA(6)-TS. The detailed evaluation and the explanation for the differences in the KIE were beyond the scope of this work. However, it was concluded that the pentafluorobenzene **56** C–H bond was broken in the RL-step of the catalytic cycle based on the primary KIE observed under the different reaction conditions tested.

The reversibility of the C–H bond activation step of the reaction was investigated. Analysis of the C_6F_5D **100** direct arylation reaction mixture by ^1H and ^{19}F NMR spectroscopy showed no formation of C_6F_5H **56** under the standard reaction condition. The reaction repeated in the presence of AcOH as a proton source resulted in the formation of C_6F_5H **56** as well as the product **58** (**Scheme 48**). However, the formation of C_6F_5H **56** was also observed in the absence of $Pd(OAc)_2$, confirming proton-deuterium exchange of polyfluoroarenes takes place without the Pd metal. The same observation was also reported by Li and co-workers.[166] This could result from a proton acid catalysed mechanism in the presence of excess AcOH and Ag salts, or via Ag-catalysed C–H bond activation.[180, 278] It is important to note that Pd was essential for the formation of the biaryl product **58**, but not for the deprotonating of deuteropentafluorobenzene **100**.

Further evidence for the proton-deuterium scrambling was observed from a reaction of 3 equivalents of C_6F_5H **56** in a 50% (v/v) mixture of DMF and D_2O heated at 60 °C (**Scheme 49**). A mixture of C_6F_5H **56**, C_6F_5D **100** and the biaryl-product **58** was observed by ^{19}F NMR spectroscopic analysis.

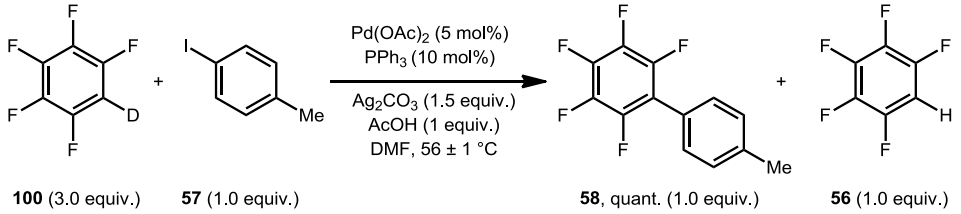

Scheme 48. Direct arylation of 4-iodotoluene **57** with deuteropentafluorobenzene **100** in the presence of acetic acid.

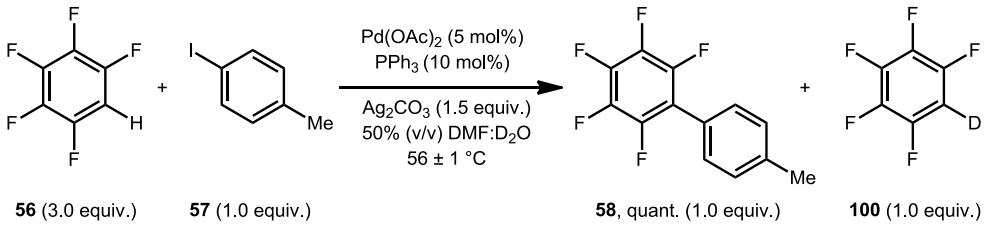

Scheme 49. Direct arylation of 4-iodotoluene **57** with pentafluorobenzene **56** in 50% (v/v) mixture of DMF and D_2O.

3.6 Influence of the Temperature on the Rate of Reaction - Kinetic Activation Parameters

For a reaction in solution phase, one of the important factors affecting the reaction rate apart from the concentration is the temperature. Chemical transformations are generally accelerated as the temperature is raised, for reasons rationalised first by the collision theory, and then by the transition-state theory. In the simplest form, the collision theory states the molecules are required to collide with enough kinetic energy and correct orientation to overcome the activation barrier of the kinetic profile. At higher temperature, more molecules have the speed and the kinetic energy necessary for the reaction, as described by Maxwell's distribution of speeds in the gas phase.[279, 280] The temperature dependence of the reaction rate based on the collision theory is commonly described by the mathematical expression called the Arrhenius equation (Eq. 33).[281, 282]

Unlike the completely elastic treatment of chemical reactions by the collision theory, transition-state theory hypothesises the formation of an activated complex between the reactants as they approach one another. The maximum potential energy is reached at the TS where the activated complex can form the product or revert to the reactants. Thus the activated complex is in quasi-equilibrium with the reactants. The rate constant then describes how the activated complex is formed and decays over the course of the reaction progress. At elevated temperature, the vibration in the activated complex is increased resulting in the accelerated frequency for the product formation. The temperature

dependence of the reaction rate based on the transition-state theory is commonly described by the mathematical expression called the Eyring equation (Eq. 34).[283, 284] Transition-state theory is suitable for describing reactions in both the gas phase and the solution phase. The activation parameters determined from temperature dependence study of the reaction rates provide invaluable information regarding the energetic states of the TS.

$$k_r = Ae^{-E_a/RT} \tag{33}$$

$$k_r = \kappa \times \frac{k_B T}{h} \times K^{\ddagger} \tag{34}$$

Where k_r = rate constant, A = pre-exponential factor, E_a = activation energy, R = gas constant, T = absolute temperature, κ = transmission coefficient, k_B = Boltzmann constant, h = Planck constant, $K^{\ddagger}$ = activation equilibrium constant.

A preliminary computational study on the reaction between pentafluorobenzene **56** and Pd catalyst was reported by Lafrance and co-workers using the B3LYP basis set.[122] The calculation was run in the absence of solvent and the trialkylphosphine ligand (PR_3) was replaced by PH_3 for convenience. The lowest activation energy (E_a) for the AMLA(6)-TS was measured for a bicarbonate complex [Pd(Ph)(HCO_3)(PH_3)] at 41 kJ mol^{-1}. Guihaume and co-workers reported computationally calculated activation energies of the inner-sphere AMLA(6) step for range of polyfluorobenzene (Ar^FH) coordinated Pd complexes, Pd(Ph)(Ar^FH)(κ^1-OAc)(PMe_3).[168] The E_a for pentafluorobenzene **56** and 1,3-difluorobenzene **26** were 60.5 kJ mol^{-1} and 77.4 kJ mol^{-1} respectively. Interestingly, high dissociation energy of 77.0 kJ mol^{-1} was required for the removal of AcOH from the product complex, Pd(Ph)(C_6F_5)(AcOH)(PMe_3). The free energy of activation ($\Delta G^{\ddagger}$(298K)) for the reaction of pentafluorobenzene **56** with [Pd(Ph)(κ^2-OAc)(PMe_3)] via AMLA(6)-TS was calculated as 93.3 kJ mol^{-1} by Gorelsky and co-workers using the B3LYP exchange correlation function.[135] An experimentally determined E_a was reported by Sun and co-workers for the coupling of 5-bromo-*m*-xylene with 4-nitropyridine-*N*-oxide.[172] In Sun's work, the inner-sphere AMLA(6) reaction mechanism was reasoned to be an energetically-viable pathway based on the close proximity in the experimental and the computationally calculated E_a (77.4 kJ mol^{-1} and 73.6 kJ mol^{-1} respectively).

The effect of temperature on the direct arylation reaction of 4-iodotoluene **57** with pentafluorobenzene **56** was studied using *in situ* FT-IR spectroscopic analysis. A typical Arrhenius temperature dependence was observed with exponential increase in the observed

rate constant with increased temperature, confirming the lack of quantum mechanical tunnelling in any significance. In order to calculate the Arrhenius parameters and the activation parameters associated with the experimentally determined rate constants $k_2(2K_D)^{-1/2}$ and k′, the reaction rate dependence study on the concentration of pentafluorobenzene **56** under pseudo-zeroth-order kinetics was repeated for temperatures in the range 40–72 °C in DMF (**Figure 42**). Temperatures above 72 °C were not tested considering that the boiling point of pentafluorobenzene **56** is 85 °C. The IR spectrum of DMF showed slight changes in its absorbance at varying temperatures. The appropriate solvent spectrum was subtracted from the reaction spectra to take the shifting solvent baseline into account. The reaction temperature was directly monitored using an electronic thermometer with a K-type thermocouple submerged in the solvent. A significant difference between the temperature of the reaction mixture and the nominal temperature of the oil bath was observed. In general, the reaction temperature was lower than the oil bath temperature and the discrepancy increased at higher temperatures. The reaction progress was followed by monitoring the IR absorbance of the product **58** at 989 cm^{-1}.

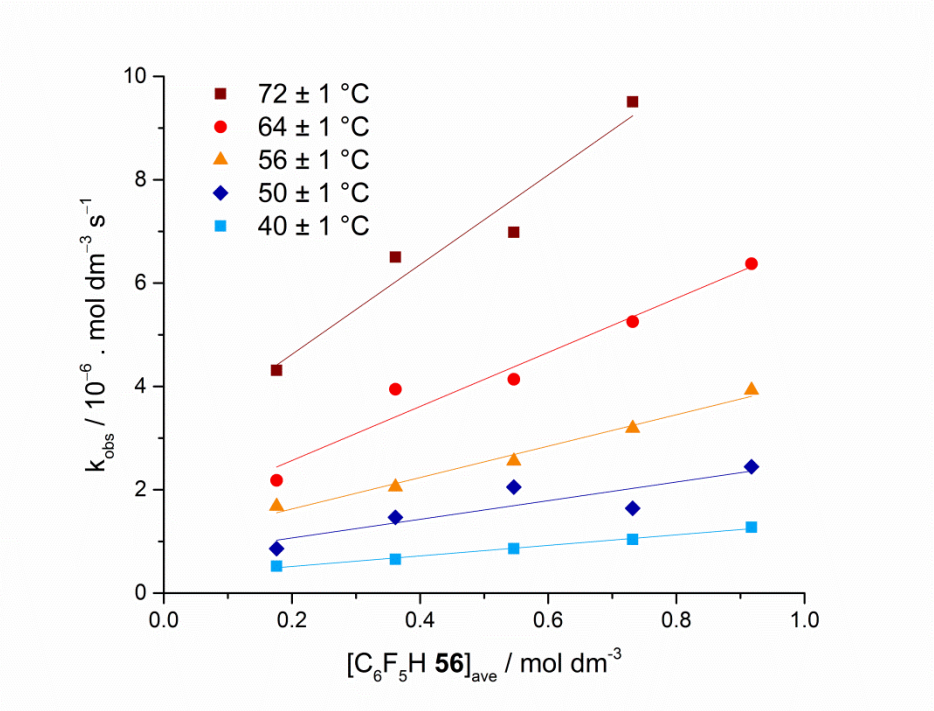

Figure 42. Plot of k_{obs} against $[C_6F_5H$ **56**$]_{ave}$ for the reaction shown in **Scheme 42** at 40 ± 1 °C, 50 ± 1 °C, 56 ± 1 °C, 64 ± 1 °C and 72 ± 1 °C. Each point represents a raw data with the linear fit lines (see Appendix 2).

The values of pentafluorobenzene **56** concentration dependent and independent rate constants (*i.e.* $k_2(2K_D)^{-1/2}$ and k′ respectively) at the experimentally tested temperatures were determined from the slope and the y-intercepts of the lines-of-best-fit (**Table 22**).

Nonzero y-intercept was observed for each data set confirming the presence of a rate constant independent of the pentafluorobenzene **56** concentration. Both rate constants were positively dependent on the reaction temperature. The experimental results were analysed to calculate the activation parameters for better understanding of the TS. Since the reaction was established to follow one-and-a-half-order rate law by RPKA and VTNA, the actual rate constants $k_2(2K_D)^{-1/2}$ and k′ at each temperature were calculated by dividing both the slope and the y-intercept by $[Pd]_{TOT}^{1/2}$.

Table 22. The values of $k_2(2K_D)^{-1/2}$ and k′ obtained from the plots of k_{obs} against $[C_6F_5H$ **56**$]_{ave}$ (**Figure 42**) at T ranging between 40–72 °C assuming half-order kinetics in Pd ($[Pd]_{TOT}$ = 0.9 mM).

Entry	Temperature / K	R^2	$k_2(2K_D)^{-1/2}$ / 10^{-4} . $dm^{3/2}$ $mol^{-1/2}$ s^{-1}	k′ / 10^{-5}. $mol^{1/2}$ $dm^{-3/2}$ s^{-1}
1	313 ± 1	0.992	0.34 ± 0.02	1.02 ± 0.11
2	323 ± 1	0.775	0.59 ± 0.18	2.32 ± 1.12
3	329 ± 1	0.984	1.00 ± 0.07	3.35 ± 0.45
4	337 ± 1	0.957	1.72 ± 0.21	4.99 ± 1.27
5	345 ± 1	0.947	2.85 ± 0.48	9.47 ± 2.39

The Arrhenius and the activation parameters for $k_2(2K_D)^{-1/2}$ and k′ were determined by graphical method using rearranged Arrhenius and Eyring equations (Eq. 35 and 36 respectively). The activation Gibbs energy ($\Delta G^{\ddagger}$) was derived using the values of activation enthalpy ($\Delta H^{\ddagger}$) and the activation entropy ($\Delta S^{\ddagger}$) obtained from the Eyring equation (Eq. 37). The Arrhenius and the Eyring plots constructed for the $k_2(2K_D)^{-1/2}$ and k′ resulted in R^2 values over 99% (**Figure 43**, see Appendix 2 for the other plots).

$$\ln k = \ln A - \frac{E_a}{R}\left(\frac{1}{T}\right) \tag{35}$$

$$\ln\frac{k}{T} = \ln\frac{k_B}{h} - \frac{\Delta H^{\ddagger}}{RT} + \frac{\Delta S^{\ddagger}}{R} \tag{36}$$

$$\Delta G^{\ddagger} = \Delta H^{\ddagger} - T\Delta S^{\ddagger} \tag{37}$$

Where k = rate constant, A = pre-exponential factor, E_a = activation energy, R = gas constant, T = absolute temperature, k_B = Boltzmann constant, h = Planck constant, $\Delta H^{\ddagger}$ = activation enthalpy, $\Delta S^{\ddagger}$ = activation entropy, $\Delta G^{\ddagger}$ = activation Gibbs energy.

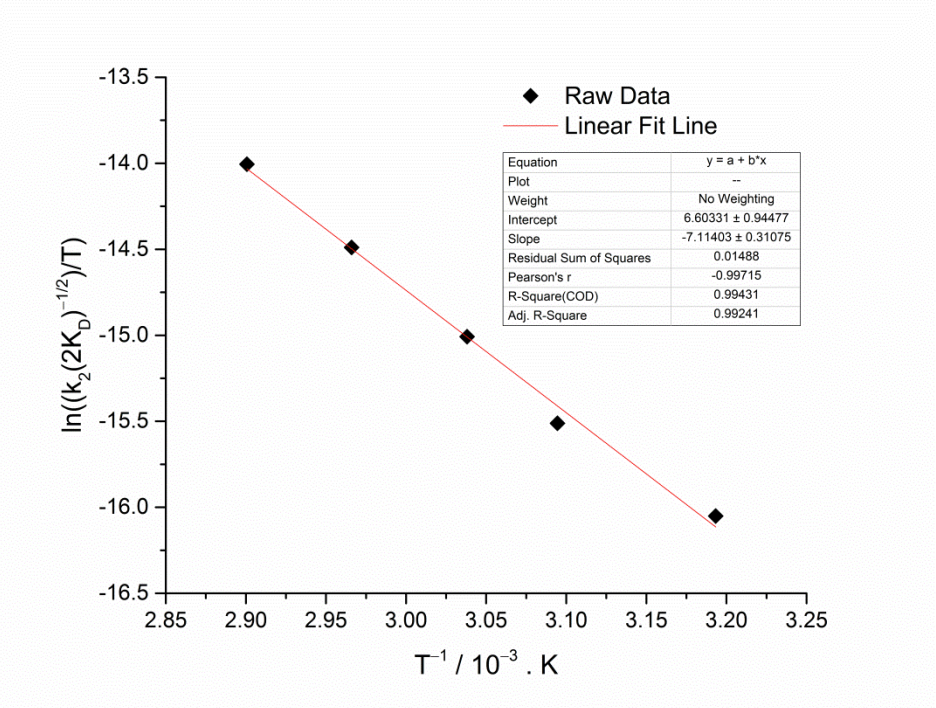

Figure 43. Selected example of the Eyring plot based on $k_2(2K_D)^{-1/2}$ value assuming half-order kinetics in the concentration of the Pd catalyst for the reaction shown in **Scheme 42**. Graph constructed using data from **Table 22**.

The rate constant k_2, dependent on the concentration of pentafluorobenzene **56** and expected to be the RL-step involving AMLA(6)-TS, could not be separated from K_D. The Arrhenius parameters A and E_a of the rate constant $k_2(2K_D)^{-1/2}$ were calculated as 6.59×10^5 and 61.9 ± 2.6 kJ mol^{-1} respectively, from the line-of-best-fit of the Arrhenius plot. The $\Delta H^{\ddagger}$ and $\Delta S^{\ddagger}$ for $k_2(2K_D)^{-1/2}$ under the same reaction condition were 59.1 ± 2.6 kJ mol^{-1} and −143 ± 8 J K^{-1} mol^{-1} respectively, from the line-of-best-fit of the Eyring plot. The negative entropy calculated suggested the entropy of the TS is less than the entropy of the original intermediate (*i.e.* TS is more-ordered than the original complex). This was expected for a AMLA(6)-TS where the composition of the TS involves coordination of reagents **56** to Pd metal centre. The Gibbs energy of activation for the model reaction was calculated as 102 ± 5 kJ mol^{-1} at 298 K. The experimentally determined thermodynamic parameters for $k_2(2K_D)^{-1/2}$ and k′ are summarised below (**Table 23**). These values can potentially be used as guidelines for performing DFT calculations. The Arrhenius and activation parameters for the rate constant k′ were similar, if not identical, to the values calculated for $k_2(2K_D)^{-1/2}$.

Table 23. Thermodynamic parameters calculated from experimentally determined $k_2(2K_D)^{-1/2}$ and k′ (**Table 22**) for half-order kinetic in Pd ($[Pd]_{TOT}$ = 0.9 mM).

Activation parameter	$k_2(2K_D)^{-1/2}$	k′
E_a [a] / kJ mol^{-1}	61.9 ± 2.6	60.9 ± 3.0
A [a] / s^{-1}	6.59 × 10^5	1.51 ×1 0^5
$\Delta H^{\ddagger}$ [b] / J mol^{-1}	59.1 ± 2.6	58.2 ± 3.0
$\Delta S^{\ddagger}$ [b] / J K^{-1} mol^{-1}	−143 ± 8	−155 ± 9
$\Delta G(298\ K)^{\ddagger}$ [b] / J mol^{-1}	102 ± 5	104 ± 6

[a] Values determined from Arrhenius plot. [b] Value determined from Eyring plot.

The kinetic parameters determined for $k_2(2K_D)^{-1/2}$ involves the two-step reaction in steady-state that are reversible.[285] Evidently, the rate law highlighted the rate dependent on the concentration of substrate **56** and rate constant k_2. The energy profile for a catalytic cycle involving an off-cycle species (C_Y) is shown below with $k_2(2K_D)^{-1/2}$ corresponding to δE (**Figure 44**).[249, 250]

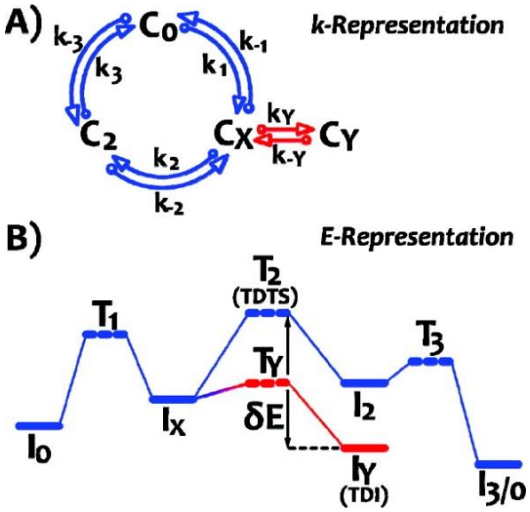

Figure 44. Catalytic cycle with off-cycle intermediate C_Y in equilibrium with on-cycle species C_X **(A)** k (rate constant)-representation and **(B)** E (energy)-representation (Reprinted with permission from S. Kozuch and J.M.L. Martin, *ACS Catal.*, 2011, **1**, 246–253. Copyright 2016 American Chemical Society.).

3.7 Linear Free-Energy Relationships of the Transition State

3.7.1 Reactivity of 1-Substituted-2,3,5,6-Tetrafluorobenzene

The structure-reactivity relationship between the electronic properties of the fluoroarenes and the reaction rates were studied to characterise the electronic state of the TS based on the Hammett equation (Eq. 38).[286, 287] This equation was empirically derived by Hammett from the effect of *meta*- and *para*-substituents on the ionisation equilibrium of benzoic acid in aqueous solution (ρ = 1). A correlation can be made between the equilibrium constants, substituent constant (σ), which depends on the electronics, and the reaction constant (ρ) which depends on reaction and the condition.

$$\log \frac{K}{K_0} = \sigma\rho \qquad (38)$$

Where K = equilibrium constant with substituent R, K_0 = equilibrium constant with R as H, σ = substituent constant, ρ = reaction constant

Values of ρ were expected to differ between mechanisms following a S_EAr pathway and a AMLA(6) pathway. A positive charge carried by the Wheland intermediate of S_EAr was expected to favour electron donating substituents giving negative value of ρ (**Figure 45**).[118] Formation of such an intermediate in the model reaction, where the C–H bond is surrounded by highly electronegative fluorine atoms, was not expected. On the other hand, AMLA(6) pathway was expected to favour electron withdrawing substituents which can stabilise the negative charge at the TS (*i.e.* formation of carbanion stabilised by the metal), resulting in positive value of ρ.[172] Since the pentafluorobenzene **56** C–H bond is broken in the RL-step of the catalytic cycle, a definitive distinction between the two hypothesised reaction pathways can be made.

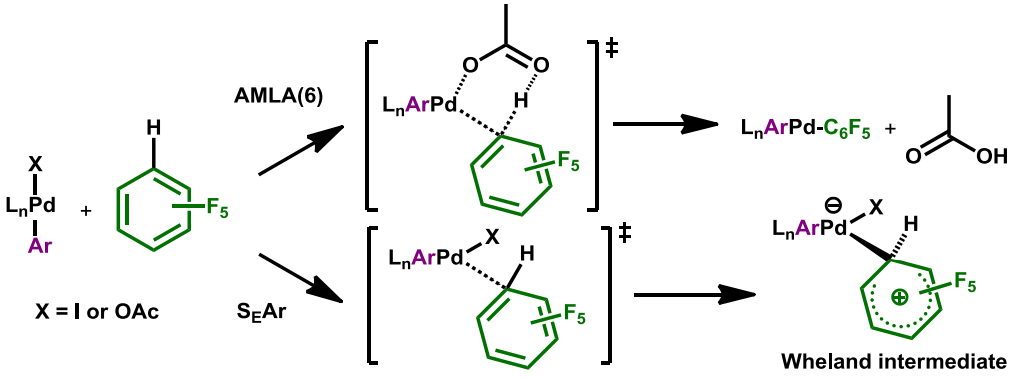

Figure 45. Possible reaction mechanism via AMLA(6) or S_EAr pathways.

The electronics of fluoroarenes were tuned by varying the substituents on the C1 position of 2,3,5,6-tetrafluorobenzene for minimum change in the steric environment of the reactive C–H bond.[288] Furthermore, this decision was based on the commercial availability of 1-substituted-2,3,5,6-tetrafluorobenzenes. Functional groups with electronic properties ranging between electron-donating dimethylamino to electron-withdrawing trifluoromethyl were selected. The reaction of these fluoroarenes achieved quantitative conversion of the starting material **57** to the desired products (*i.e.* **58**, **76**, **77**, **79** and **80**) after 24 hours of heating at 70 °C.

The structural alterations between the 1-substituted-2,3,5,6-tetrafluorobenzenes resulted in significant changes to the FT-IR spectra. The differences in the IR absorption of the compounds meant *in situ* FT-IR spectroscopic analysis was not a suitable method for consistent kinetic analysis. Alternatively, the substituent effect was analysed from relative rates obtained by competition reaction between 10 equivalents each of the 1-X-2,3,5,6-tetrafluorobenzene (where X = NMe_2, OMe, F, Cl and CF_3) and pentafluorobenzene **56** (**Scheme 50**).[289] Competition experiments were well suited as C–H bond cleavage was identified as the RL-step of the reaction. An aliquot of the crude reaction mixture was sampled after 20 hours of heating at 60 °C and analysed by ^{19}F NMR spectroscopic analysis. The relaxation delay was set to 30 s (full relaxation was between 20–25 s) for accurate signal integration of the 4-X-2,3,5,6-tetrafluorobiaryl products, P^X (where X = NMe_2 **76**, OMe **77**, F **58**, Cl **79** and CF_3 **80**) and the pentafluorobiaryl product **58**, P^F.

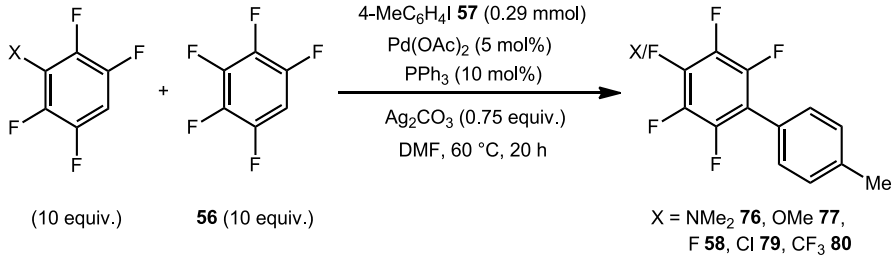

Scheme 50. Competition reaction of pentafluorobenzene **56** and 1-X-2,3,5,6-tetrafluorobenzene (where X = NMe_2, OMe, F, Cl and CF_3) heated at 60 °C for 20 h.

The original method of Hammett analysis involves the comparison of the reaction rates and equilibrium constants. The Hammett equation was modified by substitution of the relative reaction rates represented by the ratio of the two products (P^X/P^F), into the ratio of the two rate constants (k^X/k^F) (Eq. 39).[290] Faster rates were achieved with more electron-withdrawing functional group in the C1 position (**Table 24**). A linear free-energy relationship (LFER) was observed with the logarithms of the relative rates being directly proportional to the substituent constants (**Figure 46**). The resonance of the charge on the aromatic ring of the TS was taken into account by using the substituent constant σ^+ to

represent the electronic properties of these fluoroarenes. The values of σ^+ are referenced to S_N1 reaction of 4-substituted-phenyldimethyl chloromethanes.[291] The R^2 of the graphs plotted using σ^+ and σ_p were 0.954 and 0.940 respectively. The reaction constant (ρ) determined from the slope of the LFER was +0.28 ± 0.02, consistent with AMLA(6) pathway for which a small positive ρ value was expected.

$$\log\left(\frac{P^X}{P^F}\right) = \rho \cdot \sigma^+ \qquad (39)$$

Where P^X = integration of 4-X-2,3,5,6-tetrafluorobiaryl (where X = NMe_2 **76**, OMe **77**, F **58**, Cl **79** and CF_3 **80**), P^F = integration of pentafluorobiaryl **58**, ρ = reaction constant, σ^+ = substituent constant.

Table 24. The product ratio (P^X/P^F) from the reaction shown in **Scheme 50** and the substituent constants (σ^+) for X in 1-X-2,3,5,6-tetrafluorobenzenes (where X = NMe_2, OMe, F, Cl and CF_3).

Entry	X	P^x	σ^+ for X	P^X/P^F [a]
1	NMe_2	**76**	−1.70	0.33
2	OMe	**77**	−0.78	0.56
4	F	**58**	−0.07	1.00
5	Cl	**79**	+0.11	1.17
6	CF_3	**80**	+0.61	1.38

[a] Calculated from integration of ^{19}F NMR signals of the crude reaction mixture in chloroform-d with 512 scans and 30 s relaxation delay.

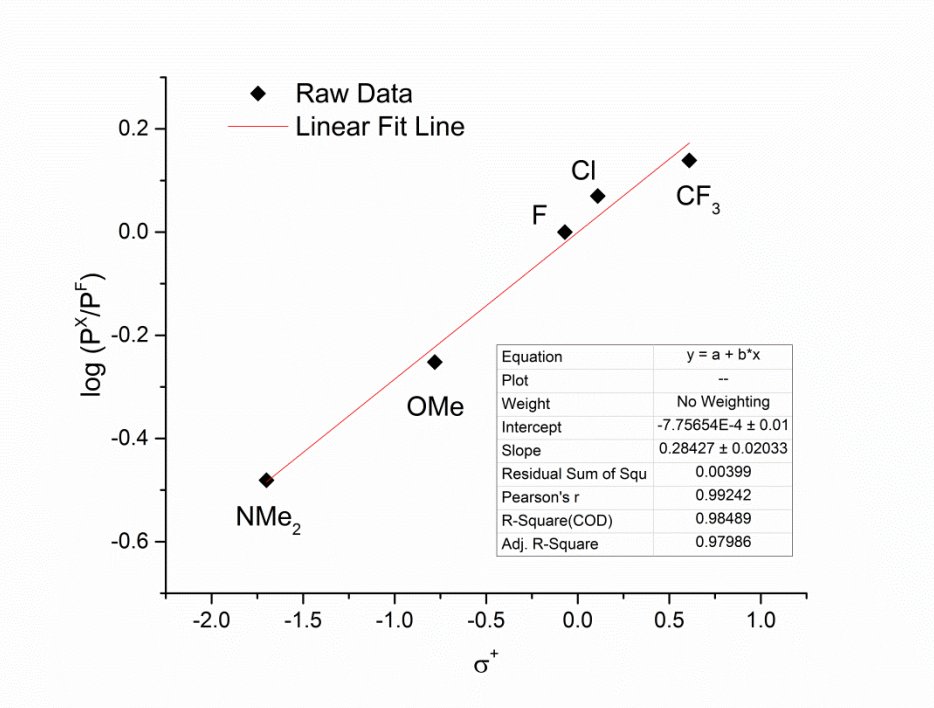

Figure 46. Hammett plot of the competition reaction shown in **Scheme 50**. Graph constructed using data from **Table 24**.

3.7.2 Reactivity of 4-Substituted-Iodoarenes

The electronic effect of the iodoarene (ArI) was studied by comparing the k_{obs} obtained for the direct arylation reactions of different 4-substituted-iodoarenes with 10-fold excess pentafluorobenzene **57** under pseudo-zeroth-order kinetics condition at 56 ± 1 °C (**Table 25**). The k_{obs} values were calculated from 5–50% formation of the products determined by following the IR bands of the respective products around 990 cm^{-1}. Slight but definite differences in the reaction rates were observed between the iodoarenes despite the zeroth-order kinetics which suggested a fast oxidative addition step for the range of substrates tested. The rates ranged between $(1.01 \pm 0.03) \times 10^{-6}$ mol dm^{-3} s^{-1} and $(1.68 \pm 0.04) \times 10^{-6}$ mol dm^{-3} s^{-1}. Therefore the rate of the RL-step was affected by the electronic nature of the iodoarene. The difference in the k_{obs} was expected to result from differences in the energies and the reactivity of the Pd^{II} complexes formed from the oxidative addition of the ArI. Unfortunately, the attempt to correlate the rates with the σ_{para} and the electronic properties of the C4-substituents was unsuccessful. Regardless of the reason behind the rate dependence on the nature of the iodoarene, this observation was in agreement with the RL-step of the catalytic cycle involving a Pd–Ar complex.[174]

Table 25. The k_{obs} for the direct arylation reaction of iodoarenes with pentafluorobenzene **56** at 56 ± 1 °C to form the C4′-substituted biaryls (where C4′ = OH **62**, NH_2 **63**, Me **58**, H **64**, F **65** and CF_3 **66**).

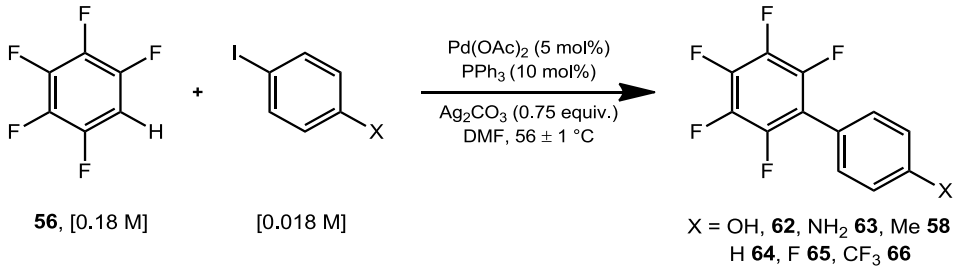

Entry	X	σ_{para}	k_{obs} [a] / 10^{-6} . mol dm^{-3} s^{-1}
1	OH **62**	−0.30	N/A
2	NH_2 **63**	−0.38	N/A
3	Me **58**	−0.14	1.68 ± 0.04
4	H **64**	0.00	1.01 ± 0.03
5	F **65**	+0.15	1.68 ± 0.04
6	CF_3 **66**	+0.53	1.13 ± 0.03

[a] k_{obs} calculated from 5–50% formation of the products **58**, **64**–**66**.

3.8 Determination of the Type of Catalyst – Homogeneous vs Heterogeneous Catalysis

3.8.1 Background

Chemical catalysts are commonly categorised as homogeneous or heterogeneous.[292] In homogeneous catalysis, the catalyst and the reaction mixture are in a single phase.[293] The catalyst is often associated with high selectivity and activity. A significant effort has been made to fine-tune electronic and steric properties at the metal centre to influence the chemoselectivity, regioselectivity, and/or enantioselectivity based on molecular design principles. The catalytic systems are easier to study and optimise, but often difficult to separate and recycle. Alternatively, in heterogeneous catalysis the catalyst is in a different phase (commonly solid) from the reagents and the reaction takes place at the interface.[294] Compared to homogeneous catalysis, heterogeneous catalysis are considered to be less selective and active, with only a fraction of the surface metal available for substrate interaction and limited by mass transfer. The development of heterogeneous catalysts is based on material design principles, and the characterisation of the active sites can be challenging. However, it is more widely applied on industrial scale due to low cost, ease of separation and recyclability.

Ranges of homogeneous and heterogeneous pre-catalysts are available today to perform different chemical transformations.[101] A strong argument for homogeneous or heterogeneous active catalyst can be made based on results obtained from a combination of different techniques designed to distinguish the nature of species involved in the catalysis.[295] However, complications arise due to the potential formation of soluble colloidal metal in homogeneous catalysts[296] and leaching of soluble metal from heterogeneous catalyst.[297] Furthermore, the classification of a reaction as purely homogeneous or heterogeneous catalysis may be an over-simplification as some have suggested catalytic cycle involving both colloidal and molecular Pd species.[298-300] Results from selected analytical techniques are presented here in an attempt to highlight the nature of catalysis involved in the Pd-mediated direct arylation reaction of 4-iodotoluene **57** with pentafluorobenzene **56**.

3.8.2 Hg^0 and PVPy Poisoning

One of the methods to distinguish between homogeneous and heterogeneous Pd catalysis is by the addition of inhibitor to the reaction. Certain additives are known to coordinate to metal species in specific oxidation states. For example, elementary mercury can quench reactions involving "naked" Pd^0 metal by forming Hg^0-Pd^0 amalgam[301-303], and polyvinyl-4-pyridine (PVPy) can act as a solubilised Pd^{II} scavenger by coordinating through its nitrogen lone-pair.[304] The reaction condition previously set as the standard condition for the modern kinetic analysis was used for comparison (**Scheme 51**). It was noticed that the reaction mixtures were coloured moss green during the reaction, and turned black only after the reaction was complete. Palladium nanoparticle catalysed reactions are often associated with black mixtures of Pd^0 commonly known as Pd black.

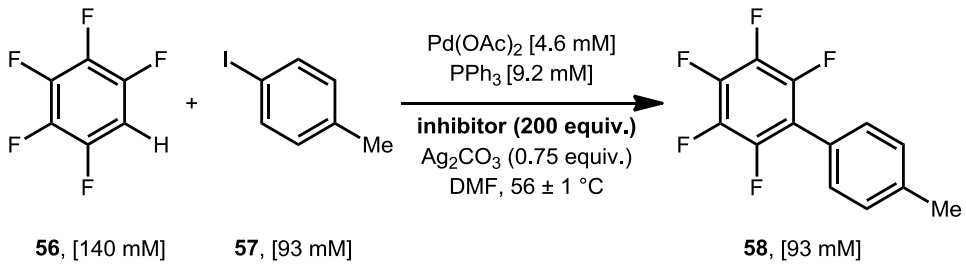

Scheme 51. Standard reaction condition selected for testing the effects of inhibitors.

For the mercury drop-test, Hg^0 (200 equivalents to Pd) was added to the reaction mixture at *ca.* 50% (*i.e.* 170 min) and *ca.* 20% (*i.e.* 70 min) starting material **57** conversion determined from past experiment under identical reaction condition. The addition of mercury at two different stages of the reaction resulted in instant quenching (**Figure 47**). The formation of Hg^0-Pd^0 amalgam does not necessarily mean the reaction was proceeding under

heterogeneous catalysis, but confirms the presence in the reaction mixture of bare Pd^0 species that are low ligated.[305] Within the proposed catalytic cycle, Pd^0 species were expected to form following the reductive elimination of the biaryl-product **58**. Therefore the result obtained from the mercury drop-test maybe interpreted as consistent with the proposed catalytic cycle assuming the rate of Hg^0-Pd^0 formation was faster than the TOF of the Pd^0 intermediates. Additionally, the quenching of the reaction could potentially result from silver precipitation as observed by addition of Hg^0 to Ag^INO_3.[306] The silver cation was understood to be necessary in the catalytic cycle for removing iodide from Pd species. To test this hypothesis, the use of tetramethylammonium acetate, an effective alternative to Ag^I salts often used in C–H bond functionalisation reactions, was considered.[198] Quantitative formation of the product **58** was previously confirmed for the reaction using $[Me_4N]OAc$ instead of Ag_2CO_3. Unfortunately, the kinetics of the reaction using the organic salt was completely different from that of the inorganic salt. Thus the role of $[Me_4N]OAc$ maybe as a phase-transfer reagent assisting in the formation of catalytic Pd nanoparticles. Further experiment using 1.5 equivalents of AgOAc is required to validate this hypothesis.

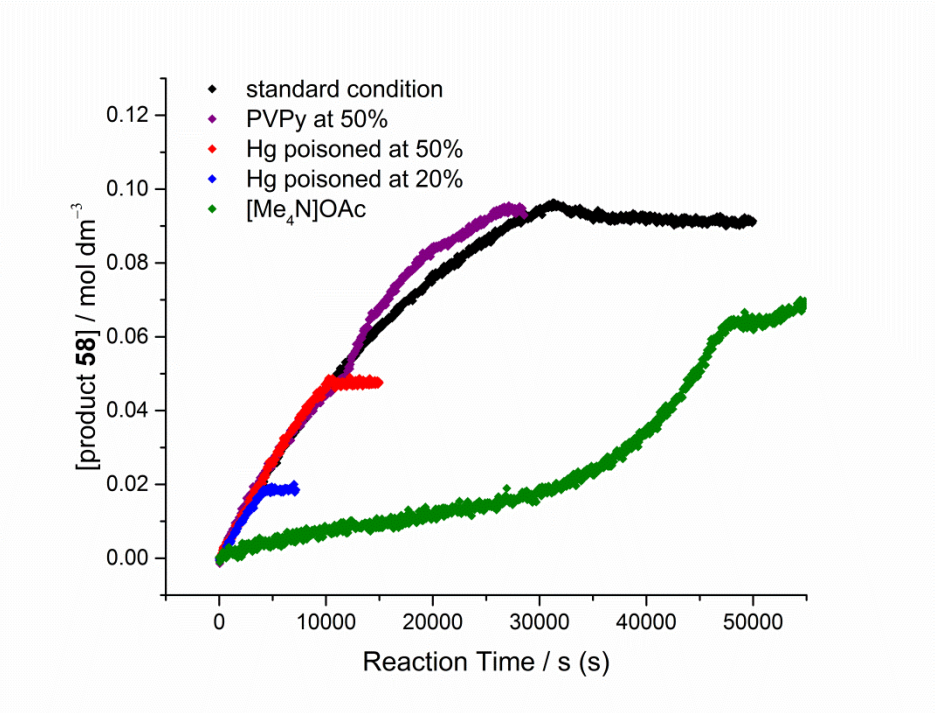

Figure 47. The kinetic profiles of the standard reaction condition shown in **Scheme 51** with **(Black)** no inhibitor, **(Purple)** addition of PVPy (200 equiv. to Pd) at *ca.* 50% conversion, **(Red)** addition of Hg (200 equiv. to Pd) at *ca.* 50% conversion, **(Blue)** addition of Hg (200 equiv. to Pd) at *ca.* 20% conversion and **(Olive)** using $[Me_4N]OAc$ instead of Ag_2CO_3.

The involvement of soluble cationic Pd^{II} species in the catalytic cycle was tested by the addition of PVPy (200 equivalents to Pd) to the reaction mixture at *ca.* 50% (*i.e.* 170 min)

starting material **57** conversion. The reaction achieved quantitative conversion of the starting material **57** with slight deviation from the kinetics of the standard condition (**Figure 47**). The result suggested a catalytic cycle without long lived Pd^{II} species for the polymer to coordinate to.[307, 308] This was inconsistent with the kinetic observation which indicates the RL-step involves the reaction of oxidative addition product Pd^{II}–Ar with pentafluorobenzene **56**. The stability of PVPy in the reaction mixture and the coordination ability to dinuclear Pd species involved in the reaction remains unknown. It is possible that the ligand stabilised catalytically active Pd^{II} species and the hypothesised off-cycle dinuclear Pd^{II} species may not bind to the polymer. It is necessary to perform control experiments to understand the stability of PVPy under the reaction condition.

3.8.3 Hot-Filtration

The involvement of soluble catalyst species were further studied by monitoring the reaction progress before and after hot-filtration[309, 310] through a pre-heated Celite®-pad at *ca.* 50% (*i.e.* 92 min) conversion of 4-iodotoluene **57**. The standard reaction condition was modified with larger excess of pentafluorobenzene **56** in anticipation of the reagent loss by evaporation during hot-filtration and the resulting deceleration of the reaction rate (**Scheme 52**). A layer of green solid was removed by the Celite®-pad (**Figure 48**) and the colourless filtrate was collected into a second reaction vessel containing the same quantity of Ag_2CO_3 as the start of the reaction. The green solid removed by filtration was identified as Ag_2CO_3 based on the appearance, confirming the low solubility of the inorganic salt in the reaction mixture at elevated temperature.

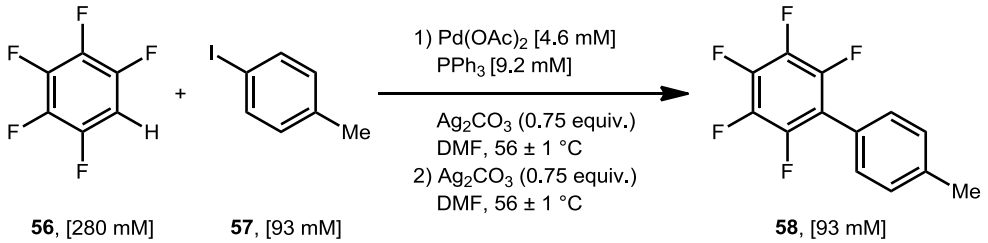

Scheme 52. Reaction condition selected for testing the effect of hot-filtration through Celite®-pad.

Monitoring the reaction after filtration, a continued formation of the product **58** was observed at a slower rate (**Figure 49**). The deceleration was expected to result from loss of catalyst and pentafluorobenzene **56** during filtration, and the dilution of the reaction mixture after washing the Celite®-pad with DMF. Loss of 4-iodotoluene **57**, pentafluroorbenzene **56** and product **58** was highlighted by the slight drop in the absorbance of the corresponding peaks. For heterogeneous catalysis involving insoluble particles, the reaction was expected to quench after the hot-filtration. Thus the result

suggests the product **58** was formed via homogeneous catalysis involving molecular Pd species or soluble nanoparticles.

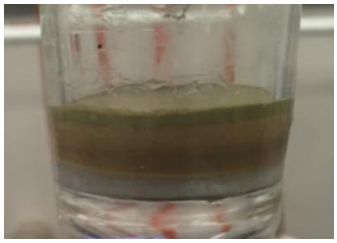

Figure 48. Photograph of the Celite®-pad after hot-filtration of the reaction shown in **Scheme 52**. The green solid collected at the top was identified as Ag_2CO_3 based on the appearance.

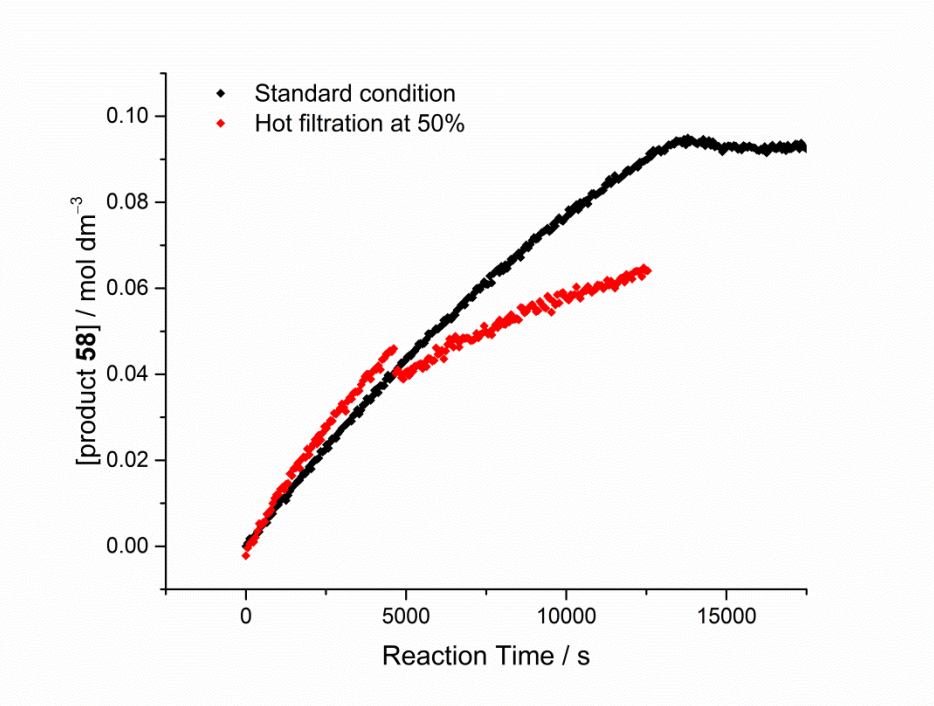

Figure 49. The kinetic profiles of the standard reaction condition shown in **Scheme 52** with **(Black)** no filtration and **(Red)** hot filtration at *ca*. 50% conversion of 4-iodotluene **57**.

3.8.4 Kinetic of Reaction Catalysed by Colloidal Pd

The formation of colloidal metal in aprotic polar solvent (*e.g.* DMF) at temperatures above 100 °C is commonly reported in "ligand-free" coupling reactions.[311, 312] Saha and co-workers observed Pd-NP formation by TEM in a C–H bond functionalisation of benzothiazole **49** with aryliodide starting with $Pd(OAc)_2$ pre-catalyst (**Scheme 53**).[313]

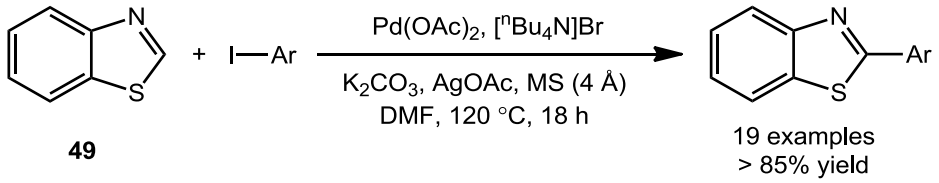

Scheme 53. Direct C–H bond arylation of benzothiazole **49** with aryliodide (Saha and co.).[313]

Storr and co-workers demonstrated that the amine ligand facilitated formation of Pd-NPs by heating $Pd(OAc)_2(NHR_2)_2$ complex in DMF at 80 °C.[314] This result suggested that the high temperature commonly required for NP formation in DMF was for generating amines via decomposition of the solvent into $NHMe_2$ and CO. The important role of solvent was also highlighted by Yano and co-workers who reported high TON cross-coupling reactions catalysed by well-defined DMF stabilised Pd-NPs, prepared by heating aqueous $PdCl_2$ solution in large excess of DMF at 140 °C for 6 hours.[315 316]

The possible role of Pd-NPs in the model reaction was considered by monitoring the reaction kinetics of direct arylation reaction using pre-formed DMF stabilised Pd-NPs solution (0.9 mM) (**Scheme 54**). The reaction required PPh_3 at the tested temperature, in agreement with the observations discussed in Chapter 2.2. Although the DMF stabilised Pd-NPs were a competent catalyst, the reaction achieved 54% conversion of 4-iodotoluene **57** after 40 h (**Figure 50**). In comparison, the reaction catalysed by $Pd(OAc)_2$ achieved quantitative conversion of substrate **57** in 3 h. The result suggested the two reactions were catalysed by different active species.

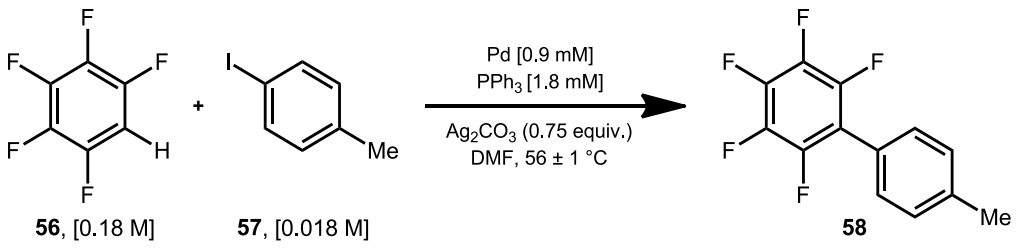

Scheme 54. Standard reaction condition selected for testing the catalytic activity of DMF stabilised Pd-NPs compared to $Pd(OAc)_2$.

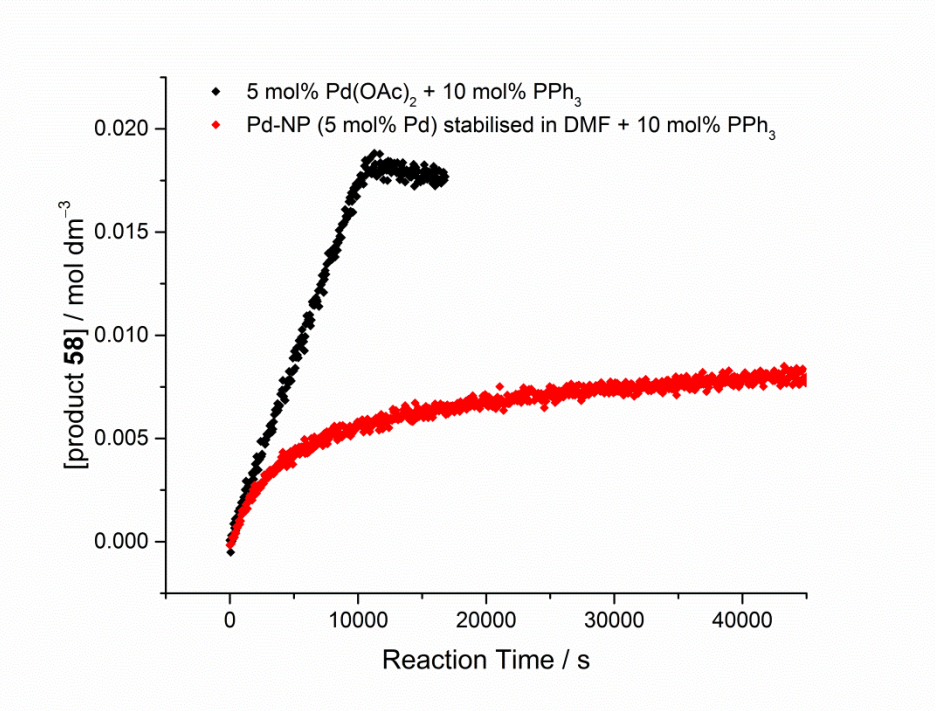

Figure 50. Reaction profile of direct arylation reaction shown in **Scheme 54** catalysed by **(Black)** $Pd(OAc)_2$ pre-catalyst and **(Red)** Pd-NPs stabilised in DMF.

3.9 Catalyst Optimisation

3.9.1 Kinetics for $Pd(OAc)_2/PPh_3$ (1:4) Catalyst System - Reaction Rate Dependence on the Concentration of Pd

The study of the effect of varying quantity of PPh_3 had demonstrated 1:4 ratio of $Pd(OAc)_2/PPh_3$ to provide the fastest reaction rate (**Figure 39**). This was most likely due to a change in the concentration of the reactive intermediates or a change in the reaction mechanism. Under the optimised catalyst system (**Scheme 55**), the equilibrium between intermediate species may shift from the off-cycle dinuclear Pd species to the on-cycle mononuclear Pd species. Consequently the reaction order with respect to $[Pd]_{TOT}$ was expected to be closer to an integer.

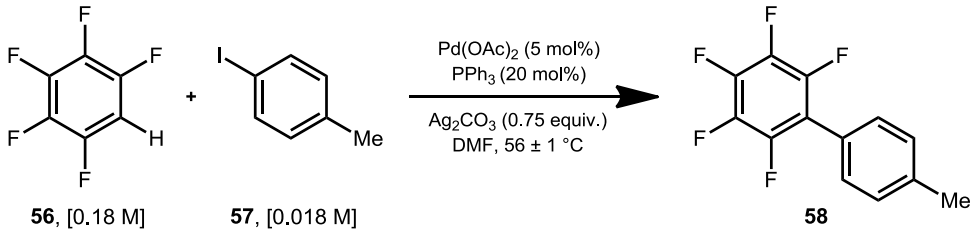

56, [0.18 M] **57**, [0.018 M] **58**

Scheme 55. Direct arylation reaction of 4-iodotoluene **57** with pentafluorobenzene **56** under the optimised catalyst condition with $Pd(OAc)_2/PPh_3$ (1:4).

In order to test this hypothesis, the rate dependence on Pd concentration under the optimised catalyst system was investigated (**Table 26**). Pseudo-zeroth-order rate constants were measured with 10-fold excess of pentafluorobenzene **56** (*i.e.* 0.18 M). A linear increase in the value of k_{obs} was observed with increased Pd concentration. The double-logarithmic plot of log k_{obs} against log $[Pd]_{TOT}$ revealed the reaction followed (0.65 ± 0.10)-order dependence with respect to $[Pd]_{TOT}$. This was lower than the order dependence observed for the catalyst system with 1:2 ratio of Pd/PPh_3.

Table 26. The k_{obs} of the reaction shown in **Scheme 55** at 56 ± 1 °C with different $[Pd]_{TOT}$ maintaining $Pd(OAc)_2/PPh_3$ (1:4) catalyst system.

Entry	$[Pd]_{TOT}$ / 10^{-3} . mol dm^{-3}	k_{obs} / 10^{-6} . mol dm^{-3} s^{-1}
1	0.93	3.73 ± 0.08
2	1.87	5.96 ± 1.02
3	2.81	6.74 ± 0.84
4	3.70	9.91 ± 1.70

The lines-of-best-fit for the experimental data of k_{obs} against $[Pd]_{TOT}$ were compared between the two catalyst systems (**Figure 51**). The slope of the optimised condition was 3 times greater than that of the standard condition. The y-intercepts were unchanged within the standard error in the experimental data. This result suggests a three-fold increase in the concentration of catalytically relevant species in the reaction mixture under the optimised catalyst system.

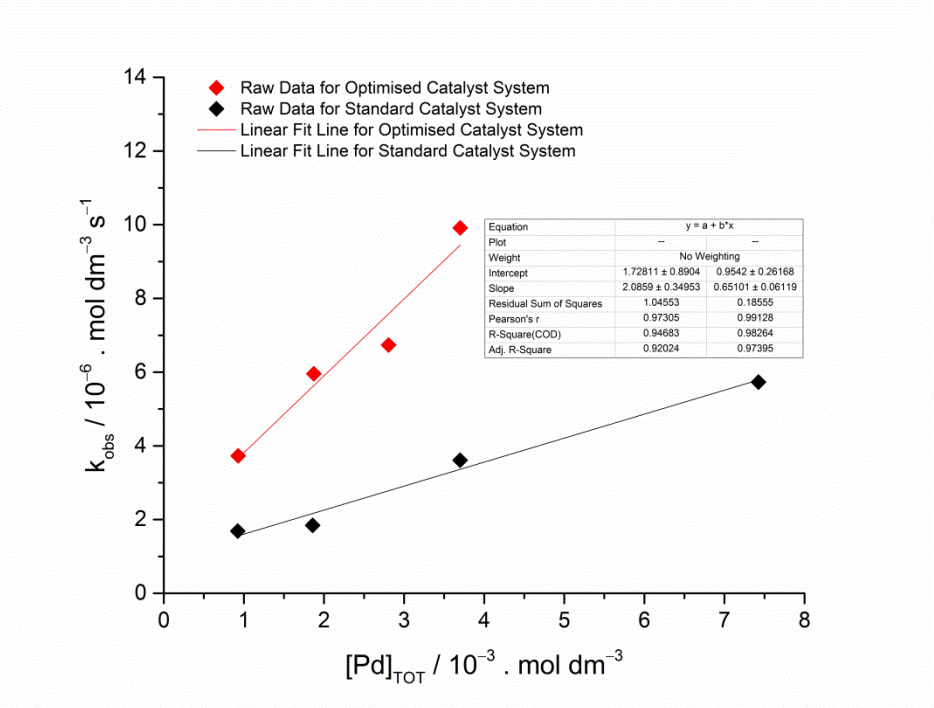

Figure 51. Plot of k_{obs} against $[Pd]_{TOT}$ catalyst system with **(Black)** 5 mol% $Pd(OAc)_2$ + 10 mol% PPh_3 and **(Red)** 5 mol% $Pd(OAc)_2$ + 20 mol% PPh_3. Graph constructed using data from **Table 12** and **Table 26**.

3.9.2 Kinetics for $Pd(OAc)_2/PPh_3$ (1:4) Catalyst System - Reaction Rate Dependence on the Concentration of Pentafluorobenzene 56

The effect of pentafluorobenzene **56** concentration between 0.18 M and 0.73 M on the observed rate constants under the optimised catalyst system was studied (**Table 27**). The catalyst concentration was kept constant at 0.93 mM. The k_{obs} showed a positive dependence on the concentration of pentafluorobenzene **56**.

Table 27. The k_{obs} of the reaction shown in **Scheme 55** at 56 ± 1 °C with different excess concentrations of pentafluorobenzene **56**.

Entry	$[C_6F_5H$ **56**$]_{ave}$ / mol dm^{-3}	k_{obs} / 10^{-6} . mol dm^{-3} s^{-1}
1	0.18	3.73 ± 0.08
2	0.36	4.18 ± 0.60
3	0.54	5.13 ± 0.30
4	0.73	5.50 ± 0.30

The lines-of-best-fit for the plot of k_{obs} against $[C_6F_5H$ **56**$]_{ave}$ were compared between the two catalyst systems (**Figure 52**). The slopes of the lines-of-best-fit were identical within the standard error, indicating the k_{obs} increased by (2.20 ± 0.71) × 10^{-6} mol dm^{-3} s^{-1}

regardless of the C_6F_5H **56** concentration. The y-intercept (k′) of the optimised condition [$(3.10 \pm 0.21) \times 10^{-6}$ mol dm^{-3} s^{-1}] was 3 times greater than the standard condition [$(1.14 \pm 0.11) \times 10^{-6}$ mol dm^{-3} s^{-1}]. This was the same increase observed for the slope of the k_{obs} against $[Pd]_{TOT}$ plot (**Figure 51**).

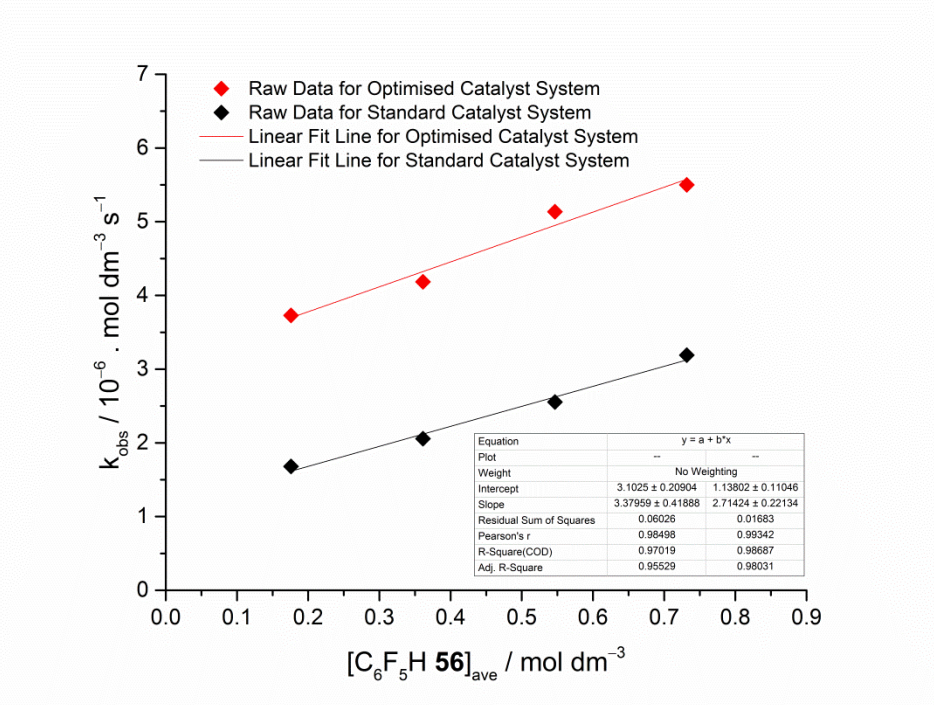

Figure 52. Plot of k_{obs} against $[C_6F_5H$ **56**$]_{ave}$ under catalyst system with **(Black)** 5 mol% $Pd(OAc)_2$ + 10 mol% PPh_3 and **(Red)** 5 mol% $Pd(OAc)_2$ + 20 mol% PPh_3. Graph constructed using data from **Table 13** and **Table 27**.

Part of the rate law independent of $[C_6F_5H$ **56**$]$ was increased by a constant value, suggesting PPh_3 is involved in a step of the catalytic cycle independent of $[C_6F_5H$ **56**$]_{ave}$. The reaction with rate constant k′ may be attributed to increased formation of either a mononuclear Pd species (*i.e.* not Pd1 in **Scheme 40**) from the off-cycle dinuclear Pd species or a $Ag(PPh_3)_n$-C_6F_5 (n = 1, 2 or 3) complex. If increased PPh_3 resulted in increased formation of Pd1, the plot of k_{obs} against $[C_6F_5H$ **56**$]$ was expected to resemble the plot of k_{obs} against $[Pd]_{TOT}$ as Pd1 was hypothesised as the active catalyst complex involved in the RL-step with pentafluorobenzene **56**. Instead, increased $[PPh_3]$ may shift the equilibrium from off-cycle dinuclear species D to the mononuclear Pd(Ar)(κ^1-OAc)$(PPh_3)_2$ **85** which is easier to form Pd1 via ligand loss than complex D.[147] The concentration of Pd(Ar)(κ^1-OAc)$(PPh_3)_2$ **85** could not be identified as it was included in the $[Pd]_{TOT}$, based on steady-state approximation. However, since $[PPh_3]$ was constant for each experimental measurement, the concentration of Pd(Ar)(κ^1-OAc)$(PPh_3)_2$ **85** was expected to be identical. Alternatively, increased $[PPh_3]$ may result in the formation of $Ag(PPh_3)_n$-C_6F_5 (n = 1, 2 or

3) complexes soluble in DMF. These Ag complexes are expected to react competitively with catalytic Pd^{II}–Ar species via transmetallation to yield $Pd^{II}(Ar)(C_6F_5)$ instead of the C–H bond activation expected for C_6F_5H **56**.

In order to distinguish between these two possibilities, the KIE of the $Pd(OAc)_2/PPh_3$ (1:4) catalyst system was determined from the k_{obs} measurements from reactions of C_6F_5H **56** [*i.e.* $(2.74 \pm 0.04) \times 10^{-6}$ mol dm^{-3} s^{-1}] and C_6F_5D **100** [(*i.e.* $(7.09 \pm 0.11) \times 10^{-7}$ mol dm^{-3} s^{-1})] in 10-fold excess. A primary KIE of $k_H/k_D = 3.86 \pm 0.12$ was observed, slightly lower that the KIE for the standard catalyst system (*i.e.* $k_H/k_D = 4.36 \pm 0.06$) with higher ratio of reaction taking place via the cleavage of pentafluorobenzene C–H bond in the RL-step. Since C–D bond resulted in the inhibition of the alternative pathway, this KIE may only reflect the reaction pathway where C–D bond cleavage is the RL-step. Therefore a reaction involving the activated pentafluorobenzene complex such as Ag-C_6F_5 cannot be ruled out as the source of nonzero y-intercept.

3.9.3 Effect of Different Trialkylphosphine on the Reaction Rate

In homogeneous catalysis, one of the most widely studied concepts is the effect of ligand on the activity of the catalyst. Korenaga and co-workers reported that electron-poor phosphine ligands improved the yield of product formation for an intramolecular AMLA(6) process.[317] Rene and co-workers also demonstrated the electron-deficient biarylphosphine as an effective ligand for the C–H bond arylation of otherwise unreactive heterocycles.[318] The effect of changing the phosphine ligand on the %conversion of 4-iodotoluene **57** (*i.e.* TON) and the observed rate constants of the catalytic cycle (*i.e.* TOF) under the model reaction condition was investigated (**Table 28**).

Table 28. The effect of phosphine ligands on the %conversion of starting material **57** and the observed rate constants for the direct arylation reaction at 56 ± 1 °C.

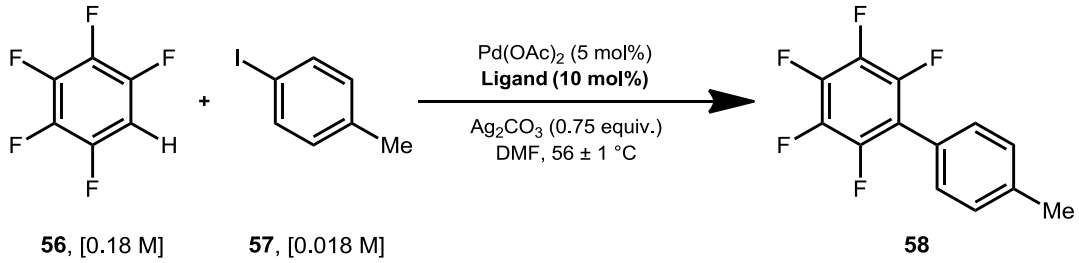

56, [0.18 M] **57**, [0.018 M] **58**

Entry	Ligand	%Conversion [a]	k_{obs} [b] / 10^{-6} . mol dm^{-3} s^{-1}
1	PPh_3	quant.	1.68 ± 0.02
2	$P(4\text{-}FC_6H_4)_3$	quant.	0.835 ± 0.014
3	$P(3,5\text{-}(CF_3)_2C_6H_3)_3$	quant.	0.705 ± 0.005
4	$P(2\text{-Furyl})_3$	quant.	1.66 ± 0.02
5	$P(2\text{-}MeOC_6H_4)_3$	89	4.37 ± 0.10
6	$P(4\text{-}MeOC_6H_4)_3$	69	1.71 ± 0.03
7	$P(2\text{-}MeC_6H_4)_3$	24	8.60 ± 1.33
8	20 mol% $P(2\text{-}MeC_6H_4)_3$	57	4.24 ± 0.21
9	PCy_3	11	0.736 ± 0.086
10	JohnPhos	23	1.33 ± 0.08

[a] Determined by integration of the methyl-peaks of the starting material **57** and the product **58** by ^1H NMR spectroscopic analysis of the reaction mixture. [b] Determined from 5–50% reaction completion monitored by *in situ* FT-IR spectroscopy.

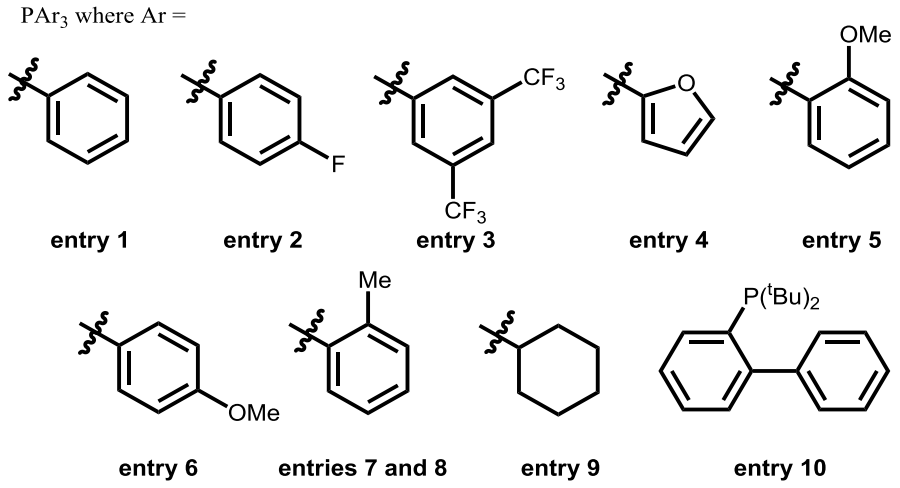

The reaction achieved quantitative conversion of 4-iodotoluene **57** to the product **58** using PPh_3, $P(3,5\text{-}(CF_3)_2C_6H_3)_3$, and $P(4\text{-}FC_6H_4)_3$ (Entries 1–3). These are considered to be relatively electron-poor phosphine ligands. An exception was observed when $P(2\text{-Furyl})_3$ was used (Entry 4). On the other hand, the catalyst stopped turning over before complete

conversion of substrate **57** when more electron-rich ligands of P(2-$OMeC_6H_4)_3$, P(4-$MeOC_6H_4)_3$, P(2-$MeC_6H_4)_3$ and PCy_3 were used (Entries 5–9). Wakioka and co-workers have previously reported the equilibrium between dinuclear and mononuclear Pd species.[319] Of the range of ligands studied, P(2-$MeOC_6H_4)_3$ was shown to shift the equilibrium most favourably towards the mononuclear species with bidentate coordination via phosphine and the methoxy-group lone pairs (**Figure 53**). Significant improvement in the reaction rate was observed with P(2-$MeOC_6H_4)_3$ (Entry 5). However, the catalyst stopped turning over after 89% conversion of substrate **57**. A similar bidentate binding mode was anticipated for P(2-Furyl)$_3$, but the reaction rate was identical to PPh_3 most likely due to the strained 4-membered ring structure required for bidentate binding.

entry 4 **entry 5**

Figure 53. Hypothesised bidentate binding modes of P(2-Furyl)$_3$ (Entry 4) and P(2-$MeOC_6H_4)_3$ (Entry 5) ligands coordinated to Pd metal centres.

An effort was made to differentiate the electronic and the steric effects of the methoxy-group of P(2-$MeOC_6H_4)_3$. The reaction with P(4-$MeOC_6H_4)_3$ resulted in both lower starting material conversion and reaction rate compared to P(2-$MeOC_6H_4)_3$, but comparable to PPh_3, within experimental error (Entry 6). The reaction with P(2-$MeC_6H_4)_3$ (Tolman cone angle of 194 ± 6 °)[320] resulted in the highest reaction rate, but with poor starting material conversion (Entry 7). Previous experiments had shown that doubling PPh_3 loading from 10 mol% to 20 mol% doubled the reaction rate. However, doubling the ligand loading of P(2-$MeC_6H_4)_3$ resulted in doubling the starting material **57** conversion, but halving the reaction rate (Entry 8). The bulky group in the *ortho*-position of the aromatic ring appears to have significant effect on both the TON and the TOF. Very poor starting material conversion was obtained for bulky phospines of PCy_3 (Entry 9) and JohnPhos (Entry 10).

Based on the limited range of trialkylphosphines tested, electron-poor phosphine ligands were shown to result in better yields of product **58** formation for the model reaction. However, the reaction rate was not inherently improved. The rate acceleration can be achieved by steric hindrance at the *ortho*-position of the aryl group with loss of product **58** yield. A range of other ligands must be tested to further establish the properties of the ligands necessary to improve the catalytic efficiency defined by TOF and TON.

One of the important roles played by the phosphine ligand when used in combination with Pd^{II} pre-catalyst such as $Pd(OAc)_2$ is as the reductant.[257] It is well understood that electron withdrawing groups on the PPh_3 results in easier reduction, and electron donating groups on the PPh_3 results in easier oxidation. Additionally, the ability of tertiary phosphine to reduce Pd^{II} into Pd^0 is known to be complicated by the changes in either the electronic or the steric factor.[194] Therefore the reduction properties of the ligands are not discussed here. However, the efficiency of the ligands was expected to be influenced by their ability to reduce Pd^{II} into active Pd^0 species for oxidative addition. This may explain why a more electronically neutral ligand such as PPh_3 provides the best overall outcome with regards to TON and TOF. It is noted here that the $O{=}PPh_3$ by-product formed from reduction of $Pd^{II}(OAc)_2$ to Pd^0 was not a competent catalyst achieving 11% conversion of the starting material **57**.

3.9.4 Reaction with Alternative Pre-Catalyst and Ag Additive

In addition to studying the effect of the different phosphine ligands, alternative pre-catalysts and Ag additives were investigated. Quantitative conversion of 4-iodotoluene **57** was observed for a reactions using $Pd(PPh_3)_4$ instead of $Pd(OAc)_2$ and Ag_2O instead of Ag_2CO_3, during the scope study on the selected model reaction (see Chapter 2). Therefore the kinetics of reactions with different combinations of pre-catalyst and additive were monitored using *in situ* FT-IR spectroscopic analysis (**Table 29**). The pseudo-zeroth-order rate constants were determined from 20–80% conversion of 4-iodotoluene **57**.

Table 29. The k_{obs} of direct arylation reaction of 4-iodotoluene **57** with pentafluorobenzene **56** at 50 ± 1 °C using Ag_2CO_3 or Ag_2O additive with $Pd(OAc)_2$ or $Pd(PPh_3)_4$ pre-catalysts.

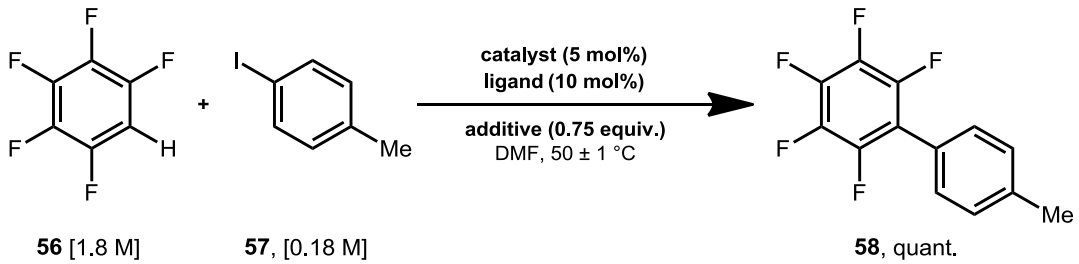

56 [1.8 M] **57**, [0.18 M] **58**, quant.

Entry	Catalyst	Ligand	Additive	k_{obs} / 10^{-5} . mol dm^{-3} s^{-1}
1	$Pd(OAc)_2$	PPh_3	Ag_2CO_3	3.05 ± 0.03
2			Ag_2O	3.78 ± 0.03
3	$Pd(PPh_3)_4$	N/A	Ag_2CO_3	9.12 ± 0.04
4			Ag_2O	0.514 ± 0.002

The kinetics of reactions catalysed by 5 mol% $Pd(OAc)_2$ and 10 mol% PPh_3 mixture were similar between the two additives (*i.e.* Ag_2CO_3 and Ag_2O). The observed rate constant for the reaction with 0.75 equivalents of Ag_2CO_3 (k_{obs} = (3.05 ± 0.03) × 10^{-5} mol dm^{-3} s^{-1}) was slightly lower than the reaction with 0.75 equivalents of Ag_2O (k_{obs} = (3.78 ± 0.03) × 10^{-5} mol dm^{-3} s^{-1}) (**Figure 54**). Assuming both reactions proceed through similar catalytic cycles involving AMLA-TS, the proximity in the k_{obs} suggested that the two Ag additives were playing the same role in the reaction. Silver carbonate is known to decompose to Ag_2O and CO_2, but when heated at 210 °C.[321] As the involvement of Ag_2O in AMLA(6)-TS is unknown, Ag_2CO_3 and Ag_2O were most likely involved in the reaction as mild bases with the acetate from $Pd(OAc)_2$ pre-catalyst acting as the inner sphere base.

For the reaction starting with 5 mol% $Pd(PPh_3)_4$ pre-catalyst, significant differences were observed between the two additives. The reaction with 0.75 equivalents of Ag_2CO_3 (k_{obs} = (9.12 ± 0.04) × 10^{-5} mol dm^{-3} s^{-1}) was about 20 times faster than the reaction with 0.75 equivalents of Ag_2O (k_{obs} = (0.514 ± 0.002) × 10^{-5} mol dm^{-3} s^{-1}). The rate for the reaction with Ag_2CO_3 was comparable to the reaction using $Pd(OAc)_2$ pre-catalyst, especially when considering the rate enhancement expected for the reaction with Pd/PPh_3 ratio of 1:4 which is *ca.* 3-times faster than reaction with Pd/PPh_3 of 1:2. While the kinetic profile provides no information on the actual mechanism, the slow rate for the reaction with Ag_2O suggested a catalytic cycle involving different active species. Assuming the C–H bond activation of pentafluorobenzene **56** proceeded only via the AMLA(6)-TS, it appears that the carboxylate anions (*i.e.* OAc^- and CO_3^{-2}) played the same role in the reaction mechanism. Further evidence for the role of acetate and the carbonate anions may be obtained by studying the kinetics of reactions using $Pd(PPh_3)_2Cl_2$ pre-catalyst.

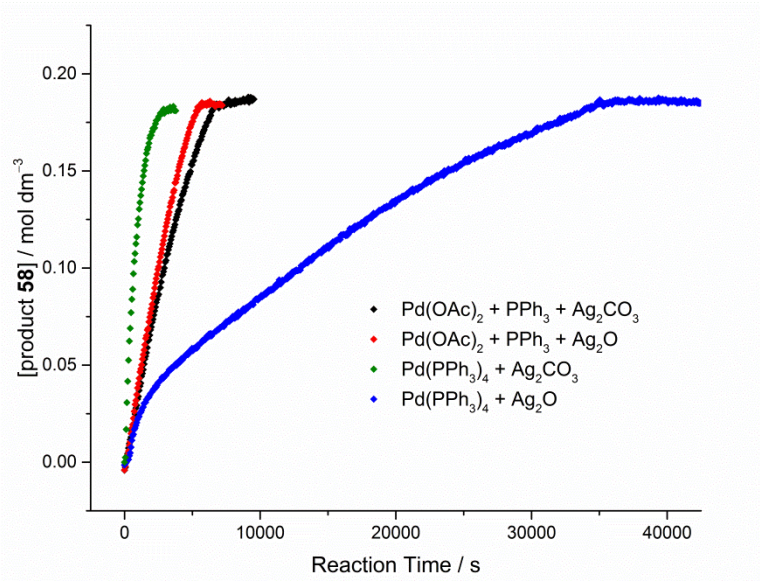

Figure 54. Reaction profiles of product **58** formation for the reactions shown in **Table 29**.

3.10 Conclusions

Experimental conditions for monitoring the reaction kinetics by *in situ* FT-IR spectroscopic analysis was established. Characteristic IR absorbances for 4-iodotoluene **57**, pentafluorobenzene **56** and the product **58** were observed at 1009 cm^{-1}, 957–944 cm^{-1} and 989 cm^{-1} respectively. The correlation between the changes in IR absorbances and the concentrations of the substrate (*i.e.* **56** and **57**) and the product **58** were demonstrated by the identical kinetic profile obtained by the %conversion determined by NMR spectroscopic analysis.

In situ FT-IR spectroscopy was used to obtain valuable kinetic data on the reaction system. The order in each substrate (*i.e.* **56** and **57**) and the catalyst was established by RPKA and VTNA at 56 ± 1 °C. The reaction kinetics followed first-order in pentafluorobenzene **56**, zeroth-order in 4-iodotoluene **57** and half-order in Pd catalyst. The reaction rate was independent of the biaryl product **58** concentration and did not suffer from significant catalyst deactivation under the conditions tested. Further kinetic studies were performed with the isolation method. A discrepancy between the order in the catalyst concentration under the pseudo-zeroth-order reaction condition (*i.e.* 0.75-order) and the modern kinetic analysis (*i.e.* 0.5-order) was noticed. The deviation from half-order in catalyst was attributed to the unusually large excess of pentafluorobenzene **56** concentration required for the isolation method. Increase in the TOF of the catalytic cycle was observed at low concentration of the Pd catalyst, indicative of off-cycle high-order Pd species being the catalyst resting state. The rate dependence on the concentration of pentafluorobenzene **56** revealed the rate law consisted of rate constants dependent (*i.e.* $k_2(2K_D)^{-1/2}$) and independent (*i.e.* k′) of the pentafluorobenzene **56** concentration. The KIE of the reaction was determined by comparing the k_{obs} for the reaction of pentafluorobenzene (C_6F_5H) **56** with that of pentafluorodeuterobenzene (C_6F_5D) **100**. At 56 ± 1 °C under pseudo-zeroth-order kinetic condition with 10-fold excess of the fluoroarene, the KIE of 4.4 ± 0.1 highlighted the RL-step of the catalytic cycle to involve C–H bond cleavage. Although the magnitude of the KIE depended inversely on the reaction temperature and the concentration of the fluoroarene, primary KIE was observed under every reaction conditions tested.

Accordingly, a rate law focused on the kinetically important region of the catalytic cycle was derived. The reaction rate was in accordance with a mechanism involving C–H bond activation of pentafluorobenzene **56** after dissociation of off-cycle dinuclear Pd species into on-cycle mononuclear Pd species. The kinetic results obtained for the direct arylation of iodobenzene **81** were consistent with 4-iodotoluene **57**, suggesting that the two substrates undergo reaction by identical mechanisms.

The effect of changing the amount of PPh_3 and Ag_2CO_3 on the reaction rate was also investigated. The optimal reaction rate was achieved for catalyst system with $Pd(OAc)_2/PPh_3$ in 1:4 ratio. Comparison of the kinetic results for the catalyst systems with $Pd(OAc)_2/PPh_3$ ratio of 1:2 and 1:4 revealed the latter condition accelerated the reaction pathway independent of pentafluorobenzene **56** concentration. Saturation kinetics in Ag_2CO_3 were observed under the model reaction conditions, allowing quasi-constant concentration of the additive during the reaction to be assumed.

The effect of temperature on the reaction rate was investigated. The pentafluorobenzene **56** concentration dependent (*i.e.* $k_2(2K_D)^{-1/2}$) and independent (*i.e.* k′) rate constants at temperatures between 40–72 °C were calculated from experimental results. A typical Arrhenius temperature dependence was observed with exponential increase in the rate constants with the reaction temperature. The thermodynamic parameter for $k_2(2K_D)^{-1/2}$ was calculated from Arrhenius and Eyring plots with the activation parameters being $\Delta H^{\ddagger}$ = 59.1 ± 2.6 J mol^{-1}, $\Delta S^{\ddagger} = -143 \pm 8$ J K^{-1} mol^{-1} and $\Delta G(298\ K)^{\ddagger}$ = 102 ± 5 J mol^{-1}. These values were proposed to characterise the reaction pathway following AMLA(6)-TS. The thermodynamic parameters for k′ was similar, if not identical to the values calculated for $k_2(2K_D)^{-1/2}$. The exact identity of the alternative reaction pathway remained uncertain.

The LFER of the electronic properties of the fluoroarene on the reaction rate was investigated based on Hammett equation. Different 1-substituted-2,3,5,6-tetrafluorobenzenes (*i.e.* NMe_2, OMe, Me, F, Cl and CF_3) were reacted with 4-iodotoluene **57** in a competition experiment with pentafluorobenzene **56**, in order to determine the relative rates. The value of ρ calculated from the gradient of the line-of-best-fit of the Hammett plot was +0.28 ± 0.02. This was consistent with the proposed AMLA(6)-TS where no significant charge build up was expected. The reaction rate was also affected by the electronic properties of 4-substituted-iodobenzene suggesting Pd–Ar species to be involved in the RL-step of the catalytic cycle.

The experimental evidence obtained from studies designed to distinguish homogeneous and heterogeneous catalysis provided insight into the nature of the catalyst. The quenching of the reaction observed by the mercury drop-test indicated the reaction involved a heterogeneous catalyst or a homogeneous catalysis with long lived Pd^0 species. The continued product formation observed following the addition of PVPy to the reaction mixture suggested the catalytic cycle had no long lived Pd^{II} species for the polymer to coordinate to. The hot-filtration demonstrated the reaction was catalysed by homogeneous species. In conclusion, the direct arylation of 4-iodotoluene **57** with pentafluorobenzene **56** involves a homogeneous catalysis with long lived Pd^0 species, but not Pd^{II} species. Further

analysis of the reaction mixture by techniques such as TEM, HPLC-MS and three-phase test are required for making clear distinction between homogeneous and heterogeneous catalysis.[322-325] However, these techniques do not differentiate reactions involving both homogeneous and heterogeneous catalysis.

The effect of phosphine ligands on the conversion of the starting material **57** and the reaction rate was investigated to understand the nature of the active catalyst. The most balanced ligand was the PPh_3 with quantitative conversion of 4-iodotoluene **57** with modest observed reaction rate of $(1.68 \pm 0.02) \times 10^{-6}$ mol dm^{-3} s^{-1}. A better reaction rate of $(4.37 \pm 0.10) \times 10^{-6}$ mol dm^{-3} s^{-1} was observed using $P(2\text{-}MeOC_6H_4)_3$ with 89% conversion of substrate **57**. The highest reaction rate of $(8.60 \pm 1.33) \times 10^{-6}$ mol dm^{-3} s^{-1} was achieved by using $P(2\text{-}MeC_6H_4)_3$, but only 24% conversion of 4-iodotoluene **57** was achieved.

Kinetic observations were also made on reactions using $Pd(PPh_3)_4$ pre-catalyst and Ag_2O additives. For reactions starting with $Pd(OAc)_2$ pre-catalyst, comparable reaction rates were obtained for both Ag_2CO_3 and Ag_2O additives. Similar reaction kinetics were observed for the reaction catalysed by $Pd(PPh_3)_4$ pre-catalyst and Ag_2CO_3. However, the reaction catalysed by $Pd(PPh_3)_4$ pre-catalyst and Ag_2O was significantly slower than other reaction conditions. The result suggested the carboxylate anions (*i.e.* acetate and carbonate) played the same role in the reaction mechanism. In the absence of carboxylate anions, the reaction appeared to react via slower reaction path.

Chapter 4: Characterisation of Catalytic Intermediates

4.1 In situ NMR Spectroscopy Studies in the Literature

Chemical kinetics provides the rate equation and the reaction order with respect to the starting materials. To complement this process the identification of the key intermediates is essential for deciphering a complete mechanism. The postulated reaction intermediates are based on experimental observations and often supported by computational calculations (*e.g.* using DFT methods).[326] The ultimate objective for the identification of catalyst intermediate is for effective reaction optimisation.

One of the most common methods for the identification of reaction intermediates is by characterising species in the reaction mixture using multiple analytical techniques.[327] The reaction mixture can be analysed in real time/*in situ* or by sampling an aliquot/*ex situ*, with the former providing a non-invasive method of analysis.[328, 329] Advances in the technology have allowed for improved methods of application. For example, mass spectrometry (MS) is not simply a way to identify the composition of the reaction mixture, but may be used to construct the kinetic profiles of low concentration intermediates.[330] Continuous monitoring of the reaction allows for time-dependent processes to be elucidated. Additionally, certain techniques like nuclear magnetic resonance (NMR) are non-destructive, whereas MS is destructive and often requires the species of interest to be charged. It is also important to be aware that the observed species maybe an artefact under the analytical condition of MS and not exist in solution. On the other hand, NMR spectroscopy can be unsuitable for detecting short-lived intermediates due to the time scale required for data collection and the averaging of the signals.[331] Combinations of multiple techniques are essential for complete mechanistic understanding.

The *in situ* FT-IR spectroscopic analysis provided a way to monitor the progress of the reaction in real time and helped in the derivation of reaction kinetics (see Chapter 3). In addition to following the absorbance of the starting materials and the product, possible reaction between $Pd(OAc)_2$ and PPh_3 was observed at high reaction concentration where the IR signal of $Pd(OAc)_2$ and PPh_3 disappeared simultaneously. However, new signals corresponding to low concentration catalytic intermediates were not observed in the FT-IR spectra, possibly due to signal overlap and low signal-to-noise ratio.

The analysis of the reaction mixture by 400 MHz NMR spectrometer resulted in broad signals due to poor shimming caused by the low solubility of Ag_2CO_3 in DMF. In order to

improve the signal resolution of the spectrum, a 400 MHz NMR spectrometer equipped with magic-angle spinning (MAS) capability was used. In NMR spectroscopy, MAS is a technique in which the sample is physically spun at a high frequency (*ca*. 1–100 kHz) at an angle Θ_m of 54.74° with respect to the direction of the magnetic field.[332-334] Nuclear dipole-dipole coupling calculated by $3\cos^2\Theta-1$ is orientation-dependent and becomes averaged to zero at the magic angle, resulting in the broad lines becoming narrower. Although MAS is often applied to solid-state NMR spectroscopy, it can also be used to improve the signal resolution of solution NMR spectrum affected by insufficient averaging of dipole-dipole interaction.[335] Therefore high-resolution magic angle spinning (HR-MAS) NMR spectroscopy was applied to obtain *in situ* spectra of the reaction mixture affected by line broadening caused by the presence of insoluble particles (**Figure 55**).

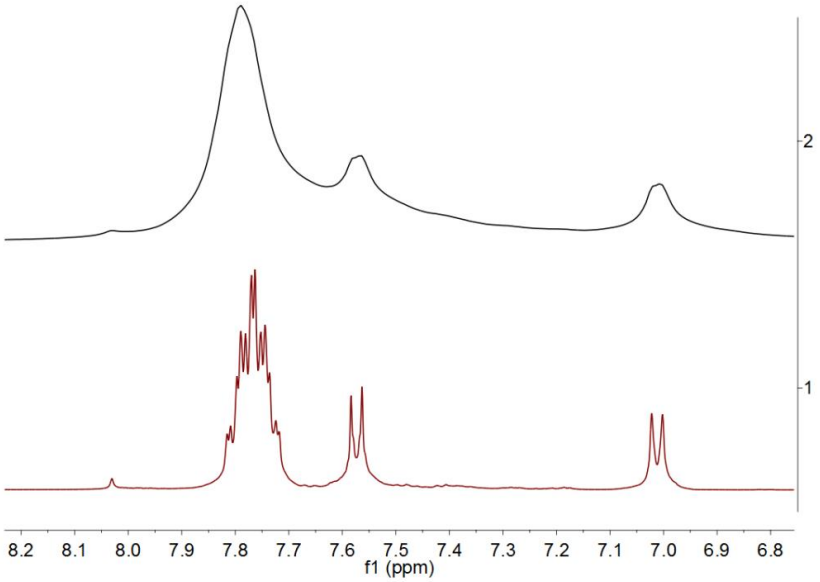

Figure 55. Stacked ^{1}H NMR spectra of the reaction mixture shown in **Scheme 58** at 285 K with **(1)** 0 Hz spin and **(2)** 3 kHz spin.

In the literature, HR-MAS NMR spectroscopy has been frequently applied for the analysis of biological samples and structural study on heterogeneous catalysts.[336-339] Posset and co-workers characterised suspension of silica supported Pd/Cu catalysts for the Sonogashira cross-coupling reaction by HR-MAS NMR spectroscopic analysis.[340] Based on the migration of the Pd along the linker observed and the loss of catalytic activity, the silica-supported Pd catalyst was shown to suffer a significant metal leaching. Combination of heterogeneous silica supported copper catalyst and a homogeneous $Pd(PPh_3)_2Cl_2$ catalyst was reported as the optimised catalyst system. Pinoie and co-workers reported the use of monoalkyltin trichloride on polystyrene as a catalyst for the transesterification of ethyl acetate and *n*-octanol.[341] HR-MAS NMR spectroscopy was used to characterise the heterogeneous catalyst in solution as well as to demonstrate its recyclability. However, the

analysis of the esterification reaction was limited to aliquots due to the reaction temperature being unsuitably high for running inside the spectrometer.

Application of HR-MAS NMR spectroscopy for real time reaction monitoring has been reported over the past few years. Roy and co-workers have reported the detailed kinetic study on the H_2SO_4-silica assisted synthesis of 2,2-di-substituted quizolin-4(3H)-ones **101** based on real time monitoring by HR-MAS NMR spectroscopic analysis (**Scheme 56**).[342] Conversion of non-protonated acetone into protonated acetone was observed indirectly as two new dimethyl proton peaks, suggesting the activation of acetone by the acid was the initial step of the reaction mechanism.

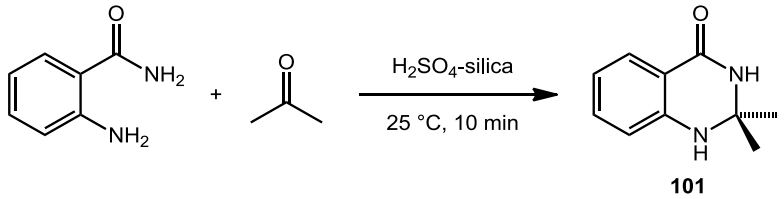

Scheme 56. H_2SO_4-silica assisted synthesis of 2,2-di-methyl quinazolin-4(3H)-one **101** (Roy and co.).[342]

Gauniyal and co-workers reported a HR-MAS NMR spectroscopy based study on the heterogeneous Cs_2CO_3 catalysed [3+3]-cyclocondensation reaction for the synthesis of pyrimido [1,2-a]indole **102** (**Scheme 57**).[343] Based on the lack of intermediate observed during the reaction, the transformation was proposed to proceed by a concerted mechanism with both N–C bonds forming simultaneously.

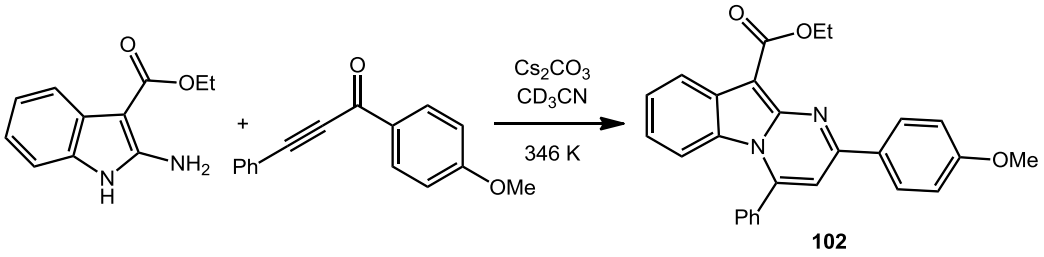

Scheme 57. Cs_2CO_3 catalysed synthesis of 2-(4-methoxyphenyl)-4-phenylpyrimido[1,2-a]indole-10-carboxylate **102** (Gauniyal and co.).[343]

4.2 Results from the in situ NMR Spectroscopy Study

The HR-MAS NMR spectroscopy was applied to monitor the direct arylation reaction of 4-iodotoluene **57** with pentafluorobenzene **56** proposed to involve a homogeneous Pd catalyst. An attempt was made to replicate the kinetic measurements previously obtained with the *in situ* FT-IR analysis by HR-MAS NMR spectroscopic analysis. Measuring out the compounds accurately as planned proved to be problematic as the maximum total volume

of the reaction mixture was constrained by the size of the rotor (*ca.* 50 µL). The use of non-deuterated DMF for stock solutions was desirable for measuring accurate substrate quantities. The resulting solvent peaks at δ 8.03, 2.93 and 2.78 affected the analysis of the ^{1}H NMR spectrum. The simultaneous subtractions of both peaks at δ 2.93 and 2.78 affected the methyl peaks at δ 2.31 used to determine the conversion of the starting material **57** to the product **58**. Attempts at subtracting the peaks individually usually affect a narrower range of the spectrum. Unfortunately, the Bruker probe attached to the solid state spectrometer did not allow sequential subtraction of the peaks. Use of stock solutions in methylene chloride-d_2 was unsuccessful, most likely due to catalyst decomposition prior to the reaction. The HR-MAS NMR spectroscopic analysis was, therefore, treated as an *operando* technique aimed at observing catalytic intermediates. The reaction condition was changed to 50 mol% $Pd(OAc)_2$ and 100 mol% PPh_3 in order to observe possible species involved in the catalytic cycle (**Scheme 58**). Once the reaction was prepared in the rotor, the first NMR spectrum was collected as soon as the spectrometer temperature was stabilised, and the peaks were shimmed appropriately. After heating at 328.4 K for 30 min, broad signals were observed at δ 7.32, 7.11 (overlapping with 4-iodotoluene **57** signal at δ 7.04) and 6.55. The peaks disappeared following the completion of the reaction. These were hypothesised to be potential intermediate species of the catalytic cycle. As a result of increased catalyst loading, the reaction rate increased and achieved quantitative conversion of 4-iodotoluene **57** to the product **58** in 83 min.

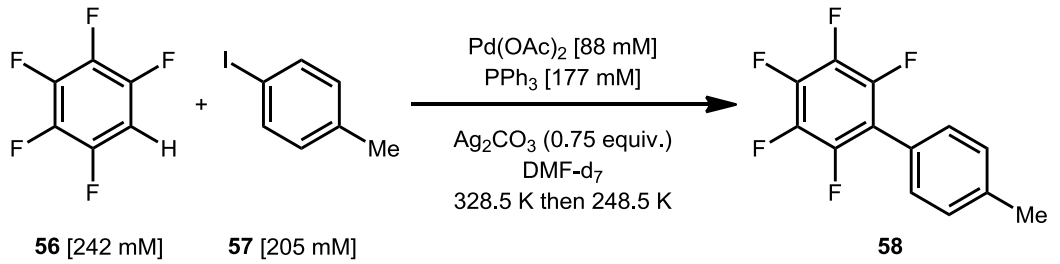

Scheme 58. Direct arylation of compound **57** monitored by HR-MAS NMR spectroscopy in DMF-d_7.

Due to the overlapping signals in the NMR spectrum of the reaction mixture, the identification of the catalytic species relied on matching the signals with isolated Pd species (*i.e.* **82a**, **83a**, **84**, **85** and **86**). However, the Pd complexes prepared for analysis contain a phenyl substituent instead of a 4-tolyl group. Therefore the experiment was continued for the reaction of pentafluorobenzene **56** with iodobenzene **81** (**Scheme 59**). The reaction mixture was studied by ^{1}H, ^{1}H-^{1}H COSY, ^{19}F, ^{31}P and ^{1}H-^{31}P HMQC NMR spectroscopic analysis at 285.0 K, 328.5 K, 308.5 K, 288.5 K, 268.5 K and 248.5 K. The reaction temperature was decreased from 328.5 K to 308.5 K after *ca.* 20% conversion of iodobenzene **81**.

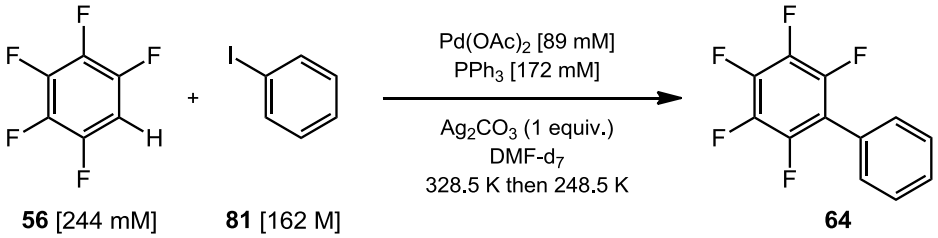

Scheme 59. Direct arylation of iodobenzene **81** with pentafluorobenzene **56** followed by HR-MAS NMR spectroscopy in DMF-d_7.

Analysis of the reaction mixture at 285.0 K revealed weak signals at δ 7.02, 6.73, 6.56 and 6.30 (**Figure 56**). Similar to the reaction of 4-iodotoluene **57**, broad signals were observed at δ 6.83 and 6.69 of the ^{1}H NMR spectrum at 328.5 K with the loss of peaks at δ 6.56 and 6.30. The peak at δ 6.73 overlapped the newly-formed broad signals. Cooling the reaction mixture to 288.5 K resulted in the reappearance of signals at δ 6.58 and 6.31, although very weak. The temperature was further lowered to 248.5 K resulting in better resolution of the broad peaks into clear triplets and the appearance of the carboxylic acid proton of the AcOH at δ 12.63. Analysis by 2D ^{1}H-^{1}H COSY NMR experiment revealed the presence of two species in the region of interest (**Figure 57**). The triplet signal at δ 6.75 was correlated with the other triplet at δ 6.91 and to a signal at δ 7.29 overlapping with other aromatic signals. A second species was observed with correlation between weak signals at δ 6.29 and 6.53. These upfield aromatic signals were assigned to the sp^2 protons of arene bound to a Pd metal with shielding from π-stacking interaction with PPh_3 ligands.[344-346]

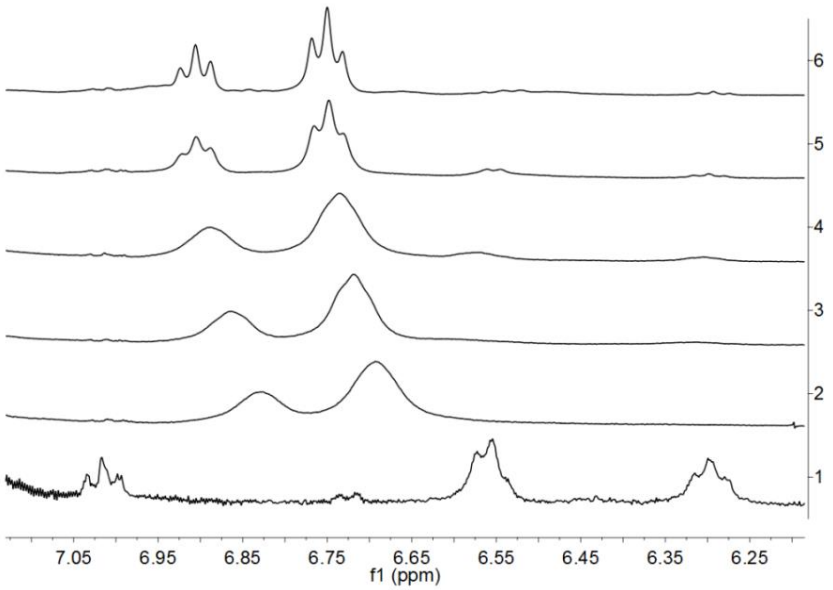

Figure 56. Stacked ^{1}H NMR spectra of the reaction shown in **Scheme 59** at **(1)** 285 K (t = 0 min), **(2)** 328 K (t = 75 min), **(3)** 308 K (t = 110 min), **(4)** 288 K (t = 135 min), **(5)** 268 K (t = 159 min) and **(6)** 248 K t = 238 min). Note t is the time since the first NMR spectrum was recorded and not the reaction time.

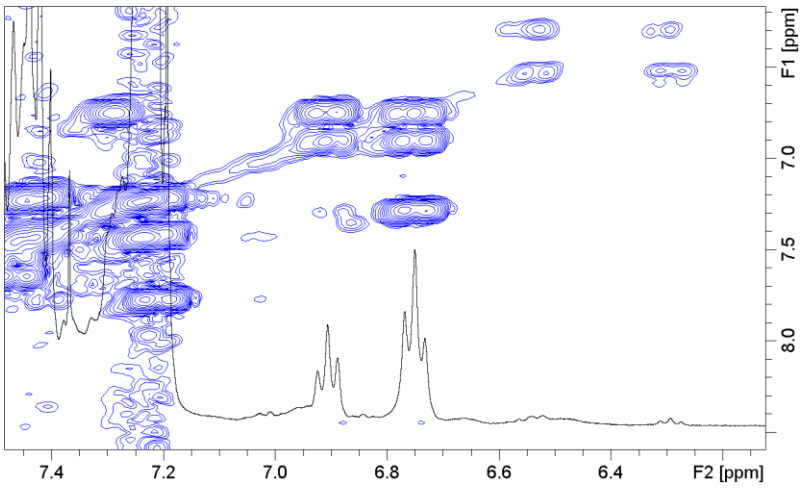

Figure 57. 2D ^{1}H-^{1}H COSY NMR spectrum of the reaction shown in **Scheme 59** at 248.5 K.

The movement of phosphines during the reaction was monitored by ^{31}P NMR spectroscopic analysis (**Figure 58**). The signal of the free PPh_3 (δ −0.5 in DMF)[257] was never observed. Upon heating the reaction to 328.5 K, the peak at δ 25.0 (assigned to $O{=}PPh_3$) increased significantly. The sharp peak at δ 14.7 (assigned to $Pd(OAc)_2(PPh_3)_2$)[347] decreased in intensity and disappeared after 1 h. Broad peaks were observed at δ 29.8 and 20.3 following the loss of sharp signals around δ 29.5 and 20.5. Cooling the reaction mixture resulted in the sharpening of these broad signals at δ 29.3 and 20.7. At 248.5 K, weak peaks were observed at δ 31.4, 26.6 and 21.1. No changes were observed to the peak at δ 25.3 and 21.5 upon cooling. Analysis by ^{1}H-^{31}P HMQC experiment was hindered by the complexity of the aromatic region of the ^{1}H NMR spectrum.

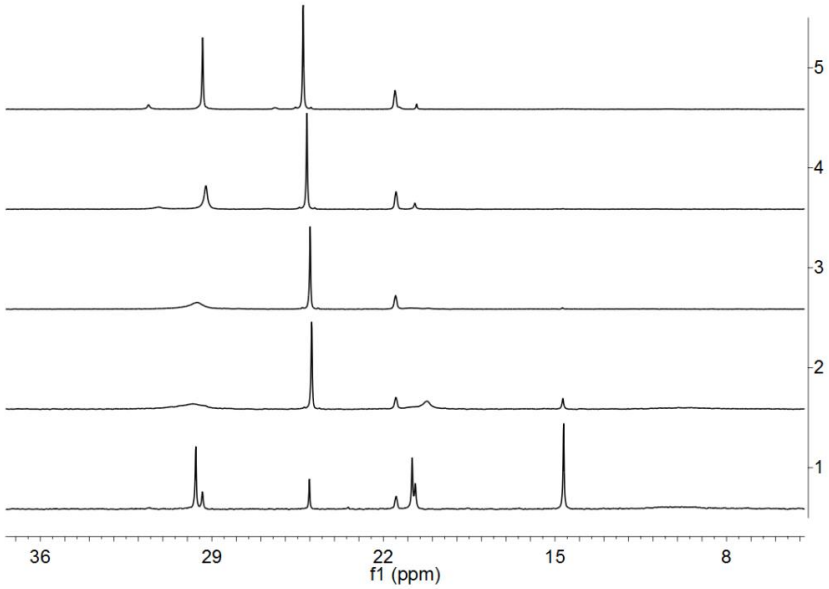

Figure 58. Stacked ^{31}P NMR spectra of the reaction shown in **Scheme 59** at **(1)** 285.0 K (t = 0 min), **(2)** 328.5 K (t = 21 min), **(3)** 328.5 K (t = 83 min), **(4)** 288.5 K (t = 138 min) and **(5)** 248.5 K (t = 243 min). Note t is the time since the first NMR spectrum was recorded and not the reaction time.

In order to replicate the conditions in which the NMR spectra were collected for the reaction mixture, the Pd species in DMF-d_7 were analysed at 285.0 K, 328.5 K, 308.5 K, 288.5 K, 268.5 K and 248.5 K. Of the five Pd species analysed, [Pd(Ph)(μ-OAc)(PPh_3)]$_2$ **84** was the only complex retaining complete structural integrity after heating. Decomposition products such as O=PPh_3 were observed for other complexes. Additionally, the dinuclear [Pd(Ph)(μ-OH)(PPh_3)]$_2$ **83a** and [Pd(Ph)(μ-I)(PPh_3)]$_2$ **86** species were observed in the ^{1}H and ^{31}P NMR spectra of mononuclear Pd(Ph)(κ^1-OAc)(PPh_3)$_2$ **85** and Pd(Ph)(I)(PPh_3)$_2$ **82a** complexes respectively. Despite the differing extents of decomposition observed, the chemical shifts of the complexes in DMF-d_7 at 248.5 K were successfully determined (**Table 30**). Comparing the phenyl protons of the Pd complexes with the intermediate observed during the reaction, it was revealed that the reaction mixture most likely contained [Pd(Ph)(μ-OAc)(PPh_3)]$_2$ **84** with trace quantities of Pd(Ph)(κ^1-OAc)(PPh_3)$_2$ **85** (**Figure 59**). The ^{31}P NMR signals of the dinuclear and the mononuclear acetate species were also observed in the reaction mixture (**Figure 60**). It is noted that the monotriphenylphosphine ligated complex Pd(Ph)(κ^2-OAc)(PPh_3) was not synthesised as isolated complex and the ^{1}H and ^{31}P NMR chemical shifts in DMF were not known.

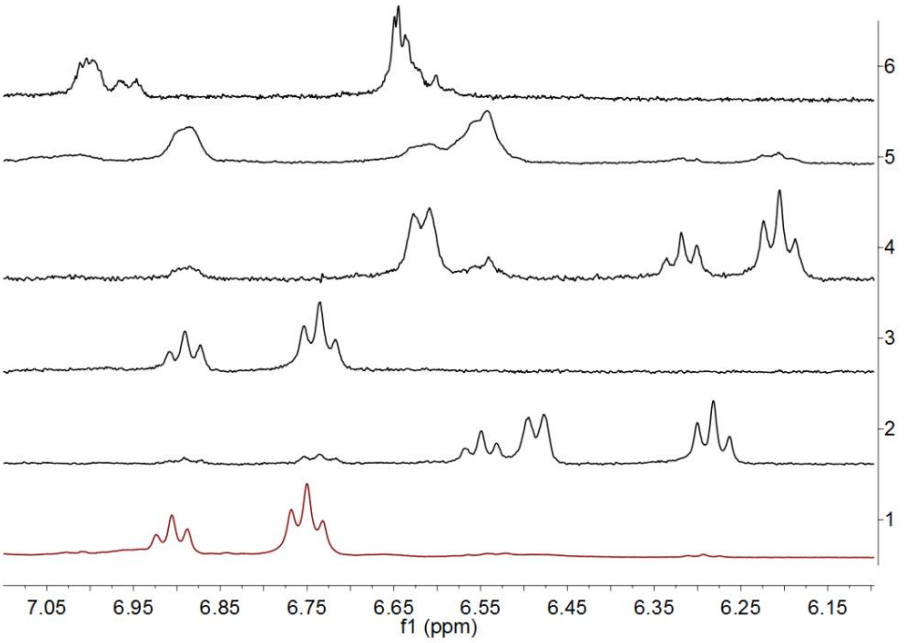

Figure 59. Stacked ^{1}H NMR spectra at 248.5 K of **(1)** the reaction shown in **Scheme 59**, **(2)** Pd(Ph)(κ^1-OAc)(PPh_3)$_2$ **85** in DMF-d_7, **(3)** [Pd(Ph)(μ-OAc)(PPh_3)]$_2$ **84** in DMF-d_7, **(4)** Pd(Ph)(I)(PPh_3)$_2$ **82a** in DMF-d_7, **(5)** [Pd(Ph)(μ-I)(PPh_3)]$_2$ **86** in DMF-d_7 and **(6)** [Pd(Ph)(μ-OH)(PPh_3)]$_2$ **83a** in DMF-d_7.

Table 30. ^{1}H and ^{31}P NMR characterisation of Pd species in DMF-d_7 at 248.5 K.

Entry	Complex	Nucleus	
		^{1}H / δ	**^{31}P** / δ
1 [a]	Pd(Ph)(κ^1-OAc)(PPh_3)$_2$ **85**	7.50–7.37 (30 H, m, PPh_3), 6.55 (1 H, t, *J* = 7.28 Hz, 4-CH), 6.49 (2 H, d, *J* = 7.52 Hz, Ph), 6.28 (2 H, t, *J* = 7.40 Hz, Ph), 0.81 (3 H, s, CH_3)	20.6 (s)
2	[Pd(Ph)(μ-OAc)(PPh_3)]$_2$ **84**	7.46 (8 H, t, *J* = 6.98 Hz, PPh_3), 7.28–7.18 (23 H, m, PPh_3+Ph), 6.89 (2 H, t, *J* = 7.10 Hz, 4-CH), 6.74 (4 H, t = 7.12 Hz, Ph), 1.13 (6 H, s, CH_3)	29.3 (s)
3 [a]	Pd(Ph)(I)(PPh_3)$_2$ **82a**	7.57–7.34 (30 H, m, PPh_3), 6.62 (2 H, d, *J* = 7.60 Hz, Ph), 6.32 (1 H, t, *J* = 7.02 Hz, 4-CH), 6.21 (1 H, t, *J* = 7.32 Hz, Ph)	33.2 (s), 22.9 (s)
4 [a, b]	[Pd(Ph)(μ-I)(PPh_3)]$_2$ **86**	7.46–7.38 (30 H, m, PPh_3), 6.91–6.87 (2 H, m, Ph), 6.62–6.53 (4 H, m, Ph), 5.91–5.90 (2 H, m , Ph)	23.9 (s)
5 [a]	[Pd(Ph)(μ-OH)(PPh_3)]$_2$ **83a**	7.53–7.38 (30 H, m, PPh_3), 7.01–6.94 (4 H, m, Ph), 6.65–6.60 (6 H, m, Ph), −0.66 to −0.67 (0.6 H, m, *cis*-OH), −1.88 (1.5 H, d, J = 2.96 Hz, *trans*-OH), −3.17 to −3.19 (0.6 H, m, *cis*-OH)	33.2 (s), 32.7 (s)
6	iodobenzene **81**	7.77 (2H, d, *J* = 7.0 Hz, 2,6-H), 7.43 (1H, t, *J* = 7.5 Hz, 4-CH), 7.22 (2H, t, *J* = 7.5 Hz, 3,5-CH)	N/A
7	pentafluorobenzene **56**	7.91 (m, CH)	N/A
8	product **64**	7.64–7.55 (m, Ph)	N/A

[a] Decomposition observed. [b] Complex was poorly soluble in DMF-d_7.

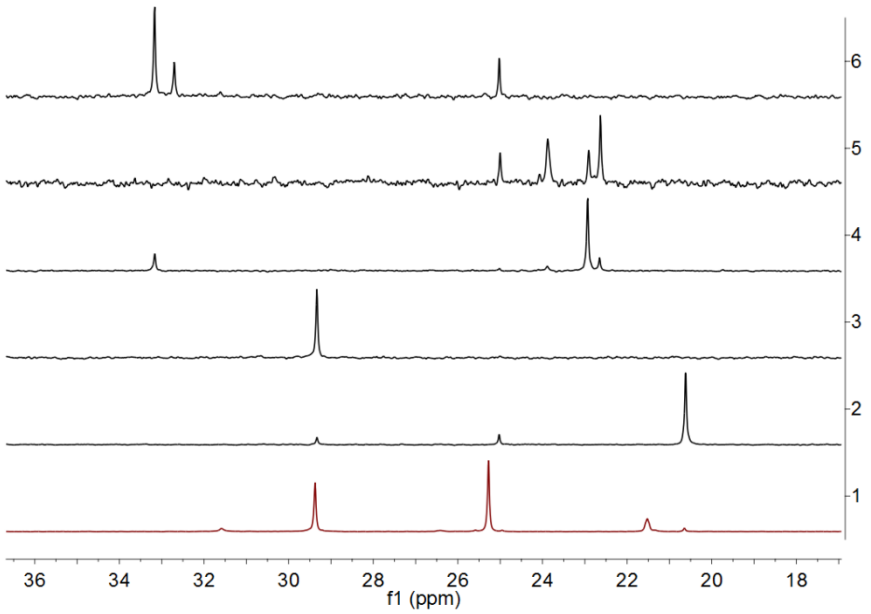

Figure 60. Stacked ^{31}P NMR spectra at 248.5 K of **(1)** the reaction shown in **Scheme 59**, **(2)** Pd(Ph)(κ^1-OAc)(PPh$_3$)$_2$ **85** in DMF-d$_7$, **(3)** [Pd(Ph)(μ-OAc)(PPh$_3$)]$_2$ **84** in DMF-d$_7$, **(4)** Pd(Ph)(I)(PPh$_3$)$_2$ **82a** in DMF-d$_7$, **(5)** [Pd(Ph)(μ-I)(PPh$_3$)]$_2$ **86** in DMF-d$_7$ and **(6)** [Pd(Ph)(μ-OH)(PPh$_3$)]$_2$ **83a** in DMF-d$_7$.

The ^{31}P NMR spectrum of the reaction mixture confirmed the presence of the dinuclear [Pd(Ph)(μ-OAc)(PPh$_3$)]$_2$ **84** and the mononuclear Pd(Ph)(κ^1-OAc)(PPh$_3$)$_2$ **85** species. Indeed, the well-resolved phenyl ring proton signals of [Pd(Ph)(μ-OAc)(PPh$_3$)]$_2$ **84** in DMF-d$_7$ at 328.5 K were broadened when the dinuclear complex was used as the catalyst for the reaction (**Scheme 60**). It was likely that the [Pd(Ph)(μ-OAc)(PPh$_3$)]$_2$ **84** involved in the reaction was in equilibrium with the mononuclear analogue. Furthermore, the use of dinuclear [Pd(Ph)(μ-OAc)(PPh$_3$)]$_2$ **84** as the catalyst for the direct arylation reaction of 4-iodotoluene **81** yielded a mixture of two biaryl products (*i.e.* **58** and **64**). Therefore, the dinuclear Pd complexes was able to react with pentafluorobenzene **56** to form the phenyl-biaryl product **64** and then to work as the catalyst to turn over 4-iodotoluene **57** to form the 4-tolyl-biaryl product **58**.

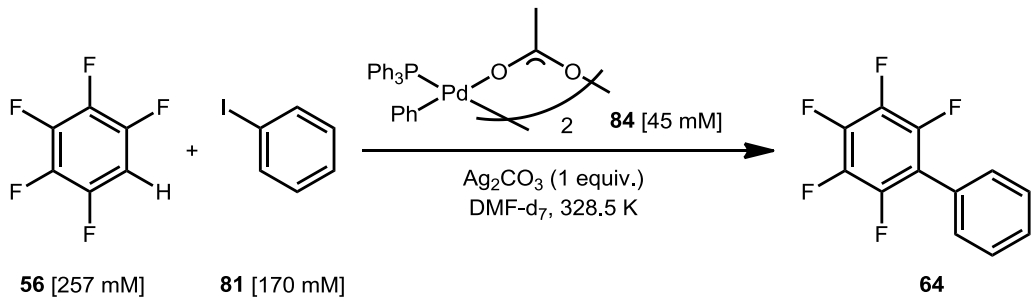

Scheme 60. Direct arylation reaction of iodobenzene **81** with pentafluorobenzene **56** catalysed by [Pd(Ph)(μ-OAc)(PPh$_3$)]$_2$ **84**.

The reaction was repeated with added PPh_3 to determine the reason for rate acceleration with increased PPh_3. The addition of 0.25 equivalents of PPh_3 resulted in the increased formation of mononuclear Pd(Ph)(κ^1-OAc)(PPh_3)$_2$ **85** as the major species with the dinuclear species **84** becoming the minor species as observed by ^{1}H NMR spectroscopic analysis (**Figure 61**). The reaction achieved 25% conversion after 1 h, confirming the rate acceleration compared to the 12% conversion achieved in the absence of added PPh_3. Increasing the quantity of PPh_3 to 0.75 equivalents resulted in increased formation of Pd(Ph)(κ^1-OAc)(PPh_3)$_2$ **85** and accelerated the reaction rate significantly (*i.e.* 57% conversion after 20 min). The addition of 0.65 equivalents of O=PPh_3 did not result in the formation of mononuclear species (**Figure 62** and **Figure 63**).

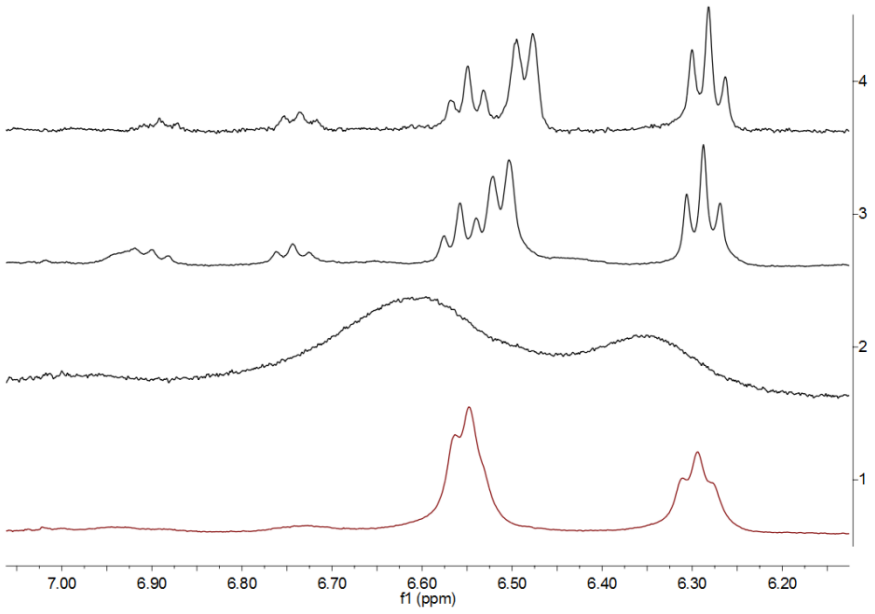

Figure 61. Stacked ^{1}H NMR spectra of the reaction shown in **Scheme 60** with 0.25 equivalents of PPh_3 added. Spectra recorded at **(1)** 285.0 K, **(2)** 328.5 K and **(3)** 248.5 K. **(4)** Pd(Ph)(κ^1-OAc)(PPh_3)$_2$ **85** in DMF-d_7 at 248.5 K.

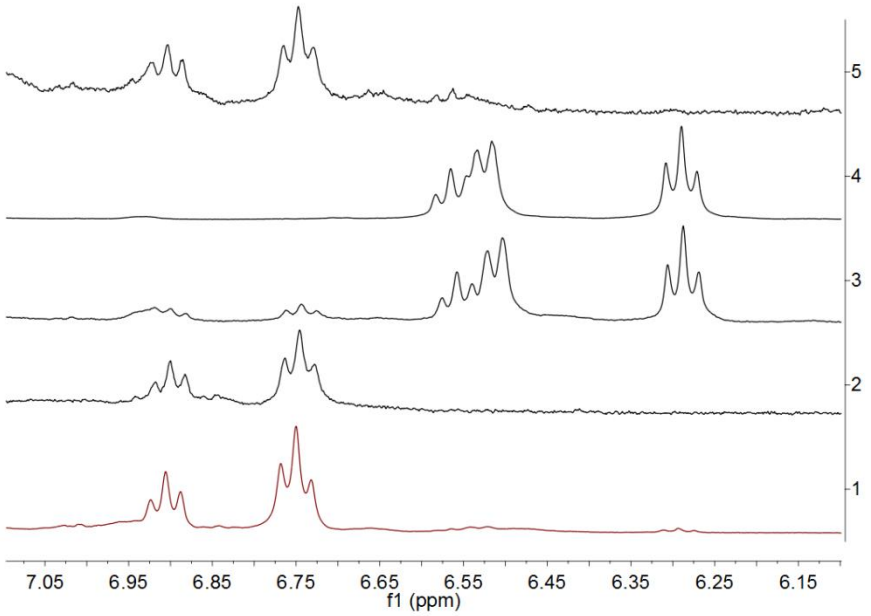

Figure 62. Stacked ^{1}H NMR spectra of the reaction mixtures at 248.5 K in DMF-d_7. Reaction catalysed by **(1)** 50 mol% $Pd(OAc)_2$ + 100 mol% PPh_3, **(2)** 25 mol% $[Pd(Ph)(\mu\text{-}OAc)(PPh_3)]_2$ **84**, **(3)** 25 mol% $[Pd(Ph)(\mu\text{-}OAc)(PPh_3)]_2$ **84** + 25 mol% PPh_3, **(4)** 25 mol% $[Pd(Ph)(\mu\text{-}OAc)(PPh_3)]_2$ **84** + 75 mol% PPh_3 and **(5)** 25 mol% $[Pd(Ph)(\mu\text{-}OAc)(PPh_3)]_2$ **84** + 65 mol% $O{=}PPh_3$.

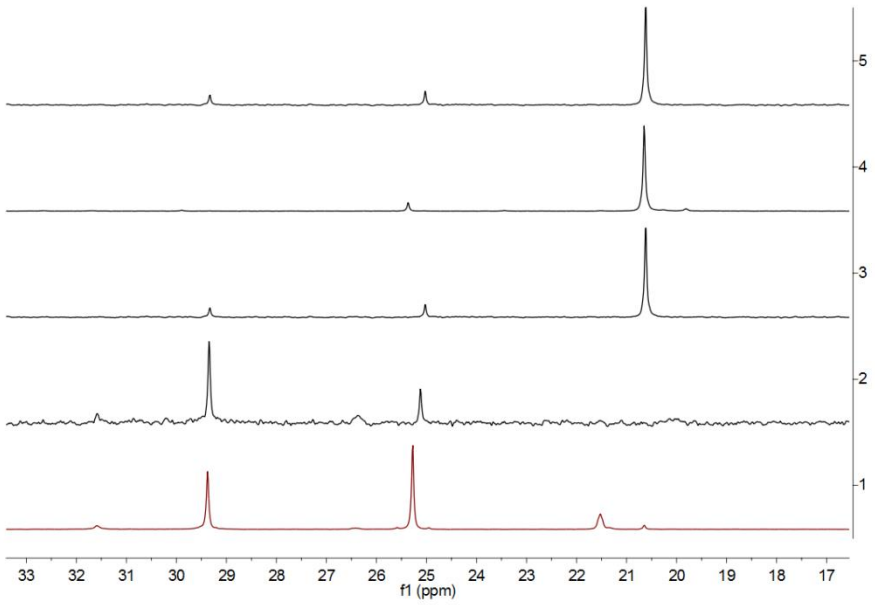

Figure 63. Stacked ^{31}P NMR spectra of the reaction mixtures at 248.5 K in DMF-d_7. Reactions catalysed by **(1)** 50 mol% $Pd(OAc)_2$ + 100 mol% PPh_3, **(2)** 25 mol% $[Pd(Ph)(\mu\text{-}OAc)(PPh_3)]_2$ **84**, **(3)** 25 mol% $[Pd(Ph)(\mu\text{-}OAc)(PPh_3)]_2$ **84** + 25 mol% PPh_3 and **(4)** 25 mol% $[Pd(Ph)(\mu\text{-}OAc)(PPh_3)]_2$ **84** + 75 mol% PPh_3. **(5)** $Pd(Ph)(\kappa^1\text{-}OAc)(PPh_3)_2$ **85** in DMF-d_7.

A mixture of $Pd(OAc)_2$ and $2PPh_3$ in DMF-d_7 was analysed. Unexpectedly, the peaks assigned to species $[Pd(Ph)(\mu\text{-}OAc)(PPh_3)]_2$ **84** were observed in addition to other peaks formed in the reaction mixture by ^1H and ^{31}P NMR spectroscopic analysis after heating at 328.5 K. The presence of tetraphenylphosphonium cation **103** was observed by LIFDI-MS (*m/z* 339.18). The formation of the Pd-phenyl bond most likely resulted from the oxidative addition of $[Ph\text{-}PPh_2OAc]^+$, generated from reduction of $Pd(OAc)_2(PPh_3)_2$ complex formed *in situ*.[194] The resulting $Pd(Ph)(OAc)(PPh_3)$ **51** complex would be capable of forming the dinuclear $[Pd(Ph)(\mu\text{-}OAc)(PPh_3)]_2$ **84** or lose PPh_4^+ **103** via reductive elimination.

The reaction catalysed by $Pd(Ph)(I)(PPh_3)_2$ **82a** was monitored by NMR spectroscopic analysis (**Scheme 61**). The 2D ^1H-^1H COSY NMR spectrum indicates the presence of two species in the reaction mixture (**Figure 64**). Singlet signals were observed in the ^{31}P NMR spectrum at δ 32.6, 29.9, 25.2, 23.4, 20.3 and 19.8. The species observed were neither $[Pd(Ph)(\mu\text{-}OAc)(PPh_3)]_2$ **84** nor $Pd(Ph)(\kappa^1\text{-}OAc)(PPh_3)_2$ **85** observed in the reaction catalysed by $Pd(OAc)_2$ and $2PPh_3$ (**Figure 65**). The peak for $Pd(Ph)(I)(PPh_3)_2$ **82a** were not observed, suggesting that the reaction was catalysed by species generated *in-situ*.

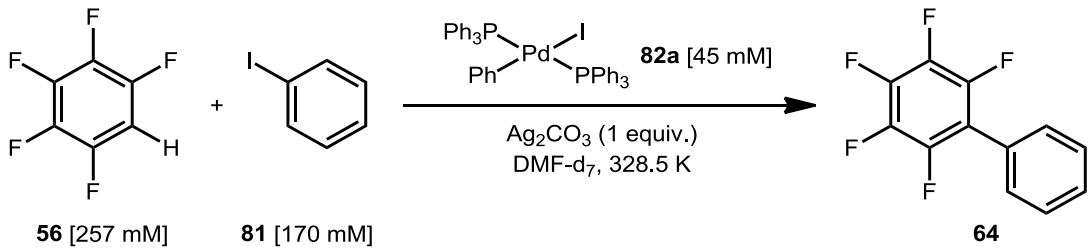

56 [257 mM] **81** [170 mM] **64**

Scheme 61. Direct arylation reaction of iodobenzene **81** with pentafluorobenzene **56** catalysed by $Pd(Ph)(I)(PPh_3)_2$ **82a**.

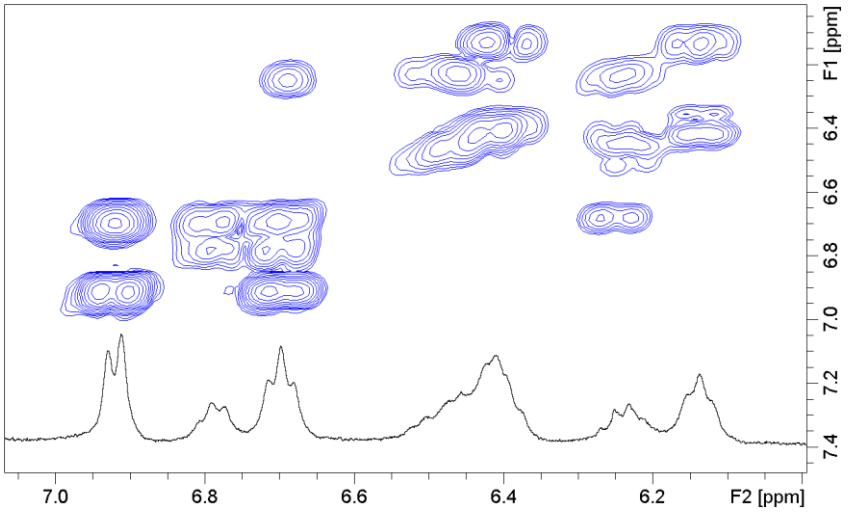

Figure 64. 2D ^1H-^1H COSY NMR spectrum of the reaction shown in **Scheme 61** at 248.5 K.

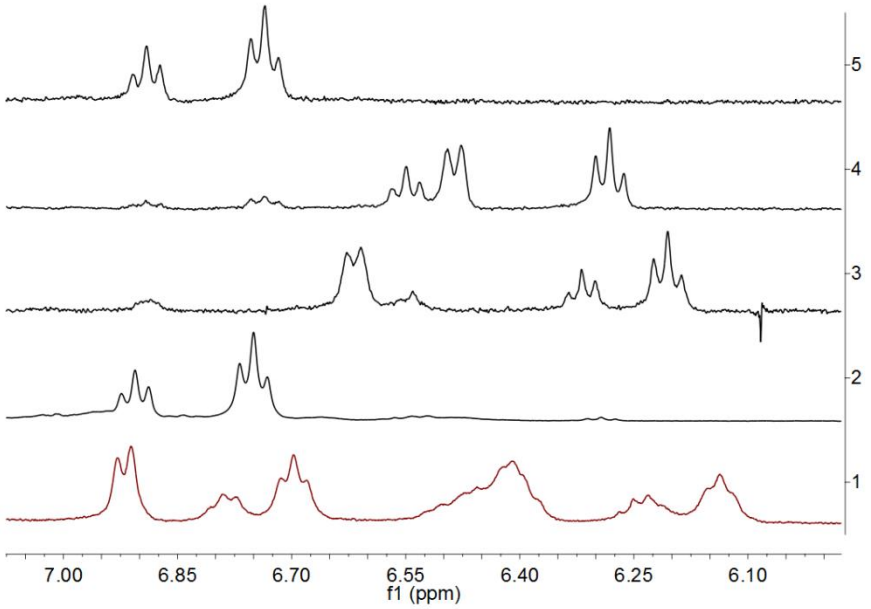

Figure 65. Stacked ^{1}H NMR spectra in DMF-d_7 at 248.5 K. **(1)** Reaction catalysed by Pd(Ph)(I)$(PPh_3)_2$ **82a**, **(2)** reaction catalysed by $Pd(OAc)_2$ and $2PPh_3$, **(3)** Pd(Ph)(I)$(PPh_3)_2$ **82a** in DMF-d_7, **(4)** Pd(Ph)(κ^1-OAc)$(PPh_3)_2$ **85** in DMF-d_7 and **(5)** [Pd(Ph)(μ-OAc)$(PPh_3)]_2$ **84** in DMF-d_7.

4.3 Mass Spectrometry Studies in the Literature

Electrospray ionization mass spectrometry (ESI-MS) has been extensively applied to the mechanistic study of homogeneous catalysis. The technique allows for a fast, selective detection of low concentration charged species in a complex reaction system. Identification of Pd-containing species is made easier by the characteristic isotopic distribution with ^{106}Pd being the most abundant isotope. The charged or chargeable species may be an inherent part of the reaction, formed inadvertently, or introduced as charge tag.[348] It must be noted that the detection of neutral species requires alternative techniques such as liquid injection field desorption ionisation mass spectrometry (LIFDI-MS).[349]

Sabino and co-workers applied ESI(+)-MS in the mechanistic study of the Mizoroki-Heck reaction of aryldiazonium salts **105** with olefin **104** (**Scheme 62**).[350] Key cationic intermediates such as the σ-aryl Pd^{II} oxidative addition products and the species prior, and post β-hydride elimination were detected successfully. Furthermore, a time-dependent dynamic ligand exchange equilibria was observed between the different oxidative addition products (*i.e.* $[Pd^{II}(Ar)(CH_3CN)_3]^+$, $[Pd^{II}(Ar)(CH_3CN)(dba)]^+$ and $[Pd^{II}(Ar)(dba)_2]^+$). The addition of olefin **104** at times with maximum concentration of each species identified $[Pd^{II}(Ar)(CH_3CN)(dba)]^+$ as the most reactive species to undergo olefin **104** insertion.

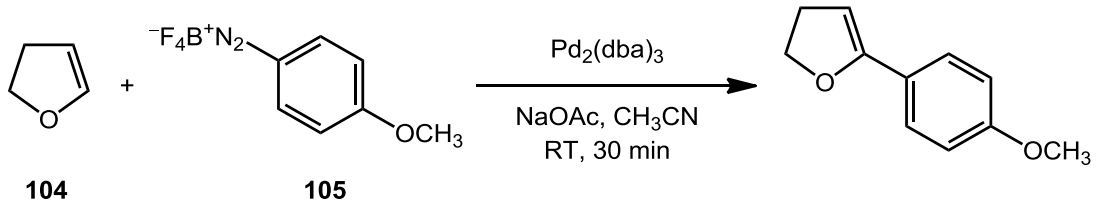

104 **105**

Scheme 62. Mizoroki-Heck reaction of olefin **104** with aryldiazonium salts **105** (Sabino and co.).[350]

Vasseur and co-workers reported ESI(+)-MS study on the dehydrogenative Mizoroki-Heck reaction of furans with acrylates.[351] Dissociation of trinuclear $Pd_2(OAc)_6$ pre-catalyst into a range of mononuclear and dinuclear Pd species was observed in the DMSO/acetate solvent system. The proposed catalytic cycle consisted of active mononuclear catalyst with the dinuclear species being off-cycle complexes. The role of dinuclear Pd species as the resting state of the catalyst was also highlighted in the ESI-MS study of the Suzuki-Miyaura reaction reported by Agrawal and co-workers.[352]

4.4 Results from the Mass Spectrometry Study

Real time analysis of the reaction mixture by HR-MAS NMR spectroscopy provided strong evidence for the involvement of dinuclear $[Pd(Ph)(\mu\text{-}OAc)(PPh_3)]_2$ **84** and mononuclear $Pd(Ph)(\kappa^1\text{-}OAc)(PPh_3)_2$ **85** complexes as catalytic intermediates. As an additional characterisation method, MS was selected for its high sensitivity compared with other analytical techniques. Although most of the catalytic species were expected to be uncharged, any iodide coordinated Pd complexes were expected to become cationic via halide loss. Furthermore, the observation of other charged species could highlight unconsidered reaction pathways. The direct arylation reaction of 4-iodotoluene **57** with pentafluorobenzene **56** under model catalytic conditions with typical reaction concentration was selected for analysis (**Scheme 63**). The experiment was run in tandem with *in situ* FT-IR spectroscopic analysis for real time kinetic data, and NMR spectroscopic analysis for kinetics and intermediate observation from the sampled aliquots of the reaction mixture. A glass syringe was used throughout to prevent contamination from plasticisers.

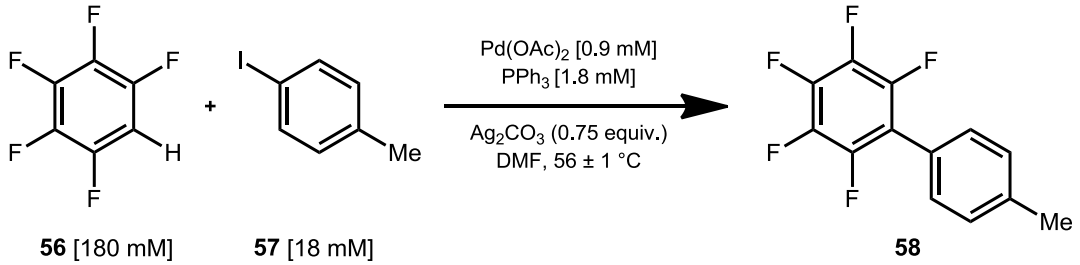

56 [180 mM] **57** [18 mM] **58**

Scheme 63. Direct arylation reaction condition selected for study by ESI-MS and LIFDI-MS.

An aliquot of the reaction mixture was collected at 22% conversion of 4-iodotoluene **57** and filtered through a Celite®-pad into two vials to give Sample 1 and Sample 2. Sample 1 was analysed without dilution and Sample 2 was diluted in acetonitrile, a molecule known to coordinate and stabilise Pd species. Both samples were analysed in positive (+) and negative (−) ion modes between *m/z* 40–1600 and *m/z* 60–1050 respectively. The spectra collected were complex and some of the signals remain unassigned.

Many cationic Pd species were observed by ESI(+)-MS (**Table 31**). In Sample 1, Pd^{II} species of $[Pd(C_6F_5)(PPh_3)]^+$ (*m/z* 534.10) and the solvent coordinated analogue (*m/z* 609.17) were detected. These complexes may have formed via AMLA pathway involving Pd^{II} species[124], or from loss of aryl group from $Pd(Ar)(C_6F_5)(PPh_3)$ during MS measurements. The oxidative addition product was observed as $[Pd(4\text{-tolyl})(PPh_3)_2]^+$ (*m/z* 721.12) with the loss of iodide. Unfortunately, the mononuclear Pd species at *m/z* 737.12, 812.19, 834.13 and 1015.21, and the dinuclear Pd species at *m/z* 993.11 and 1091.12 were not identified.

The acetonitrile-coordinated Pd species were observed for Sample 2. In addition to $[Pd(4\text{-tolyl})(PPh_3)]^+$ **60** (*m/z* 459.05), $[Pd(4\text{-tolyl})(DMF)(PPh_3)]^+$ (*m/z* 532.10) and $[Pd(4\text{-tolyl})(PPh_3)_2]^+$ (*m/z* 721.15), the oxidative addition product was detected as $[Pd(4\text{-tolyl})(CH_3CN)(PPh_3)_2]^+$ (*m/z* 500.08). The complex $[Pd(C_6F_5)(PPh_3)_2]^+$ (*m/z* 797.09) and the acetonitrile coordinated analogue (*m/z* 838.12) were also identified. The signals of mononuclear Pd species at *m/z* 737.15, 1015.24 1029.25, 1055.61, 1083.64, 1091.19 and 1293.85 were unassigned as well as the dinuclear Pd species at *m/z* 1119.09.

The quaternary phosphonium cation $[P(4\text{-tolyl})Ph_3]^+$ **60** (*m/z* 354.14) was observed in both Samples 1 and 2. This side-product was also observed in the literature for the ESI-MS study of a Pd-catalysed oxyarylation reaction of olefins in the presence of Ag_2CO_3.[353] The analysis by ESI(−)-MS was less successful. In Sample 1, mononuclear Pd species were observed at *m/z* 738.93, 770.90 and 868.94, but remained unassigned. Similarly, the mononuclear Pd species of Sample 2 at *m/z* 606.88, 868.96 were unassigned. The signal at *m/z* 501.89 was attributed to $[(Pd(CH_3CN)_2(I)_2(CO_3)]^-$ with the negative charge on the carbonate ligand. The formation of pentacoordinated anionic Pd species $[Pd^{II}(Ph)(I)(OAc)(PPh_3)_2]^-$ in the reaction mixture, starting with $Pd(OAc)_2$ pre-catalyst in DMF, was reported by Amatore and co-workers.[147] The formation of tricoordinated Pd^0 complexes with the formula $[Pd(X)(PPh_3)_2]^-$ (where X = halide, acetate and aryl anions) was also reported in the same study.

Table 31. The *m/z* of Pd-containing species detected by ESI(+)-MS and possible assignments.

Sample *	Observed *m/z*	Assignment
1	534.10	$[Pd(C_6F_5)(PPh_3)]^+$
	556.05	$[Pd(CO_3H_2)(I)(PPh_3)]^+$
	609.17	$[Pd(C_6F_5)(DMF)(PPh_3)]^+$
	721.12	$[Pd(4\text{-tolyl})(PPh_3)_2]^+$
2	459.05	$[Pd(4\text{-tolyl})(PPh_3)]^+$ **60**
	500.08	$[Pd(4\text{-tolyl})(CH_3CN)(PPh_3)]^+$
	532.10	$[Pd(4\text{-tolyl})(DMF)(PPh_3)]^+$
	721.15	$[Pd(4\text{-tolyl})(PPh_3)_2]^+$
	797.09	$[Pd(C_6F_5)(PPh_3)_2]^+$
	838.12	$[Pd(C_6F_5)(CH_3CN)(PPh_3)_2]^+$

* Sample 1 was analysed without dilution whereas Sample 2 was diluted in CH_3CN.

Vikse and co-workers reported the use of a charged substrate **107** (*i.e.* 4-iodobenzyltriphenylphosphonium hexafluorophosphate) to continuously monitor the copper-free Sonogashira reaction in real time using ESI-MS to obtain kinetic information.[354] The charge tag and the counter-ion were selected for minimum interference with the reaction while providing a strong signal. The compound **107** was synthesised following the literature procedure from 4-iodobenzyl bromide **106** (**Scheme 64**).

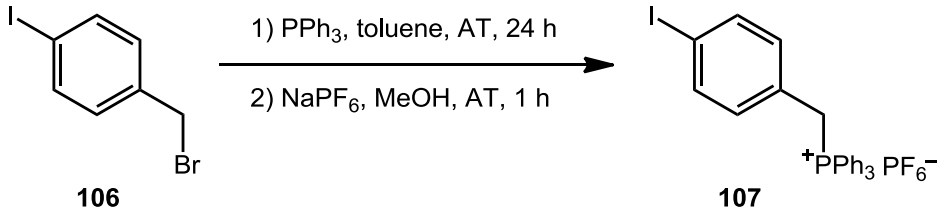

106 **107**

Scheme 64. Synthesis of 4-iodobenzyltriphenylphosphonium hexafluorophosphate **107**.

This cationic aryl phosphonium salt **107** was used instead of 4-iodotoluene **57** to improve the MS sensitivity of the intermediates and simplify the spectrum obtained (**Scheme 65**). However, the reaction of this substrate with pentafluorobenzene **56** proved to be low-yielding and slow under the standard reaction conditions. This may be due to interaction between the phosphonium salt and the Pd metal centre. An aliquot of the reaction mixture after 1 day of heating was analysed. The starting material **107** and the product **108** were observed as well as the oxidative addition Pd complex **109** (*m/z* 847.04) and the biaryl Pd complex **110** (*m/z* 887.13). These two complexes were the only Pd-containing species observed.

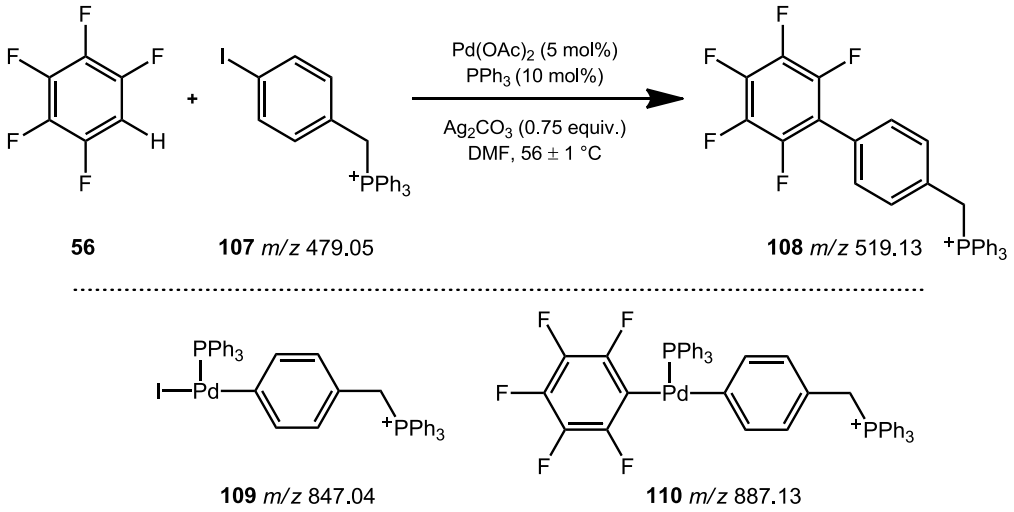

Scheme 65. Direct arylation reaction of 4-iodobenzyltriphenylphosphonium hexafluorophosphate **107** with pentafluorobenzene **56** to give the product **108**. Reaction intermediates containing Pd were observed as *m/z* 845.03 for **109** and *m/z* 885.11 for **110**.

The detection of uncharged Pd species in the reaction mixture required analysis by LIFDI-MS (*m/z* 30–1400). Identical reaction condition as the ESI-MS study was applied with the reaction progress monitored by *in situ* FT-IR and NMR spectroscopy (**Scheme 63**). The sampled reaction mixtures were injected directly into the MS without dilution as LIFDI-MS is less sensitive compared with ESI-MS. A total of six aliquots were collected at different stages of the experiment to obtain time-dependent data on the reaction composition (**Table 32**).

The first sample analysed was a solution of 4-iodotoluene **57**, $Pd(OAc)_2$ and PPh_3 in DMF (Entry 1). A series of tetra-aryl phosphonium cations $[PPh_4]^+$ **103**, $[P(4\text{-tolyl})Ph_3]^+$ **60**, $[P(4\text{-tolyl})_2Ph_2]^+$ and $[P(4\text{-tolyl})_3Ph]^+$ were detected, most likely from oxidative addition and reductive elimination of 4-iodotoluene **57** and different phosphine species to the Pd metal centre. The addition of Ag_2CO_3 and heating the mixture to 56 ± 1 °C resulted in the formation of Pd-tolyl species in addition to the phosphonium cations already observed (Entry 2). The Pd-tolyl species identified were the 4-tolyl analogues of the dinuclear $[Pd(Ph)(\mu\text{-OAc})(PPh_3)]_2$ **84** and mononuclear $Pd(Ph)(\kappa^1\text{-OAc})(PPh_3)_2$ **85** complexes previously observed by NMR spectroscopic analysis of the reaction between iodobenzene **81** and pentafluorobenzene **56**. Additionally, signals matching the *m/z* values and the isotopic pattern of anionic $[Pd(OAc)(PPh_3)_2]^-$ and $Pd(4\text{-tolyl})(\kappa^1\text{-OAc})(PPh_3)$–$Pd(PPh_3)$ complexes were detected. The mononuclear $Pd(4\text{-tolyl})(OAc)(PPh_3)$ species was still observed 5 min and 60 min into the reaction following the addition of pentafluorobenzene **56** (Entries 3 and 4). However, the signals for the dinuclear $Pd(4\text{-tolyl})(\kappa^1\text{-OAc})(PPh_3)$–$Pd(PPh_3)$ was very weak for the latter aliquot and $[Pd(4\text{-tolyl})(\mu\text{-OAc})(PPh_3)]_2$ **84b** was not

observed. The only phosphonium species observed at this stage of the reaction was [P(4-tolyl)Ph_3]$^+$ **60**. Signals matching the *m/z* of Pd(C_6F_5)(OAc)(PPh_3) and Pd(C_6F_5)(OAc)(PPh_3)$_2$ were observed after the reaction was complete (Entry 5). Analysis of the reaction mixture 40 min afterwards indicated the presence of Pd(C_6F_5)(OAc)(PPh_3), Pd(C_6F_5)$_2$(PPh_3)$_2$, and other high *m/z* Pd species that were not assigned (Entry 6). Phosphine species of P(4-tolyl)Ph_2 and [P(4-tolyl)Ph_3]$^+$ **60** were observed during and after the reaction. The formation of aryl phosphine species with a mixture of phenyl and 4-tolyl substituents is expected to result from an aryl-aryl exchange reaction between the phenyl group from the phosphine ligand and the aryl group from the oxidative addition product of the 4-iodotoluene **57** to Pd^0 metal centre (**Scheme 66**).[355] The oxidative addition and reductive elimination of the quaternary phosphonium cations must be in equilibrium to account for the formation of [P(Ph)(4-tolyl)$_3$]$^+$. Kong and co-workers have reported the reaction of Pd(4-tolyl)(I)(PPh_3)$_2$ and PPh_3 in $CDCl_3$ at 60 °C to give Pd(Ph)(I)(PPh_3)$_2$ **82a** and P(4-tolyl)Ph_2 in 90% conversion.[356] The side-reaction has been problematic for some transition metal catalysed reactions starting with Pd^0 pre-catalysts such as Pd(PPh_3)$_4$ and Pd_2(dba)$_3$.[357-359] Electron donating substituents on the aryl substituents favour the formation of quaternary phosphonium cations, most likely due to positive charge stabilisation.

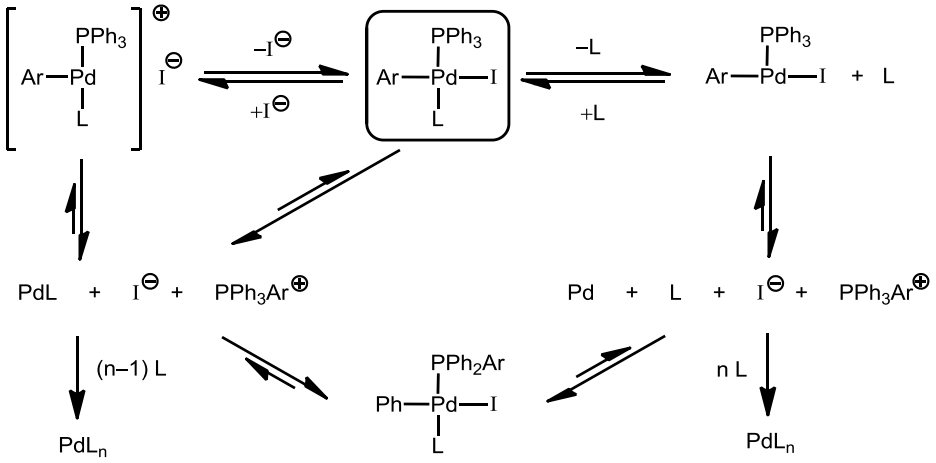

Scheme 66. Mechanism for aryl-aryl exchange reaction proposed by Goodson and co.[355]

For the reaction of iodobenzene **81** with pentafluorobenzene **56**, the phenyl group of the substrate is expected to scramble with the phenyl rings of PPh_3. Facile equilibriation of the Pd-aryl/P-aryl interchange reaction of Pd(C_6D_5)(I)(Ph_3P)$_2$ and PPh_3 in DMF has been reported by Grushin and co-workers.[360] However, the scrambled side-product **64** (*i.e.* 2,3,4,5,6-pentafluorobiphenyl) for the reaction of 4-iodotoluene **57** was never observed by ^{19}F NMR spectroscopic analysis. This is surprising considering the oxidative addition and reductive elimination of the quaternary phosphonium cations (*i.e.* [PPh_4]$^+$ **103** and [P(4-tolyl)Ph_3]$^+$ **60**) were understood to be in equilibrium.[185] Therefore these cationic species

must only exist in trace quantity during the reaction or result as the by-product of MS analysis.

Table 32. Aliquot collection time and species identified by LIFDI-MS of reaction shown in **Scheme 63**.

Entry	Collection Timing	Observed *m/z*	Assignment
1	T = 19 ± 1 °C before heating	339.05 353.05 367.08 381.11	$[PPh_4]^+$ **103** $[P(4\text{-tolyl})Ph_3]^+$ **60** $[P(4\text{-tolyl})_2Ph_2]^+$ $[P(4\text{-tolyl})_3Ph]^+$
2	T = 56 ± 1 °C t = 0 before C_6F_5H **56** addition	339.05 353.07 367.09 381.11 518.03 689.03 885.95 1038.11	$[PPh_4]^+$ **103** $[P(4\text{-tolyl})Ph_3]^+$ **60** $[P(4\text{-tolyl})_2Ph_2]^+$ $[P(4\text{-tolyl})_3Ph]^+$ $Pd(4\text{-tolyl})(OAc)(PPh_3)$ $Pd(OAc)(PPh_3)_2$ $Pd(4\text{-tolyl})(\kappa^1\text{-OAc})(PPh_3)\text{–}Pd(PPh_3)$ $[Pd(4\text{-tolyl})(\mu\text{-OAc})(PPh_3)]_2$ **84b**
3	T = 56 ± 1 °C t = 6 min 5% conversion of 4-iodotoluene **57**	353.12 518.05 886.94 1038.16	$[P(4\text{-tolyl})Ph_3]^+$ **60** $Pd(4\text{-tolyl})(OAc)(PPh_3)$ $Pd(4\text{-tolyl})(\kappa^1\text{-OAc})(PPh_3)\text{–}Pd(PPh_3)$ $[Pd(4\text{-tolyl})(\mu\text{-OAc})(PPh_3)]_2$ **84b**
4	T = 56 ± 1 °C t = 47 min 60% conversion of 4-iodotoluene **57**	277.98 353.02 517.96 887.88	$P(4\text{-tolyl})Ph_2$ $[P(4\text{-tolyl})Ph_3]^+$ **60** $Pd(4\text{-tolyl})(OAc)(PPh_3)$ $Pd(4\text{-tolyl})(\kappa^1\text{-OAc})(PPh_3)\text{–}Pd(PPh_3)$
5	T = 56 ± 1 °C t = 86 min quant. conversion of 4-iodotoluene **57**	277.98 353.04 593.90 856.02	$P(4\text{-tolyl})Ph_2$ $[P(4\text{-tolyl})Ph_3]^+$ **60** $Pd(C_6F_5)(OAc)(PPh_3)$ $Pd(C_6F_5)(\kappa^1\text{-OAc})(PPh_3)_2$
6	T = 56 ± 1 °C t = 126 min quant. conversion of 4-iodotoluene **57**	277.98 353.01 593.92 963.96	$P(4\text{-tolyl})Ph_2$ $[P(4\text{-tolyl})Ph_3]^+$ **60** $Pd(C_6F_5)(OAc)(PPh_3)$ $Pd(C_6F_5)_2(PPh_3)_2$

4.5 Stoichiometric Reaction of the Pd Complexes

The relevance of potential reaction intermediates are often examined by studying the reactivity of the isolated suspect species as reactants under stoichiometric reactions conditions.[205] In these experiments, the ability of one intermediate to form another is tested. Furthermore, the reaction kinetics of the key intermediate involved in the RL-step is expected to be consistent with the actual reaction under catalysis. Reactivity of Pd^0 and Pd^{II} complexes under representative conditions for key elementary steps of the C–C bond forming catalytic cycles have been reported for oxidative addition[361, 362], *cis-trans* isomerisation[363, 364], transmetalation[105, 242, 365-370], and reductive elimination[371-375] reactions. Reactions studied independently at stoichiometric quantity may differ from those of real catalysis, with overlooked intermediates and innocent species outside of the catalytic cycle.[100] However, such stoichiometric reactions can provide valuable insight into the possible reactive species and, ultimately, the mechanism.

A series of dinuclear and mononuclear Pd species potentially involved in the catalytic cycle were synthesised following literature procedures (see Chapter 2.6). These dinuclear and mononuclear Pd species were all possible intermediates of the catalytic cycle of interest. In catalysis, a dinuclear transition metal complex is often considered as a potential source of the active catalyst complex. However, a dinuclear chloride bridged Pd complex has been proposed by Harakat and co-workers as the active catalyst for the Wacker oxidation of alkenes based on an ESI-MS study.[209] The kinetics studied by GC showed between first- and second-order dependence on the catalyst concentration. In another study, a computational DFT calculation was applied to show dinuclear Pd^{II} as the active catalyst.[376] The μ-OH complex **83a** may form *in situ* from the water present in the DMF used as the solvent. The μ-I complex **86** can form following oxidative addition of iodobenzene **81**. The μ-OAc complex **84** was the hypothesised off-cycle dinuclear Pd species in equilibrium with the active, monomeric Pd complex. Based on the ^{31}P NMR spectra of the three Pd complexes in methylene chloride-d_2, the broad signal of iodo-bridged complex **86** suggested it was easier to cleave than the hydroxo-bridged **83a** or the acetato-bridged **84** complexes. This observation was consistent with the lack of dinuclear [Pd(Ph)(μ-OAc)(PPh_3)]$_2$ **84** dissociation in DCM reported by Wakioka and co-workers based on the FT-IR spectroscopic analysis of ν_{CO2} stretching frequencies.[175] However, the equilibrium was expected to shift towards the mononuclear complex **85** in a coordinating solvent such as DMF and at elevated temperature. All complexes showed partial solubility in DMF at room temperature with sonication. The solubility of the three complexes was tested in DMSO, MeOH, acetonitrile, dichloromethane and benzene. Both the μ-OAc **84** and μ-OH

83a complexes were fully soluble in dichloromethane and benzene. Benzene-d_6, in addition to DMF, was therefore considered as the solvent for performing kinetic experiments. Unfortunately the μ-I **86** complex was only partially soluble in dichloromethane and benzene.

The reactivity of these Pd complexes with pentafluorobenzene **56** in non-deuterated DMF and benzene-d_6 was studied. The experiments were prepared in the glove box using an NMR tube equipped with a Young's tap. For the reaction in DMF, the yield of the product **64** was calculated from the integration of ^{19}F NMR signals of the hexafluorobenzene (internal standard) singlet at δ −162.87 (6F) with the product **64** triplet-of-doublet at −163.11 (2F, 3,5-F) (**Figure 66**). The poor shimming was due to the use of non-deuterated DMF. Black precipitates were observed after heating, as expected from the Pd^0 formation following reductive elimination of the biaryl **64** from Pd^{II} intermediate formed *in situ*. A shift in the ^{19}F NMR signals of the reaction mixture with respect to hexafluoprobenzene internal standard was observed in different solvents at different temperatures. This became significant when the 3,5-fluorine atom signal of product **64** shifted up-field from δ −162.76 to −162.86 in benzene-d_6, overlapping with the hexafluorobenzene internal standard peak (*i.e.* δ −162.87) at elevated temperature. Therefore, C_6H_5F with triplet-of-triplet signal at δ −112.91 was used as the new internal standard and integrated with the 2,6- and 4-fluorine atom signals of the product **64** to determine the change in the yield during the reaction. All spectra were collected with 30 seconds of relaxation delay to achieve full relaxation of the internal standards and the product **64**.

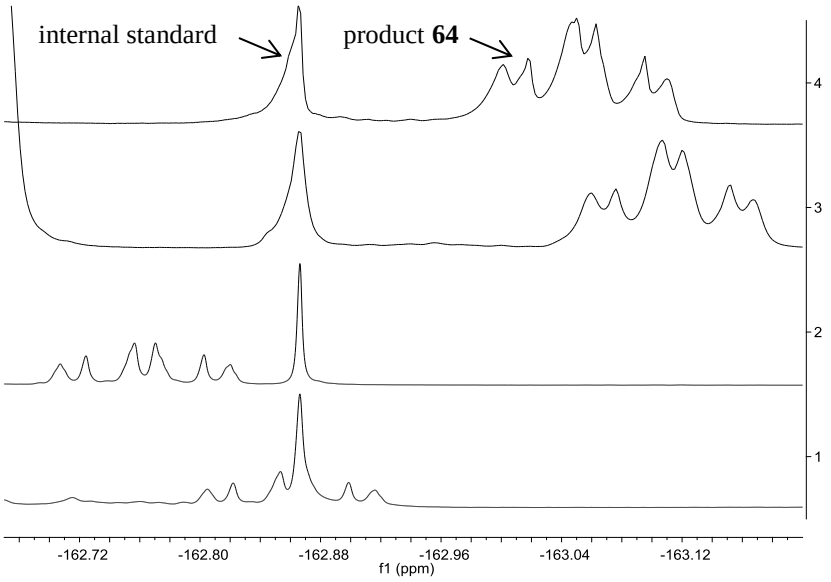

Figure 66. ^{19}F NMR spectra of reaction shown in **Scheme 67** with internal standard C_6F_6 at δ −162.87 and triplet-of-doublet peak of the product **64 (1)** in benzene-d_6 at 55.5 °C, **(2)** in benzene-d_6 at 25.0 °C, **(3)** in DMF at 55.5 °C and **(4)** in DMF at 25.0 °C.

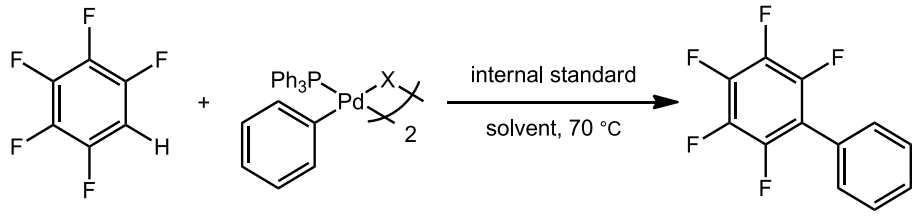

56 [180 mM] **84/83a/86** [9 mM] **64**

Scheme 67. Stoichiometric reaction of dinuclear Pd species (X = OAc **84**, OH **83a** and I **86**) and pentafluorobenzene **56** in DMF (not deuterated) or benzene-d_6.

The dinuclear species with the formula $[Pd(Ph)(\mu\text{-}X)(PPh_3)]_2$ (where X = OAc **84**, OH **83a** and I **86**) were heated at 70 °C in the presence of 20-fold excess of pentafluorobenzene **56** for 14 h in DMF (**Scheme 67**). Formation of the product **64** was observed for the reaction of $[Pd(Ph)(\mu\text{-}OAc)(PPh_3)]_2$ **84** and $[Pd(Ph)(\mu\text{-}OH)(PPh_3)]_2$ **83a** in quantitative and 60% yields respectively, but not the $[Pd(Ph)(\mu\text{-}I)(PPh_3)]_2$ **86** complex (**Table 33**, Entries 1–3). However, partial formation of the product **64** was observed in the presence of 3 equivalents of Ag_2CO_3 or 6 equivalents of AgOAc (Entries 4 and 5). No further yield improvement was observed with prolonged heating. The high reactivity of acetate-bridged complex **84** was further demonstrated by reaction with 20-fold excess 1,3-difluorobenzene **26** to form the 2,6-difluoro-1,1′-biphenyl product **30**, regioselectively, with 16% NMR yield. Formation of AcOH at δ 1.52 was observed by ^{1}H NMR spectroscopic analysis potentially from the proton of the cleaved pentafluorobenzene **56** C–H bond. This is consistent with the mechanism involving AMLA(6)-TS.[136]

The result from the reaction of hydroxo-bridged complex **83a** was interesting as the OH group is possibly acting as an intramolecular base via an AMLA(4)-TS.[143, 144] However, no water peak was observed at δ 0.40 by ^{1}H NMR spectroscopic analysis, but instead a broad peak was observed at δ 0.65. This was in contrast to the lack of reactivity for the hydroxo-bridged complex **83a** towards 2-methylthiophene **46** reported by Wakioka and co-workers.[175] The reactions were repeated in benzene-d_6 for better shimming and peak resolution. After 21 hours of heating at 70 °C showed that the reaction was less efficient compared with DMF and resulted in lower product **64** yields (Entries 1–3). These results suggested that the reaction was assisted by a polar aprotic solvent or benefited from the presence of water in the reaction mixture (*i.e.* 110 ppm).

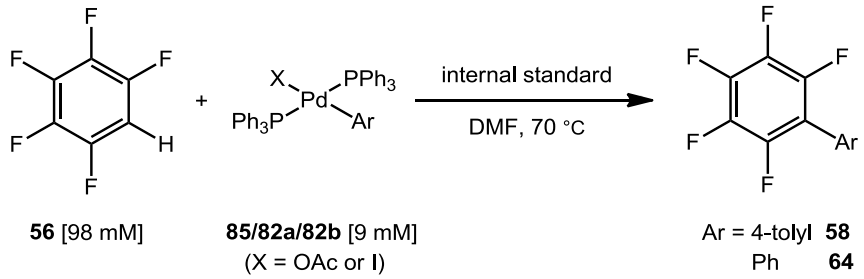

56 [98 mM] **85/82a/82b** [9 mM] (X = OAc or I) Ar = 4-tolyl **58** Ph **64**

Scheme 68. Stoichiometric reaction of mononuclear Pd species [*i.e.* Pd(Ph)(κ^1-OAc)$(PPh_3)_2$ **85**, Pd(Ph)(I)$(PPh_3)_2$ **82a**, and Pd(4-tolyl)(I)$(PPh_3)_2$ **82b**] with pentafluorobenzene **56** in DMF.

The mononuclear species Pd(Ph)(κ^1-OAc)$(PPh_3)_2$ **85**, Pd(Ph)(I)$(PPh_3)_2$ **82a**, and Pd(4-tolyl)(I)$(PPh_3)_2$ **82b** were heated at 70 °C for 14 h in the presence of 10-fold excess of pentafluorobenzene **56** (**Scheme 68**). The Pd(Ph)(κ^1-OAc)$(PPh_3)_2$ **85** complex formed the product **64** in 45% NMR yield (**Table 33**, Entry 6). The lower than expected yield of Pd(Ph)(κ^1-OAc)$(PPh_3)_2$ **85** maybe attributed to the low stability of the complex in solution compared with the dinuclear species. However, quantitative conversion of the complex was achieved in the presence of 2 equivalents of Ag_2CO_3 and 7 equivalents of AgOAc (Entries 7 and 8).

As with the dinuclear iodide complex, the mononuclear Pd(Ph)(I)$(PPh_3)_2$ **82a** complex was unreactive towards pentafluorobenzene **56** unless in the presence of Ag_2CO_3 (49%) and AgOAc (67%) (Entries 9–11). Similar results were obtained for the mononuclear Pd(4-tolyl)(I)$(PPh_3)_2$ **82b** complex (Entries 13–15). This was different from what Sun and co-workers reported for the role of base in the direct arylation reaction of pyridine *N*-oxide **37**.[172] A potential catalytic intermediate, Pd(Ph)(Br)(P^tBu_3), was reacted in stoichiometric quantity with 4-nitropyridine-*N*-oxide in the presence of different equivalents of K_2CO_3 and/or KOPiv. The yield of the product only depended on the presence of KOPiv, suggesting the pivalate anion to be the base directly involved in the C–H bond cleavage. No product **64** was formed in the mixture of Pd(Ph)(I)$(PPh_3)_2$ **82a** and $AgBF_4$ (Entry 12), confirming carboxylate anions are required for the transformation.

Table 33. NMR yields of product **58**/**64** from the stoichiometric reaction of Pd species and pentafluorobenzene **56** as shown in **Scheme 67** and **Scheme 68**.

Entry	Complex	NMR Yield (%)	
		DMF [a]	C_6D_6 [b]
1	$[Pd(Ph)(\mu\text{-}OAc)(PPh_3)]_2$ **84**	99	67
2	$[Pd(Ph)(\mu\text{-}OH)(PPh_3)]_2$ **83a**	60	18
3	$[Pd(Ph)(\mu\text{-}I)(PPh_3)]_2$ **86**	0	0
4	$[Pd(Ph)(\mu\text{-}I)(PPh_3)]_2$ **86** + $3Ag_2CO_3$	36	-
5	$[Pd(Ph)(\mu\text{-}I)(PPh_3)]_2$ **86** + 7AgOAc	22	-
6	$Pd(Ph)(\kappa^1\text{-}OAc)(PPh_3)_2$ **85**	45	-
7	$Pd(Ph)(\kappa^1\text{-}OAc)(PPh_3)_2$ **85** + $2Ag_2CO_3$	99	-
8	$Pd(Ph)(\kappa^1\text{-}OAc)(PPh_3)_2$ **85** + 7AgOAc	98	-
9	$Pd(Ph)(I)(PPh_3)_2$ **82a**	0	-
10	$Pd(Ph)(I)(PPh_3)_2$ **82a** + $2Ag_2CO_3$	49	-
11	$Pd(Ph)(I)(PPh_3)_2$ **82a** + 4AgOAc	67	-
12	$Pd(Ph)(I)(PPh_3)_2$ **82a** + $7AgBF_4$	0	-
13	$Pd(4\text{-tolyl})(I)(PPh_3)_2$ **82b**	0	-
14	$Pd(4\text{-tolyl})(I)(PPh_3)_2$ **82b** + $2Ag_2CO_3$	46	-
15	$Pd(4\text{-tolyl})(I)(PPh_3)_2$ **82b** + 4AgOAc	56	-

[a] Based on integration of C_6F_6 (internal standard) and 3,5-fluorines of the product **58**/**64**.

[b] Based on integration of C_6H_5F (internal standard) and 4-fluorines of the product **58**/**64**.

The addition of a Ag^I salt (base) assisted the formation of product (*i.e.* **58** and **64**) for the iodide-containing complexes (*i.e.* **82a**, **82b** and **86**). The halide-extracting ability of Ag^I salt was studied by reaction of $[Pd(4\text{-tolyl})(I)(PPh_3)_2]$ **82b** with Ag_2CO_3 in DMF. Analysis of the reaction mixture by ESI(+)-MS showed formation of peak at *m/z* 353.14 and 721.14 with isotopic pattern corresponding to $[P(4\text{-tolyl})Ph_3]^+$ **60** and $[Pd(4\text{-tolyl})(PPh_3)_2]^+$ species respectively. The formation of the quaternary arylphosphonium cation is thought to result from thermal decomposition of the Pd complex.[377] The RT decomposition of $[Pd(R)(I)(PPh_3)_2]$ **111** to $[PRPh_3]PF_6$ and Pd black upon addition of $AgPF_6$ was reported by Burns and co-workers (**Scheme 69**).[206]

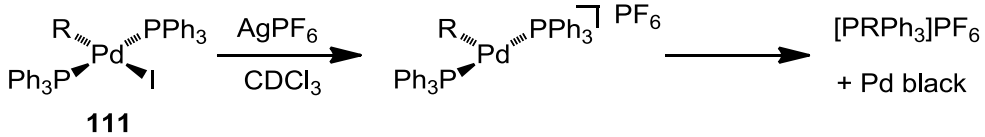

111

Scheme 69. RT decomposition of $[Pd(R)(I)(PPh_3)_2]$ **111** facilitated by $AgPF_6$ (Burns and co.).[206]

A mixture of Pd(4-tolyl)(I)(PPh_3)$_2$ **82b**, $AgBF_4$ and MeCN-d_3 in DCM-d_2 at ambient temperature resulted in a yellow solution with instantaneous precipitation of a grey solid (**Scheme 70**). Instantaneous conversion of Pd(4-tolyl)(I)(PPh_3)$_2$ **82b** to [Pd(4-tolyl)(PPh_3)$_2$]$^+$ **112** was confirmed by the changes observed in the ^{1}H and ^{31}P NMR spectroscopic analysis. The 4-tolyl aromatic protons of [Pd(4-tolyl)(PPh_3)$_2$]$^+$ **112** appeared at δ 7.27–7.50, and the methyl protons at δ 2.04. Analysis by ^{31}P NMR spectroscopy initially showed a major peak of [Pd(4-tolyl)(PPh_3)$_2$]$^+$ **112** complex at δ 21.15. Isotopic pattern corresponding to [P(4-tolyl)Ph_3]$^+$ **60** and [Pd(4-tolyl)(PPh_3)$_2$]$^+$ **112** species were detected by ESI(+)-MS analysis after three days. Decomposition of [Pd(4-tolyl)(PPh_3)$_2$]$^+$ **112** into [P(4-tolyl)Ph_3]$^+$ **60** was observed with the appearance of aromatic ^{1}H signals at δ 7.58–7.91. Additionally, the methyl signal of [Pd(4-tolyl)(PPh_3)$_2$]$^+$ **112** was completely replaced by a methyl peak of [P(4-tolyl)Ph_3]$^+$ **60** at δ 2.52 and the ^{31}P NMR peak of [P(4-tolyl)Ph_3]$^+$ **60** at δ 22.93 became the major peak after a week. The ^{19}F NMR spectra of [Pd(4-tolyl)(PPh_3)$_2$]BF_4 **112** peak at δ −153 was also replaced by a peak at δ −76 corresponding to [P(4-tolyl)Ph_3]BF_4 compound **60**. The reaction had resulted from instantaneous formation of [Pd(4-tolyl)(PPh_3)$_2$]$^+$ **112** and AgI, followed by slow reductive elimination of [P(4-tolyl)Ph_3]$^+$ **60** from the complex **112**.

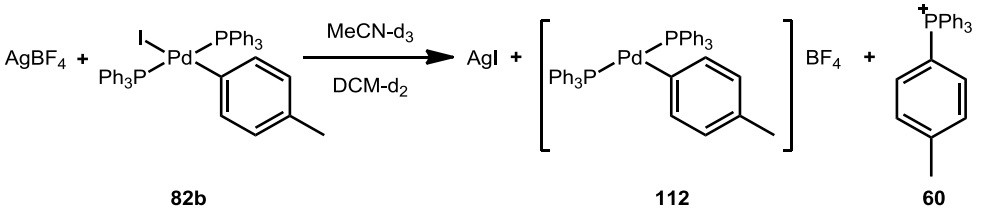

Scheme 70. Reaction of $AgBF_4$ and Pd(4-tolyl)(I)(PPh_3)$_2$ **82b** in DCM-d_2 with trace MeCN-d_3.

4.6 Kinetics of Direct Arylation Reaction of 4-Iodotoluene 57 with Pentafluorobenzene 56 Catalysed by the Isolated Pd Complexes

The kinetics of reactions in the presence of catalytic quantity of the isolated stable Pd^{II} species were monitored by *in situ* FT-IR spectroscopic analysis (**Table 34**). The k_{obs} were determined from 5–50% product **64** formation for reactions following pseudo-zeroth-order rate law. The mononuclear and the dinuclear complexes were added in 5 mol% and 2.5 mol% loading respectively, to give 5 mol% Pd-atom loading per reaction. Compared to the reactions studied under stoichiometric quantity, the catalytic condition provides a closer representation to the actual reaction of interest. As previously discussed, reaction starting with Pd species involved in the catalytic cycle should mirror the kinetics of model reaction catalysed by the 5 mol% $Pd(OAc)_2$ and 10 mol% PPh_3 mixture (Entry 1). Thus, strong evidence for the involvement of a complex in the catalysis can be obtained from the

reaction rates. It must be noted that the stability of these complexes under the exact reaction condition was unknown. However, thermal decomposition at 56 ± 1 °C was observed by HR-MAS NMR study for every complex expect for [Pd(Ph)(μ-OAc)(PPh_3)]$_2$ **84**.

Table 34. Observed rate constants for the direct arylation reaction of iodobenzene **81** with pentafluorobezene **56** catalysed by isolated Pd species (5 mol% Pd-atom).

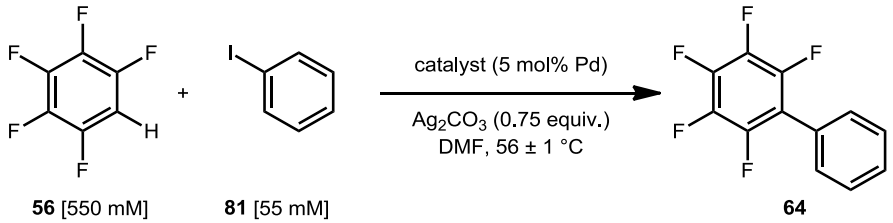

Entry	Catalyst (5 mol% Pd-atom)	k_{obs} / 10^{-6} . mol dm^{-3} s^{-1}
1	$Pd(OAc)_2$ + $2PPh_3$	9.90 ± 0.04
2	[Pd(Ph)(μ-OAc)(PPh_3)]$_2$ **84**	7.90 ± 0.05
3	[Pd(Ph)(μ-OAc)(PPh_3)]$_2$ **84** + $2PPh_3$	7.56 ± 0.06
4	[Pd(Ph)(μ-OH)(PPh_3)]$_2$ **83a**	-
5	[Pd(Ph)(μ-I)(PPh_3)]$_2$ **86**	-
6	[Pd(Ph)(μ-OH)(PPh_3)]$_2$ **83a** + 2AcOH	9.71 ± 0.10
7	[Pd(Ph)(μ-I)(PPh_3)]$_2$ **86** + 2AcOH	8.32 ± 0.05
8	Pd(Ph)(κ^1-OAc)(PPh_3)$_2$ **85**	8.52 ± 0.09
9	Pd(Ph)(I)(PPh_3)$_2$ **82a**	14.83 ± 0.01
10	$Pd(OAc)_2$ + $3PPh_3$	14.58 ± 0.01
11	Pd(Ph)(I)(PPh_3)$_2$ **82a** + AcOH	7.34 ± 0.04
12	Pd(Ph)(I)(PPh_3)$_2$ **82a** + 2AcOH	11.10 ± 0.14
13	Pd(Ph)(I)(PPh_3)$_2$ **82a** + 4AcOH	14.00 ± 0.01

The kinetic profiles and the observed rate constants for the dinuclear Pd complex catalysed reactions were compared with the base catalyst mixture of 5 mol% $Pd(OAc)_2$ and 10 mol% PPh_3 (Entry 1). Of the dinuclear Pd complexes tested, the reaction rate of [Pd(Ph)(μ-OAc)(PPh_3)]$_2$ **84** catalyst was the closest to the standard condition (Entry 2). Addition of 10 mol% PPh_3 to this reaction did not improve the reaction rate despite the expected *in situ* formation of more active mononuclear Pd(Ph)(κ^1-OAc)(PPh_3)$_2$ **85** complex (Entry 3). The [Pd(Ph)(μ-OH)(PPh_3)]$_2$ **83a** and [Pd(Ph)(μ-I)(PPh_3)]$_2$ **86** complex catalysed reactions followed first-order kinetics and proceeded significantly slower than the model catalytic conditions (**Figure 67** a). As previously observed in the stoichiometric reaction study, the [Pd(Ph)(μ-I)(PPh_3)]$_2$ **86** complex was an active catalyst in the presence of Ag_2CO_3. However, significant rate acceleration was observed for the reactions catalysed by the hydroxo- and iodo-bridged dinuclear complexes **83a** and **86** in the presence of 5 mol%

AcOH (**Figure 67** b). The pseudo-zeroth-order rate constants calculated were then similar to the model reaction (Entries 6 and 7).

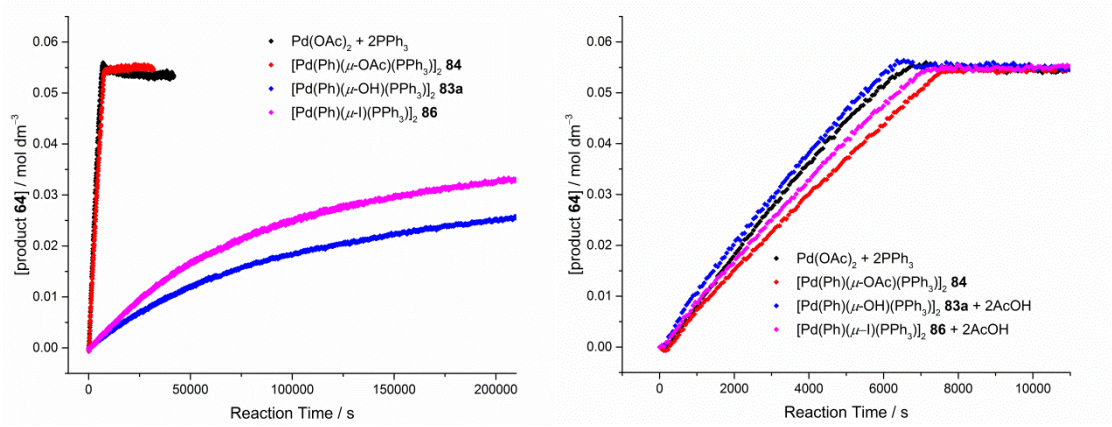

a **b**

Figure 67. Kinetic profiles showing the product **64** formation for the reactions catalysed by **(a)** the dinuclear complexes (**Table 34**, Entries 1, 2, 4 and 5) and **(b)** the dinuclear complexes with added AcOH (Entries 1, 2, 6 and 7).

The reaction rates for the mononuclear Pd complex catalysed reactions were also studied (**Table 34** and **Figure 68**). The k_{obs} for the reaction catalysed by the Pd(Ph)(κ^1-OAc)$(PPh_3)_2$ **85**, expected to be the active intermediate of the RL-step, was slower than expected (Entry 8). This may be attributed to the decomposition of the complex during the reaction. On the other hand, the reaction using the oxidative addition complex Pd(Ph)(I)$(PPh_3)_2$ **82a** as the catalyst formed the product **64** at the same rate as the reaction catalysed by 5 mol% $Pd(OAc)_2$ and 15 mol% PPh_3 catalyst mixture (Entries 9 and 10). Addition of 5 mol% AcOH to Pd(Ph)(I)$(PPh_3)_2$ **82a** catalysed reaction results in initial period of slow product **64** formation, followed by dramatic reaction rate acceleration (Entry 11). The k_{obs} determined for the later part of the reaction was comparable to the reaction under the model catalytic conditions. The addition of increased amount of AcOH (*i.e.* 10 mol% and 20 mol%) resulted in increased reaction rates (Entries 12 and 13).

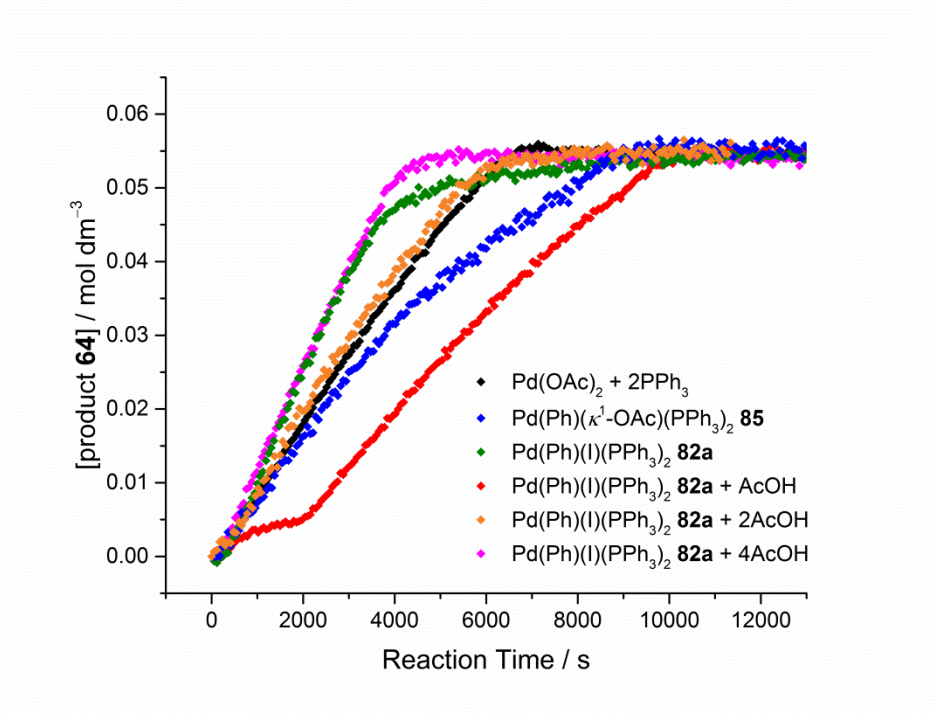

Figure 68. Kinetic profiles showing the product **64** formation for the reactions catalysed by 5 mol% of mononuclear Pd species (**Table 34**, Entries 1, 8, 9, 11–13).

The initial induction period observed for the reaction mixture with Pd(Ph)(I)(PPh$_3$)$_2$ **82a** and 5 mol% AcOH (Entry 11) was confirmed as the *in situ* formation of Pd(Ph)(κ^1-OAc)(PPh$_3$)$_2$ **85**.[257] Sequential addition of AcOH to a mixture of Pd(Ph)(I)(PPh$_3$)$_2$ **82a** and Ag_2CO_3 in DMF-d_7 was analysed by ^{31}P NMR spectroscopy and LIFDI-MS. Quantitative conversion of complex **82a** into complex **85** was observed as the ^{31}P NMR signal at δ 22.94 for **82a** was replaced by a singlet at δ 20.62 for **85** (**Figure 69**). Upon further addition of AcOH (*i.e.* 2 and 4 equivalents), additional peaks were observed including the dinuclear [Pd(Ph)(μ-OAc)(PPh$_3$)]$_2$ **84** species at δ 29.34. Pd-containing mononuclear species Pd(Ph)(OAc)(PPh$_3$) (*m/z* 503.05), Pd(Ph)(κ^1-OAc)(PPh$_3$)$_2$ **85** (*m/z* 766.14) and dinuclear species **84** (*m/z* 1010.10) were also detected successfully by LIFDI-MS. It must be noted that Ag_2CO_3 was present in much greater excess under the catalytic reaction condition and some of these species may not be formed under the catalytic reaction conditions. However, the addition of excess AcOH most likely increases the rate of the reaction by coordinating and stabilising the homogeneous Pd species formed *in situ*.[190]

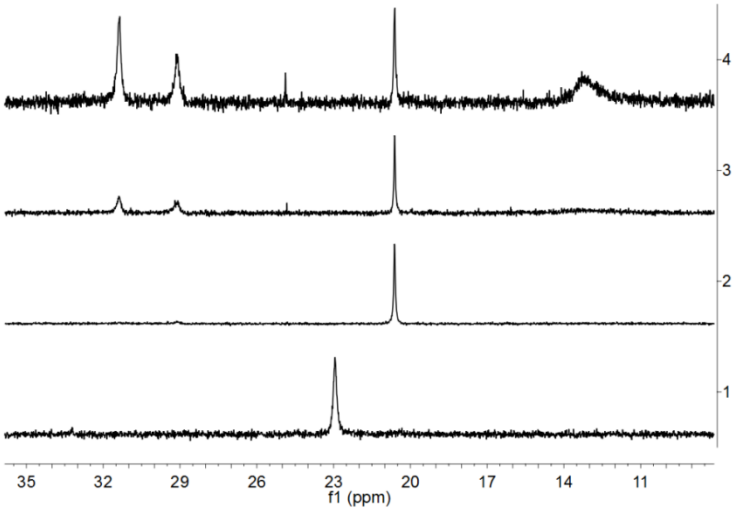

Figure 69. Stacked ^{31}P NMR spectra of Pd(Ph)(I)$(PPh_3)_2$ **82a** in DMF-d_7 with different additives. **(1)** 1.4 equiv. Ag_2CO_3, **(2)** 1.4 equiv. Ag_2CO_3 + 1 equiv. AcOH, **(3)** 2.8 equiv. Ag_2CO_3 + 2 equiv. AcOH and **(4)** 2.8 equiv. Ag_2CO_3 + 4 equiv. AcOH.

4.7 Conclusions

The direct arylation of iodoarenes (*i.e.* **57** and **81**) with pentafluorobenzene **56** was studied by range of *in situ* and *ex situ* analytical techniques to characterise the reaction intermediates. The HR-MAS NMR spectroscopic analysis was applied as an *in situ* technique for observing species formed in heterogeneous reaction mixture. The technique allowed for the observation of NMR signals belonging to potentially catalytically important intermediates. The broad signals observed by ^{1}H and ^{31}P NMR spectroscopic analysis during the reaction (at 328.5 K) were resolved at low temperature (*i.e.* 248.5 K). The peaks were identified as the phenyl proton signals of $[Pd(Ph)(\mu\text{-}OAc)(PPh_3)]_2$ **84** and $Pd(Ph)(\kappa^1\text{-}OAc)(PPh_3)_2$ **85** complexes as major and minor species respectively. Increasing the quantity of PPh_3 in the reaction mixture resulted in the mononuclear $Pd(Ph)(\kappa^1\text{-}OAc)(PPh_3)_2$ **85** complex becoming the major species and significant acceleration of the reaction rate. The Pd-aryl intermediates observed during the reaction catalysed by Pd(Ph)(I)$(PPh_3)_2$ **82a** did not match those observed during the model reaction, suggesting a reaction of different mechanism.

Charged species in the reaction mixture were analysed by *ex situ* ESI-MS analysis in both the positive and negative ion modes. The Pd^I complexes of the formula $[Pd(Ar)(PPh_3)_n]^+$ (n = 1 or 2 and Ar = 4-tolyl or C_6F_5) were detected as well as the solvent coordinated analogues. The oxidative addition product $Pd(Ar^+)(I)(PPh_3)$ **109** and the bis-aryl Pd

complex Pd(Ar^+)(C_6F_5)(PPh_3) **110** were also observed using a charge-tagged iodoarene **107** (*i.e.* 4-iodobenzyltriphenylphosphonium hexafluorophosphate).

The *ex situ* LIFDI-MS analysis of the reaction mixture allowed for the observation of Pd species such as Pd(4-tolyl)(OAc)(PPh_3) and [Pd(4-tolyl)(μ-OAc)(PPh_3)]$_2$ **84b**, expected for reaction proceeding via AMLA(6) pathway. Furthermore, multiple arylphosphine species were observed throughout the experiment highlighting the side-reactions taking place between the iodoarene and the PPh_3 in the presence of Pd.

The reactivity of the hypothesised catalytic intermediates was tested by heating stoichiometric quantity of the isolated stable Pd complexes at 70 °C in the presence of pentafluorobenzene **56**. The reaction of [Pd(Ph)(μ-OAc)(PPh_3)]$_2$ **84** resulted in quantitative conversion of the phenyl-substituent to the biaryl product **64**. The mononuclear Pd(Ph)(κ^1-OAc)(PPh_3)$_2$ **85** achieved 45% conversion to the product **64**, most likely due to decomposition in solution as observed by heating the complex in DMF-d_7. Quantitative NMR conversion was achieved in the presence of 2 equivalents of Ag_2CO_3 or 7 equivalents of AgOAc. The hydroxo-bridged complex [Pd(Ph)(μ-OH)(PPh_3)]$_2$ **83a** was also reactive, achieving 60% conversion to the product **64**. The mononuclear (*i.e.* **82a** and **82b**) and the dinuclear (*i.e.* **86**) iodide containing complexes required addition of Ag_2CO_3 or AgOAc to form the product **64**. The significant role played by the carboxylate anions were highlighted by the $AgBF_4$ being an ineffective additive.

The catalytic activities of the isolated Pd complexes were evaluated by *in situ* FT-IR spectroscopic analysis. The reaction rates and reaction profiles observed were compared with results obtained for the model reaction catalysed by 5 mol% Pd(OAc)$_2$ and 10 mol% PPh_3 mixture. Of the dinuclear Pd complexes tested, comparable k_{obs} was obtained for reaction catalysed by [Pd(Ph)(μ-OAc)(PPh_3)]$_2$ **84**. Improved reaction rate was observed for Pd(Ph)(I)(PPh_3)$_2$ **82a** catalysed reaction, although the catalytic cycle was expected to proceed via a different mechanism. Addition of less than 4 equivalents of AcOH to the reaction catalysed by this complex **82a** negatively affected the reaction rate, following quantitative conversion of complex **82a** into the acetate ligated complex **85**. The effect of higher equivalents of AcOH was not tested.

The analysis of the direct arylation of iodoarenes (*i.e.* **57** and **81**) with pentafluorobenzene **56** by HR-MAS NMR, ESI(±)-MS and LIFDI-MS all indicated the presence of the dinuclear [Pd(Ar)(μ-OAc)(PPh_3)]$_2$ **84** and mononuclear Pd(Ar)(OAc)(PPh_3)$_2$ **85** species during the reaction. The reactivity of potential Pd intermediates tested by the stoichiometric reactions and their catalytic activity suggested [Pd(Ar)(μ-OAc)(PPh_3)]$_2$ **84** as the key

intermediate. Base on the collective experimental evidence, the mononuclear Pd(Ph)(κ^2-OAc)(PPh_3) was concluded as the catalytically active on-cycle species with the dinuclear [Pd(Ar)(μ-OAc)(PPh_3)]$_2$ **84** acting as the stable off-cycle reservoir.

Chapter 5: Conclusions and Future Work

5.1 Conclusions

5.1.1 Summary of Experiments Performed

The experimental results reported in this thesis were designed to reveal mechanistic details of the metal-catalysed direct arylation reaction involving fluoroarenes. Direct arylation methodologies have rapidly developed over the last decade as cost-effective, eco-friendly and sustainable alternatives to cross-coupling reactions. One of the main challenges in the field is controlling the regioselectivity of the reaction. Fluoroarenes are attractive substrates due to the fluorine-substitution effect[11] as well as the ability to control the regioselectivity of C–H bond activation by the *ortho*-fluorine effect.[168] Understanding the reaction mechanisms are crucial for making improvements to the C–H bond functionalisation field and provides access to unique reactivities.

Initially, yields were studied to determine the limitations and the factors affecting the reaction efficiency. A series of pre-catalysts and inorganic salt additives were tested. Acetate anion and carbonate anion were determined as suitable carboxylate ligands for the reaction. The reaction was also successfully catalysed by combination of $Pd(PPh_3)_4$ catalyst and Ag_2O additive in the absence of carboxylate anion. Although the substrate scope of the reaction was somewhat limited at the studied reaction temperature, the selected model reaction did regioselectively functionalise 1,3-difluorobenzene **26** at the C2 position.

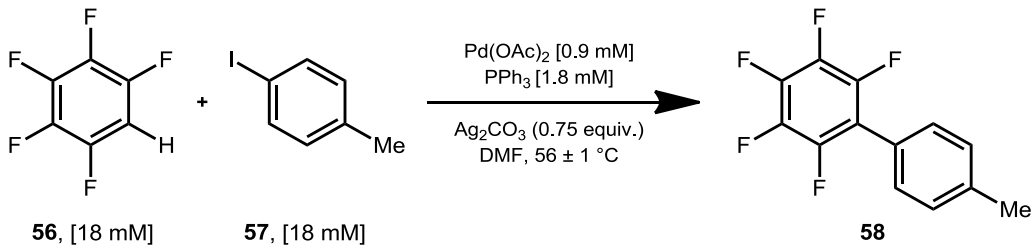

Scheme 71. The model reaction studied by *in situ* FT-IR spectroscopic analysis.

The reaction conditions and the setup were tailored for monitoring the progress by *in situ* FT-IR spectroscopic analysis (**Scheme 71**). Kinetic information regarding the relationship between the reaction rate and factors such as concentrations, temperature, C–H bond strength and the electronic properties of the substrates were established. Furthermore, the effects of using ligands other than PPh_3 were explored. The reaction was also tested for the possible involvement of heterogeneous catalysis. The catalytically relevant species were identified by *in situ* HR-MAS NMR spectroscopy, and *ex situ* ESI(±)-MS and LIFDI-MS. The reactivities of these species were confirmed by stoichiometric reactions and the ability

to act as a catalyst. From here onwards, the elementary steps of the proposed catalytic cycles are presented with experimental evidence to support the hypothesis.

5.1.2 Pre-Catalyst Activation

The model reaction conditions for the direct arylation of 4-iodotoluene **57** with pentafluorobenzene **56** were similar to the Mizoroki-Heck reaction which commonly uses a carbonate base and DMF as the solvent.[378, 379] Therefore, the mechanism and the active species involved was expected to be analogous, at least up to the oxidative addition product of the catalytic cycle.[100]

The generally-agreed first step of the catalytic cycle is the activation of the organic halide or pseudohalide by a Pd^0 species.[380, 381] For this reason, the air- and moisture-stable Pd^{II} pre-catalyst used in the model reaction must be reduced somehow to form Pd^0 species. This was highlighted by the induction period observed by *in situ* FT-IR spectroscopy when the reaction was initiated by the mixing of the liquid reagents with the solid reagents (see Chapter 6.2 General Procedures). Work by Amatore and co-workers reported rapid formation of yellow $Pd(OAc)_2(PPh_3)_2$ complex **I** from a mixture of $Pd(OAc)_2$ and 2 equivalents of PPh_3 in DMF, characterised by ^{31}P NMR and cyclic voltammetry (**Scheme 72**).[257] This divalent Pd complex was shown to undergo spontaneous intramolecular reduction with PPh_3 in DMF to form a non-isolable anionic $[Pd^0(PPh_3)(OAc)]^-$ **II**. The resulting $[AcO\text{-}PPh_3]^+$ converts to a mixture of acetic acid, $O{=}PPh_3$ and a proton in the presence of water. It was understood that the pre-catalyst exists as a trinuclear $Pd_3(OAc)_6$ but the scheme was simplified for clarity.

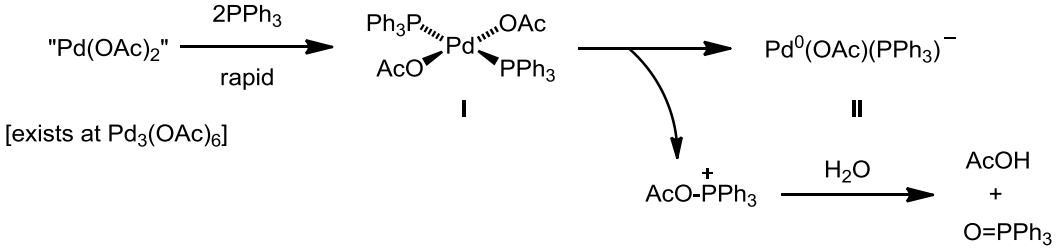

Scheme 72. The proposed activation of $Pd(OAc)_2$ by 2 equivalents of PPh_3 in DMF.

Although the $[Pd^0(OAc)(PPh_3)]^-$ complex **II** was not directly observed, indirect experimental evidence suggests the *in situ* generation of complex **II**. The formation of $Pd(OAc)_2(PPh_3)_2$ **I** in the early stages of the reaction was suspected by the colour changes observed during experimental preparation and confirmed by HR-MAS ^{31}P NMR spectroscopic analysis (observed at δ 14.6). The formation of $O{=}PPh_3$ at the expense of complex **I** was also observed in the same experiment, as well as the generation of AcOH by HR-MAS ^1H NMR spectroscopic analysis. Furthermore, $Pd(C_6F_5)(OAc)(PPh_3)_n$ (n =1 or 2)

and $[Pd(C_6F_5)(PPh_3)]^+$ were detected by LIFDI-MS and ESI(+)-MS respectively. These species may be generated via C–H bond activation of pentafluorobenzene **56** by the intermediate $[Pd^0(OAc)(PPh_3)]^-$ **II**. However, the complex **II** was expected to quickly dimerise to $[Pd^0(\mu\text{-}OAc)(PPh_3)]_2^{2-}$ **IV**, potentially solvated by DMF (**Scheme 73**).[194, 382, 383] Additionally, a complex such as $[Pd^0(DMF)(OAc)(PPh_3)]^-$ **III**, analogous to well-established active complex $[Pd^0(OAc)(PPh_3)_2]^-$, can exist in equilibrium.[207]

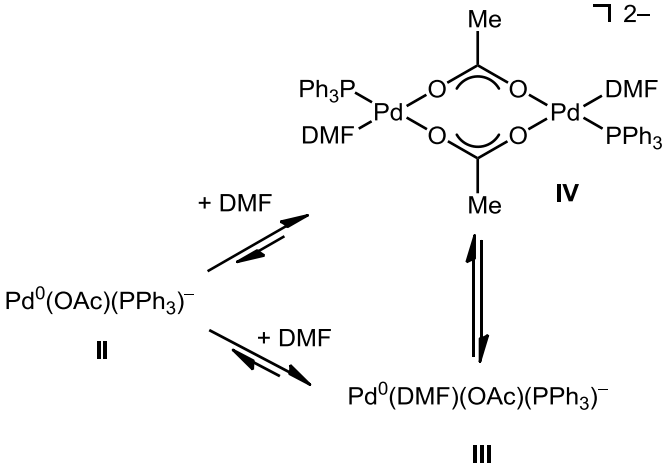

Scheme 73. The possible equilibrium of the active Pd^0 complexes.

5.1.3 Oxidative Addition and Halide Abstraction

The oxidative addition of iodobenzene **81** into $[Pd^0(OAc)(PPh_3)_2]^-$ to afford a mixture of $Pd(Ph)(I)(PPh_3)_2$ **82a** and $Pd(Ph)(\kappa^1\text{-}OAc)(PPh_3)_2$ **85** have been well documented by Amatore and co-workers.[190] Therefore, the addition of aryl iodide to $[Pd^0(DMF)(OAc)(PPh_3)]^-$ **III** was expected to result in the formation of σ-aryl Pd complex $[Pd^{II}(Ar)(I)(\kappa^1\text{-}OAc)(PPh_3)]^-$ **V** with dissociation of DMF (**Scheme 74**).[384] The halide is then abstracted by Ag^I to give $Pd^{II}(Ar)(\kappa^2\text{-}OAc)(PPh_3)$ **VI**. Such a reaction is known for the titration of $[Pd^I(I)(Cl)(PPh_3)_2]^-$ with Ag^I to yield $Pd^I(Cl)(PPh_3)_2$ and AgI.[385] The reaction is driven by the lattice energy and the insolubility of the AgI salt.

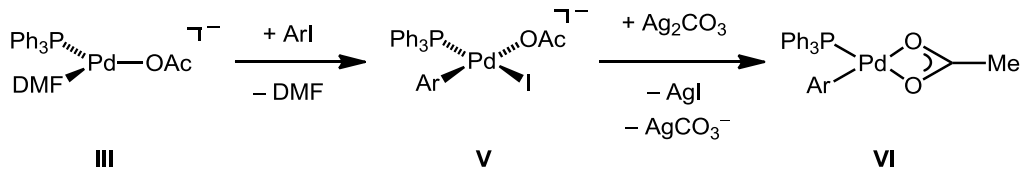

Scheme 74. The proposed oxidative addition of ArI into Pd^0 centre, followed by halide abstraction by Ag^I.

A variety of σ-aryl Pd intermediates similar to species **V** and **VI** were observed during the model reaction. The use of charge-tagged iodoarene **107** (*i.e.* 4-iodobenzyltriphenyl-

phosphonium hexafluorophosphate) allowed the detection of $Pd(Ar^+)(I)(PPh_3)$ **109** (Ar^+ = C_6H_4-4-$CH_2PPh_4^+$) by ESI(+)-MS analysis. The oxidative addition products were detected as $[Pd(Ar)(PPh_3)_n]^+$ (n = 1 or 2) species for reactions using neutral iodoarenes. The halide abstraction by Ag^I was supported by the precipitation of solid upon addition of silver salt to a solution of $Pd(Ar)(I)(PPh_3)_2$ **82b** complex in DMF. The resulting complex Pd(Ar)(κ^2-OAc)(PPh_3) **VI** was observed by LIFDI-MS, ^{1}H and ^{31}P NMR spectroscopic analysis.

The involvement of $[Pd(Ar)(I)(OAc)(PPh_3)]^-$ **V** was supported by the change in the reaction intermediates and the kinetics observed for the reaction using $Pd(Ph)(I)(PPh_3)_2$ **82a** pre-catalyst without AcO^- in the reaction mixture. This result highlighted the role of acetate-coordinated palladium species in the model reaction.

5.1.4 C–H Bond Activation

The mononuclear bidentate acetate ligated Pd complexes **VI** is known to exist in equilibrium with the dinuclear $[Pd(Ar)(\mu\text{-OAc})(PPh_3)]_2$ **VIII** in solution (**Scheme 75**). The 14-electron Pd complex **VII** was considered to be too unstable to exist as a discrete intermediate. Solvent or ligand coordinated mononuclear Pd species **IX** are also likely involved in the equilibrium, which was studied by Wakioka and co-workers.[175]

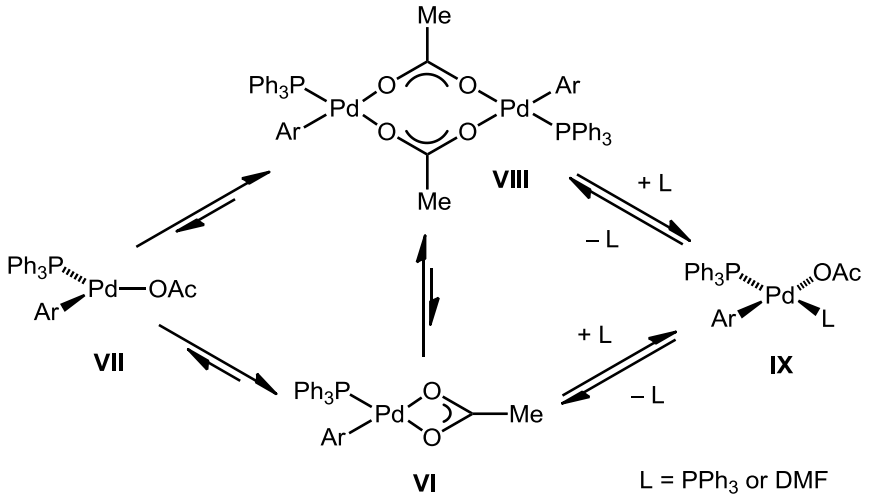

Scheme 75. The proposed equilibrium of acetate ligated σ-aryl Pd species **VI**–**IX**.

The monomeric 16-electron Pd complexes $Pd^{II}(Ar)(\kappa^2\text{-OAc})(PPh_3)$ **VI** was proposed as the active catalytic species involved in the C–H bond activation step (**Scheme 76**). The mechanism proposed is similar to the reaction postulated by published DFT calculations with the initial complex Pd(Ph)(κ^1-OAc)(DMF)(PMe_3) reacting via AMLA(6)-TS **X**.[168] However, this monomeric complex **VI** was shown to exist in pre-equilibrium with the dinuclear complex **VIII**. Reactions involving dinuclear Pd complexes similar to **VIII** are commonly characterised by half-order kinetic dependence in $[Pd]_{TOT}$.

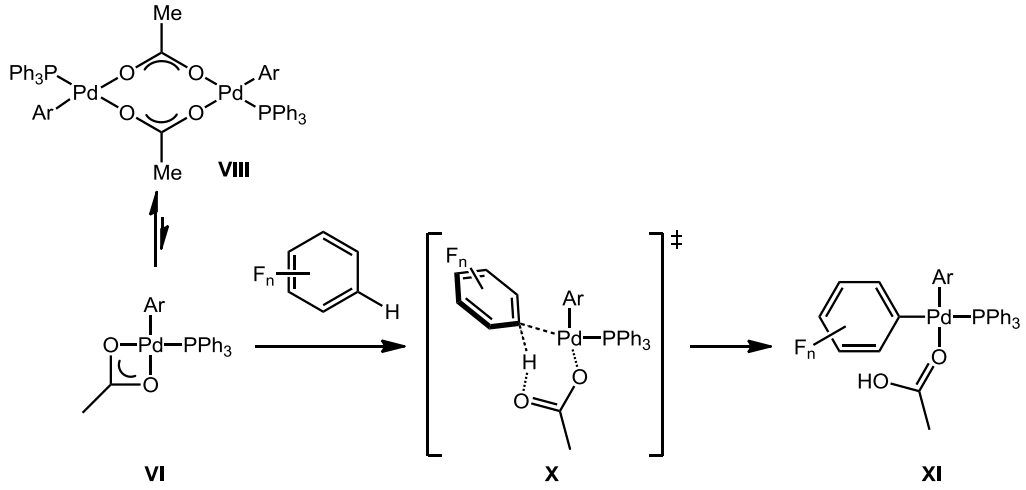

Scheme 76. The proposed C–H bond activation of fluorobenzene with Pd **VI** via AMLA(6)-TS **X**.

The proposed mechanism for the C–H bond activation step of the catalytic cycle was supported by the evidence from detailed kinetic investigations. The reaction followed first-order kinetics in pentafluorobenzene **56** and half-order kinetics in Pd, while being independent of iodoarenes (*i.e.* **57** and **81**) concentration. This result indicated that the resting state of the catalyst lies after the oxidative addition of the iodoarene to the Pd catalyst. However, since the rate was dependent on the structure of the iodoarene, the Pd species involved in the RL-step was identified as a σ-aryl Pd complex. The primary KIE identified the C–H bond activation step of pentafluorobenzene **56** as the RL-step of the catalytic cycle. A slight negative charge build up in the TS was determined from competition experiments of 1-substituted-2,3,5,6-tetrafluorobenzene with pentafluoro-benzene **56**. The largely negative activation entropy of $\Delta S^{\ddagger} = -143 \pm 8$ J K^{-1} mol^{-1} and the activation energy of $E_a = 61.9 \pm 2.6$ kJ mol^{-1} were determined from the temperature dependence of the reaction rate. In summary the RL-step of the catalytic cycle involves the C–H bond cleavage of the fluoroarene by σ-aryl Pd species via highly-ordered TS with marginal negative charge build up. These observations were in strong agreement with what is commonly associated with reaction proceeding via AMLA(6)-TS **X**.

The dinuclear species **84** (intermediate **VIII**) and the mononuclear species **85** (intermediate **IX**) were identified as the resting states of the catalytic cycle by HR-MAS NMR spectroscopic analysis and *ex situ* LIFDI-MS analysis of the reaction mixture. The catalytic abilities of these species were confirmed by using individually synthesised complexes to catalyse the model reaction. Furthermore, the stoichiometric reaction of these acetate-containing complexes with pentafluorobenzene **56** resulted in successful formation of the biaryl product **64** without requiring additives.

One of the unanswered questions is the role played by the two carboxylates present in the reaction mixture (*i.e.* acetate and bicarbonate). There are multiple possibilities: i) the bicarbonate can displace the acetate ligand prior to the RL-step, during stages of Pd^0 generation or from the oxidative addition product. The displacement may take place later on in the catalytic cycle depending on the energetic state of the Pd, ii) the carbonate may deprotonate the acetic acid by-product to regenerate acetate ligand to re-coordinate to Pd^0, iii) after the first catalytic cycle and the dissociation of acetic acid, the carbonate can coordinate to the Pd^0 to complete the catalytic cycle thereafter. At high concentration of CO_3^{2-} the first situation may be likely. Computational calculations by Sun and co-workers have shown marginal 3.3 kJ mol^{-1} energy difference favouring the AMLA(6)-TS **X** involving inner sphere acetate over carbonate ligand.[172] Despite the excess of Ag_2CO_3 added compared with the acetate ligated pre-catalyst, the poor solubility of the salt in DMF complicates determination of the concentration of carbonate in a reaction mixture. For this reason, the exact nature of the base involved in the AMLA pathway remains uncertain. Experimental results have indicated both AcO^- and CO_3^{2-} as suitable additives for the reaction. However, carbonate coordinated Pd species were not observed by ESI(−)-MS or LIFDI-MS analysis. It was concluded, therefore, the acetate anion was the base involved in the C–H bond cleavage, with CO_3^{2-} acting as a proton sponge to regenerate AcO^- from acetic acid by-product.

Under the model reaction condition catalysed by Pd/PPh_3 (1:2) system, the dinuclear species **84** (intermediate **VIII**) was observed as the major species with trace quantities of the mononuclear species **85** (intermediate **IX**) present. The addition of PPh_3 resulted in increased formation of complex **85** and rate acceleration. The rate acceleration was also observed for reactions using *ortho*-substituted phosphine ligands (*e.g.* $P(2\text{-}MeOC_6H_4)_3$ and $P(2\text{-}MeC_6H_4)_3$) expected to prevent the formation of dinuclear species such as **84**. The mononuclear **VI** complex (accessible via species **84** and **85**) was, therefore, concluded as being the catalytically active species. The dinuclear species **VIII** was postulated to act as a stable, off-cycle Pd-reservoir. In support of this hypothesis, the Pd specie **85** readily decomposed in solution at elevated temperature, whereas the Pd species **84** was stable upon heating.

5.1.5 Alternative Reaction Pathway

The proposed C–H bond activation step (referred to as path-1) was strongly supported by the experimental results. However, this mechanism on its own does not take into account the nonzero y-intercept observed for the pentafluorobenzene **56** concentration dependence

of the reaction rate. The nonzero y-intercept more specifically suggested the presence of an alternative reaction pathway (referred to as path-2).

Some observations were made regarding path-2 which was independent of the concentration of pentafluorobenzene **56**. The temperature-dependence study suggested the kinetic parameters were similar to the proposed AMLA(6)-TS (*i.e.* path-1). The reaction rate acceleration observed by the addition of PPh_3 was experimentally confirmed as the result of increased rate of path-2. This observation suggested the Pd(Ar)(κ^1-OAc)$(PPh_3)_2$ **85** (intermediate **IX**) was a path-2 intermediate. Based on limited experimental results, the magnitude of the nonzero y-intercepts was significantly reduced for reactions of deuteropentafluorobenzene **100** suggesting a path-2 inhibition.

The most likely mechanisms for path-2 was the involvement of an activated pentafluorobenzene **56** species such as $Ag(PPh_3)_n$-C_6F_5 (n = 1, 2 or 3). As reported by Whitaker and co-workers[180], these Ag complexes were able to react with catalytic Pd^{II}–Ar species **IX** via transmetallation to yield $Pd^{II}(Ar)(C_6F_5)(PPh_3)_n$ complex **XII** as the RL-step (**Scheme 77**). This mechanism was in agreement with the rate acceleration observed by the increased concentration of $Pd^{II}(Ar)(\kappa^1$-OAc$)(PPh_3)_2$ **85** (intermediate **IX**), the observed nonzero y-intercept and the energetic similarities in the two reaction pathways. However, no evidence for the formation of Ag-C_6F_5 was obtained from the ^{19}F NMR spectroscopic analysis (reported at δ −105 in THF)[181] or MS of the reaction mixture.

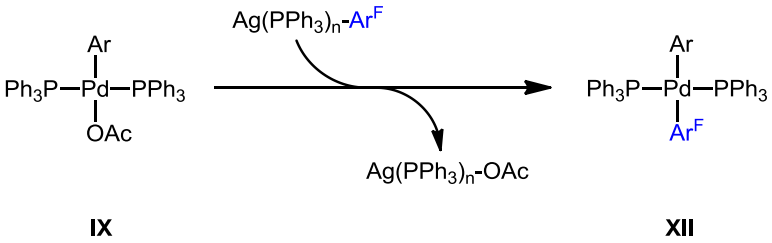

Scheme 77. Possible mechanism for path-2 involving silver species.

Alternatively the reaction of Pd(Ar)(κ^1-OAc$)(PPh_3)_2$ **IX** could proceed via a dissociative mechanism in which the ligand loss was the RL-step of the reaction (**Scheme 78**). Although this mechanism would take the nonzero y-intercept into account, it does not fit the large negative entropy of activation observed for path-2.

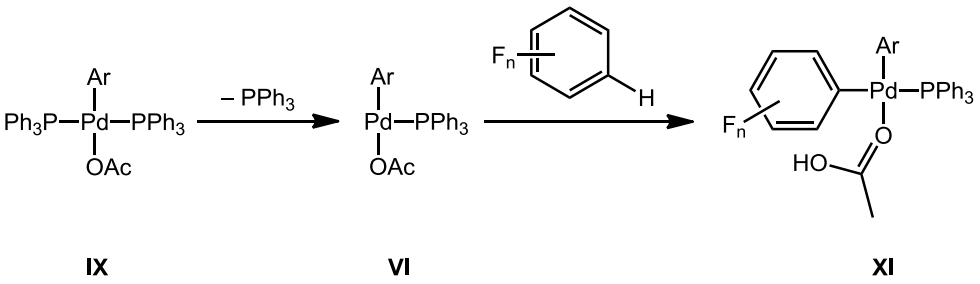

IX **VI** **XI**

Scheme 78. Possible mechanism for path-2 involving PPh_3 ligand dissociation as the RL-step.

Another possibility for path-2 was a Pd-NPs-catalysed reaction pathway. The pre-formed Pd-NPs in the presence of a stabilising polymer were catalytically active, albeit less effectively. It was recognised that the Pd-NPs formed *in situ* were expected to be more active than pre-formed Pd-NPs. A series of tests were performed to determine the role of heterogeneous catalysis in the reaction. The results were inconclusive due to the uncertainties in the experiments (*i.e.* Hg^0 drop-test and PVPy poisoning experiments). The involvement of Pd-NPs in the reaction mechanism cannot be ruled out and may contribute to the observed nonzero y-intercept.

There were a few possible explanations for the reduced contribution of path-2 to the overall rate for the reaction of deuteropentafluorobenzene **100**. While the pentafluorobenzene **56** was commercially purchased and used without purification, the synthesised deuteropentafluorobenzene **100** was purified by distillation. There might, therefore, be a promoter or an inhibitor in the commercially purchased pentafluorobenzene **56** or in the deuterated material **100**. The proposed mechanisms for the path-2 are speculative and further experimental work is required for clarification. At this stage it was not possible to propose a mechanism fully consistent with the results.

5.1.6 Reductive Elimination

Bis(phosphine)diorganopalladium complexes of the formula $Pd^{II}R_2(PR'_3)_2$ are known to thermally decompose leading to C–C bond formation.[386, 387] In this study a sequential mechanism is proposed involving the initial loss of the AcOH, generated from the C–H bond activation, from the intermediate **XI** (**Scheme 79**). The resulting tricoordinated complex **XIII** then undergoes concerted intramolecular 1,1-reductive elimination to give the Ar^F-Ar product.[388] The resulting "$Pd(PPh_3)$" **XIV** intermediate can regenerate the active catalyst $[Pd^0(CO_2R)(PPh_3)]^-$ **I** by coordination of carboxylate to complete the catalytic cycle, or precipitate out as Pd black.[176]

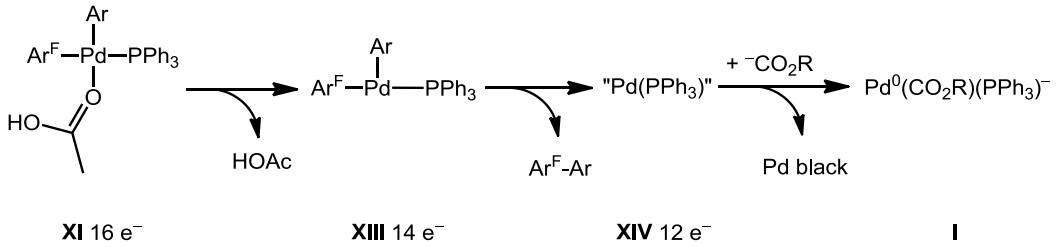

Scheme 79. The proposed reductive elimination step of the catalytic cycle (R = Me or OAg).

Intermediate **XI** was not directly observed experimentally, although complex **XIII** was detected by ESI(+)-MS as $Pd(Ar^{+})(C_6F_5)(PPh_3)$ **110** (Ar^{+} = C_6H_4-4-$CH_2PPh_4^{+}$) using a charge-tagged iodoarene cation **107** as the substrate. No kinetic information regarding the step was obtained as it follows that the C–H bond activation step was identified as the RL-step of the catalytic cycle.

5.1.7 Overall Catalytic Cycle

The elementary steps discussed in the previous sections were combined to propose a catalytic cycle for the direct arylation reaction of iodoarene with fluorobenzene (**Scheme 80**). It was discovered that the key step in the catalytic cycle involved equilibrium between on-cycle mononuclear Pd complex and off-cycle dinuclear Pd species. All of the active and inactive Pd species co-exists in endergonic equilibria during the multistep catalytic process. The proposed mechanism for the reaction is consistent with the experimental results and provides strong evidence for the AMLA(6)-TS. The alternative reaction pathway was attributed to the transmetallation reaction of $Ag(PPh_3)_n$-C_6F_5 species. Although these species were not observed during the reaction, it is a plausible reaction pathway which agreed most strongly with the kinetic observations.

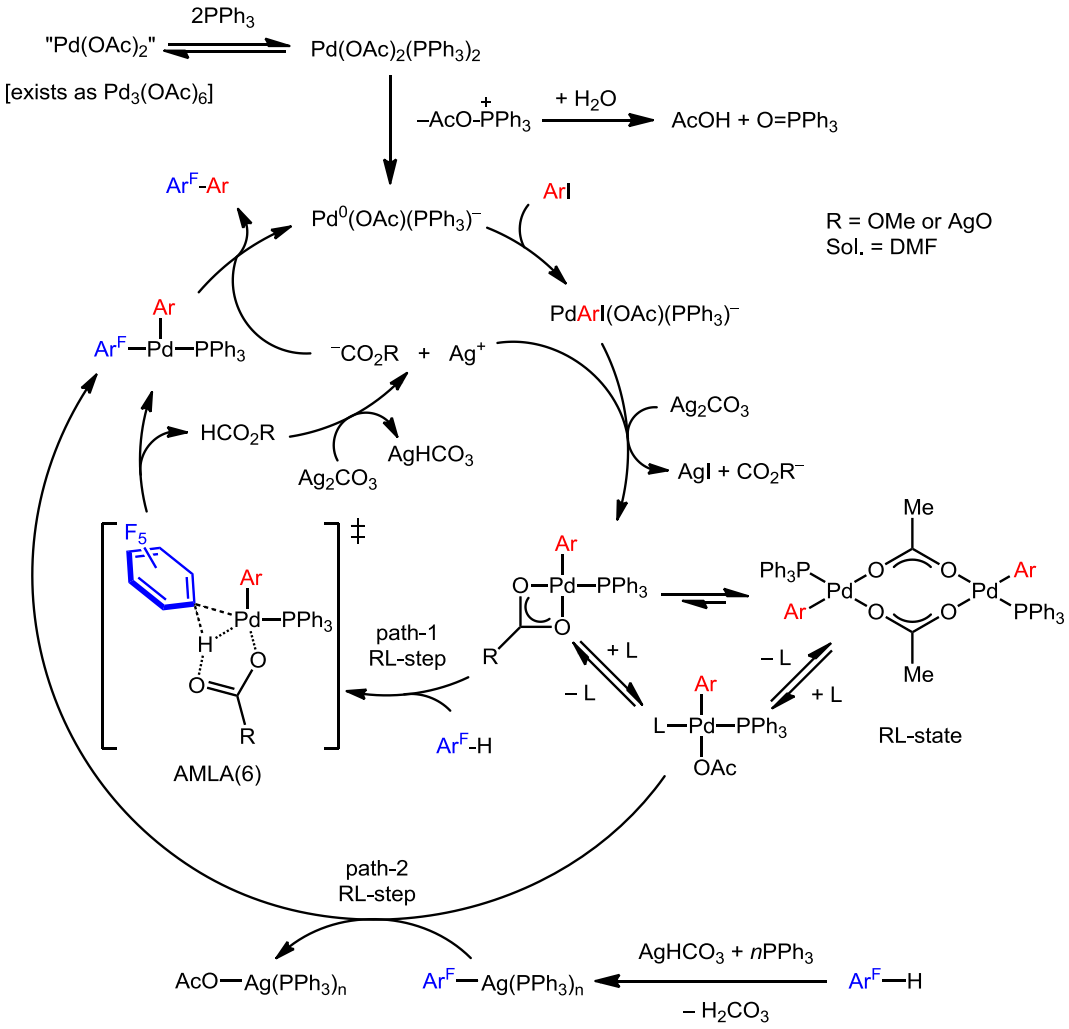

Scheme 80. The proposed 2-path mechanism for the Pd-catalysed direct arylation of iodoarene with polyfluorobenzene**.**

5.2 Future Work

5.2.1 Continued Mechanistic Study on the Model Reaction

Despite best efforts to cover as many mechanistic aspects of the direct arylation reaction of fluoroarenes, there are still uncertainties in the proposed catalytic cycle. Firstly, experiments focussing on the characterisation of the RL-step independent of the concentration of pentafluorobenzene **56** are necessary to support the proposed involvement of $Ag(PPh_3)_n$-C_6F_5 species. The isolated pentafluorophenylsilver **113** can be prepared following the procedure reported by Sun and co-workers (**Scheme 81**).[389] The reactivity of the complex under the model reaction condition can then be studied in detail.

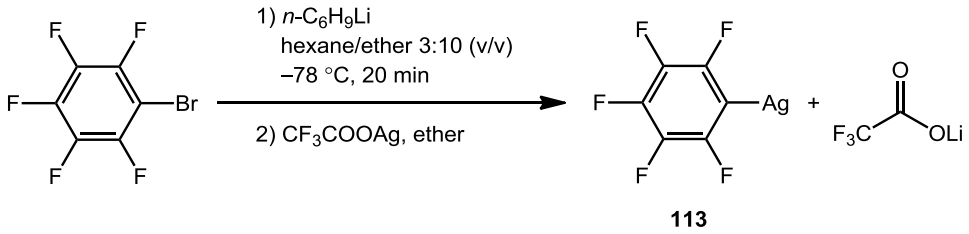

Scheme 81. Literature procedures for the synthesis of perfluorophenylsilver **113** (Sun and co.).[389]

The kinetic behaviour detailed in the model reaction suggests the catalytic cycle is mostly homogeneous in nature. However, based on the reasonable reactivity of Pd-NPs on PVP, the sigmoidal kinetic profile for the reaction using [Me_4N]OAc additive and the report of polyfluoroarene C–H bond functionalisation catalysed by Pd-NCs[127], it is not possible to unequivocally deny the possible involvement of Pd aggregates in the reaction. Firstly, it is necessary to determine the formation of NPs during the reaction by using transmission electron microscopy (TEM). The possible leaching of operationally homogeneous catalyst from the Pd-NPs can be tested by the three-phase test,[301, 390] studying the direct arylation of free pentafluorobenzene **56** with iodoarene attached to a solid support **114** (**Scheme 82**). Successful formation of the product **115** would indicate the Pd-NPs suffers from leaching. Additionally, the catalytic ability of different NPs can be probed to investigation the possible role of Pd-NPs.

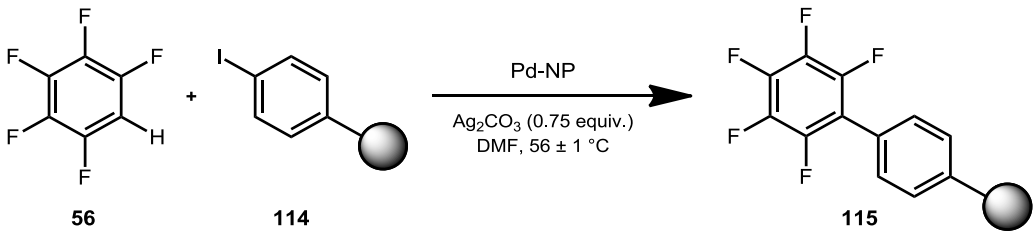

Scheme 82. Suggested reaction condition for the three-phase test of the model reaction.

Additional experiments are also required to explore the rate dependence on the concentration of deuteropentafluorobenzene **100**. Rationalisation of the apparent reduced contribution of path-2 to the overall rate of the reaction is expected to provide evidence on the nature of path-2. Additionally, this would allow the TS geometry of the RL-step to be characterised following the TDKIE analysis reported by Kwart and co-workers.[276] Obtaining the rate constants for the concentrations of deuteropentafluorobenzene **100** between the 4 data points shown below can be beneficial (**Figure 70**).

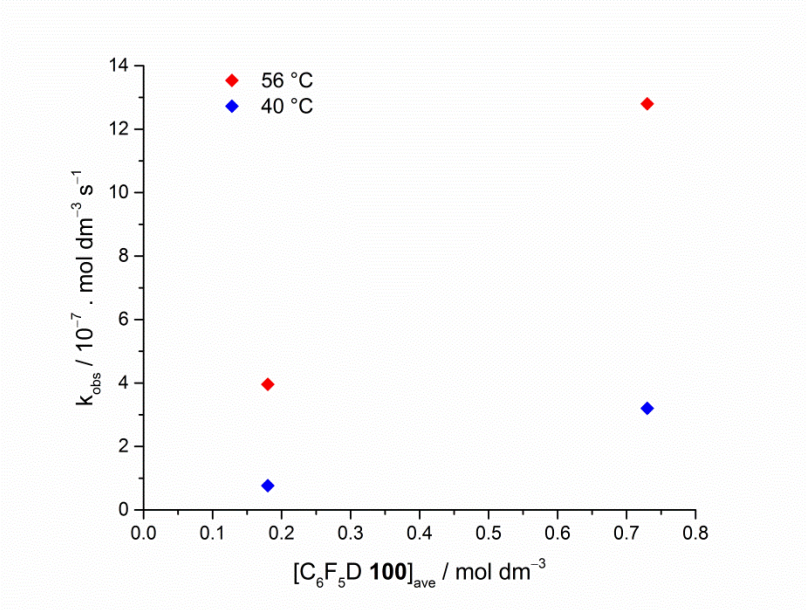

Figure 70. The preliminary results on the rate dependence on $[C_6F_5D$ **100**$]_{ave}$.

It is important to study the equilibrium between the dinuclear Pd species and the mononuclear Pd species, determined to play a significant role in the catalytic cycle, in further detail. The favoured formation of the dinuclear species **84** over the mononuclear species **85** was based on the ^{1}H and ^{31}P NMR spectroscopic analysis of the isolated Pd complexes in DMF-d_7. This was in agreement with the study reported by Wakioka and co-workers on the equilibrium between dinuclear **45** and mononuclear **51** species in DCM (**Scheme 83**).[175] Formation of the mononuclear species **51** is expected under the reaction condition with elevated temperature (*e.g.* 56 °C). By determining the equilibrium constant (K_D), it would be possible to determine the second order rate constant (k_2) for the C–H bond activation step (*i.e.* $k_2(2K_D)^{-1/2} = (5.73 \pm 0.43) \times 10{-}4$ $dm^{3/2}$ $mol^{-1/2}$ s^{-1}).

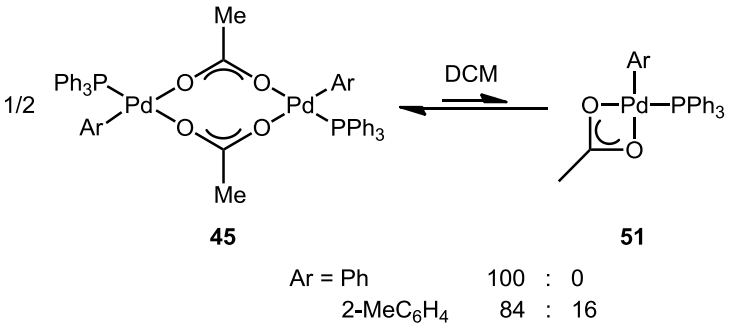

Scheme 83. Equilibrium between dinuclear **45** and mononuclear **51** Pd-OAc species in DCM studied by FT-IR spectroscopy (Wakioka and co.).[175]

Another aspect of the reaction that was not studied in detail was the role played by the solvent in the reaction mechanism. The research focussed on the use of DMF as the solvent due to the lack of solvent peak in the region of the IR spectrum of interest for monitoring

the reaction by *in situ* FT-IR spectroscopic analysis. Based on the results obtained from testing the effect of the solvent on the yield of the product **58** formation, propylene carbonate was shown as a less hazardous alternative to DMF (see Chapter 2.4). The reaction in water could also be tested, as the original methodology[126] was performed in water.

The mechanistic study could benefit greatly from computational calculations using DFT methods, based on the proposed catalytic cycle (**Scheme 80**) and the experimentally determined kinetic parameters (See Chapter 3). Furthermore, the roles played by the two carboxylate ligands could also be clarified, in addition to comparing mechanism involving inner-sphere and outer-sphere C–H bond activation.

5.2.2 Exploring the Possibility of AMLA(4) Pathway

During testing, the use of different palladium pre-catalyst and base additives, the combination of $Pd(PPh_3)_4$ and Ag_2O was observed to be effective. Similar to Ag_2CO_3, Ag_2O is often attributed to act as a base, a mild oxidant and halogen scavenger.[391] Hirabayashi and co-workers reported the cross-coupling of organosilicon reagents **116** using $Pd(PPh_3)_4$ pre-catalyst and Ag_2O additive (**Scheme 84**).[392] The transmetallation step of the catalytic cycle was proposed to involve 6-membered TS **118**. Similar reaction mechanism may be possible for the reaction of pentafluorobenzene **56** with the Ar^F–H bond instead of R–Si bond.

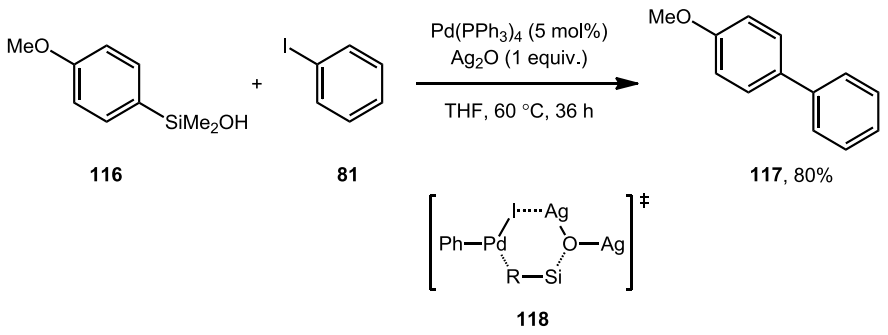

Scheme 84. Pd-catalysed Hiyama cross-coupling reaction promoted by silver(I) oxide with proposed transmetallation via 6-membered TS **118** (Hiyama and co.).[392]

A similar mechanism may exist for the reaction of $Pd(Ar)(I)(PPh_3)_2$ **82a** in the presence of Ag_2O. Alternatively, the model reaction may involve hydroxide anion generated from the reaction of Ag_2O with the H_2O present in the DMF (*i.e.* 110 ppm).[393] This could result in the formation of arylpalladium hydroxide complex involved in AMLA(4)-TS. The possibility of such TS **119** was observed in the stoichiometric reaction of $[Pd(Ph)(\mu\text{-}OH)(PPh_3)]_2$ **83a** with pentafluorobenzene **56** which resulted in successful product **64**

formation (**Scheme 85**). For further experiments, use of [Pd(4-tolyl)(μ-OH)(PPh_3)]$_2$ **83b** would be beneficial with the methyl proton to follow by ^{1}H NMR spectroscopic analysis.

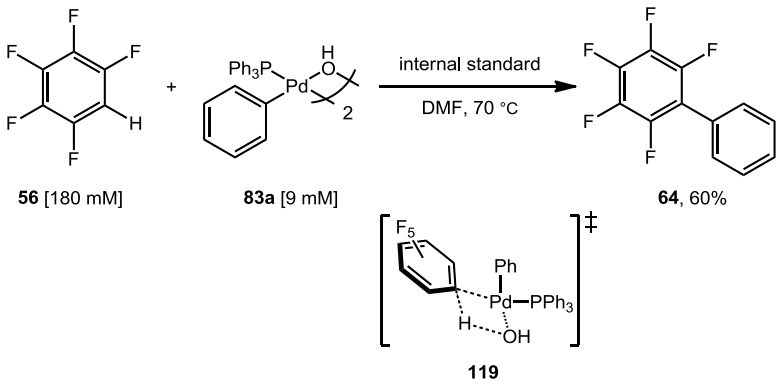

Scheme 85. Stoichiometric reaction of Pd(Ph)(μ-OH)(PPh_3)]$_2$ **83a** with pentafluorobenzene **56**.

5.2.3 Mechanism of Dehydrogenative Arylation of Fluoroarenes

Through the progressive development of C–C bond forming reactions, dehydrogenative arylation is emerging as a viable synthetic strategy for certain substrates.[394, 395] The Pd-catalysed dehydrogenative arylation of fluoroarenes were reported by Li and co-workers.[166] The proposed mechanism involved the deprotonation of pentafluorobenzene **56** and the formation of polyfluoroarylpalladium species **120**. The intermediate **120** then reacted via AMLA(6)-TS followed by reductive elimination of the biaryl product **64**. The similarities in the reaction conditions with the direct arylation reaction of polyfluoroarenes suggest the experimental procedures detailed in the thesis can be directly applied in the mechanistic investigation of this reaction.

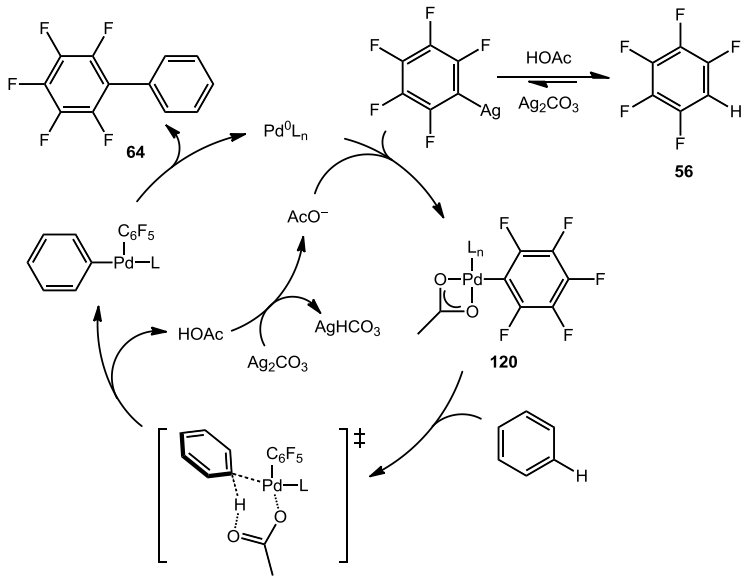

Scheme 86. The Pd^0/Pd^{II} catalytic cycle proposed for the dehydrogenative arylation of pentafluorobenzene **56** (Li and co.).[166]

Chapter 6: Experimental

6.1 General Information on Chemicals and Instruments

Solvents and Reagents

Unless stated otherwise, all reagents were purchased from commercial sources (Acros Organics, Alfa Aesar, Fischer Scientific, Fluorochem, Sigma-Aldrich or TCI) and used without further purification. $Pd(OAc)_2$ was purchased from Precious Metals Online. PPh_3 was recrystallized from ethanol and dried over P_2O_5. Iodobenzene **81**, pentafluorobenzene **56**, 1,3-difluorobenzene **26** and pentafluorobromobenzene **99** were degassed by three cycles of freeze-pump-thaw and stored over 3 Å molecular sieves. Extra dry DMF (99.8%, water < 50 ppm) purchased from Acros Organics was degassed by bubbling with nitrogen gas under sonication for 30 minutes and stored in an ampoule over 3 Å molecular sieves. Other dry solvents (*e.g.* benzene, methanol) were collected from the solvent purification system and distilled under argon. Chloroform-d was dried by stirring over CaH_2 for 24 h, degassed by three cycles of freeze-pump-thaw and distilled at high vacuum (0.03 mm Hg). The synthesised Pd complexes were stored at −20 °C in the freezer inside the glove box.

Reaction Conditions

Room temperature reactions were carried out at temperatures between 15–25 °C without thermostatic control. Air and moisture sensitive procedures were carried out using oven- or flame-dried glassware, inside dry argon filled glove box (< 0.5 ppm O_2) or using standard Schlenk line (10^{-2} mbar) techniques connected to oxygen-free argon or nitrogen gas. Nitrogen gas from the liquid nitrogen tank was dried by passing through a column of sodium hydroxide pellets and silica prior to use.

Flash Chromatography

Merck aluminium backed thin-layer chromatography (TLC) plates with silica gel 60 F254 were used for TLC. The spots were visualised using ultraviolet lights (λ_{max} = 254 nm). Retention factors (R_f) are reported to two decimal places with the solvent system used for purification. Fluka 60 silica gel (35–75 μm particle size) was used for flash column chromatography.

Nuclear Magnetic Resonance (NMR) Spectroscopy

Solution NMR spectra were recorded using Jeol ECX400 MHz or Jeol ECS400 MHz (^{1}H 400 MHz; ^{13}C 101 MHz; ^{19}F 376 MHz; ^{31}P 162 MHz) spectrometers (from JEOL Ltd, Japan). Higher frequency NMR spectra were recorded using Bruker AMX 500 (^{1}H 500 MHz; ^{2}H 77 MHz; ^{13}C 126 MHz; ^{19}F 471 MHz; ^{31}P 202 MHz) spectrometer (from Bruker Co., Germany). Solution phase NMR of suspensions (*i.e.* HR-MAS NMR) were recorded using a Bruker Avance III HD spectrometer (from Bruker Co., Germany) equipped with 4 mm MAS BB/BB/1H/19F H8906–20/0003. The spectra were measured at rotation frequencies of 3 kHz. Unless stated otherwise, the NMR spectra were measured at temperatures between 22–25 °C. The chemical shifts are quoted in parts per million (ppm, δ) relative to tetramethylsilane (TMS). Residual protio solvent resonances of DMF-d_7 (δ_H 8.03), benzene-d_6 (δ_H 7.16), chloroform-d (δ_H 7.26) and dichloromethane-d_2 (δ_H 5.32) were used as internal reference for proton (^{1}H) NMR spectra and reported to two decimal places. Residual deutero solvent resonance of benzene (δ_H 7.26) was used as internal reference for deuterium (^{2}H) NMR spectra and reported to two decimal places. Carbon-13 (^{13}C) NMR spectra were internally referenced to residual solvent resonances of chloroform-d (δ_C 77.2) and benzene-d_6 (δ_C 128.1) and reported to one decimal place. Fluorine-19 (^{19}F) NMR spectra were externally referenced to $CFCl_3$ with ^{1}H decoupling and reported to two decimal places. Phosphorus-31 (^{31}P) NMR spectra were externally referenced to H_3PO_4 with ^{1}H decoupling and reported to one decimal place. Coupling constants (*J*) are reported to ±0.5 Hz. Peak multiplicities are described as singlet (s), doublet (d), triplet (t), quartet (q), quintet (quin), sextet (sext), heptet (hept), multiplet (m), apparent (app) or broad (br). MestReNova™ version 6.0.2-5475 and Bruker TopSpin™ version 3.2 and 3.5 were used to analyse the generated NMR spectrum.

Mass (MS) Spectrometry

Electrospray ionisation (ESI) mass spectrometry was measured using a Bruker micrOTOF spectrometer (from Bruker Daltonics Co., Germany). The *m/z* values were accurate to four decimal places. Electrospray spectrometry (EI) mass spectrometry and liquid injected field desorption ionization (LIFDI) mass spectrometry were measured using Waters GCT Premier mass spectrometer (from Waters Co., USA). The *m/z* values were accurate to two decimal places. Mass-to-charge ratio (*m/z*) was reported in Daltons (Da) with the percentage abundance of the ion. For compounds with multiple isotopic peaks, the most abundant ion was reported. Naturally occurring isotopes of Pd are ^{102}Pd, ^{104}Pd, ^{105}Pd, ^{106}Pd, ^{108}Pd and ^{110}Pd. The isotope distribution plots were made using OriginPro™ 2016 (from Origin Lab Co., USA) version b9.3.226 (64-bit).

Infrared (IR) Spectroscopy

A solid phase IR spectrum was prepared by means of a KBr disc, and a liquid phase IR spectrum prepared in CaF_2 solution cell was recorded using a Unicam Research Series FT-IR spectrometer. WinFIRST software was used to process and analyse the data. A solid phase IR spectrum, obtained by method of ATR, was recorded using an ALPHA FT-IR spectrometer (from Bruker Optics, Germany). OPUS (build 7.2.139.1294) was used to process and analyse the data. Results are presented as absorption maxima in wavenumbers (ν_{max} cm^{-1}) and described as weak (w), medium (med), strong (st) or broad (br).

In situ FT-IR spectra were recorded using K6 Conduit (16 mm probe) with a SiComp (silicon ATR sensor)-fitted ReactIR™ iC10 (from Mettler-Toledo AutoChem, Inc., USA). Spectra were collected every minute between 4000–650 cm^{-1} at resolution of 4 cm^{-1} with 167 scans min^{-1}. Obtained data were analysed using MC-IR™ version 4.0 and Microsoft Excel 2010 version 14.7106.5003 (32-bit). The results were presented using Origin Pro 2016 (from Origin Lab Co., USA) version b9.3.226 (64-bit).

Thermometer

A Tenma 72-7715 (from Farnell, UK) thermometer connected to a K-type thermocouple with 0.2% ± 0.6 °C accuracy calibrated in an ice bath at 0 °C. The thermocouple was submerged in the solvent to monitor the temperature of the reaction mixture.

Melting Points

Stuart™ digital SMP3 (from Stuart Equipment, UK) with resolution of 0.1 °C and accuracy ±0.5 °C at 20 °C, ±1.5 °C at 360 °C, was used to measure the melting points of synthesised compounds. Decomposition temperatures (dec.) were quoted for Pd complexes.

Elemental Analysis

Elemental (CHN) analysis was run on Exeter Analytical CE-440 Elemental Analyser. The percentages were an average of three runs and recorded to two decimal places.

Testing the Water Content in the Solvents

The water content of the DMF was determined using Mettler Toledo DL32 Karl Fischer Coulometer (from Fischer Scientific, UK) with double platinum pin electrodes.

6.2 General Procedures

General Procedure A: Synthesis of Fluorinated Biaryls

A light-protected Schlenk tube with Ag_2CO_3 (0.186 g, 0.68 mmol, 0.75 equiv.), PPh_3 (24 mg, 0.092 mmol, 10 mol%) and $Pd(OAc)_2$ (10 mg, 0.045 mmol, 5 mol%) was evacuated and backfilled with atmosphere of nitrogen three times. To this, haloarene (0.9 mmol, 1 equiv.) was added against the flow of nitrogen, followed by the fluoroarene (1.35–2.70 mmol, 1.5–3 equiv.) and 2.5 cm^3 DMF. The mixture was heated at 70 °C for 24 hours under atmosphere of nitrogen. After the crude mixture had cooled to ambient temperature, it was extracted with 80 cm^3 EtOAc and 40 cm^3 deionized water. The aqueous phase was back-extracted with EtOAc (2 × 40 cm^3), dried over Na_2SO_4, filtered and solvent removed under vacuum to give a crude product.

General Procedure B: Synthesis of 1,3-Difluoro Biaryls

A light-protected Schlenk tube with Ag_2CO_3 (93 mg, 0.34 mmol, 0.75 equiv.), PPh_3 (18 mg, 0.069 mmol, 15 mol%) and $Pd(OAc)_2$ (5 mg, 0.022 mmol, 5 mol%) was evacuated and backfilled with atmosphere of nitrogen three times. To this, haloarene (0.45 mmol, 1 equiv.) was added against the flow of nitrogen, followed by the fluoroarene (4.5 mmol, 10 equiv.) and 2.5 cm^3 DMF. The mixture was heated at 75 °C for 24 hours under atmosphere of nitrogen. After the crude mixture had cooled to ambient temperature, it was extracted with 80 cm^3 EtOAc and 40 cm^3 deionized water. The aqueous phase was back-extracted with EtOAc (2 × 40 cm^3), dried over Na_2SO_4, filtered and solvent removed under vacuum to give a crude product.

General Procedure C: Using *in situ* FT-IR Spectroscopy to Monitor the Kinetics of a Reaction Initiated by the Addition of Pentafluorobenzene 56

A light-protected three-necked 100 cm^3, round-bottom flask equipped with a stir bar was fitted to the IR probe with the second neck connected to the Schlenk line and the third neck sealed with a rubber septum. The flask was evacuated and refilled with nitrogen (× 3) before configuring the probe under nitrogen atmosphere. The IR instrument was set up by collecting second atmosphere background, followed by the solvent background of DMF. Data collection was started immediately after the set up. Reagents were added in the order of iodoarene, PPh_3, $Pd(OAc)_2$, and Ag_2CO_3 with 30 minutes gap between the addition of $Pd(OAc)_2$ and Ag_2CO_3. The mixture was heated in a pre-heated oil bath at 60 °C. The reaction was initiated by the addition of pentafluorobenzene **56**. The total volume of the mixture was maintained at 9.7 cm^3. The reaction mixture was stabilised at 56 ± 1 °C and

temperature measured using the digital thermometer, and stirred at a constant rate under continuous flow of nitrogen. The reaction progress was monitored following the IR signals of iodobenzene **81** (1016 cm^{-1} and 998 cm^{-1}), 4-iodotoluene **57** (1009 cm^{-1}), product **58** (989 cm^{-1}) and pentafluorobenzene **56** (957 cm^{-1} and 944 cm^{-1}).

General Procedure D: Using i*n situ* FT-IR Spectroscopy to Monitor the Kinetics of a Reaction Initiated by Mixing the Liquid and Solid Reagents of the Reaction

A light-protected three-necked 100 cm^3, round-bottom flask equipped with a stir bar was fitted to the IR probe with the second neck connected to the Schlenk line and the third neck sealed with a rubber septum. The round-bottom flask was charged with the solid reagents (*e.g.* pre-catalyst, Ag_2CO_3 and ligand in certain examples). The flask was evacuated and refilled with nitrogen (× 3) before configuring the probe and starting the data collection. A DMF (8.0 cm^3) solution of iodobenzene **81** and pentafluorobenzene **56** in a Schlenk tube was transferred into the round-bottom flask using a cannula. The Schlenk tube and the needle were rinsed with DMF, making the total volume of the mixture to 9.76 cm^3. The reaction was heated in a pre-heated oil bath at 60 °C and stirred at a constant rate under continuous flow of nitrogen. The temperature of the reaction mixture was stabilised at 56 ± 1 °C after *ca.* 10 min monitoring using the digital thermometer. The reaction progress was monitored following the IR signals of iodobenzene **81** (1016 cm^{-1} and 998 cm^{-1}), 4-iodotoluene **57** (1009 cm^{-1}), product **58** (989 cm^{-1}) and pentafluorobenzene **56** (957 cm^{-1} and 944 cm^{-1}).

6.3 Synthetic Procedures and Compound Data

Synthesis of 2,3,4,5,6-pentafluoro-4′-(methyl)biphenyl (58)

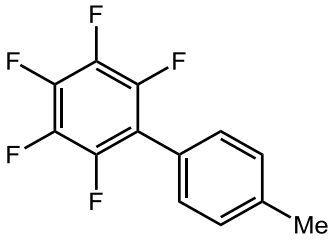

Pentafluorobenzene **56** (150 μL, 227 mg, 1.35 mmol, 1.5 equiv.) and 4-iodotoluene **57** (196 mg, 0.899 mmol, equiv.) were reacted following the general procedure A. Purification by flash chromatography (SiO_2, R_f = 0.53, petroleum-ether 40–60 °C) gave the product **58** (195 mg, 84%) as a white crystalline solid; m.p. 118.9–119.4 °C (lit.[126] 111–113 °C); ν_{max}/cm^{-1} (disc, KBr) 3043 (C–H aromatic str.), 2927 (CH_3 str.), 1514 (–CH=CH– str.), 1491 (C=C aromatic str.), 1062 (C–F str.), 988 (=C–H in-plane bend), 821 (=C–H oop bend); ^{1}H NMR (400 MHz, 16 scans, C_6D_6): δ = 7.10 (2 H, d, *J* = 8.0 Hz, 2′,6′-H), 6.97 (2 H, d, *J* = 8.0 Hz, 3′,5′-H), 2.06 (3 H, s, 4′-CH_3); ^{13}C NMR (100 MHz, 1024 scans, $CDCl_3$): δ = 144.3 (dm, *J* = 246.5 Hz, CF), 140.4 (dm, *J* = 233.5, 4-CF), 139.6 (s), 138.0 (dm, *J* = 250.5 Hz, CF), 130.1 (dt, *J* = 2.0, 1.0 Hz, 2′,6′-C), 129.6 (s, 3′,5′-C), 123.6–123.5 (m), 116.1 (dt, *J* = 16.5, 3.5 Hz), 21.5 (s, CH_3); ^{19}F NMR (376 MHz, 64 scans, C_6D_6): δ = −143.50 (2F, dd, *J* = 23.5, 8.0 Hz, 2,6-F), −156.20 (1 F, t, *J* = 21.5 Hz, 4-F), −162.27 (2 H, ddd, *J* = 23.5, 21.5, 8.0 Hz, 3,5-F); MS (EI) *m/z* (%) 258.0461 ($[M]^+$, 100) ($C_{13}H_7F_5$ requires 258.0468).

The analytical data obtained were in agreement with the literature.[126]

(*Lab book reference number*: GMHP-1-10)

Synthesis of 4,4′-(dimethyl)biphenyl (59)

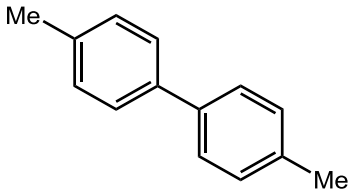

A mixture of 4-iodotoluene **57** (437 mg, 2.0 mmol, 1 equiv.), $Pd(OAc)_2$ (22 mg, 5 mol%) PPh_3 (52 mg, 10 mol%), Ag_2CO_3 (607 mg, 2.2 mmol, 1.1 equiv.) and benzoin (255 mg, 1.2 mmol, 0.6 equiv.) in 3 cm^3 DMF was heated at 120 °C for 5 hours under atmosphere of argon. The reaction mixture rapidly changed colour from yellow to black upon heating. The crude mixture was worked-up as described in the general procedure. Purification by flash chromatography (SiO_2, R_f = 0.21, petroleum-ether 40–60 °C) gave the product **55** (77 mg, 42%) as a white solid; m.p. 104.6–106.0 °C (lit.[396] 119–120 °C); ν_{max}/cm^{-1} (disc, KBr) 3029 (C–H aromatic str.), 2918 (CH_3 str.), 1510 (–CH=CH– str.), 808 (=C–H oop bend); ^1H NMR (400 MHz, 32 scans, CD_2Cl_2): δ = 7.49 (4 H, d, *J* = 8.0 Hz, 2,2′,6,6′-H), 7.25 (4 H, d, *J* = 8.0 Hz, 3,3′,5,5′-H), 2.39 (6 H, s, CH_3); ^{13}C NMR (100 MHz, 1024 scans, CD_2Cl_2): δ =138.6 (s), 137.4 (s), 130.0 (s, 3,3′,5,5′-H), 127.1 (s, 2,2′,6,6′-CH), 21.3 (s, CH_3); MS (EI) *m/z* (%) 182.1102 ($[M]^+$, 100) ($C_{14}H_{14}$ requires 182.1096).

A literature procedure was followed for the synthesis of this compound.[184] The analytical data obtained were in agreement with the literature.

(*Lab book reference number*: GMHP-2-69, GMHP-2-71)

Synthesis of 2,3,4,5,6-pentafluorobiphenyl (64)

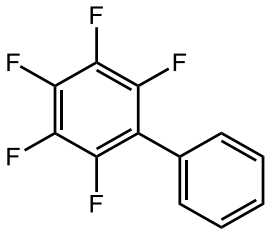

Pentafluorobenzene **56** (150 μL, 227 mg, 1.35 mmol, 1.5 equiv.) and iodobenzene **81** (100 μL, 0.894 mmol, 1 equiv.) were reacted following the general procedure A. Purification by flash chromatography (SiO_2, R_f = 0.51, petroleum-ether 40–60 °C) gave the product **64** (182 mg, 84%) as a white crystalline solid; m.p. 111.6–112.3 °C (lit.[397] 111–112 °C); ν_{max}/cm^{-1} (disc, KBr) 3054 (C–H aromatic str.), 2987 (CH_3 str.), 1526 (–CH=CH– str.), 1496 (C=C aromatic str.), 1063 (C–F str.), 984 (=C–H in-plane bend), 853 (=C–H oop bend); ^{1}H NMR (400 MHz, 8 scans, $CDCl_3$): δ = 7.53–7.45 (3 H, m, 2′,4′,6’-H), 7.44–7.41 (2H, m, 3′,5′-H); ^{13}C NMR (100 MHz, 1024 scans, $CDCl_3$): δ = 144.3 (dm, *J* = 247.5 Hz, CF), 140.5 (dm, *J* = 248.5 Hz, 4-CF), 138.0 (dm, *J* =250.5 Hz, CF), 130.3 (t, *J* = 1.5 Hz, 3′,5′-CH), 129.5 (s, 4′-H), 128.9 (s, 2′,6’-H), 126.5 (q, *J* = 2.0 Hz), 116.1 (td, *J* = 17.5, 4.0 Hz); ^{19}F NMR (376 MHz, 64 scans, $CDCl_3$): δ = −143.17 (2 F, dd, *J* = 23.0, 8.0 Hz, 2,6-F), −155.53 (1 F, t, *J* = 21.0 Hz, 4-F), −162.09 to −162.24 (2 F, m, 3,5-F); MS (EI) *m/z* (%) 244.0311 ([M]$^+$, 100) ($C_{12}H_5F_5$ requires 244.0311).

The analytical data obtained were in agreement with the literature.[91]

(*Lab book reference number*: GMHP-3-158)

Synthesis of 2,3,4,5,6-pentafluoro-4′-(nitro)biphenyl (67)

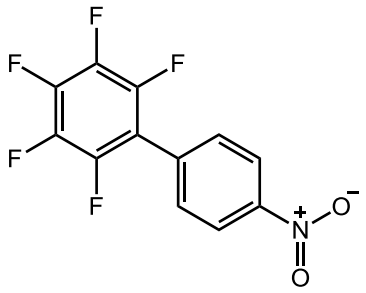

Pentafluorobenzene **56** (150 μL, 227 mg, 1.35 mmol, 1.5 equiv.) and 4-iodonitrobenzene (224 mg, 0.90 mmol, 1 equiv.) were reacted following the general procedure A. Purification by flash chromatography (R_f = 0.21, petroleum-ether 40–60 °C : EtOAc / 50 : 1) gave the product **67** (203 mg, 78%) as a white crystalline solid; m.p. 93.4–93.9 °C (lit.[126] 86–88 °C); ν_{max}/cm^{-1} (disc, KBr) 3115 (C-H aromatic str.), 1523 and 1495 (NO_2), 1348 (C–H str.), 1064 (C–F str.), 989 (=C–H in-plane bend), 866 and 840 (=C–H oop bend); ^{1}H NMR (400 MHz, 8 scans, $CDCl_3$): δ = 8.36 (2 H, dtd, *J* = 9.0, 2.3, 0.5 Hz, 3′,5′-H), 7.66–7.63 (2 H, dm, *J* = 8.5 Hz, 2′,6′-H); ^{13}C NMR (100 MHz, 1024 scans, $CDCl_3$, 22.2 °C): δ = 148.4 (s, 4′-C), 144.1 (dm, *J* = 250.0 Hz, CF), 141.4 (dm, *J* = 256.5 Hz, 4-CF), 138.2 (dm, *J* = 252.5 Hz, CF), 133.1–133.0 (m), 131.4 (td, *J* = 2.0, 1.0 Hz, 2′,6′-C), 124.0 (s, 3′,5′-C), 113.9 (td, J = 16.5, 4.0 Hz); ^{19}F NMR (376 MHz, 64 scans, $CDCl_3$): δ = −142.38 to −142.46 (2 F, m, 2,6-F), −152.38 (1 F, tt, *J* = 21.0, 1.5 Hz, 4-F), −160.63 to −160.76 (2 F, m, 3,5-F); MS (EI) *m/z* (%) 289.0177 ($[M]^+$, 100) ($C_{12}H_4F_5NO_2$ requires 289.0162).

The analytical data obtained were in agreement with the literature.[126]

(*Lab book reference number*: GMHP-3-161)

Synthesis of 2,3,4,5,6-pentafluoro-4′-(trifluoromethyl)biphenyl (66)

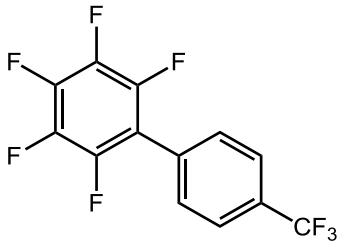

Pentafluorobenzene **56** (150 μL, 227 mg, 1.35 mmol, 1.5 equiv.) and 4-iodobenzotrifluoride (130 μL, 0.885 mmol, 1 equiv.) were reacted following the general procedure A. Purification by flash chromatography (SiO_2, R_f = 0.42, hexane) gave the product **66** (187 mg, 68%) as a white crystalline solid; m.p. 60.1–61.7 °C (lit.[398] 59–60 °C); ν_{max}/cm^{-1} (disc, KBr) 2930 (C–H aromatic str.), 1533 (–CH=CH– str.), 1489 (C=C aromatic str.), 1327, 1164, 1063 (C–F str.), 988 (=C–H in-plane bend), 848 (=C–H oop bend); ^{1}H NMR (400 MHz, 16 scans, C_6D_6): δ = 7.30 (2 H, d, *J* = 8.0 Hz, 2′,6′-H), 6.95 (2 H, d, *J* = 8.0 Hz, 3′,5′-H); ^{13}C NMR (100 MHz, 1024 scans, $CDCl_3$): δ = 144.3 (dm, *J* = 249.0 Hz, CF), 141.2 (dm, *J* = 255.5 Hz, 4-CF), 138.2 (dm, *J* = 252.0 Hz, CF), 131.6 (q, *J* = 33.0 Hz), 130.8 (td, *J* = 2.0, 0.5 Hz, 3′,5′-C), 130.3 (s), 125.9 (q, *J* = 4.0 Hz, 2′,6′-C), 124.0 (q, *J* = 272.5 Hz, CF_3), 114.7 (td, *J* = 17.0, 4.2 Hz); ^{19}F NMR (376 MHz, 64 scans, C_6D_6): δ = −62.60 (1 F, s, CF_3), −143.69 to −143.77 (2 F, m, 2,6-F), −154.54 (1 F, tt, *J* = 21.5, 1.5 Hz, 4-F), −161.83 to −161.97 (2 H, m, 3,5-F); MS (EI) *m/z* (%) 312.0190 ($[M]^+$, 100) ($C_{13}H_4F_8$ requires 312.0185).

The analytical data obtained were in agreement with the literature.[91]

(*Lab book reference number*: GMHP-5-278)

Synthesis of 2,3,4,5,6-pentafluoro-4′-(fluoro)biphenyl (65)

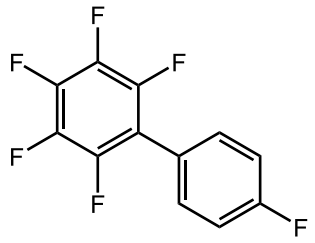

Pentafluorobenzene **56** (150 μL, 227 mg, 1.35 mmol, 1.6 equiv.) and 1-fluoro-4-iodobenzene (100 μL, 0.867 mmol, 1 equiv.) were reacted following the general procedure A. Purification by flash chromatography (SiO_2, R_f = 0.39, hexane) gave the product **65** (185 mg, 81%) as a white crystalline solid; m.p. 115.5–116.4 °C (lit.[91] 116–118 °C); ν_{max}/cm^{-1} (ATR) 2918 (C–H aromatic str.), 1489 (C=C aromatic str.), 982 (C–F str.), 843 (=C–H oop bend); ^{1}H NMR (400 MHz, 32 scans, C_6D_6): δ = 6.92–6.88 (2 H, m, 3′,5′-H), 6.79–6.73 (2 H, m, 2′,6′-H); ^{13}C NMR (100 MHz, 4096 scans, $CDCl_3$): δ = 163.2 (d, *J* = 250.0 Hz, 4′-CF), 144.3 (dm, *J* = 247.5 Hz, 2,6-CF), 140.6 (dm, *J* = 254.5 Hz, 4-CF), 138.1 (dm, *J* =251.5 Hz, 3,5-CF), 132.2 (dtd, *J* = 8.5 Hz, 2.0, 0.5 Hz, 3′,5′-C), 122.4–122.3 (m), 116.1 (d, *J* = 22.0, 2′,6′-C), 115.1 (td, *J* = 17.5, 4.4 Hz); ^{19}F NMR (376 MHz, 64 scans, C_6D_6): δ = −111.21 (1 F, tt, *J* = 8.5, 5.5 Hz, 4′-F), −144.02 (2 F, dd, *J* = 23.0, 8.0 Hz, 2,6-F), −155.85 (1 F, t, J = 21.5 Hz,4-F), −162.35 to −162.50 (2 F, m, 3,5-F).

The analytical data obtained were in agreement with the literature.[91]

(*Lab book reference number*: GMHP-5-281)

Synthesis of 2,3,5,6-tetrafluoro-4′-(methyl)biphenyl (70^{I})

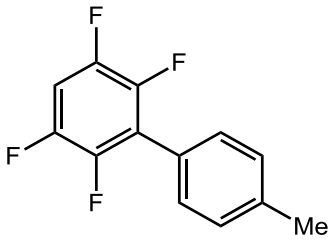

The reaction of 1,2,4,5-tetrafluorobenzene (300 μL, 403 mg, 2.69 mmol, 3 equiv.) and 4-iodotoluene **57** (197 mg, 0.904 mmol, 1 equiv.) was prepared following the general procedure A. Purification by flash chromatography (SiO_2, R_f =0.33, petroleum-ether 40–60 °C) gave the major product **70^{I}** (126 mg, 58%) as a white solid; m.p. 85.2–86.6 °C (lit.[122] 88–89 °C); ν_{max}/cm^{-1} (disc, KBr) 3078 (C–H aromatic str.), 2926 (CH_3 str.), 1502 (–CH=CH– str.), 1490 (C=C aromatic str.), 1175 (C–F str.), 930 (=C–H in-plane bend), 814 (=C–H oop bend); ^{1}H NMR (400 MHz, 8 scans, $CDCl_3$): δ = 7.36 (2 H, d *J* = 8.5 Hz, 2′,6′-H), 7.31 (2 H, d, *J* = 8.0 Hz, 3′,5′-H), 7.05 (1 H, tt, *J* = 9.5, 7.5 Hz, 4-H), 2.43 (3 H, s, CH_3); ^{13}C NMR (100 MHz, 1024 scans, $CDCl_3$): δ = 146.4 (dm, *J* = 247.0 Hz, CF), 144.0 (dm, *J* = 242.0 Hz, CF), 139.4 (s), 130.1 (t, *J* = 2.0 Hz, 2′,6′-C), 129.5 (s, 3′,5′-C), 124.6 (t, *J* = 2.5 Hz), 121.7 (t, *J* = 17.0 Hz), 104.4 (tt, *J* = 22.5, 0.5 Hz), 21.5 (s, CH_3); ^{19}F NMR (376 MHz, 64 scans, $CDCl_3$): δ = −139.25 (2 F, ddd, *J* = 22.5, 13.0, 9.5 Hz, 2,6-F), −143.86 to –143.97 (2 F, m, 3,5-F); MS (EI) *m/z* (%) 240.0568 ([M]$^+$, 100) ($C_{13}H_8F_4$ requires 240.0562).

The analytical data obtained were in agreement with the literature.[122]

(*Lab book reference number*: GMHP-3-128)

Synthesis of 1,4-di(4′,4″-tolyl)-2,3,5,6-tetrafluorobenzene (70^{II})

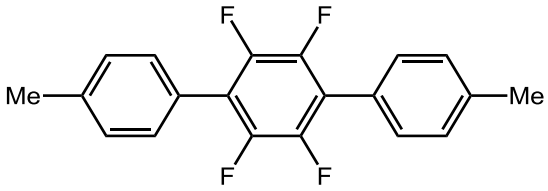

The compound was obtained as the minor product in the 2,3,5,6-tetrafluoro-4′-(methyl)biphenyl **70^{I}** reaction. Purification by flash column chromatography (SiO_2, R_f = 0.17, petroleum-ether 40–60 °C) gave the product **70^{II}** (33 mg, 11%) as a white solid; m.p. 221.3–222.9 °C (lit.[122] 210–212 °C); ν_{max}/cm^{-1} (disc, KBr) 3041 (C–H aromatic str.), 2926 (CH_3 str.), 1475 (C=C aromatic str.), 1193 (C–F str.), 971 (=C–H in-plane bend), 818 (=C–H oop bend); ^{1}H NMR (400 MHz, 16 scans, CD_2Cl_2): δ = 7.41 (4 H, d, *J* = 8.0 Hz, 2′,2″,6′,6″-H), 7.34 (4 H, d, *J* = 8.0 Hz, 3′,3″,5′,5″-H), 2.43 (6 H, s, CH_3); ^{19}F NMR (376 MHz, 64 scans, CD_2Cl_2): δ = −145.35 (4 F, s, 2,3,5,6-F); MS (EI) *m/z* (%) 330.1032 ([M]$^+$, 100) ($C_{20}H_{14}F_4$ requires 330.1032).

The analytical data obtained were in agreement with the literature.[122]

(*Lab book reference number*: GMHP-3-128)

Synthesis of 2,4,6-trifluoro-4′-(methyl)biphenyl (71^{I})

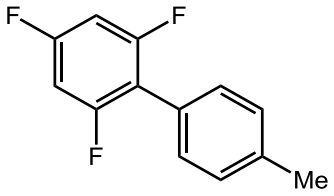

The reaction of 1,3,5-trifluorobenzene (280 μL, 358 mg, 2.71 mmol, 3 equiv.) and 4-iodotoluene **57** (197 mg, 0.904 mmol, 1 equiv.) was prepared following the general procedure A. Purification by flash chromatography (SiO_2, R_f = 0.45, petroleum-ether 40–60 °C) gave the major product **71^{I}** (114 mg, 57%) as a white solid; m.p. 70.9–71.6 °C (lit.[122] 74–75 °C); ν_{max}/cm^{-1} (disc, KBr) 3038 (C–H aromatic str.), 2922 (CH_3 str.), 1596 (–CH=CH– str.), 1486, 1438 and 1404 (C=C aromatic str.), 1123 (C–F str.), 1029 and 999 (=C–H in-plane bend), 840 and 818 (=C–H oop bend); ^{1}H NMR (400 MHz, 16 scans, C_6D_6): δ = 7.32 (2 H, d, *J* = 8.0 Hz, 2′,6′-H), 6.99 (2 H, dd, *J* = 8.0, 0.5 Hz, 3′,5′-H), 6.28 (2 H, td, *J* = 8.0, 1.0 Hz, 3,5-H), 2.06 (3 H, s, CH_3); ^{13}C NMR (100 MHz, 1024 scans, $CDCl_3$): δ = 161.7 (dt, *J* = 249.0, 15.5 Hz, 4-CF), 160.4 (ddd, *J* = 249.0, 15.0, 10.0 Hz, 2,6-CF), 138.4 (s), 130.2 (t, *J* = 1.5 Hz, 2′,6′-C), 129.3 (s, 3′,5′-C), 125.4 (s), 115.1 (td, *J* = 19.5, 5.0 Hz), 100.8–100.3 (m, 3,5-C), 21.4 (s, CH_3); ^{19}F NMR (376 MHz, 64 scans, C_6D_6): δ = −109.63 (1 F, tt, *J* = 9.0, 6.0 Hz, 4-F), –111.21 (2 F, t, *J* = 6.5 Hz, 2,6-F); MS (EI) *m/z* (%) 222.0655 ($[M]^+$, 100) ($C_{13}H_9F_3$ requires 222.0656).

The analytical data obtained were in agreement with the literature.[122]

(*Lab book reference number*: GMHP-3-127)

Synthesis of 1,3-di(4′,4′′-tolyl)-2,4,6-trifluorobenzene (71^{II})

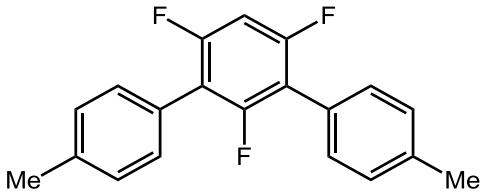

The compound was obtained as the minor product in the 2,4,6-trifluoro-4′-(methyl)biphenyl **71^{I}** reaction. Purification by flash chromatography (SiO_2, R_f = 0.23, petroleum-ether 40–60 °C) gave the minor product **71^{II}** (27 mg, 19%) as a white solid; m.p. 81.5–83.1 °C (lit.[122] 84–85 °C); ν_{max}/cm^{-1} (disc, KBr) 3024 (C-H aromatic str.), 2924 (CH_3 str.), 1598 (–CH=CH– str.), 1483–1397 (C=C aromatic str.), 1142 (C–F str.), 1038 and 1017 (=C–H in-plane bend), 833 and 817 (=C–H oop bend); ^{1}H NMR (400 MHz, 32 scans, C_6D_6): δ = 7.33 (4 H, d, *J* = 7.6 Hz, 2′,2′′,6′,6′′-H), 7.02 (4 H, d, *J* = 8.0 Hz, 3′,3′′,5′,5′′-H), 6.47 (1 H, td, *J* = 9.5, 2.0 Hz, 5-H), 2.08 (6H, s, CH_3); ^{13}C NMR (100 MHz, 4096 scans, $CDCl_3$): δ = 158.9 (ddd, *J* = 248.5, 15.5, 10.0 Hz, 3,5-CF), 157.4 (dt, *J* = 248.5, 9.5 Hz, 2-CF), 138.4 (s, C), 130.3 (dd, *J* = 3.0, 1.5 Hz, 2′,2′′,6′,6′′-H), 129.3 (s, 3′,3′′,5′,5′′ -CH), 125.8 (s, C), 115.2 (td, *J* = 21.0, 2.0 Hz, C), 100.5 (td, *J* = 27.0, 4.0 Hz, 5-C), 21.5 (CH_3); ^{19}F NMR (376 MHz, 64 scans, C_6D_6): δ = −113.26 (2 F, dd, J = 9.5, 6.5 Hz, 4,6-F), −114.89 (1 F, td, J = 6.5, 1.0 Hz, 2-F); MS (EI) *m/z* (%) 312.1127 ($[M]^+$, 100) ($C_{20}H_{15}F_3$ requires 312.1126).

The analytical data obtained were in agreement with the literature.[122]

(*Lab book reference number*: GMHP-3-127)

Synthesis of 1,3,5-tri(4′,4″,4‴-tolyl)-2,4,6-trifluorobenzene (71^{III})

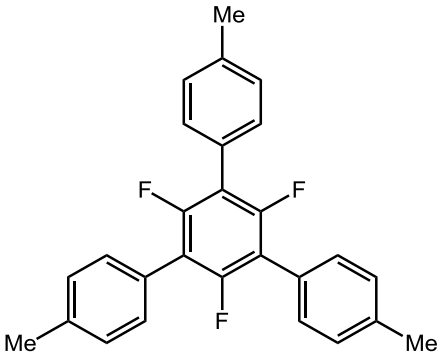

The compound was obtained as the minor product in the 2,4,6-trifluoro-4′-methyl-1,1′-biphenyl **71^{I}** reaction. Purification by flash chromatography (SiO_2, R_f = 0.1, petroleum-ether 40–60 °C : Et_2O / 100 : 1) gave the minor product **71^{III}** (5 mg, 4%) as a white solid; m.p. 185.9–190.1 °C (lit.[122] 186–187 °C); ν_{max}/cm^{-1} (disc, KBr) 3034 (C–H aromatic str.), 2965 (CH_3 str.), 1608 (–CH=CH– str.), 1458 and 1401 (C=C aromatic str.), 1262 (s), 1040 (C–F str.), 808 (=C–H oop bend); ^{1}H NMR (400 MHz, 16 scans, $CDCl_3$): δ = 7.39 (6 H, d, J = 8.0 Hz, 2′,2″,2‴,6′,6″,6‴-H), 7.28 (6H, d, J = 8.0 Hz, 3′,3″,3‴,5′,5″,5‴-H), 2.41 (9 H, s, CH_3); ^{19}F NMR (376 MHz, 64 scans, $CDCl_3$): δ = −116.92 (3 F, s, 2,4,6-F); MS (EI) *m/z* (%) 402.1591 ($[M]^+$, 100) ($C_{27}H_{21}F_3$ requires 402.1595).

The analytical data obtained were in agreement with the literature.[122]

(*Lab book reference number*: GMHP-3-127)

Synthesis of 2,6-difluoro-4′-methyl-1,1′-biphenyl (28)

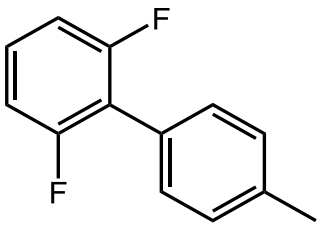

The reaction of 1,3-difluorobenzene **26** (450 μL, 523 mg, 4.59 mmol, 11 equiv.) and 4-iodotoluene **57** (94 mg, 0.431 mmol, 1 equiv.) was prepared following the general procedure B. Purification by silica-gel packed column chromatography (R_f = 0.28, petroleum-ether 40–60 °C) gave the product **28** (60 mg, 68%) as a white solid; m.p. 32.4–36.6 (lit.[122] 39–40 °C); ν_{max}/cm^{-1} (ATR) 3017 (C–H aromatic str.), 2927 (CH_3 str.), 1460 (C=C aromatic str.), 1227 (C–F str.), 993 (=C–H in-plane bend), 816 (=C–H oop bend); ^{1}H NMR (400 MHz, 32 scans, CD_2Cl_2): δ = 7.36 (2 H, dt, *J* = 8.0, 1.5 Hz), 7.34–7.26 (3 H, m), 7.04–6.97 (2 H, m), 2.42 (3H, s, CH_3); ^{13}C NMR (100 MHz, 1024 scans, CD_2Cl_2): δ = 160.7 (dd, *J* = 247.5, 7.0 Hz, 2,6-CF), 138.9 (s, C), 130.6 (t, *J* = 2.0 Hz, CH), 129.5 (s, CH), 129.3 (t, *J* = 10.5 Hz, 4-C), 126.7 (s, C), 119.0 (t, *J* = 19.0 Hz, C1), 112.1 (dd, *J* = 19.5, 7.0 Hz, 3,5-C), 21.6 (s, CH_3); ^{19}F NMR (376 MHz, 64 scans, CD_2Cl_2): δ = −115.27 (2 F, td, *J* = 6.5, 1.0 Hz, 2,6-F); MS (EI) *m/z* (%) 204.0752 ($[M]^+$, 100) ($C_{13}H_{10}F_2$ requires 204.0751).

The analytical data obtained were in agreement with the literature.[122]

(*Lab book reference number*: GMHP-7-456)

Synthesis of 2,6-difluoro-1,1′-biphenyl (30)

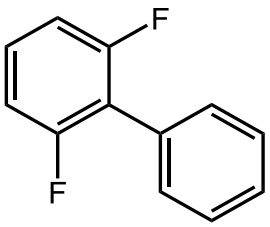

The reaction of 1,3-difluorobenzene **26** (450 μL, 523 mg, 4.59 mmol, 10 equiv.) and iodobenzene **81** (50 μL, 0.447 mmol, 1 equiv.) was prepared following the general procedure B. Purification by silica-gel packed column chromatography (R_f = 0.38, petroleum-ether 40–60 °C) gave the product **30** (70 mg, 82%) as a white solid; m.p. 91.9–93.7 °C (lit.[399] 93–94 °C); ν_{max}/cm^{-1} (ATR) 3061 (C–H aromatic str.), 1462 (C=C aromatic str.), 1227 (C–F str.), 992 (=C–H in-plane bend), 783 (=C–H oop bend); ^{1}H NMR (400 MHz, 32 scans, CD_2Cl_2): δ = 7.51–7.40 (5 H, m, 2′,3′,4′,5′,6′-H), 7.36–7.29 (1 H, m, 4-CH), 7.06–6.98 (2 H, m, 3,5-CH); ^{13}C NMR (100 MHz, 1024 scans, CD_2Cl_2): δ = 160.7 (dd, *J* = 247.5, 7.5 Hz, 2,6-CF), 131.0–130.7 (m, CH), 129.8 (s, 4-C), 129.6 (t, *J* = 10.5 Hz, CH), 128.9–128.7 (m, 2 overlapping CH), 119.0 (t, *J* = 19.0 Hz, C), 112.4–111.9 (m, 3,5-CH); ^{19}F NMR (376 MHz, 64 scans, CD_2Cl_2): δ = 115.26 (t, *J* = 7.0 Hz, 2,6-F).

The analytical data obtained were in agreement with the literature.[399]

(*Lab book reference number*: GMHP-7-453)

Synthesis of 2,3,5,6-tetrafluoro-4,4′-(dimethyl)biphenyl (78)

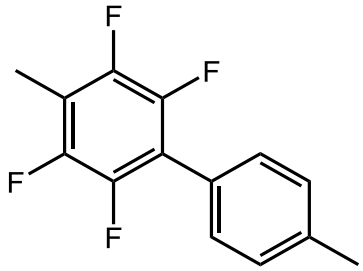

The reaction of 2,3,5,6-tetrafluorotoluene (165 μL, 222 mg, 1.35 mmol, 1.5 equiv.) and 4-iodotoluene **57** (198 mg, 0.908 mmol, 1 equiv.) was prepared following the general procedure A. Purification by flash chromatography (SiO_2, R_f =0.38, petroleum-ether 40–60 °C) gave the product **78** (214 mg, 93%) as a white crystalline solid; m.p. 65.3–66.6 °C (lit.[122] 67–68 °C); ν_{max}/cm^{-1} (ATR) 2924 (CH_3 str.), 1473 (C=C aromatic str.), 1062 (C–F str.), 921 (=C–H in-plane bend), 813 (=C–H oop bend); ^{1}H NMR (400 MHz, 16 scans, C_6D_6): δ = 7.27 (2 H, dt, *J* = 6.5, 1.4 Hz, 2′,6′-H), 6.99 (2 H, d, *J* = 8.0 Hz 3′,5′-H), 2.07 (3 H, s, 4′-CH_3), 1.81 (3 H, t, *J* = 2.0 Hz, 4-CH_3); ^{13}C NMR (100 MHz, 1024 scans, $CDCl_3$): δ = 145. 4 (dddd, *J* = 244.0, 14.5, 7.5, 4.0 Hz, CF), 143.7 (dddd, *J* = 245.5, 14.5, 5.5, 4.0 Hz, CF), 139.1 (s), 130.1 (t, *J* = 2.0 Hz, 2′,6′-C), 129.4 (s, 3′,5′-C), 124.9 (t, *J* = 2.5 Hz), 118.1 (t, *J* = 17.0 Hz), 114.9 (t, *J* = 19.5 Hz), 21.4 (s, 4′-CH_3), 7.6 (tt, *J* = 3.5, 2.0 Hz, 4-CH_3); ^{19}F NMR (376 MHz, 64 scans, C_6D_6): δ = −144.45 (2 H, ddq, *J* = 23.0, 13.0, 2.0 Hz, 3,5-F), −145.81 (2 H, dd, *J* = 22.5, 12.5 Hz, 2,6-F); MS (EI) *m/z* (%) 254.0720 ($[M]^+$, 100) ($C_{14}H_{10}F_4$ requires 254.0719).

The analytical data obtained were in agreement with the literature.[122]

(*Lab book reference number*: GMHP-6-364, GMHP-7-441)

Synthesis of 2,3,5,6-tetrafluoromethoxy-4′-(methyl)biphenyl (77)

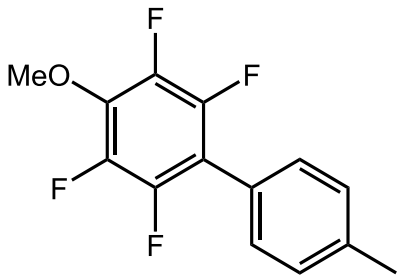

The reaction of 2,3,5,6-tetrafluoroanisole (190 μL, 246 mg, 1.36 mmol, 1.5 equiv.) and 4-iodotoluene **57** (198 mg, 0.908 mmol) was prepared following the general procedure A. Purification by flash chromatography (SiO_2, R_f =0.16, petroleum-ether 40–60 °C) gave the product **77** (227 mg, 92%) as a white solid; m.p. 43.6–45.0 °C (lit.[122] 49–51 °C); ν_{max}/cm^{-1} (disc, KBr) 2953 and 2925 (CH_3 str.), 1501 (–CH=CH- str.), 1487 (C=C aromatic str.), 1095 (C–F str.), 981 (=C–H in-plane bend), 825 (=C–H oop bend); ^{1}H NMR (400 MHz, 16 scans, C_6D_6): δ = 7.22 (2 H, d, *J* = 8.0 Hz, 2′,6′-H), 6.99 (2 H, d, *J* = 8.0 Hz, 3′,5′-H), 3.50 (3 H, t, *J* = 1.0 Hz, OCH_3), 2.07 (3 H, s, CH_3); ^{13}C NMR (100 MHz, 1024 scans, $CDCl_3$): δ = 144.5 (dm, *J* = 245.5 Hz, CF), 141.3 (ddt, *J* = 246.5, 16.0, 4.5 Hz, CF), 139.0 (s), 137.4 (tt, *J* = 12.0, 3.5 Hz, 4-C), 130.2 (t, *J* = 2.0 Hz, 2′,6′-C), 129.4 (s, 3′,5′-C), 124.4 (t, *J* = 2.0 Hz), 114.4 (t, *J* = 17.5 Hz), 62.3 (t, *J* = 3.5 Hz, OCH_3), 21.4 (s, CH_3); ^{19}F NMR (376 MHz, 64 scans, C_6D_6): δ = −145.47 (2 F, dd, *J* = 22.5, 9.0 Hz, 2,6-F), −158.45 (2 F, dd, *J* = 22.5, 8.5 Hz, 3,5-F); MS (EI) *m/z* (%) 270.0679 ($[M]^+$, 100) ($C_{14}H_{10}F_4O$ requires 270.0668).

The analytical data obtained were in agreement with the literature.[122]

(*Lab book reference number*: GMHP-5-253, GMHP-7-442)

Synthesis of 2,3,5,6-tetrafluorochloro-4′-(methyl)biphenyl (79)

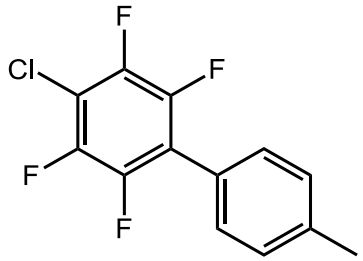

The reaction of 1-chloro-2,3,5,6-tetrafluorobenzene (165 μL, 254 mg, 1.38 mmol, 1.5 equiv.) with 4-iodotoluene **57** (198 mg, 0.909 mmol, 1 equiv.) was prepared following the general procedure A. Purification by flash chromatography (SiO_2, R_f =0.40, petroleum-ether 40–60 °C) gave the product **79** as a white crystalline solid (237 mg, 95%); m.p. 126.5–128.0 °C; ν_{max}/cm^{-1} (ATR) 3033 (C–H aromatic str.), 2926 (CH_3 str.), 1466 (C=C aromatic str.), 967 (=C–H in-plane bend), 819 (=C–H oop bend); ^{1}H NMR (400 MHz, 16 scans, C_6D_6): δ = 7.13 (2 H, dt, *J* = 6.5, 1.5 Hz, 2′,6′-H), 6.97 (2 H, d, *J* = 8.0 Hz, 3′,5′-H), 2.06 (3 H, s, CH_3); ^{13}C NMR (100 MHz, 1024 scans, $CDCl_3$): δ = 144.5 (dddd, *J* = 249.0, 16.5, 4.5, 2.5 Hz, CF), 144.3 (dddd, *J* = 248.0, 12.5, 6.0, 5.0 Hz, CF), 139.7 (s), 130.1 (t, *J* = 2.0 Hz, 2′,6′-C), 129.6 (s, 3′,5′-C), 123.8 (t, *J* = 2.0 Hz), 119.7 (t, *J* = 17.0 Hz), 110.9 (tt, *J* = 19.0, 3.0 Hz), 21.5 (s, CH_3); ^{19}F NMR (376 MHz, 64 scans, C_6D_6): δ = −141.89 (2 F, td, *J* = 12.0, 4.0 Hz, 2,6-F), −143.12 to −143.22 (2 F, m, 3,5-F); MS (EI) *m/z* (%) 274. 0172 ($[M]^+$, 100) ($C_{13}H_7ClF_4$ requires 274.01722).

(*Lab book reference number*: GMHP-5-270, GMHP-7-455)

Synthesis of 2,3,5,6-tetrafluoro(trifluoromethyl)-4′-(methyl)biphenyl (80)

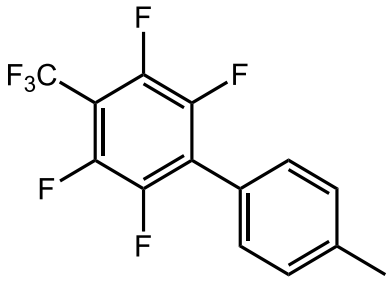

The reaction of 2,3,5,6-tetrafluorobenzotrifluoride (185 μL, 296 mg, 1.36 mmol, 1.5 equiv.) with 4-iodotoluene **57** (198 mg, 0.908 mmol, 1 equiv.) was prepared following the general procedure A. Purification by flash chromatography (SiO_2, R_f =0.38, petroleum-ether 40–60 °C) gave the major product **80** (259 mg, 93 %) as a white crystalline solid; m.p. 116.5−118.0 °C (lit.[126] 111–114 °C); ν_{max}/cm^{-1} (disc, KBr) 3044 (C–H aromatic str.), 2927 (CH_3 str.), 1477 (C=C aromatic str.), 1339, 1146 (C–F str.), 988 (=C–H in-plane bend), 825 (=C–H oop bend); ^{1}H NMR (400 MHz, 16 scans, C_6D_6): δ = 7.09 (2 H, d, *J* = 8.1 Hz, 2′,6′-H), 6.95 (2 H, d, *J* = 8.0 Hz, 3′,5′-H), 2.05 (3 H, s, 4-H); ^{13}C NMR (100 MHz, 1024 scans, $CDCl_3$): δ = 144.6 (dm, *J* = 258.5 Hz, CF), 144.3 (ddt, *J* = 248.5, 13.0, 4.5 Hz, CF), 140.4 (s), 130.0 (t, *J* = 2.0 Hz, 2′,6′-C), 129.7 (s, 3′,5′-C), 125.1 (t, *J* = 16.5 Hz), 123.2 (s), 122.5–119.7 (dm, *J* = 275.0 Hz, CF_3), 108.9–107.8 (m), 21.5 (CH_3); ^{19}F NMR (376 MHz, 64 scans, C_6D_6): δ = −55.94 (3 F, t, *J* = 21.5 Hz, CF_3), −141.35 to −141.49 (2 F, m, 3,5-F), –142.17 (2 F, td, *J* = 15.0, 5.5 Hz, 2,6-F); MS (EI) *m/z* (%) 308.0416 ($[M]^+$, 100) ($C_{14}H_7F_7$ requires 308.0436).

The analytical data obtained were in agreement with the literature.[126]

(*Lab book reference number*: GMHP-5-256, GMHP-7-443)

Synthesis of 2,3,5,6-tetrafluoro(dimethylamino)-4′-(methyl)biphenyl (76)

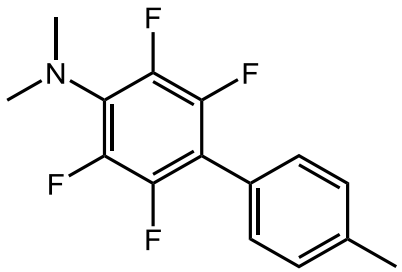

The reaction of 2,3,5,6-tetrafluoro-*N*,*N*-dimethylaniline **121** (200 μL, 266 mg, 1.38 mmol, 1.5 equiv.) and 4-iodotoluene **57** (197 mg, 0.904 mmol, 1 equiv.) was prepared following the general procedure A. Purification by flash chromatography (SiO_2, R_f =0.07 petroleum-ether 40–60 °C) gave the major product **76** (232 mg, 91%) as a white solid; m.p. 116.5−118.0 °C (lit.[126] 111–113 °C); ν_{max}/cm^{-1} (ATR) 2923 (CH_3 str.), 1640, 1512 (–CH=CH– str.), 1480 (C=C aromatic str.), 1221 (C–F str.), 1056 (C–H str.), 972 (=C–H in-plane bend), 827 (=C–H oop bend); ^{1}H NMR (400 MHz, 16 scans, C_6D_6): δ = 7.32 (2 H, dt, *J* = 8.0, 1.5 Hz, 2′,6′–H), 7.00 (2 H, dt, *J* = 8.0, 0.5 Hz, 3′,5′-H), 2.59 (6 H, t, *J* = 2.0 Hz, $N(CH_3)_2$), 2.07 (3 H, s, CH_3); ^{13}C NMR (100 MHz, 1024 scans, $CDCl_3$): δ = 144.9 (dddd, *J* = 198.0, 18.0, 9.0, 5.0 Hz), 142.4 (dddd, *J* = 194.0, 15.5, 6.5, 4.0 Hz, CF), 138.6 (s), 130.2 (t, *J* = 2.0 Hz, 2′,6′-C), 129.4 (s, 3′,5′-C), 128.6 (s), 125.1–125.0 (m), 112.9 (t , *J* = 17.5 Hz), 43.5 (t, *J* = 4.0 Hz, $N(CH_3)_2$), 21.5 (s, CH_3); ^{19}F NMR (376 MHz, 64 scans, C_6D_6): δ = −146.27 to −146.35 (2 F, m, 2,6-F), −151.96 to −152.05 (2 F, m, 3,5-F); MS (EI) *m/z* (%) 283.0986 ($[M]^+$, 100) ($C_{15}H_{13}F_4N$ requires 283.0984).

The analytical data obtained were in agreement with the literature.[126]

(*Lab book reference number*: GMHP-6-365, GMHP-7-469)

Synthesis of pentafluorodeuterobenzene (100)

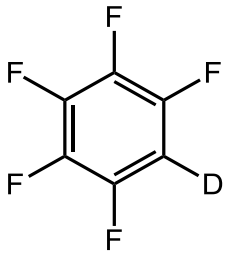

Magnesium-turnings (5.50 g, 0.23 mol, 1.4 equiv.), and 160 cm^3 of dry diethylether were sequentially added to a three-neck round-bottom flask equipped with condenser under atmosphere of nitrogen. The reaction was initiated by quick addition of 6 cm^3 dry pentafluorobromobenzene **99** (20 cm^3, 40 g, 0.16 mol, 1 equiv.) followed by slow, dropwise addition. After two hours of stirring, D_2O (14 cm^3, 15 g, 0.77 mol, 4.8 equiv.) was added to the brown reaction mixture and stirred for 30 min. The yellow organic phase was dried over Mg_2SO_4, solvent removed on the rotary evaporator and purified by distillation under continuous flow of nitrogen at 100 °C. The product **100** was obtained as colourless oil (7 cm^3, 11 g, 40%); b.p. 84 °C; density 1.532 g cm^3; ν_{max}/cm^{-1} (CaF_2 cell, DCM) 1642 and 1516 (–CH=CH– str.), 1069 (C–F str.), 1018 and 1006 (=C–H in-plane bend); ^{2}H NMR (76 MHz, 16 scans, C_6H_6): δ = 5.83 (s); ^{13}C NMR (126 MHz, 6729 scans, $CDCl_3$): δ = 146.4 (dm, *J* = 249.5 Hz, CF), 142.0 (dtt, *J* = 254.0, 13.5, 5.0 Hz, CF), 137.8 (dm, *J* = 250.5 Hz, CF), 101.1–100.3 (m, CD); ^{19}F NMR (471 MHz, 16 scans, $CDCl_3$): δ = −136.44 (2 F, dd, *J* = 21.5, 8.5 Hz, 2,6-F), −151.15 (1 F, t, *J* = 20.0 Hz, 4-F), −159.55 (2 F, td, *J* = 21.0, 8.5 Hz, 3,5-F).

A literature procedure was followed for the synthesis of this compound.[264] The analytical data obtained were in agreement with the literature.

(*Lab book reference number*: GMHP-5-254, GMHP- 6-341)

Synthesis of 2,3,5,6-tetrafluoro-*N*,*N*-dimethylaniline (121)

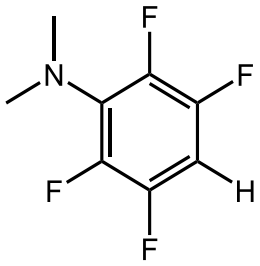

A mixture of pentafluorobenzene **56** (2.6 cm^3, 3.9 g, 0.023 mol) and 33% w/w ethanolic dimethylamine (5.0 cm^3) were heated in pressure tube at 75 °C for 20 hours. Once the crude mixture was cooled to room temperature, 200 cm^3 Et_2O and 40 cm^3 deionized water were added for liquid-liquid extraction. The aqueous phase was back-extracted with Et_2O (2 × 200 cm^3). The combined organic phase was dried over Na_2SO_4, filtered and solvent removed under vacuum to give the product **121** as clear yellow oil (1.9 g, 43%). The product contained 10% of 2,3,4,5-tetrafluoro-*N*,*N*-dimethylaniline; ν_{max}/cm^{-1} (ATR) 2981 (C–H aromatic str.), 2889 (CH_3 str.), 1641 (–CH=CH– str.), 1499 (C=C aromatic str.), 1055 (C–F str.), 933 (=C–H in-plane bend), 813 (=C–H oop bend); ^{1}H NMR (400 MHz, 32 scans, $CDCl_3$): δ =6.63 (1 H, tt, *J* = 10.0, 7.0 Hz, 1-CH), 2.95 (6H, t, *J* = 2.0 Hz, $N(CH_3)_2$); ^{13}C NMR (100 MHz, 1024 scans, $CDCl_3$): δ = 146.8 (dm, *J* = 245.5 Hz, CF), 142.3 (dm, *J* = 244.0 Hz, CF), 132.2 (tt, *J* = 10.5, 2.5 Hz), 97.9 (tm, *J* = 23.0 Hz), 43.3–43.2 (m, Me); ^{19}F NMR (376 MHz, 128 scans, $CDCl_3$): δ = −141.06 to –141.17 (2 F, m, CF), −151.59 to −151.68 (2 F, m, CF).

A literature procedure was followed for the synthesis of this compound.[400] The analytical data obtained were in agreement with the literature.

(*Lab book reference number*: GMHP-6-361, GMHP-7-467)

Synthesis of 4-iodobenzyltriphenylphosphonium bromide (122)

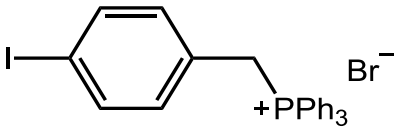

An oven-dried Schlenk tube was charged with 4-iodobenzylbromide (780 mg, 2.63 mmol, 1 equiv.) and PPh_3 (717 mg, 2.73 mmol, 1 equiv.). Dry toluene (*ca.* 10 cm^3) was transferred into the Schlenk tube using a double-pointed needle and the colourless solution was stirred for 21 hrs at ambient temperature under atmosphere of N_2. The solvent was removed from the opaque reaction mixture by filter cannula, and the resulting white solid was washed with dry toluene (*ca.* 10 cm^3 × 5) to give the product **122** (322 mg, 22%) as a white solid; m.p. 248.1–250.7 °C (lit.[354] 248 °C); ν_{max}/cm^{-1} (ATR) 3009 (C–H aromatic str.), 2902 (CH_2 str.), 1485 (–CH=CH– str.), 1437 (C=C aromatic str.), 1110 (=C–H in-plane bend), 692, 495 (C–I str.); ^{1}H NMR (400 MHz, 8 scans, $CDCl_3$): δ = 7.80–7.74 (9 H, m, 2,4,6-Ph), 7.62 (6 H, td, *J* = 7.5, 3.5 Hz, 3,5-Ph), 7.41 (2H, d, *J* = 7.5 Hz, 3,5-CH), 6.92 (2H, dd, *J* = 8.5, 2.5 Hz, 2,6-CH), 5.53 (2H, d, *J* = 14.5 Hz, CH_2); ^{13}C NMR (100 MHz, 1024 scans, $CDCl_3$): δ = 137.9 (d, *J* = 3.0 Hz, 3,5-Bn), 135.1 (d, *J* = 3.0 Hz, 4-Ph), 134.6 (d, *J* = 10.0 Hz, 2,6-Ph), 133.7 (d, *J* = 5.5 Hz, 2,6-Bn), 130.3 (d, *J* = 12.6 Hz, 3,5-Ph), 127.2 (d, *J* = 9.0 Hz, 1-Bn), 117.8 (d, *J* = 86.0 Hz, 1-Ph), 94.6 (d, *J* =5.0 Hz, 4-Bn), 30.3 (d, *J* = 46.5 Hz, CH_2); ^{31}P NMR (162 MHz, 64 scans, $CDCl_3$): δ = 23.7 (s); MS (ESI(+)) *m/z* (%) 479.0407 ($[M–Br]^+$, 100) ($C_{25}H_{21}IP$ requires 479.0426).

A literature procedure was followed for the synthesis of this compound.[354] The analytical data obtained were in agreement with the literature.

(*Lab book reference number*: GMHP-7-481)

Synthesis of 4-iodobenzyltriphenylphosphonium hexafluorophosphate (107)

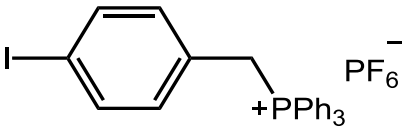

Dry methanol (*ca.* 5 cm^3) was added to a Schlenk tube charged with 4-iodobenzyl-triphenylphosphonium bromide **122** (187 mg, 0.334 mmol, 1 equiv.) and sodium hexafluorophosphate (115 mg, 0.685 mmol, 2.1 equiv.). The mixture was stirred for 1 h under atmosphere of nitrogen before removing the solvent under vacuum. The resulting solid was washed with dry methanol (*ca.* 3 × 3 cm^3) to give the product **107** (54 mg, 26%) as a white solid; m.p. 235.8–238.1 °C (lit.[354] 248 °C); ν_{max}/cm^{-1} (ATR) 3050 (C–H aromatic str.), 2933 (CH_2 str.), 1486, 1437, 1108, 827, 556 ; ^{1}H NMR (400 MHz, 16 scans, $CDCl_3$): δ = 7.80 (3 H, td, *J* = 7.0, 1.0 Hz, 4-Ph), 7.64 (6H, td, *J* = 8.0, 3.5 Hz, 2,6-Ph), 7.54–7.45 (8 H, m, 3,5-Ph + 3,5-CH), 6.65 (2H, dd, *J* = 8.5, 2.5 Hz, 2,6-CH), 4.52 (2H, d, *J* = 14.5 Hz, CH_2); ^{13}C NMR (100 MHz, 4094 scans, $CDCl_3$): δ = 138.3 (d, *J* = 3.0 Hz, 3,5-Ph or 3.5-CH), 135.6 (d, *J* = 3.0 Hz, 4-Ph), 134.1 (d, *J* = 9.5 Hz, 3,5-Ph or 3.5-CH), 133.0 (d, *J* = 5.5 Hz, 2,6-CH), 130.5 (d, *J* = 12.5 Hz, 2,6-Ph), 126.4 (d, *J* = 8.5 Hz, C), 117.0 (d, *J* = 86.0 P–C), 95.0 (d, *J* = 5.0 Hz, C), 30.0 (d, *J* = 49.0 Hz, CH_2); ^{19}F NMR (376 MHz, 64 scans, $CDCl_3$): δ = −71.17 (s), −73.07 (s); ^{31}P NMR (162 MHz, $CDCl_3$, 21.1°C): δ = 23.9 (s), −143.63 (sext, J = 714 Hz, PF_6^-); MS (ESI(+)) *m/z* (%) 479.0407 ($[M–PF_6]^+$, 100) ($C_{25}H_{21}IP$ requires 479.0426).

A literature procedure was followed for the synthesis of this compound.[354] The analytical data obtained were in agreement with the literature.

(*Lab book reference number*: GMHP-7-483)

Synthesis of tetraphenylphosphonium iodide (103)

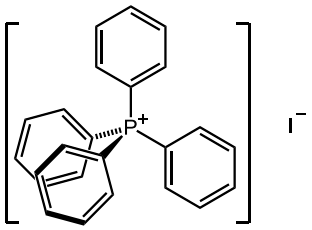

A solution of iodobenzene **81** (225 μL, 410 mg, 2.01 mmol, 1 equiv.), PPh_3 (526 mg, 2.00 mmol, 1 equiv.) and $Pd(OAc)_2$ (5 mg, 1 mol%) in toluene (3 cm^3) was heated at 120 °C under continuous flow of nitrogen for 25 h. The reaction mixture was filtered and washed with benzene to give the product **103** (950 mg, quant.) grey solid; ν_{max}/cm^{-1} (ATR) 1584, 1480, 1434, 1106, 996, 720, 686, 522; ^{1}H NMR (400 MHz, 16 scans, DMF-d_7, 11.9 °C): δ = 8.08–8.03 (4 H, m, 4-Ph), 7.91–7.87 (16 H, m, 2,3,5,6-Ph); ^{13}C NMR (100 MHz, 4094 scans, $CDCl_3$): δ = 135.9 (d, *J* = 3.0 Hz, 4-CH), 134.6 (d, *J* = 10.5 Hz, 3,5-CH), 131.0 (d, *J* = 13.0 Hz, 2,6-CH), 117.5 (d, J = 89.5 Hz, P–C); ^{31}P NMR (162 MHz, 256 scans, DMF-d_7, 11.9 °C): δ = 22.7 (s); MS (ESI(+)) *m/z* (%) 339.1293 ($[M-I]^+$, 100) ($C_{24}H_{20}P$ requires 339.1303).

A literature procedure was followed for the synthesis of this compound.[401] The analytical data obtained were in agreement with the literature.

(*Lab book reference number*: GMHP-7-498)

Synthesis of triphenyl(4-tolyl)phosphonium iodide (60)

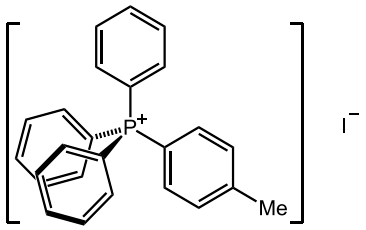

A solution of 4-iodotoluene **57** (437 mg, 2.01 mmol, 1 equiv.), PPh_3 (525 mg, 2.00 mmol, 1 equiv.) and $Pd(OAc)_2$ (5 mg, 1 mol%) in toluene (3 cm^3) was heated at 120 °C under continuous flow of nitrogen for 25 h. The reaction mixture was filtered and washed with benzene to give the product **60** (887 mg, 92%) white solid; m.p. 209.8–212.4 °C (lit.[401] 214 °C); ν_{max}/cm^{-1} (ATR) 3434, 3048, 1598, 1434, 1107, 723, 691, 527; ^{31}P NMR (162 MHz, 256 scans, DMF-d_7, 11.9 °C): δ = 22.4 (s); MS (ESI(+)) *m/z* (%) 353.1452 ($[M-I]^+$, 100) ($C_{25}H_{22}P$ requires 353.1459).

A literature procedure was followed for the synthesis of this compound.[401] The analytical data obtained were in agreement with the literature.

(*Lab book reference number*: GMHP-7-499)

Synthesis of bis(triphenylphosphine)palladium(dichloride) (123)

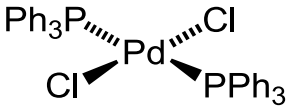

A yellow suspension of $PdCl_2$ (1.51 g, 8.50 mmol, 1 equiv.) in anhydrous DMSO (150 cm^3) was stirred until fully dissolved. PPh_3 (4.46 g, 17.0 mol, 2 equiv.) was added to the resulting orange solution. The reaction mixture was heated at 90 °C for 6 hours under continuous flow of argon, cooled to room temperature, filtered and washed with DMSO (2 × 10 cm^3) and Et_2O (5 × 50 cm^3). The product **123** (5.25 g, 88%) was obtained as a yellow solid; ^1H NMR (400 MHz, 16 scans, $CDCl_3$): δ = 7.74–7.68 (12 H, m, 2,6-C_6H_5P), 7.46–7.36 (18 H, m, 3,4,5-C_6H_5P); ^{31}P NMR (162 MHz, 128 scans, $CDCl_3$): δ = 23.9 (s); MS (LIFDI) m/z (%) 702.03 ($[M]^+$, 100) ($PdC_{36}H_{30}Cl_2P_2$ requires 702.02).

A literature procedure was followed for the synthesis of this compound.[402] The analytical data obtained were in agreement with the literature.

(*Lab book reference number*: GMHP-2-54, GMHP-4-177)

Synthesis of tetrakis(triphenylphosphine)palladium (124)

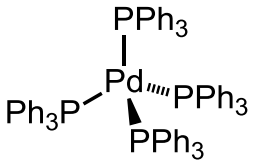

A yellow suspension of $PdCl_2$ (0.502 g, 2.83 mmol, 1 equiv.) and PPh_3 (3.71 g, 14.1 mmol, 5 equiv.) in anhydrous DMSO (40 cm^3) under atmosphere of argon was heated until fully dissolved into an orange solution (*ca.* 160 °C). The heat was removed and hydrazine monohydrate (0.55 cm^3, 0.568 g, 11.3mmol, 4 equiv.) was slowly added over a minute, resulting in a bubbling green mixture. The reaction mixture was cooled to RT, filtered under atmosphere of argon and the solid washed with EtOH (3 × 10 cm^3) and diethyl ether (3 × 10 cm^3). The product **124** (3.06 g, 94%) was obtained as a yellow crystalline solid which gradually darkened into orange when left open to air for a few days; ^{1}H NMR (400 MHz, 16 scans, $CDCl_3$): δ = 7.73–7.61 (24 H, m, 3,5-C_6H_5P), 7.39–7.30 (36 H, m, 2,4,6-C_6H_5P); ^{31}P NMR (202 MHz, 4096 scans, C_6D_6): δ = 24.7 (s); MS (LIFDI) *m/z* (%) 892.31 ($[M-PPh_3]^+$, 100) ($PdC_{54}H_{45}P_3$ requires 892.18).

A literature procedure was followed for the synthesis of this compound.[403] The analytical data obtained were in agreement with the literature.

(*Lab book reference number*: GMHP-3-120)

Synthesis of dinuclear di(*μ*-hydroxo)-bis(phenyl)-di(triphenylphosphine)palladium(II), $[Pd(C_6H_5)(\mu\text{-}OH)(PPh_3)]_2$ (83a)

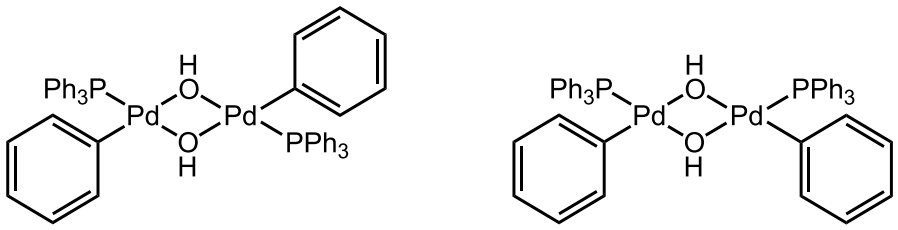

Separate solutions of KOH (4.07 g, 0.0726 mol, 51 equiv.) in deionised water (4 cm^3) and iodobenzene **81** (340 μL, 620 mg, 3.04 mmol, 2.1 equiv.) in benzene (20 cm^3) were degassed by two freeze-pump-thaw cycles. The degassed liquids were charged to apparatus with $Pd(PPh_3)_2Cl_2$ **123** (1.00 g, 1.43 mmol, 1 equiv.) to give a yellow suspension which was then refluxed (*ca.* 83 °C) under atmosphere of argon for 3 hours. During this time, the mixture changed colour from orange to green, and then colourless, with black precipitate. The organic phase was separated while hot and the aqueous phase was washed with warm benzene (5 × 4 cm^3). The combined colourless organic phase was filtered through a cotton plug, removing the black solids from yellow solution, and the solvent was removed under vacuum to give cream-coloured crude product. Washing the solid with acetone (4 × 4 cm^3) yielded the product **83a** of a 1:3 mixture of *cis* and *trans* isomers (0.539 g, 81%) as a white solid; ν_{max}/cm^{-1} (ATR) 3608 and 3603 (OH str., shp), 3047 (C–H aromatic str.), 1564 (–CH=CH– str.), 1435 (C=C aromatic str.), 1096 (=C–H in-plane bend); ^1H NMR (500 MHz, 16 scans, CD_2Cl_2): δ = 7.51–7.33 (18 H, m, 2,4,6-C_6H_5P), 7.28–7.24 (12 H, m, 3,5-C_6H_5P), 7.00 (4H, d, J = 6.1 Hz, 2,6-C_6H_5Pd), 6.66–6.62 (6H, m, 3,4,5-C_6H_5Pd), −0.59 (0.23 H, s, *cis*-OH), −1.80 (1.35 H, s, *trans*-OH), −3.51 (0.21 H, s, *cis*-OH); ^{31}P (202 MHz, 128 scans, CD_2Cl_2): δ = 33.23 (3 P, s, *trans*), 32.7 (1 P, s, *cis*); MS (LIFDI) *m/z* (%) 926.09 ($[M]^+$, 100) ($Pd_2C_{48}H_{42}O_2P_2$ requires 926.08).

A literature procedure was followed for the synthesis of this compound.[211] The analytical data obtained were in agreement with the literature.

(*Lab book reference number*: GMHP-3-115, GMHP-5-265, GMHP-5-311)

Synthesis of di(*μ*-hydroxo)-bis(4-tolyl)-di(triphenylphosphine)palladium(II) dimer, [Pd(4-tolyl)(*μ*-OH)(PPh_3)]$_2$ (83b)

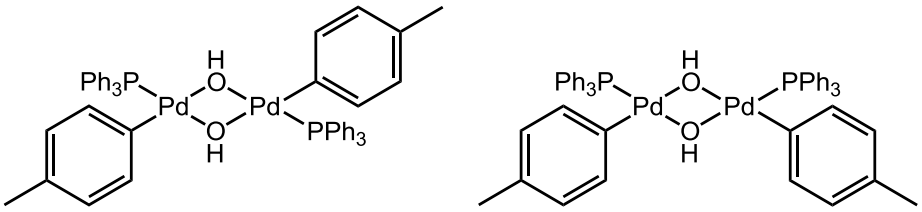

A white suspension of [Pd(Ph)(*μ*-OH)(PPh_3)]$_2$ **83a** (0.400 g, 0.433 mmol, 1 equiv.) and 4-iodotoluene **57** (0.387 g, 1.78 mmol, 4.1 equiv.) in benzene (10 cm^3) was degassed by two freeze-pump-thaw cycles. The mixture was then stirred under 1 atm of CO for 24 hours after complete dissolution. The resulting red solution was degassed and refilled with argon before addition of 4-iodotoluene **57** (0.381 g, 1.75 mmol, 4 equiv.) and a solution of KOH (2.64 g, 47.1 mmol, 109 equiv.) in degassed deionised water (3.96 cm^3). The mixture was stirred for 19 hours, extracted with warm benzene (open to air), filtered, and solvent removed under vacuum. The yellow solid was washed with acetone (5 × 2 cm^3) to give the 1:4 mixture of *cis-trans* isomers **83b** (206 mg, 50%) as a cream coloured solid; ν_{max}/cm^{-1} (ATR) 3638 (OH str.), 3048 (C–H aromatic str.), 2981 (CH_3 str.), 1479 (–CH=CH– str.), 1434 (C=C aromatic str.), 1093 (=C–H in-plane bend); ^{1}H NMR (400 MHz, 8 scans, $CDCl_3$): δ = 7.50–7.19 (30 H, m, C_6H_5P), 6.90 (4 H, d, *J* = 7.0 Hz, 2,6-C_6H_5), 6.47 (4 H, d, *J* = 7.5 Hz, 3,5-C_6H_5), 2.08–2.03 (6 H, m, (CH_3)C_6H_4Pd-*cis* and *trans*), −0.30 (0.14H, s, OH-*cis*), −1.49 (1.17 H, s, OH-*trans*), −3.41 (0.11 H, s, OH-*cis*); ^{13}C NMR (100 MHz, 1024 scans, $CDCl_3$): δ = 137.4 (s), 134.4 (d, *J* = 12.0 Hz), 134.3 (d, *J* = 12.0 Hz), 131.6 (d, *J* = 4.0 Hz), 131.3 (s), 131.1 (s), 128.3 (d, *J* = 11.0 Hz), 127.9 (d, *J* = 36.5 Hz), 21.2 (s, *cis* or *trans*-CH_3), 20.8 (s, *cis* or *trans*-CH_3); ^{31}P NMR (202 MHz, 32 scans, $CDCl_3$): δ = 33.4 (3 P, s, *trans*), 32.77 (1 P, s, *cis*); MS (LIFDI) *m/z* (%) 954.14 ($[M]^+$, 100) ($Pd_2C_{50}H_{46}O_2P_2$ requires 954.10).

A literature procedure was followed for the synthesis of this compound.[211] The analytical data obtained were in agreement with the literature.

(*Lab book reference number*: GMHP-3-137, GMHP-4-237, GMHP-5-269)

Synthesis of di(*μ*-acetato)-bis(phenyl)-di(triphenylphosphine)palladium(II) dimer, [Pd(Ph)(*μ*-OAc)(PPh_3)]$_2$ (84)

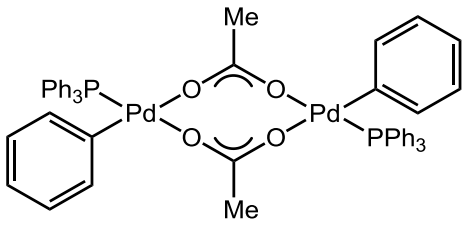

Glacial AcOH (45 μL, 47 mg, 0.79 mmol, 3.2 equiv.), degassed by bubbling through with nitrogen, was added to a white suspension of [Pd(Ph)(*μ*-OH)(PPh_3)]$_2$ **83a** (226 mg, 0.244 mmol, 1 equiv.) in dry benzene (*ca.* 8 cm^3). The reaction mixture quickly turned into clear yellow solution. The solvent was removed under vacuum and the resulting solid was washed with hexane (4 × 4 cm^3) to give the product **84** (186 mg, 76%) as a cream-coloured solid; ν_{max}/cm^{-1} (ATR) 3054 (C–H aromatic str.), 1581 and 1558 (CO str.), 1434 and 1415 (CO str.), 1097 (=C–H in-plane bend), 692 (s); ^{1}H NMR (500 MHz, 64 scans, C_6D_6): δ = 7.78 (4 H, dd, *J* = 7.5, 3.5 Hz, 2,6-C_6H_5Pd), 7.51–7.47 (12 H, m, 2,6-C_6H_5P), 7.00 (2 H, t, *J* = 7.0 Hz, 4-C_6H_5Pd), 6.93–6.88 (10 H, m, 4-C_6H_5P and 3,5-C_6H_5Pd), 6.84 (12 H, td, *J* = 7.5, 2.0 Hz, 3,5-C_6H_5P), 1.59 (6 H, s, $O_2C(CH_3)$); ^{13}C NMR (125 MHz, 14731 scans, C_6D_6): δ = 180.3 (s), 150.0 (d, *J* = 5.5 Hz), 138.3 (d, *J* = 4.5 Hz), 135.2 (d, *J* = 11.5 Hz), 131.0 (s), 130.5 (s), 130.2 (d, *J* = 1.5 Hz), 127.3 (d, *J* = 1.5 Hz), 123.5 (s), 24.6 (d, J = 2.5 Hz); ^{31}P NMR (202 MHz, 512 scans, C_6D_6): δ = 29.9 (s); MS (LIFDI) *m/z* (%) 1010.12 ([M]$^+$, 100) ($Pd_2P_2O_4C_{52}H_{46}$ requires 1010.10).

A literature procedure was followed for the synthesis of this compound.[212] The analytical data obtained were in agreement with the literature.

(*Lab book reference number*: GMHP-7-445, GMHP-5-292)

Synthesis of di(*μ*-acetato)-bis(4-tolyl)-di(triphenylphosphine)palladium(II) dimer, [Pd(4-tolyl)(*μ*-OAc)(PPh_3)]$_2$ (84b)

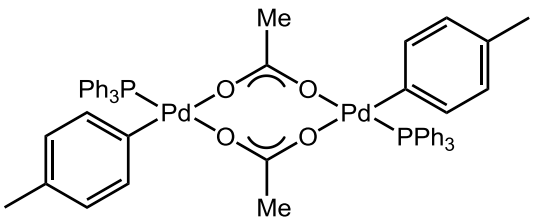

Addition of degassed glacial AcOH (3 μL, 0.05 mmol, 3.8 equiv.) to a white suspension of [Pd(4-tolyl)(*μ*-OH)(PPh_3)]$_2$ **83b** (12 mg, 0.013 mmol, 1 equiv.) in dry benzene (0.5 cm^3) resulted in clear yellow solution. The solvent was removed under vacuum and the resulting solid washed with hexane (3 × 1 cm^3) to give the product **84b** (12 mg, 89 %) as a cream coloured solid; ν_{max}/cm^{-1} (ATR) 3052 (C–H aromatic str.), 2923 (CH_3 str.), 1566 and 1414 (CO str.); ^{1}H NMR (500 MHz, 8 scans, C_6D_6): δ = 7.66–7.65 (4 H, m, 2,6-MeC_6H_4Pd), 7.51 (12 H, dd, *J* = 10.5, 8.0 Hz, 2,6-C_6H_5P), 6.93 (6 H, dd, *J* = 7.5, 6.0 Hz, 4-C_6H_5P), 6.86 (12 H, t, *J* = 6.5 Hz, 3.5-C_6H_5P), 6.75 (4 H, d, *J* = 7.5 Hz, 3,5-MeC_6H_4Pd), 2.26 (6 H, s, Me), 1.59 (6 H, s, $O_2C(CH_3)$); ^{31}P NMR (203 MHz, 64 scans, C_6D_6): δ = 29.7 (9P, s), 29.0 (1P, s); MS (LIFDI) *m/z* (%) 1038.28 ($[M]^+$, 100) ($Pd_2C_{54}H_{50}O_4P_2$ requires 1038.13).

A literature procedure was followed for the synthesis of this compound.[212] The analytical data obtained were in agreement with the literature.

(*Lab book reference number*: GMHP-4-214, GMHP-4-245)

Synthesis of di(μ-iodo)-bis(phenyl)-di(triphenylphosphine)palladium(II) dimer, $[Pd(Ph)(\mu\text{-}I)(PPh_3)]_2$ (86)

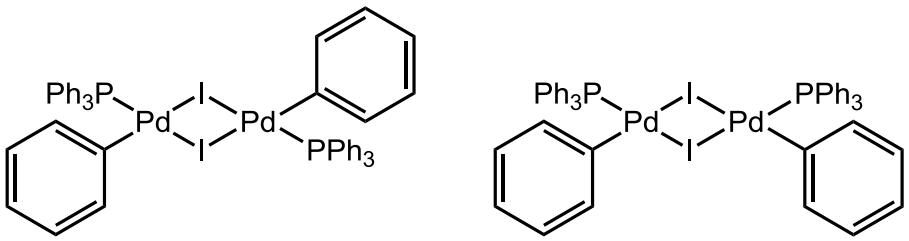

A solution of $[Pd(Ph)(\mu\text{-}OH)(PPh_3)]_2$ **83a** (148 mg, 0.160 mmol, 1 equiv.) in dichloromethane (1.5 cm^3) was added to a solution of sodium iodide (0.994 g, 6.6 mmol, 41 equiv.) in acetone (4.5 cm^3) to give a yellow solution. The precipitate formed by addition of water (0.5 cm^3) was collected by vacuum filtration and washed with water (× 3), acetone (× 3) and pentane (× 3) to give the product **86** (144 mg, 79%) as a yellow solid; ν_{max}/cm^{-1} (ATR) 3046 (C–H aromatic str.), 1560 (–CH=CH– str.), 1425 (C=C aromatic str.), 1094 (=C–H in-plane bend); ^1H NMR (500 MHz, 32 scans, CD_2Cl_2): δ = 7.48 (12 H, dd, J = 10.5, 8.5 Hz, 2,6-C_6H_5P), 7.38 (6 H, t, J = 7.0 Hz, 4-C_6H_5P), 7.28 (12 H, t, J = 7.0 Hz, 3,5-C_6H_5P), 7.02 (4 H, d, J = 4.0 Hz, 2,6-C_6H_5Pd), 6.63–6.57 (6 H, m, 3,4,5-C_6H_5Pd); ^{31}P NMR (202 MHz, 1024 scans, CD_2Cl_2, 25.3 °C): δ = 27.4 (br); ^{31}P NMR (202 MHz, 256 scans, CD_2Cl_2, −20.3 °C): δ = 28.3 (1 P, *cis*-P), 27.6 (2 P, *trans*-P); MS (ESI(+)) *m/z* (%) 707.1285 ($[M-(I+(PPh_3)_2Pd(Ph)I)]^+$, 100) ($Pd_2C_{42}H_{35}P_2$ requires 707.1249).

A literature procedure was followed for the synthesis of this compound.[211] The analytical data obtained were in agreement with the literature.

(*Lab book reference number*: GMHP-5-312)

Synthesis of iodo-bis(triphenylphosphine)-(phenyl)palladium(II), $Pd(Ph)(I)(PPh_3)_2$ (82a)

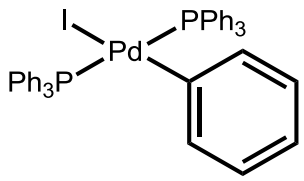

Degassed iodobenzene **81** (23 µL, 41 mg, 0.20 mmol, 1 equiv.) was added to a suspension of $Pd(PPh_3)_4$ **124** (232 mg, 0.20 mmol, 1 equiv.) in dry benzene (*ca.* 3 cm^3). The black reaction mixture was stirred for 20 h under atmosphere of nitrogen, filtered and washed with hexane (5 × 5 cm^3) to give the product **82a** (72 mg, 43%) as a grey coloured solid; ν_{max}/cm^{-1} (ATR) 3052 (C–H aromatic str.), 1558 (–CH=CH– str.), 1434 (C=C aromatic str.), 1095 (=C–H in-plane bend), 688, 495; ^1H NMR (500 MHz, 64 scans, $CDCl_3$): δ = 7.51 (12 H, d, *J* = 5.5 Hz, 2,6-C_6H_5P), 7.32 (6 H, t, *J* = 7.0 Hz, 4-C_6H_5P), 7.26–7.23 (12 H, m, 3,5-C_6H_5P), 6.61 (2 H, d, *J* = 6.5 Hz, 2,6-C_6H_5Pd), 6.34 (1H, t, *J* = 7.0 Hz, 4-C_6H_5Pd), 6.22 (2 H, t, *J* = 7.0 Hz, 3,5-C_6H_5Pd); ^{13}C NMR (126 MHz, 16048 scans, $CDCl_3$): δ = 136.1 (t, *J* = 5.0 Hz, CH), 135.0 (t, *J* = 6.0 Hz, CH), 132.3 (t, *J* = 23.0 Hz, CH), 129.8 (s, CH), 127.9 (t, *J* = 5.0, CH), 122.0 (s, CH). ^{31}P NMR (202 MHz, 128 scans, $CDCl_3$): δ = 22.9 (s); MS (ESI(+)) *m/z* (%) 707.1253 ($[M-I]^+$, 100) ($PdC_{42}H_{35}P_2$ requires 707.1249).

A literature procedure was followed for the synthesis of this compound.[242] The analytical data obtained were in agreement with the literature.

(*Lab book reference number*: GMHP-6-426, GMHP-7-444)

Synthesis of iodo-bis(triphenylphosphine)-(4-tolyl)palladium(II), Pd(4-tolyl)(I)(PPh_3)$_2$ (82b)

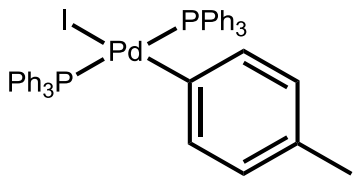

A solution of 4-iodotoluene **57** (88 mg, 0.40 mmol, 3.1 equiv.) in DCM (60 cm^3), degassed by three cycles of freeze-pump-thaw, was added to $Pd_2dba_3.CHCl_3$ (137 mg, 0.13 mmol, 1 equiv.) and PPh_3 (140 mg, 0.53 mmol, 4.1 equiv.) under atmosphere of nitrogen. The clear violet solution had changed colour to clear yellow after stirring for 1 hour. The solvent was removed under vacuum, and the resulting yellow solid was washed with diethylether (5 × 15 cm^3) to give the product **82b** (180 mg, 80%) as a grey coloured solid; ν_{max}/cm^{-1} (ATR) 3050 (C–H aromatic str.), 2981 (CH_3 str.), 1478 (–CH=CH– str.), 1432 (C=C aromatic str.), 1094 (=C–H in-plane bend), 688, 507; ^{1}H NMR (500 MHz, 64 scans, $CDCl_3$): δ = 7.52–7.48 (12 H, m, 2,6-C_6H_5P), 7.31 (6 H, t, *J* = 7.5 Hz, 4-C_6H_5P), 7.23 (12 H, t, *J* = 7.5 Hz, 3,5-C_6H_5P), 6.42 (2 H, dt, *J* = 8.0, 2.0 Hz, 2,6-C_6H_5Pd), 6.08 (2 H, d, *J* = 7.5 Hz, 3,5-C_6H_5Pd), 1.92 (3H, s); ^{31}P NMR (202 MHz, 128 scans, $CDCl_3$): δ = 22.5 (s); MS (LIFDI) *m/z* (%) 848.08 ($[M]^+$, 100) ($PdC_{43}H_{37}IP_2$ requires 848.05).

A literature procedure was followed for the synthesis of this compound.[206] The analytical data obtained were in agreement with the literature.

(*Lab book reference number*: GMHP-6-400, GMHP-6-422)

Synthesis of bis(triphenylphosphine)-(phenyl)palladium(II)acetate, Pd(Ph)(κ^1-OAc)(PPh_3)$_2$ (85)

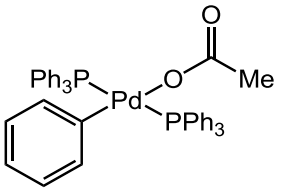

To a white suspension of [Pd(Ph)(μ-OAc)(PPh_3)]$_2$ **84** (101 mg, 0.110 mmol, 1 equiv.) in dry benzene (*ca.* 6 cm^3) was added PPh_3 (70 mg, 0.27 mmol, 2.5 equiv.). The reaction mixture was stirred at room temperature to give a colourless solution. The volume of the solution was reduced to *ca.* 2cm^3 and ice cold dry hexane (5 × 2 cm^3) was added to give white precipitate after 1 h. The crystals were washed with ice-cold hexane (2 cm^3 × 6) to yield the product **85** (100 mg, 65%) as white solid; ν_{max}/cm^{-1} (ATR) 3051 (C–H aromatic str.), 1604(CO st.), 1434 (C=C aromatic str.), 1372 (C–O str.), 1096 (=C–H in-plane bend), 690, 508; ^{1}H NMR (500 MHz, 32 scans, C_6D_6): δ = 7.70 (12 H, br, 2,6-C_6H_5P), 7.04–6.95 (20 H, m, 3,4,5-C_6H_5P + 2,6-C_6H_5Pd), 6.59 (1 H, t, *J* = 7.0 Hz , 4-C_6H_5Pd), 6.41 (2 H, t, *J* = 7.5 Hz, 3,5-C_6H_5Pd), 1.41 (3H, s, $O_2C(CH_3)$); ^{31}P NMR (202 MHz, 128 scans, C_6D_6): δ = 21.3 (s); MS (LIFDI) *m/z* (%) 766.12 ([M]$^+$, 100) ($PdC_{44}H_{38}O_2P_2$ requires 766.14).

A literature procedure was followed for the synthesis of this compound.[212] The analytical data obtained were in agreement with the literature.

(*Lab book reference number*: GMHP-6-388, GMHP-7-446)

6.4 Monitoring Reaction Progress by in situ FT-IR Spectroscopy

6.4.1 Reaction Progress Kinetic Analysis and Variable Time Normalisation Analysis of the Direct Arylation of 4-Iodotoluene 57 with Pentafluorobenzene 56

Reaction at standard condition (Table 10, Entry 1)

A mixture of 4-iodotoluene **57** (197 mg, 117µL, 0.904 mmol, 1 equiv.), pentafluorobenzene **56** (150 µL, 227 mg, 1.35 mmol, 1.5 equiv.), $Pd(OAc)_2$ (10 mg [a], 0.045 mmol, 5 mol%), PPh_3 (24 mg [b], 0.091 mmol, 10 mol%) and Ag_2CO_3 (185 mg, 0.671 mmol, 0.74 equiv.) in DMF (9.4 cm^3 total volume) was prepared following general procedure C. The reaction progress was monitored by *in situ* FT-IR spectroscopy. Quantitative conversion of starting material **57** was achieved.

[a] Using 500 µL of 0.09 M $Pd(OAc)_2$ stock solution made from stirring 20 mg $Pd(OAc)_2$ (0.089 mmol) in 1 cm^3 DMF for 10 min.

[b] Using 500 µL of 0.18 M PPh_3 stock solution made from stirring 47 mg PPh_3 (0.18 mmol) in 1 cm^3 DMF for 5 min.

(*Lab book reference number*: GMHP-7-474)

Reaction at different ["excess"] condition 1 (Table 10, Entry 2)

A mixture of 4-iodotoluene **57** (197 mg, 117 µL, 0.904 mmol, 1 equiv.), pentafluorobenzene **56** (100 µL, 151 mg, 0.901 mmol, 1 equiv.), $Pd(OAc)_2$ (10 mg [a], 0.045 mmol, 5 mol%), PPh_3 (24 mg [b], 0.091 mmol, 10 mol%) and Ag_2CO_3 (187 mg, 0.678 mmol, 0.75 equiv.) in DMF (9.45 cm^3 total volume) was prepared following general procedure C. The reaction progress was monitored by *in situ* FT-IR spectroscopy. Quantitative conversion of starting material **57** was achieved.

[a] Using 500 µL of 0.09 M $Pd(OAc)_2$ stock solution made from stirring 20 mg $Pd(OAc)_2$ (0.089 mmol) in 1 cm^3 DMF for 10 min.

[b] Using 500 µL of 0.18 M PPh_3 stock solution made from stirring 47 mg PPh_3 (0.18 mmol) in 1 cm^3 DMF for 5 min.

(*Lab book reference number*: GMHP-7-477)

Reaction at different ["excess"] condition 2 (Table 10, Entry 3)

A mixture of 4-iodotoluene **57** (196 mg, 117 µL, 0.899 mmol, 1 equiv.), pentafluorobenzene **56** (300 µL, 454 mg, 2.70 mmol, 3 equiv.), $Pd(OAc)_2$ (10 mg [a], 0.045 mmol, 5 mol%), PPh_3 (24 mg [b], 0.091 mmol, 10 mol%) and Ag_2CO_3 (186 mg, 0.675 mmol, 0.75 equiv.) in DMF (9.25 cm^3 total volume) was prepared following general procedure C. The reaction progress was monitored by *in situ* FT-IR spectroscopy. Quantitative conversion of starting material **57** was achieved.

[a] Using 500 µL of 0.09 M $Pd(OAc)_2$ stock solution made from stirring 20 mg $Pd(OAc)_2$ (0.089 mmol) in 1 cm^3 DMF for 10 min.

[b] Using 500 µL of 0.18 M PPh_3 stock solution made from stirring 47 mg PPh_3 (0.18 mmol) in 1 cm^3 DMF for 5 min.

(*Lab book reference number*: GMHP-7-473)

Reaction at different ["excess"] condition 3 (Table 10, Entry 4)

A mixture of 4-iodotoluene **57** (593 mg, 353 µL, 2.72 mmol, 2 equiv.), pentafluorobenzene **56** (100 µL, 151 mg, 0.90 mmol, 1 equiv.), $Pd(OAc)_2$ (10 mg [a], 0.045 mmol, 5 mol%), PPh_3 (24 mg [b], 0.091 mmol, 10 mol%) and Ag_2CO_3 (185 mg, 0.671 mmol, 0.75 equiv.) in DMF (9.215 cm^3 total volume) was prepared following general procedure C. The reaction progress was monitored by *in situ* FT-IR spectroscopy. Quantitative conversion of starting material **57** was achieved.

[a] Using 500 µL of 0.09 M $Pd(OAc)_2$ stock solution made from stirring 20 mg $Pd(OAc)_2$ (0.089 mmol) in 1 cm^3 DMF for 10 min.

[b] Using 500 µL of 0.18 M PPh_3 stock solution made from stirring 47 mg PPh_3 (0.18 mmol) in 1 cm^3 DMF for 5 min.

(*Lab book reference number*: GMHP-7-480)

Reaction at different catalyst concentration 1 (Table 10, Entry 5)

A mixture of 4-iodotoluene **57** (197 mg, 117 µL, 0.904 mmol, 1 equiv.), pentafluorobenzene **56** (150 µL, 227 mg, 1.35 mmol, 1.5 equiv.), $Pd(OAc)_2$ (20 mg, 9 µL, 0.089 mmol, 10 mol%), PPh_3 (47 mg, 43 µL, 0.18 mmol, 20 mol%) and Ag_2CO_3 (186 mg, 0.675 mmol, 0.75 equiv.) in DMF (9.35 cm^3 total volume) was prepared following general procedure C. The reaction progress was monitored by *in situ* FT-IR spectroscopy. Quantitative conversion of starting material **57** was achieved.

(*Lab book reference number*: GMHP-7-475)

Reaction at different catalyst concentration 2

A mixture of 4-iodotoluene **57** (196 mg, 117 µL, 0.899 mmol, 1 equiv.), pentafluorobenzene **56** (150 µL, 227 mg, 1.35 mmol, 1.5 equiv.), $Pd(OAc)_2$ (30 mg, 14 µL, 0.13 mmol, 15 mol%), PPh_3 (71 mg, 65 µL, 0.27 mmol, 30 mol%) and Ag_2CO_3 (187 mg, 0.678 mmol, 0.75 equiv.) in DMF (9.32 cm^3 total volume) was prepared following general procedure C. The reaction progress was monitored by *in situ* FT-IR spectroscopy. Quantitative conversion of starting material **57** was achieved.

(*Lab book reference number*: GMHP-7-476)

Reaction at the same ["excess"] (Table 10, Entry 6)

A mixture of 4-iodotoluene **57** (98 mg, 58 µL, 0.45 mmol, 1 equiv.), pentafluorobenzene **56** (100 µL, 151 mg, 0.90 mmol, 2 equiv.), $Pd(OAc)_2$ (10 mg [a], 0.045 mmol, 5 mol%), PPh_3 (24 mg [b], 0.091 mmol, 10 mol%) and Ag_2CO_3 (186 mg, 0.675 mmol, 1.5 equiv.) in DMF (9.51 cm^3 total volume) was prepared following general procedure C. The reaction progress was monitored by *in situ* FT-IR spectroscopy. Quantitative conversion of starting material **57** was achieved.

[a] Using 500 µL of 0.09 M $Pd(OAc)_2$ stock solution made from stirring 20 mg $Pd(OAc)_2$ (0.089 mmol) in 1 cm^3 DMF for 10 min.

[b] Using 500 µL of 0.18 M PPh_3 stock solution made from stirring 47 mg PPh_3 (0.18 mmol) in 1 cm^3 DMF for 5 min.

(*Lab book reference number*: GMHP-7-478)

Reaction at the same ["excess"] with product added to the reaction mixture (Table 10, Entry 7)

A mixture of 4-iodotoluene **57** (98 mg, 58 µL, 0.45 mmol, 1 equiv.), pentafluorobenzene **56** (100 µL, 151 mg, 0.90 mmol, 2 equiv.), 2,3,4,5,6-tetrafluoro-4′-(methyl)biphenyl **58** (116 mg, 320 µL, 0.45 mmol, 1equiv.), $Pd(OAc)_2$ (10 mg [a], 0.045 mmol, 5 mol%), PPh_3 (24 mg [b], 0.091 mmol, 10 mol%) and Ag_2CO_3 (186 mg, 0.675 mmol, 1.5 equiv.) in DMF (9.475 cm^3 total volume) was prepared following general procedure C. The reaction progress was monitored by *in situ* FT-IR spectroscopy. Quantitative conversion of starting material **57** was achieved.

[a] Using 500 µL of 0.09 M $Pd(OAc)_2$ stock solution made from stirring 20 mg $Pd(OAc)_2$ (0.089 mmol) in 1 cm^3 DMF for 10 min.

[b] Using 500 µL of 0.18 M PPh_3 stock solution made from stirring 47 mg PPh_3 (0.18 mmol) in 1 cm^3 DMF for 5 min.

(*Lab book reference number*: GMHP-7-479)

6.4.2 Kinetic Analysis of the Direct Arylation of 4-Iodotoluene 57 with Pentafluorobenzene 56 by Isolation Method

Order with respect to Pd catalyst with $Pd(OAc)_2/PPh_3$ 1:2 pre-catalyst

A mixture of 4-iodotoluene **57** (39 mg, 0.18 mmol, 1 equiv.), pentafluorobenzene **56** (0.2 cm^3, 0.3 g, 1.8 mmol, 10 equiv.), $Pd(OAc)_2$ (see below), PPh_3 (see below) and Ag_2CO_3 (37 mg, 0.13 mmol, 0.75 equiv.) in DMF (9.5 cm^3 total volume) were prepared following the general procedure C. The reaction progress was monitored by *in situ* FT-IR spectroscopy (**Figure 71**).

1. $Pd(OAc)_2$ (0.4 mg [a], 1.8×10^{-6} mol, 1.0 mol%), PPh_3 (0.94 mg [b], 3.6×10^{-6} mol, 2.0 mol%). [a] Using 120 µL of 0.015 M $Pd(OAc)_2$ stock solution made from stirring 20 mg $Pd(OAc)_2$ (0.089 mmol) in 6 cm^3 DMF for 10 min. [b] Using 120 µL of 0.03 M PPh_3 stock solution made from stirring 47 mg PPh_3 (0.18 mmol) in 6 cm^3 DMF for 5 min; 77% conversion of starting material **57** was achieved with $k_{obs} = (3.52 \pm 0.03) \times 10^{-7}$ mol dm^{-3} s^{-1} (**Table 12**, Entry 1). (*Lab book reference number*: GMHP-5-304)
2. $Pd(OAc)_2$ (1.0 mg [a], 4.5×10^{-6} mol, 2.5 mol%), PPh_3 (2.4 mg [b], 9.0×10^{-6} mol, 5.0 mol%). [a] Using 100 µL of 45 mM $Pd(OAc)_2$ stock solution made from stirring 20 mg $Pd(OAc)_2$ (0.089 mmol) in 2 cm^3 DMF for 10 min. [b] Using 100 µL of 90 mM PPh_3 stock solution made from stirring 47 mg PPh_3 (0.18 mmol) in 2 cm^3 DMF for 5 min; Quantitative conversion of starting material **57** was achieved with $k_{obs} = (7.90 \pm 0.06) \times 10^{-7}$ mol dm^{-3} s^{-1} (**Table 12**, Entry 2). (*Lab book reference number*: GMHP-6-345)
3. $Pd(OAc)_2$ (2 mg [a], 9×10^{-6} mol, 5.0 mol%), PPh_3 (4.7 mg [b], 1.8×10^{-5} mol, 10 mol%). [a] Using 150 µL of 0.059 M $Pd(OAc)_2$ stock solution made from stirring 20 mg $Pd(OAc)_2$ (0.089 mmol) in 1.5 cm^3 DMF for 10 min. [b] Using 150 µL of 0.12 M PPh_3 stock solution made from stirring 47 mg PPh_3 (0.18 mmol) in 1.5 cm^3 DMF for 5 min; Quantitative conversion of starting material **57** was achieved with k_{obs} =

(1.69 ± 0.02) × 10^{-6} mol dm^{-3} s^{-1} (**Table 12**, Entry 3). (*Lab book reference number*: GMHP-4-233)

4. $Pd(OAc)_2$ (4.0 mg [a], 0.018 mmol, 10 mol%), PPh_3 (9.4 mg, 0.036 mmol, 20 mol%). [a] Using 400 µL of 45 mM $Pd(OAc)_2$ stock solution made from stirring 20 mg $Pd(OAc)_2$ (0.089 mmol) in 2 cm^3 DMF for 10 min. [b] Using 400 µL of 90 mM PPh_3 stock solution made from stirring 47 mg PPh_3 (0.18 mmol) in 2 cm^3 DMF for 5 min; Quantitative conversion of starting material **57** was achieved with k_{obs} = (1.84 ± 0.04) × 10^{-6} mol dm^{-3} s^{-1} (**Table 12**, Entry 4). (*Lab book reference number*: GMHP-5-272)
5. $Pd(OAc)_2$ (8.1 mg [a], 0.036 mmol, 20 mol%), PPh_3 (18.9 mg, 0.072 mmol, 40 mol%). [a] Using 800 µL of 45 mM $Pd(OAc)_2$ stock solution made from stirring 20 mg $Pd(OAc)_2$ (0.089 mmol) in 2 cm^3 DMF for 10 min. [b] Using 800 µL of 90 mM PPh_3 stock solution made from stirring 47 mg PPh_3 (0.18 mmol) in 2 cm^3 DMF for 5 min; Quantitative conversion of starting material **57** was achieved with k_{obs} = (3.61 ± 0.13) × 10^{-6} mol dm^{-3} s^{-1} (**Table 12**, Entry 5). (*Lab book reference number*: GMHP-5-273)
6. $Pd(OAc)_2$ (16 mg, 0.071 mmol, 0.4 equiv.), PPh_3 (38 mg, 0.014 mmol, 0.8 equiv.); Quantitative conversion of starting material **57** was achieved with k_{obs} = (5.73 ± 0.23) × 10^{-6} mol dm^{-3} s^{-1} (**Table 12**, Entry 6). (*Lab book reference number*: GMHP-5-274)
7. $Pd(OAc)_2$ (32 mg, 0.14 mmol, 0.8 equiv.), PPh_3 (76 mg, 0.29 mmol, 1.6 equiv.); Quantitative conversion of starting material **57** was achieved with k_{obs} = (1.14 ± 0.01) × 10^{-5} mol dm^{-3} s^{-1} (**Table 12**, Entry 7). (*Lab book reference number*: GMHP-5-275)

Order with respect to pentafluorobenzene 56 for $Pd(OAc)_2$/PPh_3 1:2 pre-catalyst

A mixture of 4-iodotoluene **57** (39 mg, 0.18 mmol, 1 equiv.), pentafluorobenzene **56** (see below), $Pd(OAc)_2$ (2 mg [a], 8.9 × 10^{-6} mol, 5 mol%), PPh_3 (4.7 mg [b], 0.018 mmol, 10 mol%) and Ag_2CO_3 (37 mg, 0.13 mmol, 0.75 equiv.) in DMF (see below) was prepared following general procedure C. The reaction progress was monitored by *in situ* FT-IR spectroscopy (**Figure 72**).

[a] Using 200 µL of 45 mM $Pd(OAc)_2$ stock solution made from stirring 20 mg $Pd(OAc)_2$ (0.089 mmol) in 2 cm^3 DMF for 10 min.

[b] Using 200 µL of 90 mM PPh_3 stock solution made from stirring 47 mg PPh_3 (0.18 mmol) in 2 cm^3 DMF for 5 min.

1. Pentafluorobenzene **56** (0.2 cm^3, 1.8 mmol, 0.3 g, 10 equiv.), DMF (9.5 cm^3 total volume); Quantitative conversion of starting material **57** was achieved with k_{obs} = (1.68 ± 0.02) × 10^{-6} mol dm^{-3} s^{-1} (**Table 13**, Entry 1). (*Lab book reference number*: GMHP-4-233)
2. Pentafluorobenzene **56** (0.4 cm^3, 0.6 g, 3.6 mmol, 20 equiv.), DMF (9.3 cm^3 total volume); Quantitative conversion of starting material **57** was achieved with k_{obs} = (2.06 ± 0.03) × 10^{-6} mol dm^{-3} s^{-1} (**Table 13**, Entry 2). (*Lab book reference number*: GMHP-6-395)
3. Pentafluorobenzene **56** (0.6 cm^3, 0.9 g, 5.4 mmol, 30 equiv.), DMF (9.1 cm^3 total volume); Quantitative conversion of starting material **57** was achieved with k_{obs} = (2.56 ± 0.04) × 10^{-6} mol dm^{-3} s^{-1} (**Table 13**, Entry 3). (*Lab book reference number*: GMHP-4-235)
4. Pentafluorobenzene **56** (0.8 cm^3, 1.2 g, 7.2 mmol, 40 equiv.), DMF (8.9 cm^3 total volume); Quantitative conversion of starting material **57** was achieved with k_{obs} = (3.19 ± 0.06) × 10^{-6} mol dm^{-3} s^{-1} (**Table 13**, Entry 4). (*Lab book reference number*: GMHP-4-236)
5. Pentafluorobenzene **56** (1 cm^3, 1.5 g, 9 mmol, 50 equiv.), DMF (8.7 cm^3 total volume); Quantitative conversion of starting material **57** was achieved with k_{obs} = (4.04 ± 0.07) × 10^{-6} mol dm^{-3} s^{-1} (**Table 13**, Entry 5). (*Lab book reference number*: GMHP-4-234)

Order with respect to Pd catalyst with $Pd(OAc)_2$/PPh_3 1:4 pre-catalyst

A mixture of 4-iodotoluene **57** (39 mg, 0.18 mmol, 1 equiv.), pentafluorobenzene **56** (0.2 cm^3, 0.3 g, 1.8 mmol, 10 equiv.), $Pd(OAc)_2$ (see below), PPh_3 (see below) and Ag_2CO_3 (37 mg, 0.13 mmol, 0.75 equiv.) in DMF (9.5 cm^3 total volume) were prepared following the general procedure C. The reaction progress was monitored by *in situ* FT-IR spectroscopy.

1. $Pd(OAc)_2$ (2 mg [a], 9 × 10^{-6} mol, 5.0 mol%), PPh_3 (9.4 mg [b], 0.036 mmol, 20 mol%). [a] Using 200 µL of 45 mM $Pd(OAc)_2$ stock solution made from stirring 20 mg $Pd(OAc)_2$ (0.089 mmol) in 2 cm^3 DMF for 10 min. [b] Using 400 µL of 90 mM PPh_3 stock solution made from stirring 47 mg PPh_3 (0.18 mmol) in 2 cm^3 DMF for 5 min; Quantitative conversion of starting material **57** was achieved with k_{obs} = (3.73 ± 0.08) × 10^{-6} mol dm^{-3} s^{-1} (**Table 26**, Entry 1). (*Lab book reference number*: GMHP-6-349)
2. $Pd(OAc)_2$ (4 mg [a], 0.018 mmol, 10 mol%), PPh_3 (19 mg [b], 0.073 mmol, 40 mol%). [a] Using 400 µL of 45 mM $Pd(OAc)_2$ stock solution made from stirring 20 mg $Pd(OAc)_2$ (0.089 mmol) in 2 cm^3 DMF for 10 min. [b] Using 400 µL of 0.18 M PPh_3

stock solution made from stirring 48 mg PPh_3 (0.18 mmol) in 1 cm^3 DMF for 5 min; Quantitative conversion of starting material **57** was achieved with k_{obs} = (5.96 ± 1.02) × 10^{-6} mol dm^{-3} s^{-1} (**Table 26**, Entry 2). (*Lab book reference number*: GMHP-7-503)

3. $Pd(OAc)_2$ (6 mg [a], 0.027 mmol, 15 mol%), PPh_3 (28 mg [b], 0.11 mmol, 60 mol%). [a] Using 600 µL of 45 mM $Pd(OAc)_2$ stock solution made from stirring 20 mg $Pd(OAc)_2$ (0.089 mmol) in 2 cm^3 DMF for 10 min. [b] Using 600 µL of 0.18 M PPh_3 stock solution made from stirring 48 mg PPh_3 (0.18 mmol) in 1 cm^3 DMF for 5 min; Quantitative conversion of starting material **57** was achieved with k_{obs} = (6.74 ± 0.84) × 10^{-6} mol dm^{-3} s^{-1} (**Table 26**, Entry 3). (*Lab book reference number*: GMHP-7-502)
4. $Pd(OAc)_2$ (8.1 mg [a], 0.036 mmol, 20 mol%), PPh_3 (38 mg, 0.14 mmol, 0.8 equiv.). [a] Using 800 µL of 45 mM $Pd(OAc)_2$ stock solution made from stirring 20 mg $Pd(OAc)_2$ (0.089 mmol) in 2 cm^3 DMF for 10 min; Quantitative conversion of starting material **57** was achieved with k_{obs} = (9.91 ± 1.70) × 10^{-6} mol dm^{-3} s^{-1} (**Table 26**, Entry 4). (*Lab book reference number*: GMHP-7-509)

Order with respect to pentafluorobenzene 56 for $Pd(OAc)_2$/PPh_3 1:4 pre-catalyst

A mixture of 4-iodotoluene **57** (39 mg, 0.18 mmol, 1 equiv.), pentafluorobenzene **56** (see below), $Pd(OAc)_2$ (2 mg [a], 8.9 × 10^{-6} mol, 5 mol%), PPh_3 (9.4 mg [b], 0.036 mmol, 20 mol%) and Ag_2CO_3 (37 mg, 0.13 mmol, 0.75 equiv.) in DMF (see below) was prepared following general procedure C. The reaction progress was monitored by *in situ* FT-IR spectroscopy.

[a] Using 200 µL of 45 mM $Pd(OAc)_2$ stock solution made from stirring 20 mg $Pd(OAc)_2$ (0.089 mmol) in 2 cm^3 DMF for 10 min.

[b] Using 200 µL of 0.18 M PPh_3 stock solution made from stirring 47 mg PPh_3 (0.18 mmol) in 1 cm^3 DMF for 5 min.

1. Pentafluorobenzene **56** (0.2 cm^3, 0.3 g, 1.8 mmol, 10 equiv.), DMF (9.5 cm^3 total volume); Quantitative conversion of starting material **57** was achieved with k_{obs} = (3.73 ± 0.08) × 10^{-6} mol dm^{-3} s^{-1} (**Table 27**, Entry 1). (*Lab book reference number*: GMHP-6-349)
2. Pentafluorobenzene **56** (0.4 cm^3, 0.6 g, 3.6 mmol, 20 equiv.), DMF (9.3 cm^3 total volume); Quantitative conversion of starting material **57** was achieved with k_{obs} = (4.18 ± 0.60) × 10^{-6} mol dm^{-3} s^{-1} (**Table 27**, Entry 2). (*Lab book reference number*: GMHP-7-504)

3. Pentafluorobenzene **56** (0.6 cm^3, 0.9 g, 5.4 mmol, 30 equiv.), DMF (9.1 cm^3 total volume); Quantitative conversion of starting material **57** was achieved with k_{obs} = (5.13 ± 0.30) × 10^{-6} mol dm^{-3} s^{-1} (**Table 27**, Entry 3). (*Lab book reference number*: GMHP-7-506)
4. Pentafluorobenzene **56** (0.8 cm^3, 1.2 g, 7.2 mmol, 40 equiv.), DMF (8.9 cm^3 total volume); Quantitative conversion of starting material **57** was achieved with k_{obs} = (5.50 ± 0.30) × 10^{-6} mol dm^{-3} s^{-1} (**Table 27**, Entry 4). (*Lab book reference number*: GMHP-7-507)

6.4.3 Kinetic Analysis of the Direct Arylation of Iodobenzene 81 with Pentafluorobenzene 56 by Isolation Method

Order with respect to Pd catalyst

A mixture of iodobenzene **81** (60 µL, 0.54 mmol, 1 equiv.), pentafluorobenzene **56** (0.6 cm^3, 0.9 g, 5.4 mmol, 10 equiv.), $Pd(OAc)_2$ (see below), PPh_3 (see below) and Ag_2CO_3 (111 mg, 0.40 mmol, 0.75 equiv.) in DMF (9.1 cm^3 total volume) was prepared following general procedure C. The reaction progress was monitored by *in situ* FT-IR spectroscopy (**Figure 73**).

1. $Pd(OAc)_2$ (6 mg [a], 0.027 mmol, 5 mol%), PPh_3 (14 mg [b], 0.054 mmol, 10 mol%). [a] Using 300 µL of 0.09 M $Pd(OAc)_2$ stock solution made from stirring 20 mg $Pd(OAc)_2$ (0.089 mmol) in 1 cm^3 DMF for 10 min. [b] Using 300 µL of 0.18 M PPh_3 stock solution made from stirring 47 mg PPh_3 (0.18 mmol) in 1 cm^3 DMF for 5 min); Quantitative conversion of starting material **81** was achieved with k_{obs} = (9.99 ± 0.11) × 10^{-6} mol dm^{-3} s^{-1} (**Table 15**, Entry 1). (*Lab book reference number*: GMHP-5-287)
2. $Pd(OAc)_2$ (12 mg, 0.053 mmol, 10 mol%), PPh_3 (28 mg, 0.11 mmol, 20 mol%); Quantitative conversion of starting material **81** was achieved with k_{obs} = (1.61 ± 0.01) × 10^{-5} mol dm^{-3} s^{-1} (**Table 15**, Entry 2). (*Lab book reference number*: GMHP-5-293)
3. $Pd(OAc)_2$ (24 mg, 0.11 mmol, 20 mol%), PPh_3 (56 mg, 0.22 mmol, 40 mol%); Quantitative conversion of starting material **81** was achieved with k_{obs} = (2.18 ± 0.03) × 10^{-5} mol dm^{-3} s^{-1} (**Table 15**, Entry 3). (*Lab book reference number*: GMHP-5-290)
4. $Pd(OAc)_2$ (37 mg, 0.16 mmol, 30 mol%), PPh_3 (85 mg, 0.32, 60 mol%); Quantitative conversion of starting material **81** was achieved with k_{obs} = (2.41 ±

0.04) × 10^{-5} mol dm^{-3} s^{-1} (**Table 15**, Entry 4). (*Lab book reference number*: GMHP-5-322)

Order with respect to pentafluorobenzene 56

A mixture of iodobenzene **81** (60 µL, 0.54 mmol, 1 equiv.), pentafluorobenzene **56** (see below), $Pd(OAc)_2$ (6 mg [a], 0.027 mmol, 5 mol%), PPh_3 (14 mg [b], 0.054 mmol, 10 mol%) and Ag_2CO_3 (111 mg, 0.40 mmol) in DMF (see below) was prepared following general procedure C. The reaction progress was monitored by *in situ* FT-IR spectroscopy (**Figure 74**).

[a] Using 300 µL of 0.09 M $Pd(OAc)_2$ stock solution made from stirring 20 mg $Pd(OAc)_2$ (0.089 mmol) in 1 cm^3 DMF for 10 min.

[b] Using 300 µL of 0.18 M PPh_3 stock solution made from stirring 47 mg PPh_3 (0.18 mmol) in 1 cm^3 DMF for 5 min.

1. Pentafluorobenzene **56** (0.6 cm^3, 0.9 g, 5.4 mmol, 10 equiv.), DMF (9.1 cm^3 total volume); Quantitative conversion of starting material **81** was achieved with k_{obs} = (9.99 ± 0.11) × 10^{-6} mol dm^{-3} s^{-1} (**Table 16**, Entry 1). (*Lab book reference number*: GMHP-5-287)
2. Pentafluorobenzene **56** (1.2 cm^3, 1.8 g, 0.011 mol, 20 equiv.), DMF (8.5 cm^3 total volume); Quantitative conversion of starting material **81** was achieved with k_{obs} = (1.24 ± 0.02) × 10^{-5} mol dm^{-3} s^{-1} (**Table 16**, Entry 2). (*Lab book reference number*: GMHP-5-289)
3. Pentafluorobenzene **56** (1.8 cm^3, 2.7 g, 0.016 mol, 30 equiv.), DMF (7.9 cm^3 total volume); Quantitative conversion of starting material **81** was achieved with k_{obs} = (1.57 ± 0.02) × 10^{-5} mol dm^{-3} s^{-1} (**Table 16**, Entry 3). (*Lab book reference number*: GMHP-5-288)
4. Pentafluorobenzene **56** (2.4 cm^3, 3.6 g, 0.022 mol, 40 equiv.), DMF (7.3 cm^3 total volume); Quantitative conversion of starting material **81** was achieved with k_{obs} = (2.07 ± 0.05) × 10^{-5} mol dm^{-3} s^{-1} (**Table 16**, Entry 4). (*Lab book reference number*: GMHP-5-286)

6.4.4 Kinetic Analysis of the Direct Arylation of 4-Substituted-Iodobenzene with Pentafluorobenzene 56

A mixture of 4-substituted-iodoarene (see below), pentafluorobenzene **56** (200 µL, 0.3 g, 1.8 mmol, 10 equiv.), $Pd(OAc)_2$ (2 mg [a], 8.9 × 10^{-6} mol, 5 mol%), PPh_3 (4.7 mg [b], 0.018 mmol, 10 mol%) and Ag_2CO_3 (37 mg, 0.13 mmol, 0.75 equiv.) in DMF (9.5 cm^3 total

volume) was prepared following general procedure C. The reaction progress was monitored by *in situ* FT-IR spectroscopy (**Figure 88**).

[a] Using 200 µL of 45 mM $Pd(OAc)_2$ stock solution made from stirring 20 mg $Pd(OAc)_2$ (0.089 mmol) in 2 cm^3 DMF for 10 min.

[b] Using 200 µL of 90 mM PPh_3 stock solution made from stirring 47 mg PPh_3 (0.18 mmol) in 2 cm^3 DMF for 5 min.

1. OH (39 mg, 0.18 mmol, 1 equiv.); 0% conversion to product **62** (**Table 25**, Entry 1). (*Lab book reference number*: GMHP-7-510)
2. NH_2 (39 mg, 0.18 mmol, 1 equiv.); 0% conversion to product **63** (**Table 25**, Entry 2). (*Lab book reference number*: GMHP-7-500)
3. Me (39 mg, 0.18 mmol, 1 equiv.); Quantitative conversion of starting material to product **58** was achieved with $k_{obs} = (1.68 \pm 0.04) \times 10^{-6}$ mol dm^{-3} s^{-1} (**Table 25**, Entry 3). (*Lab book reference number*: GMHP-4-233)
4. H (20 µL, 36 mg, 0.18 mmol, 1 equiv.); Quantitative conversion of starting material to product **64** was achieved with $k_{obs} = (1.01 \pm 0.03) \times 10^{-6}$ mol dm^{-3} s^{-1} (**Table 25**, Entry 4). (*Lab book reference number*: GMHP-5-276)
5. F (21 µL, 40 mg, 0.18 mmol, 1 equiv.); Quantitative conversion of starting material to product **65** was achieved with $k_{obs} = (1.68 \pm 0.04) \times 10^{-6}$ mol dm^{-3} s^{-1} (**Table 25**, Entry 5). (*Lab book reference number*: GMHP-7-501)
6. CF_3 (27 µL, 49 mg, 0.18 mmol, 1 equiv.); Quantitative conversion of starting material to product **66** was achieved with $k_{obs} = (1.13 \pm 0.03) \times 10^{-6}$ mol dm^{-3} s^{-1} (**Table 25**, Entry 6). (*Lab book reference number*: GMHP-5-285)

6.4.5 Temperature Dependence of the Direct Arylation of 4-Iodotoluene 57 with Pentafluorobenzene 56

A mixture of 4-iodotoluene **57** (39 mg, 0.18 mmol, 1 equiv.), pentafluorobenzene **56** (see below), $Pd(OAc)_2$ (2 mg [a], 8.9×10^{-6} mol, 5 mol%), PPh_3 (4.7 mg [b], 0.018 mmol, 10 mol%) and Ag_2CO_3 (37 mg, 0.13 mmol, 0.75 equiv.) in DMF (see below) was prepared following general procedure C. The reaction progress was monitored by *in situ* FT-IR spectroscopy. Graphical representation of the overall experimental results was presented as **Figure 42**.

[a] Using 200 µL of 45 mM $Pd(OAc)_2$ stock solution made from stirring 20 mg $Pd(OAc)_2$ (0.089 mmol) in 2 cm^3 DMF for 10 min.

[b] Using 200 µL of 90 mM PPh_3 stock solution made from stirring 47 mg PPh_3 (0.18 mmol) in 2 cm^3 DMF for 5 min.

Reactions heated at 40.0 ± 1 °C (Figure 75)

1. Pentafluorobenzene **56** (0.2 cm^3, 0.3 g, 1.8 mmol, 10 equiv.), DMF (9.5 cm^3 total volume); Quantitative conversion of starting material **57** was achieved with k_{obs} = (5.22 ± 0.04) × 10^{-7} mol dm^{-3} s^{-1}. (*Lab book reference number*: GMHP-4-241)
2. Pentafluorobenzene **56** (0.4 cm^3, 0.6 g, 3.6 mmol, 20 equiv.), DMF (9.3 cm^3 total volume); Quantitative conversion of starting material **57** was achieved with k_{obs} = (6.53 ± 0.06) × 10^{-7} mol dm^{-3} s^{-1}. (*Lab book reference number*: GMHP-5-327)
3. Pentafluorobenzene **56** (0.6 cm^3, 0.9 g, 5.4 mmol, 30 equiv.), DMF (9.1 cm^3 total volume); Quantitative conversion of starting material **57** was achieved with k_{obs} = (8.60 ± 0.06) × 10^{-7} mol dm^{-3} s^{-1}. (*Lab book reference number*: GMHP-6-396)
4. Pentafluorobenzene **56** (0.8 cm^3, 1.2 g, 7.2 mmol, 40 equiv.), DMF (8.9 cm^3 total volume); Quantitative conversion of starting material **57** was achieved with k_{obs} = (1.04 ± 0.02) × 10^{-6} mol dm^{-3} s^{-1}. (*Lab book reference number*: GMHP-5-333)
5. Pentafluorobenzene **56** (1 cm^3, 1.5 g, 9 mmol, 50 equiv.), DMF (8.7 cm^3 total volume); Quantitative conversion of starting material **57** was achieved with k_{obs} = (1.27 ± 0.01) × 10^{-6} mol dm^{-3} s^{-1}. (*Lab book reference number*: GMHP-5-335)

Reactions heated at 50 ± 1 °C (Figure 76)

1. Pentafluorobenzene **56** (0.2 cm^3, 0.3 g, 1.8 mmol, 10 equiv.), DMF (9.5 cm^3 total volume); Quantitative conversion of starting material **57** was achieved with k_{obs} = (8.61 ± 0.06) × 10^{-7} mol dm^{-3} s^{-1}. (*Lab book reference number*: GMHP-5-321)
2. Pentafluorobenzene **56** (0.4 cm^3, 0.6 g, 3.6 mmol, 20 equiv.), DMF (9.3 cm^3 total volume); Quantitative conversion of starting material **57** was achieved with k_{obs} = (1.46 ± 0.02) × 10^{-6} mol dm^{-3} s^{-1}. (*Lab book reference number*: GMHP-5-328)
3. Pentafluorobenzene **56** (0.6 cm^3, 0.9 g, 5.4 mmol, 30 equiv.), DMF (9.1 cm^3 total volume); Quantitative conversion of starting material **57** was achieved with k_{obs} = (2.05 ± 0.02) × 10^{-6} mol dm^{-3} s^{-1}. (*Lab book reference number*: GMHP-5-331)
4. Pentafluorobenzene **56** (0.8 cm^3, 1.2 g, 7.2 mmol, 40 equiv.), DMF (8.9 cm^3 total volume); Quantitative conversion of starting material **57** was achieved with k_{obs} = (1.64 ± 0.02) × 10^{-6} mol dm^{-3} s^{-1}. (*Lab book reference number*: GMHP-5-329)
5. Pentafluorobenzene **56** (1 cm^3, 1.5 g, 9 mmol, 50 equiv.), DMF (8.7 cm^3 total volume); Quantitative conversion of starting material **57** was achieved with k_{obs} = (2.44 ± 0.04) × 10^{-6} mol dm^{-3} s^{-1}. (*Lab book reference number*: GMHP-5-336)

Reactions heated at 64 ± 1 °C (Figure 77)

1. Pentafluorobenzene **56** (0.2 cm^3, 0.3 g, 1.8 mmol, 10 equiv.), DMF (9.5 cm^3 total volume); Quantitative conversion of starting material **57** was achieved with k_{obs} = (2.18 ± 0.03) × 10^{-6} mol dm^{-3} s^{-1}. (*Lab book reference number*: GMHP-6-338)
2. Pentafluorobenzene **56** (0.4 cm^3, 0.6 g, 3.6 mmol, 20 equiv.), DMF (9.3 cm^3 total volume); Quantitative conversion of starting material **57** was achieved with k_{obs} = (3.95 ± 0.08) × 10^{-6} mol dm^{-3} s^{-1}. (*Lab book reference number*: GMHP-6-342)
3. Pentafluorobenzene **56** (0.6 cm^3, 0.9 g, 5.4 mmol, 30 equiv.), DMF (9.1 cm^3 total volume); Quantitative conversion of starting material **57** was achieved with k_{obs} = (4.14 ± 0.10) × 10^{-6} mol dm^{-3} s^{-1}. (*Lab book reference number*: GMHP-6-343)
4. Pentafluorobenzene **56** (0.8 cm^3, 1.2 g, 7.2 mmol, 40 equiv.), DMF (8.9 cm^3 total volume); Quantitative conversion of starting material **57** was achieved with k_{obs} = (5.25 ± 0.14) × 10^{-6} mol dm^{-3} s^{-1}. (*Lab book reference number*: GMHP-6-337)
5. Pentafluorobenzene **56** (1 cm^3, 1.5 g, 9 mmol, 50 equiv.), DMF (8.7 cm^3 total volume); Quantitative conversion of starting material **57** was achieved with k_{obs} = (6.37 ± 0.29) × 10^{-6} mol dm^{-3} s^{-1}. (*Lab book reference number*: GMHP-6-344)

Reactions heated at 72 ± 1 °C (Figure 78)

1. Pentafluorobenzene **56** (0.2 cm^3, 1.8 mmol, 0.3 g, 10 equiv.), DMF (9.5 cm^3 total volume); Quantitative conversion of starting material **57** was achieved with k_{obs} = (4.31 ± 0.10) × 10^{-6} mol dm^{-3} s^{-1}. (*Lab book reference number*: GMHP-4-242)
2. Pentafluorobenzene **56** (0.4 cm^3, 0.6 g, 3.6 mmol, 20 equiv.), DMF (9.3 cm^3 total volume); Quantitative conversion of starting material **57** was achieved with k_{obs} = (6.50 ± 0.30) × 10^{-6} mol dm^{-3} s^{-1}. (*Lab book reference number*: GMHP-5-330)
3. Pentafluorobenzene **56** (0.6 cm^3, 0.9 g, 5.4 mmol, 30 equiv.), DMF (9.1 cm^3 total volume); Quantitative conversion of starting material **57** was achieved with k_{obs} = (6.98 ± 0.24) × 10^{-6} mol dm^{-3} s^{-1}. (*Lab book reference number*: GMHP-5-332)
4. Pentafluorobenzene **56** (0.8 cm^3, 1.2 g, 7.2 mmol, 40 equiv.), DMF (8.9 cm^3 total volume); Quantitative conversion of starting material **57** was achieved with k_{obs} = (9.51 ± 1.01) × 10^{-6} mol dm^{-3} s^{-1}. (*Lab book reference number*: GMHP-5-334)
5. Pentafluorobenzene **56** (1 cm^3, 1.5 g, 9 mmol, 50 equiv.), DMF (8.7 cm^3 total volume); Quantitative conversion of starting material **57** was achieved with k_{obs} = (8.12 ± 0.28) × 10^{-6} mol dm^{-3} s^{-1}. (*Lab book reference number*: GMHP-6-401)

6.4.6 Kinetic Isotope Effect of the Direct Arylation of 4-Iodotoleuene 57 with Deuteropentafluorobenzene 100

A mixture of 4-iodotoluene **57** (39 mg, 0.18 mmol, 1 equiv.), deuteropentafluorobenzene **100** (see below), $Pd(OAc)_2$ (2 mg [a], 8.9×10^{-6} mol, 5 mol%), PPh_3 (4.7 mg [b], 0.018 mmol, 10 mol%) and Ag_2CO_3 (37 mg, 0.13 mmol, 0.75 equiv.) in DMF (9.5 cm^3 total volume) was prepared following general procedure C. The reaction progress was monitored by *in situ* FT-IR spectroscopy. The IR signals of 2,3,4,5,6-pentafluoro-4′-(methyl)biphenyl product **58** at 989 cm^{-1} was monitored and the k_{obs} were used to calculate the KIE values.

[a] Using 200 µL of 45 mM $Pd(OAc)_2$ stock solution made from stirring 20 mg $Pd(OAc)_2$ (0.089 mmol) in 2 cm^3 DMF for 10 min.

[b] Using 200 µL of 90 mM PPh_3 stock solution made from stirring 47 mg PPh_3 (0.18 mmol) in 2 cm^3 DMF for 5 min.

Reactions heated at 40 ± 1 °C

1. C_6F_5D **100** (0.2 cm^3, 0.3 g, 1.8 mmol, 10 equiv.); Quantitative conversion of starting material **57** was achieved with $k_{obs} = (7.65 \pm 0.02) \times 10^{-8}$ mol dm^{-3} s^{-1} (**Figure 82** and **Table 21**, Entry 2). (*Lab book reference number*: GMHP-6-340)
2. C_6F_5D **100** (0.8 cm^3, 1.2 g, 7.2 mmol, 40 equiv.); Quantitative conversion of starting material **57** was achieved with $k_{obs} = (3.20 \pm 0.02) \times 10^{-7}$ mol dm^{-3} s^{-1} (**Figure 83** and **Table 21**, Entry 4). (*Lab book reference number*: GMHP-6-339)

Reactions heated at 56 ± 1 °C

1. C_6F_5D **100** (0.2 cm^3, 0.3 g, 1.8 mmol, 10 equiv.); Quantitative conversion of starting material **57** was achieved with $k_{obs} = (3.96 \pm 0.02) \times 10^{-7}$ mol dm^{-3} s^{-1} (**Figure 41** and **Table 21**, Entry 6). (*Lab book reference number*: GMHP-5-296 and GMHP-6-356)
2. C_6F_5D **100** (0.8 cm^3, 1.2 g, 7.2 mmol, 40 equiv.); Quantitative conversion of starting material **57** was achieved with $k_{obs} = (1.28 \pm 0.01) \times 10^{-6}$ mol dm^{-3} s^{-1} (**Figure 84** and **Table 21**, Entry 8). (*Lab book reference number*: GMHP-6-358)

6.4.7 Kinetic Analysis of the Direct Arylation of 4-Iodotoluene 57 with Pentafluorobenzene 56 using Different Quantity of PPh_3

A mixture of 4-iodotoluene **57** (39 mg, 0.18 mmol, 1 equiv.), pentafluorobenzene **56** (200 µL, 0.3 g, 1.8 mmol, 10 equiv.), $Pd(OAc)_2$ (2 mg [a], 8.9×10^{-6} mol, 5 mol%), trialkylphosphine (see below) and Ag_2CO_3 (37 mg, 0.13 mmol, 0.75 equiv.) in DMF (9.5

cm^3 total volume) was prepared following general procedure C. The reaction progress was monitored by *in situ* FT-IR spectroscopy (**Figure 86**).

[a] Using 200 µL of 45 mM $Pd(OAc)_2$ stock solution made from stirring 20 mg $Pd(OAc)_2$ (0.089 mmol) in 2 cm^3 DMF for 10 min.

1. PPh_3 (2.4 mg [b], 0.009 mmol, 5 mol%), [b] Using 100 µL of 90 mM PPh_3 stock solution made from stirring 47 mg PPh_3 (0.18 mmol) in 2 cm^3 DMF for 5 min.; 76% conversion of starting material **57** achieved with $k_{obs} = (6.04 \pm 0.07) \times 10^{-7}$ mol dm^{-3} s^{-1} (**Table 18**, Entry 1). (*Lab book reference number*: GMHP-6-348)
2. PPh_3 (4.7 mg, 0.018 mmol, 10 mol%), [b] Using 150 µL of 120 mM PPh_3 stock solution made from stirring 47 mg PPh_3 (0.18 mmol) in 1.5 cm^3 DMF for 5 min.; Quantitative conversion of starting material **57** achieved with $k_{obs} = (1.68 \pm 0.02) \times 10^{-6}$ mol dm^{-3} s^{-1} (**Table 18**, Entry 2). (*Lab book reference number*: GMHP-4-233)
3. PPh_3 (7.1 mg, 0.027 mmol, 15 mol%), [b] Using 300 µL of 90 mM PPh_3 stock solution made from stirring 47 mg PPh_3 (0.18 mmol) in 2 cm^3 DMF for 5 min.; Quantitative conversion of starting material **57** achieved with $k_{obs} = (2.78 \pm 0.03) \times 10^{-6}$ mol dm^{-3} s^{-1} (**Table 18**, Entry 3). (*Lab book reference number*: GMHP-6-367)
4. PPh_3 (9.4 mg, 0.036 mmol, 20 mol%), [b] Using 400 µL of 90 mM PPh_3 stock solution made from stirring 47 mg PPh_3 (0.18 mmol) in 2 cm^3 DMF for 5 min.; Quantitative conversion of starting material **57** achieved with $k_{obs} = (3.73 \pm 0.08) \times 10^{-6}$ mol dm^{-3} s^{-1} (**Table 18**, Entry 4). (*Lab book reference number*: GMHP-6-349)
5. PPh_3 (12 mg, 0.046 mmol, 25 mol%), [b] Using 250 µL of 180 mM PPh_3 stock solution made from stirring 48 mg PPh_3 (0.18 mmol) in 1 cm^3 DMF for 5 min.; Quantitative conversion of starting material **57** achieved with $k_{obs} = (2.72 \pm 0.05) \times 10^{-6}$ mol dm^{-3} s^{-1} (**Table 18**, Entry 5). (*Lab book reference number*: GMHP-6-380)
6. PPh_3 (14 mg, 0.054 mmol, 30 mol%), [b] Using 300 µL of 180 mM PPh_3 stock solution made from stirring 48 mg PPh_3 (0.18 mmol) in 1 cm^3 DMF for 5 min.; Quantitative conversion of starting material **57** achieved with $k_{obs} = (2.67 \pm 0.04) \times 10^{-6}$ mol dm^{-3} s^{-1} (**Table 18**, Entry 6). (*Lab book reference number*: GMHP-6-357)
7. PPh_3 (19 mg, 0.072 mmol, 40 mol%), [b] Using 400 µL of 180 mM PPh_3 stock solution made from stirring 48 mg PPh_3 (0.18 mmol) in 1 cm^3 DMF for 5 min.; Quantitative conversion of starting material **57** achieved with $k_{obs} = (2.71 \pm 0.06) \times 10^{-6}$ mol dm^{-3} s^{-1} (**Table 18**, Entry 7). (*Lab book reference number*: GMHP-6-350)

6.4.8 Kinetic Analysis of the Direct Arylation of 4-Iodotoluene 57 with Pentafluorobenzene 56 using Different Quantity of Ag_2CO_3

A mixture of 4-iodotoluene **57** (39 mg, 0.18 mmol, 1 equiv.), pentafluorobenzene **56** (200 µL, 0.3 g, 1.8 mmol, 10 equiv.), $Pd(OAc)_2$ (2 mg [a], 8.9×10^{-6} mol, 5 mol%), PPh_3 (4.7 mg [b], 0.018 mmol, 10 mol%) and Ag_2CO_3 (see below) in DMF (9.5 cm^3 total volume) was prepared following general procedure C. The reaction progress was monitored by *in situ* FT-IR spectroscopy (**Figure 87**).

[a] Using 200 µL of 45 mM $Pd(OAc)_2$ stock solution made from stirring 20 mg $Pd(OAc)_2$ (0.089 mmol) in 2 cm^3 DMF for 10 min.

[b] Using 200 µL of 90 mM PPh_3 stock solution made from stirring 47 mg PPh_3 (0.18 mmol) in 2 cm^3 DMF for 5 min.

1. Ag_2CO_3 (4.7 mg, 0.1 equiv.); 9% conversion of starting material **57** achieved with $k_{obs} = (4.24 \pm 0.40) \times 10^{-7}$ mol dm^{-3} s^{-1} (**Table 19**, Entry 1). (*Lab book reference number*: GMHP-6-392)
2. Ag_2CO_3 (12 mg, 0.24 equiv.); 39% conversion of starting material **57** achieved with $k_{obs} = (7.85 \pm 0.15) \times 10^{-7}$ mol dm^{-3} s^{-1} (**Table 19**, Entry 2). (*Lab book reference number*: GMHP-6-379)
3. Ag_2CO_3 (25 mg, 0.49 equiv.); Quantitative conversion of starting material **57** achieved with $k_{obs} = (1.35 \pm 0.01) \times 10^{-6}$ mol dm^{-3} s^{-1} (**Table 19**, Entry 3). (*Lab book reference number*: GMHP-6-381)
4. Ag_2CO_3 (37 mg, 0.74 equiv.); Quantitative conversion of starting material **57** achieved with $k_{obs} = (1.68 \pm 0.02) \times 10^{-6}$ mol dm^{-3} s^{-1} (**Table 19**, Entry 4). (*Lab book reference number*: GMHP-4-233)
5. Ag_2CO_3 (73 mg, 1.47 equiv.); Quantitative conversion of starting material **57** achieved with $k_{obs} = (1.65 \pm 0.02) \times 10^{-6}$ mol dm^{-3} s^{-1} (**Table 19**, Entry 5). (*Lab book reference number*: GMHP-6-382)
6. Ag_2CO_3 (112 mg, 2.24 equiv.); Quantitative conversion of starting material **57** achieved with $k_{obs} = (1.71 \pm 0.01) \times 10^{-6}$ mol dm^{-3} s^{-1} (**Table 19**, Entry 6). (*Lab book reference number*: GMHP-6-383)

6.4.9 Poisoning the Direct Arylation of 4-Iodotoluene 57 with Pentafluorobenzene 56 by Mercury Drop-Test

A mixture of 4-iodotoluene **57** (197 mg, 0.904 mmol, 1 equiv.), pentafluorobenzene **56** (150 µL, 227 mg, 1.35 mmol, 1.5 equiv.), $Pd(OAc)_2$ (10 mg, 0.045 mmol, 5 mol%), PPh_3

(24 mg, 0.091 mmol, 10 mol%) and Ag_2CO_3 (188 mg, 0.68 mmol, 0.75 equiv.) in DMF (9.4 cm^3 total volume) was prepared following general procedure C. The reaction progress was monitored by *in situ* FT-IR spectroscopy (**Figure 47**). Mercury (135 µL, 1.83 g, 9.1 mmol, 200 equiv. of Pd) was added to the reaction mixture at 20% (*ca.* 64 min) or 50% (*ca.* 170 min) conversion of the starting material **57** to the product **58**. The reaction was quenched instantaneously upon addition of Hg.

Hg addition at 20% Conversion (*Lab book reference number*: GMHP-7-515)

Hg addition at 50% Conversion (*Lab book reference number*: GMHP-7-512)

6.4.10 Poisoning the Direct Arylation of 4-Iodotoluene 57 with Pentafluorobenzene 56 by Addition of PVPy

A mixture of 4-iodotoluene **57** (196 mg, 0.899 mmol, 1 equiv.), pentafluorobenzene **56** (150 µL, 227 mg, 1.35 mmol, 1.5 equiv.), $Pd(OAc)_2$ (11 mg, 0.049 mmol, 5 mol%), PPh_3 (24 mg, 0.091 mmol, 10 mol%) and Ag_2CO_3 (187 mg, 0.68 mmol, 0.75 equiv.) in DMF (9.4 cm^3 total volume) was prepared following general procedure C. The reaction progress was monitored by *in situ* FT-IR spectroscopy (**Figure 47**). Polvinyl-4-pyridine (0.962 g, 9.1 mmol, 200 equiv. of Pd) was added to the reaction mixture at 50% (*ca.* 170 min) conversion of the starting material **57** to the product **58**. The reaction was unaffected by the addition of PVPy.

(*Lab book reference number*: GMHP-7-517)

6.4.11 Hot-Filtration of the Direct Arylation of 4-Iodotoluene 57 with Pentafluorobenzene 56

A mixture of 4-iodotoluene **57** (194 mg, 0.890 mmol, 1 equiv.), pentafluorobenzene **56** (150 µL, 227 mg, 1.35 mmol, 1.5 equiv.), $Pd(OAc)_2$ (11 mg, 0.049 mmol, 5 mol%), PPh_3 (24 mg, 0.091 mmol, 10 mol%) and Ag_2CO_3 (188 mg, 0.68 mmol, 0.75 equiv.) in DMF (9.4 cm^3 total volume) was prepared following general procedure C. The reaction progress was monitored by *in situ* FT-IR spectroscopy (**Figure 49**). At 50% (*ca.* 170 min) conversion of the starting material **57** to the product **58**, the hot reaction mixture was filtered through heated Celite®-pad. A layer of green precipitate was removed by the Celite®-pad and the colourless filtrate was collected into a second reaction vessel containing the same quantity of Ag_2CO_3 (188 mg, 0.68 mmol, 0.75 equiv.) as the start of the reaction. The original reaction vessel and the Celite® pad were washed out with DMF until approximately 10 cm^3 of solution was present. The reaction mixture was sealed under continuous flow of nitrogen gas, re-heated in the oil bath to 56 ± 1 °C and monitored by *in*

situ FT-IR spectroscopic analysis (**Figure 49**). Continued formation of the product **58** was observed after performing hot-filtration.

(*Lab book reference number*: GMHP-7-518)

6.4.12 Reaction Kinetics of the Direct Arylation of Iodobenzene 81 with Pentafluorobenzene 56 using Different Pd Pre-Catalysts

Reactions with a pre-catalyst

A mixture of iodobenzene **81** (60 µL, 109 mg, 0.536 mmol, 1 equiv.), pentafluorobenzene **56** (600 µL, 908 mg, 5.41 mmol, 10 equiv.), pre-catalysts (0.0265 mmol Pd atom, 5 mol% Pd atom) and Ag_2CO_3 (111 mg, 0.403 mmol, 0.75 equiv.) in DMF (9.1 cm^3 total volume) was prepared following general procedure D. The reaction progress was monitored using *in situ* FT-IR spectroscopy (**Figure 67** a, **Figure 67** b and **Figure 68**). The pre-catalysts tested and the quantities used are provided below.

1. Pd(Ph)(κ^1-OAc)$(PPh_3)_2$ **85** (21 mg, 0.027 mmol, 5 mol%); Quantitative conversion of starting material **81** was achieved wtih k_{obs} = (8.52 ± 0.09) × 10^{-6} mol dm^{-3} s^{-1} (**Table 34**, Entry 8). (*Lab book reference number*: GMHP-7-448)
2. Pd(Ph)(I)$(PPh_3)_2$ **82a** (23 mg, 0.027 mmol, 5 mol%); Quantitative conversion of starting material **81** was achieved with k_{obs} = (14.83 ± 0.01) × 10^{-6} mol dm^{-3} s^{-1} (**Table 34**, Entry 9). (*Lab book reference number*: GMHP-7-465)
3. [Pd(Ph)(μ-OAc)(PPh_3)]$_2$ **84** (14 mg, 0.014 mmol, 2.5 mol%); Quantitative conversion of starting material **81** was achieved with k_{obs} = (7.90 ± 0.05) × 10^{-6} mol dm^{-3} s^{-1} (**Table 34**, Entry 2). (*Lab book reference number*: GMHP-7-431)
4. [Pd(Ph)(μ-OH)(PPh_3)]$_2$ **83a** (12 mg, 0.013 mmol, 2.5 mol%) (**Table 34**, Entry 4). (*Lab book reference number*: GMHP-7-432)
5. [Pd(Ph)(μ-I)(PPh_3)]$_2$ **86** (15 mg, 0.013 mmol, 2.5 mol%) (**Table 34**, Entry 5). (*Lab book reference number*: GMHP-7-435)

Reactions with a pre-catalyst and a ligand

A mixture of iodobenzene **81** (60 µL, 109 mg, 0.536 mmol, 1 equiv.), pentafluorobenzene **56** (600 µL, 908 mg, 5.41 mmol, 10 equiv.), pre-catalysts (0.0265 mmol Pd atom, 5 mol% Pd atom), PPh_3 (see below) and Ag_2CO_3 (111 mg, 0.403 mmol, 0.75 equiv.), in DMF (9.1 cm^3 total volume) was prepared following general procedure D. The reaction was monitored using *in situ* FT-IR spectroscopy. The pre-catalysts tested and the quantities used are provided below.

1. $Pd(OAc)_2$ (6.0 mg, 0.027 mmol, 5 mol%) and PPh_3 (14 mg, 0.053 mmol, 10 mol%); Quantitative conversion of starting material **81** was achieved with k_{obs} = (9.90 ± 0.04) × 10^{-6} mol dm^{-3} s^{-1} (**Table 34**, Entry 1). (*Lab book reference number*: GMHP-7-429)
2. $Pd(OAc)_2$ (5.9 mg, 0.027 mmol, 5 mol%) and PPh_3 (21 mg, 0.080 mmol, 15 mol%); Quantitative conversion of starting material **81** was achieved with k_{obs} = (14.58 ± 0.01) × 10^{-6} mol dm^{-3} s^{-1} (**Table 34**, Entry 10). (*Lab book reference number*: GMHP-7-452)
3. $[Pd(Ph)(\mu\text{-}OAc)(PPh_3)]_2$ **84** (14 mg, 0.014 mmol, 2.5 mol%) and PPh_3 (7 mg, 0.027 mmol, 5 mol%); Quantitative conversion of starting material **81** was achieved with k_{obs} = (7.56 ± 0.06) × 10^{-6} mol dm^{-3} s^{-1} (**Table 34**, Entry 3). (*Lab book reference number*: GMHP-7-436)

Reactions with a pre-catalyst and an AcOH

A mixture of iodobenzene **81** (60 µL, 109 mg, 0.536 mmol, 1 equiv.), pentafluorobenzene **56** (600 µL, 908 mg, 5.41 mmol, 10 equiv.), pre-catalysts (0.0265 mmol Pd atom, 5 mol% Pd atom), AcOH (see below) and Ag_2CO_3 (111 mg, 0.403 mmol, 0.75 equiv.), in DMF (9.1 cm^3 total volume) was prepared following general procedure D. The reaction progress was monitored using *in situ* FT-IR spectroscopy. Stock solution of 0.54 M AcOH was made from 155 µL degassed glacial AcOH (163 mg, 2.71 mmol) in 5 cm^3 DMF. The pre-catalysts tested and the quantities used are provided below.

1. $Pd(Ph)(I)(PPh_3)_2$ **82a** (22 mg, 0.026 mmol, 5 mol%) and AcOH (50 µL of 0.54 M stock, 1.55 µL, 1.63 mg, 0.0271 mmol, 5 mol%); Quantitative conversion of starting material **81** was achieved with k_{obs} = (7.34 ± 0.04) × 10^{-6} mol dm^{-3} s^{-1} (**Table 34**, Entry 11). (*Lab book reference number*: GMHP-7-450)
2. $Pd(Ph)(I)(PPh_3)_2$ **82a** (23 mg, 0.026 mmol, 5mol%) and AcOH (100 µL of 0.54 M stock, 3.1 µL, 3.25 mg, 0.0542 mmol, 10 mol%); Quantitative conversion of starting material **81** was achieved with k_{obs} = (11.10 ± 0.14) × 10^{-6} mol dm^{-3} s^{-1} (**Table 34**, Entry 12). (*Lab book reference number*: GMHP-7-508)
3. $Pd(Ph)(I)(PPh_3)_2$ **82a** (23 mg, 0.026 mmol, 5mol%) and AcOH (200 µL of 0.54 M stock, 6.2 µL, 6.5 mg, 0.11 mmol, 20 mol%); Quantitative conversion of starting material **81** was achieved with k_{obs} = (14.00 ± 0.01) × 10^{-6} mol dm^{-3} s^{-1} (**Table 34**, Entry 13). (*Lab book reference number*: GMHP-7-464)
4. $[Pd(Ph)(\mu\text{-}OH)(PPh_3)]_2$ **83a** (12 mg, 0.013 mmol, 2.5 mol%) and AcOH (50 µL of 0.54 M stock, 1.55 µL, 1.63 mg, 0.0271 mmol, 5 mol%); Quantitative conversion

of starting material **81** was achieved with k_{obs} = (9.71 ± 0.10) × 10^{-6} mol dm^{-3} s^{-1} (**Table 34**, Entry 6). (*Lab book reference number*: GMHP-7-439)

5. [Pd(Ph)(μ-I)(PPh_3)]$_2$ **86** (15 mg, 0.013 mmol, 2.5 mol%) and AcOH (50 µL of 0.54 M stock, 1.55 µL, 1.63 mg, 0.0271 mmol, 5 mol%); Quantitative conversion of starting material **81** was achieved with k_{obs} = (8.32 ± 0.05) × 10^{-6} mol dm^{-3} s^{-1} (**Table 34**, Etnry 7). (*Lab book reference number*: GMHP-7-438)

6.4.13 Reaction Kinetics of the Direct Arylation of 4-Iodotoluene 57 with Pentafluorobenzene 56 using Different Trialkylphosphines

A mixture of 4-iodotoluene **57** (39 mg, 0.18 mmol, 1 equiv.), pentafluorobenzene **56** (200 µL, 0.3 g, 1.8 mmol, 10 equiv.), $Pd(OAc)_2$ (2 mg [a], 8.9 × 10^{-6} mol, 5 mol%), trialkylphosphine (see below) and Ag_2CO_3 (37 mg, 0.13 mmol, 0.75 equiv.) in DMF (9.5 cm^3 total volume) was prepared following general procedure C. The reaction progress was monitored by *in situ* FT-IR spectroscopy (**Figure 89**).

[a] Using 200 µL of 45 mM $Pd(OAc)_2$ stock solution made from stirring 20 mg $Pd(OAc)_2$ (0.089 mmol) in 2 cm^3 DMF for 10 min.

1. $P(4\text{-}FC_6H_4)_3$ (5.7 mg [b], 0.018 mmol, 10 mol%), [b] Using 200 µL of 90 mM $P(4\text{-}FC_6H_4)_3$ stock solution made from stirring 29 mg $P(4\text{-}FC_6H_4)_3$ (0.09 mmol) in 1 cm^3 DMF for 5 min.; Quantitative conversion of starting material **57** was achieved with k_{obs} = (8.35 ± 0.14) × 10^{-7} mol dm^{-3} s^{-1} (**Table 28**, Entry 2). (*Lab book reference number*: GMHP-6-412)
2. $P(3,5\text{-}(CF_3)_2C_6H_3)_3$ (12 mg [b], 0.018 mmol, 10 mol%), [b] Using 500 µL of 37 mM $P(3,5\text{-}(CF_3)_2C_6H_3)_3$ stock solution made from stirring 25 mg $P(3,5\text{-}(CF_3)_2C_6H_3)_3$ (0.037 mmol) in 1 cm^3 DMF for 5 min.; Quantitative conversion of starting material **57** was achieved with k_{obs} = (7.05 ± 0.05) × 10^{-7} mol dm^{-3} s^{-1} (**Table 28**, Entry 3). (*Lab book reference number*: GMHP-6-409)
3. $P(2\text{-Furyl})_3$ (4.2 mg [b], 0.018 mmol, 10 mol%), [b] Using 200 µL of 90 mM $P(2\text{-Furyl})_3$ stock solution made from stirring 42 mg $P(2\text{-Furyl})_3$ (0.18 mmol) in 2 cm^3 DMF for 5 min.; Quantitative conversion of starting material **57** was achieved with k_{obs} = (1.66 ± 0.02) × 10^{-6} mol dm^{-3} s^{-1} (**Table 28**, Entry 4). (*Lab book reference number*: GMHP−6-427)
4. $P(2\text{-}MeOC_6H_4)_3$ (6.5 mg [b], 0.018 mmol, 10 mol%), [b] Using 600 µL of 31 mM $P(2\text{-}MeOC_6H_4)_3$ stock solution made from stirring 13 mg $P(2\text{-}MeOC_6H_4)_3$ (0.37 mmol) in 1.2 cm^3 DMF for 5 min.; 89% conversion of starting material **57** was achieved

with k_{obs} = (4.37 ± 0.10) × 10^{-6} mol dm^{-3} s^{-1} (**Table 28**, Entry 5). (*Lab book reference number*: GMHP-6-406)

5. P(4-$MeOC_6H_4$)$_3$ (6.5 mg [b], 0.018 mmol, 10 mol%), [b] Using 600 µL of 31 mM P(4-$MeOC_6H_4$)$_3$ stock solution made from stirring 13 mg P(4-$MeOC_6H_4$)$_3$ (0.37 mmol) in 1.2 cm^3 DMF for 5 min.; 69% conversion of starting material **57** was achieved with k_{obs} = (1.71 ± 0.03) × 10^{-6} mol dm^{-3} s^{-1} (**Table 28**, Entry 6). (*Lab book reference number*: GMHP-6-414)
6. P(2-MeC_6H_4)$_3$ (5.5 mg [b], 0.018 mmol, 10 mol%), [b] Using 200 µL of 90 mM P(2-MeC_6H_4)$_3$ stock solution made from stirring 55 mg P(2-MeC_6H_4)$_3$ (0.18 mmol) in 2 cm^3 DMF for 5 min.; 24% conversion of starting material **57** was achieved with k_{obs} = (8.60 ± 1.33) × 10^{-6} mol dm^{-3} s^{-1} (**Table 28**, Entry 7). (*Lab book reference number*: GMHP-6-413)
7. P(2-MeC_6H_4)$_3$ (11 mg [b], 0.036 mmol, 20 mol%); [b] Using 400 µL of 90 mM P(2-MeC_6H_4)$_3$ stock solution made from stirring 55 mg P(2-MeC_6H_4)$_3$ (0.18 mmol) in 2 cm^3 DMF for 5 min.; 57% conversion of starting material **57** was achieved with k_{obs} = (4.24 ± 0.21) × 10^{-6} mol dm^{-3} s^{-1} (**Table 28**, Entry 8). (*Lab book reference number*: GMHP-6-418)
8. PCy_3 (5.1mg [b], 0.018 mmol, 10 mol%), [b] Using 200 µL of 90 mM P(2-MeC_6H_4)$_3$ stock solution made from stirring 51 mg P(2-MeC_6H_4)$_3$ (0.18 mmol) in 2 cm^3 DMF for 5 min.; 11% conversion of starting material **57** was achieved with k_{obs} = (7.36 ± 0.86) × 10^{-7} mol dm^{-3} s^{-1} (**Table 28**, Entry 9). (*Lab book reference number*: GMHP-6-407)
9. JohnPhos (5.4 mg [b], 0.018 mmol, 10 mol%); [b] Using 400 µL of 45 mM P(2-MeC_6H_4)$_3$ stock solution made from stirring 27 mg JohnPhos (0.09 mmol) in 2 cm^3 DMF for 5 min.; 23% conversion of starting material **57** was achieved with k_{obs} = (1.33 ± 0.08) × 10^{-6} mol dm^{-3} s^{-1} (**Table 28**, Entry 10). (*Lab book reference number*: GMHP-6-419)

6.4.14 Comparing the Reaction Progress Followed by *in situ* FT-IR Spectroscopy and *ex situ* NMR Spectroscopy

A mixture of 4-iodotoluene **57** (41 mg, 0.19 mmol, 1 equiv.), pentafluorobenzene **56** (0.2 cm^3, 1.8 mmol, 10 equiv.), Ag_2CO_3 (38 mg, 0.14 mmol, 0.74 equiv.), $Pd(OAc)_2$ (2 mg, 8.9 × 10^{-6} mol, 5 mol%) and PPh_3 (4.8 mg, 1.8 × 10^{-5} mol, 10 mol%) in DMF (9.5 cm^3 total volume) was prepared following general procedure C. The reaction progress was monitored by *in situ* FT-IR spectroscopy (**Figure 15**). An aliquot of the reaction mixture was collected

at *ca.* 30 min intervals, filtered through a Celite®-plug and analysed by ^{1}H NMR spectroscopy to determine the %conversion of starting material **57** to product **58**.

[a] Using 200 µL of 45 mM $Pd(OAc)_2$ stock solution made from stirring 20 mg $Pd(OAc)_2$ (0.089 mmol) in 2 cm^3 DMF for 10 min.

[b] Using 200 µL of 90 mM PPh_3 stock solution made from stirring 47 mg PPh_3 (0.18 mmol) in 2 cm^3 DMF for 5 min.

(*Lab book reference number*: GMHP-6-385)

6.5 Experiments Based on Solution Phase NMR spectroscopy

6.5.1 Competition Experiment Between Pentafluorobenzene 56 and 4-Substituted-2,3,5,6-Tetrafluorobenzene in the Direct Arylation of 4-Iodotoluene 57

A light-protected Schlenk tube with $Pd(OAc)_2$ (3.3 mg, 0.015 mmol, 5 mol%), PPh_3 (7.6 mg, 0.029 mmol, 10 mol%) and Ag_2CO_3 (59 mg, 0.21 mmol, 0.75 equiv.) was evacuated and backfilled with atmosphere of nitrogen three times. The Schlenk tube was charged with 4-iodotoluene **57** (62 mg. 0.29 mmol, 1 equiv.) and DMF (2.5 cm^3). Pentafluorobenzene **56** (320 µL, 484 mg, 2.88 mmol, 10 equiv.) and 4-X-2,3,5,6-tetrafluorobenzene (see below) were added simultaneously. The crude reaction mixture was heated at 60 °C and analysed after 20 hours by ^{19}F NMR spectroscopic analysis. The ratios of the products were determined from the integration of the spectra run with 20 seconds of relaxation delay. Quantitative conversion of 4-iodotoleuene **57** was observed.

1. X = NMe_2 **121** (490 µL, 652 mg, 3.38 mmol, 12 equiv.); 25% yield of biaryl **76** by NMR spectroscopic analysis with 75% yield of biary **58** (**Figure 211**, **Figure 212** and **Table 24**, Entry 1). (*Lab book reference number*: GMHP-6-365)
2. X = OMe (405 µL, 524 mg, 2.91 mmol, 10 equiv.); 36% yield of biaryl **77** by NMR spectroscopic analysis with 64% yield of biaryl **58** (**Figure 213**, **Figure 214** and **Table 24**, Emtry 2). (*Lab book reference number*: GMHP-5-253)
3. X = Cl (345 µL, 531 mg, 2.88 mmol, 10 equiv.); 54% yield of biaryl **79** by NMR spectroscopic analysis with 46% yield of biaryl **54** (**Figure 215**, **Figure 216** and **Table 24**, Entry 5). (*Lab book reference number*: GMHP-5-270)
4. X = CF_3 (395 µL, 632 mg, 2.90 mmol, 10 equiv.); 58% yield of biaryl **80** by NMR spectroscopic analysis with 42% yield of biaryl **58** (**Figure 217**, **Figure 218**and **Table 24**, Emtry 6). (*Lab book reference number*: GMHP-5-250)

6.5.2 Stoichiometric Reaction of Pre-Synthesised Stable Pd Complexes

Reaction of dinuclear species with pentafluorobenzene 56 in non-deuterated DMF

The reaction was prepared inside an argon-filled glove box. The Pd complex (see below), pentafluorobenzene **56** (11 µL, 17 mg, 9.9×10^{-5} mol, 20 equiv.), hexafluorobenzene internal standard (10 µL, 8.66×10^{-7} mol [a]) and DMF (to 0.55 cm^3 mark) were placed in an NMR tube equipped with J. Young's valve and heated in an oil bath at 70 °C. The yields of the reactions were determined from the ^{19}F NMR peaks integration of the product **64** and the internal standard.

[a] Using a stock solution of 0.086 M hexafluorobenzene in DMF.

1. $[Pd(Ph)(\mu\text{-}OAc)(PPh_3)]_2$ **84** (5.1 mg, 5.1×10^{-6} mol, 1 equiv.); Quantitative yield by NMR spectroscopic analysis (**Table 33**, Entry 1). (*Lab book reference number*: GMHP-5-315)
2. $[Pd(Ph)(\mu\text{-}OH)(PPh_3)]_2$ **83a** (4.7 mg, 5.1×10^{-6} mol, 1 equiv.); 60% yield by NMR spectroscopic analysis (**Table 33**, Entry 2). (*Lab book reference number*: GMHP-5-313)
3. $[Pd(Ph)(\mu\text{-}I)(PPh_3)]_2$ **86** (6.0 mg, 5.2×10^{-6} mol, 1 equiv.); 0% yield by NMR spectroscopic analysis (**Table 33**, Entry 3). (*Lab book reference number*: GMHP-5-314)

Reaction of dinuclear species in the presence of Ag additives in DMF:

4. $[Pd(Ph)(\mu\text{-}I)(PPh_3)]_2$ **86** (5.6 mg, 4.9×10^{-6} mol, 1 equiv.) and Ag_2CO_3 (4.0 mg, 1.5×10^{-5} mol, 3 equiv.); 36% yield by NMR spectroscopic analysis (**Table 33**, Entry 4). (*Lab book reference number*: GMHP-6-411)
5. $[Pd(Ph)(\mu\text{-}I)(PPh_3)]_2$ **86** (5.6 mg, 4.8×10^{-6} mol, 1 equiv.) and AgOAc (5.3 mg, 3.2×10^{-5} mol, 7 equiv.); 22% yield by NMR spectroscopic analysis (**Table 33**, Entry 5). (*Lab book reference number*: GMHP-6-416)

Reaction of dinuclear species with pentafluorobenzene 56 in benzene-d_6

The reaction was prepared inside an argon-filled glove box. The Pd complex (see below), pentafluorobenzene **56** (11 µL, 17 mg, 9.9×10^{-5} mol, 20 equiv.), fluorobenzene internal standard (5 µL, 2.4×10^{-6} mol [a]) and benzene-d_6 (to 0.55 cm^3 mark) were placed in an NMR tube equipped with J. Young's valve and heated in an oil bath at 70 °C. The yields of the reactions were determined from the ^{19}F NMR peaks integration of the product **64** and the internal standard.

[a] Using a stock solution of 0.48 M fluorobenzene in benzene-d_6.

1. [Pd(Ph)(μ-OAc)(PPh_3)]$_2$ **84** (5.1 mg, 5.1 × 10^{-6} mol, 1 equiv.); 67% yield by NMR spectroscopic analysis (**Table 33**, Entry 1). (*Lab book reference number*: GMHP-5-317 and 319)
2. [Pd(Ph)(μ-OH)(PPh_3)]$_2$ **83a** (4.6 mg, 5.0 × 10^{-6} mol, 1 equiv.); 18% yield by NMR spectroscopic analysis (**Table 33**, Entry 2). (*Lab book reference number*: GMHP-5-318)
3. [Pd(Ph)(μ-I)(PPh_3)]$_2$ **86** (6.0 mg, 5.2 × 10^{-6} mol, 1 equiv.); 0% yield by NMR spectroscopic analysis (**Table 33**, Entry 3). (*Lab book reference number*: GMHP-5-320)

Reaction of mononuclear species with pentafluorobenzene 56 in DMF

The reaction was prepared inside an argon-filled glove box. The Pd complex (see below), pentafluorobenzene **56** (6 µL, 9 mg, 5.4 × 10^{-5} mol, 10 equiv.), hexafluorobenzene internal standard (5 µL, 4.33 × 10^{-7} mol [a]) and DMF (to 0.55 cm^3 mark) were placed in an NMR tube equipped with J. Young's valve and heated in an oil bath at 70 °C. The yields of the reactions were determined from the ^{19}F NMR peaks integration of the product **64** and the internal standard.

[a] Using a stock solution of 0.086 M hexafluorobenzene in DMF.

1. Pd(Ph)(κ^1-OAc)(PPh_3)$_2$ **85** (3.7 mg, 4.8 × 10^{-6} mol, 1 equiv.); 45% yield by NMR spectroscopic analysis (**Table 33**, Entry 6). (*Lab book reference number*: GMHP-6-391)
2. Pd(Ph)(I)(PPh_3)$_2$ **82a** (5.8 mg, 6.9 × 10^{-6} mol, 1 equiv.); 0% yield by NMR spectroscopic analysis (**Table 33**, Entry 9). (*Lab book reference number*: GMHP-7-493)
3. Pd(4-tolyl)(I)(PPh_3)$_2$ **82b** (4.0 mg, 4.7 × 10^{-6} mol, 1 equiv.); 0% yield by NMR spectroscopic analysis (**Table 33**, Entry 13). (*Lab book reference number*: GMHP-6-424)

Reaction of mononuclear species in the presence of Ag additives in DMF:

4. Pd(Ph)(κ^1-OAc)(PPh_3)$_2$ **85** (3.6 mg, 4.7 × 10^{-6} mol, 1 equiv.) and Ag_2CO_3 (2.8 mg, 1.0 × 10^{-5} mol, 2 equiv.); 99% yield by NMR spectroscopic analysis (**Table 33**, Entry 7). (*Lab book reference number*: GMHP-7-496)

5. Pd(Ph)(κ^1-OAc)(PPh_3)$_2$ **85** (4.3 mg, 5.6×10^{-6} mol, 1 equiv.) and AgOAc (6.5 mg, 3.9×10^{-5} mol, 7 equiv.); 98% yield by NMR spectroscopic analysis (**Table 33**, Entry 8). (*Lab book reference number*: GMHP-7-519)
6. Pd(Ph)(I)(PPh_3)$_2$ **82a** (4.7 mg, 5.6×10^{-6} mol) and Ag_2CO_3 (2.6 mg, 9.4×10^{-6} mol, 2 equiv.); 49% yield by NMR spectroscopic analysis (**Table 33**, Entry 10). (*Lab book reference number*: GMHP-7-494)
7. Pd(Ph)(I)(PPh_3)$_2$ **82a** (4.5 mg, 5.4×10^{-6} mol) and AgOAc (3.7 mg, 2.2×10^{-5} mol, 4 equiv.); 67% yield by NMR spectroscopic analysis (**Table 33**, Entry 11). (*Lab book reference number*: GMHP-7-495)
8. Pd(Ph)(I)(PPh_3)$_2$ **82a** (3.9 mg, 4.7×10^{-6} mol) and $AgBF_4$ (6.8 mg, 3.5×10^{-5} mol, 7 equiv.); 0% yield by NMR spectroscopic analysis (**Table 33**, Entry 12). (*Lab book reference number*: GMHP-7-505)
9. Pd(4-tolyl)(I)(PPh_3)$_2$ **82b** (4.0 mg, 4.7×10^{-6} mol, 1 equiv.) and Ag_2CO_3 (2.2 mg, 8.0×10^{-6} mol, 2 equiv.); 46% yield by NMR spectroscopic analysis (**Table 33**, Entry 14). (*Lab book reference number*: GMHP-6-420)
10. Pd(4-tolyl)(I)(PPh_3)$_2$ **82b** (4.0 mg, 4.7×10^{-6} mol) and AgOAc (3.1 mg, 1.9×10^{-5} mol, 4 equiv.); 56% yield by NMR spectroscopic analysis (**Table 33**, Entry 15). (*Lab book reference number*: GMHP-6-421)

6.6 Analysis of Catalytic Intermediates by in situ HR-MAS NMR Spectroscopy

6.6.1 Following the Reaction Progress of Direct Arylation of 4-Iodotoluene 57 with Pentafluorobenzene 56

The rotor for the solid-state NMR spectroscopy was charged with $Pd(OAc)_2$ (1.1 mg, 4.9×10^{-6} mol, 50 mol%), PPh_3 (2.6 mg, 9.9×10^{-6} mol, 100 mol%), Ag_2CO_3 (2.4 mg, 8.7×10^{-6} mol, 1 equiv.), 4-iodotoluene **57** (2.1 mg, 9.6×10^{-6} mol, 1 equiv.), DMF-d_7 (50 µL) and pentafluorobenzene **56** (1.5 µL, 2.3 mg, 1.4×10^{-5} mol, 1.6 equiv.) respectively. The mixture was heated at 328.5 K inside the spectrometer and the progress was monitored by ^{1}H and ^{31}P NMR spectroscopic analysis at *ca.* 17 min intervals until reaction completion without decreasing the temperature.

(*Lab book reference number*: GMHP-6-386)

6.6.2 Observing the Reaction Intermediates of the Direct Arylation of 4-Iodotoluene 57 with Pentafluorobenzene 56

The rotor for the solid-state NMR spectroscopy was charged with $Pd(OAc)_2$ (1.1 mg, 4.9×10^{-6} mol, 50 mol%), PPh_3 (2.6 mg, 9.9×10^{-6} mol, 100 mol%), Ag_2CO_3 (2.3 mg, 8.3×10^{-6} mol, 1 equiv.), 4-iodotoluene **57** (2.5 mg, 1.1×10^{-5} mol, 1 equiv.), DMF-d_7 (50 µL) and pentafluorobenzene **56** (1.5 µL, 2.3 mg, 1.4×10^{-5} mol, 1.6 equiv.) respectively. The mixture, initially at 285.0 K, was heated at 328.5 K inside the spectrometer until *ca.* 20% conversion of the starting material was achieved. At this point the reaction was cooled to 308.5 K, 288.5 K, 268.5 K and 248.5 K in sequential order. The mixture was studied by 1D (^{1}H, ^{19}F and ^{31}P) and 2D (^{1}H-^{1}H COSY and ^{1}H-^{31}P HMQC) NMR spectroscopic analysis at each temperature presented above (*i.e.* 285.0, 328.5, 308.5, 288.5, 268.5 and 244.5 K).

(*Lab book reference number*: GMHP-6-417)

6.6.3 Observing the Reaction Intermediates of the Direct Arylation of Iodobenzene 92 with Pentafluorobenzene 56

The rotor for the solid-state NMR spectroscopy was charged with $Pd(OAc)_2$ (1.1 mg, 4.9×10^{-6} mol, 50 mol%), PPh_3 (2.5 mg, 9.5×10^{-6} mol, 100 mol%), Ag_2CO_3 (2.4 mg, 8.7×10^{-6} mol, 1 equiv.), iodobenzene **81** (1 µL, 1.8 mg, 8.9×10^{-6} mol, 1 equiv.), DMF-d_7 (50 µL) and pentafluorobenzene **56** (1.5 µL, 2.3 mg, 1.4×10^{-5} mol, 1.6 equiv.) respectively. The mixture, initially at 285.0 K, was heated at 328.5 K inside the spectrometer until *ca.* 20% conversion of the starting material was achieved. At this point the reaction was cooled to 308.5 K, 288.5 K, 268.5 K and 248.5 K in sequential order. The mixture was studied by 1D (^{1}H, ^{19}F and ^{31}P) and 2D (^{1}H-^{1}H COSY and ^{1}H-^{31}P HMQC) NMR spectroscopic analysis at each temperatures (*i.e.* 285.0, 328.5, 308.5, 288.5, 268.5 and 244.5 K).

(*Lab book reference number*: GMHP-7-449)

6.6.4 Direct Arylation of the Iodobenzene 81 with Pentafluorobenzene 56 Catalysed by $[Pd(Ph)(\mu\text{-}OAc)(PPh_3)]_2$ 84

The rotor for the solid-state NMR spectroscopy was charged with $[Pd(Ph)(\mu\text{-}OAc)(PPh_3)]_2$ **84** (2.4 mg, 2.4×10^{-6} mol, 50 mol% Pd atom), Ag_2CO_3 (2.4 mg, 8.7×10^{-6} mol, 1 equiv.), iodobenzene **81** (1 µL, 1.8 mg, 8.9×10^{-6} mol, 1 equiv.), DMF-d_7 (50 µL) and pentafluorobenzene **56** (1.5 µL, 2.3 mg, 1.4×10^{-5} mol, 1.6 equiv.) respectively. The mixture, initially at 285.0 K, was heated at 328.5 K inside the spectrometer until *ca.* 20% conversion of the starting material was achieved. At this point the reaction was cooled to

308.5 K, 288.5 K, 268.5 K and 248.5 K in sequential order. The mixture was studied by 1D (^{1}H, ^{19}F and ^{31}P) and 2D (^{1}H-^{1}H COSY and ^{1}H-^{31}P HMQC) NMR spectroscopic analysis at each temperatures (*i.e.* 285.0, 328.5, 308.5, 288.5, 268.5 and 244.5 K).

(*Lab book reference number*: GMHP-7-461)

Reaction catalysed by [Pd(Ph)(μ-OAc)(PPh$_3$)]$_2$ 84 and phosphine ligand

1. [Pd(Ph)(μ-OAc)(PPh$_3$)]$_2$ **84** (2.4 mg, 2.4 × 10^{-6} mol, 50 mol% Pd atom), PPh$_3$ (0.6 mg, 2.3 × 10^{-6} mol, 25 mol%) (*Lab book reference number*: GMHP-7-466)
2. [Pd(Ph)(μ-OAc)(PPh$_3$)]$_2$ **84** (2.4 mg, 2.4 × 10^{-6} mol, 50 mol% Pd atom), PPh$_3$ (1.7 mg, 6.6 × 10^{-6} mol, 75 mol%) (*Lab book reference number*: GMHP-7-471)
3. [Pd(Ph)(μ-OAc)(PPh$_3$)]$_2$ **84** (2.4 mg, 2.4 × 10^{-6} mol, 50 mol% Pd atom), O=PPh$_3$ (1.6 mg, 5.7 × 10^{-6} mol, 65 mol%) (*Lab book reference number*: GMHP-7-470)

6.6.5 Characterisation of Pre-Synthesised Pd Complexes in DMF-d$_7$ at the Reaction Temperatures

The rotor for the solid-state NMR spectroscopy was charged with pre-synthesised Pd complexes (listed below) and DMF-d$_7$ (50 µL). The samples were analysed at 285.0 K, 328.5 K, 308.5 K, 288.5 K, 268.5 K and 248.5 K in sequential order.

1. [Pd(Ph)(μ-OAc)(PPh$_3$)]$_2$ **84** (*Lab book reference number*: GMHP-7-445-P)
2. [Pd(Ph)(μ-OH)(PPh$_3$)]$_2$ **83a** (*Lab book reference number*: GMHP-5-311-P)
3. [Pd(Ph)(μ-I)(PPh$_3$)]$_2$ **86** (*Lab book reference number*: GMHP-5-312-P)
4. Pd(Ph)(κ^1-OAc)(PPh$_3$)$_2$ **85** (*Lab book reference number*: GMHP-7-446-P)
5. Pd(Ph)(I)(PPh$_3$)$_2$ **82a** (*Lab book reference number*: GMHP-7-444-P)

6.7 Analysis of Catalytic Intermediates by ex situ Mass Spectrometry

6.7.1 Observation of Reactive Intermediates in the Direct Arylation of 4-Iodotoluene 57 with Pentafluorobenzene 56 by ESI-MS

A mixture of 4-iodotoluene **57** (39 mg, 0.18 mmol, 1 equiv.), pentafluorobenzene **56** (400 µL, 0.6 g, 3.6 mmol, 20 equiv.), Pd(OAc)$_2$ (2 mg [a], 8.9 × 10^{-6} mol, 5 mol%), PPh$_3$ (4.7 mg [b], 0.018 mmol, 10 mol%) and Ag$_2$CO$_3$ (37 mg, 0.13 mmol, 0.75 equiv.) in DMF (9.3 cm^3 total volume) was prepared following general procedure C. The reaction progress was monitored by *in situ* FT-IR spectroscopy. An aliquot of the reaction mixture was collected and filtered through a Celite®-plug. Half of the sample was diluted in DMF (Sample 1) and

the other half was diluted in acetonitrile (Sample 2). The two solutions were analysed by ESI-MS in the positive and negative modes.

[a] Using 200 µL of 45 mM $Pd(OAc)_2$ stock solution made from stirring 20 mg $Pd(OAc)_2$ (0.089 mmol) in 2 cm^3 DMF for 10 min.

[b] Using 200 µL of 90 mM PPh_3 stock solution made from stirring 47 mg PPh_3 (0.18 mmol) in 2 cm^3 DMF for 5 min.

(*Lab book reference number*: GMHP-6-397)

6.7.2 Observation of Reactive Intermediates in the Direct Arylation of 4-Iodotoluene 57 with Pentafluorobenzene 56 by LIDFI-MS

A mixture of 4-iodotoluene **57** (391 mg, 1.8 mmol, 1 equiv.), pentafluorobenzene **56** (1 cm^3, 1.5 g, 9.0 mmol, 5 equiv.), $Pd(OAc)_2$ (21 mg, 0.094 mol, 5 mol%), PPh_3 (48 mg, 0.18 mmol, 10 mol%) and Ag_2CO_3 (375 mg, 1.4 mmol, 0.75 equiv.) in DMF (8.5 cm^3 total volume) was prepared following general procedure C. The reaction progress was monitored by *in situ* FT-IR spectroscopy. An aliquot of the reaction mixture was collected, filtered through a Celite®-plug and the solution directly analysed by LIFDI-MS without dilution.

(*Lab book reference number*: GMHP-7-492)

Appendices

Appendix 1: Derivations of the Equations

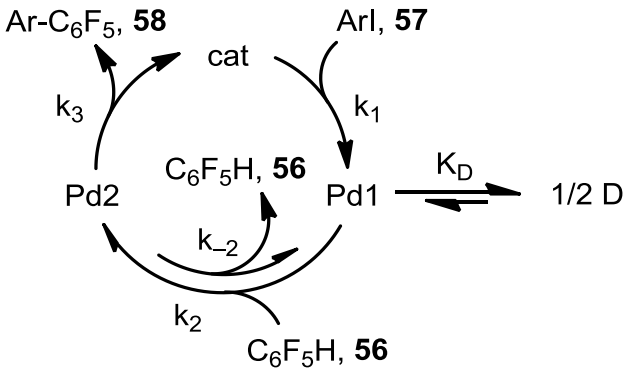

Scheme 87. Simplified catalytic cycle for the direct arylation of iodoarene with fluoroarene. (ArI **57** + C_6F_5H **56** –> Ar-C_6F_5 **58**).

Rate Law with Dominant Dinuclear Species

If 4a term is dominant in Eq. 12, *i.e.* $4a > b^2 > 2b$

$$rate = \frac{+d[P]}{dt} = \frac{2k_3[Pd]_{TOT}}{\sqrt{4a[Pd]_{TOT}}} \tag{12}$$

$$4a[Pd]_{TOT} = 4 \times 2K_D \left(\frac{k_3 + k_{-2}}{k_2[C_6F_5H\ \mathbf{56}]}\right)^2 [Pd]_{TOT}$$

$$\sqrt{4a[Pd]_{TOT}} = {K_D}^{1/2} 2\sqrt{2} {[Pd]_{TOT}}^{1/2} \left(\frac{k_3 + k_{-2}}{k_2[C_6F_5H\ \mathbf{56}]}\right)$$

$$rate = \frac{+d[P\ \mathbf{58}]}{dt} = \frac{2k_3[Pd]_{TOT} k_2[C_6F_5H\ \mathbf{56}]}{{K_D}^{1/2} 2\sqrt{2} {[Pd]_{TOT}}^{1/2} (k_3 + k_{-2})}$$

$$rate = \frac{+d[P\ \mathbf{58}]}{dt} = \frac{k_2 k_3 {[Pd]_{TOT}}^{1/2} [C_6F_5H\ \mathbf{56}]}{{K_D}^{1/2} \sqrt{2} (k_3 + k_{-2})}$$

If $k_3 > k_{-2}$

$$rate = \frac{+d[P\ \mathbf{58}]}{dt} = \frac{k_2 {[Pd]_{TOT}}^{1/2} [C_6F_5H\ \mathbf{56}]}{{K_D}^{1/2} \sqrt{2}}$$

Integrated Rate Law for Zeroth-Order Reaction

$$rate = k_{obs} \tag{20}$$

$$\frac{-d[ArI\ \mathbf{57}]}{dt} = k_{obs}$$

$$-d[ArI\ \mathbf{57}] = -k_{obs}dt$$

$$\int_{[ArI\ \mathbf{57}]_0}^{[ArI\ \mathbf{57}]_t} d[ArI\ \mathbf{57}] = \int_0^t -k_{obs}dt$$

$$[ArI\ \mathbf{57}]_t - [ArI\ \mathbf{57}]_0 = -k_{obs}t$$

$$[ArI\ \mathbf{57}]_t = -k_{obs}t + [ArI\ \mathbf{57}]_0 \tag{21}$$

$$where\ k_{obs} = k_r[C_6F_5H\ \mathbf{56}]_{ave}[Pd]_{TOT}{}^{1/2} \tag{22}$$

Integrated Rate Law for First-Order Reaction

$$rate = k_{obs}[C_6F_5H\ \mathbf{56}] \tag{17}$$

$$\frac{-d[C_6F_5H\ \mathbf{56}]}{dt} = k_{obs}[C_6F_5H\ \mathbf{56}]$$

$$\int_{[C_6F_5H\ \mathbf{56}]_0}^{[C_6F_5H\ \mathbf{56}]_t} \frac{1}{[C_6F_5H\ \mathbf{56}]} d[C_6F_5H\ \mathbf{56}] = \int_0^t -k_{obs}dt$$

$$ln\left(\frac{[C_6F_5H\ \mathbf{56}]_t}{[C_6F_5H\ \mathbf{56}]_0}\right) = -k_{obs}t$$

$$ln[C_6F_5H\ \mathbf{56}]_t - ln[C_6F_5H\ \mathbf{56}]_0 = -k_{obs}t$$

$$ln[C_6F_5H\ \mathbf{56}]_t = -k_{obs}t + ln[C_6F_5H\ \mathbf{56}]_0 \tag{18}$$

$$where\ k_{obs} = k_r[Pd]_{TOT}{}^{1/2} \tag{19}$$

Alternatively

$$[C_6F_5H\ \mathbf{56}]_t = [C_6F_5H\ \mathbf{56}]_0 e^{-k_{obs}t}$$

Appendix 2: In situ FT-IR Spectroscopy Data

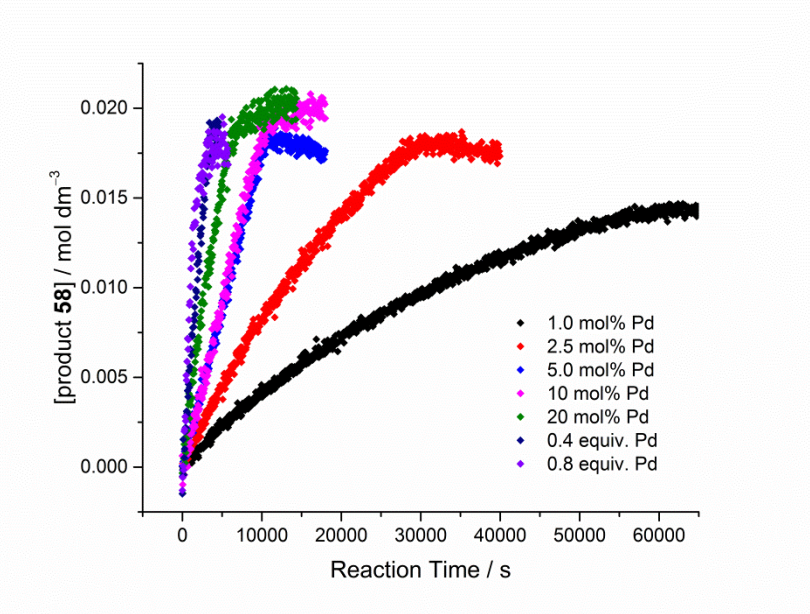

Figure 71. Reaction profiles of the product **58** formation for the direct arylation of 4-iodotoluene **57** (0.018 M) with pentafluorobenzene **56** (0.18 M), catalysed by range of $Pd(OAc)_2/PPh_3$ (1:2) pre-catalyst loadings (1.0 mol% to 0.8 equiv.) at 56 ± 1 °C. These experimental data were used to construct **Figure 34**.

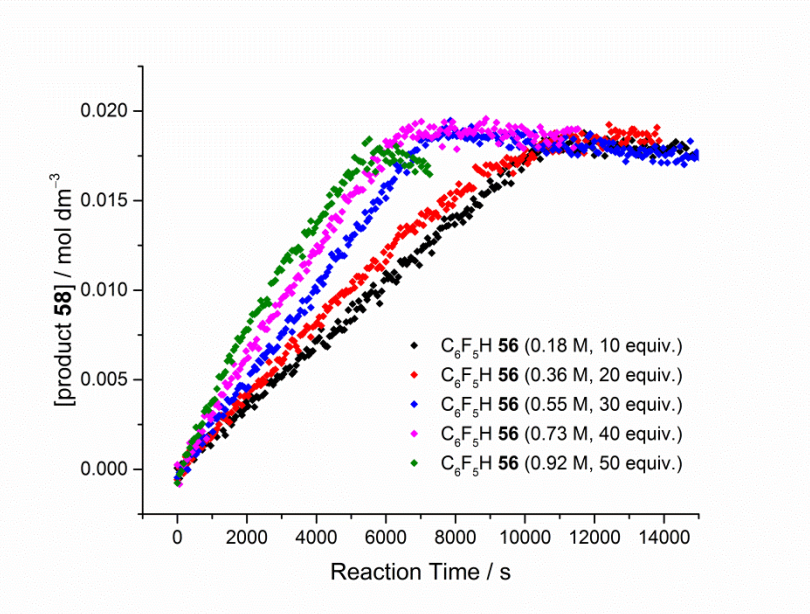

Figure 72. Reaction profiles of the product **58** formation for the direct arylation of 4-iodotoluene **57** (0.018 M) with range of pentafluorobenzene **56** concentrations (0.18–0.92 M), catalysed by $Pd(OAc)_2/PPh_3$ (5 mol% : 10 mol%) pre-catalyst at 56 ± 1 °C. These experimental data were used to construct **Figure 36**.

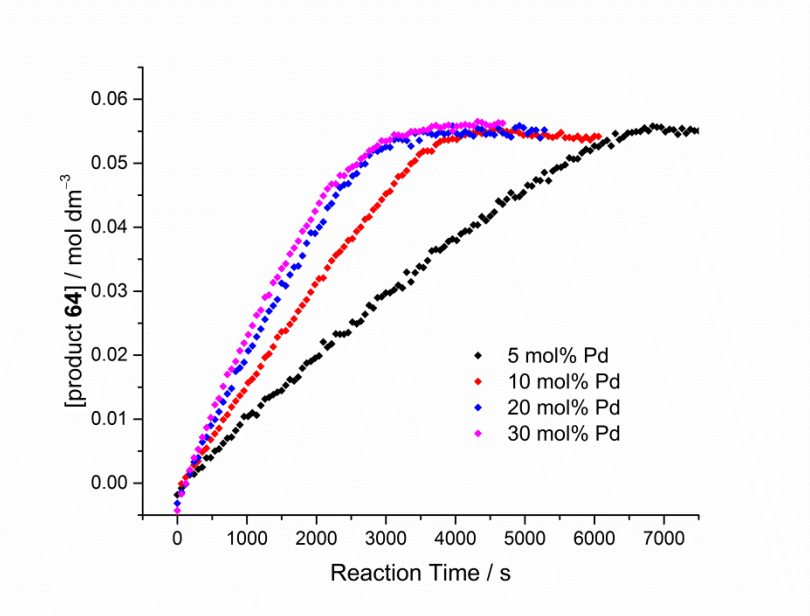

Figure 73. Reaction profiles of the product **64** formation for the direct arylation of iodobenzene **81** (0.05 M) with pentafluorobenzene **56** (0.55 M), catalysed by range of $Pd(OAc)_2/PPh_3$ (1:2) pre-catalyst loadings (5–30 mol%) at 56 ± 1 °C. These experimental data were used to construct **Figure 37**.

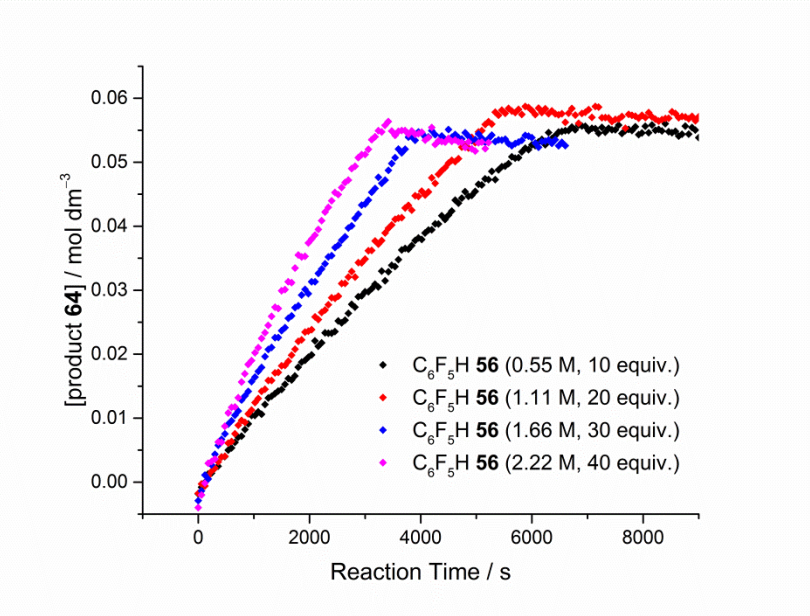

Figure 74. Reaction profiles of the product **64** formation for the direct arylation of iodobenzene **81** (0.055 M) with range of pentafluorobenzene **56** concentrations (0.55–2.22 M), catalysed by $Pd(OAc)_2/PPh_3$ (5 mol% : 10 mol%) pre-catalyst at 56 ± 1 °C. These experimental data were used to construct**Figure 38**.

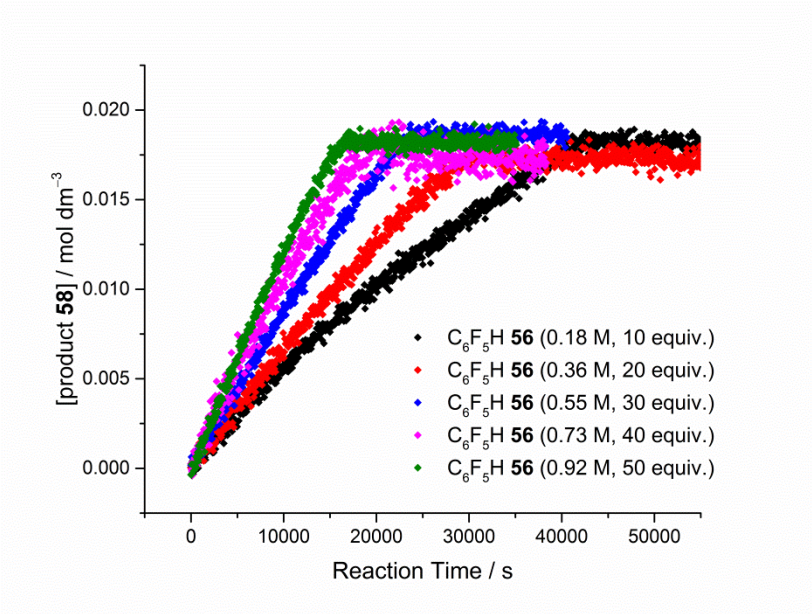

Figure 75. Reaction profiles of the product **58** formation for the direct arylation of 4-iodotoluene **57** (0.018 M) with range of pentafluorobenzene **56** concentrations (0.18–0.92 M), catalysed by $Pd(OAc)_2/PPh_3$ (5 mol% : 10 mol%) pre-catalyst at 40 ± 1 °C. These experimental data were used to construct **Figure 42**.

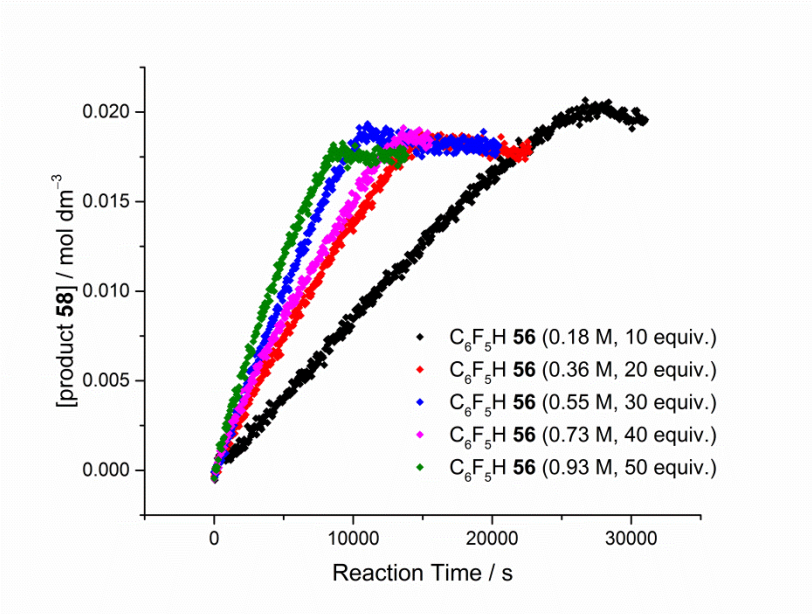

Figure 76. Reaction profiles of the product **58** formation for the direct arylation of 4-iodotoluene **57** (0.018 M) with range of pentafluorobenzene **56** concentrations (0.18–0.93 M), catalysed by $Pd(OAc)_2/PPh_3$ (5 mol% : 10 mol%) pre-catalyst at 50 ± 1 °C. These experimental data were used to construct**Figure 42**.

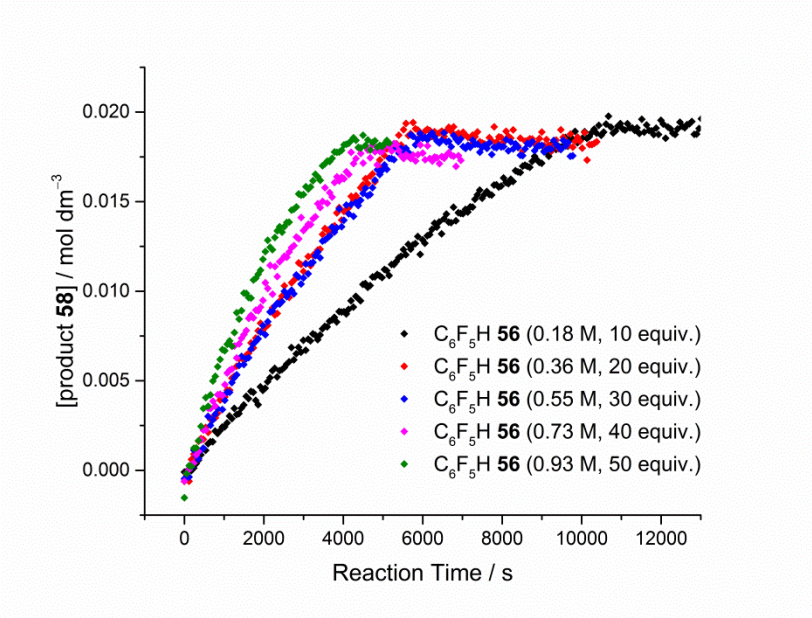

Figure 77. Reaction profiles of the product **58** formation for the direct arylation of 4-iodotoluene **57** (0.018 M) with range of pentafluorobenzene **56** concentrations (0.18–0.93 M), catalysed by $Pd(OAc)_2/PPh_3$ (5 mol% : 10 mol%) pre-catalyst at 64 ± 1 °C. These experimental data were used to construct **Figure 42**.

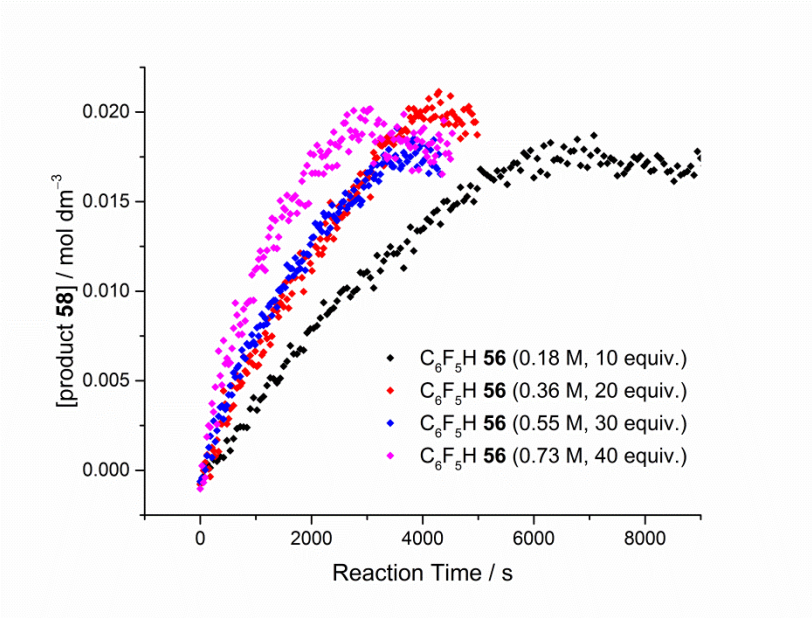

Figure 78. Reaction profiles of the product **58** formation for the direct arylation of 4-iodotoluene **57** (0.018 M) with range of pentafluorobenzene **56** concentrations (0.18–0.73 M), catalysed by $Pd(OAc)_2/PPh_3$ (5 mol% : 10 mol%) pre-catalyst at 72 ± 1 °C. These experimental data were used to construct **Figure 42**.

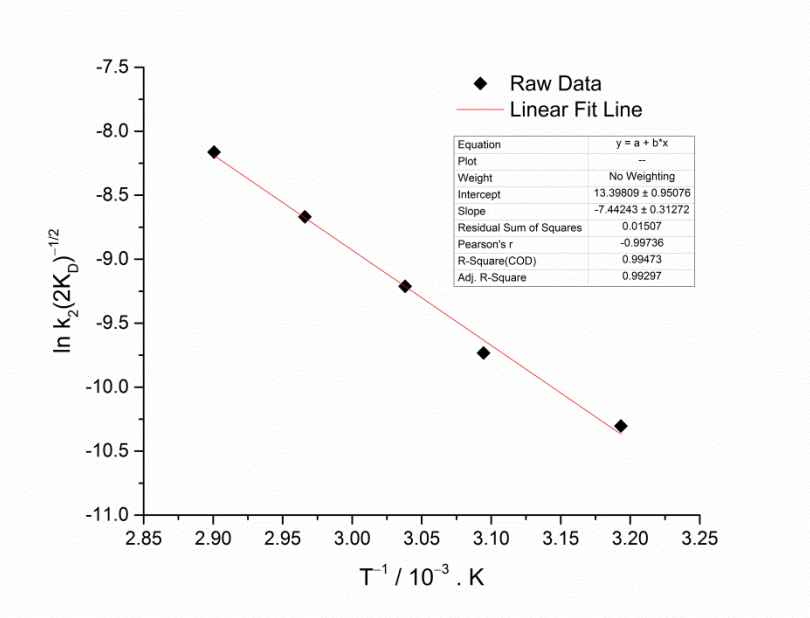

Figure 79. Arrhenius plot of the $k_2(2K_D)^{-1/2}$ rate constants for the direct arylation of 4-iodotoluene **57** with pentafluorobenzene **56**. The rate constants were determined from the slopes of graph plotting k_{obs} against concentrations of pentafluorobenzene **56** at temperatures between 40–72 °C (**Figure 42**).

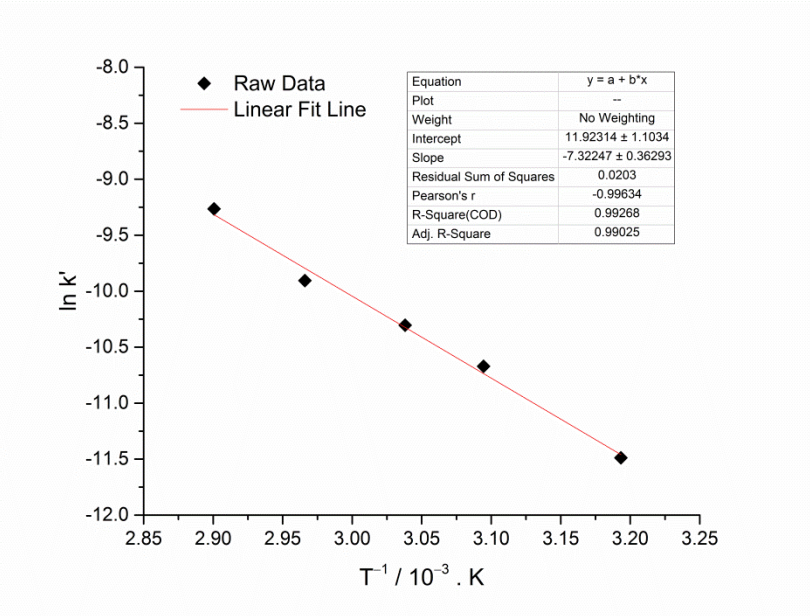

Figure 80. Arrhenius plot of the k′ rate constant for the direct arylation of 4-iodotoluene **57** with pentafluorobenzene **56**. The rate constant was determined from the y-intercepts of graph plotting k_{obs} against concentrations of pentafluorobenzene **56** at temperatures between 40–72 °C (**Figure 42**).

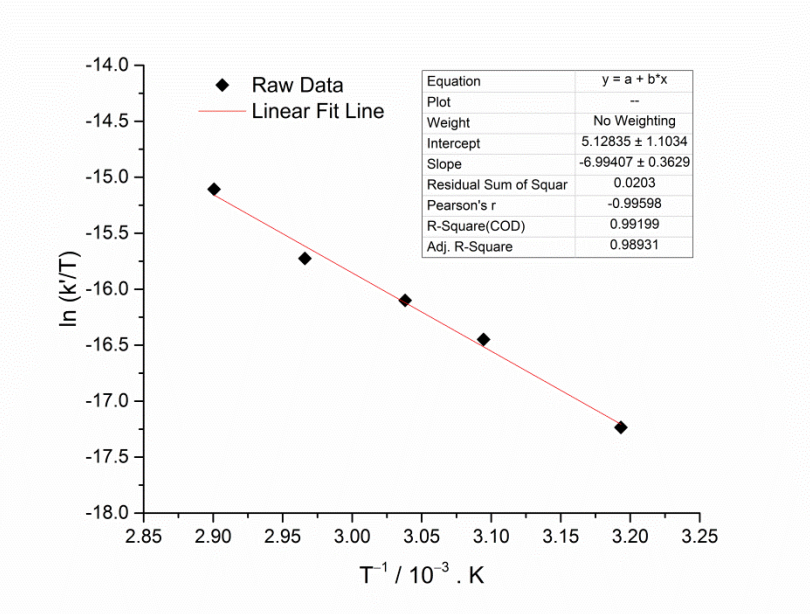

Figure 81. Eyring plot of the k′ rate constant for the direct arylation of 4-iodotoluene **57** with pentafluorobenzene **56**. The rate constant was determined from the y-intercepts of graph plotting k_{obs} against concentrations of pentafluorobenzene **56** at temperatures between 40–72 °C (**Figure 42**).

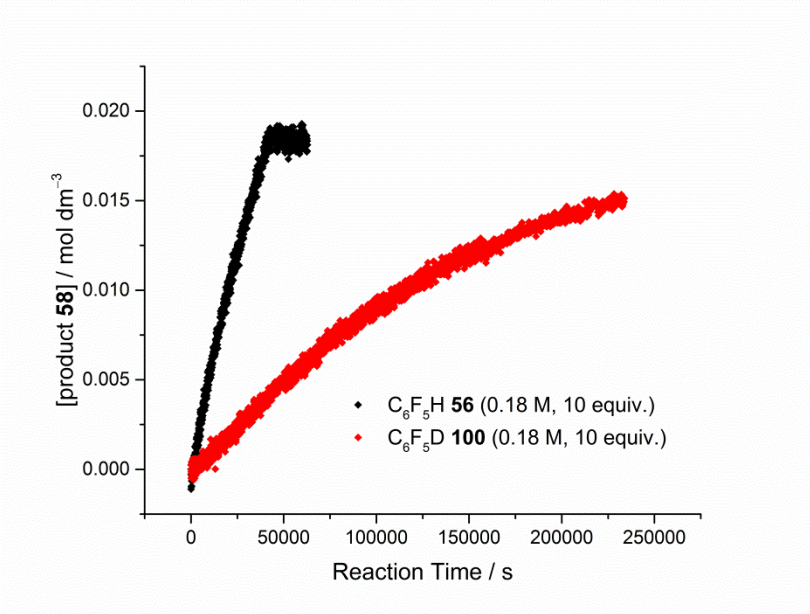

Figure 82. Reaction profiles of the product **58** formation for the direct arylation of 4-iodotoleuen **57** (0.018 M) with pentafluorobenzene **56** (0.18 M) or deuteropentafluorobenzene **100** (0.18 M), catalysed by $Pd(OAc)_2/PPh_3$ (5 mol% : 10 mol%) pre-catalyst at 40 ± 1 °C.

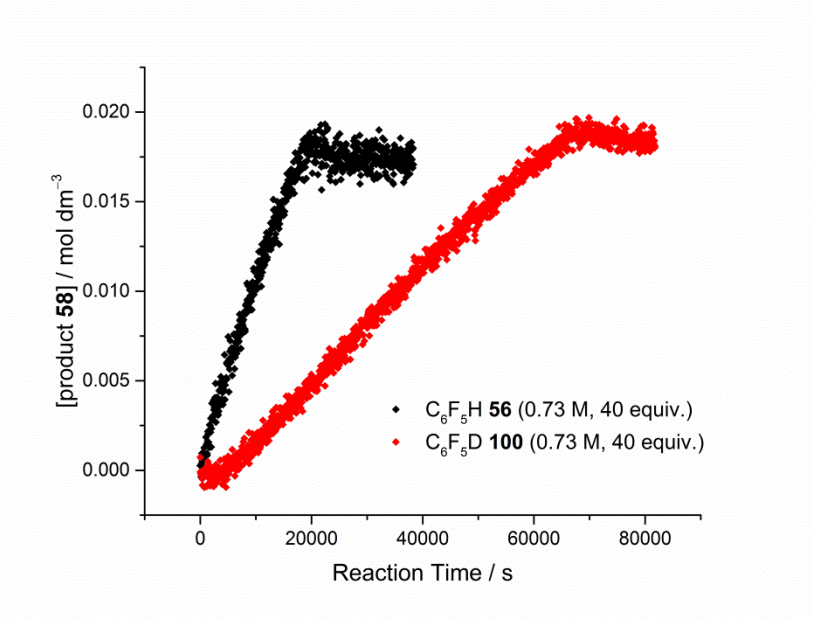

Figure 83. Reaction profiles of the product **58** formation for the direct arylation of 4-iodotoleuen **57** (0.018 M) with pentafluorobenzene **56** (0.73 M) or deuteropentafluorobenzene **100** (0.73 M), catalysed by $Pd(OAc)_2/PPh_3$ (5 mol% : 10 mol%) pre-catalyst at 40 ± 1 °C.

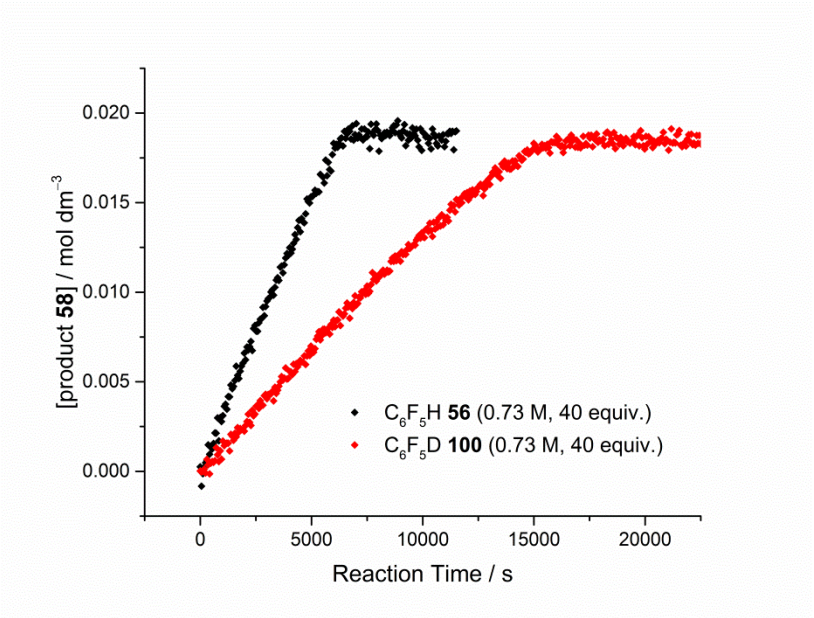

Figure 84. Reaction profiles of the product **58** formation for the direct arylation of 4-iodotoleuen **57** (0.018 M) with pentafluorobenzene **56** (0.73 M) or deuteropentafluorobenzene **100** (0.73 M), catalysed by $Pd(OAc)_2/PPh_3$ (5 mol% : 10 mol%) pre-catalyst at 56 ± 1 °C.

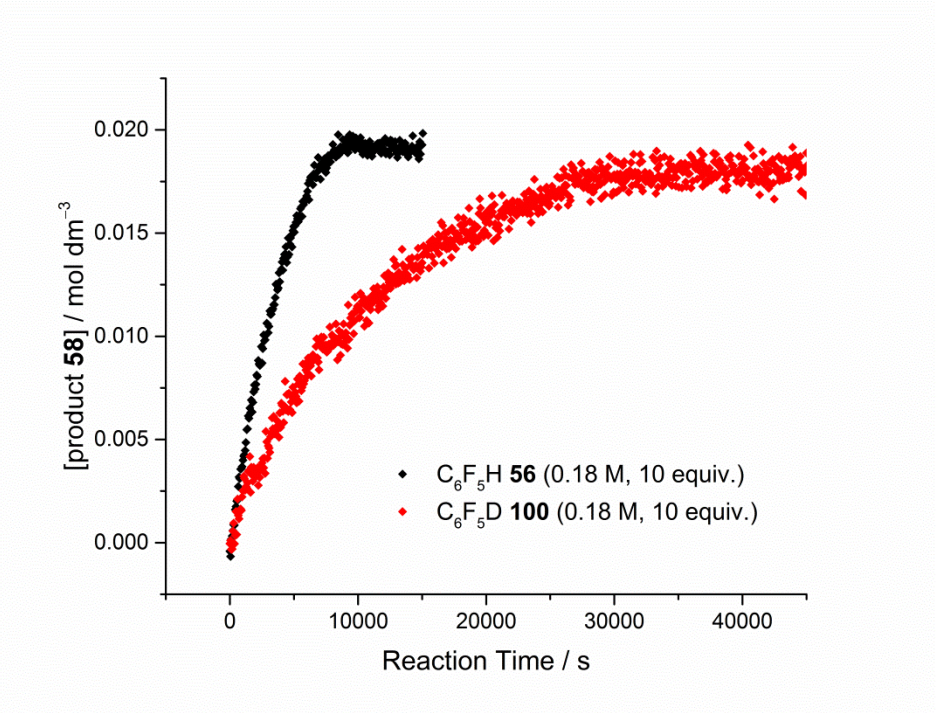

Figure 85. Reaction profiles of the product **58** formation for the direct arylation of 4-iodotoleuen **57** (0.018 M) with pentafluorobenzene **56** (0.18 M) or deuteropentafluorobenzene **100** (0.18 M), catalysed by $Pd(OAc)_2/PPh_3$ (5 mol% : 20 mol%) pre-catalyst at 56 ± 1 °C.

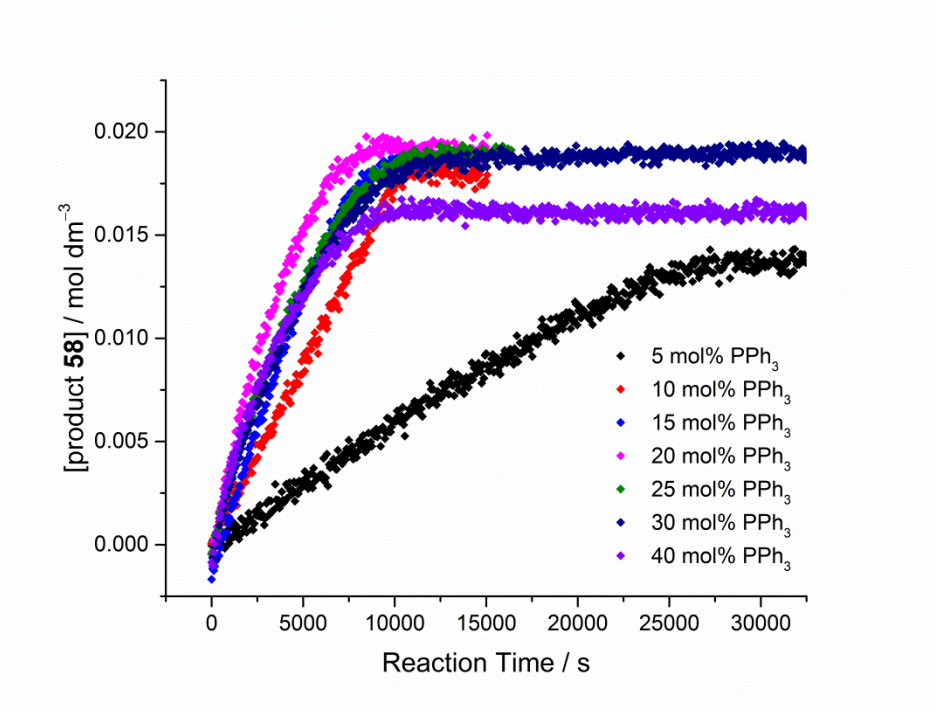

Figure 86. Reaction profiles of the product **58** formation for the direct arylation of 4-iodotoluene **57** (0.018 M) with pentafluorobenzene **56** (0.18 M) shown in **Table 18**, catalysed by $Pd(OAc)_2$ (5 mol%) and range of PPh_3 loading (5–40 mol%) at 56 ± 1 °C.

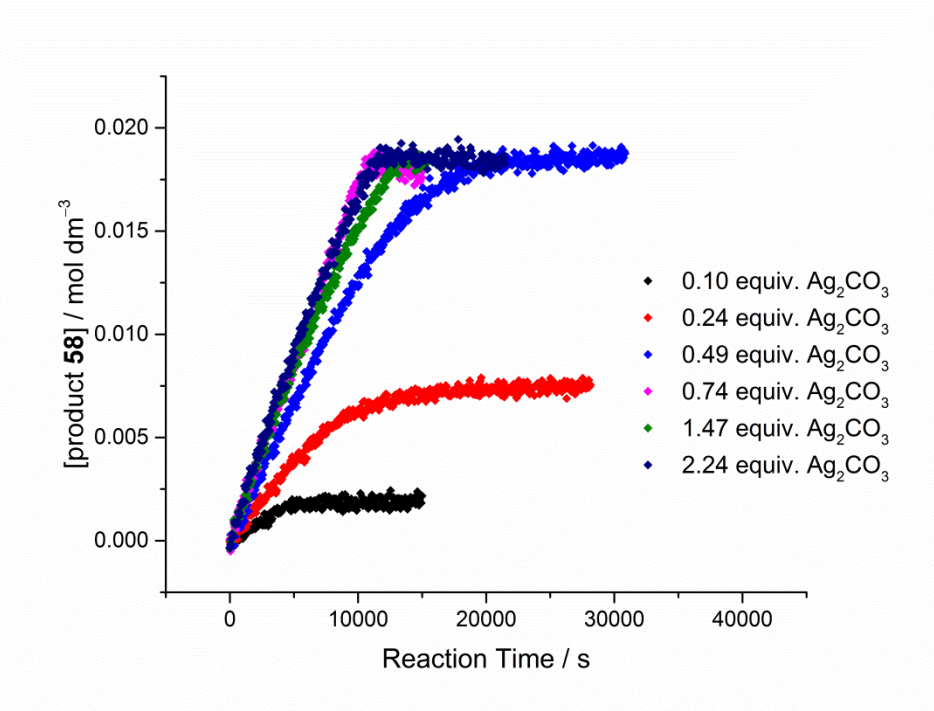

Figure 87. Reaction profiles of the product **58** formation for the direct arylation of 4-iodotoluene **57** (0.018 M) with pentafluorobenzene **56** (0.18 M) shown in **Table 19**, catalysed by $Pd(OAc)_2/PPh_3$ (5 mol% : 10 mol%) at 56 ± 1 °C with range of silver carbonate quantity (0.1–2.24 equiv.).

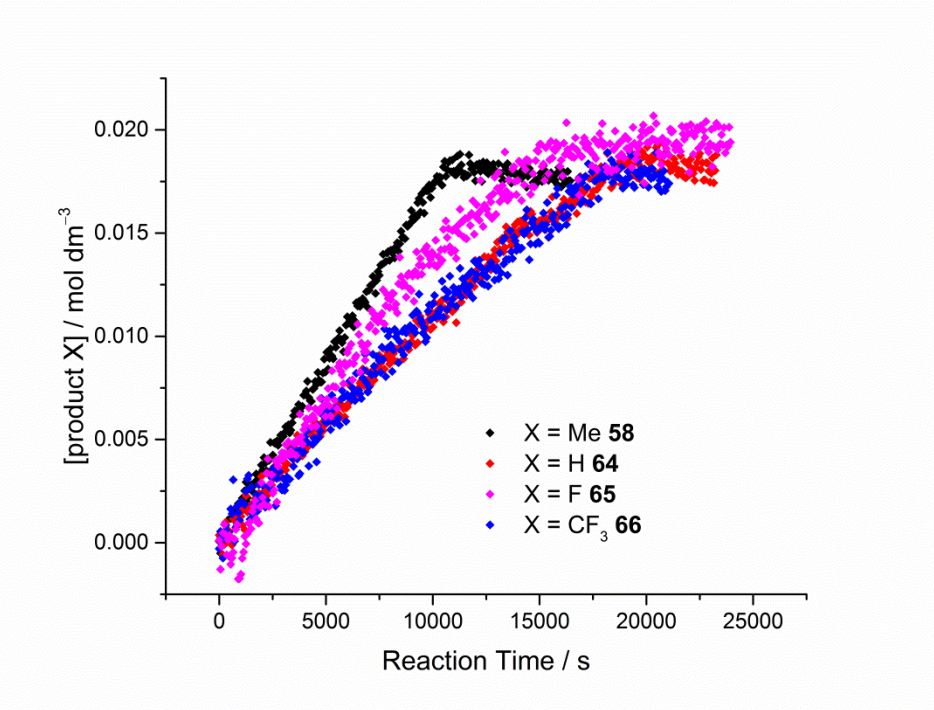

Figure 88. Reaction profiles of the product biaryl (**58**, **64**–**66**) formation for the direct arylation of different 4-substituted-iodobenzenes (0.018 M) with pentafluorobenzene **56** (0.18 M) shown in **Table 25**, catalysed by $Pd(OAc)_2/PPh_3$ (5 mol% : 10 mol%) pre-catalyst at 56 ± 1 °C.

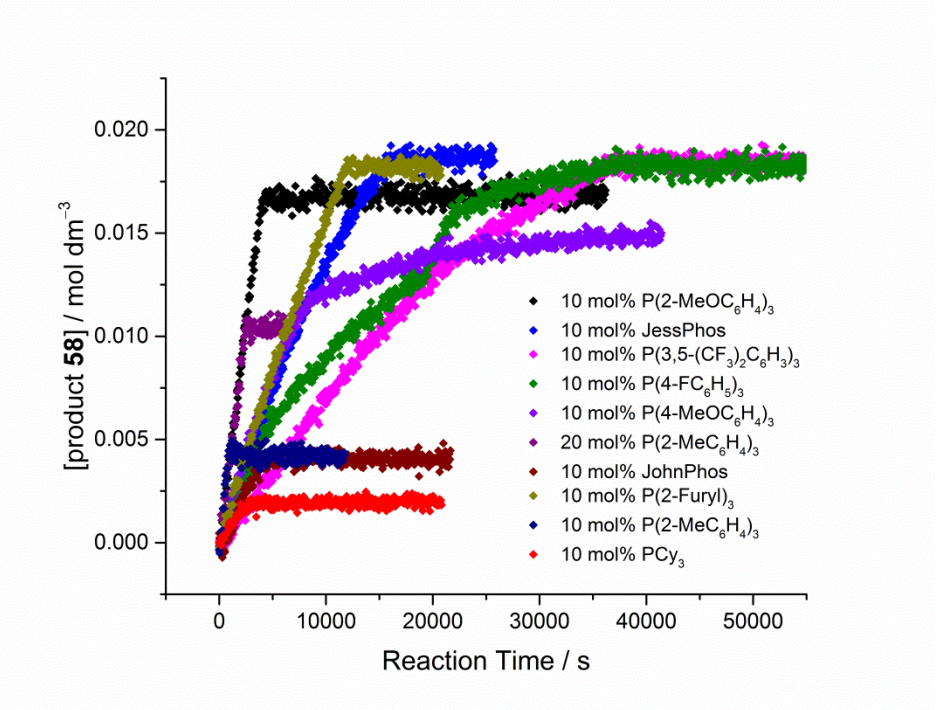

Figure 89. Reaction profiles of the product **58** formation for the direct arylation of 4-iodotoluene **57** (0.018 M) with pentafluorobenzene **56** (0.18 M) shown in **Table 28**, catalysed by $Pd(OAc)_2$ (5 mol%) and different trialkylphosphine ligands (10 mol%) at 56 ± 1 °C.

Appendix 3: ESI-MS and LIFDI-MS Data

Mononuclear and Dinuclear Palladium Complexes

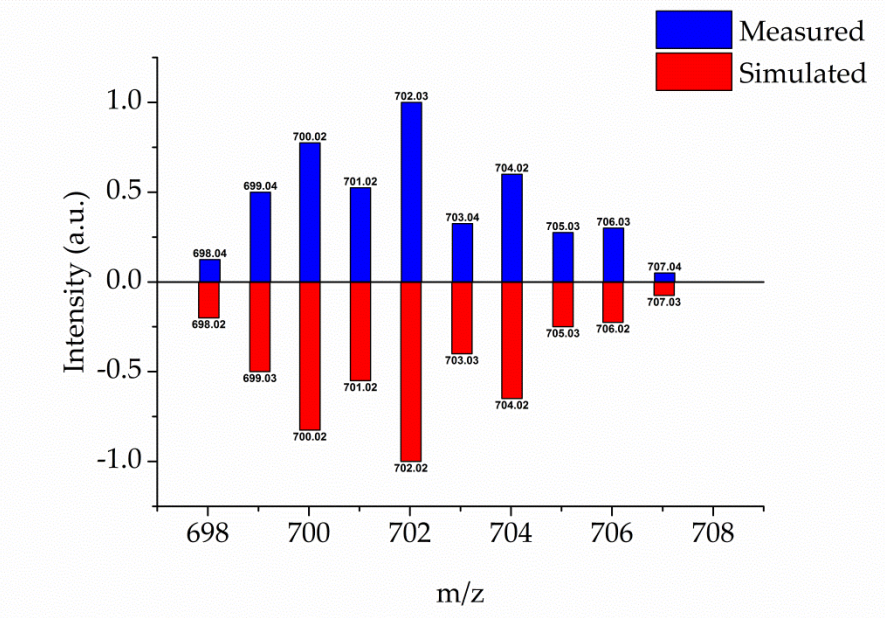

Figure 90. LIFDI-MS spectrum of $Pd(PPh_3)_2Cl_2$ **123** ($PdC_{36}H_{30}Cl_2P_2$ requires 702.02, *mass spectrum reference*: rnp52720gp).

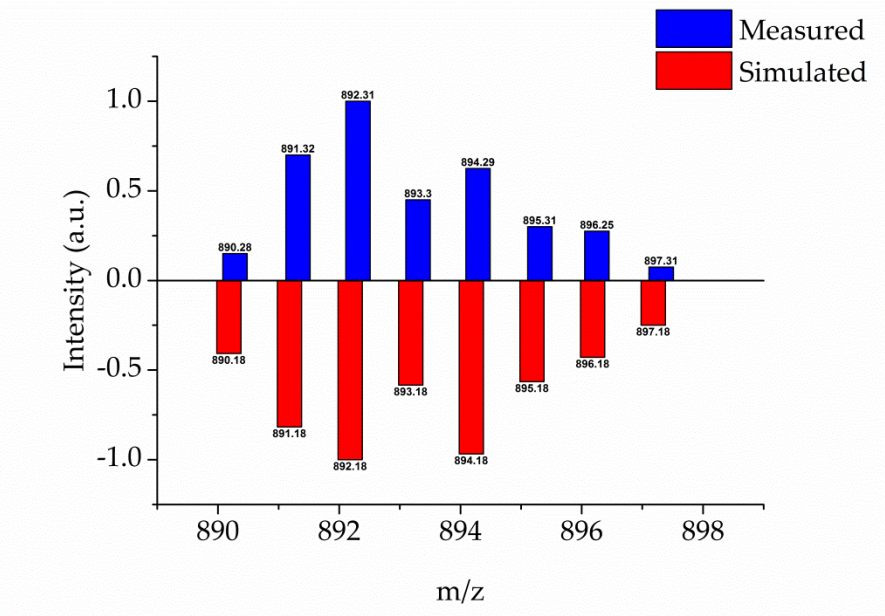

Figure 91. LIFDI-MS spectrum of $Pd(PPh_3)_4$ **124**, observed as $Pd(PPh_3)_3$ ($PdC_{54}H_{45}P_3$ requires 892.18, *mass spectrum reference*: rnp45650gp).

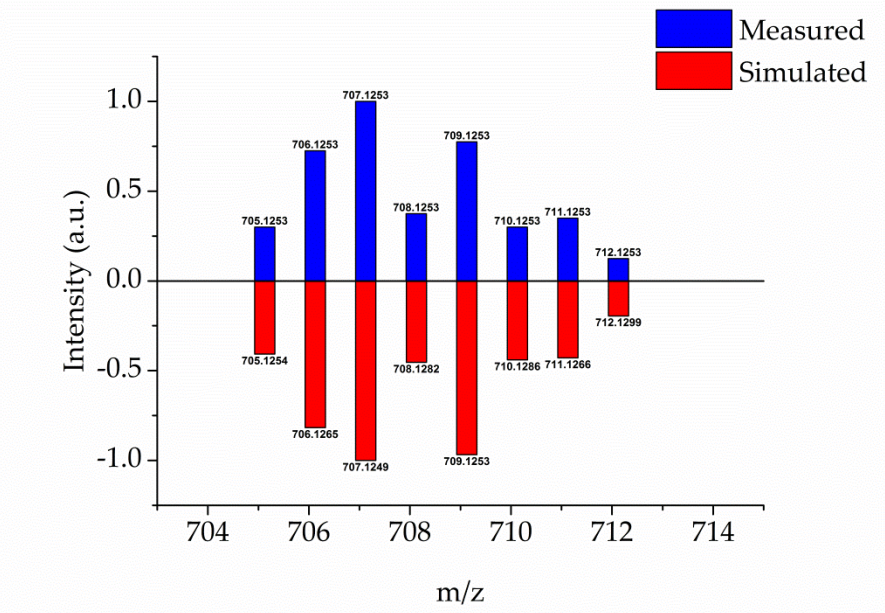

Figure 92. ESI(+)-MS spectrum of $Pd(Ph)(I)(PPh_3)_2$ **82a** observed as $[Pd(Ph)(PPh_3)_2]^+$ ($PdC_{42}H_{35}P_2Pd$ requires 707.1249, *mass spectrum reference*: rnp59402gp).

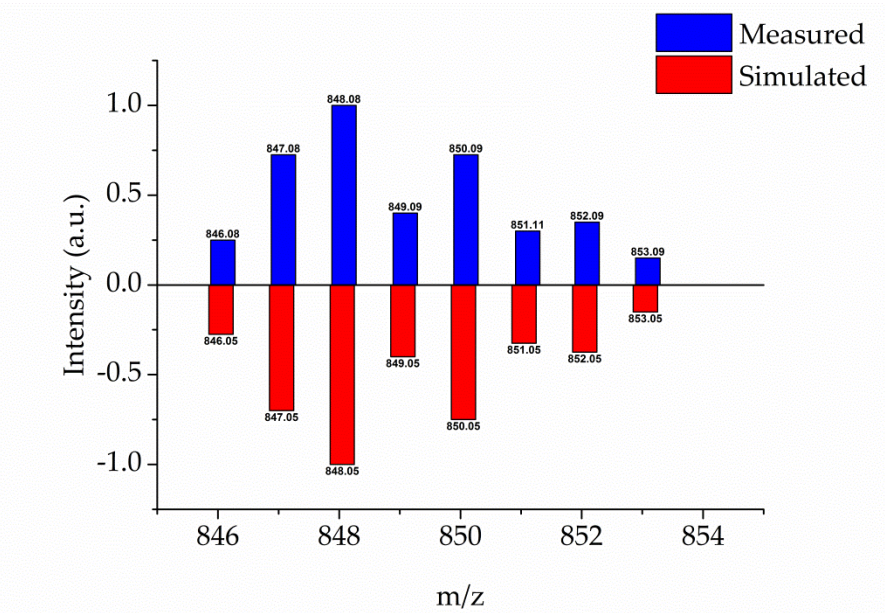

Figure 93. LIFDI-MS spectrum of $Pd(4\text{-tolyl})(I)(PPh_3)_2$ **82b** ($PdC_{43}H_{37}IP_2$ requires 848.05, *mass spectrum reference*: rnp53152gp).

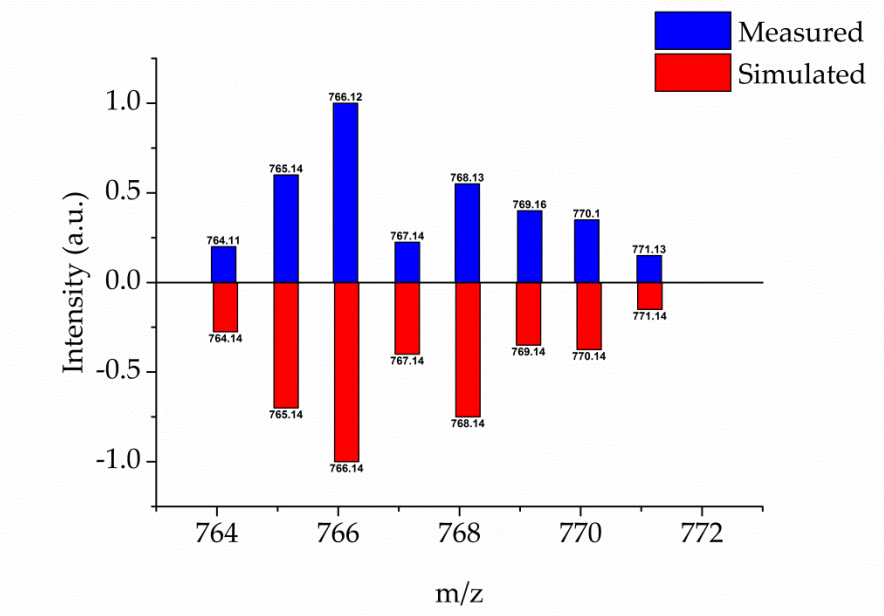

Figure 94. LIFDI-MS spectrum of Pd(Ph)(κ^1-OAc)(PPh_3)$_2$ **85** ($PdC_{44}H_{38}O_2P_2$ requires 766.14, *mass spectrum reference*: rnp55338gp).

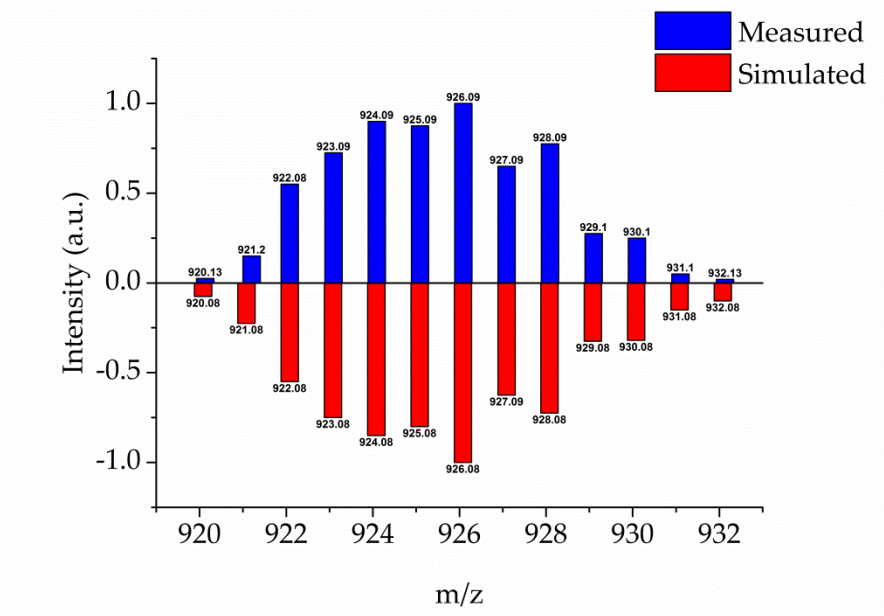

Figure 95. LIFDI-MS spectrum of [Pd(Ph)(μ-OH)(PPh_3)]$_2$ **83a** ($Pd_2C_{48}H_{42}O_2P_2$ requires 926.08, *mass spectrum reference*: rnp44378gp).

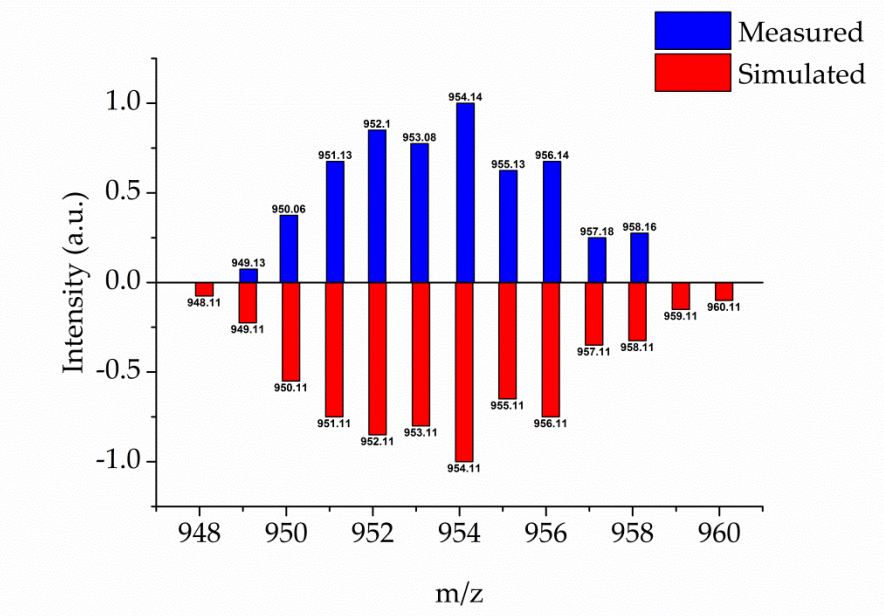

Figure 96. LIFDI-MS spectrum of [Pd(4-tolyl)(μ-OH)(PPh_3)]$_2$ **83b** ($Pd_2C_{50}H_{46}O_2P_2$ requires 954.10, *mass spectrum reference*: rnp44377gp).

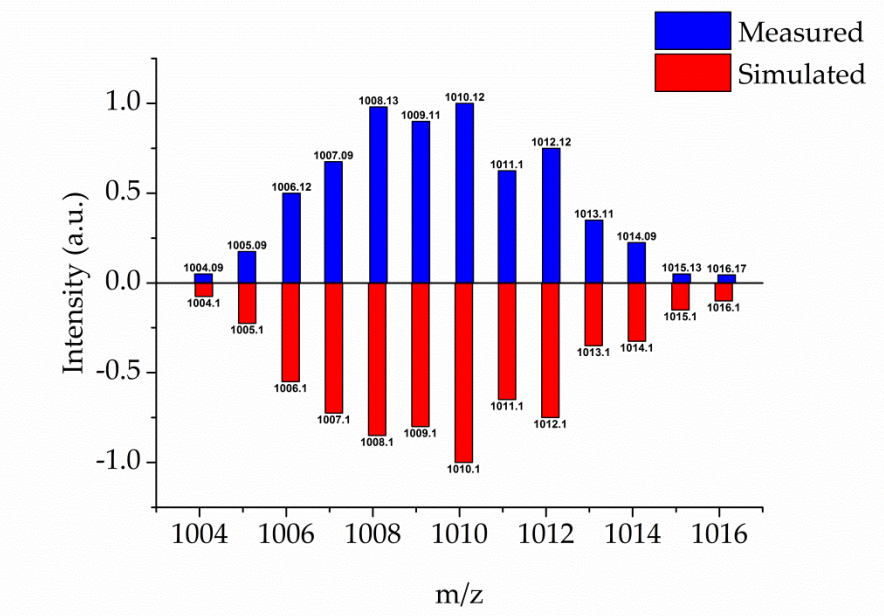

Figure 97. LIFDI-MS spectrum of [Pd(Ph)(μ-OAc)(PPh_3)]$_2$ **84** ($Pd_2C_{52}H_{46}O_4P_2$ requires 1010.10, *mass spectrum reference*: rnp48470gp).

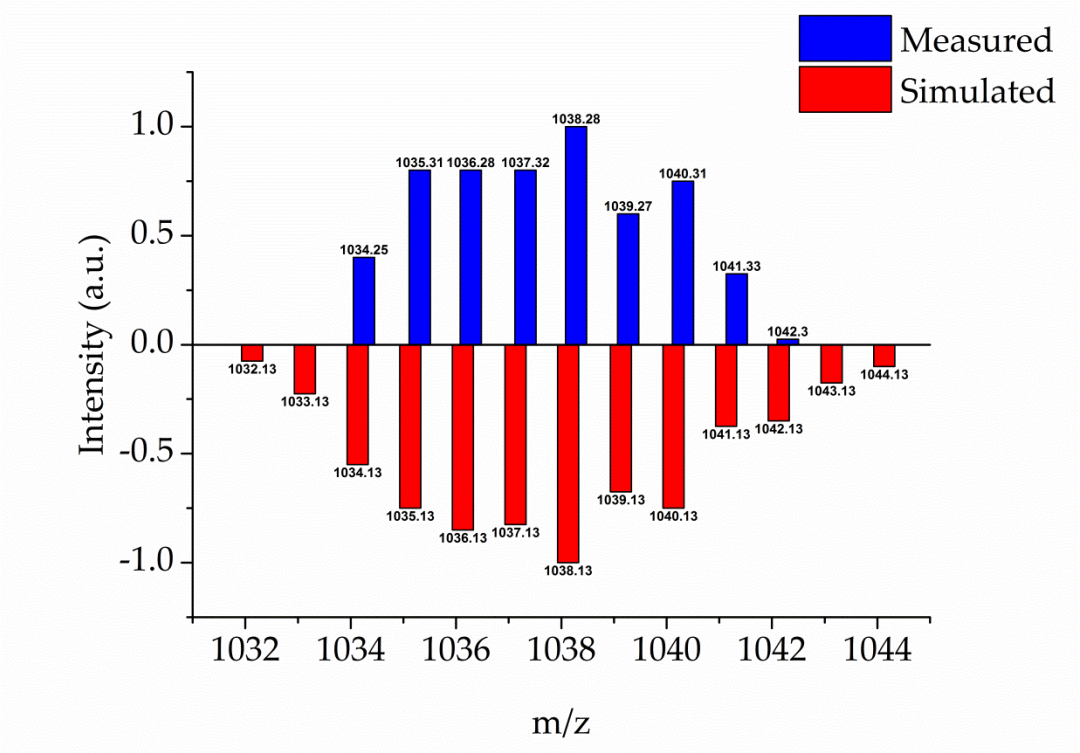

Figure 98. LIFDI-MS spectrum of [Pd(4-tolyl)(μ-OAc)(PPh_3)]$_2$ **84b** ($Pd_2C_{54}H_{50}O_4P_2$ requires 1038.13, *mass spectrum reference*: rnp45749gp).

Ex situ Analysis of the Reaction Mixture by ESI(±)-MS

Lab book reference number: GMHP-6-397

Analysis by ESI(+)-MS

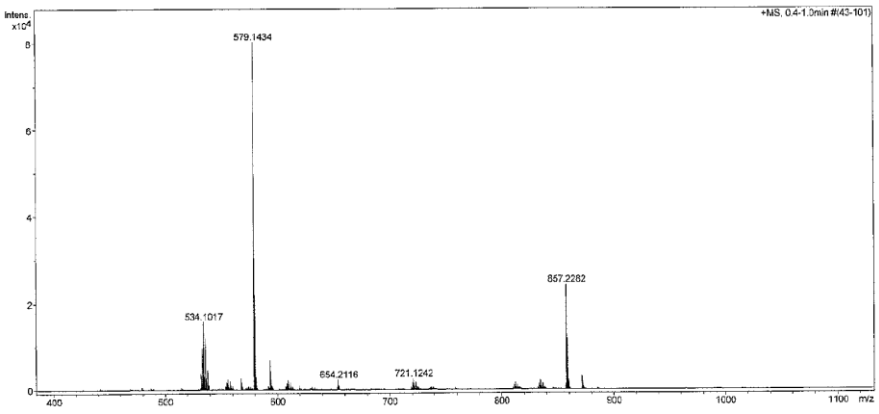

Figure 99. ESI(+)-MS between *m/z* 375–1125 for the reaction aliquot collected from **Scheme 63** at 22% conversion and diluted in DMF (*mass spectrum reference*: rnp52881gp).

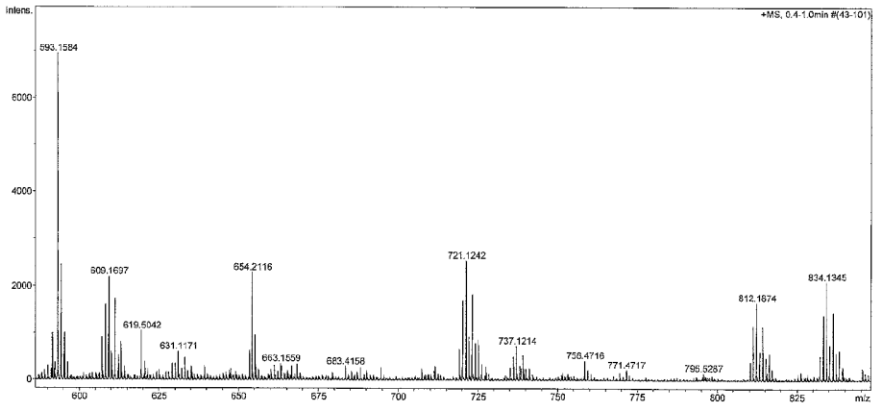

Figure 100. ESI(+)-MS between *m/z* 590–845 for the reaction aliquot collected from **Scheme 63** at 22% conversion and diluted in DMF (*mass spectrum reference*: rnp52881gp).

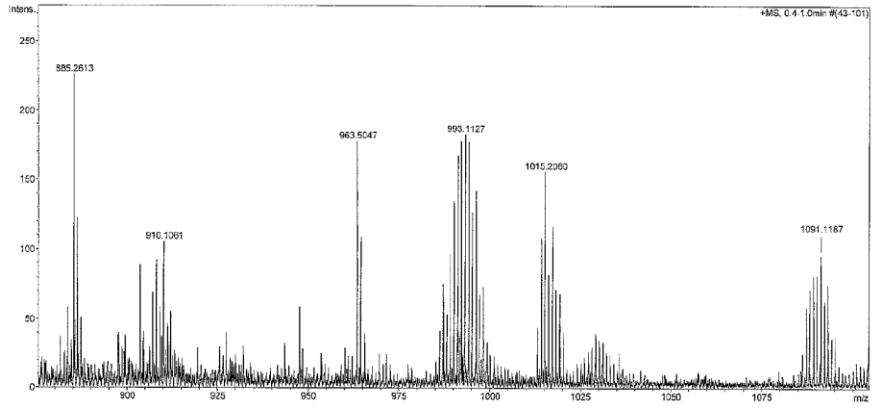

Figure 101. ESI(+)-MS between *m/z* 900–1100 for the reaction aliquot collected from **Scheme 63** at 22% conversion and diluted in DMF (*mass spectrum reference*: rnp52881gp).

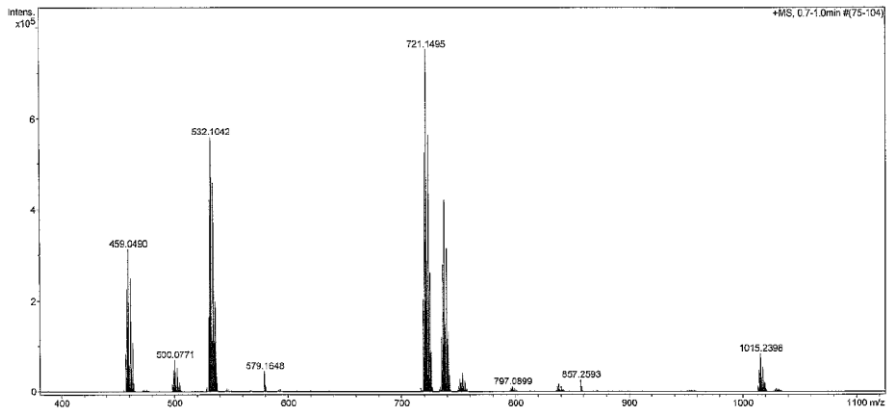

Figure 102. ESI(+)-MS between *m/z* 375–1125 for the reaction aliquot collected from **Scheme 63** at 22% conversion and diluted in acetonitrile (*mass spectrum reference*: rnp52882gp).

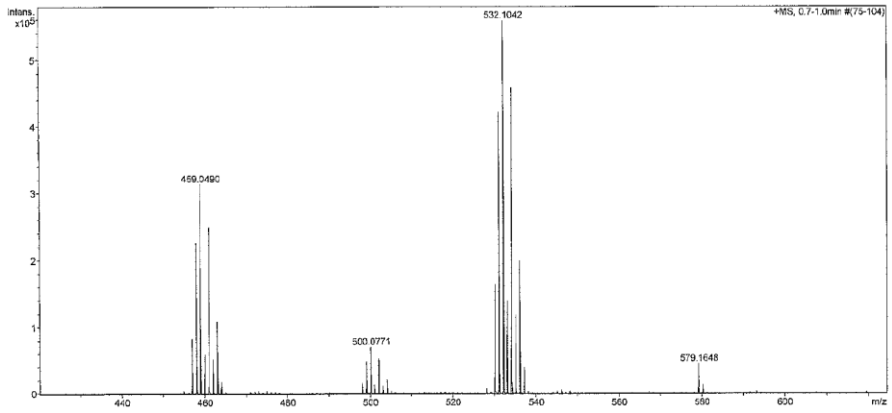

Figure 103. ESI(+)-MS between *m/z* 420–620 for the reaction aliquot collected from **Scheme 63** at 22% conversion and diluted in acetonitrile (*mass spectrum reference*: rnp52882gp).

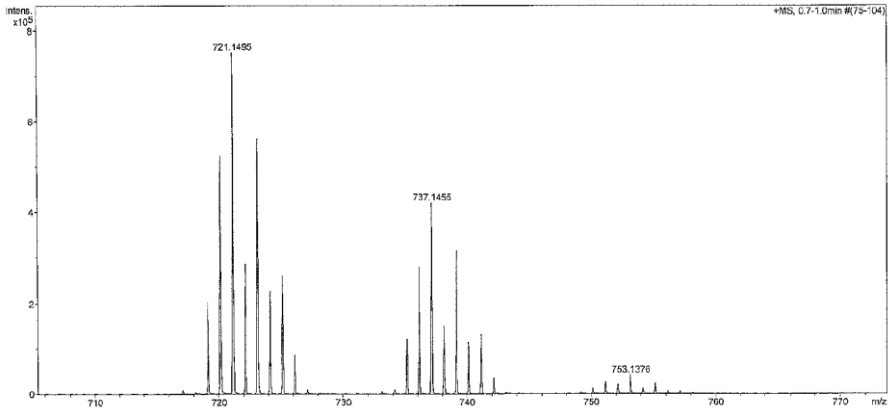

Figure 104. ESI(+)-MS between *m/z* 706–772 for the reaction aliquot collected from **Scheme 63** at 22% conversion and diluted in acetonitrile (*mass spectrum reference*: rnp52882gp).

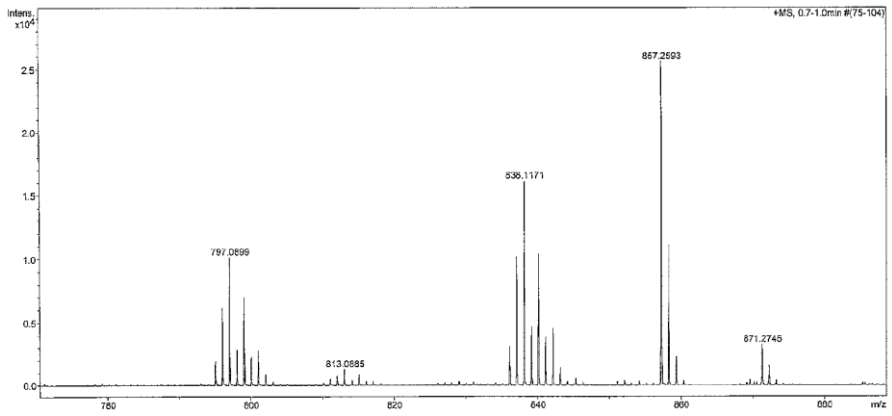

Figure 105. ESI(+)-MS between *m/z* 770–890 for the reaction aliquot collected from **Scheme 63** at 22% conversion and diluted in acetonitrile (*mass spectrum reference*: rnp52882gp).

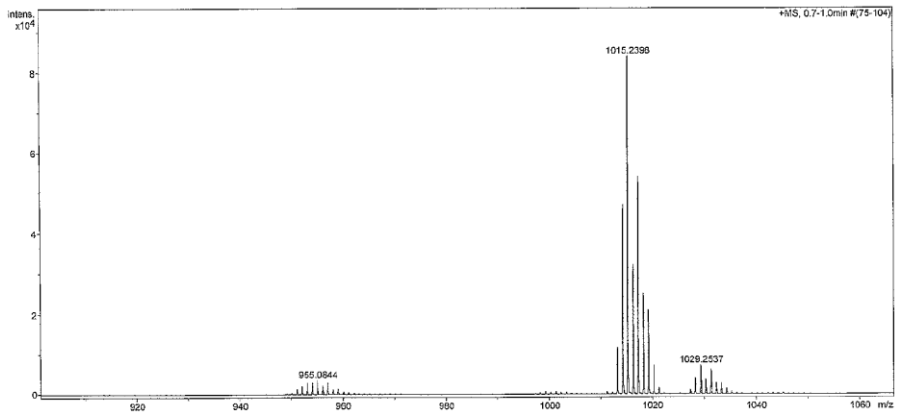

Figure 106. ESI(+)-MS between *m/z* 910–1060 for the reaction aliquot collected from **Scheme 63** at 22% conversion and diluted in acetonitrile (*mass spectrum reference*: rnp52882gp).

Analysis by ESI(−)-MS

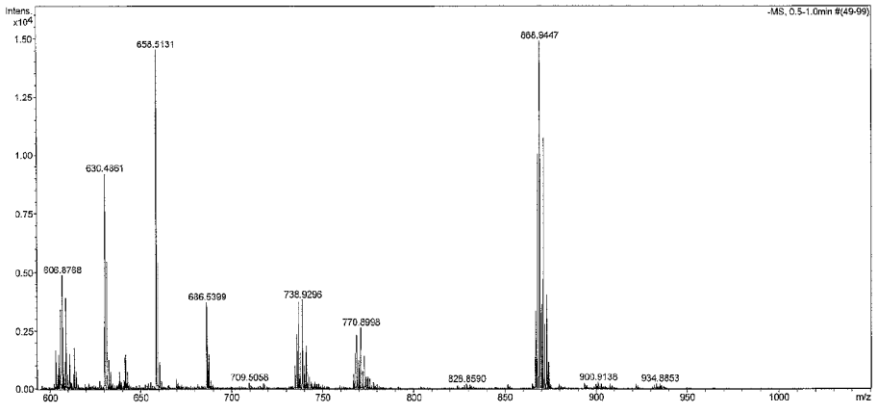

Figure 107. ESI(−)-MS between *m/z* 600–1050 for the reaction aliquot collected from **Scheme 63** at 22% conversion and diluted in DMF (*mass spectrum reference*: rnp52881gp).

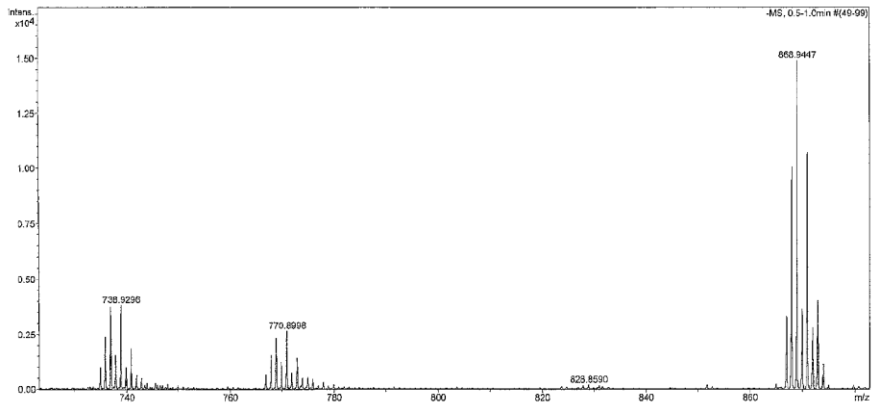

Figure 108. ESI(−)-MS between *m/z* 720–880 for the reaction aliquot collected from **Scheme 63** at 22% conversion and diluted in DMF (*mass spectrum reference*: rnp52881gp).

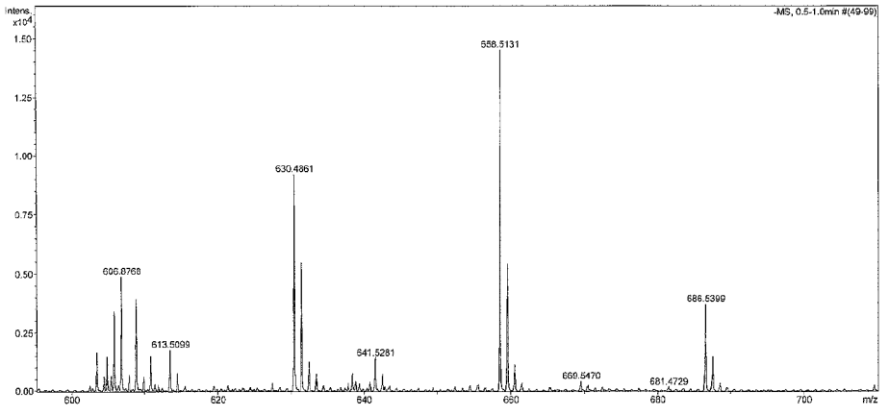

Figure 109. ESI(−)-MS between *m/z* 595–710 for the reaction aliquot collected from **Scheme 63** at 22% conversion and diluted in DMF (*mass spectrum reference*: rnp52881gp).

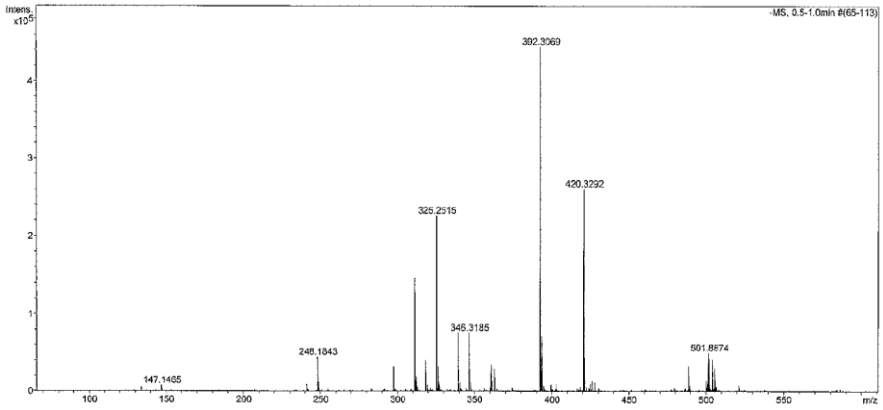

Figure 110. ESI(−)-MS between *m/z* 50–600 for the reaction aliquot collected from **Scheme 63** at 22% conversion and diluted in acetonitrile (*mass spectrum reference*: rnp52882gp).

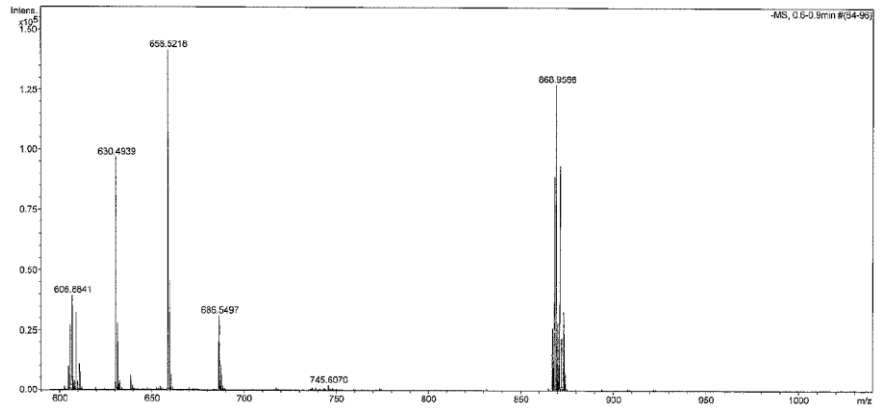

Figure 111. ESI(−)-MS between *m/z* 590–1040 for the reaction aliquot collected from **Scheme 63** at 22% conversion and diluted in acetonitrile (*mass spectrum reference*: rnp52882gp).

Ex situ Analysis of the Reaction Mixture by LIFDI-MS

Lab book reference number: GMHP-7-492

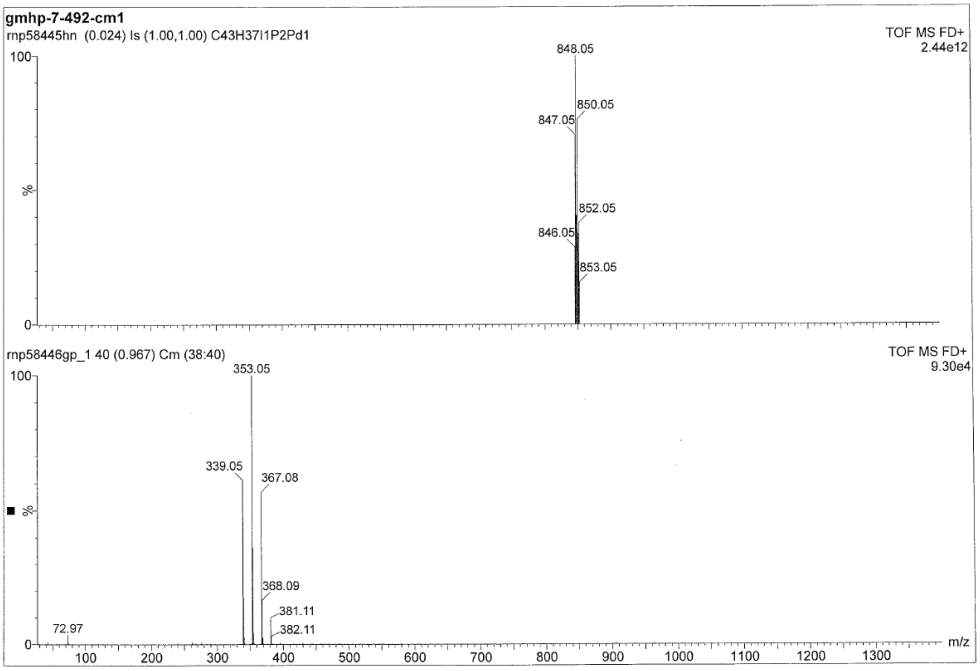

Figure 112. LIFDI-MS of 4-iodotluene **57**, $Pd(OAc)_2$, PPh_3 and Ag_2CO_3 mixture in DMF at 19 ± 1 °C (*mass spectrum reference*: rnp58445hn).

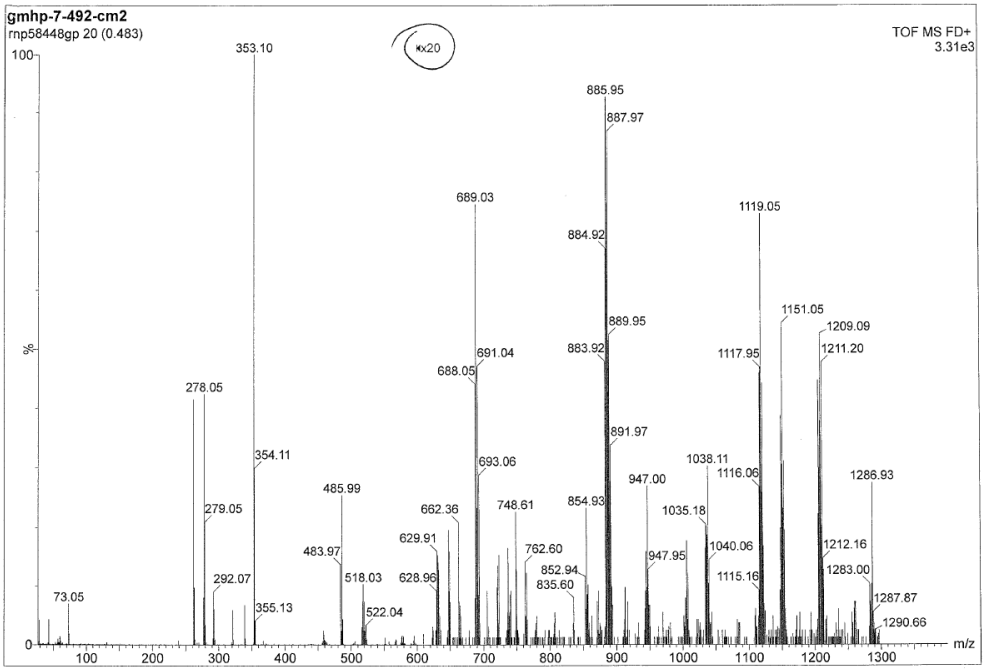

Figure 113. LIFDI-MS of 4-iodotluene **57**, $Pd(OAc)_2$, PPh_3 and Ag_2CO_3 mixture in DMF at 56 ± 1 °C (*mass spectrum reference*: rnp58448gp).

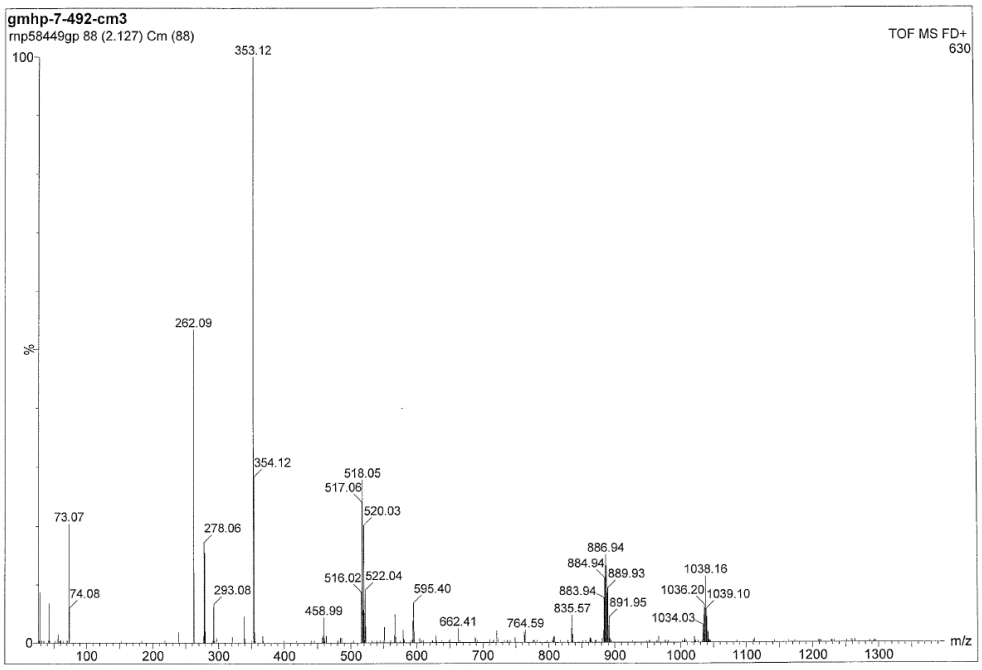

Figure 114. LIFDI-MS of an reaction aliquot collected from **Scheme 63** after 6 min (5% conversion) of heating a 4-iodotluene **57**, pentafluorobenzene **56**, $Pd(OAc)_2$, PPh_3 and Ag_2CO_3 mixture in DMF at 56 ± 1 °C (*mass spectrum reference*: rnp58449gp).

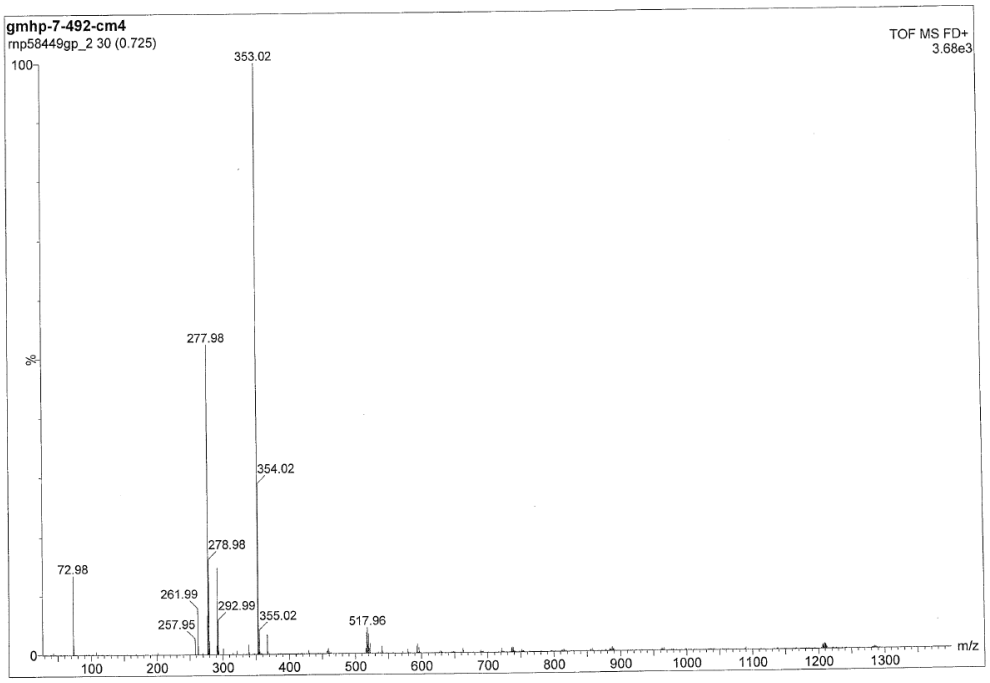

Figure 115. LIFDI-MS of an reaction aliquot collected from **Scheme 63** after 47 min (60% conversion) of heating a 4-iodotluene **57**, pentafluorobenzene **56**, $Pd(OAc)_2$, PPh_3 and Ag_2CO_3 mixture in DMF at 56 ± 1 °C (*mass spectrum reference*: rnp58449gp).

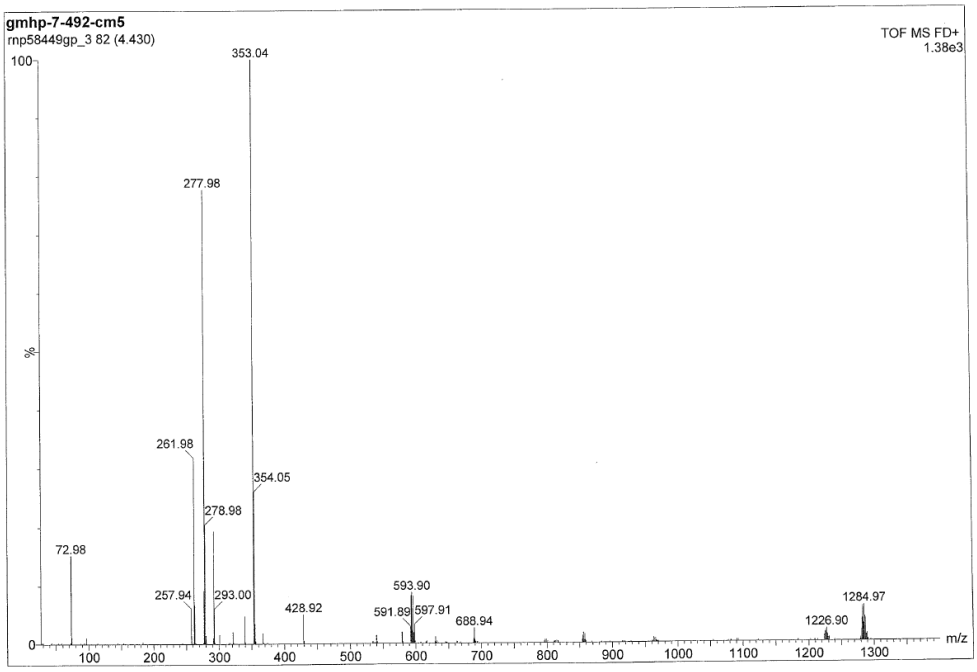

Figure 116. LIFDI-MS of an reaction aliquot collected from **Scheme 63** after 86 min (quant. conversion) of heating a 4-iodotluene **57**, pentafluorobenzene **56**, $Pd(OAc)_2$, PPh_3 and Ag_2CO_3 mixture in DMF at 56 ± 1 °C (*mass spectrum reference*: rnp58449gp).

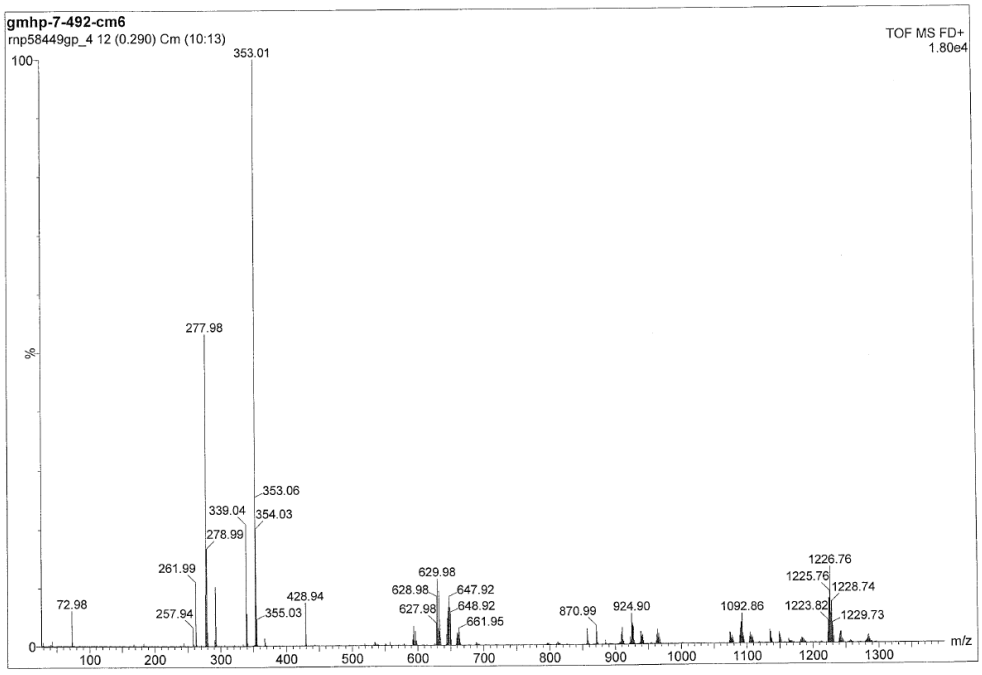

Figure 117. LIFDI-MS of an reaction aliquot collected from **Scheme 63** after 126 min (quant. conversion) of heating a 4-iodotluene **57**, pentafluorobenzene **56**, $Pd(OAc)_2$, PPh_3 and Ag_2CO_3 mixture in DMF at 56 ± 1 °C (*mass spectrum reference*: rnp58449gp).

Appendix 4: NMR Spectroscopy Data

NMR Spectra of Synthesised Compounds

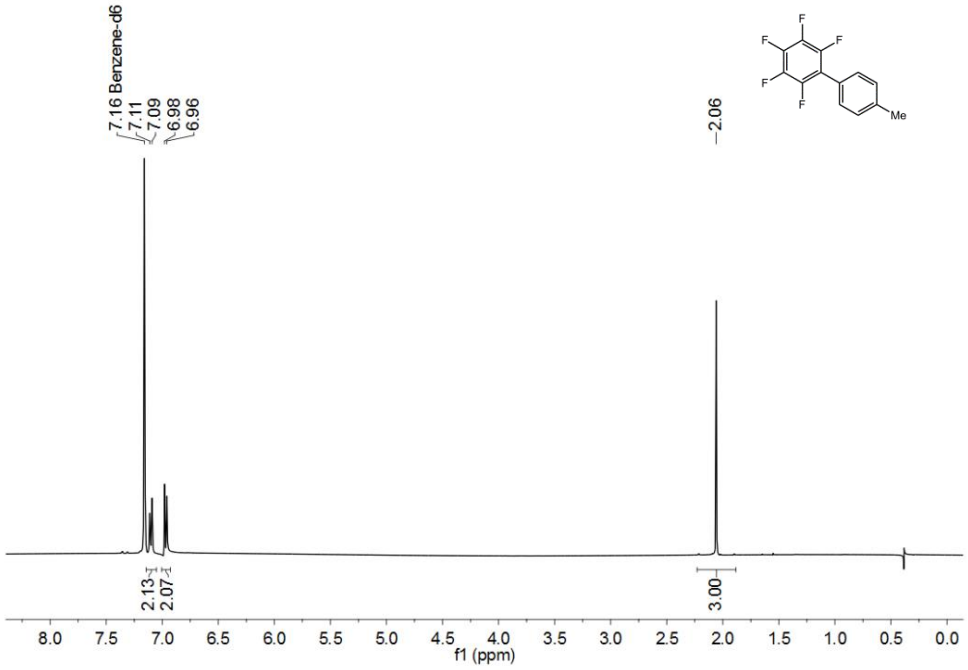

Figure 118. ^{1}H NMR spectrum of 2,3,4,5,6-pentafluoro-4′-(methyl)biphenyl **58** in benzene-d_6 (*JDF file reference*: a8355gmp).

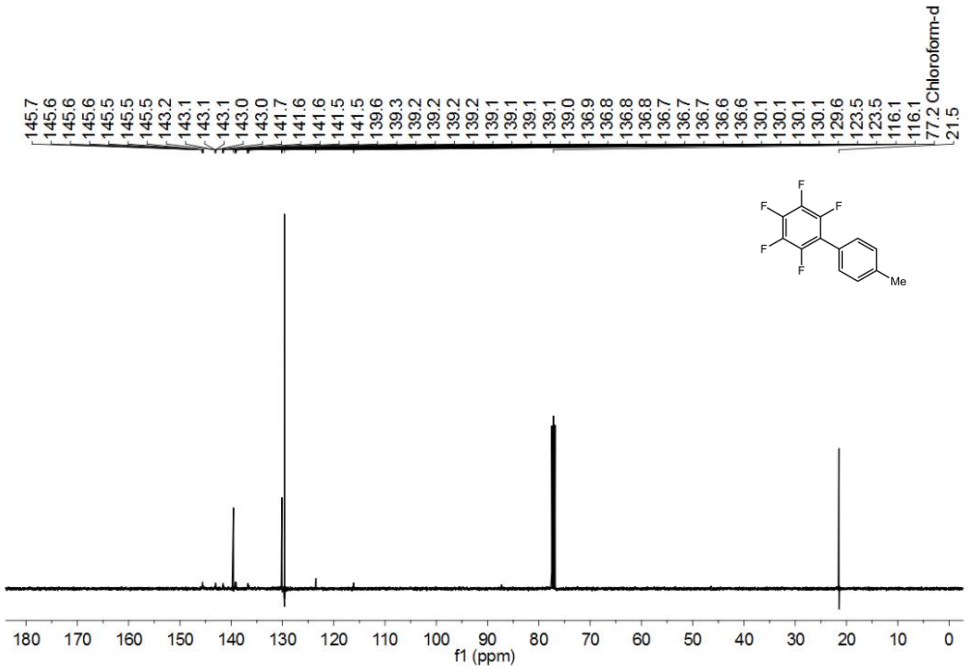

Figure 119. ^{13}C NMR spectrum of 2,3,4,5,6-pentafluoro-4′-(methyl)biphenyl **58** in chloroform-d (*JDF file reference*: a8356gmp).

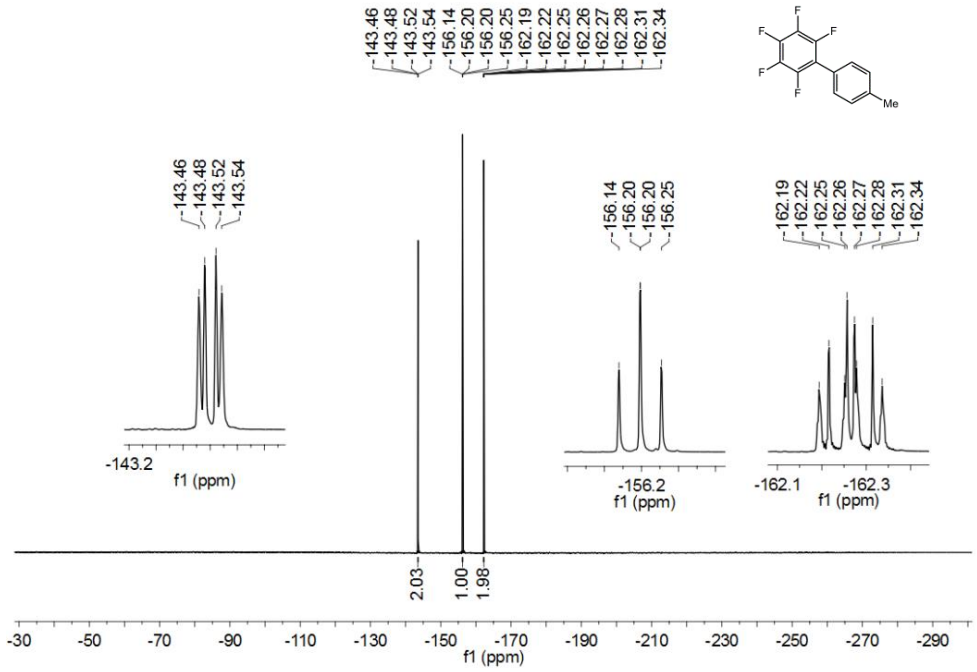

Figure 120. ^{19}F NMR spectrum of 2,3,4,5,6-pentafluoro-4′-(methyl)biphenyl **58** in benzene-d_6 (*JDF file reference*: a8355gmp).

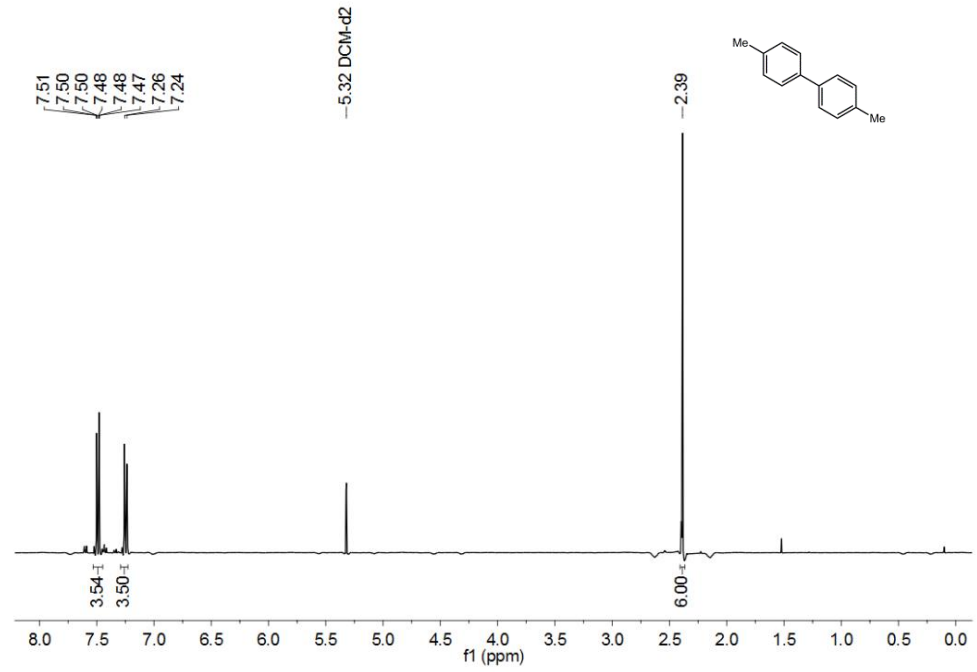

Figure 121. ^{1}H NMR spectrum of 4,4′-(dimethyl)biphenyl **59** in methylene chloride-d_2 (*JDF file reference*: a8907gmp).

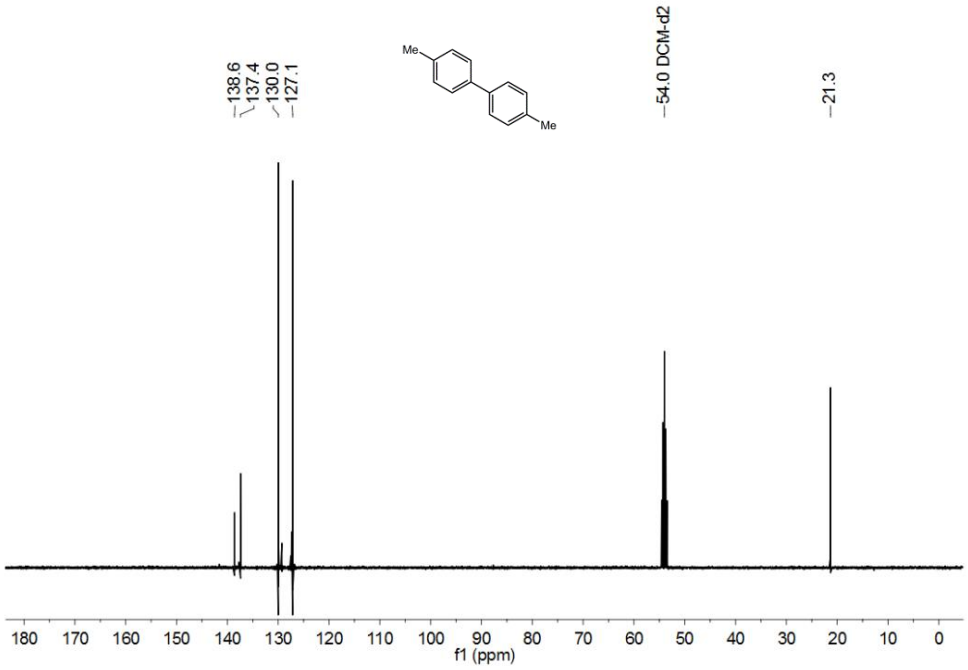

Figure 122. ^{13}C NMR spectrum of 4,4′-(dimethyl)biphenyl **59** in methylene chloride-d_2 (*JDF file reference*: a8907gmp).

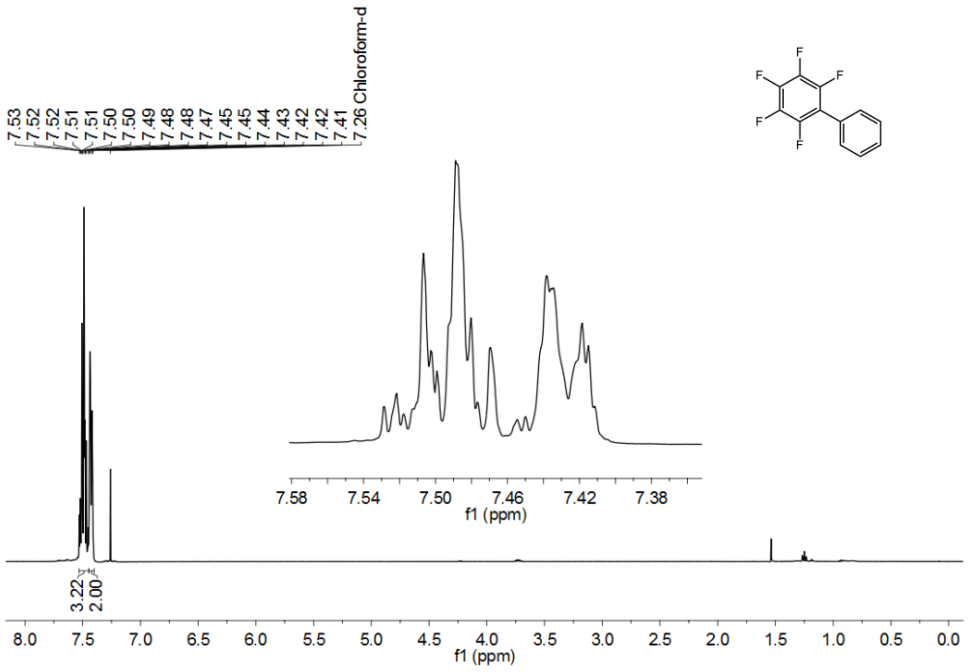

Figure 123. ^{1}H NMR spectrum of 2,3,4,5,6-pentafluorobiphenyl **64** in chloroform-d (*JDF file reference*: a8189gmp).

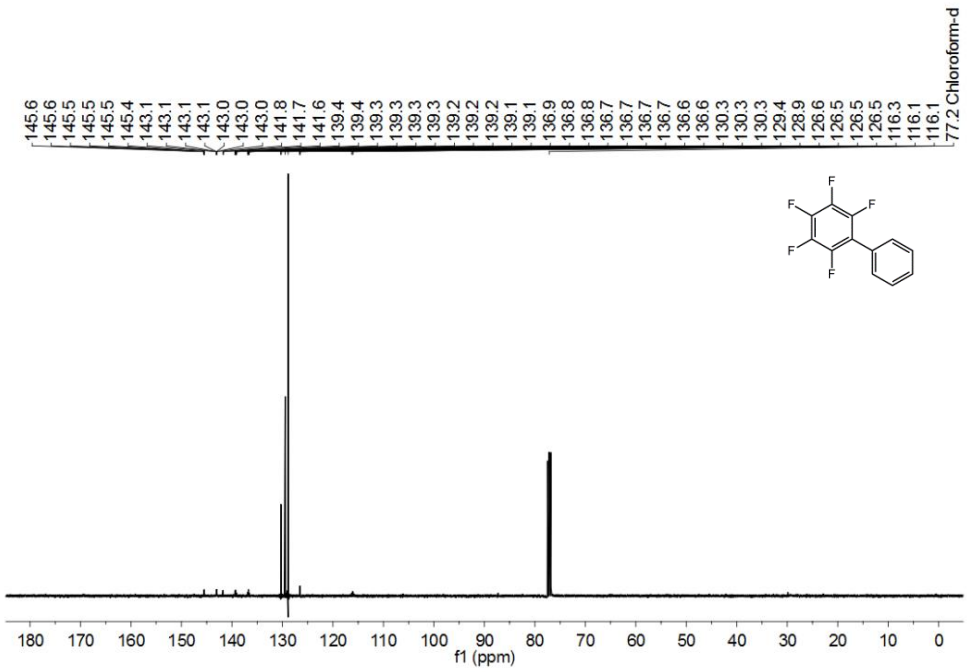

Figure 124. ^{13}C NMR spectrum of 2,3,4,5,6-pentafluorobiphenyl **64** in chloroform-d (*JDF file reference*: a8189gmp).

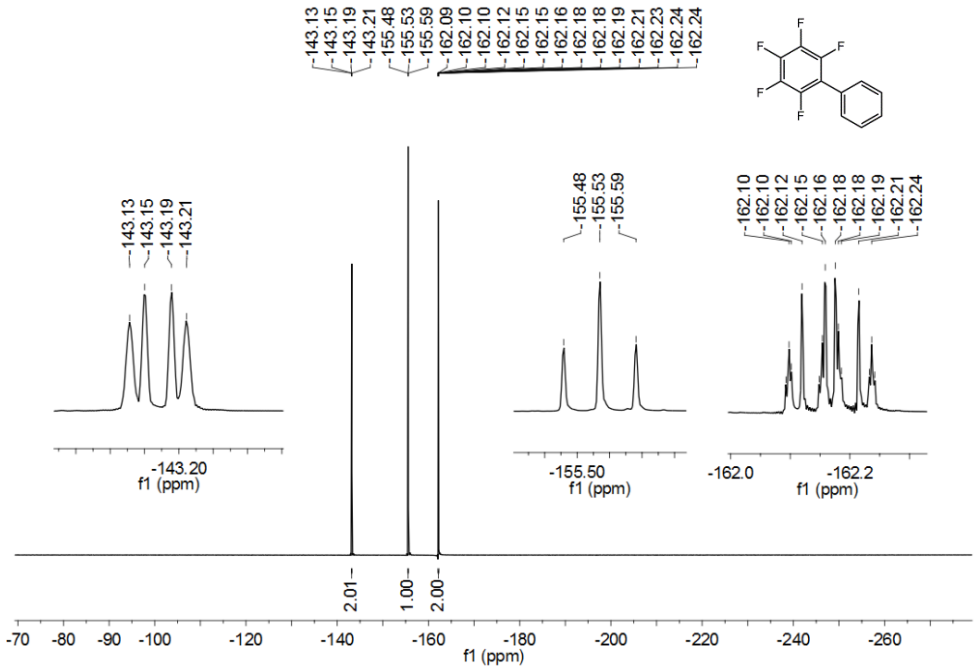

Figure 125. ^{19}F NMR spectrum of 2,3,4,5,6-pentafluorobiphenyl **64** in chloroform-d (*JDF file reference*: a8189gmp).

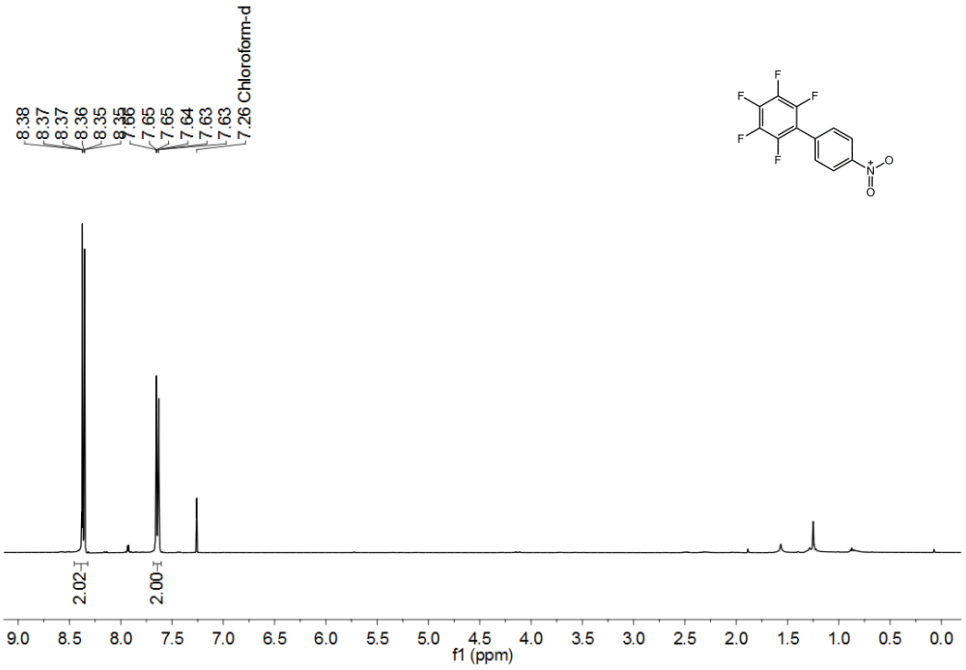

Figure 126. ^{1}H NMR spectrum of 2,3,4,5,6-pentafluoro-4′-(nitro)biphenyl **67** in chloroform-d (*JDF file reference*: a8368gmp).

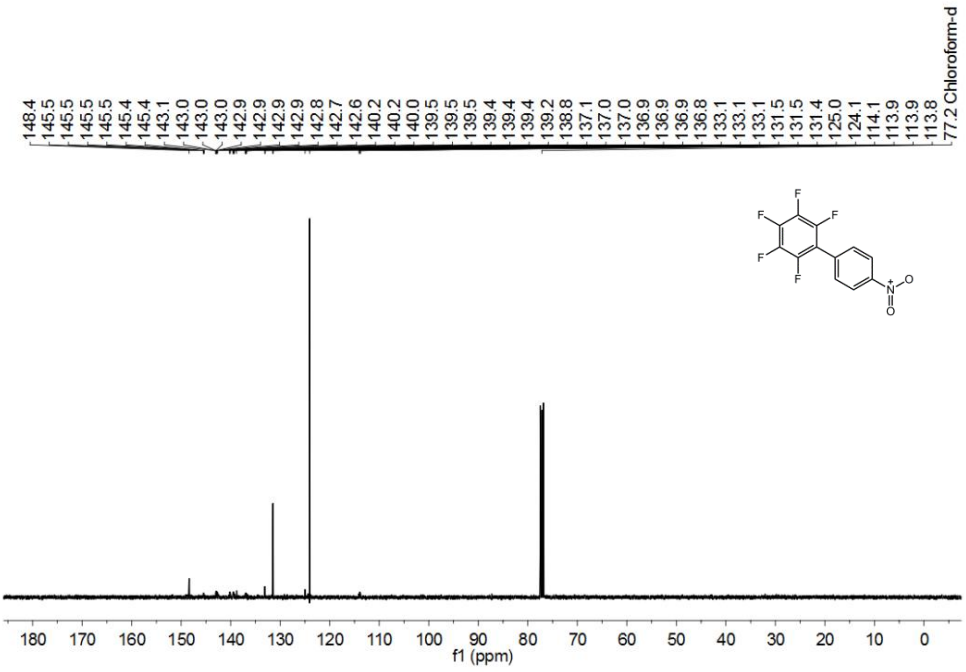

Figure 127. ^{13}C NMR spectrum of 2,3,4,5,6-pentafluoro-4′-(nitro)biphenyl **67** in chloroform-d (*JDF file reference*: a8368gmp).

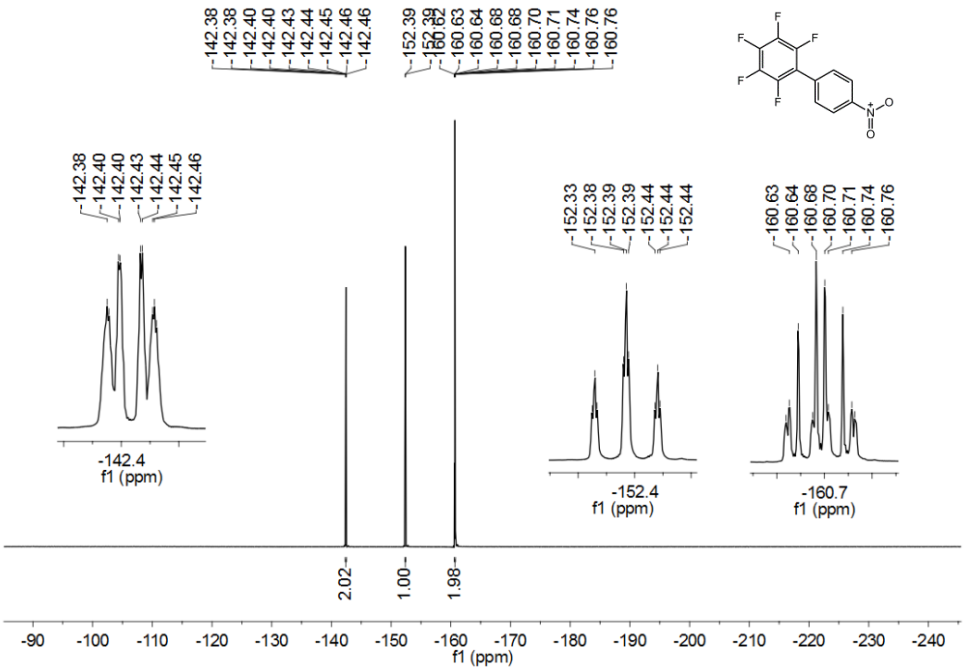

Figure 128. ^{19}F NMR spectrum of 2,3,4,5,6-pentafluoro-4′-(nitro)biphenyl **67** in chloroform-d (*JDF file reference*: a8368gmp).

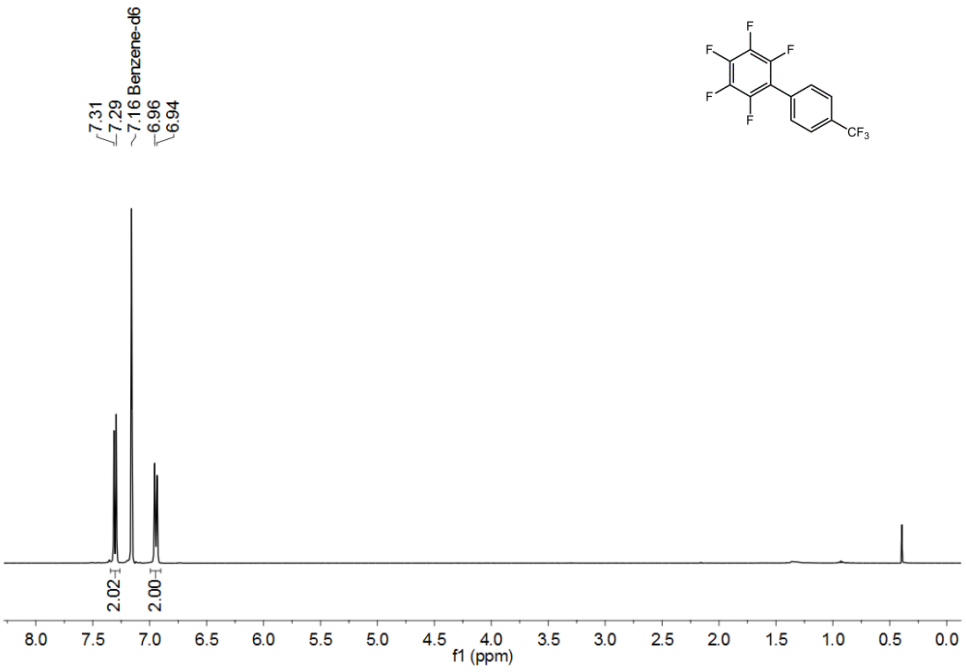

Figure 129. ^{1}H NMR spectrum of 2,3,4,5,6-pentafluoro-4′-(tifluoromethyl)biphenyl **66** in benzene-d_6 (*JDF file reference*: a8366gmp).

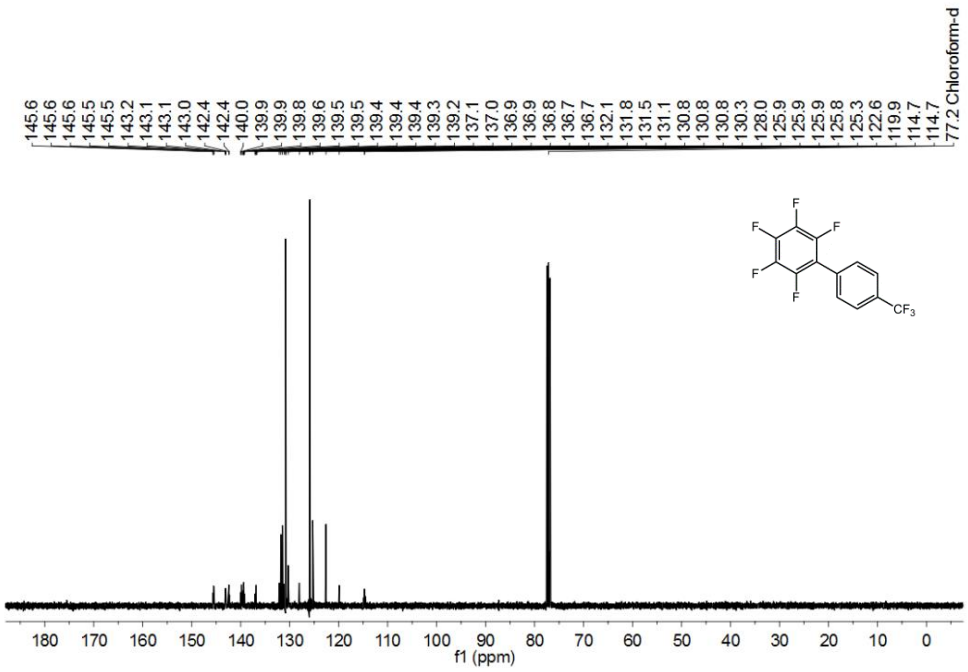

Figure 130. ^{13}C NMR spectrum of 2,3,4,5,6-pentafluoro-4′-(tifluoromethyl)biphenyl **66** in chloroform-d (*JDF file reference*: a8365gmp).

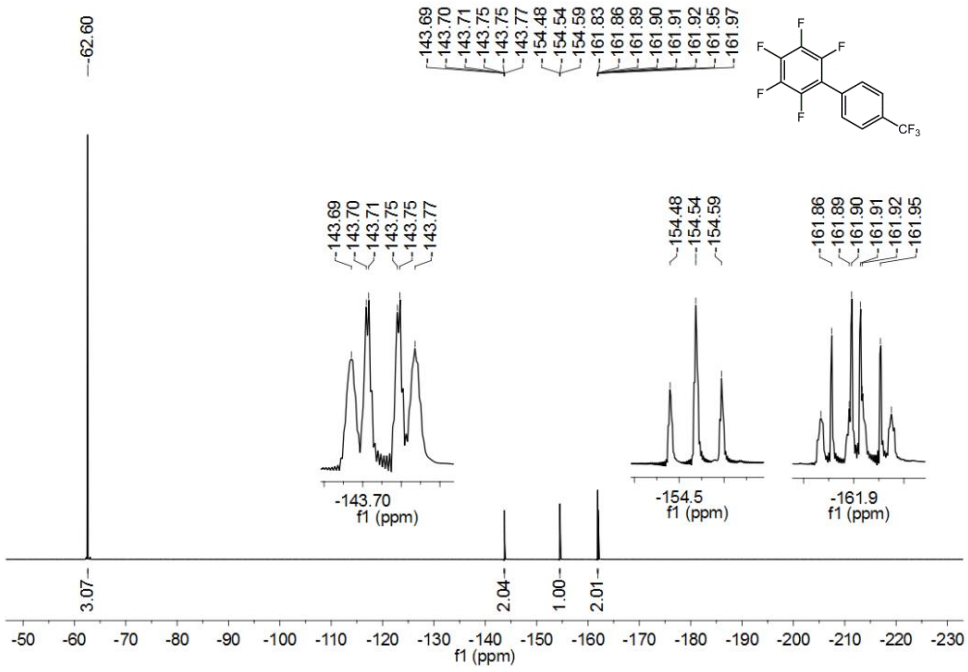

Figure 131. ^{19}F NMR spectrum of 2,3,4,5,6-pentafluoro-4′-(tifluoromethyl)biphenyl **66** in benzene-d_6 (*JDF file reference*: a8366gmp).

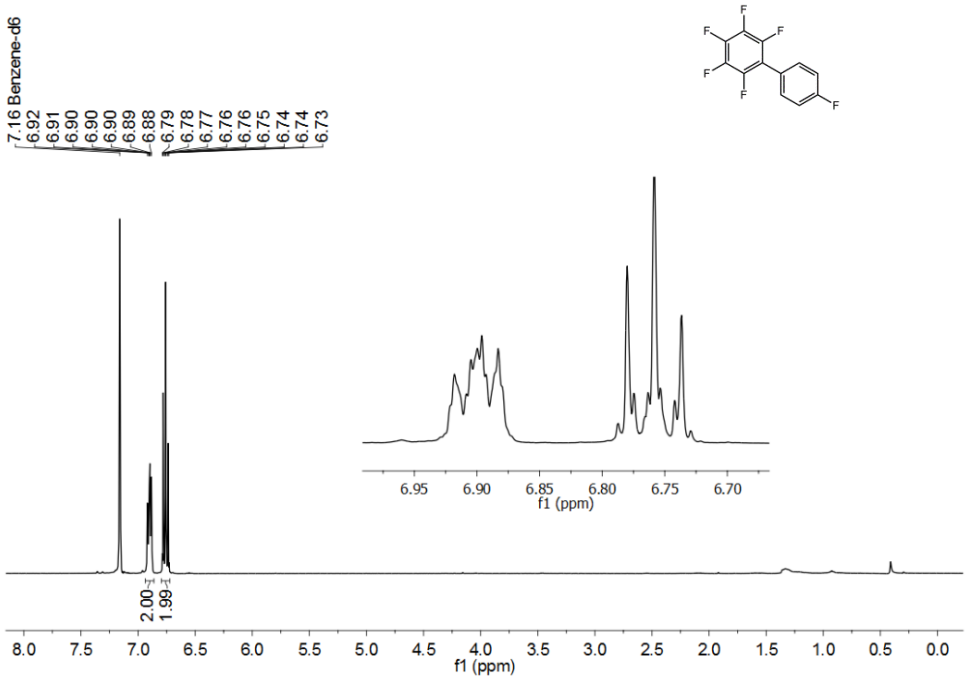

Figure 132. ^{1}H NMR spectrum of 2,3,4,5,6-pentafluoro-4′-(fluoro)biphenyl **65** in benzene-d_6 (*JDF file reference*: a8095gmp).

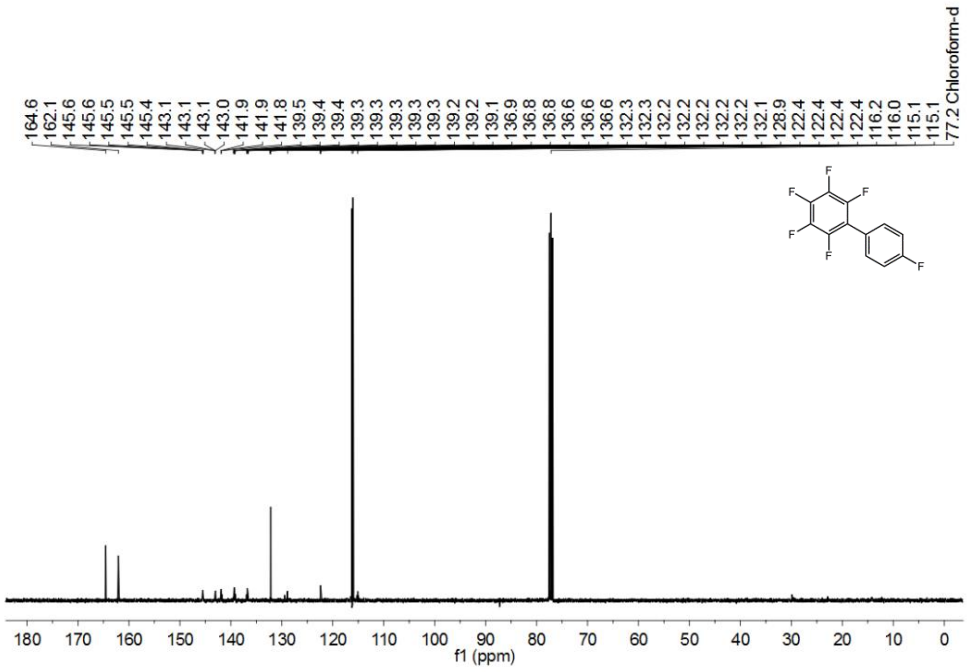

Figure 133. ^{13}C NMR spectrum of 2,3,4,5,6-pentafluoro-4′-(fluoro)biphenyl **65** in chloroform-d (*JDF file reference*: a8774gmp).

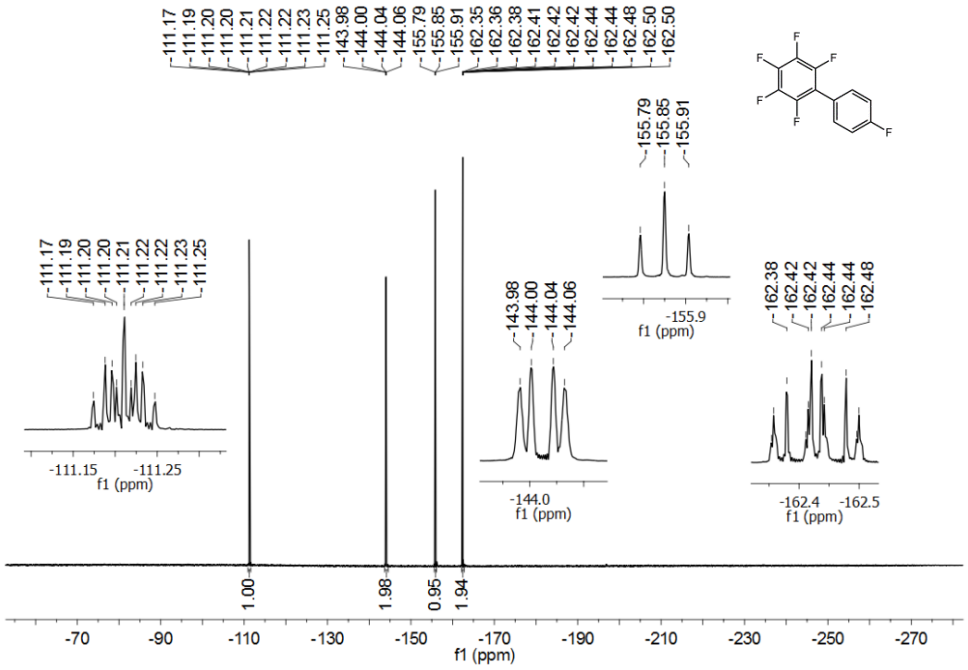

Figure 134. ^{19}F NMR spectrum of 2,3,4,5,6-pentafluoro-4′-(fluoro)biphenyl **65** in benzene-d_6 (*JDF file reference*: a8775gmp).

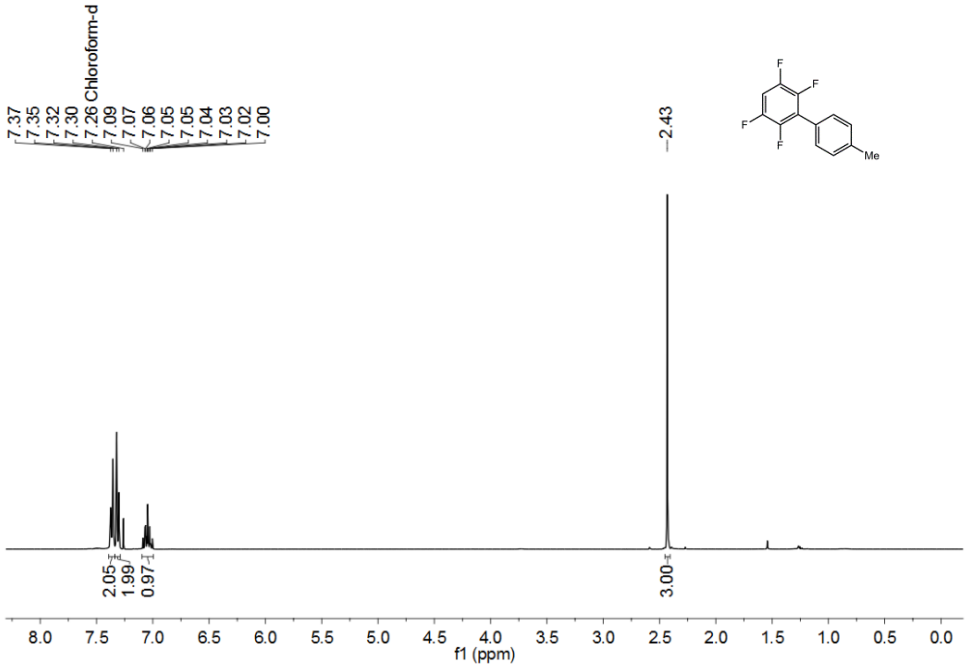

Figure 135. ^{1}H NMR spectrum of 2,3,5,6-tetrafluoro-4′-(methyl)biphenyl **70^{I}** in chloroform-d (*JDF file reference*: a8360gmp).

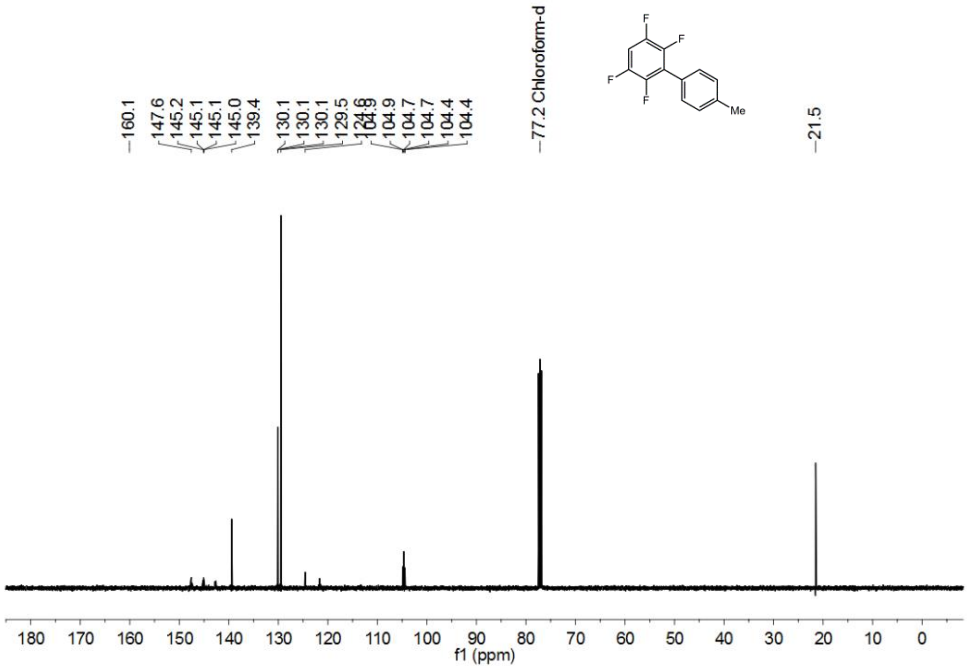

Figure 136. ^{13}C NMR spectrum of 2,3,5,6-tetrafluoro-4′-(methyl)biphenyl **70^{I}** in chloroform-d (*JDF file reference*: a8360gmp).

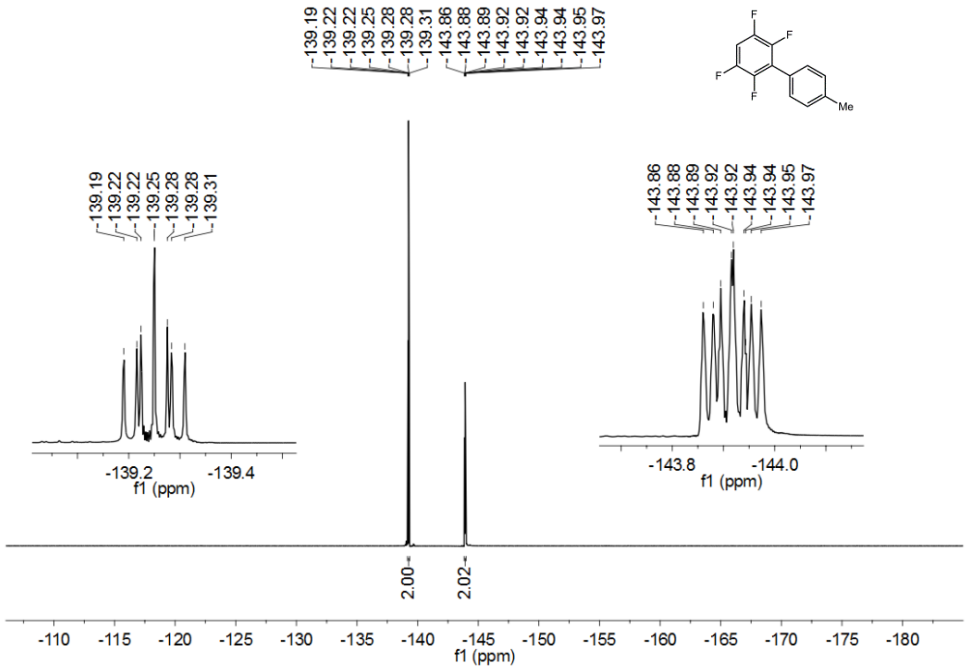

Figure 137. ^{19}F NMR spectrum of 2,3,5,6-tetrafluoro-4′-(methyl)biphenyl **70^{I}** in chloroform-d (*JDF file reference*: a8360gmp).

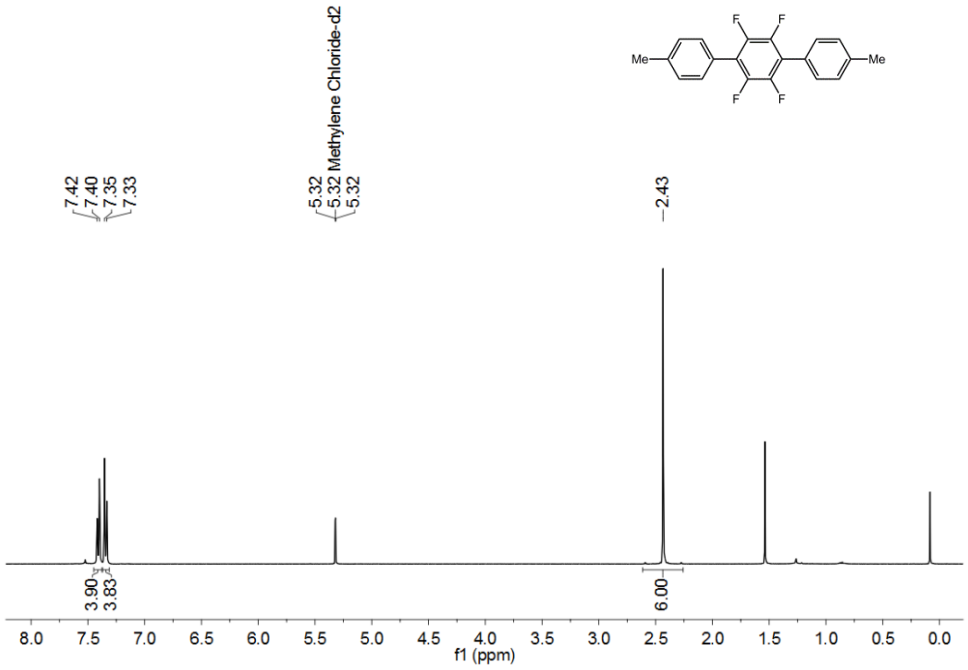

Figure 138. ^{1}H NMR spectrum of 1,4-di(4′,4″-tolyl)-2,3,5,6-tetrafluorobenzene **70^{II}** in methylene chloride-d_2 (*JDF file reference*: k3655gmp).

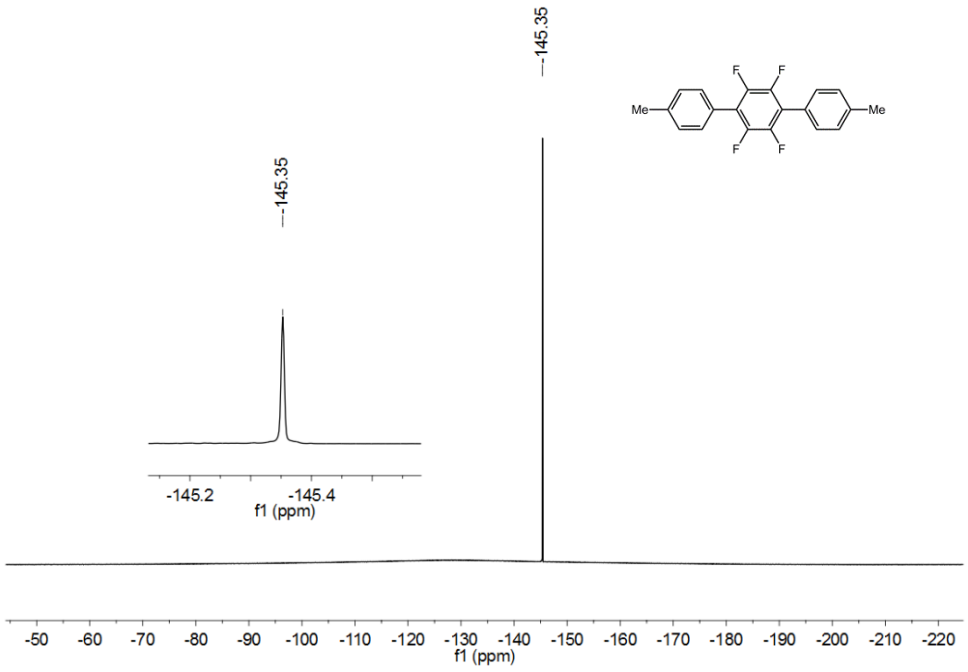

Figure 139. ^{19F}F NMR spectrum of 1,4-di(4′,4″-tolyl)-2,3,5,6-tetrafluorobenzene **70^{II}** in methylene chloride-d_2 (*JDF file reference*: k3655gmp).

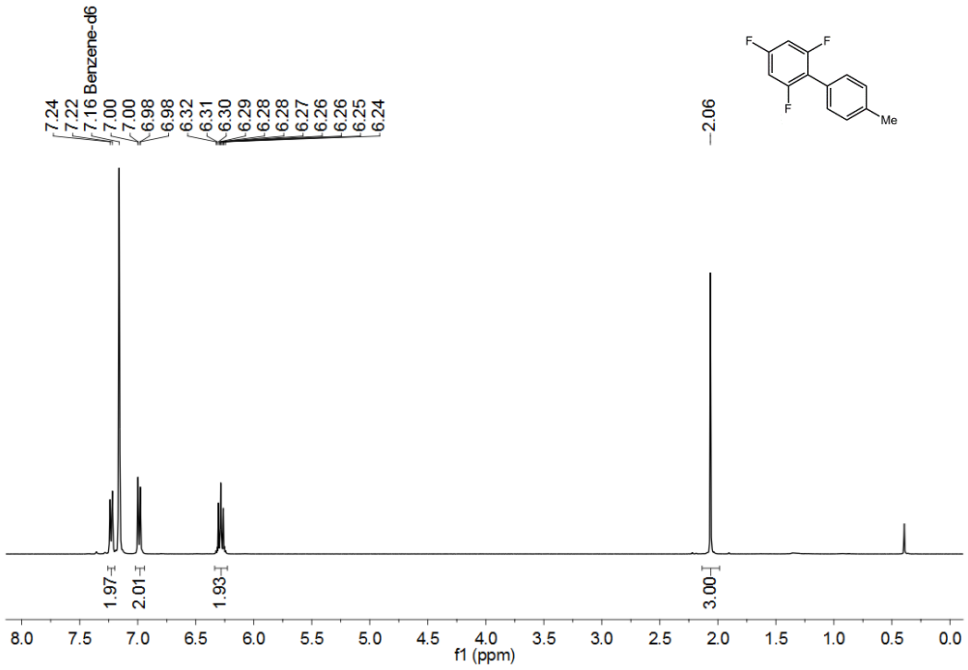

Figure 140. ^{1}H NMR spectrum of 2,4,6-trifluoro-4′-(methyl)biphenyl **71^{I}** in benzene-d_6 (*JDF file reference*: a8179gmp).

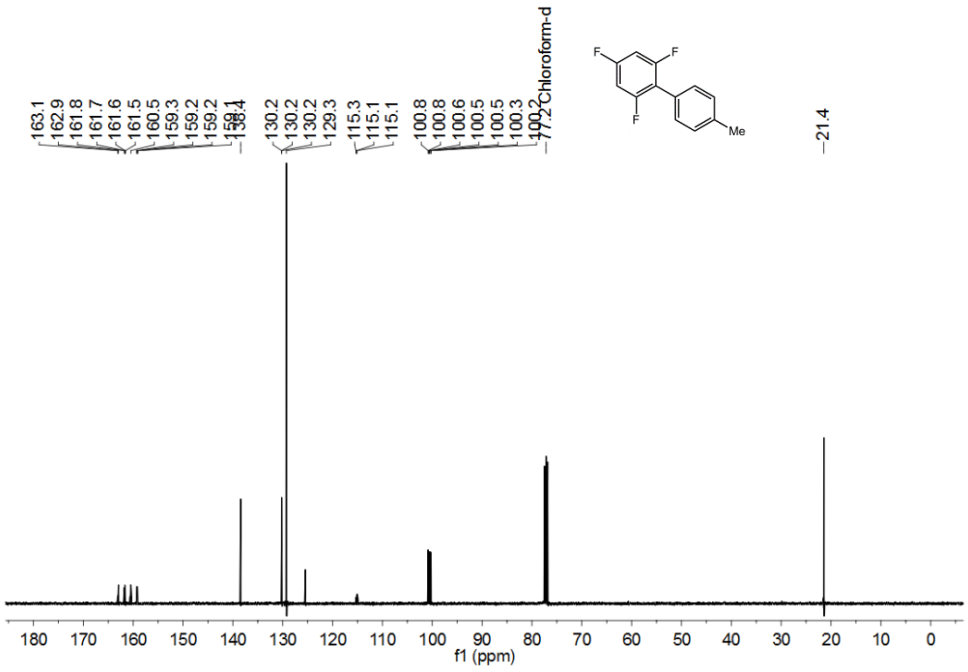

Figure 141. ^{13}C NMR spectrum of 2,4,6-trifluoro-4′-(methyl)biphenyl **71^{I}** in chloroform-d (*JDF file reference*: a8188gmp).

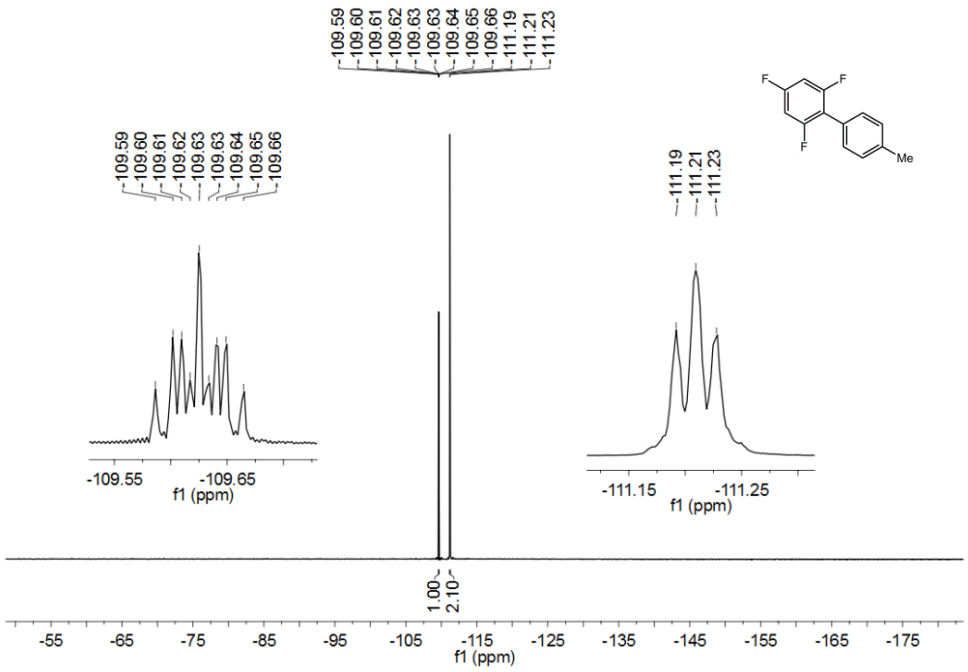

Figure 142. ^{19}F NMR spectrum of 2,4,6-trifluoro-4′-(methyl)biphenyl **71^{I}** in benzene-d$_6$ (*JDF file reference*: a8179gmp).

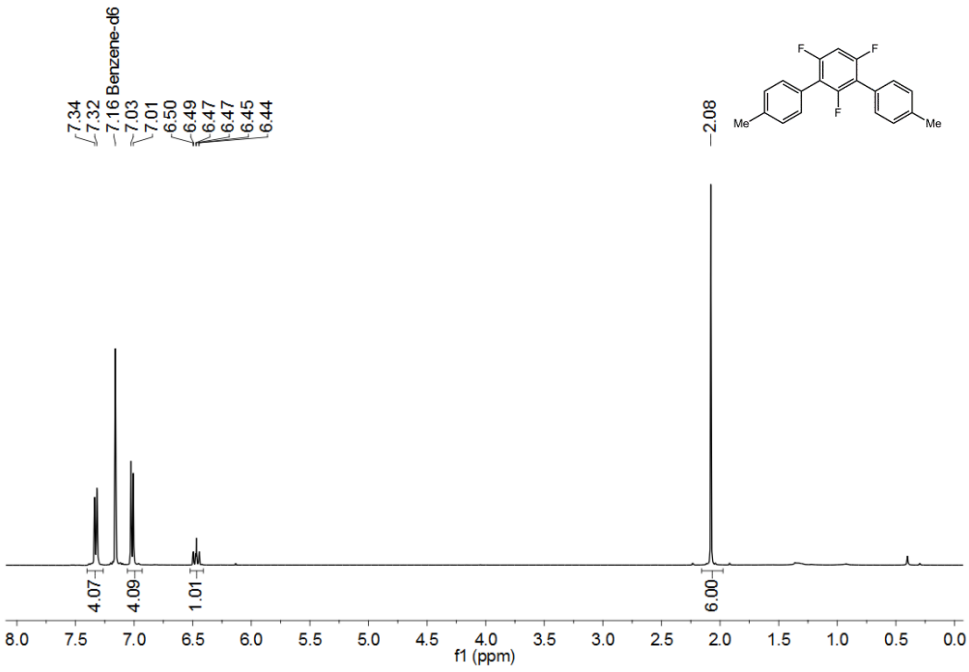

Figure 143. ^{1}H NMR spectrum of 1,3-di(4′,4″-tolyl)-2,4,6-trifluorobenzene **71^{II}** in benzene-d$_6$ (*JDF file reference*: a8788gmp).

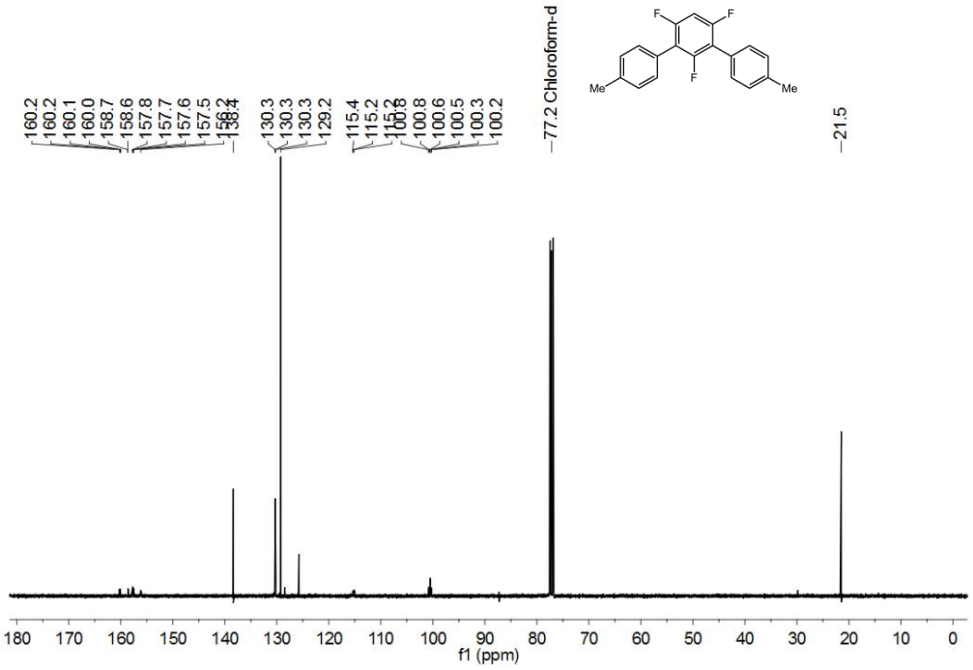

Figure 144. ^{13}C NMR spectrum of 1,3-di(4′,4″-tolyl)-2,4,6-trifluorobenzene **71^{II}** in chloroform-d (*JDF file reference*: a8771gmp).

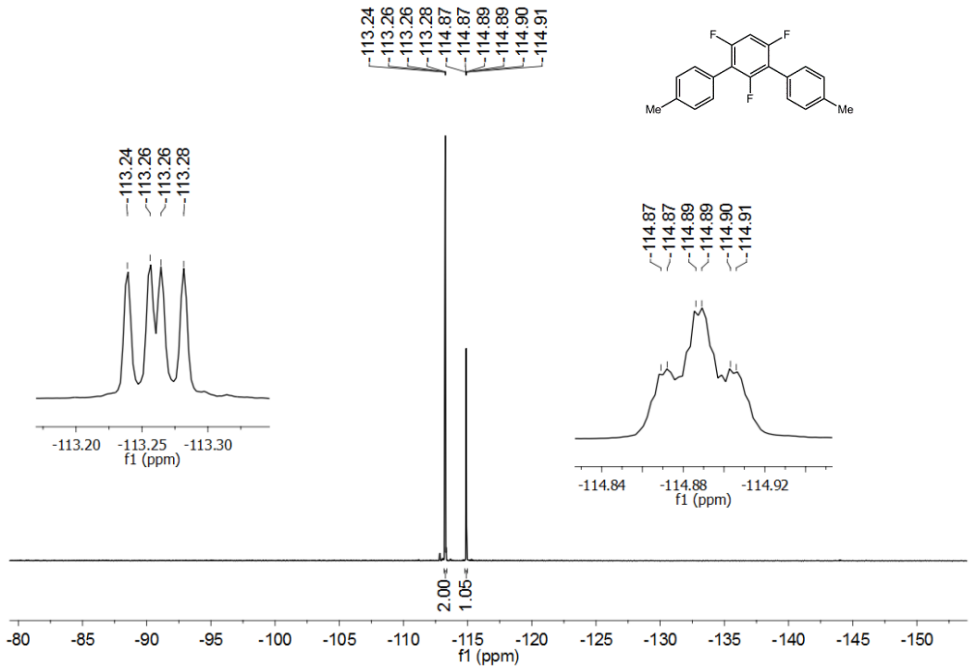

Figure 145. ^{19}F NMR spectrum of 1,3-di(4′,4″-tolyl)-2,4,6-trifluorobenzene **71^{II}** in benzene-d_6 (*JDF file reference*: a8788gmp).

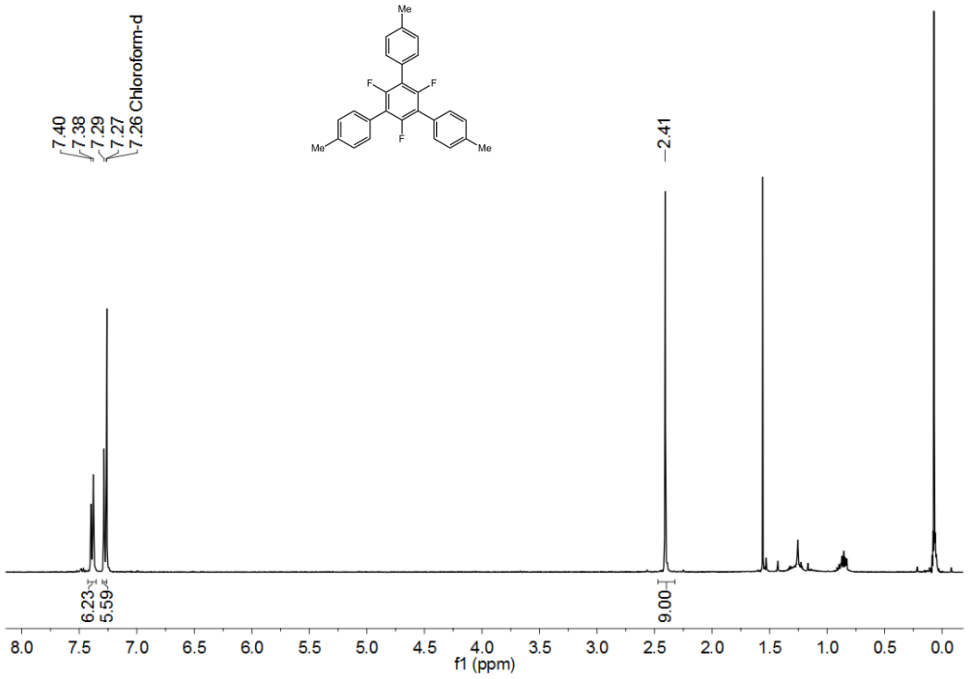

Figure 146. ^{1}H NMR spectrum of 1,3,5-tri(4′,4″,4‴-tolyl)-2,4,6-trifluorobenzene **71^{III}** in chloroform-d (*JDF file reference*: k3762gmp).

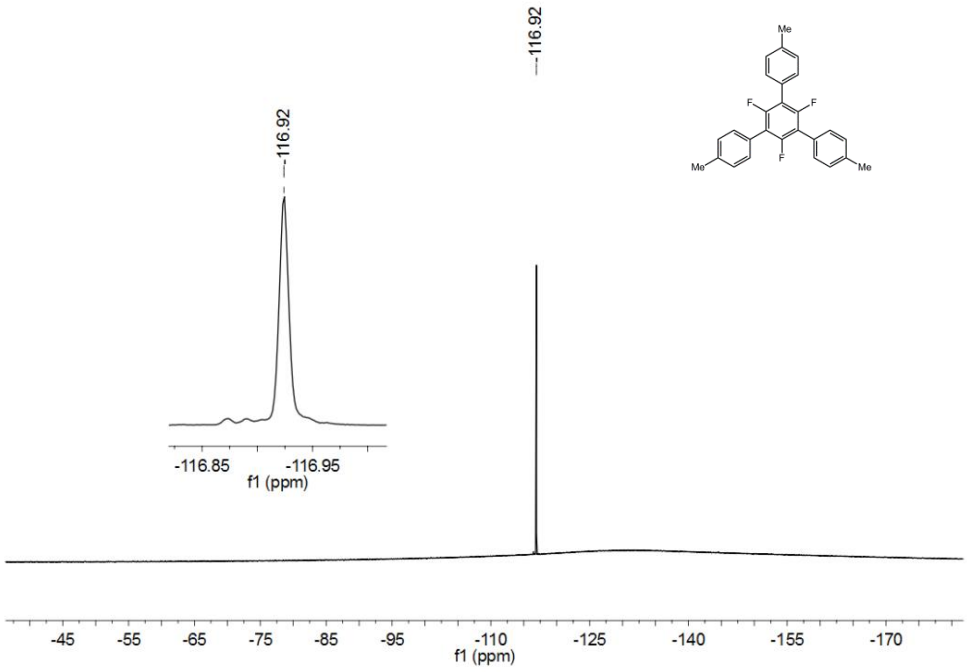

Figure 147. ^{19}F NMR spectrum of 1,3,5-tri(4′,4″,4‴-tolyl)-2,4,6-trifluorobenzene **71^{III}** in chloroform-d (*JDF file reference*: k3762gmp).

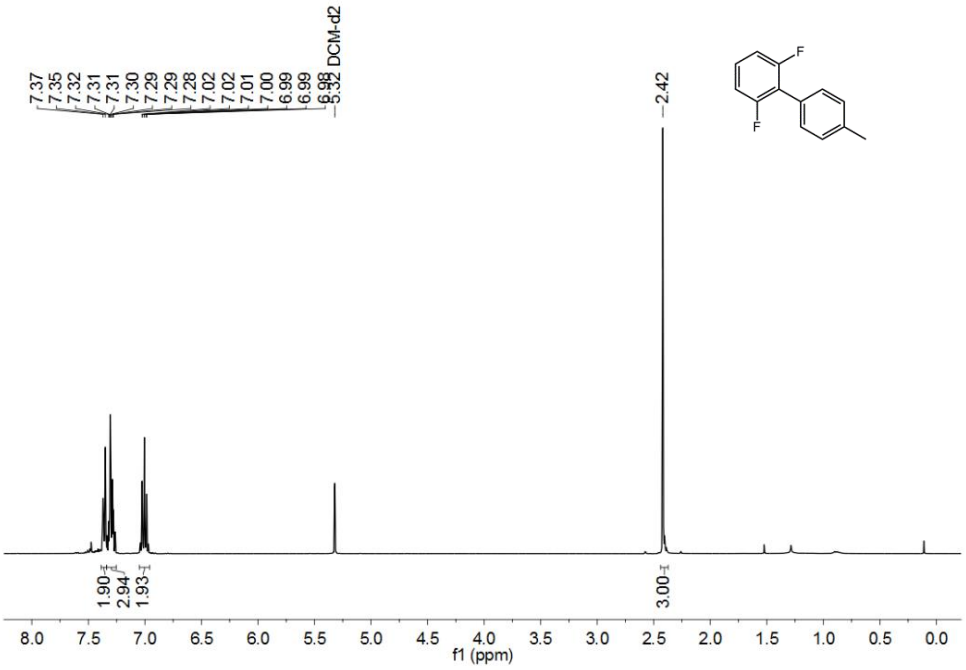

Figure 148. ^{1}H NMR spectrum of 2,6-difluoro-4′-(methyl)biphenyl **28** in methylene chloride-d_2 (*JDF file reference*: a8906gmp).

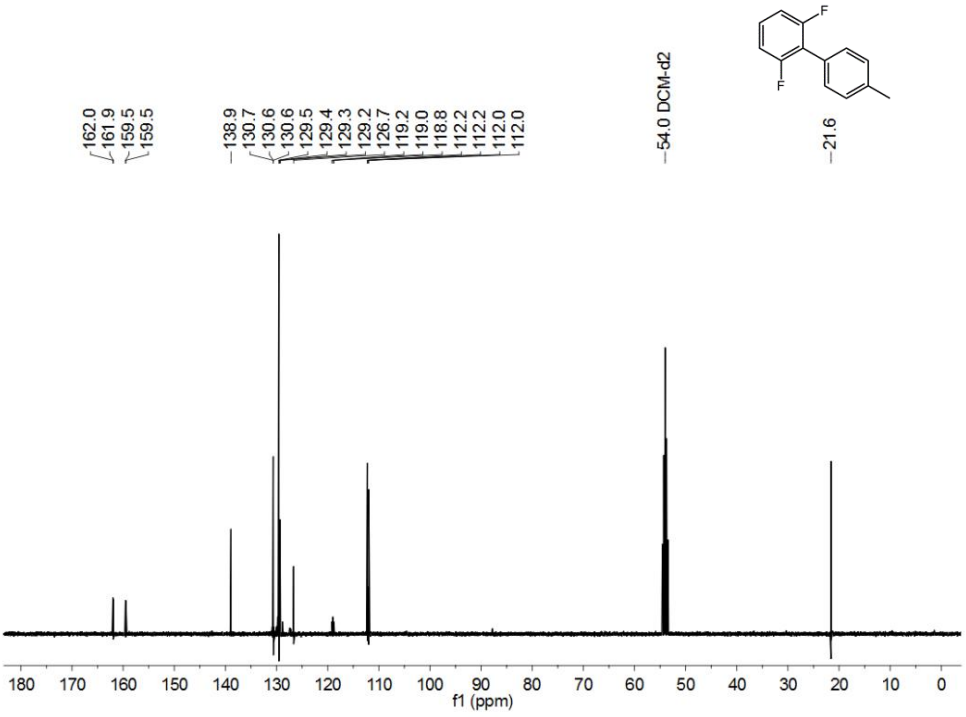

Figure 149. ^{13}C NMR spectrum of 2,6-difluoro-4′-(methyl)biphenyl **28** in methylene chloride-d_2 (*JDF file reference*: a8906gmp).

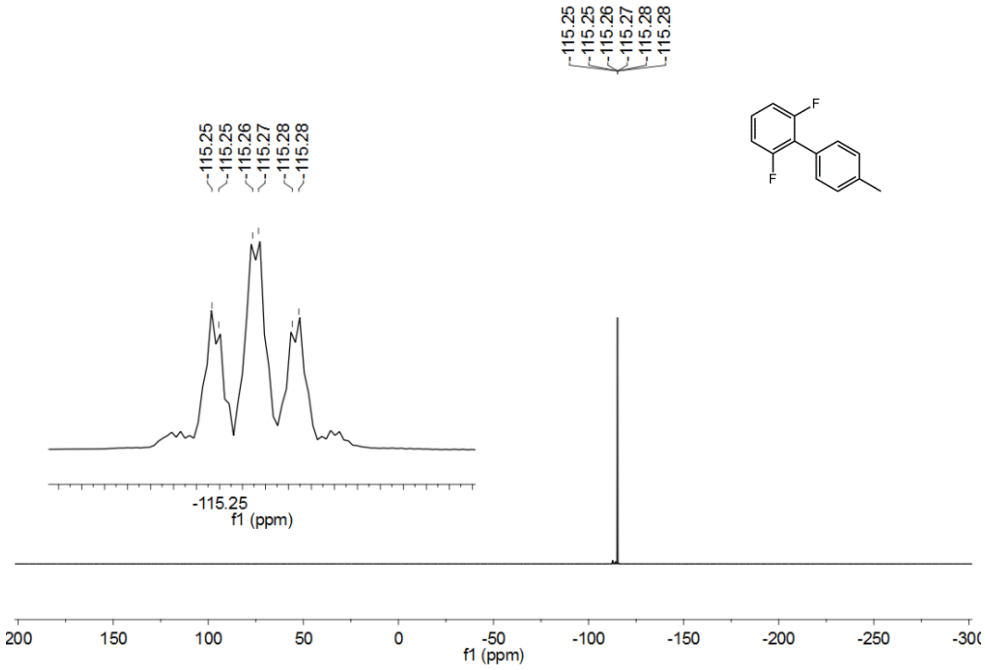

Figure 150. ^{19}F NMR spectrum of 2,6-difluoro-4′-(methyl)biphenyl **28** in methylene chloride-d_2 (*JDF file reference*: a8906gmp).

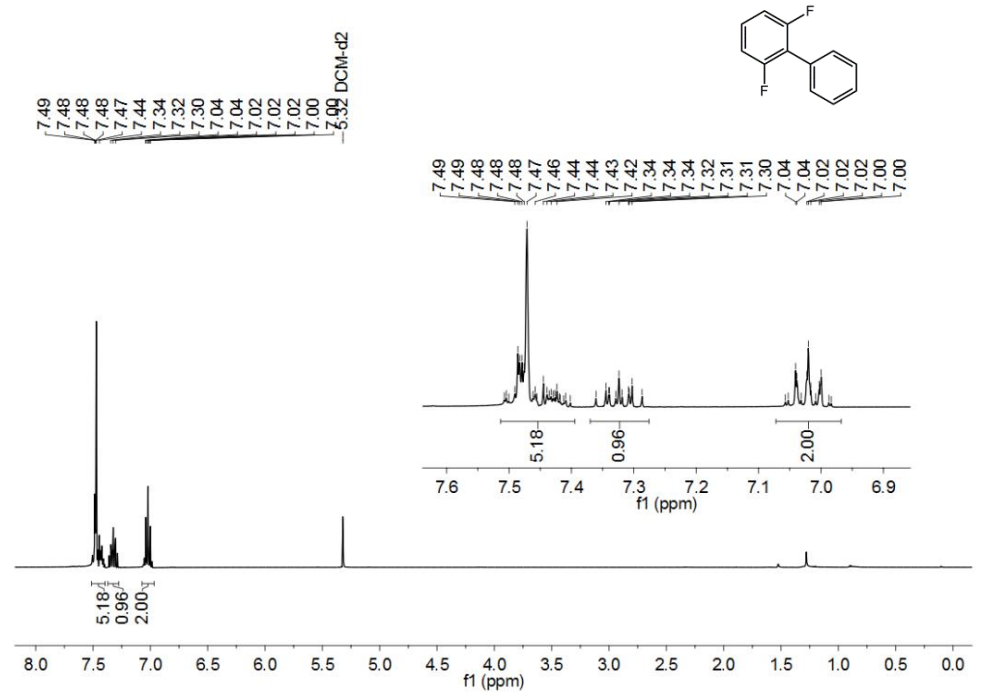

Figure 151. ^{1}H NMR spectrum of 2,6-(difluoro)biphenyl **30** in methylene chloride-d_2 (*JDF file reference*: a8908gmp).

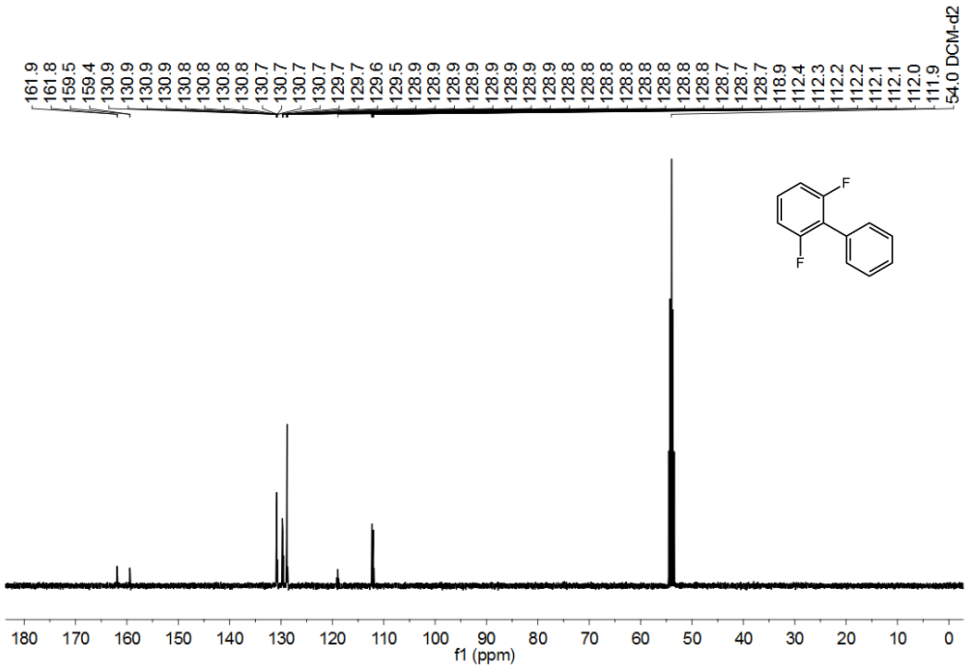

Figure 152. ^{13}C NMR spectrum of 2,6-(difluoro)biphenyl **30** in methylene chloride-d_2 (*JDF file reference*: a8908gmp).

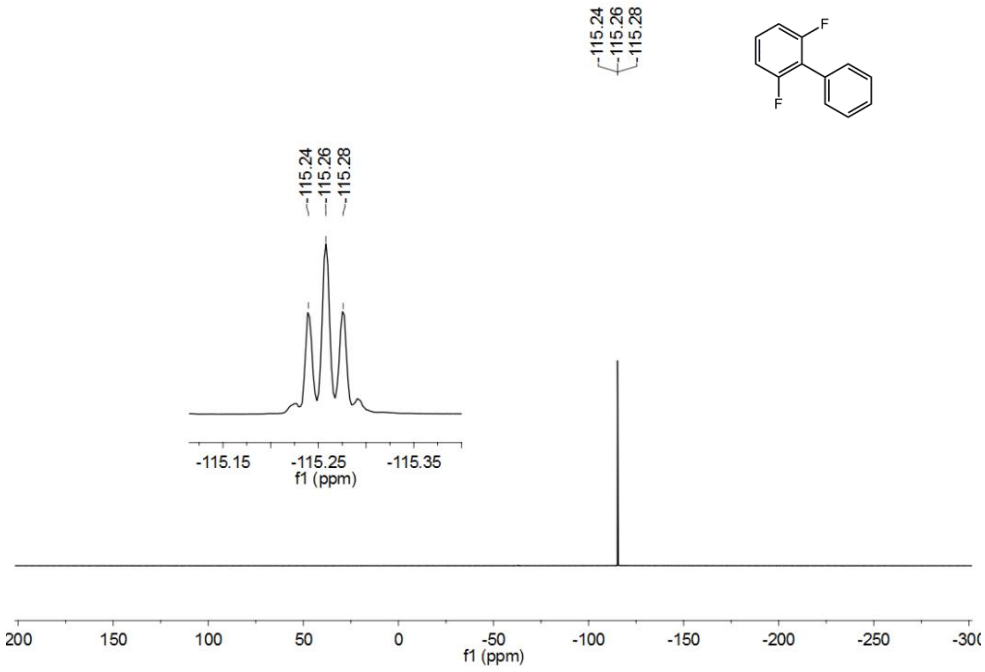

Figure 153. ^{19}F NMR spectrum of 2,6-(difluoro)biphenyl **30** in methylene chloride-d_2 (*JDF file reference*: a8908gmp).

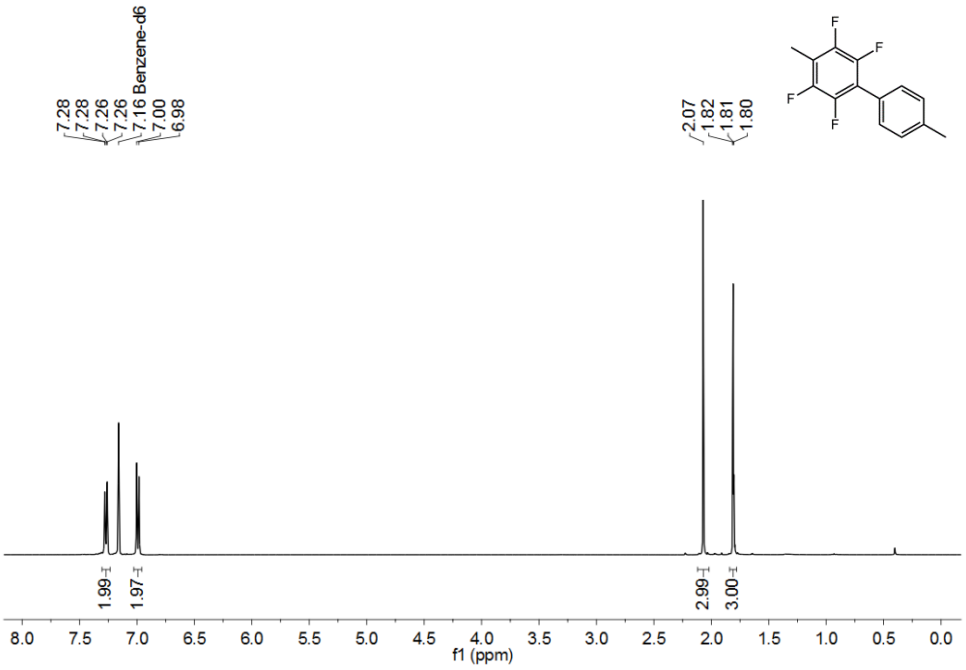

Figure 154. ^{1}H NMR spectrum of 2,3,5,6-tetrafluoro-4,4′-(dimethyl)biphenyl **78** in benzene-d_6 (*JDF file reference*: a8362gmp).

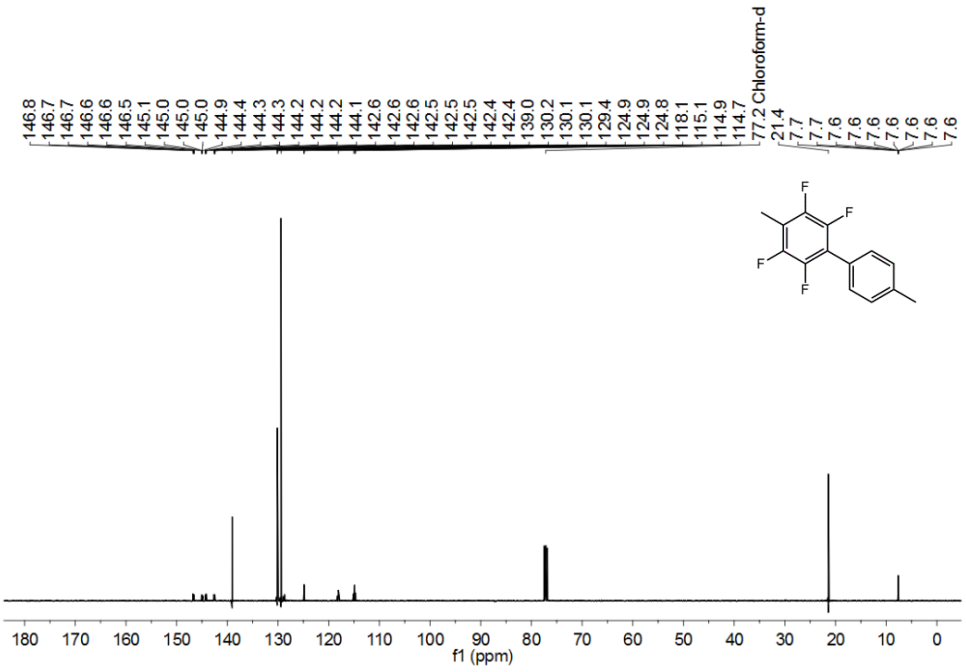

Figure 155. ^{13}C NMR spectrum of 2,3,5,6-tetrafluoro-4,4′-(dimethyl)biphenyl **78** in chloroform-d (*JDF file reference*: a8361gmp).

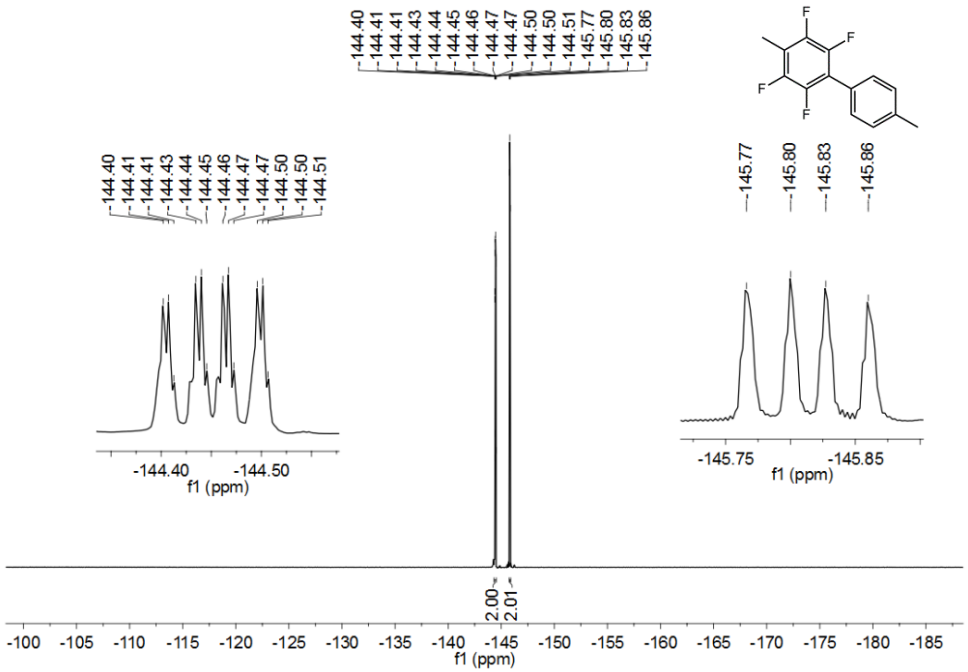

Figure 156. ^{19}F NMR spectrum of 2,3,5,6-tetrafluoro-4,4′-(dimethyl)biphenyl **78** in benzene-d_6 (*JDF file reference*: a8362gmp).

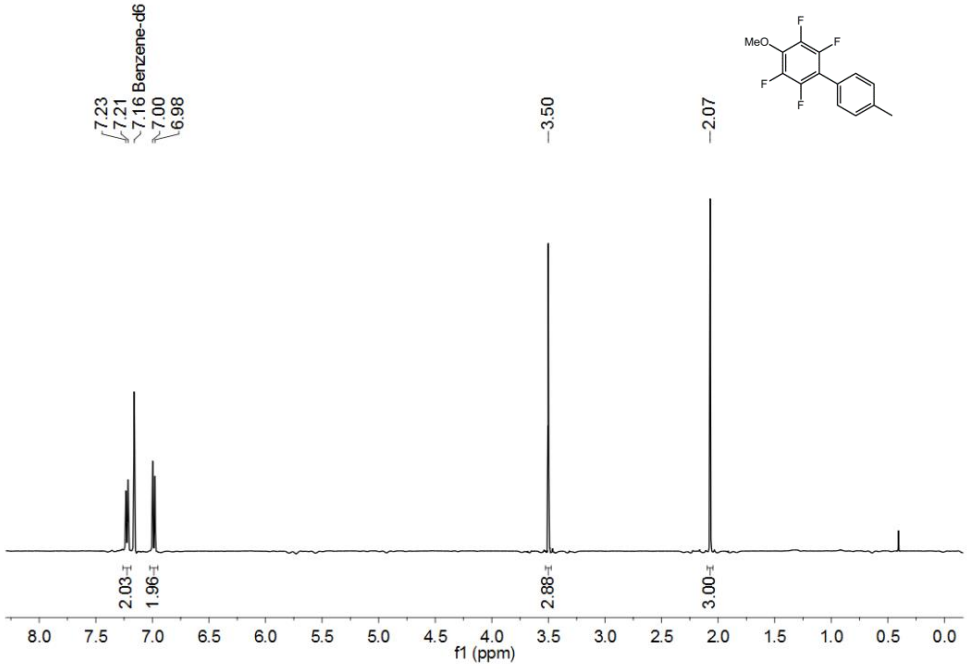

Figure 157. ^{1}H NMR spectrum of 2,3,5,6-tetrafluoromethoxy-4′-(methyl)biphenyl **77** in benzene-d_6 (*JDF file reference*: a8363gmp).

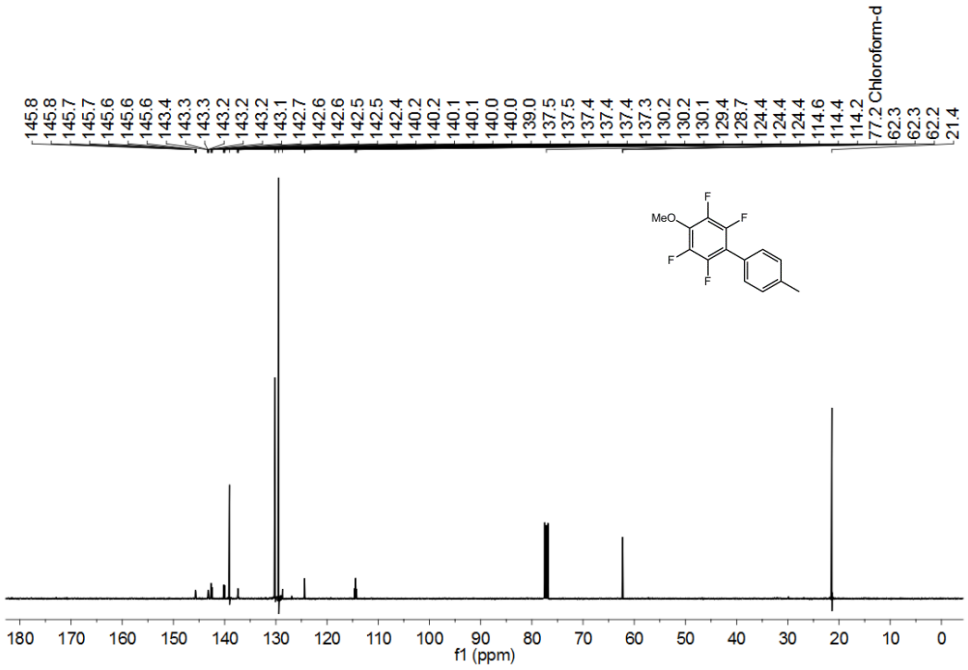

Figure 158. ^{13}C NMR spectrum of 2,3,5,6-tetrafluoromethoxy-4′-(methyl)biphenyl **77** in chloroform-d (*JDF file reference*: a8364gmp).

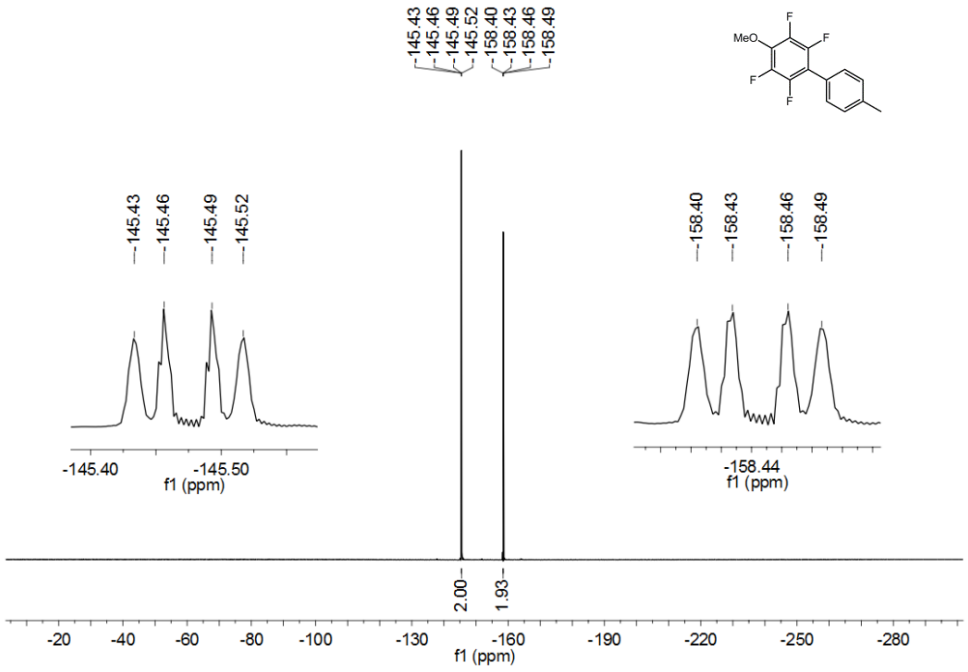

Figure 159. ^{19}F NMR spectrum of 2,3,5,6-tetrafluoromethoxy-4′-(methyl)biphenyl **77** in benzene-d_6 (*JDF file reference*: a8363gmp).

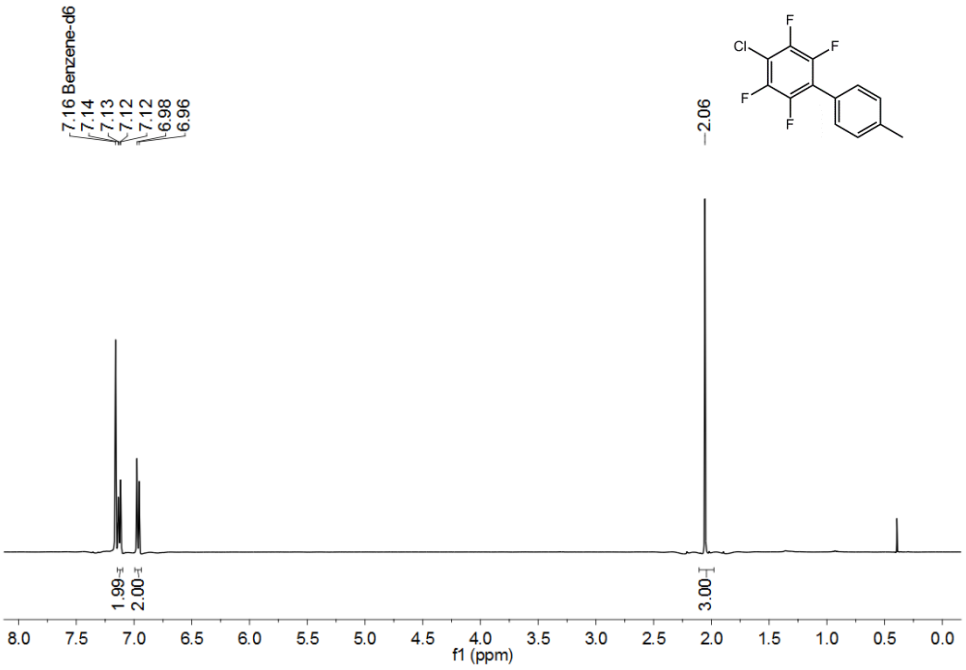

Figure 160. ^{1}H NMR spectrum of 2,3,5,6-tetrafluorochloro-4′-(methyl)biphenyl **79** in benzene-d_6 (*JDF file reference*: a8372gmp).

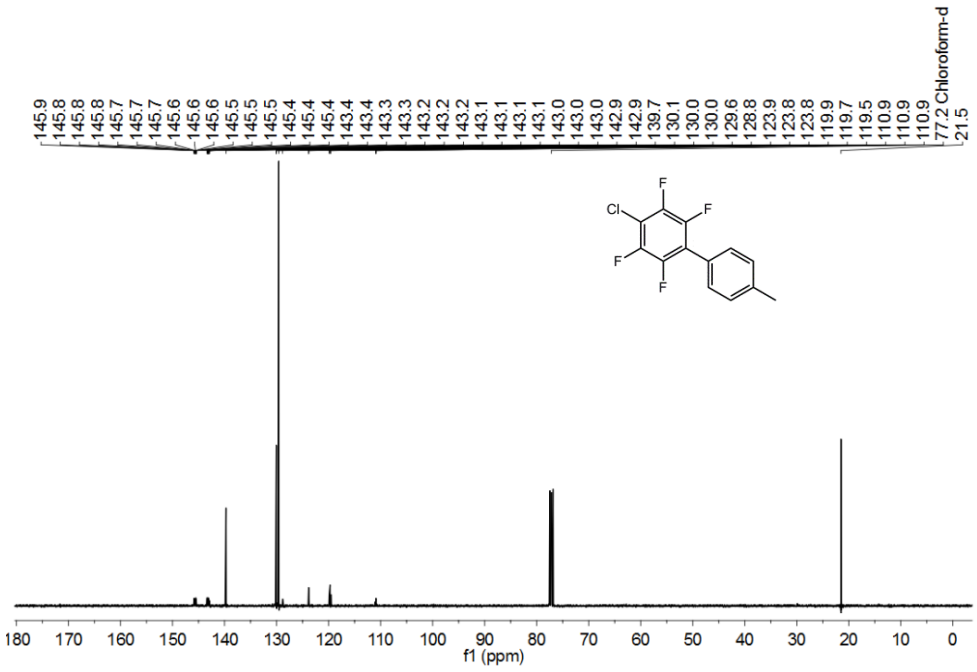

Figure 161. ^{13}C NMR spectrum of 2,3,5,6-tetrafluorochloro-4′-(methyl)biphenyl **79** in chloroform-d (*JDF file reference*: a8367gmp).

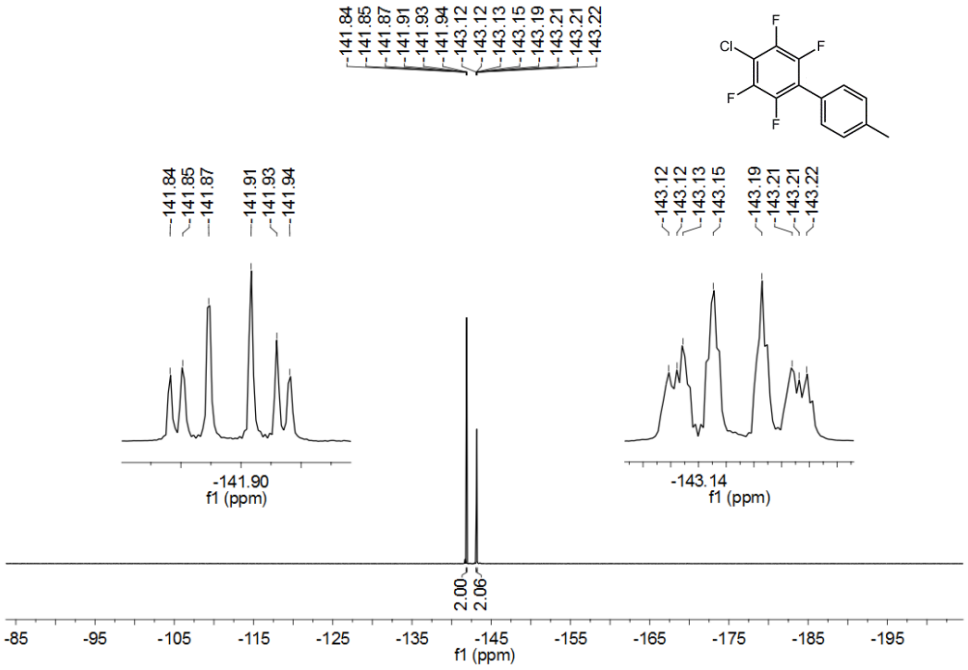

Figure 162. ^{19}F NMR spectrum of 2,3,5,6-tetrafluorochloro-4′-(methyl)biphenyl **79** in benzene-d_6 (*JDF file reference*: a8372gmp).

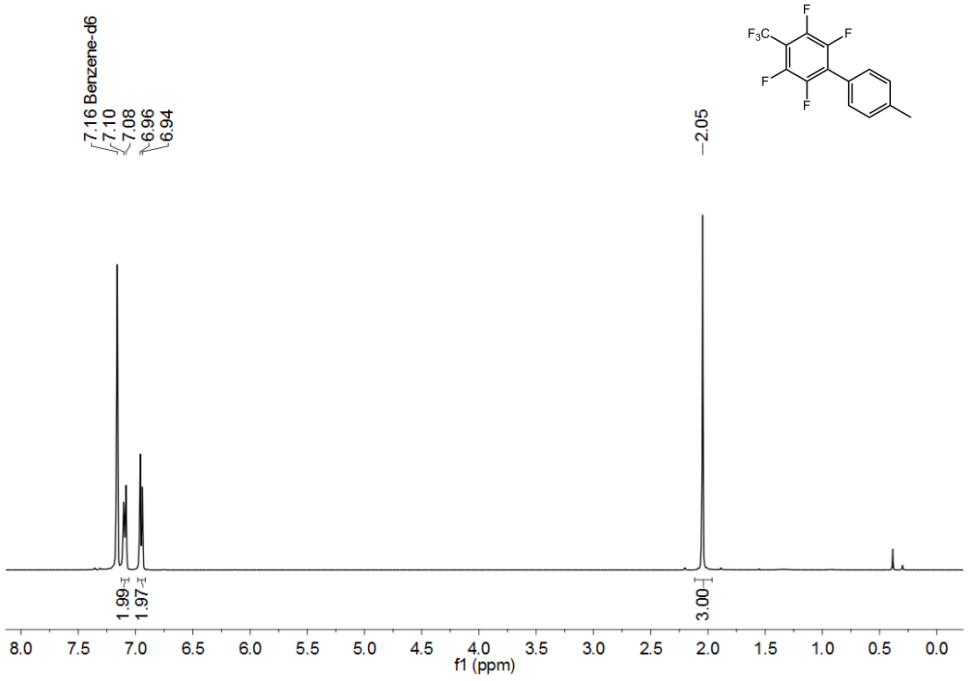

Figure 163. ^{1}H NMR spectrum of 2,3,5,6-tetrafluoro(trifluoromethyl)-4′-(methyl)biphenyl **80** in benzene-d_6 (*JDF file reference*: a8358gmp).

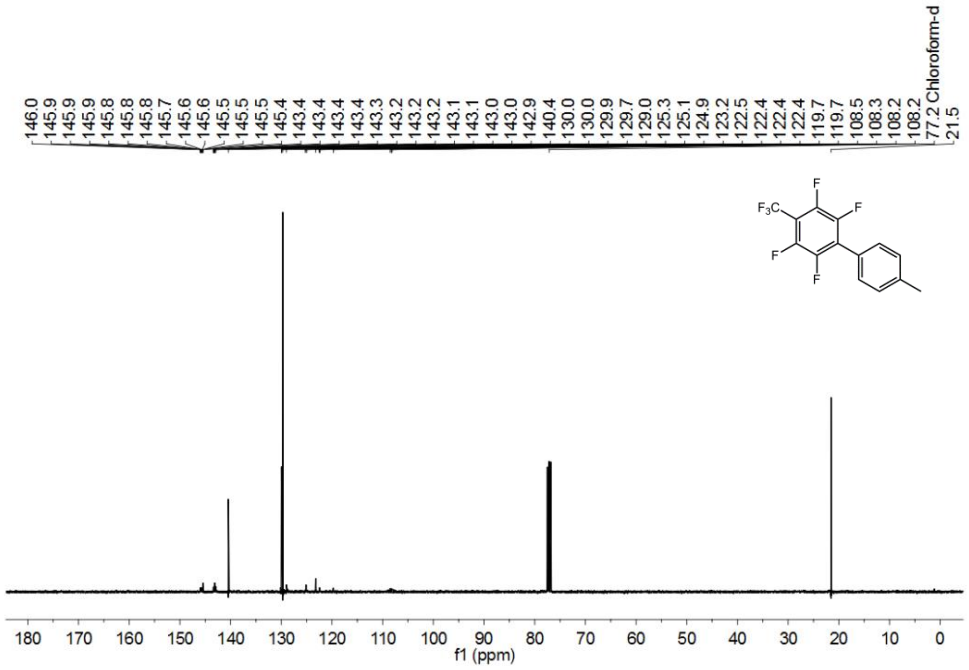

Figure 164. ^{13}C NMR spectrum of 2,3,5,6-tetrafluoro(trifluoromethyl)-4′-(methyl)biphenyl **80** in chloroform-d (*JDF file reference*: a8357gmp).

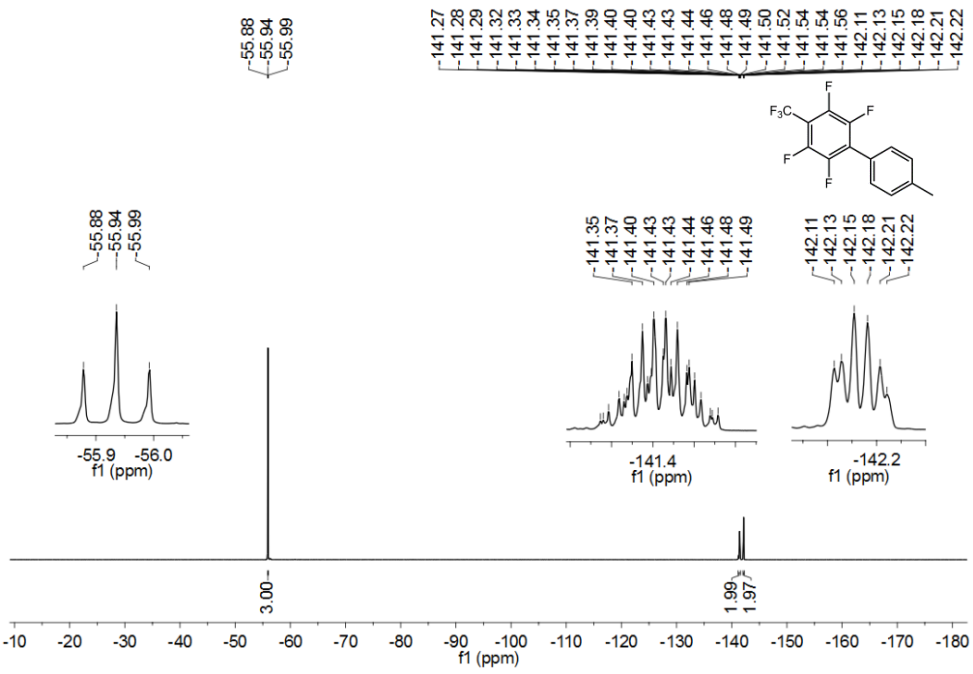

Figure 165. ^{19}F NMR spectrum of 2,3,5,6-tetrafluoro(trifluoromethyl)-4′-(methyl)biphenyl **80** in benzene-d_6 (*JDF file reference*: a8358gmp).

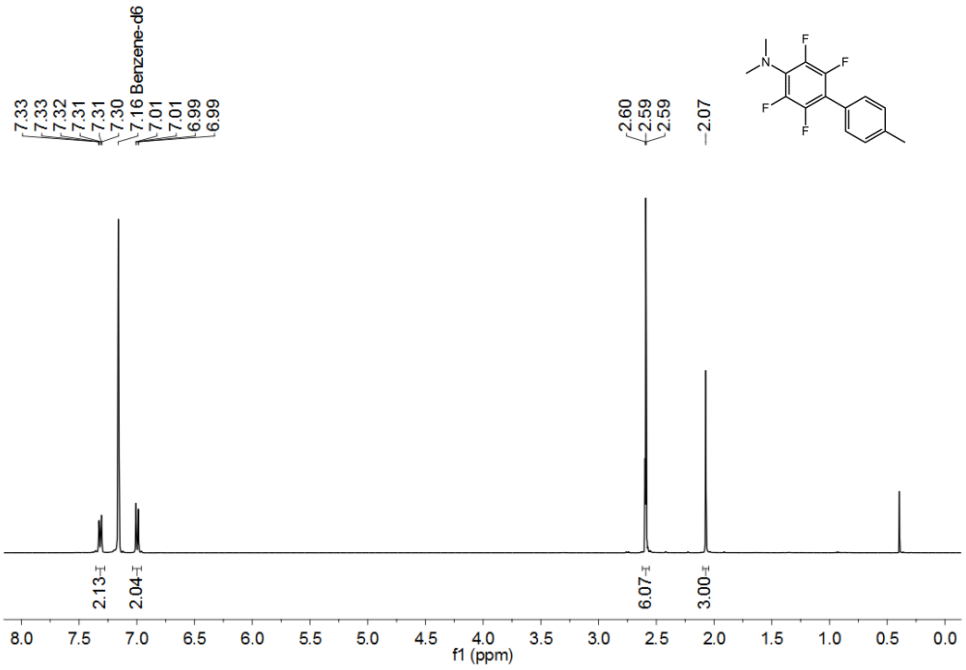

Figure 166. ^{1}H NMR spectrum of 2,3,5,6-tetrafluoro(dimethylamino)-4′-(methyl)biphenyl **76** in benzene-d_6 (*JDF file reference*: a8371gmp).

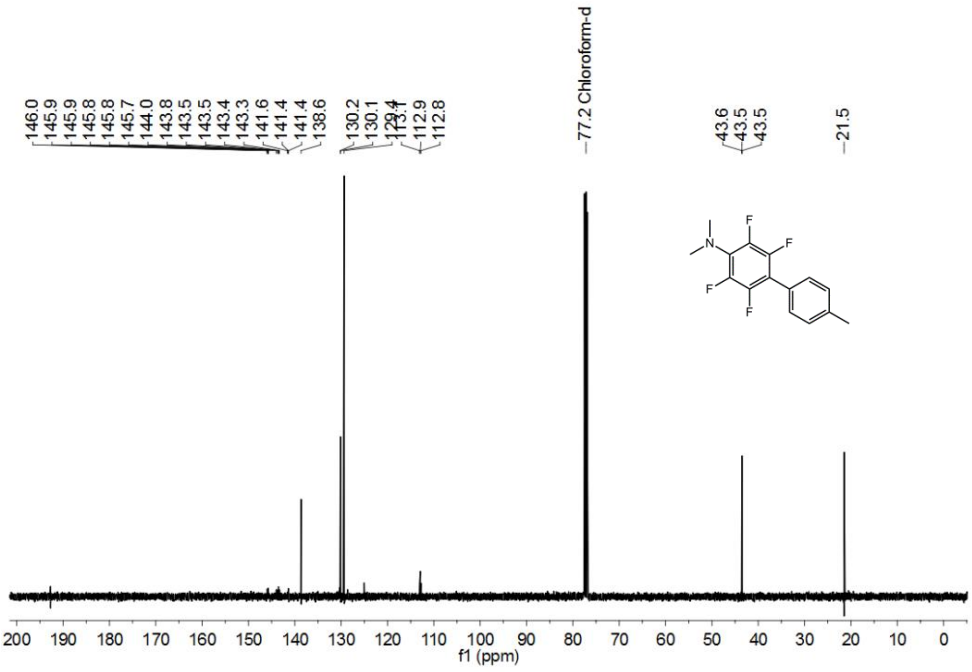

Figure 167. ^{13}C NMR spectrum of 2,3,5,6-tetrafluoro(dimethylamino)-4′-(methyl)biphenyl **76** in chloroform-d (*JDF file reference*: a8370gmp).

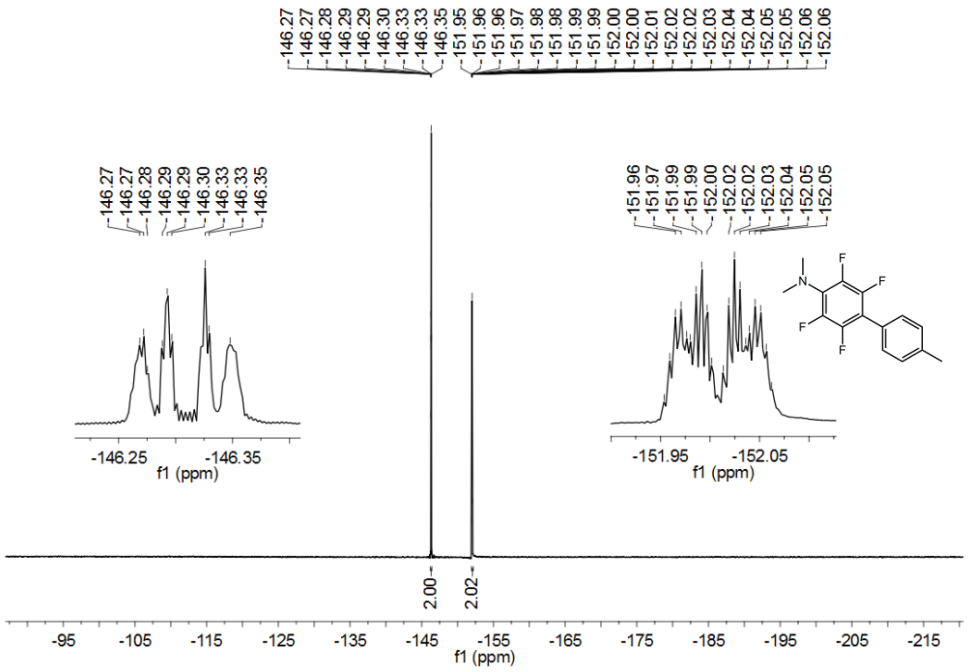

Figure 168. ^{19}F NMR spectrum of 2,3,5,6-tetrafluoro(dimethylamino)-4′-(methyl)biphenyl **76** in benzene-d_6 (*JDF file reference*: a8371gmp).

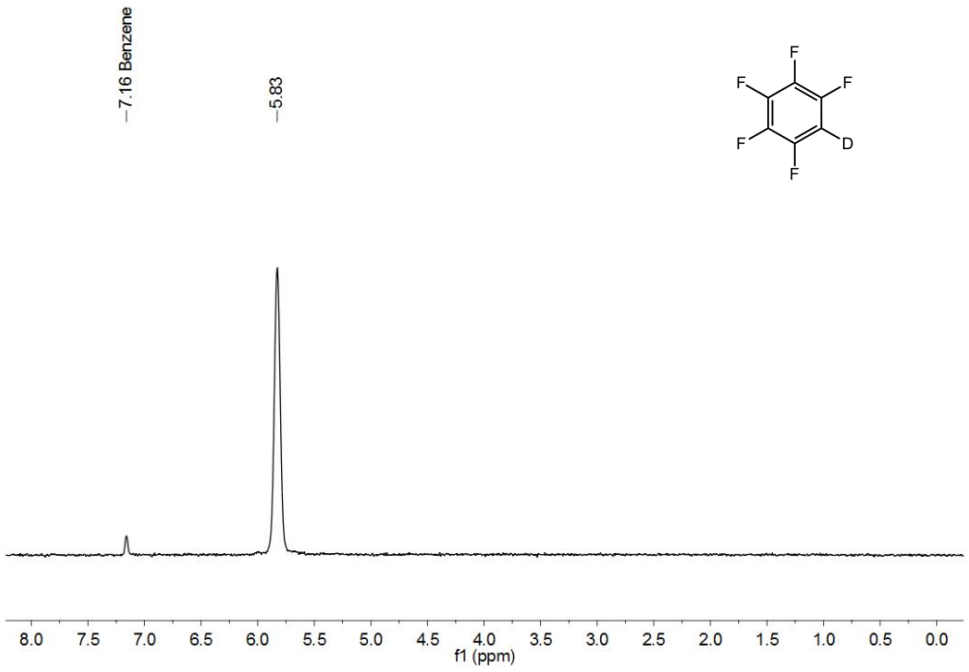

Figure 169. ^{2}H NMR spectrum of deuteropentafluorobenzene **100** in benzene (spectrum collected on AV500, saved as 1 under folder GMHP-4-254-P3).

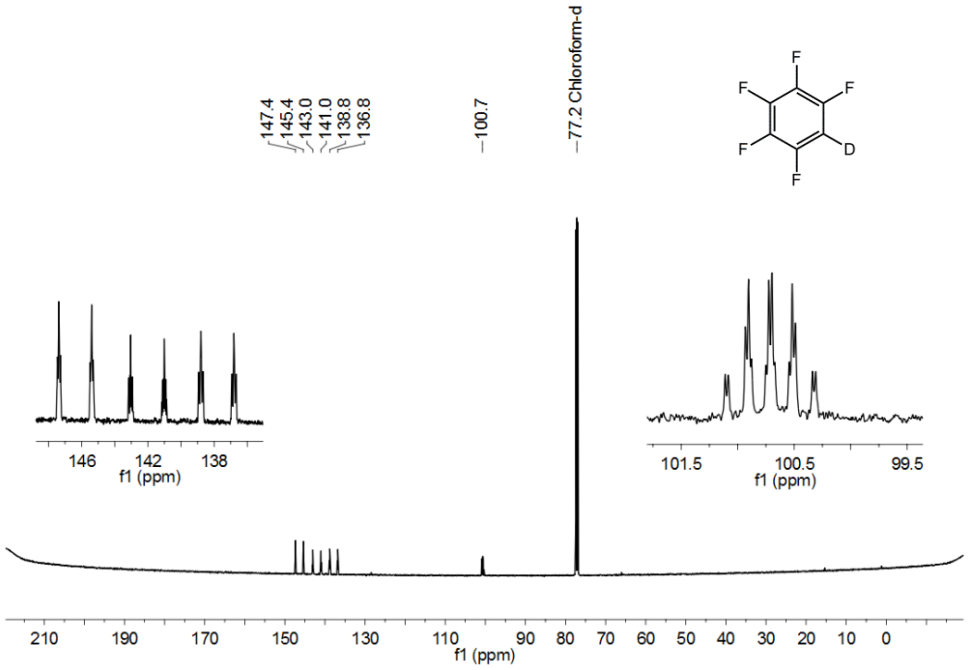

Figure 170. ^{13}C NMR spectrum of deuteropentafluorobenzene **100** in chloroform-d (spectrum collected on AV500, saved as 3 under folder GMHP-4-254-P4).

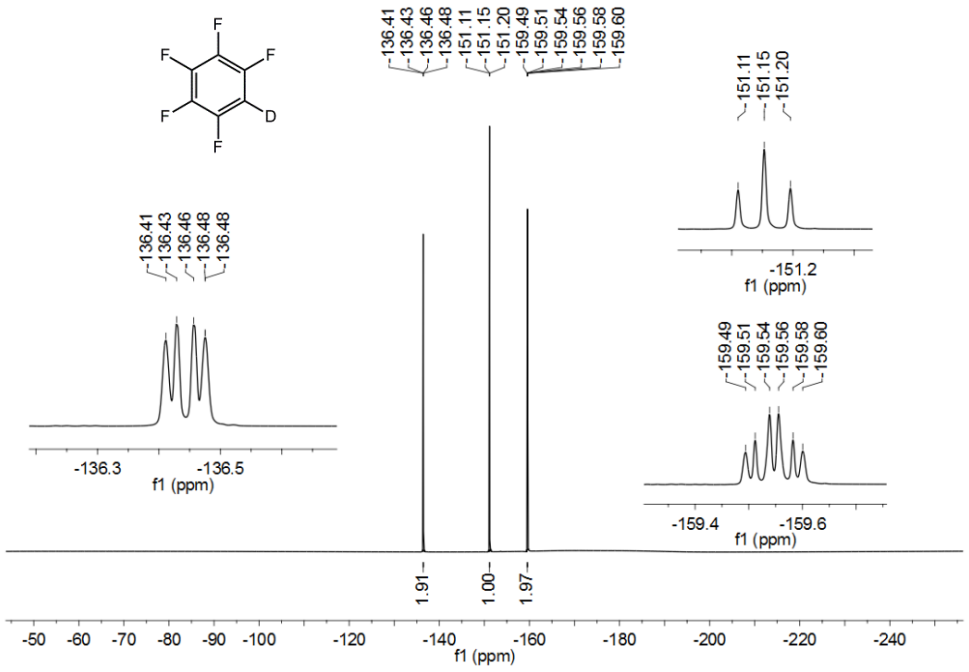

Figure 171. ^{19}F NMR spectrum of deuteropentafluorobenzene **100** in chloroform-d (spectrum collected on AV500, saved as 3 under folder GMHP-6-341-P).

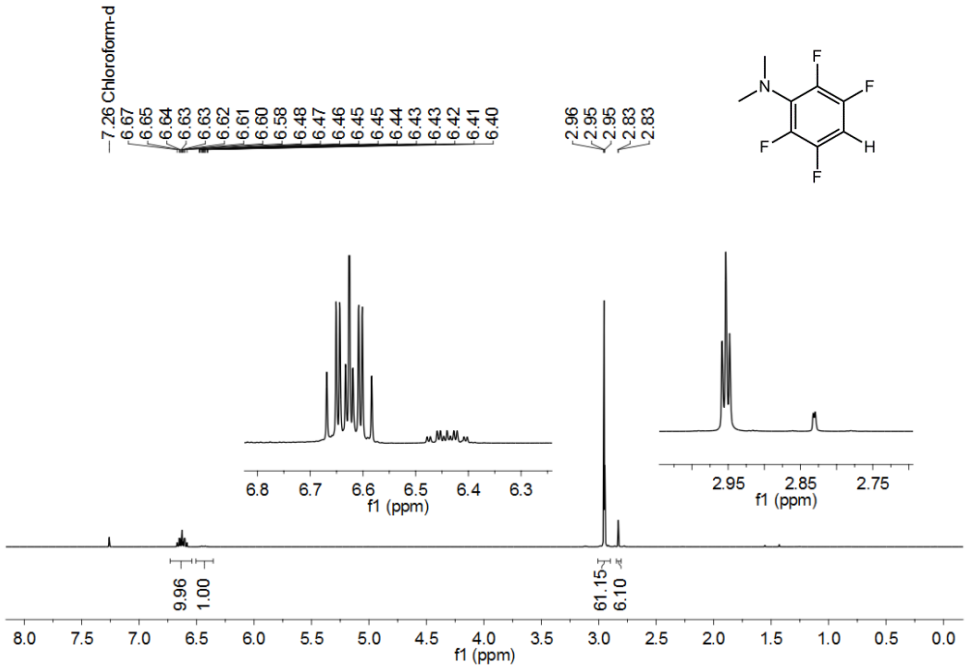

Figure 172. ^{1}H NMR spectrum of 2,3,5,6-tetrafluoro-*N*,*N*-dimethylaniline **121** in chloroform-d (*JDF file reference*: a8713gmp).

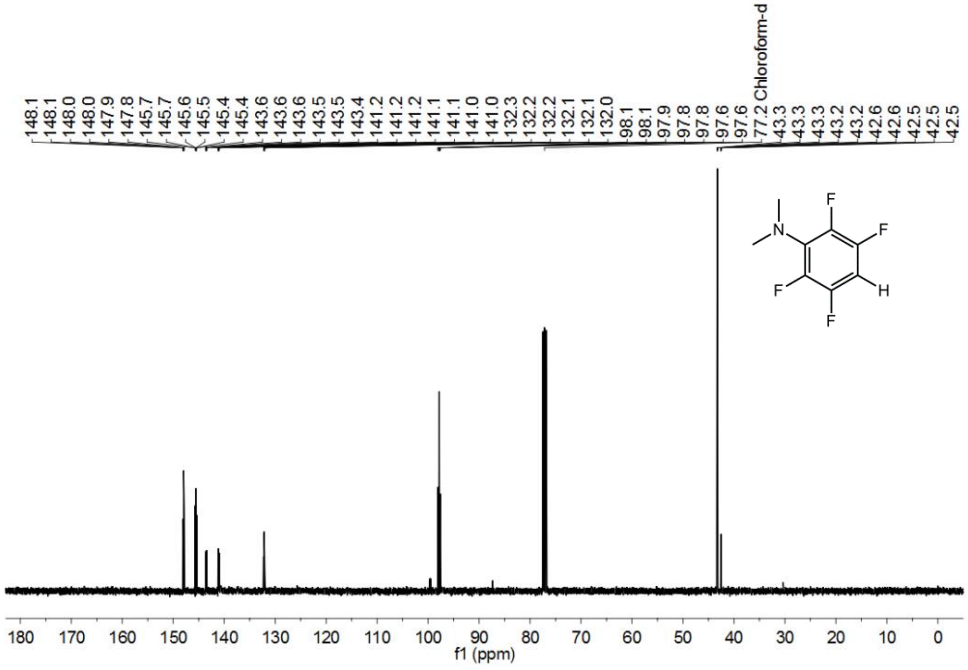

Figure 173. ^{13}C NMR spectrum of 2,3,5,6-tetrafluoro-*N*,*N*-dimethylaniline **121** in chloroform-d (*JDF file reference*: a8714gmp).

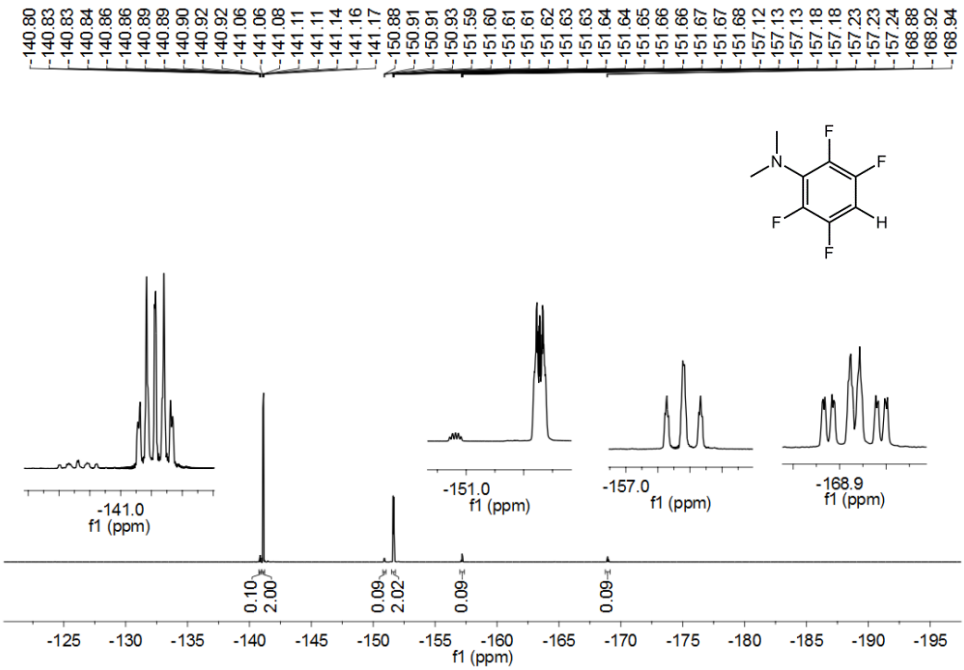

Figure 174. ^{19}F NMR spectrum of 2,3,5,6-tetrafluoro-*N*,*N*-dimethylaniline **121** in chloroform-d (*JDF file reference*: a8713gmp).

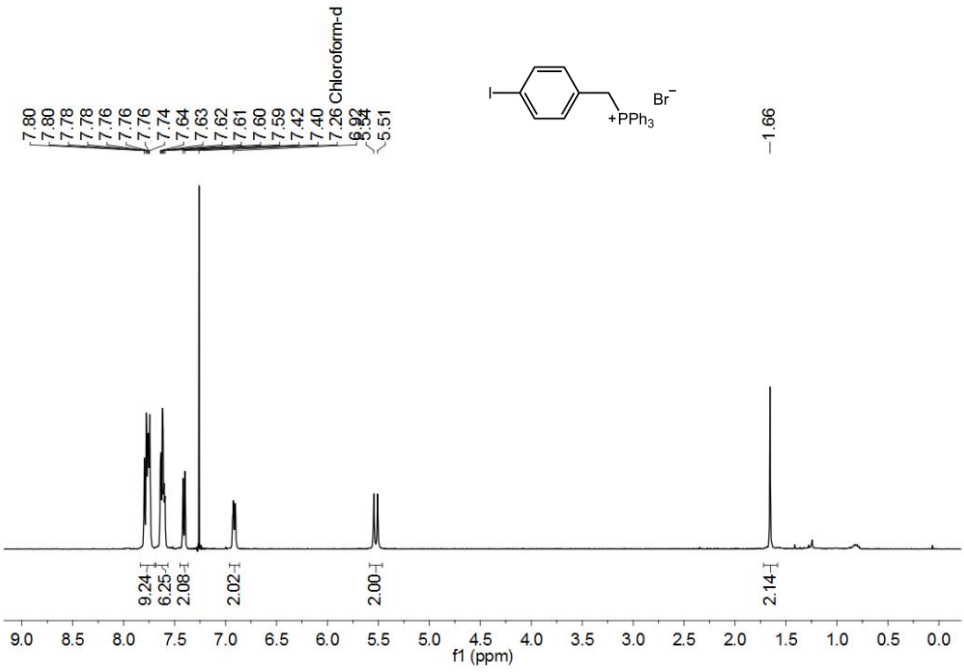

Figure 175. ^{1}H NMR spectrum of 4-iodobenzyltriphenylphosphonium bromide **122** in chloroform-d (*JDF file reference*: r2499gmp).

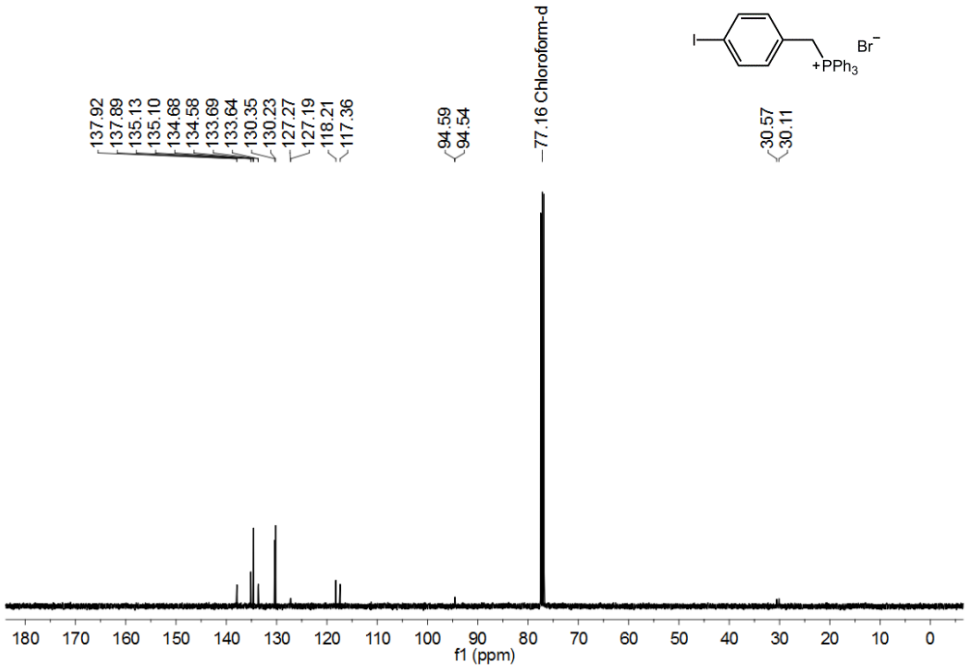

Figure 176. ^{13}C NMR spectrum of 4-iodobenzyltriphenylphosphonium bromide **122** in chloroform-d (*JDF file reference*: r2636gmp).

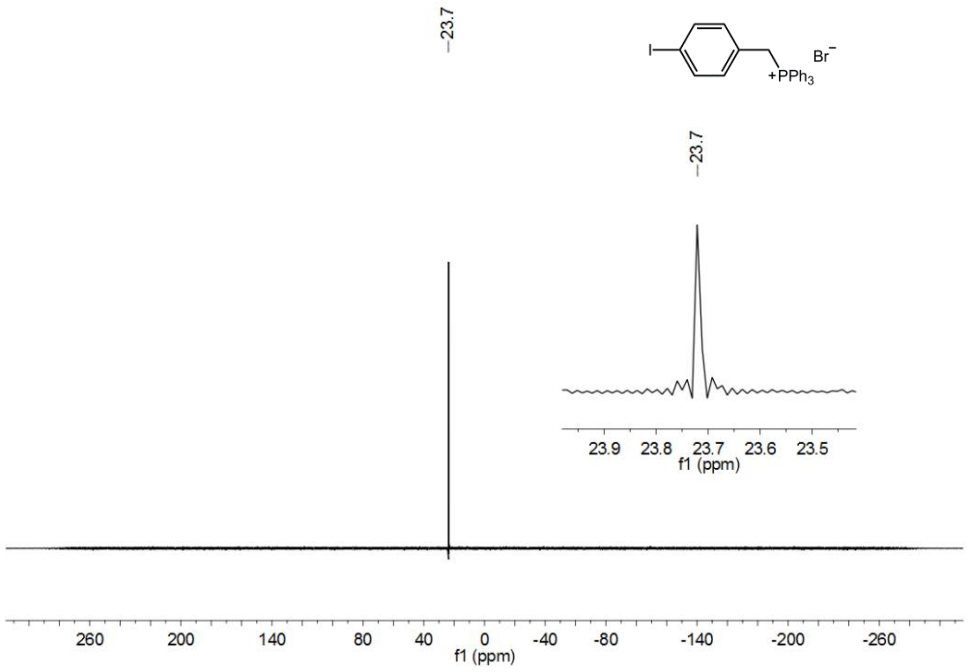

Figure 177. ^{31}P NMR spectrum of 4-iodobenzyltriphenylphosphonium bromide **122** in chloroform-d (*JDF file reference*: r2499gmp).

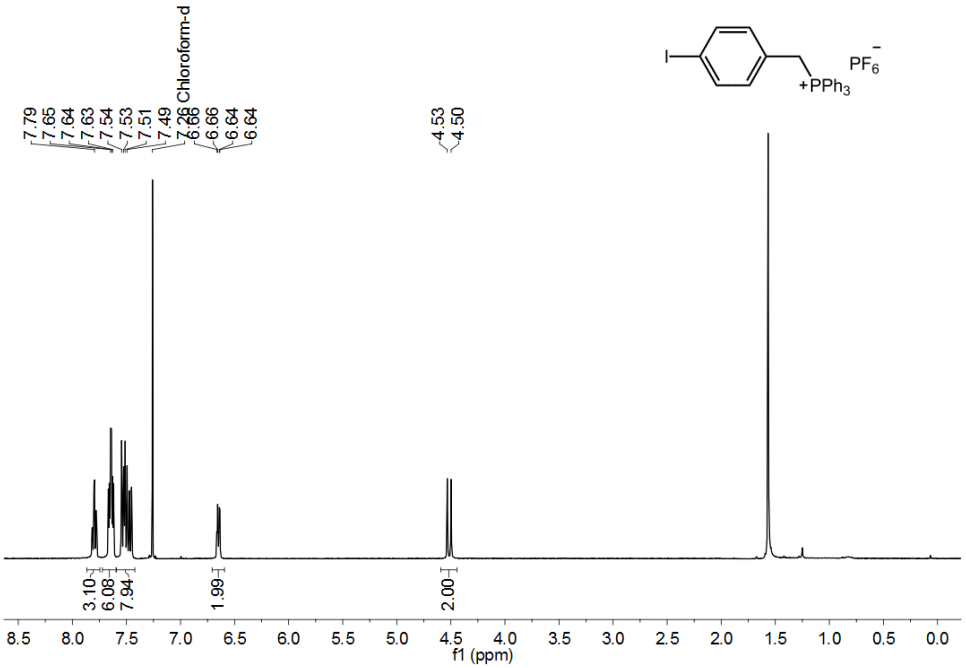

Figure 178. ^{1}H NMR spectrum of 4-iodobenzyltriphenylphosphonium hexafluorophosphate **107** in chloroform-d (*JDF file reference*: b4633gmp).

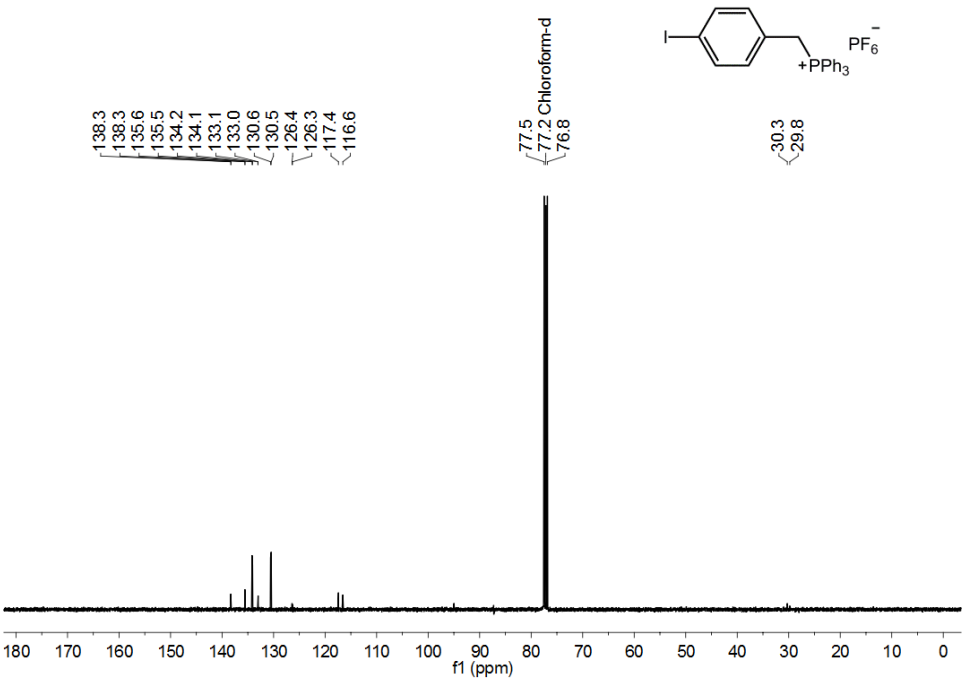

Figure 179. ^{13}C NMR spectrum of 4-iodobenzyltriphenylphosphonium hexafluorophosphate **107** in chloroform-d (*JDF file reference*: b4633gmp).

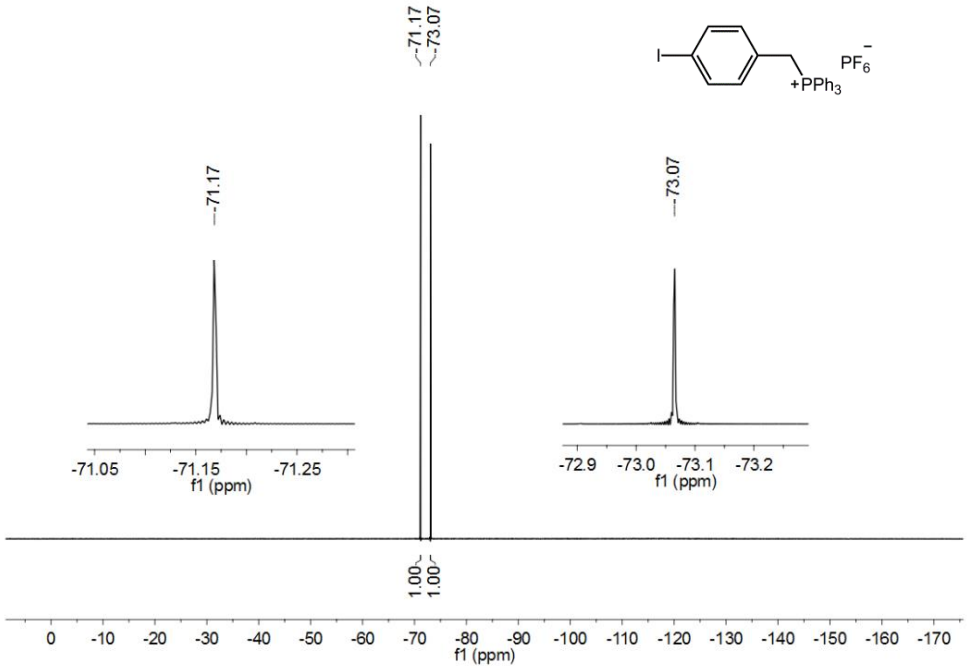

Figure 180. ^{19}F NMR spectrum of 4-iodobenzyltriphenylphosphonium hexafluorophosphate **107** in chloroform-d (*JDF file reference*: b1682gmp).

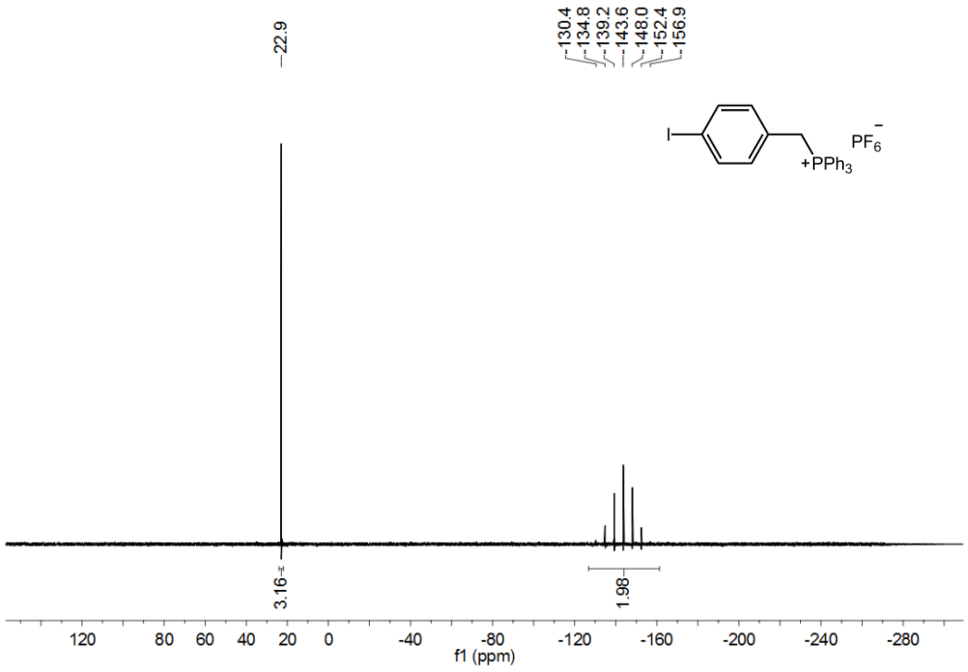

Figure 181. ^{31}P NMR spectrum of 4-iodobenzyltriphenylphosphonium hexafluorophosphate **107** in chloroform-d (*JDF file reference*: b1682gmp).

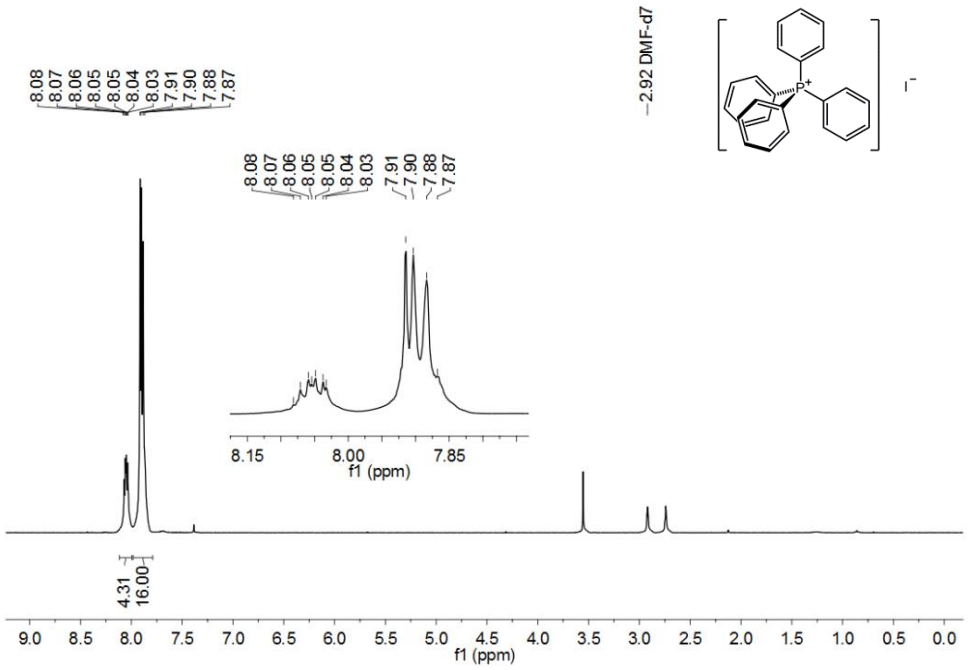

Figure 182. ^{1}H NMR spectrum of tetraphenylphosphonium iodide **103** in DMF-d_7 (spectrum collected on Avance III HD, saved as 3 under folder GMHP-7-498-Pa).

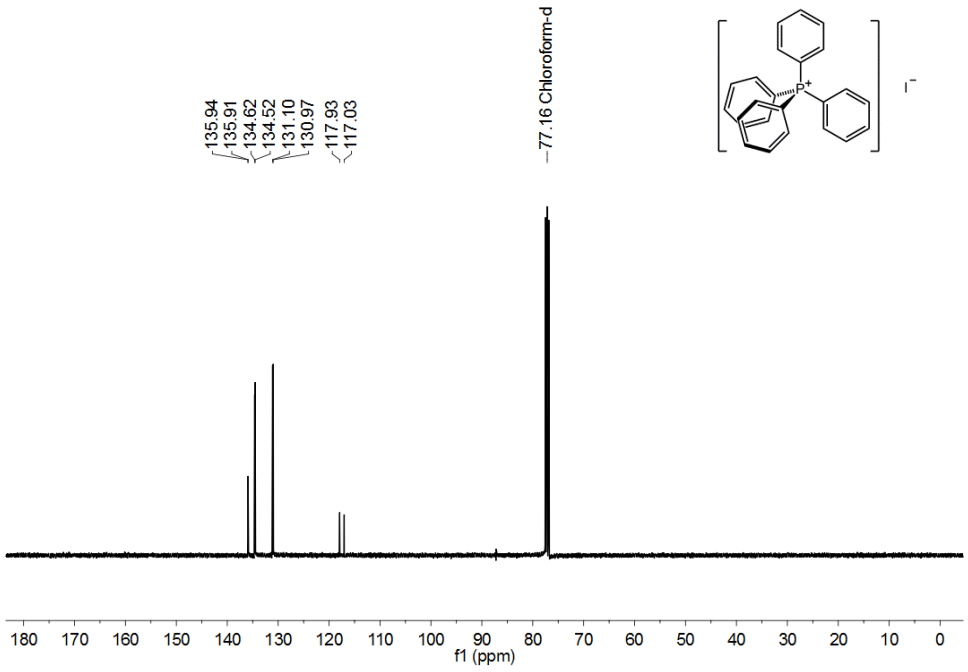

Figure 183. ^{13}C NMR spectrum of tetraphenylphosphonium iodide **103** in chloroform-d (*JDF file reference*: b4632gmp).

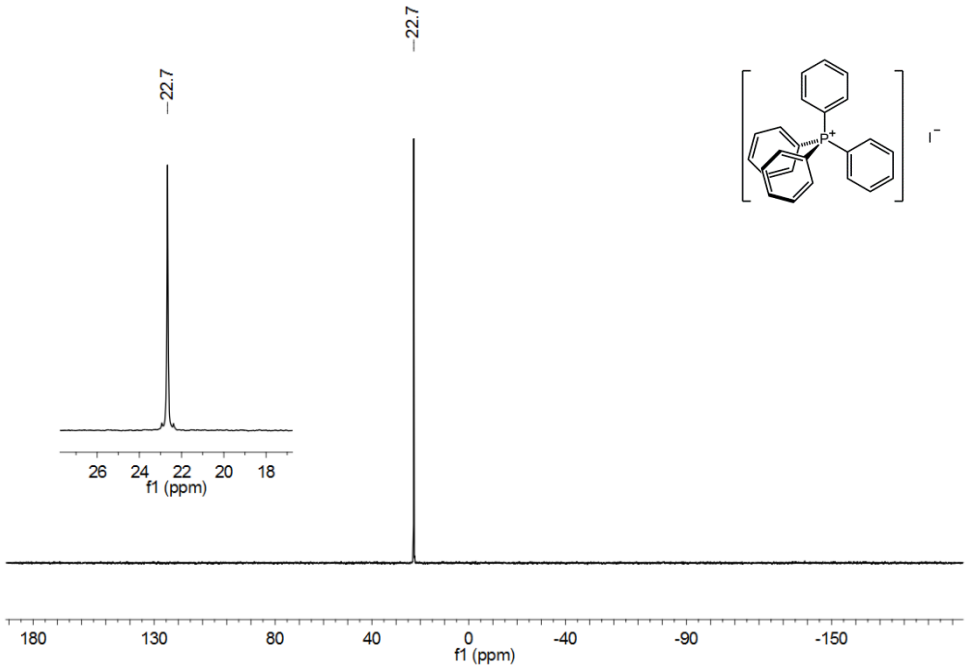

Figure 184. ^{31}P NMR spectrum of tetraphenylphosphonium iodide **103** in DMF-d_7 (spectrum collected on Avance III HD, saved as 4 under folder GMHP-7-498-Pa).

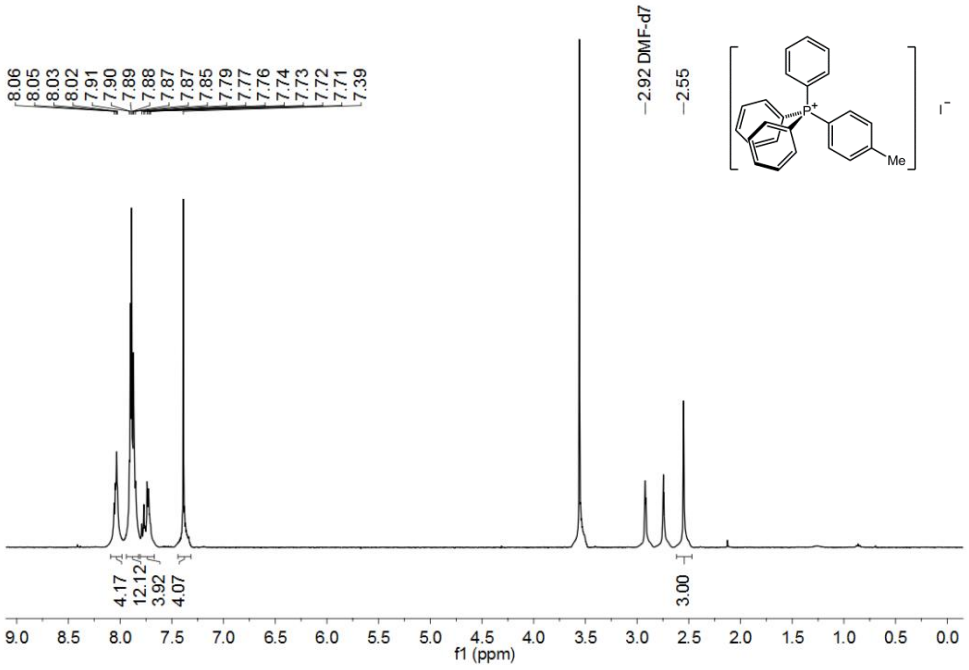

Figure 185. ^{1}H NMR spectrum of triphenyl(4-tolyl)phosphonium iodide **60** in DMF-d_7 (spectrum collected on Avance III HD, saved as 3 under folder GMHP-7-499-P).

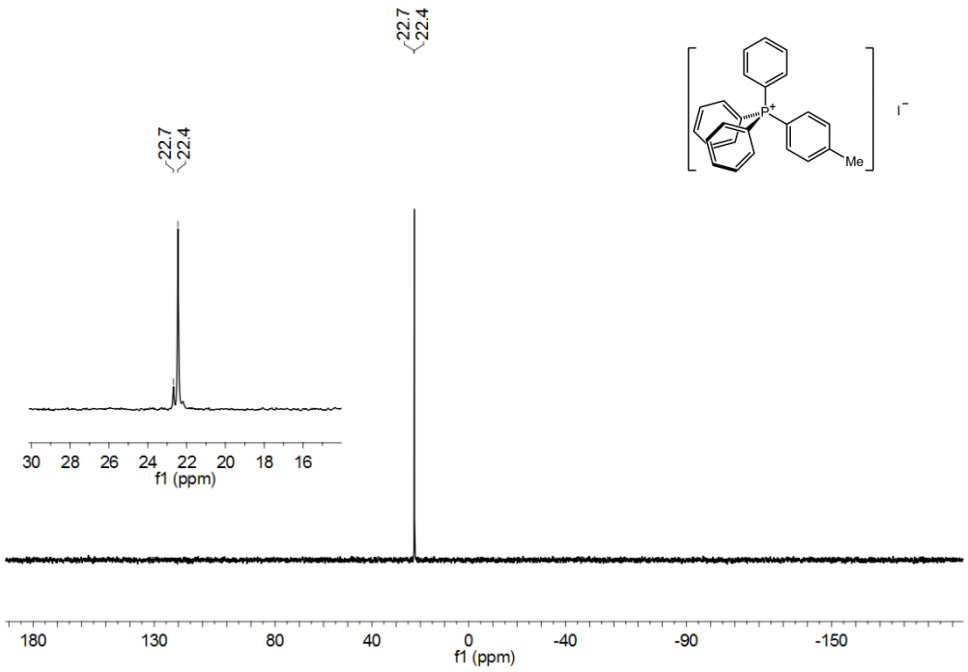

Figure 186. ^{31}P NMR spectrum of triphenyl(4-tolyl)phosphonium iodide **60** in DMF-d_7 (spectrum collected on Avance III HD, saved as 4 under folder GMHP-7-499-P).

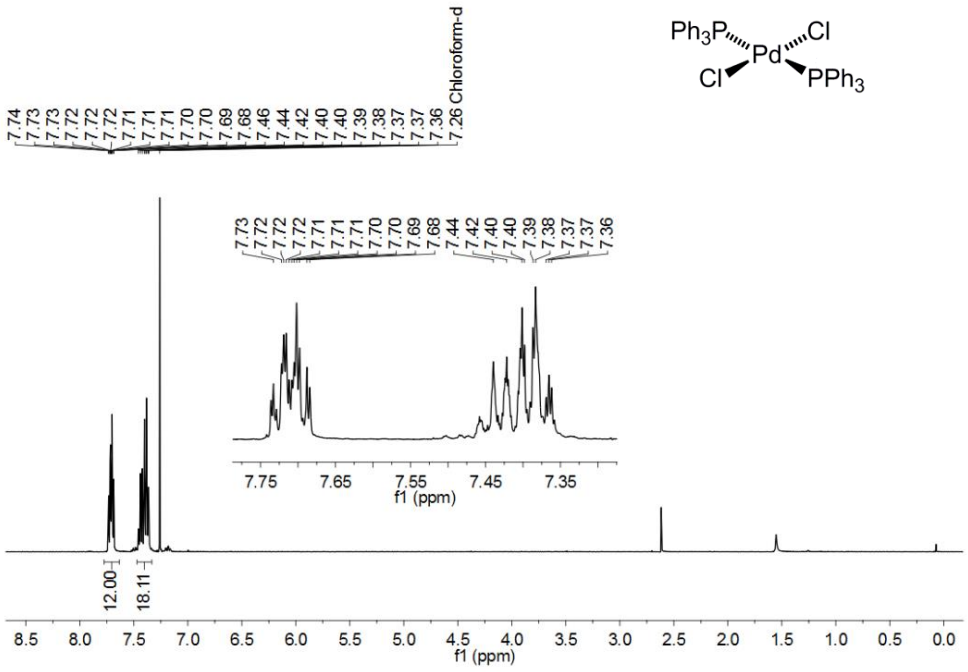

Figure 187. ^{1}H NMR spectrum of bis(triphenylphosphine)palladium(dichloride) **123** in chloroform-d (*JDF file reference*: j7853gmp).

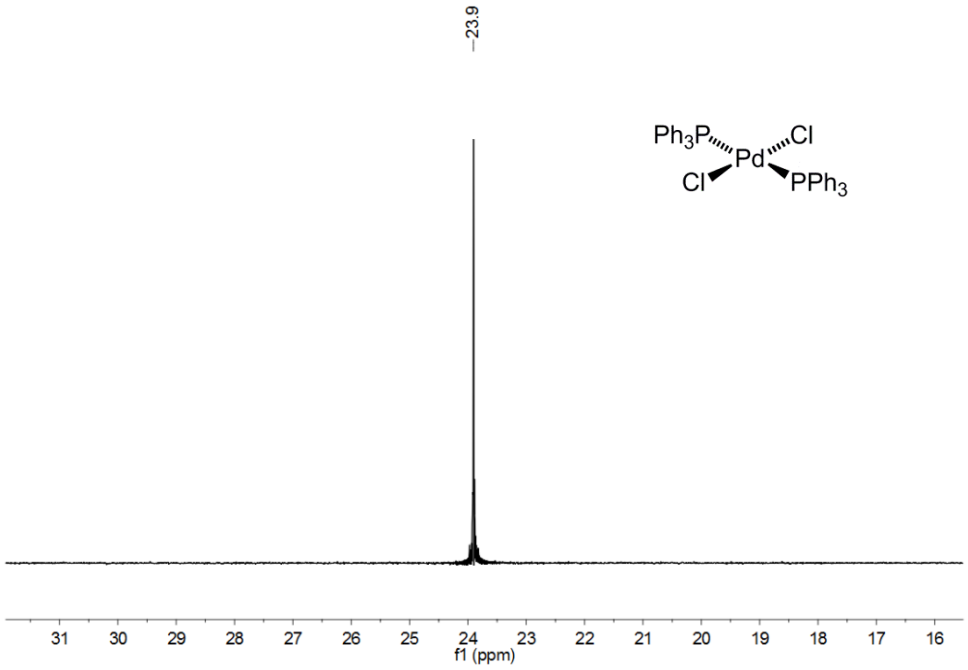

Figure 188. ^{31}P NMR spectrum of bis(triphenylphosphine)palladium(dichloride) **123** in chloroform-d (*JDF file reference*: b3767gmp).

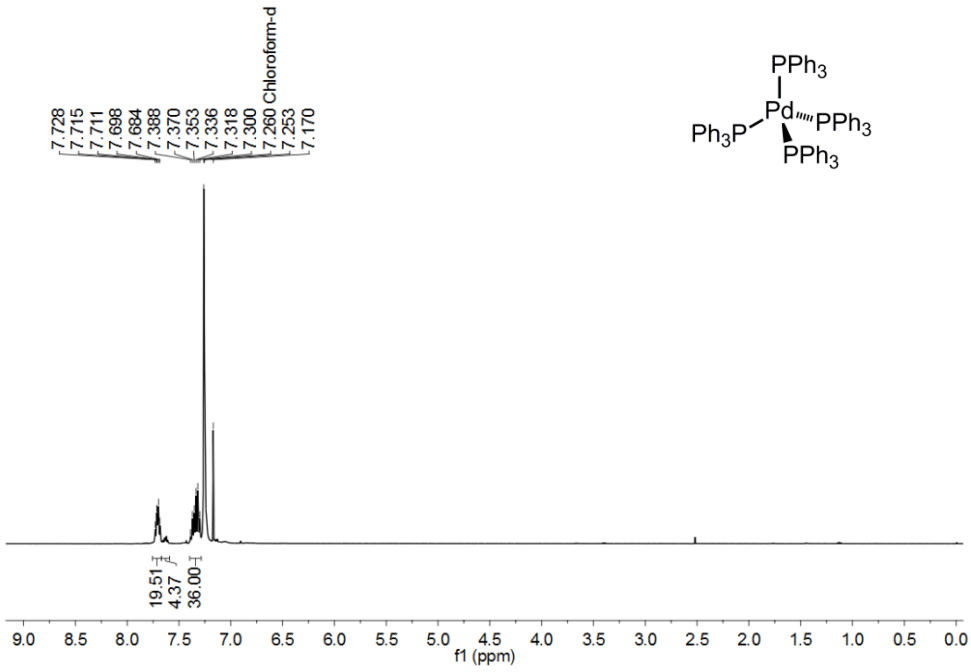

Figure 189. ^{1}H NMR spectrum of tetrakis(triphenylphosphine)palladium **124** in chloroform-d (*JDF file reference*: k3246gmp).

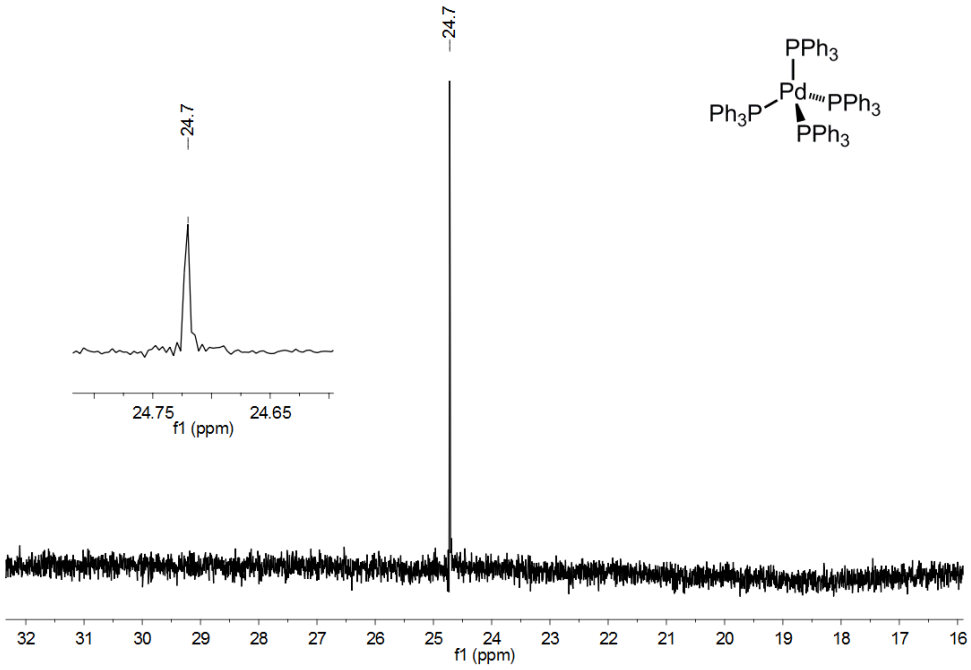

Figure 190. ^{31}P NMR spectrum of tetrakis(triphenylphosphine)palladium **124** in benzene-d_6 (spectrum collected on AV500, saved as 1 under folder GMHP-2-120-P).

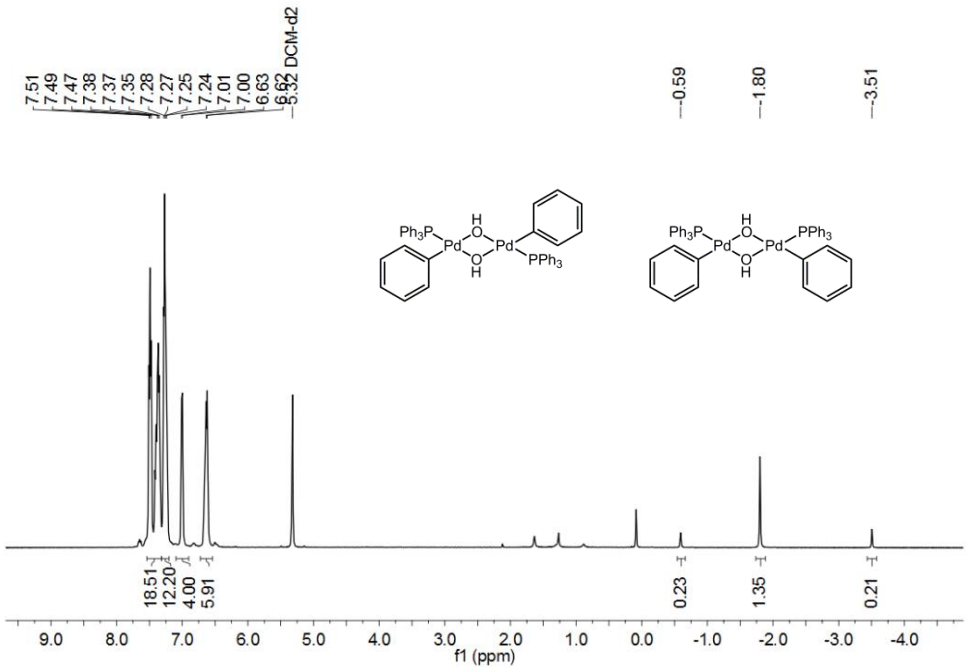

Figure 191. ^{1}H NMR spectrum of $[Pd(C_6H_5)(\mu\text{-}OH)(P(C_6H_5)_3)]_2$ **83a** in methylene chloride-d_2 (spectrum collected on AV500, saved as 1 under folder GMHP-5-311-P2).

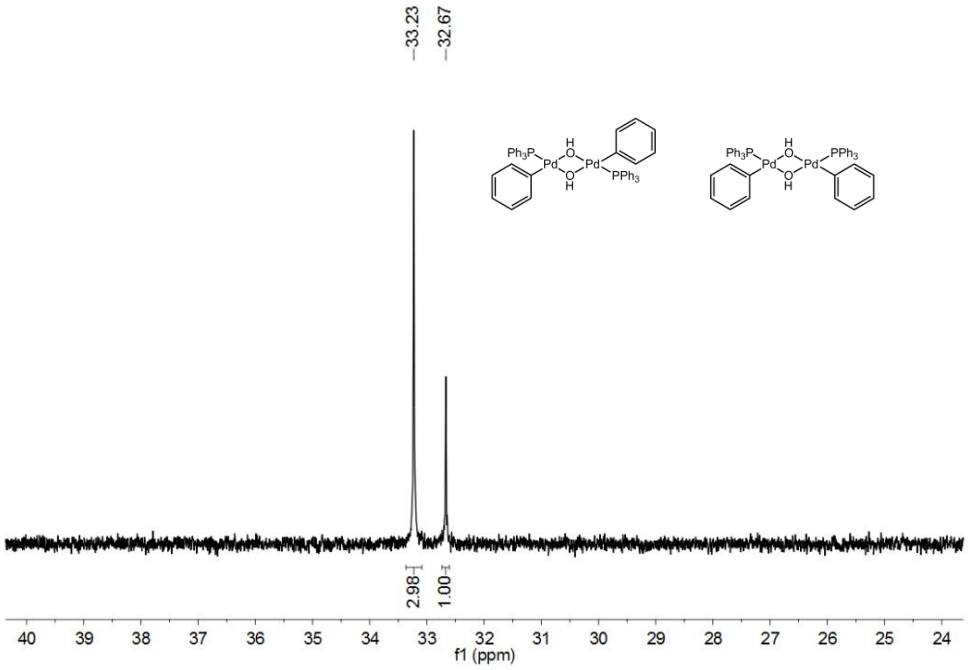

Figure 192. ^{31}P NMR spectrum of $[Pd(Ph)(\mu\text{-}OH)(PPh_3)]_2$ **83a** in methylene chloride-d_2 (spectrum collected on AV500, saved as 3 under folder GMHP-5-311-P2).

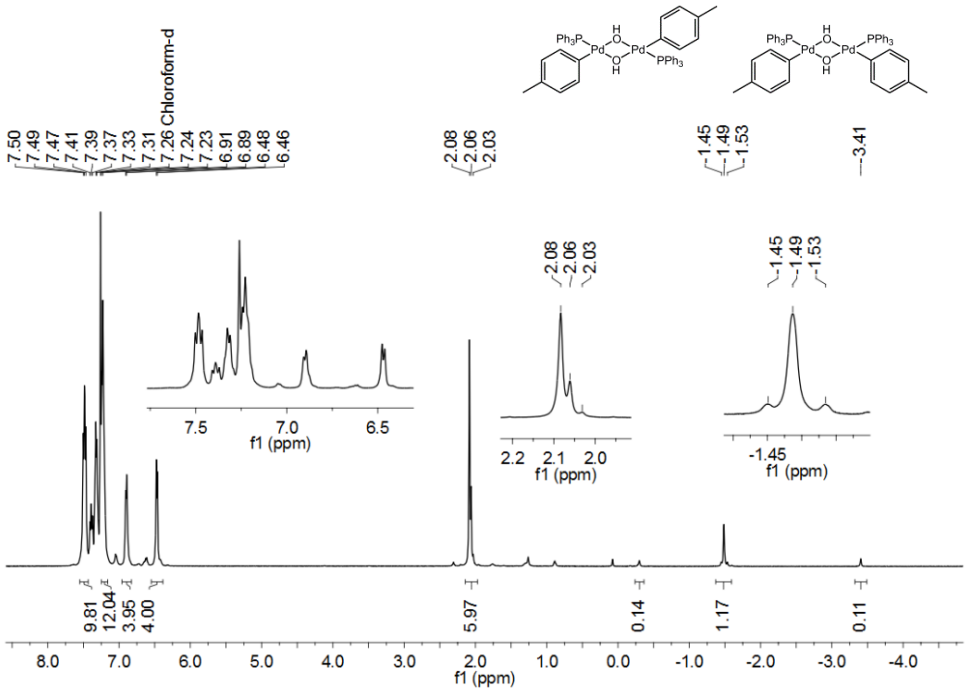

Figure 193. ^{1}H NMR spectrum of $[Pd(4\text{-}MeC_6H_4)(\mu\text{-}OH)(P(C_6H_5)_3)]_2$ **83b** in chloroform-d (spectrum collected on AV500, run by ds933 saved as GMHP-3-137-P-recryst under folder GPO_001a).

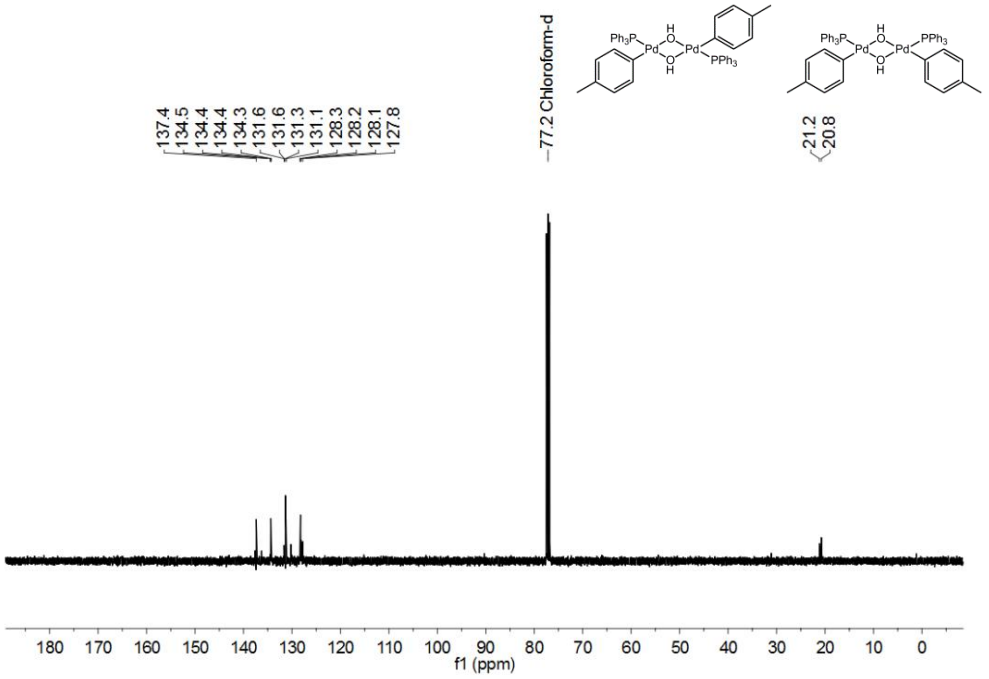

Figure 194. ^{13}C NMR spectrum of $[Pd(4\text{-}MeC_6H_4)(\mu\text{-}OH)(P(C_6H_5)_3)]_2$ **83b** in chloroform-d (*JDF file reference*: b8378gmp).

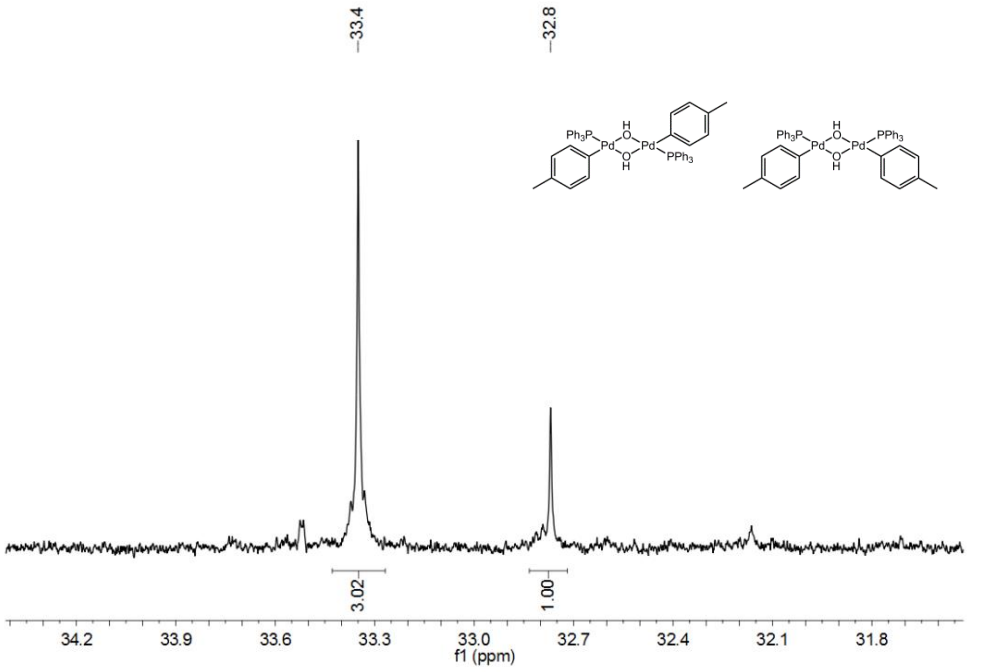

Figure 195. ^{31}P NMR spectrum of $[Pd(4\text{-tolyl})(\mu\text{-}OH)(PPh_3)]_2$ **83b** in chloroform-d (spectrum collected on AV500, saved as 2 under folder GMHP-4-269).

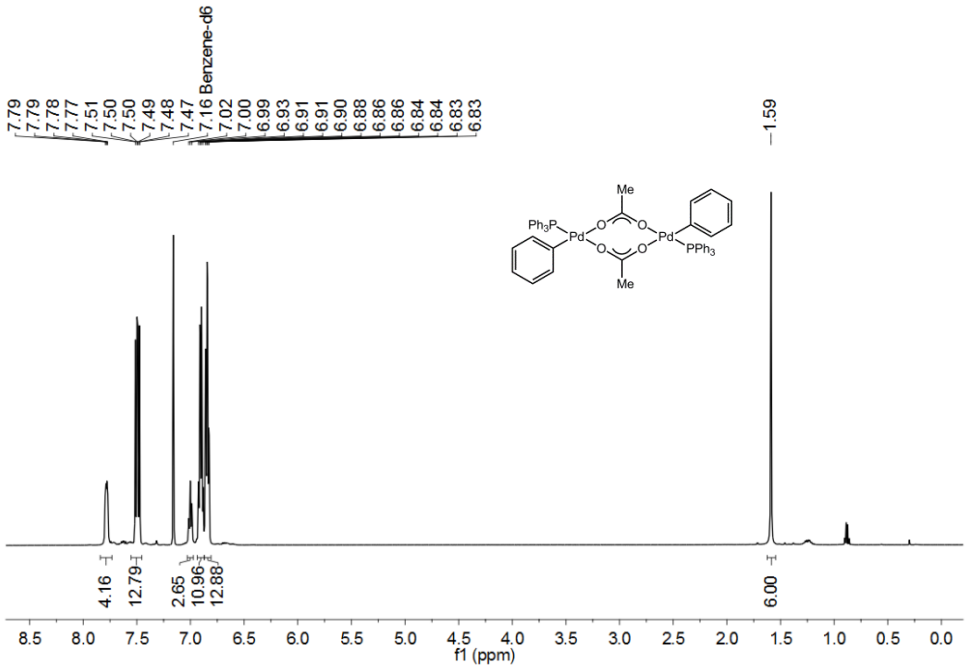

Figure 196. ^{1}H NMR spectrum of $[Pd(C_6H_5)(\mu\text{-}O_2CMe)(P(C_6H_5)_3)]_2$ **84** in benzene-d_6 (spectrum collected on AV500, saved as 7 under folder GMHP-5-292-P).

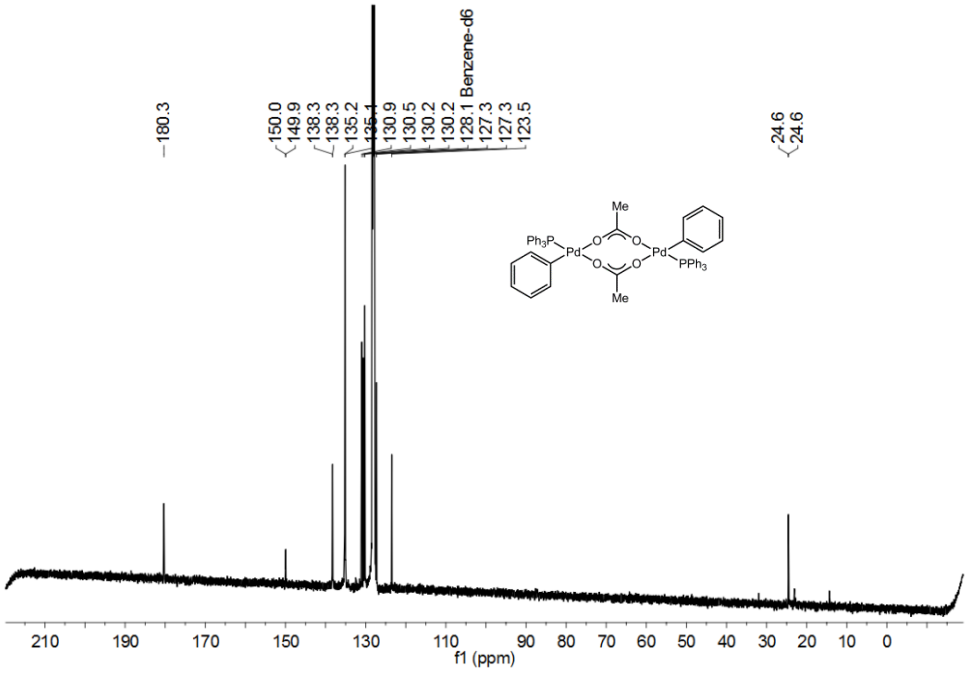

Figure 197. ^{13}C NMR spectrum of $[Pd(C_6H_5)(\mu\text{-}O_2CMe)(P(C_6H_5)_3)]_2$ **84** in benzene-d_6 (spectrum collected on AV500, saved as 6 under folder GMHP-5-292-P).

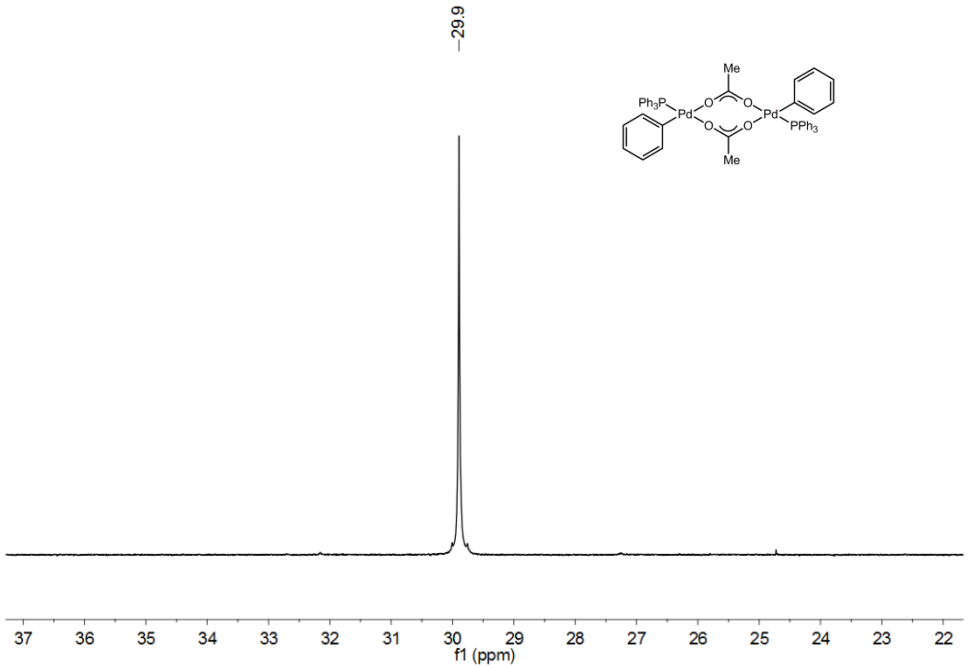

Figure 198. ^{31}P NMR spectrum of [Pd(Ph)(μ-OAc)(PPh_3)]$_2$ **84** in benzene-d_6 (spectrum collected on AV500, saved as 2 under folder GMHP-5-292-P).

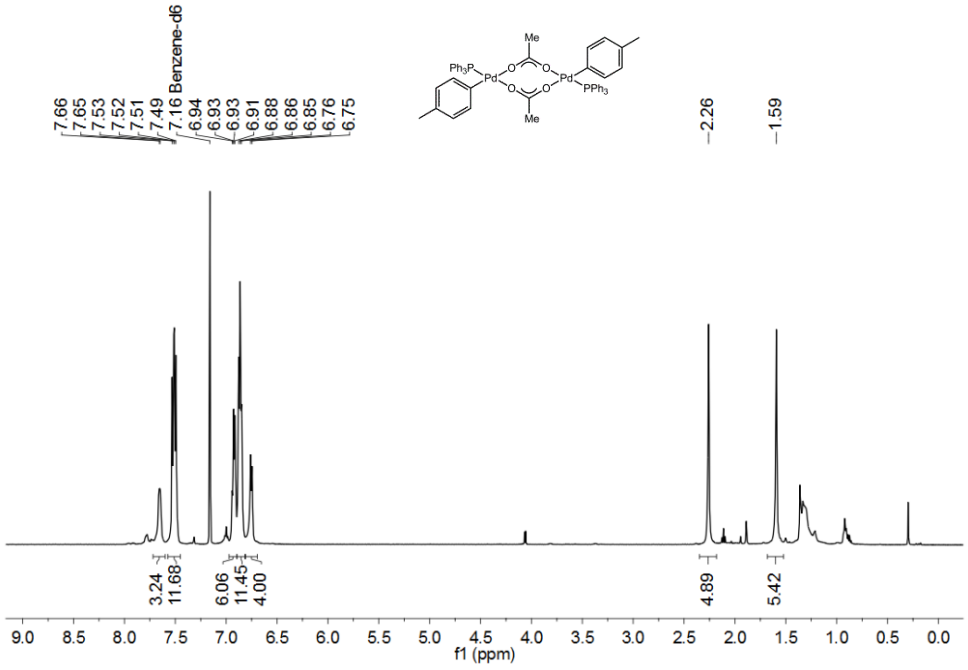

Figure 199. ^{1}H NMR spectrum of [Pd(4-MeC_6H_4)(μ-O_2CMe)($P(C_6H_5)_3$)]$_2$ **84b** in benzene-d_6 (spectrum collected on AV500, saved as 1 under folder GMHP-4-245).

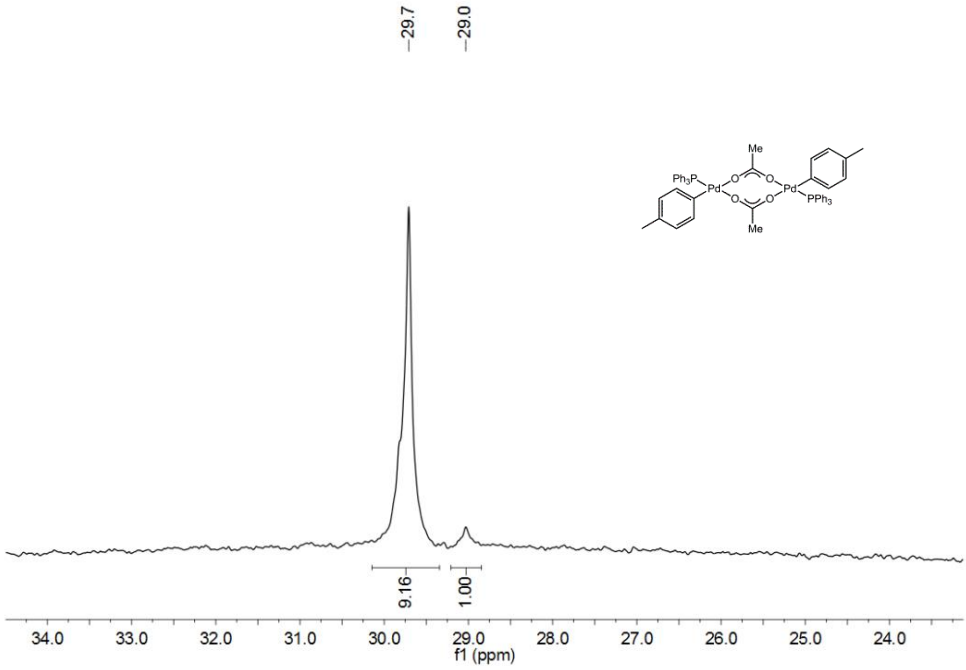

Figure 200. ^{31}P NMR spectrum of [Pd(4-tolyl)(μ-OAc)(PPh_3)]$_2$ **84b** in benzene-d_6 (spectrum collected on AV500, saved as 5 under folder GMHP-4-214-P).

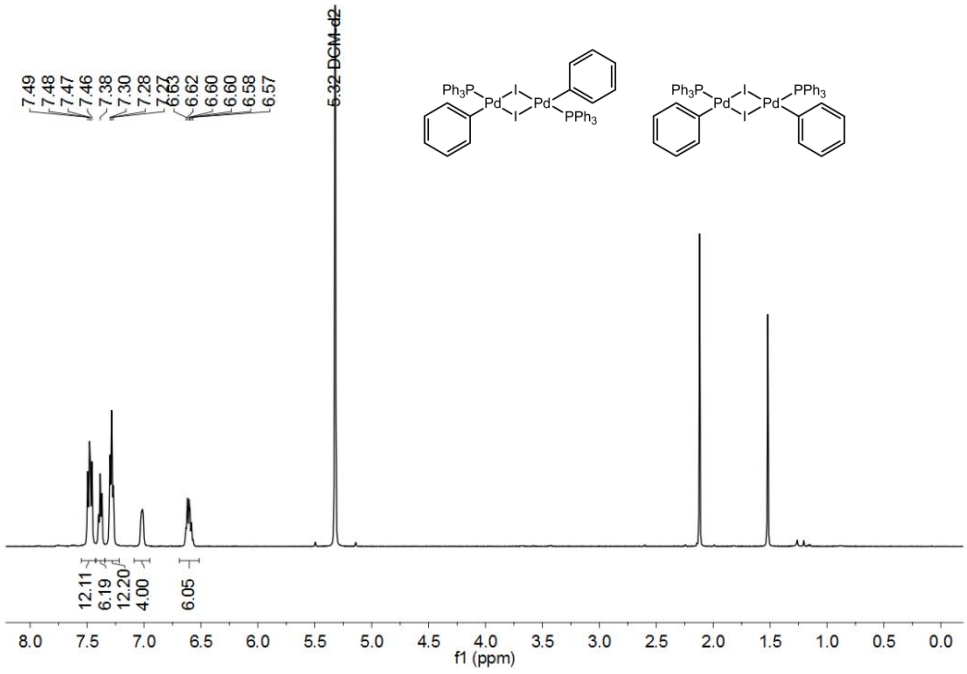

Figure 201. ^{1}H NMR spectrum of [Pd(C_6H_5)(μ-I)($P(C_6H_5)_3$)]$_2$ **86** in methylene chloride-d_2 (spectrum collected on AV500, saved as 11 under folder GMHP-5-312-P).

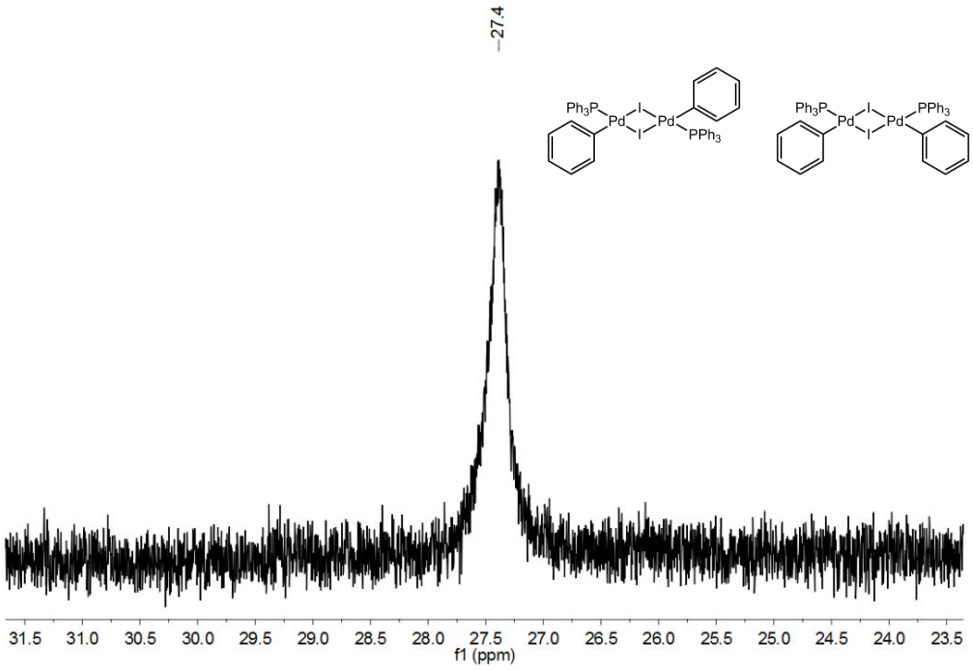

Figure 202. ^{31}P NMR spectrum of [Pd(Ph)(μ-I)(PPh$_3$)]$_2$ **86** in methylene chloride-d$_2$ (spectrum collected on AV500, saved as 15 under folder GMHP-5-312-P).

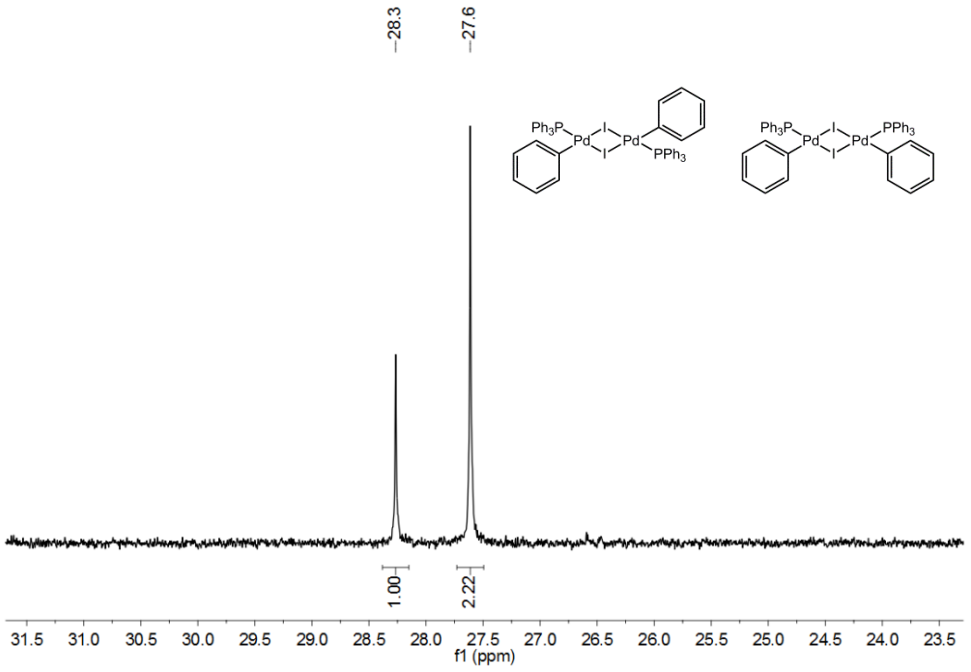

Figure 203. ^{31}P NMR spectrum of [Pd(Ph)(μ-I)(PPh$_3$)]$_2$ **86** in methylene chloride-d$_2$ at −20 °C (spectrum collected on AV500, saved as 20 under folder GMHP-5-312-P).

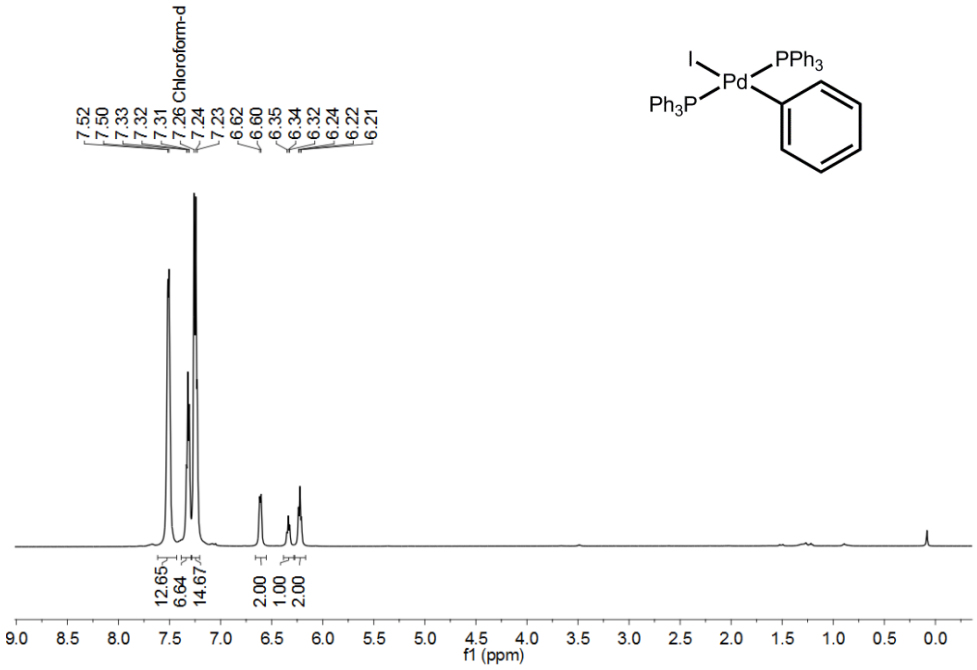

Figure 204. ^{1}H NMR spectrum of Pd(C_6H_5)(I)(P(C_6H_5)$_3$)$_2$ **82a** in chloroform-d (spectrum collected on AV500, saved as 10 under folder GMHP-6-426).

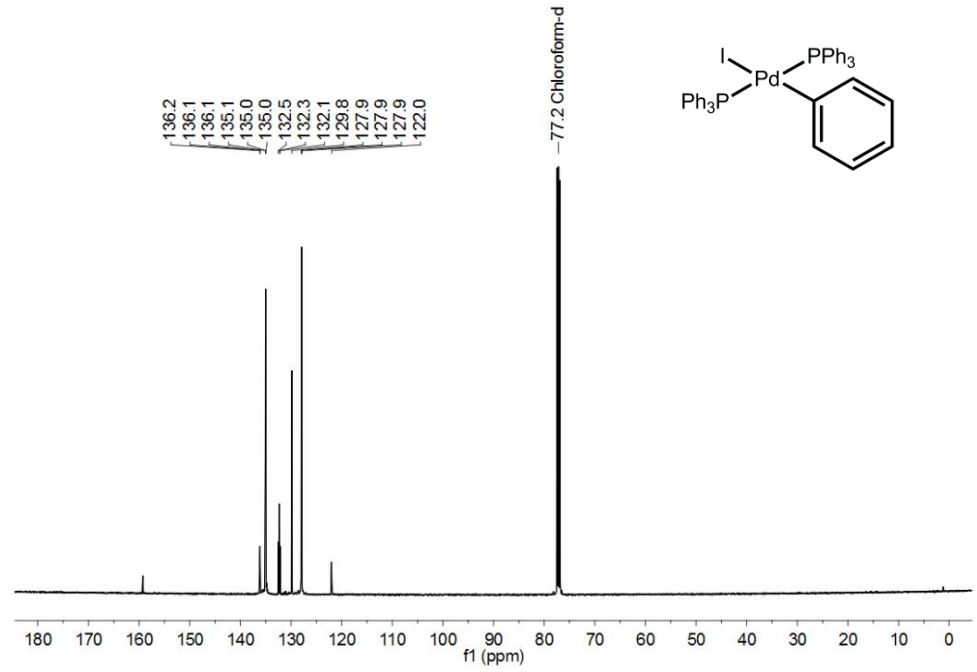

Figure 205. ^{13}C NMR spectrum of Pd(C_6H_5)(I)(P(C_6H_5)$_3$)$_2$ **82a** in chloroform-d (spectrum collected on AV500, saved as 15 under folder GMHP-6-426).

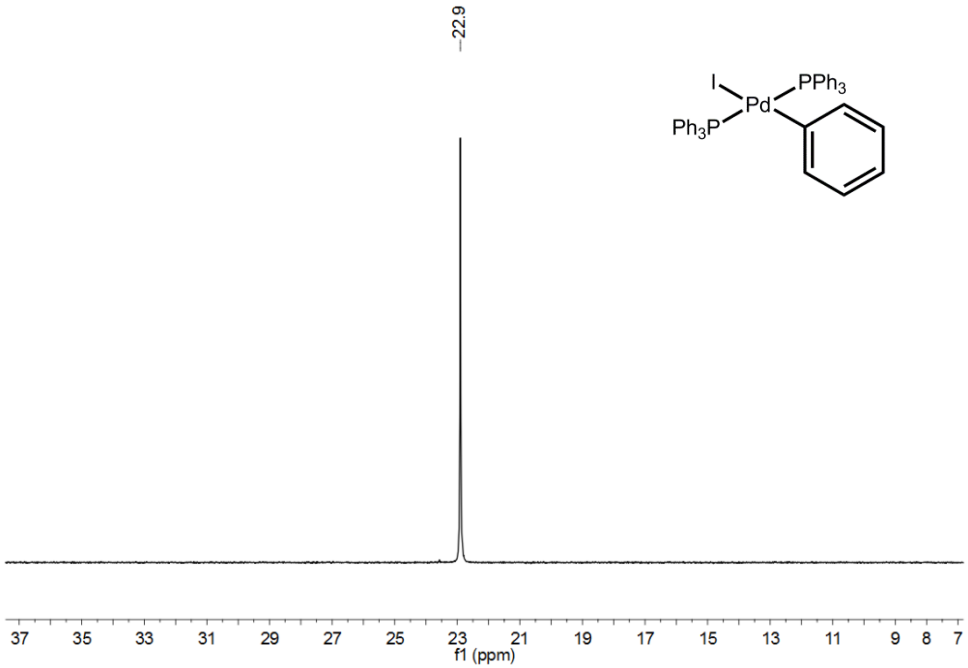

Figure 206. ^{31}P NMR spectrum of $Pd(Ph)(I)(PPh_3)_2$ **82a** in chloroform-d (spectrum collected on AV500, saved as 11 under folder GMHP-6-426).

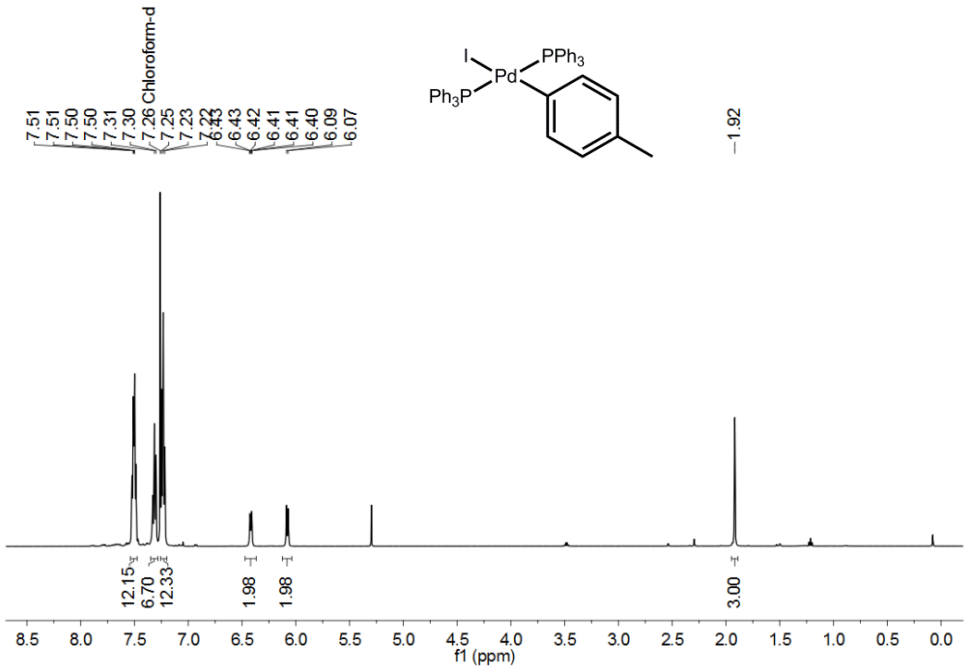

Figure 207. ^{1}H NMR spectrum of $Pd(4\text{-}MeC_6H_5)(I)(P(C_6H_5)_3)_2$ **82b** in chloroform-d (spectrum collected on AV500, saved as 10 under folder GMHP-6-422).

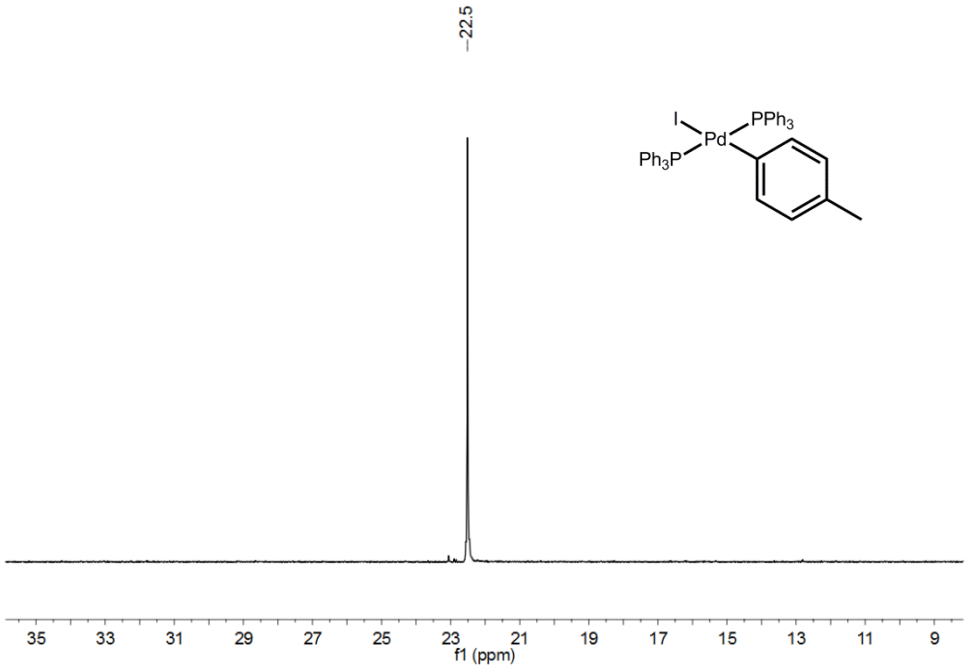

Figure 208. ^{31}P NMR spectrum of Pd(4-tolyl)(I)(PPh_3)$_2$ **82b** in chloroform-d (spectrum collected on AV500, saved as 11 under folder GMHP-6-422).

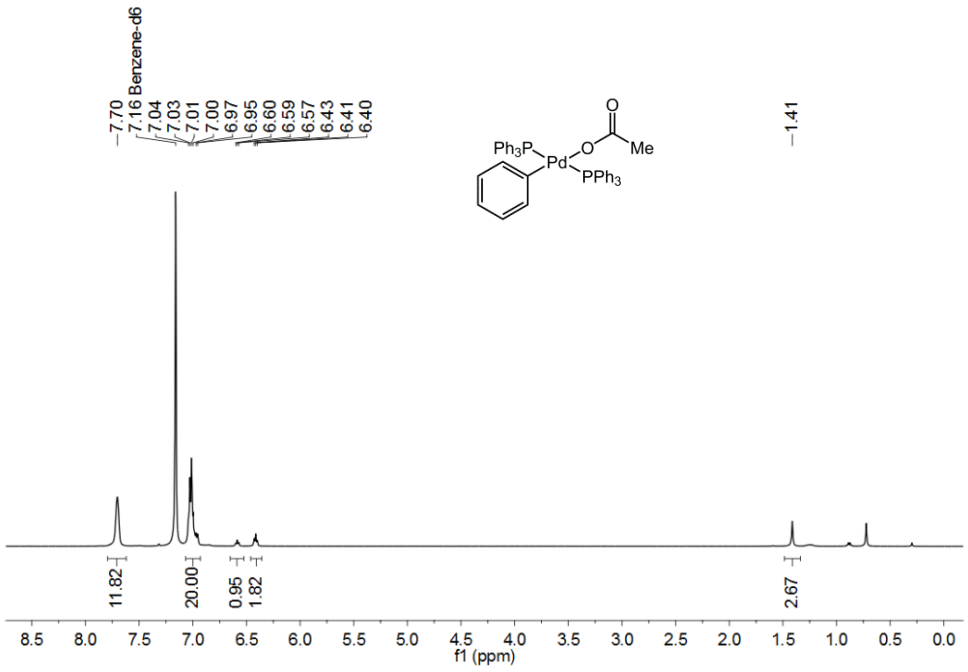

Figure 209. ^{1}H NMR spectrum of Pd(C_6H_5)(κ^1-O_2CMe)($P(C_6H_5)_3$)$_2$ **85** in benzene-d_6 (spectrum collected on AV500, saved as 1 under folder GMHP-6-388-P).

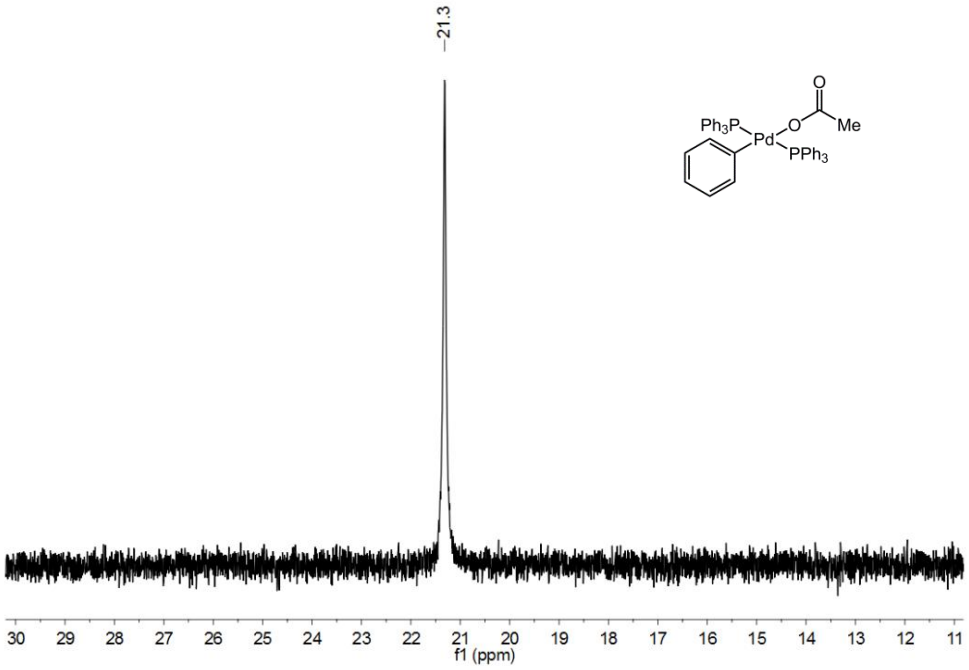

Figure 210. ^{31}P NMR spectrum of Pd(Ph)(κ^1-OAc)(PPh_3)$_2$ **85** in benzene-d_6 (spectrum collected on AV500, saved as 2 under folder GMHP-6-388-P).

^{19}F NMR Spectra from the Competition Hammett Experiments

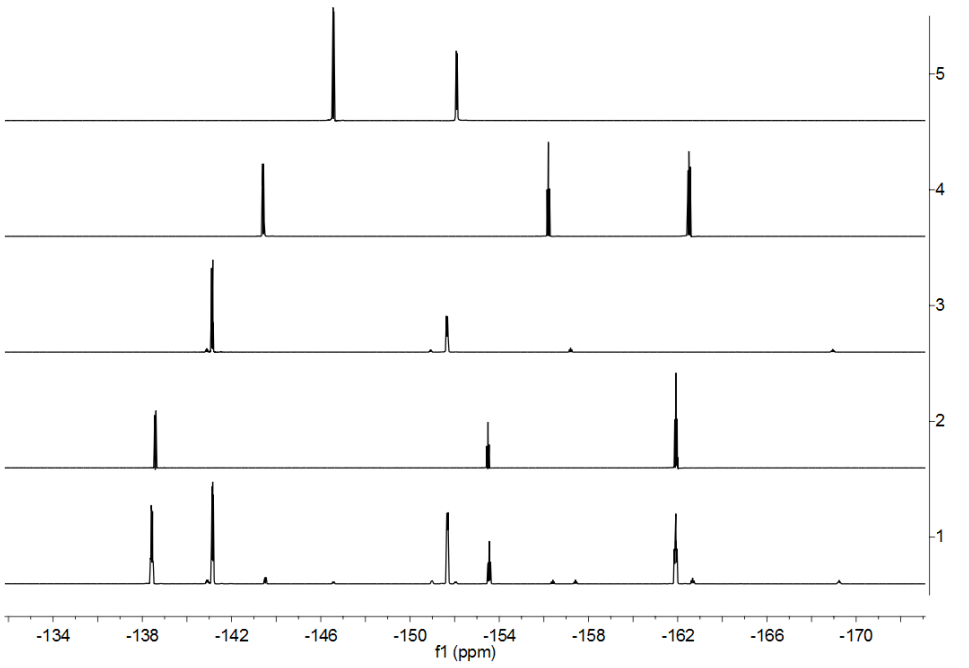

Figure 211. Stacked ^{19}F NMR spectra of **(1)** the reaction mixture (*Lab book reference number*: GMHP-6-365, *JDF file reference*: d6334gmp), **(2)** pentafluorobenzene **56** (*JDF file reference*: d6073gmp), **(3)** $(Me_2N)C_6F_4H$ **121** (*JDF file reference*: a8713gmp), **(4)** P^F **58** (*JDF file reference*: a8356gmp) and **(5)** P^X (X = NMe_2) **76** (*JDF file reference*: a8370gmp).

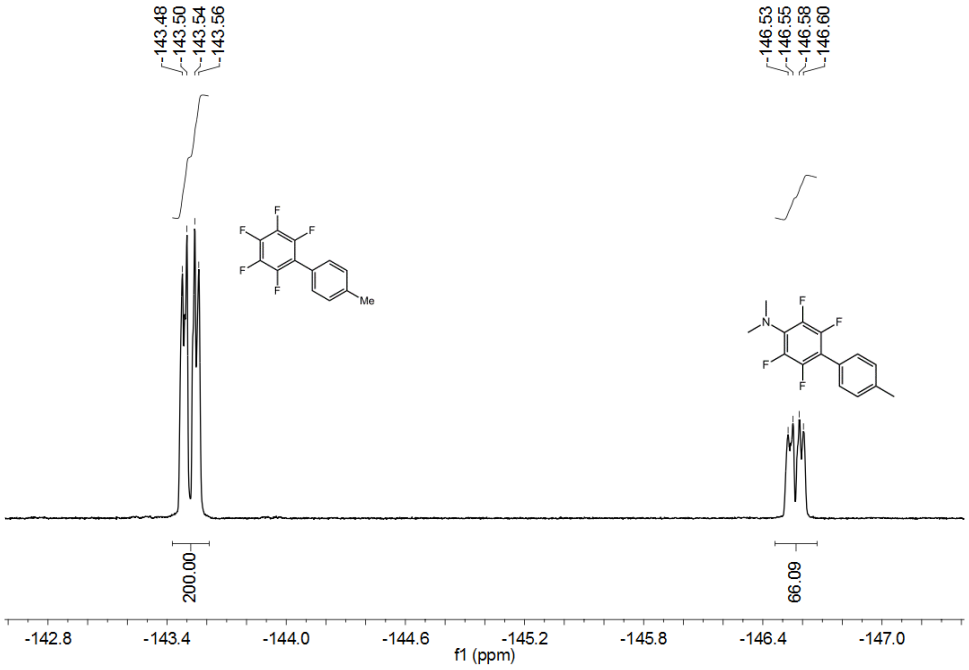

Figure 212. ^{19}F NMR spectrum of the reaction mixture with integration of P^F **58** (200) and P^X (X = NMe_2) **76** (66) peaks (*JDF file reference*: d6334gmp).

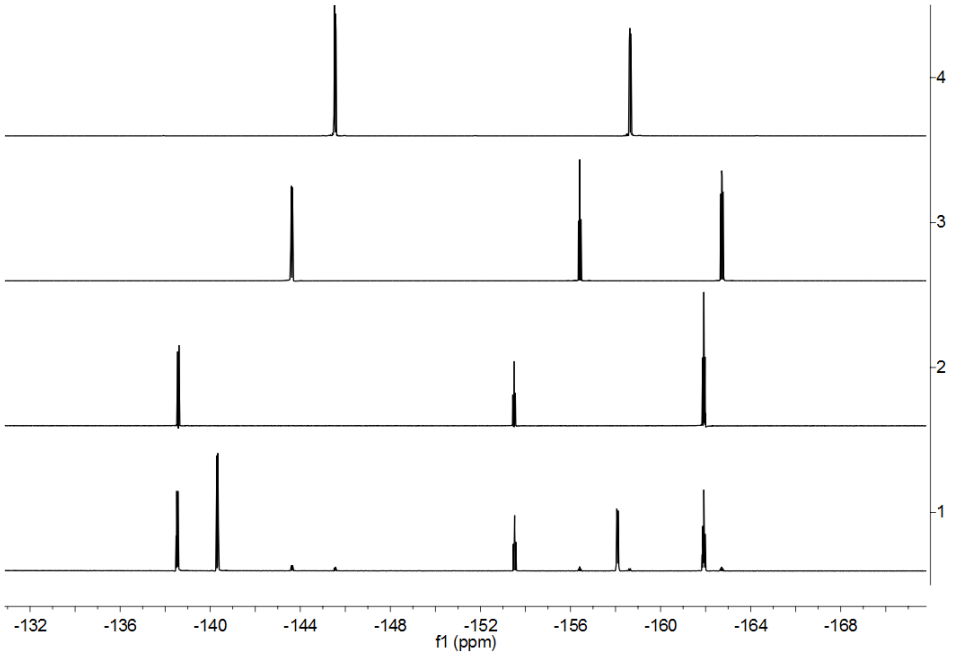

Figure 213. Stacked ^{19}F NMR spectra of **(1)** the reaction mixture (*Lab book reference number*: GMHP-5-253, *JDF file reference*: c4247gmp), **(2)** pentafluorobenzene **56** (*JDF file reference*: d6073gmp), **(3)** P^F **58** (*JDF file reference*: a8356gmp) and **(4)** P^X (X = OMe) **77** (*JDF file reference*: a8364gmp).

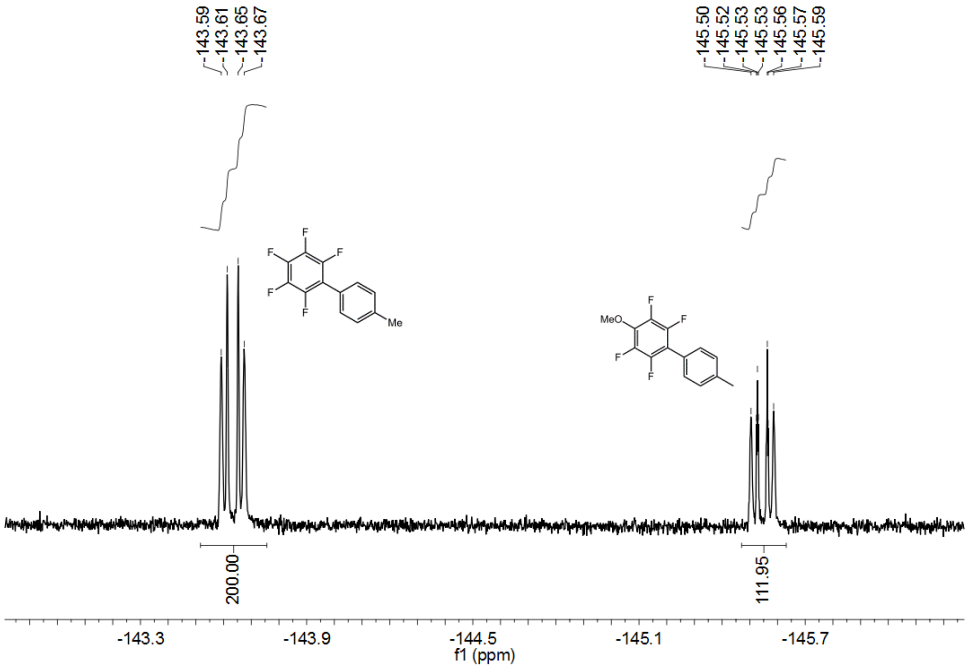

Figure 214. ^{19}F NMR spectrum of the reaction mixture with integration of P^{F} **58** (200) and P^{X} (X = OMe) **77** (112) peaks (*JDF file reference*: c4247gmp).

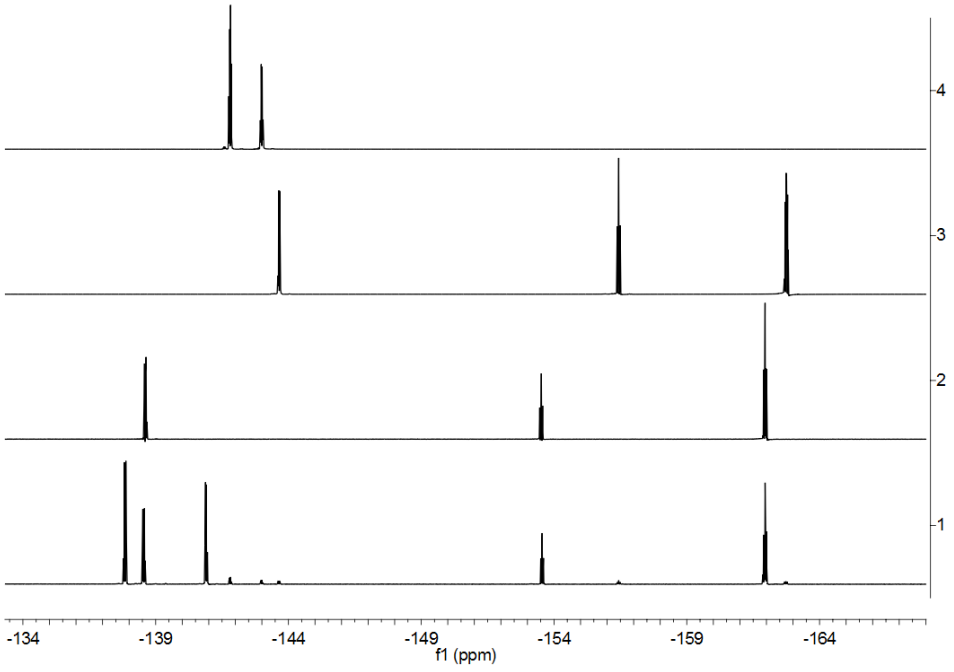

Figure 215. Stacked ^{19}F NMR spectra of **(1)** the reaction mixture (*Lab book reference number*: GMHP-5-270, *JDF file reference*: c5539gmp), **(2)** pentafluorobenzene **56** (*JDF file reference*: d6073gmp), **(3)** P^{F} **58** (*JDF file reference*: a8356gmp) and **(4)** P^{X} (X = Cl) **79** (*JDF file reference*: a8367gmp).

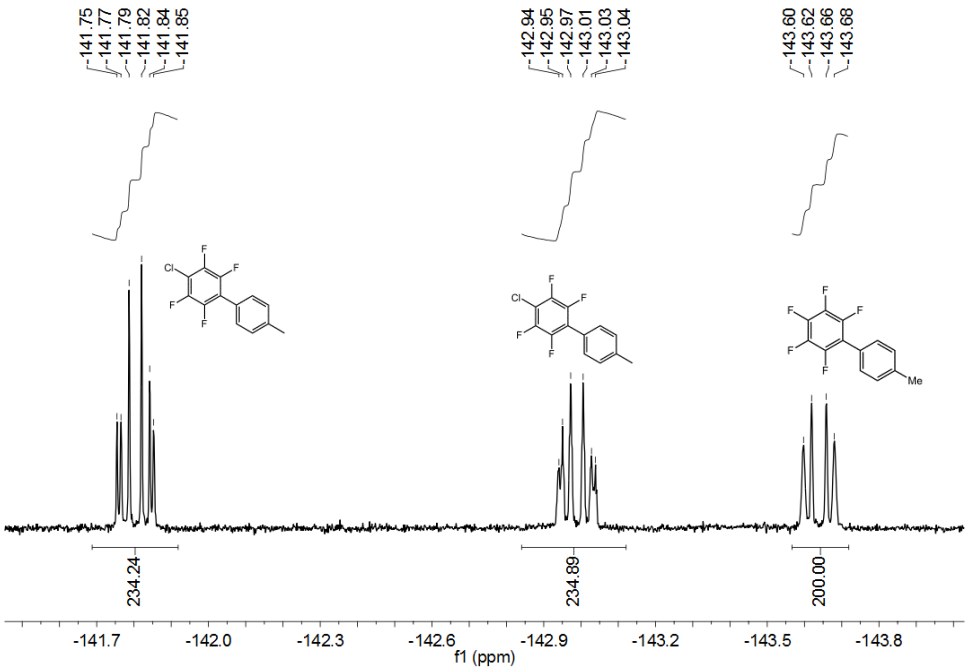

Figure 216. ^{19}F NMR spectrum of the reaction mixture with integration of P^F **58** (200) and P^X (X = Cl) **79** (235) peaks (*JDF file reference*: c5539gmp).

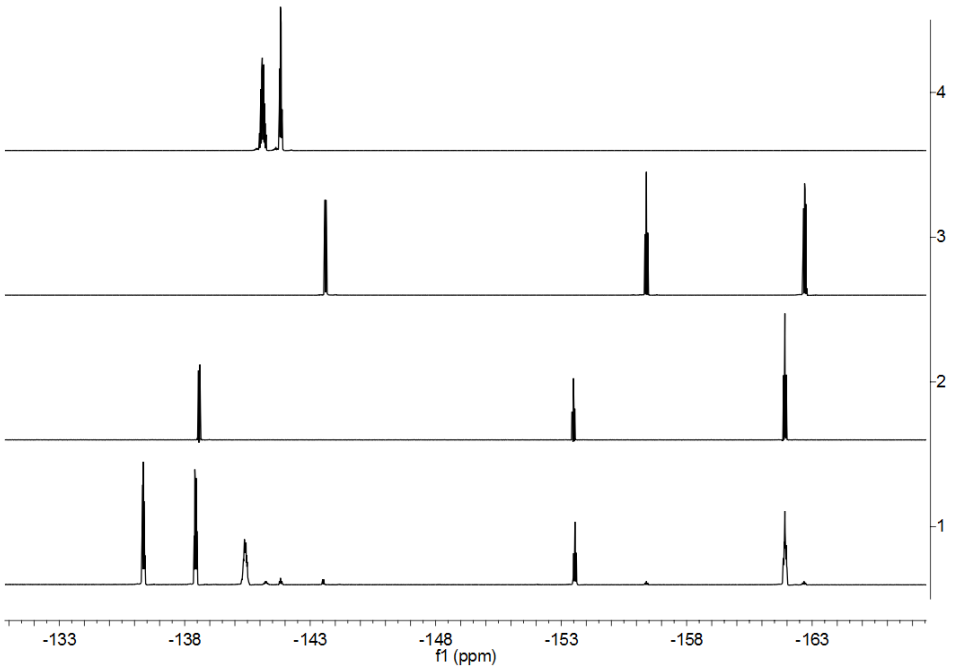

Figure 217. Stacked ^{19}F NMR spectra of **(1)** the reaction mixture (*Lab book reference number*: GMHP-5-250, *JDF file reference*: c4007gmp), **(2)** pentafluorobenzene **56** (*JDF file reference*: d6073gmp), **(3)** P^F **58** (*JDF file reference*: a8356gmp) and **(4)** P^X (X = CF_3) **80** (*JDF file reference*: a8357gmp).

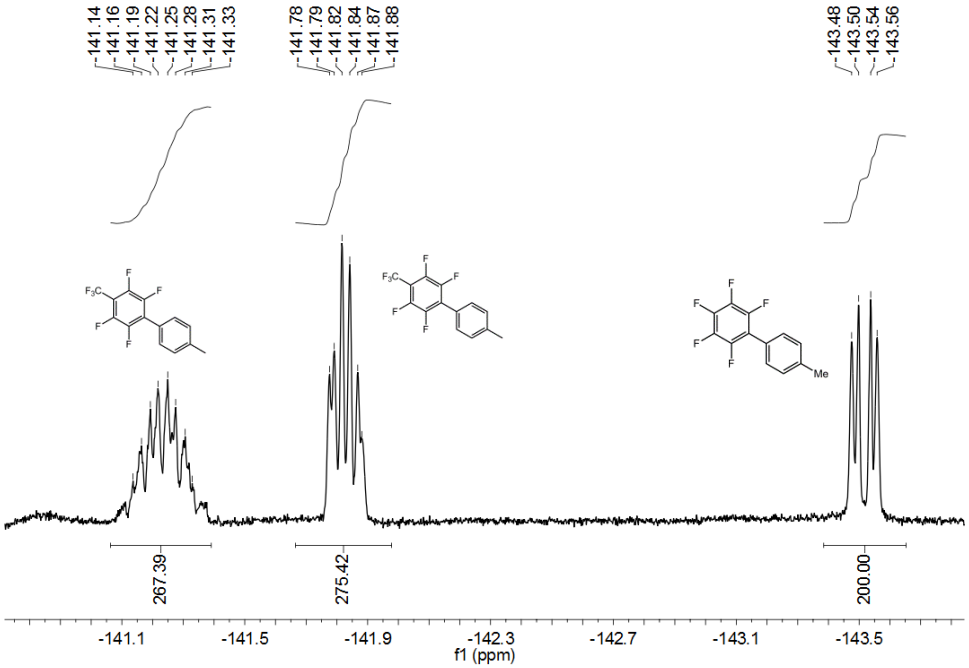

Figure 218. ^{19}F NMR spectrum of the reaction mixture with integration of P^F **58** (200) P^X (X = CF_3) **80** (275) peaks (*JDF file reference*: c4007gmp).

Abbreviations

^{1}H NMR	proton nuclear magnetic resonance
^{13}C NMR	carbon 13 nuclear magnetic resonance
^{19}F NMR	fluorine 19 nuclear magnetic resonance
^{2}H NMR	deuterium nuclear magnetic resonance
^{31}P NMR	phosphorus 31 nuclear magnetic resonance
°	degree
°C	degree Celsius
$\Delta H^{\ddagger}$	enthalpy of activation
$\Delta S^{\ddagger}$	entropy of activation
$\Delta G^{\ddagger}$	Gibbs free energy of activation
α	alpha
β	beta
γ	gamma
δ	chemical shift (in ppm)
ε	molar extinction coefficient
Θ_m	magic angle, 54.74 °
κ	kappa
λ	wavenumbers
μ	eta
μL	microliter
ν_{max}	frequencies of the maxima
ν(t)	rate
ρ	reaction constant
σ	substituent constant
τ	mean reaction time
Å	angstrom
A	absorbance or pre-exponential factor
[A]	concentration of species A
Ac	acetyl
AMLA(4)	4 membered ambiphilic metal-ligand activation
AMLA(6)	6 membered ambiphilic metal-ligand activation
aq.	aqueous
Ar	aryl
Ar^{F}	fluorinated aryl

ATR	attenuated total reflectance
atm	standard atmosphere
Au	absorbance units
ave.	average
Bn	benzyl
b.p.	boiling point
br	broad
BT	benzothiazole
Bu	butyl
ca.	circa, a Latin word meaning “approximately”
cat.	catalyst
cf.	confer, a Latin word meaning “compare”
CMD	concerted metalation deprotonation
cm^{-1}	wavenumbers
cm^3	cubic centimetre
COSY	correlation spectroscopy
Cy	cyclohexyl
d	doublet
Da	Daltons
DA	direct arylation
DCM	dichloromethane
dd	doublet of doublets
DFT	density functional theory
DG	directing group
DIEA	*N*,*N*-diisopropylethylamine
DMAc	*N*,*N*-dimethylacetamide
DMF	*N*,*N*-dimethylformamide
dt	doublet of triplets
E_a	activation energy
e.g.	exempli grantia, a Latin word meaning “for example”
EI	electron impact
equiv.	equivalents
ESI	electrospray ionisation
Et	ethyl
et al.	et alii, a Latin word meaning “and co-workers”
etc.	et cetera, a Latin word meaning “and the rest”

ex situ	a Latin meaning “off-site”
FT	Fourier transform
h	hour
h	Planck constant (6.626×10^{-34} J s)
HMQC	heteronuclear multi-quantum coherence spectroscopy
HR	high resolution
Hz	hertz
IES	internal electrophilic substitution
i.e.	id est, a Latin word meaning “that is”
IES	internal electrophilic substitution
IR	infrared
in situ	a Latin word meaning “on-site”
J	coupling constant
J	joules
JohnPhos	(2-biphenyl)di-*tert*-butylphosphine
K	kelvin
kHz	kilohertz
kJ	kilojoules
k	rate constant
K	equilibrium constant
k_B	Boltzmann constant (1.381×10^{-23} J K^{-1})
k_D	rate constant for reaction involving deuterium
k_H	rate constant for reaction involving proton
k_{obs}	observed rate constant
K_{sp}	solubility constant
KIE	kinetic isotope effect
LIFDI	liquid injection field desorption ionisation
lit.	literature
m	multiplets
m-	meta
M	mol dm^{-3}
$[M^+]$	molecular ion
MAS	magic-angle spinning
Me	methyl
med	medium
mg	miligram

MHz	megahertz
min	minutes
MI	mass intensity
mmol	milimole(s)
mol	mole(s)
m.p.	melting point
MS	mass spectrometry
Mw	molecular weight
m/z	mass-to-charge ratio
NMP	*N*-methyl-2-pyrrolidone
NPs	nanoparticles
o-	ortho
operando	a Latin word meaning “working”
p-	para
PAD	peripheral arterial disease
PET	positron emission tomography
Ph	Phenyl, C_6H_5
pin	pinacol ester
Piv	pivaloyl
ppm	parts per million
Pr	propyl
PVP	poly(*N*-vinyl-2-pyrolidone)
PVPy	polyvinyl-4-pyridine
q	quintet
quart	quartet
quant.	quantitative
R	alkyl, aryl or ideal gas constant (8.314 J K^{-1} mol^{-1})
R^2	coefficient of determinant
R_f	retention factor
RPKA	reaction progress kinetic analysis
RL	rate-limiting
RT	room-temperature
s	singlet or seconds
shp	sharp
str.	stretching
t	triplet

t-	tertiary
$t_{1/2}$	half-life
T	temperature in °C or K
TEM	transmission electron microscopy
Tf	trifluoromethanesulfonic
THF	tetrahydrofuran
TLC	this-layer chromatography
TOF	turnover frequency
TON	turnover number
TOT	total
TS	transition state
UV	ultraviolet
Vis	visible
vs	versus, a Latin word meaning “over against”
VTNA	variable time normalisation analysis
w	weak

References

1. T. Fujiwara and D. O'Hagan, *J. Fluor. Chem.*, 2014, **167**, 16–29.

2. P. Jeschke, *Chembiochem*, 2004, **5**, 570–589.

3. T. Okazoe, *Proc. Jpn. Acad. Ser. B-Phys. Biol. Sci.*, 2009, **85**, 276–289.

4. W. K. Hagmann, *J. Med. Chem.*, 2008, **51**, 4359–4369.

5. S. Purser, P. R. Moore, S. Swallow and V. Gouverneur, *Chem. Soc. Rev.*, 2008, **37**, 320–330.

6. C. Heidelberger, N. K. Chaudhuri, P. Danneberg, D. Mooren, L. Griesbach, R. Duschinsky, R. J. Schnitzer, E. Pleven and J. Scheiner, *Nature*, 1957, **179**, 663–666.

7. R. Martino, V. Gilard, F. Desmoulin and M. Malet-Martino, *Chemotherapy*, 2006, **52**, 215–219.

8. H. Chen, S. Viel, F. Ziarelli and L. Peng, *Chem. Soc. Rev.*, 2013, **42**, 7971–7982.

9. I. A. Ashton, K. O. Abulnaja, K. E. Pallett, D. J. Cole and J. L. Harwood, *Phytochem.*, 1994, **35**, 587–590.

10. I. M. Chalmers, B. J. Cathcart, W. W. Buchanan, E. B. Kumar and W. C. Dick, *Ann. Rheum. Dis.*, 1972, **31**, 319–324.

11. B. E. Smart, *J. Fluor. Chem.*, 2001, **109**, 3–11.

12. D. O'Hagan, *Chem. Soc. Rev.*, 2008, **37**, 308–319.

13. H. J. Bohm, D. Banner, S. Bendels, M. Kansy, B. Kuhn, K. Muller, U. Obst-Sander and M. Stahl, *Chembiochem*, 2004, **5**, 637–643.

14. R. Paulini, K. Muller and F. Diederich, *Angew. Chem., Int. Ed.*, 2005, **44**, 1788–1805.

15. K. Mueller, C. Faeh and F. Diederich, *Science*, 2007, **317**, 1881–1886.

16. J. HernandezTrujillo and A. Vela, *J. Phys. Chem.*, 1996, **100**, 6524–6530.

17. A. Matsushima, T. Fujita, T. Nose and Y. Shimohigashi, *J. Biochem.*, 2000, **128**, 225–232.

18. S. K. Khetan and T. J. Collins, *Chem. Rev.*, 2007, **107**, 2319–2364.

19. A. Bondi, *J. Phys. Chem.*, 1964, **68**, 441–451.

20. S. S. Batsanov, *Inorg. Mater.*, 2001, **37**, 871–885.

21. D. Ohagan and H. S. Rzepa, *Chem. Commun.*, 1997, 645–652.

22. Y. R. Luo, *Comprehensive Handbook of Chemical Bond Energies*, CRC Press, 2007.

23. B. K. Park, N. R. Kitteringham and P. M. O'Neill, *Annu. Rev. Pharmacol. Toxicol.*, 2001, **41**, 443–470.

24. A. T. Proudfoot, S. M. Bradberry and J. A. Vale, *Toxicol. Rev.*, 2006, **25**, 213–219.

25. H. W. Roesky, *Nat Chem*, 2010, **2**, 240–240.

26. G. Resnati, *Tetrahedron*, 1993, **49**, 9385–9445.

27. C. D. Murphy, *Biotechnol. Lett.*, 2010, **32**, 351–359.

28. D. B. Harper and D. Ohagan, *Nat. Prod. Rep.*, 1994, **11**, 123–133.

29. M. Shimizu and T. Hiyama, *Angew. Chem., Int. Ed.*, 2005, **44**, 214–231.

30. M. G. Campbell and T. Ritter, *Chem. Rev.*, 2015, **115**, 612–633.

31. T. Furuya, C. A. Kuttruff and T. Ritter, *Curr. Opin. Drug Discov. Dev.*, 2008, **11**, 803–819.

32. L. J. Allen, J. M. Muhuhi, D. C. Bland, R. Merzel and M. S. Sanford, *J. Org. Chem.*, 2014, **79**, 5827–5833.

33. S. D. Schimler, S. J. Ryan, D. C. Bland, J. E. Anderson and M. S. Sanford, *J. Org. Chem.*, 2015, **80**, 12137–12145.

34. T. Fujimoto, F. Becker and T. Ritter, *Org. Process Res. Dev.*, 2014, **18**, 1041–1044.

35. T. Fujimoto and T. Ritter, *Org. Lett.*, 2015, **17**, 544–547.

36. G. Balz and G. Schiemann, *Ber. Dtsch. Chem. Ges.*, 1927, **60**, 1186–1190.

37. V. V. Grushin, *Acc. Chem. Res.*, 2010, **43**, 160–171.

38. K. L. Hull, W. Q. Anani and M. S. Sanford, *J. Am. Chem. Soc.*, 2006, **128**, 7134–7135.

39. X. S. Wang, T. S. Mei and J. Q. Yu, *J. Am. Chem. Soc.*, 2009, **131**, 7520–7521.

40. T. Furuya, A. S. Kamlet and T. Ritter, *Nature*, 2011, **473**, 470–477.

41. D. A. Watson, M. J. Su, G. Teverovskiy, Y. Zhang, J. Garcia-Fortanet, T. Kinzel and S. L. Buchwald, *Science*, 2009, **325**, 1661–1664.

42. A. C. Sather, H. G. Lee, V. Y. De la Rosa, Y. Yang, P. Muller and S. L. Buchwald, *J. Am. Chem. Soc.*, 2015, **137**, 13433–13438.

43. N. Ichiishi, A. J. Canty, B. F. Yates and M. S. Sanford, *Org. Lett.*, 2013, **15**, 5134–5137.

44. N. D. Ball, J. W. Kampf and M. S. Sanford, *J. Am. Chem. Soc.*, 2010, **132**, 2878–2879.

45. N. D. Ball, J. B. Gary, Y. D. Ye and M. S. Sanford, *J. Am. Chem. Soc.*, 2011, **133**, 7577–7584.

46. C. N. Neumann and T. Ritter, *Angew. Chem., Int. Ed.*, 2015, **54**, 3216–3221.

47. E. Lee, A. S. Kamlet, D. C. Powers, C. N. Neumann, G. B. Boursalian, T. Furuya, D. C. Choi, J. M. Hooker and T. Ritter, *Science*, 2011, **334**, 639–642.

48. T. Mizoroki, K. Mori and A. Ozaki, *Bull. Chem. Soc. Jpn.*, 1971, **44**, 581–581.

49. R. F. Heck and J. P. Nolley, *J. Org. Chem.*, 1972, **37**, 2320–2322.

50. I. P. Beletskaya and A. V. Cheprakov, *Chem. Rev.*, 2000, **100**, 3009–3066.

51. E. Negishi, *J. Organomet. Chem.*, 2002, **653**, 34–40.

52. J. P. Corriu and J. P. Masse, *J. Chem. Soc.-Chem. Commun.*, 1972, 144–144.

53. K. Tamao, Y. Kiso, K. Sumitani and M. Kumada, *J. Am. Chem. Soc.*, 1972, **94**, 9268–9269.

54. K. Tamao, K. Sumitani, Y. Kiso, M. Zembayashi, A. Fujioka, S. Kodama, I. Nakajima, A. Minato and M. Kumada, *Bull. Chem. Soc. Jpn.*, 1976, **49**, 1958–1969.

55. L. Cassar, *J. Organomet. Chem.*, 1975, **93**, 253–257.

56. S. I. Murahashi, *J. Organomet. Chem.*, 2002, **653**, 27–33.

57. K. Sonogashira, Y. Tohda and N. Hagihara, *Tetrahedron Lett.*, 1975, 4467–4470.

58. K. Sonogashira, *J. Organomet. Chem.*, 2002, **653**, 46–49.

59. R. R. Tykwinski, *Angew. Chem., Int. Ed.*, 2003, **42**, 1566–1568.

60. A. O. King, N. Okukado and E. I. Negishi, *J. Chem. Soc.-Chem. Commun.*, 1977, 683–684.

61. E. Negishi, A. O. King and N. Okukado, *J. Org. Chem.*, 1977, **42**, 1821–1823.

62. E. Erdik, *Tetrahedron*, 1992, **48**, 9577–9648.

63. D. Milstein and J. K. Stille, *J. Am. Chem. Soc.*, 1978, **100**, 3636–3638.

64. J. K. Stille, *Angew. Chem.-Int. Edit. Engl.*, 1986, **25**, 508–523.

65. T. N. Mitchell, *Synthesis*, 1992, **1992**, 803–815.

66. N. Miyaura and A. Suzuki, *J. Chem. Soc.-Chem. Commun.*, 1979, 866–867.

67. N. Miyaura, T. Yanagi and A. Suzuki, *Synth. Commun.*, 1981, **11**, 513–519.

68. J. P. Wolfe, R. A. Singer, B. H. Yang and S. L. Buchwald, *J. Am. Chem. Soc.*, 1999, **121**, 9550–9561.

69. N. Miyaura and A. Suzuki, *Chem. Rev.*, 1995, **95**, 2457–2483.

70. Y. Hatanaka and T. Hiyama, *J. Org. Chem.*, 1988, **53**, 918–920.

71. S. E. Denmark, D. Wehrli and J. Y. Choi, *Org. Lett.*, 2000, **2**, 2491–2494.

72. S. E. Denmark and C. S. Regen, *Acc. Chem. Res.*, 2008, **41**, 1486–1499.

73. C. Torborg and M. Beller, *Adv. Synth. Catal.*, 2009, **351**, 3027–3043.

74. B. Li, R. A. Buzon and Z. Zhang, *Org. Process Res. Dev.*, 2007, **11**, 951–955.

75. S. Zegar, C. Tokar, L. A. Enache, V. Rajagopol, W. Zeller, M. O'Connell, J. Singh, F. W. Muellner and D. E. Zembower, *Org. Process Res. Dev.*, 2007, **11**, 747–753.

76. C. Seechurn, M. O. Kitching, T. J. Colacot and V. Snieckus, *Angew. Chem., Int. Ed.*, 2012, **51**, 5062–5085.

77. R. J. Harper, C. Tamborski and E. J. Soloski, *J. Org. Chem.*, 1964, **29**, 2385–2389.

78. D. Kurauchi, K. Hirano, H. Kato, T. Saito, K. Miyamoto and M. Uchiyama, *Tetrahedron*, 2015, **71**, 5849–5857.

79. A. C. Albeniz, P. Espinet, B. Martin-Ruiz and D. Milstein, *J. Am. Chem. Soc.*, 2001, **123**, 11504–11505.

80. A. C. Albeniz, P. Espinet, B. Martin-Ruiz and D. Milstein, *Organometallics*, 2005, **24**, 3679–3684.

81. R. N. Loy and M. S. Sanford, *Org. Lett.*, 2011, **13**, 2548–2551.

82. M. Havelkova, D. Dvorak and M. Hocek, *Synthesis-Stuttgart*, 2001, 1704–1710.

83. T. Thiemann, K. Umeno, D. Ohira, E. Inohae, T. Sawada and S. Mataka, *New J. Chem.*, 1999, **23**, 1067–1070.

84. N. Y. Adonin, A. Y. Shabalin and V. V. Bardin, *J. Fluor. Chem.*, 2014, **168**, 111–120.

85. T. Saeki, Y. Takashima and K. Tamao, *Synlett*, 2005, 1771–1774.

86. T. Ahrens, J. Kohlmann, M. Ahrens and T. Braun, *Chem. Rev.*, 2015, **115**, 931–972.

87. A. D. Sun and J. A. Love, *Dalton Trans.*, 2010, **39**, 10362–10374.

88. H. Amii and K. Uneyama, *Chem. Rev.*, 2009, **109**, 2119–2183.

89. T. Braun and R. N. Perutz, *Chem. Commun.*, 2002, 2749–2757.

90. T. Braun, R. N. Perutz and M. I. Sladek, *Chem. Commun.*, 2001, 2254–2255.

91. T. Korenaga, T. Kosaki, R. Fukumura, T. Ema and T. Sakai, *Org. Lett.*, 2005, **7**, 4915–4917.

92. J. Chen and A. Cammers-Goodwin, *Tetrahedron Lett.*, 2003, **44**, 1503–1506.

93. G. Zou, Y. K. Reddy and J. R. Falck, *Tetrahedron Lett.*, 2001, **42**, 7213–7215.

94. V. V. Bardin, A. Y. Shabalin and N. Y. Adonin, *Beilstein J. Org. Chem.*, 2015, **11**, 608–616.

95. H. J. Frohn, N. Y. Adonin, V. V. Bardin and V. F. Starichenko, *J. Fluor. Chem.*, 2002, **117**, 115–120.

96. G. A. Molander and B. Biolatto, *J. Org. Chem.*, 2003, **68**, 4302–4314.

97. H. J. Frohn, N. Y. Adonin, V. V. Bardin and V. F. Starichenko, *Tetrahedron Lett.*, 2002, **43**, 8111–8114.

98. H. J. Frohn, N. Y. Adonin, V. V. Bardin and V. F. Starichenko, *J. Fluor. Chem.*, 2003, **122**, 195–199.

99. T. Kinzel, Y. Zhang and S. L. Buchwald, *J. Am. Chem. Soc.*, 2010, **132**, 14073–14075.

100. C. Amatore and A. Jutand, *J. Organomet. Chem.*, 1999, **576**, 254–278.

101. N. T. S. Phan, M. Van Der Sluys and C. W. Jones, *Adv. Synth. Catal.*, 2006, **348**, 609–679.

102. A. J. Reay and I. J. S. Fairlamb, *Chem. Commun.*, 2015, **51**, 16289–16307.

103. V. Farina, B. Krishnan, D. R. Marshall and G. P. Roth, *J. Org. Chem.*, 1993, **58**, 5434–5444.

104. V. Farina, *Pure Appl. Chem.*, 1996, **68**, 73–78.

105. A. L. Casado and P. Espinet, *J. Am. Chem. Soc.*, 1998, **120**, 8978–8985.

106. A. L. Casado, P. Espinet and A. M. Gallego, *J. Am. Chem. Soc.*, 2000, **122**, 11771–11782.

107. P. Espinet and A. M. Echavarren, *Angew. Chem., Int. Ed.*, 2004, **43**, 4704–4734.

108. C. Amatore, A. Jutand and G. Le Duc, *Chemistry*, 2011, **17**, 2492–2503.

109. G. T. Crisp, *Chem. Soc. Rev.*, 1998, **27**, 427–436.

110. W. Cabri and I. Candiani, *Acc. Chem. Res.*, 1995, **28**, 2–7.

111. D. J. C. Constable, P. J. Dunn, J. D. Hayler, G. R. Humphrey, J. L. Leazer, R. J. Linderman, K. Lorenz, J. Manley, B. A. Pearlman, A. Wells, A. Zaks and T. Y. Zhang, *Green Chem.*, 2007, **9**, 411–420.

112. D. Alberico, M. E. Scott and M. Lautens, *Chem. Rev.*, 2007, **107**, 174–238.

113. T. Ishiyama, J. Takagi, K. Ishida, N. Miyaura, N. R. Anastasi and J. F. Hartwig, *J. Am. Chem. Soc.*, 2002, **124**, 390–391.

114. C. S. Yeung and V. M. Dong, *Chem. Rev.*, 2011, **111**, 1215–1292.

115. L. Ackermann, R. Vicente and A. R. Kapdi, *Angewandte Chemie*, 2009, **48**, 9792–9826.

116. L. Ackermann, *Chem. Rev.*, 2011, **111**, 1315–1345.

117. C. H. Park, V. Ryabova, I. V. Seregin, A. W. Sromek and V. Gevorgyan, *Org. Lett.*, 2004, **6**, 1159–1162.

118. B. S. Lane, M. A. Brown and D. Sames, *J. Am. Chem. Soc.*, 2005, **127**, 8050–8057.

119. M. Lafrance and K. Fagnou, *J. Am. Chem. Soc.*, 2006, **128**, 16496–16497.

120. L. C. Campeau, S. Rousseaux and K. Fagnou, *J. Am. Chem. Soc.*, 2005, **127**, 18020–18021.

121. X. W. Ma, Y. Liu, P. Liu, J. W. Xie, B. Dai and Z. Y. Liu, *Appl. Organomet. Chem.*, 2014, **28**, 180–185.

122. M. Lafrance, C. N. Rowley, T. K. Woo and K. Fagnou, *J. Am. Chem. Soc.*, 2006, **128**, 8754–8756.

123. X. C. Cambeiro, N. Ahlsten and I. Larrosa, *J. Am. Chem. Soc.*, 2015, **137**, 15636–15639.

124. M. Simonetti, G. J. P. Perry, X. C. Cambeiro, F. Julia-Hernandez, J. N. Arokianathar and I. Larrosa, *J. Am. Chem. Soc.*, 2016, **138**, 3596–3606.

125. H. Q. Do and O. Daugulis, *J. Am. Chem. Soc.*, 2008, **130**, 1128–1129.

126. F. Chen, Q. Q. Min and X. Zhang, *J. Org. Chem.*, 2012, **77**, 2992–2998.

127. M. Cao, D. Wu, W. Su and R. Cao, *J. Catal.*, 2015, **321**, 62–69.

128. S. Fan, J. Yang and X. Zhang, *Org. Lett.*, 2011, **13**, 4374–4377.

129. A. D. Ryabov, *Chem. Rev.*, 1990, **90**, 403–424.

130. M. S. McClure, B. Glover, E. McSorley, A. Millar, M. H. Osterhout and F. Roschangar, *Org. Lett.*, 2001, **3**, 1677–1680.

131. B. Glover, K. A. Harvey, B. Liu, M. J. Sharp and M. F. Tymoschenko, *Org. Lett.*, 2003, **5**, 301–304.

132. W. J. Li, D. P. Nelson, M. S. Jensen, R. S. Hoerrner, G. J. Javadi, D. Cai and R. D. Larsen, *Org. Lett.*, 2003, **5**, 4835–4837.

133. J. X. Wang, J. A. McCubbin, M. Z. Jin, R. S. Laufer, Y. Y. Mao, A. P. Crew, M. J. Mulvihill and V. Snieckus, *Org. Lett.*, 2008, **10**, 2923–2926.

134. R. S. Sanchez and F. A. Zhuravlev, *J. Am. Chem. Soc.*, 2007, **129**, 5824–2825.

135. S. I. Gorelsky, D. Lapointe and K. Fagnou, *J. Am. Chem. Soc.*, 2008, **130**, 10848–10849.

136. Y. Boutadla, D. L. Davies, S. A. Macgregor and A. I. Poblador-Bahamonde, *Dalton Trans.*, 2009, 5887–5893.

137. Y. Boutadla, D. L. Davies, S. A. Macgregor and A. I. Poblador-Bahamonde, *Dalton Trans.*, 2009, 5820–5831.

138. S. Winstein and T. G. Traylor, *J. Am. Chem. Soc.*, 1955, **77**, 3747–3752.

139. C. W. Fung, M. Khorramdelvahed, R. J. Ranson and R. M. G. Roberts, *J. Chem. Soc.-Perkin Trans. 2*, 1980, 267–272.

140. J. M. Davidson and C. Triggs, *J. Chem. Soc. A*, 1968, 1324–1330.

141. A. D. Ryabov, I. K. Sakodinskaya and A. K. Yatsimirsky, *J. Chem. Soc.-Dalton Trans.*, 1985, 2629–2638.

142. D. L. Davies, S. M. A. Donald and S. A. Macgregor, *J. Am. Chem. Soc.*, 2005, **127**, 13754–13755.

143. W. J. Tenn, K. J. H. Young, G. Bhalla, J. Oxgaard, W. A. Goddard and R. A. Periana, *J. Am. Chem. Soc.*, 2005, **127**, 14172–14173.

144. J. Oxgaard, W. J. Tenn, III, R. J. Nielsen, R. A. Periana and W. A. Goddard, III, *Organometallics*, 2007, **26**, 1565–1567.

145. D. Lapointe and K. Fagnou, *Chem. Lett.*, 2010, **39**, 1119–1126.

146. L. Ackermann, R. Vicente and A. Althammer, *Org. Lett.*, 2008, **10**, 2299–2302.

147. C. Amatore and A. Jutand, *Acc. Chem. Res.*, 2000, **33**, 314–321.

148. T. W. Lyons and M. S. Sanford, *Chem. Rev.*, 2010, **110**, 1147–1169.

149. X. Chen, K. M. Engle, D. H. Wang and J. Q. Yu, *Angewandte Chemie*, 2009, **48**, 5094–5115.

150. G. P. McGlacken and L. M. Bateman, *Chem. Soc. Rev.*, 2009, **38**, 2447–2464.

151. D. Kalyani, N. R. Deprez, L. V. Desai and M. S. Sanford, *J. Am. Chem. Soc.*, 2005, **127**, 7330–7331.

152. M. R. Yadav, R. K. Rit and A. K. Sahoo, *Chem.-Eur. J.*, 2012, **18**, 5541–5545.

153. R. K. Rit, M. R. Yadav and A. K. Sahoo, *Org. Lett.*, 2012, **14**, 3724–3727.

154. N. Uhlig and C. J. Li, *Chem.-Eur. J.*, 2014, **20**, 12066–12070.

155. J. Cornella, M. Righi and I. Larrosa, *Angew. Chem., Int. Ed.*, 2011, **50**, 9429–9432.

156. J. F. Luo, S. Preciado and I. Larrosa, *J. Am. Chem. Soc.*, 2014, **136**, 4109–4112.

157. R. B. Bedford, S. J. Coles, M. B. Hursthouse and M. E. Limmert, *Angew. Chem., Int. Ed.*, 2003, **42**, 112–114.

158. D. Leow, G. Li, T. S. Mei and J. Q. Yu, *Nature*, 2012, **486**, 518–522.

159. P. Wang, M. E. Farmer, X. Huo, P. Jain, P. X. Shen, M. Ishoey, J. E. Bradner, S. R. Wisniewski, M. D. Eastgate and J. Q. Yu, *J. Am. Chem. Soc.*, 2016, **138**, 9269–9276.

160. Y.-F. Yang, G.-J. Cheng, P. Liu, D. Leow, T.-Y. Sun, P. Chen, X. Zhang, J.-Q. Yu, Y.-D. Wu and K. N. Houk, *J. Am. Chem. Soc.*, 2014, **136**, 344–355.

161. H. X. Dai, G. Li, X. G. Zhang, A. F. Stepan and J. Q. Yu, *J. Am. Chem. Soc.*, 2013, **135**, 7567–7571.

162. L. Wan, N. Dastbaravardeh, G. Li and J. Q. Yu, *J. Am. Chem. Soc.*, 2013, **135**, 18056–18059.

163. Y. J. Liu, H. Xu, W. J. Kong, M. Shang, H. X. Dai and J. Q. Yu, *Nature*, 2014, **515**, 389–393.

164. N. Kuhl, M. N. Hopkinson, J. Wencel-Delord and F. Glorius, *Angew. Chem., Int. Ed.*, 2012, **51**, 10236–10254.

165. D. Garcia-Cuadrado, P. de Mendoza, A. A. C. Braga, F. Maseras and A. M. Echavarren, *J. Am. Chem. Soc.*, 2007, **129**, 6880–6886.

166. H. Li, J. Liu, C. L. Sun, B. J. Li and Z. J. Shi, *Org. Lett.*, 2011, **13**, 276–279.

167. C. Y. He, S. L. Fan and X. G. Zhang, *J. Am. Chem. Soc.*, 2010, **132**, 12850–12852.

168. J. Guihaume, E. Clot, O. Eisenstein and R. N. Perutz, *Dalton Trans.*, 2010, **39**, 10510–10519.

169. S. I. Gorelsky, *Coord. Chem. Rev.*, 2013, **257**, 153–164.

170. A. Vigalok, O. Uzan, L. J. W. Shimon, Y. Ben-David, J. M. L. Martin and D. Milstein, *J. Am. Chem. Soc.*, 1998, **120**, 12539–12544.

171. J. S. Cannon, L. F. Zou, P. Liu, Y. Lan, D. J. O'Leary, K. N. Houk and R. H. Grubbs, *J. Am. Chem. Soc.*, 2014, **136**, 6733–6743.

172. H.-Y. Sun, S. I. Gorelsky, D. R. Stuart, L.-C. Campeau and K. Fagnou, *J. Org. Chem.*, 2010, **75**, 8180–8189.

173. Y. Tan, F. Barrios-Landeros and J. F. Hartwig, *J. Am. Chem. Soc.*, 2012, **134**, 3683–3686.

174. S. Duric, F. D. Sypaseuth, S. Hoof, E. Svensson and C. C. Tzschucke, *Chem.-Eur. J.*, 2013, **19**, 17456–17463.

175. M. Wakioka, Y. Nakamura, Q. Wang and F. Ozawa, *Organometallics*, 2012, **31**, 4810–4816.

176. M. Wakioka, Y. Nakamura, Y. Hihara, F. Ozawa and S. Sakaki, *Organometallics*, 2013, **32**, 4423–4430.

177. E. Ferrer Flegeau, C. Bruneau, P. H. Dixneuf and A. Jutand, *J. Am. Chem. Soc.*, 2011, **133**, 10161–10170.

178. I. Fabre, N. von Wolff, G. Le Duc, E. F. Flegeau, C. Bruneau, P. H. Dixneuf and A. Jutand, *Chem.-Eur. J.*, 2013, **19**, 7595–7604.

179. P. Ricci, K. Kraemer, X. C. Cambeiro and I. Larrosa, *J. Am. Chem. Soc.*, 2013, **135**, 13258–13261.

180. D. Whitaker, J. Burés and I. Larrosa, *J. Am. Chem. Soc.*, 2016, **138**, 8384–8387.

181. M. D. Lotz, N. M. Camasso, A. J. Canty and M. S. Sanford, *Organometallics*, 2016, **36**, 165–171.

182. M.-A. Légaré, M.-A. Courtemanche, É. Rochette and F.-G. Fontaine, *Science*, 2015, **349**, 513–516.

183. S. Kozuch and J. M. L. Martin, *ACS Catal.*, 2012, **2**, 2787–2794.

184. B. R. Park, K. H. Kim, T. H. Kim and J. N. Kim, *Tetrahedron Lett.*, 2011, **52**, 4405–4407.

185. D. R. Fahey and J. E. Mahan, *J. Am. Chem. Soc.*, 1976, **98**, 4499–4503.

186. M. A. Delarosa, E. Velarde and A. Guzman, *Synth. Commun.*, 1990, **20**, 2059–2064.

187. M. Beller, H. Fischer, K. Kuhlein, C. P. Reisinger and W. A. Herrmann, *J. Organomet. Chem.*, 1996, **520**, 257–259.

188. A. Biffis, M. Zecca and M. Basato, *J. Mol. Catal. A-Chem.*, 2001, **173**, 249–274.

189. D. Astruc, *Inorg. Chem.*, 2007, **46**, 1884–1894.

190. C. Amatore, E. Carre, A. Jutand, M. A. Mbarki and G. Meyer, *Organometallics*, 1995, **14**, 5605–5614.

191. C. Amatore, E. Carre and A. Jutand, *Acta Chem. Scand.*, 1998, **52**, 100–106.

192. M. Garcia-Melchor, A. A. C. Braga, A. Lledos, G. Ujaque and F. Maseras, *Acc. Chem. Res.*, 2013, **46**, 2626–2634.

193. J.-M. Weibel, A. Blanc and P. Pale, *Chem. Rev.*, 2008, **108**, 3149–3173.

194. C. Amatore, E. Carre, A. Jutand and M. A. Mbarki, *Organometallics*, 1995, **14**, 1818–1826.

195. X. Fang, Y. Y. Huang, X. Q. Chen, X. X. Lin, Z. S. Bai, K. W. Huang, Y. F. Yuan and Z. Q. Weng, *J. Fluor. Chem.*, 2013, **151**, 50–57.

196. S. Takemoto and V. V. Grushin, *J. Am. Chem. Soc.*, 2013, **135**, 16837–16840.

197. G. Biedermann and L. G. Sillen, *Acta Chem. Scand.*, 1960, **14**, 717–725.

198. C. Arroniz, J. G. Denis, A. Ironmonger, G. Rassias and I. Larrosa, *Chem. Sci.*, 2014, **5**, 3509–3514.

199. D. Prat, A. Wells, J. Hayler, H. Sneddon, C. R. McElroy, S. Abou-Shehada and P. J. Dunn, *Green Chem.*, 2016, **18**, 288–296.

200. Niosh, *Am. Ind. Hyg. Assoc. J.*, 1991, **52**, A162–A160, A162.

201. C. Fischmeister and H. Doucet, *Green Chem.*, 2011, **13**, 741–753.

202. O. Rene and K. Fagnou, *Org. Lett.*, 2010, **12**, 2116–2119.

203. B. Schaffner, F. Schaffner, S. P. Verevkin and A. Borner, *Chem. Rev.*, 2010, **110**, 4554–4581.

204. L. A. Adrio, B. N. Nguyen, G. Guilera, A. G. Livingston and K. K. Hii, *Catal. Sci. Tech.*, 2012, **2**, 316–323.

205. J. S. Mathew, M. Klussmann, H. Iwamura, F. Valera, A. Futran, E. A. C. Emanuelsson and D. G. Blackmond, *J. Org. Chem.*, 2006, **71**, 4711–4722.

206. M. J. Burns, R. J. Thatcher, R. J. K. Taylor and I. J. S. Fairlamb, *Dalton Trans.*, 2010, **39**, 10391–10400.

207. C. Amatore, A. A. Bahsoun, A. Jutand, G. Meyer, A. N. Ntepe and L. Ricard, *J. Am. Chem. Soc.*, 2003, **125**, 4212–4222.

208. C. Markert, M. Neuburger, K. Kulicke, M. Meuwly and A. Pfaltz, *Angew. Chem., Int. Ed.*, 2007, **46**, 5892–5895.

209. D. Harakat, J. Muzart and J. Le Bras, *RSC Adv.*, 2012, **2**, 3094–3099.

210. R. A. Widenhoefer and S. L. Buchwald, *Organometallics*, 1996, **15**, 2755–2763.

211. V. V. Grushin and H. Alper, *Organometallics*, 1993, **12**, 1890–1901.

212. V. V. Grushin, C. Bensimon and H. Alper, *Organometallics*, 1995, **14**, 3259–3263.

213. M. Aufiero, T. Scattolin, F. Proutiere and F. Schoenebeck, *Organometallics*, 2015, **34**, 5191–5195.

214. F. Zaera, *Chem. Soc. Rev.*, 2014, **43**, 7624–7663.

215. G. Mul, G. M. Hamminga and J. A. Moulijn, *Vib. Spectrosc.*, 2004, **34**, 109–121.

216. A. Vimont, F. Thibault-Starzyk and M. Daturi, *Chem. Soc. Rev.*, 2010, **39**, 4928–4950.

217. C. He, G. H. Zhang, J. Ke, H. Zhang, J. T. Miller, A. J. Kropf and A. W. Lei, *J. Am. Chem. Soc.*, 2013, **135**, 488–493.

218. N. S. Sheikh, D. Leonori, G. Barker, J. D. Firth, K. R. Campos, A. J. H. M. Meijer, P. O'Brien and I. Coldham, *J. Am. Chem. Soc.*, 2012, **134**, 5300–5308.

219. J. E. Lynch, S. M. Riseman, W. L. Laswell, D. M. Tschaen, R. P. Volante, G. B. Smith and I. Shinkai, *J. Org. Chem.*, 1989, **54**, 3792–3796.

220. A. Pintar, J. Batista and J. Levec, *Analyst*, 2002, **127**, 1535–1540.

221. D. G. Blackmond, *Angew. Chem., Int. Ed.*, 2005, **44**, 4302–4320.

222. D. Steele and D. H. Whiffen, *Spectrochim. Acta*, 1960, **16**, 368–375.

223. D. A. Long and D. Steele, *Spectrochim. Acta*, 1963, **19**, 1947–1954.

224. C. Garrigoulagrange, J. M. Lebas and M. L. Josien, *Spectrochim. Acta*, 1958, **12**, 305–320.

225. J. H. S. Green, *Spectrochim. Acta A*, 1970, **A 26**, 1503–1513.

226. F. Meunier and M. Daturi, *Catal. Today*, 2006, **113**, 1–2.

227. M. A. Banares, *Catal. Today*, 2005, **100**, 71–77.

228. J. Burés, *Angew. Chem., Int. Ed.*, 2016, **55**, 2028–2031.

229. J. Burés, *Angew. Chem.*, 2016, **128**, 16318–16321.

230. S. Shekhar, P. Ryberg, J. F. Hartwig, J. S. Mathew, D. G. Blackmond, E. R. Strieter and S. L. Buchwald, *J. Am. Chem. Soc.*, 2006, **128**, 3584–3591.

231. A. P. Smalley and M. J. Gaunt, *J. Am. Chem. Soc.*, 2015, **137**, 10632–10641.

232. E. R. Strieter, D. G. Blackmond and S. L. Buchwald, *J. Am. Chem. Soc.*, 2005, **127**, 4120–4121.

233. S. P. Mathew, S. Gunathilagan, S. M. Roberts and D. G. Blackmond, *Org. Lett.*, 2005, **7**, 4847–4850.

234. P. Dydio, R. J. Detz and J. N. H. Reek, *J. Am. Chem. Soc.*, 2013, **135**, 10817–10828.

235. M. Colladon, A. Scarso, P. Sgarbossa, R. A. Michelin and G. Strukul, *J. Am. Chem. Soc.*, 2007, **129**, 7680–7689.

236. S. B. Kedia and M. B. Mitchell, *Org. Process Res. Dev.*, 2009, **13**, 420–428.

237. G. P. F. van Strijdonck, M. D. K. Boele, P. C. J. Kamer, J. G. de Vries and P. van Leeuwen, *Eur. J. Inorg. Chem.*, 1999, 1073–1076.

238. A. K. Cook and M. S. Sanford, *J. Am. Chem. Soc.*, 2015, **137**, 3109–3118.

239. T. Rosner, J. Le Bars, A. Pfaltz and D. G. Blackmond, *J. Am. Chem. Soc.*, 2001, **123**, 1848–1855.

240. M. Kitamura, S. Suga, H. Oka and R. Noyori, *J. Am. Chem. Soc.*, 1998, **120**, 9800–9809.

241. S. S. Woodard, M. G. Finn and K. B. Sharpless, *J. Am. Chem. Soc.*, 1991, **113**, 106–113.

242. E. Negishi, T. Takahashi, S. Baba, D. E. Vanhorn and N. Okukado, *J. Am. Chem. Soc.*, 1987, **109**, 2393–2401.

243. W. Ostwald, *Lehrbuch Der Allgemeinen Chemie*, Engelmann, 1902.

244. E. Vitz, *J. Chem. Educ.*, 1998, **75**, 1661–1663.

245. W. F. Coleman, *J. Chem. Educ.*, 1996, **73**, 243–245.

246. W. E. Roseveare, *J. Am. Chem. Soc.*, 1931, **53**, 1651–1661.

247. S. D. Kirik, R. F. Mulagaleev and A. I. Blokhin, *Acta Crystallogr. Sect. C-Cryst. Struct. Commun.*, 2004, **60**, M449–M450.

248. M. Boudart, A. Aldag, J. E. Benson, Doughart.Na and C. G. Harkins, *J. Catal.*, 1966, **6**, 92–99.

249. S. Kozuch and S. Shaik, *Acc. Chem. Res.*, 2011, **44**, 101–110.

250. S. Kozuch and J. M. L. Martin, *ACS Catal.*, 2011, **1**, 246–253.

251. I. J. S. Fairlamb, A. R. Kapdi, A. F. Lee, G. Sanchez, G. Lopez, J. L. Serrano, L. Garcia, J. Perez and E. Perez, *Dalton Trans.*, 2004, 3970–3981.

252. M. T. Reetz and J. G. de Vries, *Chem. Commun.*, 2004, 1559–1563.

253. A. H. M. de Vries, J. Mulders, J. H. M. Mommers, H. J. W. Henderickx and J. G. de Vries, *Org. Lett.*, 2003, **5**, 3285–3288.

254. H. A. Dieck and R. F. Heck, *J. Am. Chem. Soc.*, 1974, **96**, 1133–1136.

255. R. F. Heck, *Acc. Chem. Res.*, 1979, **12**, 146–151.

256. R. F. Heck, *Org. React.*, 1982, **27**, 345–390.

257. C. Amatore, A. Jutand and M. A. Mbarki, *Organometallics*, 1992, **11**, 3009–3013.

258. M. Camalli, F. Caruso, S. Chaloupka, P. N. Kapoor, P. S. Pregosin and L. M. Venanzi, *Helv. Chim. Acta*, 1984, **67**, 1603–1611.

259. M. Anand, R. B. Sunoj and H. F. Schaefer, *J. Am. Chem. Soc.*, 2014, **136**, 5535–5538.

260. D. R. Lide, *CRC Handbook of Chemistry and Physics : a Ready-Reference Book of Chemical and Physical Data*, CRC Press, Boca Raton, Fla., 2009.

261. R. Alexander, E. C. F. Ko, Y. C. Mac and A. J. Parker, *J. Am. Chem. Soc.*, 1967, **89**, 3703–3712.

262. J. Bigeleisen and M. G. Mayer, *J. Chem. Phys.*, 1947, **15**, 261–267.

263. E. M. Simmons and J. F. Hartwig, *Angew. Chem., Int. Ed.*, 2012, **51**, 3066–3072.

264. S. A. Johnson, E. T. Taylor and S. J. Cruise, *Organometallics*, 2009, **28**, 3842–3855.

265. R. Apweiler, R. Armstrong, A. Bairoch, A. Cornish-Bowden, P. J. Halling, J. H. S. Hofmeyr, C. Kettner, T. S. Leyh, J. Rohwer, D. Schomburg, C. Steinbeck and K. Tipton, *Nat. Chem. Biol.*, 2010, **6**, 785–785.

266. K. Francis and A. Kohen, *Perspect. Sci.*, 2014, **1**, 110–120.

267. H. S. Johnston, W. A. Bonner and D. J. Wilson, *J. Chem. Phys.*, 1957, **26**, 1002–1006.

268. F. Abu-Hasanayn, A. S. Goldman and K. Krogh-Jespersen, *J. Phys. Chem.*, 1993, **97**, 5890–5896.

269. R. S. Sikorski, L. Wang, K. A. Markham, P. T. R. Rajagopalan, S. J. Benkovic and A. Kohen, *J. Am. Chem. Soc.*, 2004, **126**, 4778–4779.

270. R. P. Bell, *Trans. Faraday Soc.*, 1959, **55**, 1–4.

271. M. J. Sutcliffe and N. S. Scrutton, *Eur. J. Biochem.*, 2002, **269**, 3096–3102.

272. A. Kohen, R. Cannio, S. Bartolucci and J. P. Klinman, *Nature*, 1999, **399**, 496–499.

273. Z. D. Nagel and J. P. Klinman, *Chem. Rev.*, 2006, **106**, 3095–3118.

274. F. G. Bordwell and W. J. Boyle, *J. Am. Chem. Soc.*, 1971, **93**, 512–514.

275. F. H. Westheimer, *Chem. Rev.*, 1961, **61**, 265–273.

276. H. Kwart, *Acc. Chem. Res.*, 1982, **15**, 401–408.

277. H. Kwart and M. C. Latimore, *J. Am. Chem. Soc.*, 1971, **93**, 3770–3771.

278. D. Munz, M. Webster-Gardiner, R. Fu, T. Strassner, W. A. Goddard and T. B. Gunnoe, *ACS Catal.*, 2015, **5**, 769–775.

279. J. C. Maxwell, *Philos. Mag. Series 4*, 1860, **19**, 19–32.

280. J. C. Maxwell, *Philos. Mag. Series 4*, 1860, **20**, 21–37.

281. S. A. Arrhenius, *Z. Phys. Chem.*, 1889, **4**, 96–116.

282. S. A. Arrhenius, *Z. Phys. Chem.*, 1889, **4**, 226–248.

283. H. Eyring, *J. Chem. Phys.*, 1935, **3**, 107–115.

284. W. F. K. Wynne-Jones and H. Eyring, *J. Chem. Phys.*, 1935, **3**, 492–502.

285. S. Kozuch and J. M. L. Martin, *Chemphyschem*, 2011, **12**, 1413–1418.

286. L. P. Hammett, *J. Am. Chem. Soc.*, 1937, **59**, 96–103.

287. L. P. Hammett, *Chem. Rev.*, 1935, **17**, 125–136.

288. C. Hansch, A. Leo and R. W. Taft, *Chem. Rev.*, 1991, **91**, 165–195.

289. J. H. Schauble, G. J. Walter and J. G. Morin, *J. Org. Chem.*, 1974, **39**, 755–760.

290. H. M. Yau, A. K. Croft and J. B. Harper, *Chem. Commun.*, 2012, **48**, 8937–8939.

291. H. C. Brown and Y. Okamoto, *J. Am. Chem. Soc.*, 1958, **80**, 4979–4987.

292. J. Schwartz, *Acc. Chem. Res.*, 1985, **18**, 302–308.

293. D. J. Cole-Hamilton, *Science*, 2003, **299**, 1702–1706.

294. L. X. Yin and J. Liebscher, *Chem. Rev.*, 2007, **107**, 133–173.

295. J. A. Widegren and R. G. Finke, *J. Mol. Catal. A-Chem.*, 2003, **198**, 317–341.

296. D. Astruc, F. Lu and J. R. Aranzaes, *Angew. Chem., Int. Ed.*, 2005, **44**, 7852–7872.

297. M. Pagliaro, V. Pandarus, R. Ciriminna, F. Beland and P. D. Cara, *Chemcatchem*, 2012, **4**, 432–445.

298. J. G. de Vries, *Dalton Trans.*, 2006, 421–429.

299. C. C. Cassol, A. P. Umpierre, G. Machado, S. I. Wolke and J. Dupont, *J. Am. Chem. Soc.*, 2005, **127**, 3298–3299.

300. J. Hu and Y. B. Liu, *Langmuir*, 2005, **21**, 2121–2123.

301. R. H. Crabtree, *Chem. Rev.*, 2012, **112**, 1536–1554.

302. D. R. Anton and R. H. Crabtree, *Organometallics*, 1983, **2**, 855–859.

303. G. M. Whitesides, M. Hackett, R. L. Brainard, J. Lavalleye, A. F. Sowinski, A. N. Izumi, S. S. Moore, D. W. Brown and E. M. Staudt, *Organometallics*, 1985, **4**, 1819–1830.

304. S. Klingelhofer, W. Heitz, A. Greiner, S. Oestreich, S. Forster and M. Antonietti, *J. Am. Chem. Soc.*, 1997, **119**, 10116–10120.

305. C. S. Consorti, F. R. Flores and J. Dupont, *J. Am. Chem. Soc.*, 2005, **127**, 12054–12065.

306. H. J. Dietz, Google Patents, 1964.

307. K. Q. Yu, W. Sommer, M. Weck and C. W. Jones, *J. Catal.*, 2004, **226**, 101–110.

308. K. Q. Yu, W. Sommer, J. M. Richardson, M. Weck and C. W. Jones, *Adv. Synth. Catal.*, 2005, **347**, 161–171.

309. J. E. Hamlin, K. Hirai, A. Millan and P. M. Maitlis, *J. Mol. Catal.*, 1980, **7**, 543–544.

310. R. A. Sheldon, M. Wallau, I. Arends and U. Schuchardt, *Acc. Chem. Res.*, 1998, **31**, 485–493.

311. A. Alimardanov, L. S. V. de Vondervoort, A. H. M. de Vries and J. G. de Vries, *Adv. Synth. Catal.*, 2004, **346**, 1812–1817.

312. M. T. Reetz and E. Westermann, *Angew. Chem., Int. Ed.*, 2000, **39**, 165–168.

313. D. Saha, L. Adak and B. C. Ranu, *Tetrahedron Lett.*, 2010, **51**, 5624–5627.

314. T. E. Storr, C. G. Baumann, R. J. Thatcher, S. De Ornellas, A. C. Whitwood and I. J. Fairlamb, *J. Org. Chem.*, 2009, **74**, 5810–5821.

315. M. Hyotanishi, Y. Isomura, H. Yamamoto, H. Kawasaki and Y. Obora, *Chem. Commun.*, 2011, **47**, 5750–5752.

316. H. Yano, Y. Nakajima and Y. Obora, *J. Organomet. Chem.*, 2013, **745**, 258–261.

317. T. Korenaga, N. Suzuki, M. Sueda and K. Shimada, *J. Organomet. Chem.*, 2015, **780**, 63–69.

318. O. Rene and K. Fagnou, *Adv. Synth. Catal.*, 2010, **352**, 2116–2120.

319. M. Wakioka, Y. Nakamura, M. Montgomery and F. Ozawa, *Organometallics*, 2015, **34**, 198–205.

320. C. A. Tolman, *J. Am. Chem. Soc.*, 1970, **92**, 2956–2965.

321. I. D. Jurberg, *Synlett*, 2011, 3053–3054.

322. J. P. Collman, K. M. Kosydar, M. Bressan, W. Lamanna and T. Garrett, *J. Am. Chem. Soc.*, 1984, **106**, 2569–2579.

323. J. Rebek, *Tetrahedron*, 1979, **35**, 723–731.

324. J. Rebek, D. Brown and S. Zimmerman, *J. Am. Chem. Soc.*, 1975, **97**, 454–455.

325. L. Zhang, Z. P. Li, Y. Zhang, M. C. Paau, Q. Hu, X. J. Gong, S. M. Shuang, C. Dong, X. G. Peng and M. M. F. Choi, *Talanta*, 2015, **131**, 632–639.

326. R. O. Jones, *Rev. Mod. Phys.* , 2015, **87**, 897–923.

327. B. Cornils and W. A. Herrmann, *Applied Homogeneous Catalysis with Organometallic Compounds*, VCH Weinheim etc., 1996.

328. B. Heaton, *Mechanisms in Homogeneous Catalysis: A Spectroscopic Approach*, Wiley, 2006.

329. J. A. Rodriguez, J. C. Hanson and P. J. Chupas, *In-situ Characterization of Heterogeneous Catalysts*, Wiley, 2013.

330. L. S. Santos, *Reactive Intermediates: MS Investigations in Solution*, Wiley, 2009.

331. A. T. Bell, *NMR Techniques in Catalysis*, Taylor & Francis, 1994.

332. E. R. Andrew, A. Bradbury and R. G. Eades, *Nature*, 1958, **182**, 1659–1659.

333. I. J. Lowe, *Phys. Rev. Lett.*, 1959, **2**, 285–287.

334. E. R. Andrew and R. G. Eades, *Discuss. Faraday Soc.*, 1962, 38–42.

335. T. M. Alam and J. E. Jenkins, in *Advanced Aspects of Spectroscopy*, ed. M. A. Farrukh, InTech, 2012.

336. E. M. Ratai, S. Pilkenton, M. R. Lentz, J. B. Greco, R. A. Fuller, J. P. Kim, J. He, L. L. Cheng and R. G. Gonzalez, *NMR Biomed.*, 2005, **18**, 242–251.

337. J. L. Griffin, M. Bollard, J. K. Nicholson and K. Bhakoo, *NMR Biomed.*, 2002, **15**, 375–384.

338. J. H. Chen, E. B. Sambol, P. DeCarolis, R. O'Connor, R. C. Geha, Y. V. Wu and S. Singer, *Magn. Reson. Med.*, 2006, **55**, 1246–1256.

339. V. M. Mastikhin, *Colloid Surf. A*, 1993, **78**, 143–166.

340. T. Posset and J. Blumel, *J. Am. Chem. Soc.*, 2006, **128**, 8394–8395.

341. V. Pinoie, K. Poelmans, H. E. Miltner, I. Verbruggen, M. Biesemans, G. Van Assche, B. Van Mele, J. C. Martins and R. Willem, *Organometallics*, 2007, **26**, 6718–6725.

342. A. D. Roy, K. Jayalakshmi, S. Dasgupta, R. Roy and B. Mukhopadhyay, *Magn. Reson. Chem.*, 2008, **46**, 1119–1126.

343. H. M. Gauniyal, S. Gupta, S. K. Sharma and U. Bajpai, *Synth. Commun.*, 2013, **43**, 2090–2099.

344. A. G. Jarvis, P. E. Sehnal, S. E. Bajwa, A. C. Whitwood, X. B. Zhang, M. S. Cheung, Z. Y. Lin and I. J. S. Fairlamb, *Chem.-Eur. J.*, 2013, **19**, 6034–6043.

345. X. F. Mei and C. Wolf, *J. Org. Chem.*, 2005, **70**, 2299–2305.

346. E. Bosch, C. L. Barnes, N. L. Brenrian, G. L. Eakins and B. E. Breyfogle, *J. Org. Chem.*, 2008, **73**, 3931–3934.

347. J. A. Goodfellow, T. A. Stephenson and M. C. Cornock, *J. Chem. Soc.-Dalton Trans.*, 1978, 1195–1200.

348. K. L. Vikse, Z. Ahmadi and J. S. McIndoe, *Coord. Chem. Rev.*, 2014, **279**, 96–114.

349. H. B. Linden, *Eur. J. Mass Spectrom.*, 2004, **10**, 459–468.

350. A. A. Sabino, A. H. L. Machado, C. R. D. Correia and M. N. Eberlin, *Angew. Chem., Int. Ed.*, 2004, **43**, 2514–2518.

351. A. Vasseur, D. Harakat, J. Muzart and J. Le Bras, *J. Org. Chem.*, 2012, **77**, 5751–5758.

352. D. Agrawal, D. Schroder and C. M. Frech, *Organometallics*, 2011, **30**, 3579–3587.

353. C. D. Buarque, V. D. Pinho, B. G. Vaz, M. N. Eberlin, A. J. M. da Silva and P. R. R. Costa, *J. Organomet. Chem.*, 2010, **695**, 2062–2067.

354. K. L. Vikse, Z. Ahmadi, C. C. Manning, D. A. Harrington and J. S. McIndoe, *Angew. Chem., Int. Ed.*, 2011, **50**, 8304–8306.

355. F. E. Goodson, T. I. Wallow and B. M. Novak, *J. Am. Chem. Soc.*, 1997, **119**, 12441–12453.

356. K. C. Kong and C. H. Cheng, *J. Am. Chem. Soc.*, 1991, **113**, 6313–6315.

357. F. Y. Kwong, C. W. Lai, M. Yu and K. S. Chan, *Tetrahedron*, 2004, **60**, 5635–5645.

358. D. F. Okeefe, M. C. Dannock and S. M. Marcuccio, *Tetrahedron Lett.*, 1992, **33**, 6679–6680.

359. B. E. Segelstein, T. W. Butler and B. L. Chenard, *J. Org. Chem.*, 1995, **60**, 12–13.

360. V. V. Grushin, *Organometallics*, 2000, **19**, 1888–1900.

361. J. F. Fauvarque, F. Pfluger and M. Troupel, *J. Organomet. Chem.*, 1981, **208**, 419–427.

362. J. F. Hartwig and F. Paul, *J. Am. Chem. Soc.*, 1995, **117**, 5373–5374.

363. A. L. Casado and P. Espinet, *Organometallics*, 1998, **17**, 954–959.

364. F. Ozawa, T. Ito, Y. Nakamura and A. Yamamoto, *Bull. Chem. Soc. Jpn.*, 1981, **54**, 1868–1880.

365. J. F. Fauvarque and A. Jutand, *Bull. Soc. Chim. Fr.*, 1976, 765–770.

366. J. F. Fauvarque and A. Jutand, *J. Organomet. Chem.*, 1977, **132**, C17–C19.

367. J. M. Brown and K. K. Hii, *Angew. Chem.-Int. Edit. Engl.*, 1996, **35**, 657–659.

368. K. K. Hii, T. D. W. Claridge and J. M. Brown, *Angew. Chem.-Int. Edit. Engl.*, 1997, **36**, 984–987.

369. M. Portnoy, Y. Bendavid, I. Rousso and D. Milstein, *Organometallics*, 1994, **13**, 3465–3479.

370. C. M. Andersson, A. Hallberg and G. D. Daves, *J. Org. Chem.*, 1987, **52**, 3529–3536.

371. J. M. Brown and P. J. Guiry, *Inorg. Chim. Acta*, 1994, **220**, 249–259.

372. M. S. Driver and J. F. Hartwig, *J. Am. Chem. Soc.*, 1997, **119**, 8232–8245.

373. R. A. Widenhoefer, H. A. Zhong and S. L. Buchwald, *J. Am. Chem. Soc.*, 1997, **119**, 6787–6795.

374. A. Gillie and J. K. Stille, *J. Am. Chem. Soc.*, 1980, **102**, 4933–4941.

375. E. Negishi, T. Takahashi and K. Akiyoshi, *J. Organomet. Chem.*, 1987, **334**, 181–194.

376. B. E. Haines and D. G. Musaev, *ACS Catal.*, 2015, **5**, 830–840.

377. S. K. Bhargava, S. H. Priver, A. C. Willis and M. A. Bennett, *Organometallics*, 2012, **31**, 5561–5572.

378. R. F. Heck, *J. Am. Chem. Soc.*, 1968, **90**, 5518–5526.

379. A. De Meijere and F. E. Meyer, *Angew. Chem., Int. Ed.*, 1994, **33**, 2379–2411.

380. P. Fitton, M. P. Johnson and J. E. McKeon, *Chem. Commun. (London)*, 1968, 6–7.

381. P. Fitton and E. A. Rick, *J. Organomet. Chem.*, 1971, **28**, 287–291.

382. F. Ozawa, A. Kubo and T. Hayashi, *Chem. Lett.*, 1992, 2177–2180.

383. F. Proutiere and F. Schoenebeck, *Angew. Chem., Int. Ed.*, 2011, **50**, 8192–8195.

384. L. J. Goossen, D. Koley, H. L. Hermann and W. Thiel, *Organometallics*, 2005, **24**, 2398–2410.

385. C. Amatore, A. Jutand and A. Suarez, *J. Am. Chem. Soc.*, 1993, **115**, 9531–9541.

386. G. W. Parshall, *J. Am. Chem. Soc.*, 1974, **96**, 2360–2366.

387. D. Milstein and J. K. Stille, *J. Am. Chem. Soc.*, 1979, **101**, 4981–4991.

388. M. Perez-Rodriguez, A. A. C. Braga, M. Garcia-Melchor, M. H. Perez-Temprano, J. A. Casares, G. Ujaque, A. R. de Lera, R. Alvarez, F. Maseras and P. Espinet, *J. Am. Chem. Soc.*, 2009, **131**, 3650–3657.

389. K. K. Sun and W. T. Miller, *J. Am. Chem. Soc.*, 1970, **92**, 6985–6987.

390. J. Rebek and F. Gavina, *J. Am. Chem. Soc.*, 1974, **96**, 7112–7114.

391. C. Gibard, *Synlett*, 2014, **25**, 2375–2376.

392. E. Hirabayashi, A. Mori, J. Kawashima, M. Suguro, Y. Nishihara and T. Hiyama, *J. Org. Chem.*, 2000, **65**, 5342–5349.

393. H. L. Johnston, F. Cuta and A. B. Garrett, *J. Am. Chem. Soc.*, 1933, **55**, 2311–2325.

394. S. A. Girard, T. Knauber and C. J. Li, *Angew. Chem., Int. Ed.*, 2014, **53**, 74–100.

395. S. J. Lou, Y. J. Mao, D. Q. Xu, J. Q. He, Q. Chen and Z. Y. Xu, *ACS Catal.*, 2016, **6**, 3890–3894.

396. C. H. Cho, M. Sun, Y. S. Seo, C. B. Kim and K. Park, *J. Org. Chem.*, 2005, **70**, 1482–1485.

397. P. H. Oldham, G. H. Williams and B. A. Wilson, *J. Chem. Soc. C*, 1971, 1094–1098.

398. H. J. Frohn, A. Klose and V. V. Bardin, *J. Fluor. Chem.*, 1993, **64**, 201–215.

399. S. Rosner and S. L. Buchwald, *Angewandte Chemie*, 2016, **55**, 10463–10467.

400. J. Burdon, Hollyhea.Wb and J. C. Tatlow, *J. Chem. Soc.*, 1965, 6336–6342.

401. T. Migita, T. Nagai, K. Kiuchi and M. Kosugi, *Bull. Chem. Soc. Jpn.*, 1983, **56**, 2869–2870.

402. N. M. Chaignon, I. J. S. Fairlamb, A. R. Kapdi, R. J. K. Taylor and A. C. Whitwood, *J. Mol. Catal. A-Chem.*, 2004, **219**, 191–199.

403. D. R. Coulson, L. C. Satek and S. O. Grim, in *Inorg. Synth.*, John Wiley & Sons, Inc., 2007, pp. 121–124.